Studies on Mg^{2+} and Coenzyme B_{12} Induced Conformational Changes in Coenzyme B_{12} Riboswitches from *E. coli* and *D. hafniense*

DISSERTATION

zur

Erlangung der naturwissenschaftlichen Doktorwürde

(Dr. sc. nat.)

vorgelegt der

Mathematisch-naturwissenschaftlichen Fakultät

der

Universität Zürich

von

Pallavi Choudhary

aus

Indien

Promotionskomitee

Prof. Dr. Roland K. O. Sigel (Vorsitz, Leitung der Dissertation)

Prof. Dr. Gilles Gasser

Prof. Dr. Nathan Luedtke

Zürich 2014

Acknowledgements

I would like to express my sincere gratitude to my Ph.D. advisor, Prof. Dr. Roland K. O. Sigel for giving me the opportunity to explore the manifold facets of the fascinating world of riboswitches. I am grateful to him for his kind support, great mentorship, welcoming my ideas and his perennial enthusiasm.

My special thanks to the members of my Ph.D. committee Prof. Dr. Gilles Gasser and Prof. Dr. Nathan Luedtke for kindly acting as referees.

I thank Dr. Julien Maillard and Prof. Christof Holliger from the Department of Enviromental Biotechnology, Ècole Polytechnique Fédérale de Lausanne (EPFL) for a wonderful collaborative project on the B_{12} riboswitches from *Desulfitobacterium*. Many thanks to Dr. Julien Maillard for his constant support right from start to the end of this project.

I am very thankful to the Functional Genomics Center, ETH/UZH, Zürich (FGCZ) for their kind support throughout our work on the Biacore T100. Thanks to Dr. Stefan Schauer (FGCZ) for his timely help and constant supervision during the SPR experiments.

For the financial support, I thank the European Research Council (ERC starting grant to RKOS), the Swiss National Science Foundation (to RKOS), the COST Action CM1105, University of Zürich and the Graduate School of Chemical and Molecular Sciences, Zürich (CMSZH).

I would also like to thank all the members of the Sigel group for their great support throughout my research.

Big thank you to Dr. Sofia Gallo for helping me in the *btuB* project, for all the insightful discussions, for correcting my manuscripts and for guiding me in almost every aspect related to my Ph.D. work.

Many thanks to Maria Pechlaner, Joachim Schnabl, Maximiliane Korth and Silke Johannsen for their great support. My very special thanks to Maria Pechlaner for translating my thesis summary to German and for always being there to help me out. Thanks also to Miriam Skilandat for correcting my thesis chapter and to Alessia Duerst for her help in my projects.

Thanks to my lab-mates of lab 34F76, Michelle Schaffer, Joachim Schnabl and Anastasia Musiari for a great friendly atmosphere in the lab and for their unquestionable help. Special thanks to my friend, Bhaumik Dave for his timely help in the lab and good times on/off the campus. Thanks to Marianthi Zampakou for cheerful times in the lab.

I would also like to extend my appreciation to Prof. Dr. Eva Freisinger and her group for their help on the 'F' floor. Many thanks to our institute, ACI and all the ACI members for their help whenever needed. Special thanks to Manfred Jöhri for his patience to solve the computer related problems.

Many thanks to Leiloma, who made me feel at home away from home.

I definitely would not have come this far without the support of my friends and my family.

I owe genuine thanks to my best friends, Sheetal and Rakesh for their friendship, motivation and fair criticism throughout many years. I am grateful to both of them for sharing my joys, bearing my burdens and always guiding me. I will never be able to thank Rakesh enough for all his help related to the discussions on the experiments and corrections of thesis

chapters. I thank my friends in Zürich- Manoj, Dheeraj, Kiran and Abhijeet, for the wonderful moments that we spent together.

My thesis is dedicated to my dear parents. I acknowledge them for their love, encouragement and their faith in me. Many thanks to my siblings, Madhav and Aarti, for their constant support right from my childhood. Special thanks to Aarti for her wise advice, emotional support and all the fun times. I thank my sister-in-law, Sujata and my adorable niece, Risa for their affection. From thousands of miles away, my family made my life much easier here in Zürich.

Very special thanks to Mangesh, who with his unconditional love, supreme care and vibrant positivity turned each day beautiful. I truly appreciate his patience and great support especially during the writing phase.

Last but not least, I thank all my teachers for sharing their knowledge and inculcating many aspects of science and life.

Table of Contents

List of Abbreviations

AdoCbl	Adenosylcobalamine
Ado-Cobi	Adenosylcobinamide
AdoFactA	Adenosyl factor A
AqCbl	Aquo-cobalamine
dG	Deoxy-guanine
DMB	Dimethylbenzimidazole
DNA	Deoxy-ribonucleic acid
E. coli	*Escherichia coli*
ER	Endoplasmic reticulum
FMN	Flavin mononucleotide
FRET	Förster Energy Resonance Transfer
GlcN6P	Glucosamine-6-phosphate
KL	Kissing Loop
KT	Kink-turn
LB	Luria-Bertani
lncRNA	long non-coding RNA
miRNA	micro RNA
Moco	Molybdenum cofactor
mRNA	Messenger RNA
ncRNA	non-coding RNA
nt	nucleotide
NTP	Nucleoside 5'-triphosphate
PAGE	Polyacrylamide Gel Electrophoresis
PK	Pseudoknot
preQ1	pre-Quenosine-1
RBPs	RNA binding proteins
RBS	Ribosome binding site
R_g	Radius of gyration
RNA	Ribonucleic acid
RNAP	RNA polymerase
rRNA	Ribosomal RNA
SAM	S-Adenosylmethionine

SD	Shine-Dalgarno sequence
SE	Standard Error
snoRNA	small nucleolar RNA
snRNA	small nuclear RNA
SPR	Surface Plasmon Resonance
SRP	Signal recognition particle
THF	Tetrahydrofolate
TPP	Thiamine pyrophosphate
tRNA	transfer RNA
Tuco	Tungsten cofactor
UTR	Untranslated region
$VitB_{12}$	Vitamin B_{12}

1 Introduction

In 1944, DNA was proposed to be an important component of the genetic material and possibly the only one (1). Watson and Crick further in 1953 proposed the structural model for DNA showing that DNA can carry out self replication which is a crucial requirement for being the genetic material (2,3). However, the idea how DNA could directly define the sequence of proteins was still a mystery due to different locations of these macromolecules inside cells i.e. nucleus for DNA and cytoplasm for proteins. The discovery of microsomes- the cytoplasmic particles composed of RNA and proteins- as a site for protein synthesis led to an emergence of a third molecule in decoding the DNA sequence i.e. RNA (4,5). Therefore, a relation between DNA, RNA and proteins appeared as a solution to the process of decoding the nucleotide sequence from DNA into amino acid sequence of proteins. A term, 'central dogma of molecular biology' was then coined by F. Crick giving early insights into a connection between the process of transcription of mRNA from DNA and translation of mRNA into corresponding proteins (6).

However, the one directional central dogma did not appear to be followed religiously by certain cellular machinery as it was proposed by F. Crick. The events that mainly challenged the concept of central dogma were the discovery of prions (7-9), chaperons (in protein folding) (10-12) and the RNA dependent DNA polymerase- reverse transcriptase (13,14). Moreover, viruses were shown to carry RNA as their genetic material instead of a conventional DNA (15). Further in 1981, Thomas Cech and co-workers showed that the precursor transcript coding for 26S rRNA *Tetrahymena thermophila* contains a 413 nucleotide long IVS/ intron that catalyzes a self splicing reaction to produce the mature transcript (16). In 1983, Altmann and coworkers found that the RNA moiety of enzyme RNase P catalyzes the maturation of tRNA (17). The dual role of RNA as a genome and as a catalyst led Walter Gilbert to propose the existence of an RNA world where RNA was predicted to be the first entity arising in a pre-biotic environment even before the onset of DNA and proteins (18).

The functional diversity of RNA was subsequently expanded and can be categorized into two main groups being coding RNA (mRNA) and non-coding RNA. Non-coding RNAs like Group I and II introns, RNase P, snRNA (of the spliceosome), snoRNAs, tRNA, rRNA, SRP-RNA are involved in RNA processing, protein synthesis and co-translational protein targeting to ER (eukaryotes)/ plasma membrane (prokaryotes) (17,19-23). Other set of non-coding RNAs called as regulatory RNAs are involved in the regulation of gene expression at transcriptional or translational level e.g. miRNA, lncRNA and riboswitches (24-26). All of the above mentioned functions of RNA are largely influenced by their secondary and tertiary structures that enable RNAs for intra-molecular/ inter-molecular interactions as well as facilitate their interaction with RBPs and with ligands.

1.1 RNA architecture

1.1.1 Basic components

Nucleic acids are the polymers of nucleotides that consist of three basic components- a) a pentose sugar b) a nitrogenous base and c) a phosphate (Figure 1.1A). The nitrogen containing bases of nucleic acids are purines (Adenine and Guanine) and pyrimidines (Cytosine, Thymine, Uracil). A nucleoside triphosphate (NTP) is formed by linking the C1' of the pentose to the N9 of purine or N1 of pyrimidine and C5' of sugar to a triphosphate moiety. A polymeric chain of nucleotides is formed by covalently linking the 3'- hydroxyl group of one nucleotide unit to the 5'- α- phosphate of the next nucleotide through the formation of a 3'-5'-phosphodiester bond (Figure 1.1B). The polymerization reaction is catalysed by DNA and RNA polymerases with the release of inorganic pyrophosphate (PPi) from the NTP. The covalent backbone of nucleic acids thus consists of alternating phosphate and pentose residues. The phosphodiester linkages have the same orientation along the strand of nucleic acids giving each strand a distinct 5' end and a 3' end.

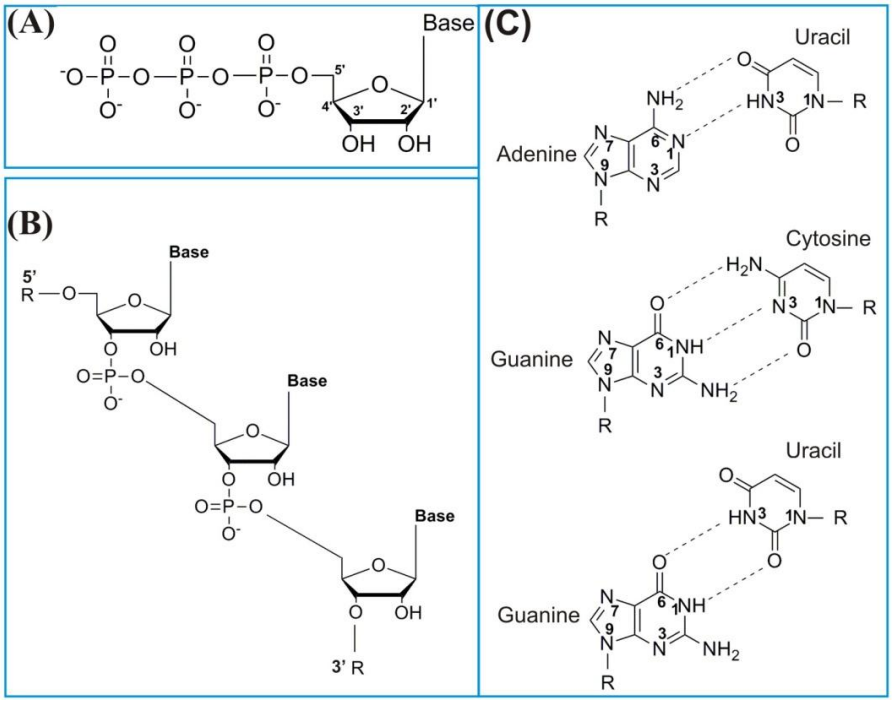

Figure 1.1: Basic components of the RNA structure: (A) A nucleoside tri-phosphate (NTP) unit in RNA consisting of a nitrogenous base, a ribose sugar and a tri-phosphate moiety. (B) A tri-nucleotide RNA strand in which the nucleotides are linked by the formation of 3'-5'- phosphate bridges. (C) Common base pairs in RNA. Shown are the Watson-Crick base pairs (Adenine-Uracil, Guanine-Cytosine) and a G-U wobble pair.

DNA and RNA are composed of the same purines but vary in their pyrimidine composition. DNA has Cytosine and Thymine as its pyrimidine content whereas RNA contains Cytosine and Uracil. The pentose sugar varies as well being 2'-deoxy-ribose in DNA and ribose in RNA. Moreover, the relative orientation of C2' and C3' of the ribose with respect to the plane of C5' is different in DNA and RNA. DNA contains C2' endo conformation in contrast to the C3' endo conformation seen in RNA. Another major difference lies in the double stranded helices of DNA and RNA as DNA predominantly forms B form helix whereas RNA helices are organized in A form with deep, narrow major grooves and shallow minor groove.

The formation of a helix needs base pairing between the complementary nucleotides of the two strands of nucleic acids (Figure 1.1C). DNA and RNA both follow a standard Watson-Crick base pairing with the hydrogen bonds between their purines and pyrimidines (A-T, G-C, A-U base pairing). RNA however, can also adopt other patterns of base pairing like a wobble base pair (between G and U), sheared G-A pair and Hoogsteen base pairs (27-32). The network of hydrogen bonding interactions stabilizes the conformation of nucleic acids.

1.1.2 Structural organization

RNA structure can be categorized into three basic levels of organization similar to proteins primary, secondary and tertiary structure. Primary structure refers to the sequential order of nucleotides in RNA. However, it may not necessarily correspond to the DNA sequence of the gene encoding RNA as many of the biologically functional RNA undergo post-transcriptional modifications. As the transcribed RNA is single stranded, it can undergo intra-molecular interactions mainly through the formation of Watson-Crick base pairs between the complementary nucleotides. Such interactions form the secondary structure of RNA that contains the base paired as well as the intervening unpaired regions. Although RNA predominantly forms A helix, other secondary structural elements such as hairpins, bulges, internal loops and junctions are common as well (Figure 1.2) (33).

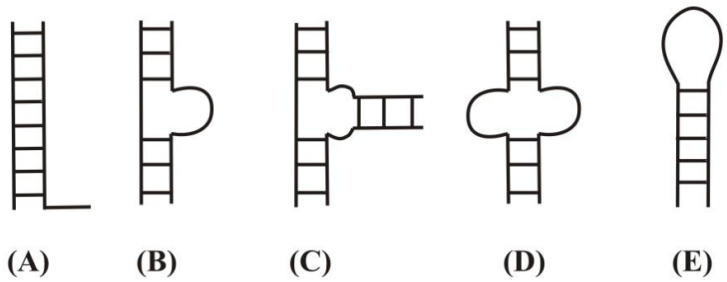

Figure 1.2: Secondary structural elements of RNA: The base pairing interactions within RNA lead to the formation of helical regions and the intervening unpaired regions represented by helix (A), bulge (B), junction (C), internal loop (D) and hairpin stem-loop (E). Figure adapted from ref. (33).

The secondary structure of RNA can be predicted using the folding programmes like mfold. These programmes calculate the probable base pairing scheme in RNA that would result into the secondary structure with the lowest free energy (34). The predicted secondary structure can be confirmed by enzymatic (RNase) or chemical probing of ^{32}P-end labelled RNA (35). These probes modify RNA at solvent accessible regions that are not involved in Watson-Crick base pairing and therefore map the unpaired and paired regions in the RNA.

Tertiary structural elements involve a specific interaction between the secondary structural motifs of RNA. Such interactions can take place between two helical regions, between paired and unpaired motifs as well as within the unpaired regions. The commonly occurring tertiary motifs in RNA are coaxial stacks, adenosine platforms, tetraloops, ribose zippers, pseudoknots and loop-loop interactions (33,36). All of these interactions stabilize the tertiary fold of RNA and therefore form a biologically functional RNA molecule that is recognized by proteins, ligands and other RNA molecules. The tertiary interactions within the RNA can be modelled by comparative sequence analysis and solved at high resolution by techniques like NMR spectroscopy and X-ray crystallography.

1.1.3 RNA folding and the role of metal ions

RNA is a polyanionic molecule due to its negatively charged phosphate backbone. Therefore, the folding of RNA into its secondary and tertiary structural motifs causes an accumulation of negative charge in space (37). The RNA folding thus requires charge screening to compensate the electrostatic repulsion and to bring the structural elements in proximity. This task is mainly fulfilled by monovalent and divalent cations like K^+ and Mg^{2+} due to their high intracellular concentrations (Figure 1.3) (38-41). However other monovalent ions like Na^+ and Li^+ can also fold certain RNAs (42). The diffuse binding of metal ions to RNA is observed more commonly than site specific binding and it contributes to the stabilization of RNA secondary/tertiary structures through non- specific charge screening (39,43,44). The formation of secondary structure can be stimulated by almost any monovalent/divalent cation or by cationic polyamines. However, some of the tertiary interactions are dependent on a strict requirement for metal ions, mostly Mg^{2+} (37,45-47). Due to its small size and high charge density, Mg^{2+} is preferred for charge neutralization in RNA. Mg^{2+} can interact site specifically with RNA in both outer sphere and inner sphere manner (48). In case of outer sphere interaction, water ligands of hexahydrate Mg^{2+} interact with the phosphate backbone and the RNA bases whereas the direct interaction between Mg^{2+} and RNA is established through inner sphere co-ordination (38,44,49).

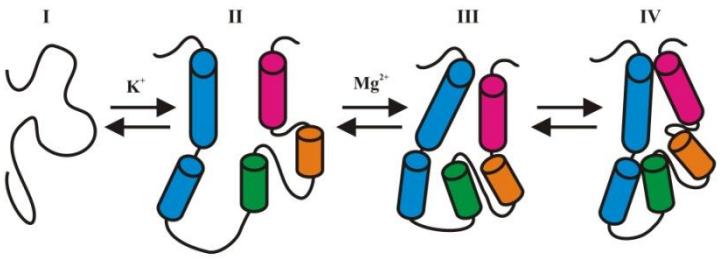

Figure 1.3: Metal ion induced folding of RNA: Association of monovalent ions (K^+) with the unfolded RNA (I) leads to the formation of secondary structure (II). The formation of tertiary structure (III) is promoted by divalent metal ions (Mg^{2+}). However, further conformational rearrangements might occur in the tertiary structure to form the native active tertiary structure (IV).

While monovalent and divalent cations contribute to the structural stabilization of RNA, trivalent ions are not the natural cofactors for RNA. They however, can be used for structural mapping of metal ion binding sites in RNA e.g Tb^{3+} and other lanthanide ions (50-54). Tb^{3+} especially has been used as a closer mimic to Mg^{2+} as it can replace Mg^{2+} with high affinity due to its higher charge. Once bound to RNA, Tb^{3+} carries out the hydrolytic cleavage of RNA backbone at physiological pH due to its pK_a being 7.4 and therefore, enables the mapping of metal ion binding sites on a near native/native conformation of RNA molecule (53).

Metal ions are not only needed for the stabilization of RNA structure but also for the catalysis of ribozymes (41,48,55), for interaction with ligands (56-60) and for gene regulation as shown by the Mg^{2+} sensing riboswitch (61).

1.2 Regulatory RNAs in bacteria

Alteration of gene expression is extremely crucial for a cell to survive changing environmental conditions. Regulatory non-coding RNAs (ncRNA) serve this purpose and affect all the steps of gene expression via similar mechanisms in all organisms. RNA regulators offer several benefits to the cell over protein regulators. The regulatory RNAs are more economical to produce as they are shorter than most of the mRNAs and are produced without an extra step of translation in contrast to protein regulators. Moreover, as most of the regulatory RNAs act post-transcriptionally, they can rapidly shut off or turn on the gene expression as compared to protein regulators. Regulatory RNAs in bacteria are often small transcripts, sRNA (~ 50 to 300 nt) that are encoded either in *cis* – on the opposite DNA strand of the target RNA or in *trans* – located separately from the genes encoding their target RNA (62-65). Depending on the nature of their target mRNA, sRNA can follow various mechanisms to alter the expression of their target gene(s). The regulation involves base pairing between the sRNA to their target mRNA due to extensive (in *cis* encoded) or limited (in *trans* encoded) complementarities. This class of non-coding RNA is called antisense RNA that regulates the gene expression via translation inhibition or activation, transcription termination and also by RNase mediated degradation of mRNA (26). The other class of ncRNA binds to proteins and modulate their activities related to gene expression (26,66). Considering the diversity of the target mRNA affected by regulatory RNAs, the search for new mechanisms employed by these RNA began. In 2002, another class of non-coding, *cis* acting regulatory RNA elements were discovered in bacteria called riboswitches.

1.2.1 Brief history of riboswitch discovery

Artificial short RNA sequences that could bind ATP, amino acids, antibiotics and organic dyes were discovered through *in vitro* evolution in 1990 (67,68). These short RNA segments were named aptamers that bind to their target molecule with high affinity and specificity. The discovery of aptamers led to the questions if natural evolution created similar RNA segments with some specific functions in the cellular machinery.

The role of certain non-coding RNA sequences as natural aptamers in cellular regulation led to the discovery of riboswitches in bacteria (69-72). Riboswitches represent those RNA elements of the RNA world that react to changing environmental conditions and therefore, constitute a widespread means of genetic regulation at mRNA level in prokaryotes. These RNA elements are located commonly in the 5' UTR of mRNA and are able to bind their cognate ligand with unusually high specificity and high affinity notably, without the aid of accessory protein factors (73,74). Binding of metabolites lead to regulation of the gene coding for mostly the transporters/ enzymes involved in cellular regulation of the bound ligand (74-76).

1.2.2 Framework of riboswitches

Structurally, a ribowitch consists of two domains, the aptamer and the expression platform (EP) (Figure 1.4) (74,77). An aptamer region is responsible for recognition of the ligand and is evolutionarily conserved across the species (73,78). A compact three dimensional fold adopted by the aptamer facilitates recognition of the ligand with high specificity. A more variable domain of the riboswitch is an expression platform situated downstream from the aptamer. An expression platform is a regulatory domain of the riboswitch which harbours two mutually exclusive secondary structures that constitute the ON and OFF state of the riboswitch (79). The aptamer and expression platform share a stretch of sequence called switching sequence (Figure 1.4). A metabolite binding to the aptamer alters its conformation and a signal is transmitted to the EP through structural changes in the switching sequence (74,77). This leads to destabilization of one of the competing structures in the EP that either shuts off or activates gene expression.

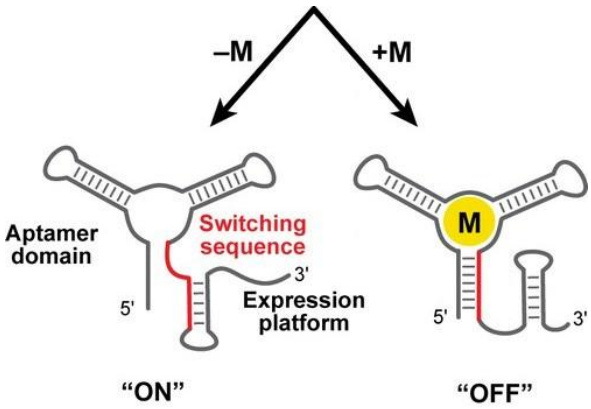

Figure 1.4: Structure of riboswitches: An aptamer and an expression platform of the riboswitch are connected together by a switching sequence (red). Addition of metabolite (M) induces conformational rearrangements in the switching sequence followed by the changes in the expression platform. The 'OFF' state of the riboswitch is thus stabilized over the 'ON' state. Figure taken from ref. (79).

Metabolite dependent changes in the riboswitches were monitored mainly by a classical method called as in-line probing that indicates the local structure at each inter-nucleotide linkage (Figure 1.5) (70,80). This method exploits the self cleavage reaction of RNA where the 2'-hydroxyl group attacks the adjacent phosphorous center. The cleavage reaction takes place when the attacking 2'-hydroxyl group, the phosphorous center and leaving 5' oxygen of the phosphodiester linkage are in a linear or 'in-line' geometry with each other (80). The linkages within highly structured regions of RNA (base paired helices) resist in-line cleavage due to the absence of in-line geometry whereas, the dynamic regions of RNA (loops, junctions) adopt in-line geometry through random motions and therefore undergo enhanced rate of spontaneous cleavage (74,80).

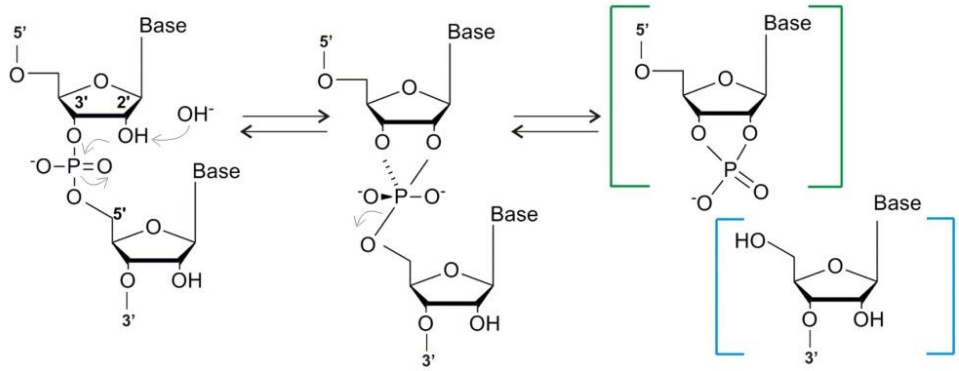

Figure 1.5: Mechanism for self-cleavage reaction in RNA: The 'in-line' nucleophilic attack by 2' oxygen on the adjacent phosphorous center cleaves the inter-nucleotide linkage in RNA resulting into the formation of 2',3'-cyclic phosphate (green bracket) and 5' hydroxyl termini (blue bracket). Figure partially adapted from ref. (74,80).

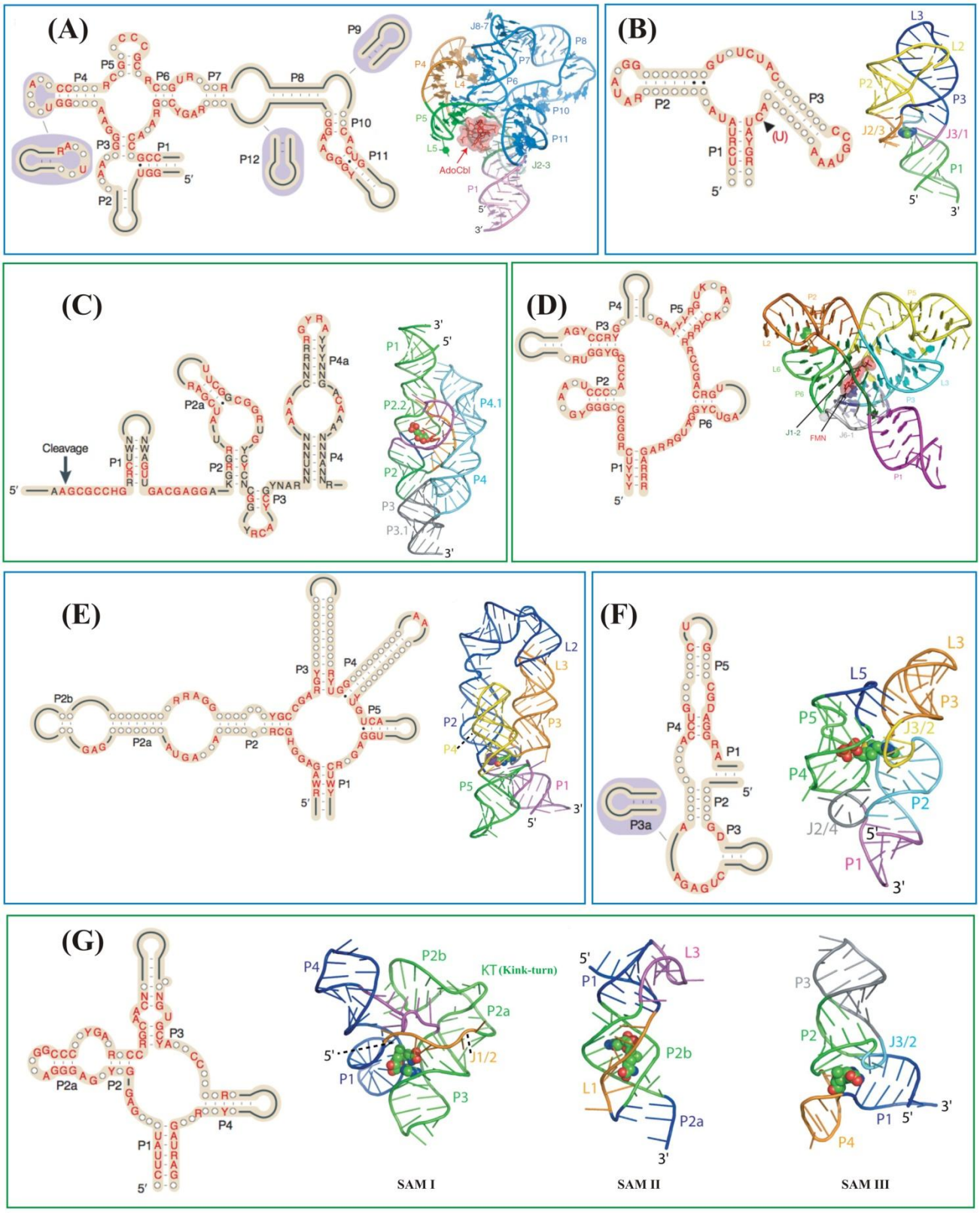

Figure 1.6: Secondary and tertiary structures of known riboswitch classes: Shown are the consensus sequences and tertiary structures for AdoCbl (A), purine (B), GlcN6P (C), FMN (D), lysine (E), TPP (F) and SAM (G) binding riboswitches. On the secondary structure of the riboswitches, the nucleotides in red are conserved in at least 90% of the representatives and a circle indicates a nucleotide of any base identity. The alternative secondary structural motifs are shown in blue ovals. The tertiary structures of riboswitches in their metabolite bound form are shown as ribbon diagrams. The metabolites are represented as spheres unless indicated. In case of purine binding riboswitches (B), C to U mutation (marked by an arrow) changes the specificity of adenine riboswitch to guanine. Figure adapted from ref. (74, 78).

The riboswitches binding to diverse array of ligands have been discovered in the bacterial genomes (Figure 1.6). The reported riboswitches bind mainly to coenzymes and cofactors (AdoCbl, TPP, THF, FMN, SAM, Moco, Tuco), nucleobases (guanine, adenine, preQ1, c-di-GMP,dG), amino acids (lysine, glycine, glutamine), metal ions (Mg^{2+}) and phosphoamine sugar (GlcN6P) (81,82). All of these metabolites/ligands regulate the essential pathways for survival of bacteria.

1.2.3 Modes of gene regulation by riboswitches

The genetic regulation by riboswitches is operational mainly at the transcriptional or translational level for most of the riboswitches (Figure 1.7). The transcriptional control is manifested by the formation or destabilization of the intrinsic terminator. An intrinsic terminator contains an extended stem-loop structure followed by a stretch of six or more U residues that abort transcription by stalling the RNA polymerase (74,75,77). The conformational change in aptamer upon ligand binding is transduced to the expression platform through a switching sequence which is incorporated either into the terminator or anti-terminator stem. The repression or activation of the gene transcription is mediated by abortion of transcription or through transcription elongation respectively. The translational control of mRNAs depends on the accessibility of the ribosome binding site (RBS) or the Shine –Dalgarno (SD) sequence (74,77,79,81). The ligand induced conformational change in aptamer either presents or sequesters the SD sequence from the 30S ribosomal subunit, resulting into the translation initiation or inhibition.

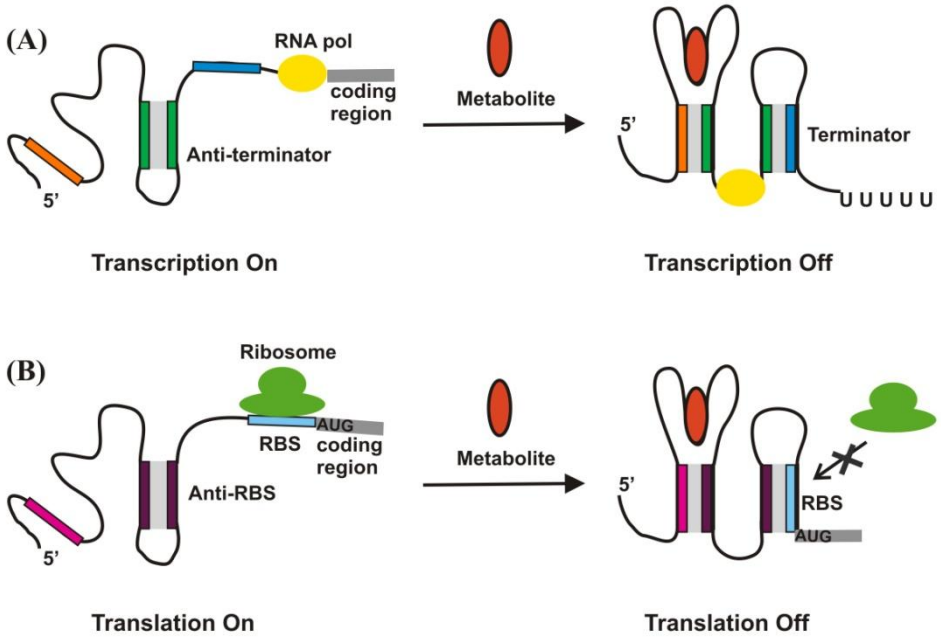

Figure 1.7: Mechanism of gene-regulation by riboswitches: (A) In a transcriptional control, metabolite (orange) binding induces the formation of an intrinsic terminator in the expression platform and thereby, aborts the transcription of the gene by stalling the RNA polymerase (yellow). (B) Metabolite binding inhibits translation of the mRNA by sequestering the ribosome binding site (RBS) within the expression platform and thereby prevents ribosome (green) binding. Helical regions are shown as rectangles along with the base paired (grey) regions within.

Apart from the transcriptional and translational control, recently other mechanisms like the self cleavage of mRNA, mRNA degradation, trans-regulation and intron splicing are reported in bacterial/plant regulatory RNAs that lack the transcriptional/translational regulatory elements (83). A riboswitch-ribozyme, *glmS* is located in the 5' UTR of the gene encoding glucosamine-6-phosphate (GlcN6P) synthetase in Gram positive bacteria (84). The similarity between global

conformations of ligand bound and ligand unbound structures of *glmS* ribozyme suggested that *glmS* ribozyme does not undergo ligand induced conformational changes unlike other riboswitches (84-86). Binding of GlcN6P triggers an autocatalytic cleavage reaction near the 5' end of the transcript, producing a 2'-3' cyclic phosphate and a 5'hydroxyl termini (87-89). This reaction is followed by RNase J1 mediated degradation of 3' cleaved product that includes coding region for *glmS* and prevents the synthesis of GlcN6P (90). Therefore, through combined actions of self cleavage and mRNA degradation, *glmS* ribozyme controls the level of GlcN6P, a cell wall component in Gram positive bacteria (91).

The Mg^{2+} sensing riboswitch, *mgtA* (in γ proteobacteria) mediates the regulation of gene expression through the process of mRNA degradation. Gene *mgtA* codes for a Mg^{2+} transporter and therefore, under high Mg^{2+} conditions, forms an alternative stem-loop structure in the 5' UTR that abolishes transcription of the gene (92). Along with transcriptional attenuation, the RNase E mediated degradation of the *mgtA* transcript affects its stability and in turn reduces the expression of a transporter, MgtA (93). A *trans* regulation is displayed by a riboswitch that functions as a small non-coding RNA and regulate the expression of distally located target mRNA. Along with the regulation of their own downstream genes, two SAM riboswitches- *SreA* and *SreB* in *Listeria monocytogenes* can bind to the distal part of *prfA* untranslated RNA and downregulate the expression of major virulence regulator, PrfA (94). TPP binding riboswitches are found in the 5' UTR (fungi) and 3' UTR (*Arabidopsis thaliana)* of the genes involved in thiamine metabolism (78,95-98). These riboswitches are located within an intron of the mRNA and regulate the expression of downstream genes through TPP induced splicing mechanism (78,95-98).

Most of the riboswitches function in isolation, controlling the gene expression through single metabolite binding to a single aptamer domain. However, some genetic systems harbour a tandem arrangement of aptamers or complete riboswitches to fine-tune the fluctuating metabolite concentration to the gene expression regulation. The glycine riboswitch regulates the expression of gene products that catabolises excessive glycine as an energy source. Therefore, to allow increased sensitivity to changing glycine concentration, the glycine riboswitch consists of two similar aptamer domains arranged consecutively (99,100). These tandem aptamers recognize glycine in a co-operative fashion such that glycine binding at one aptamer domain increases affinity towards glycine at the other aptamer domain, exerting an efficient regulation of glycine metabolism (99-101).

Along with tandem aptamers, tandem riboswitches that recognize two distinct ligands have also been reported e.g in *Bacillus clausii*, SAM I and AdoCbl riboswitches are arrayed tandemly along with their separate intrinsic terminators (102). These riboswitches regulate the expression of MetE, a less efficient enzyme synthesizing methionine from homocysteine (103). In contrast, MetH, a more efficient enzyme in methionine synthesis uses methylcobalamine (an AdoCbl derivative) for catalysis (104). Therefore, when SAM or AdoCbl are in excess, the less efficient route to methionine synthesis is shut off.

Although most of the riboswitches exhibit the 'OFF' switch upon ligand binding, repressing the synthesis of transporters/enzymes at high ligand concentration, there are two exceptions. The adenine binding riboswitch that regulates the expression of *ydhL* gene of *B. subtilis* undergoes an 'ON' switch at high adenine concentration (105). *ydhL* codes for purine transporter (106) and therefore, expels the excess adenine through positive regulation of the transporter at high adenine levels. Similarly, lysine regulating *LYS* elements in *T. tencongenesis* and *F. nucleatum* activates the expression of lysine catabolising genes and transporters at high lysine concentration (107).

1.2.4 Architecture of riboswitches

Although there are no clear evolutionary relationships between the different classes of riboswitch, the basic riboswitch architecture seems to follow certain common structural trends and shares the architectural principles as that of other large cellular RNAs. Most of the riboswitches consist of coaxial stacks or their bundles connected by junctions and pseudoknots (PK) with three-way junctions being the most common riboswitch scaffold. The helical elements in riboswitches are often arranged with other recurrent structural motifs in RNA like A-minor triples, kink-turn (KT), kissing-loop (KL) and T-loop interactions (108-110). Specifically the T-loop-PK interactions are observed in FMN and AdoCbl binding riboswitches (59, 109). These structural motifs are extremely essential for riboswitch function as their deletion renders the riboswitch non-functional under physiological conditions.

All riboswitches depend on metal ions for their function. Metal ions are not only involved in riboswitch folding and stabilization of the RNA conformation but also assist in ligand-riboswitch interactions by neutralizing the negatively charged moieties of ligands (56,58,59,86,112-115). Another element of commonality between riboswitches is that most of the ligand binding pockets are located close to the switching sequences. Since the alternative pairing of the switching sequences depends upon the presence of ligand, the close proximity of the bound ligand and the switching element facilitates the transduction of the signal to the expression platform. Also, the global conformation of most riboswitches is organized by long range tertiary interactions induced or stabilized by ligand binding.

1.2.5 Binary system of riboswitch classification

On the basis of the architecture of the ligand binding pocket and ligand induced conformational changes, riboswitches were recently grouped into two categories, i.e. Type I and Type II riboswitches (Figure 1.8) (79). Type I riboswitches consist of a pre-organized tertiary structure with a single, localized binding pocket. Ligand induced conformational changes in RNA are restricted to a region within and adjacent to a binding pocket as in the case of adenine, guanine, SAM II riboswitches and the *glmS* ribozyme (57,116-123). Type II riboswitches consist of a bipartite binding pocket brought together by ligand induced tertiary structure. These riboswitches therefore undergo global conformational changes in addition to local changes within the binding pocket e.g. SAM I, TPP and Mg^{2+} sensors (114,124-126). Sometimes the distinction between two types is less obvious for some riboswitches e.g. the THF sensor similar to a Type I riboswitch adopts a pre-formed ligand binding pocket but undergoes a large conformational change upon ligand binding like Type II riboswitches (127).

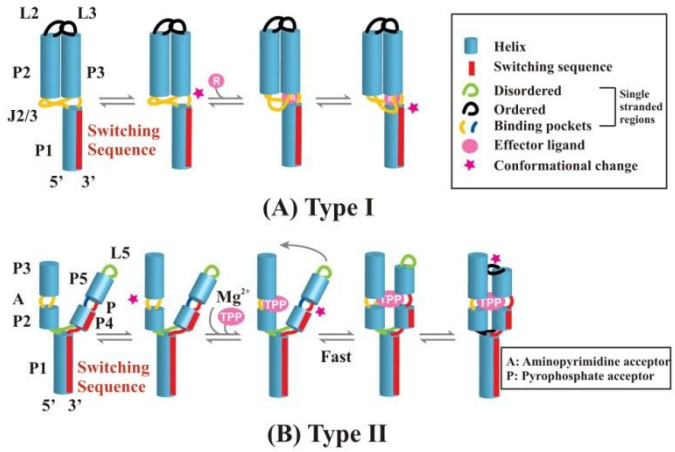

Figure 1.8: Conformational changes in Type I and Type II riboswitches: (A) In case of Type I riboswitches (e.g. purine riboswitches), the overall global fold of the riboswitch is preformed in the absence of ligand except for the binding pocket (gold). The conformational changes (asterisk) in the binding pocket allow ligand (R) (pink) binding followed by the locking of the binding pocket around the ligand. (B) The global architecture is not preformed in Type II riboswitches (e.g. in TPP riboswitch). Binding of TPP and Mg^{2+} to the aminopyrimidine acceptor (A) (gold) and pyrophosphate acceptor (P) (blue) respectively leads to the conformational changes in the riboswitch at the three way junction as well as near P3 and L5. Helical regions are shown as cylinders and single-stranded regions as lines. Figure taken from ref. (79).

Also, this binary system of riboswitch classification is paradoxical when the distinctive gradation in the response of the aptamer to ligand binding is considered. This is demonstrated by SAXS studies carried out on the aptamer domains in different solution conditions (128,129). The aptamers of riboswitches undergo a range of global conformational response depending upon the environmental conditions e.g. the SAM I aptamer exhibits a distinctive ligand free extended and ligand bound compact conformation with 2.5 mM Mg^{2+} similar to the c-di-GMP aptamer (129). However, under more stabilizing Mg^{2+} conditions (10 mM), the SAM I aptamer collapses into a compact conformation similar to the ligand bound conformation even in the absence of ligand (129). The TPP aptamer domains from *E. coli* and *A. thaliana* vary in the R_g for their metabolite free conformations however the R_g for their ligand bound conformation are similar (129). On the contrary, the global conformation of lysine riboswitch is insensitive to the presence of ligand although conformational change was clearly evident with varying Mg^{2+} concentrations in the absence of ligand (129). The FMN aptamer domain notably is globally insensitive to both ligand and Mg^{2+} concentrations (129). Therefore, Type I c-di-GMP undergoes a global change whereas Type II aptamers of SAM I and TPP have a range of response to ligand binding and Mg^{2+} concentrations.

1.2.6 Ligand recognition by riboswitches

Riboswitches recognize their cognate ligands through specific mechanisms that depend upon the architecture of the aptamer domains but mostly seem to employ recurrent molecular strategies due to the characteristic chemical nature of RNA. These interactions mainly involve base stacking, base pairing and metal-ion mediated interactions (Figure 1.9). The riboswitches binding to nucleobases or planar heterocycles mainly employ stacking and base pairing interactions e.g. riboswitches binding to TPP, FMN, SAM, purines, c-di-GMP and preQ1 (59,118,123,130-132). Notably, the replacement of C to U is adequate to alter the ligand specificity of the riboswitch from G to A (105). Some riboswitches employ metal ion mediated interactions with their ligands along with base stacking and base pairing. The pyrophosphate moiety of TPP and the phosphate groups of FMN, c-di-GMP, GlcN6P are recognized indirectly through the interactions mediated by divalent cations (57,59,60,125,132). However, metal ion mediated interactions are not restricted to phosphate containing ligands and divalent cations. Monovalent cations like K^+ co-ordinates the carboxylate group of the lysine and therefore, lysine riboswitch is strictly dependent upon K^+ for ligand recognition (113). The specificity towards K^+ is so high that the riboswitch exhibits 50 to 100 fold weaker affinity towards lysine if K^+ is replaced with Na^+ or Mg^{2+} (113).

The structural organization of the aptamer, the molecular mechanisms employed in ligand recognition and the functional groups of cognate ligand allow riboswitches to distinguish their cognate ligands from related analogues. Most of the riboswitch's aptamer bind their ligands with an apparent dissociation constant (K_D) ranging from low nanomolar to low micromolar indicative of a high affinity interaction. The TPP aptamer recognizes TPP with 1000 fold higher affinity than TMP, thiamine or its analogues (71). Similarly, the FMN riboswitch binds with 1000 fold weaker affinity to riboflavin if it lacks a phosphate group (72). The SAM and B_{12} aptamers strongly distinguish the ligands that lack or modify the methionine and 5'-deoxy-5'-adenosyl moieties respectively (70,133). The lysine aptamer forms a binding pocket that stereospecifically binds L-lysine and also distinguishes the length/nature of alkyl side chain (134). Similarly, the *glmS* ribozyme-riboswitch exhibits 1000 fold rate enhancement in the self cleavage with GlcN6P as compared to its related ligand, glucose-6-phosphate and glucosamine (84)

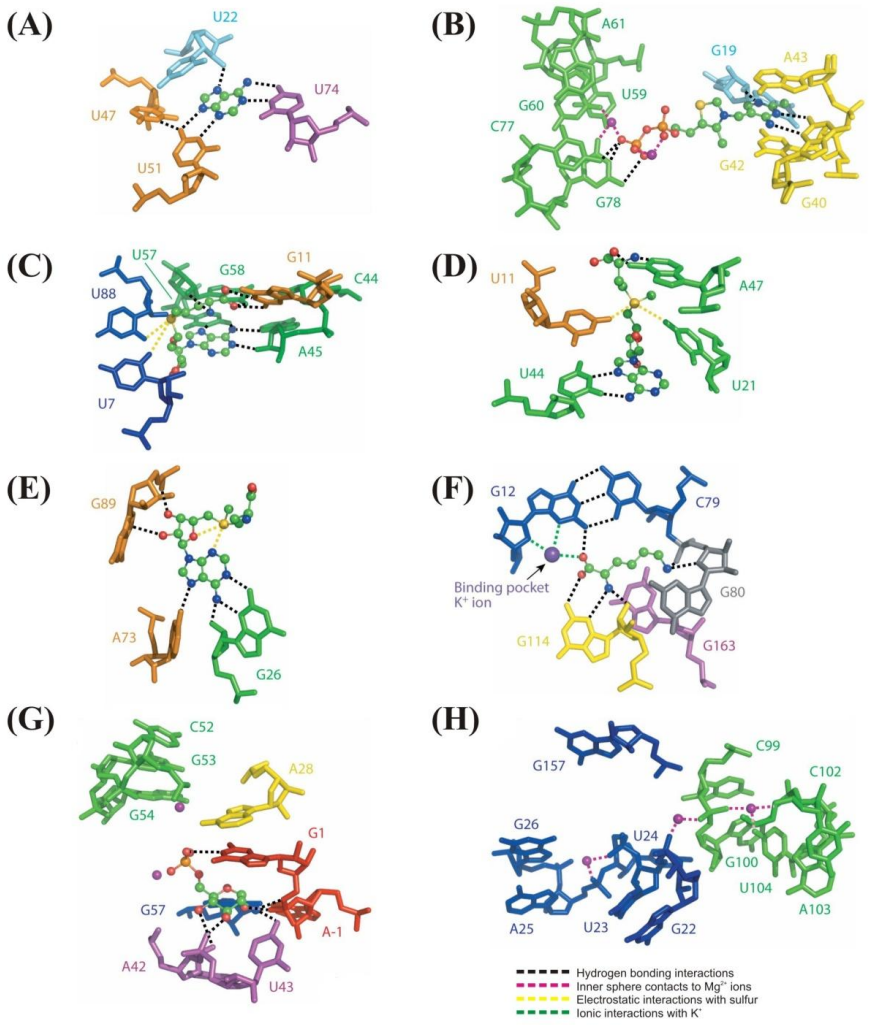

Figure 1.9: Molecular interactions between the ligand and aptamer: Shown are the subset of key interactions in adenine (A), TPP (B), SAM-I (C), SAM-II (D), SAM-III (E), lysine (F), GlcN6P (G) and Mg^{2+} (H) binding riboswitches. Figure taken from ref. (78).

1.2.7 Process of gene regulation by riboswitches

Regulation of gene expression by riboswitches can be divided into three distinct stages

1. **Folding:** Aptamer folds into its initial structure
2. **Metabolite sensing:** Aptamer recognizes the ligand
3. **Regulation:** Conformational change in the aptamer affecting the gene expression.

Studies on aptamer folding by various methods like NMR, SAXS, FRET, sm FRET, single molecule force microscopy have demonstrated that aptamers follow distinct strategies to achieve a folded state. Most of the folding models suggest the critical Mg^{2+} mediated tertiary contacts within the aptamer prior to ligand binding (56,120,135,136). These Mg^{2+} mediated interactions pre-organize the ligand binding pocket and facilitate the formation of binding compatible conformation of the aptamer that sense and bind its cognate ligand.

Metabolite sensing by the riboswitches can be explained by three different models depending upon the mode of interaction between the ligand and the aptamer (Figure 1.10).

(A) Induced fit: The ligand binding pocket is dynamic to allow the ligand to access the interior of the pocket, followed by the pocket closure. Therefore, ligand induces the ligand free state of the aptamer to adopt a new conformation which is more complementary to the ligand (121).

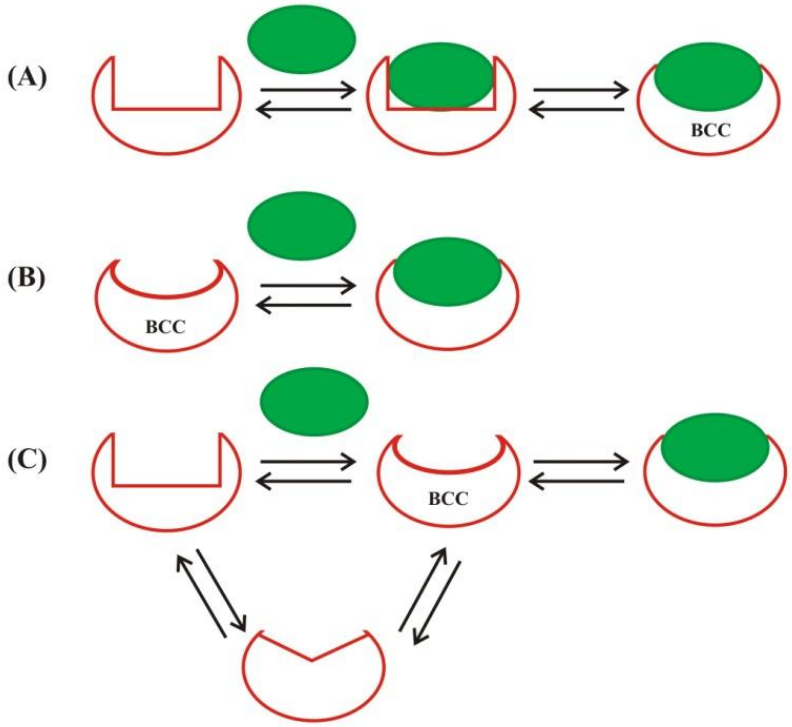

(B) Lock and key: Ligand binding is driven by inherent complementarities between the ligand and the aptamer. Such a binding mode is displayed by ligands that bind to a semi-open binding pocket and therefore, might not need conformational re-arrangements in the aptamer to access the metabolite (127).

(C) Conformational selection: A ligand binding competent conformation is selected by the ligand from the dynamic ensemble of multiple conformations (137).

Figure 1.10: Models for metabolite sensing by riboswitches: (A) Induced fit model involves ligand (green) induced changes in the riboswitch (red) to form a binding competent conformation (BCC). (B) In lock and key model, ligand (green) binds to the riboswitch (red) without any conformational changes. (C) In conformational selection model, ligand (green) selects the BCC that pre-exists with other conformations of the riboswitch (red). Figure partially adapted from ref. (81).

The structures of the riboswitches in their ligand free and ligand bound form facilitated the understanding of the metabolite recognition by the aptamers. The riboswitches like TPP and c-di-GMP I differ in their ligand free and ligand bound conformations and therefore appeal more to an induced fit model (125,131,138). Other riboswitches do not undergo large conformational changes upon ligand binding and hence fit more to the lock and key binding model e.g. lysine riboswitch, *glmS* ribozyme (57,113,139). However, according to the solution data, the conformational selection model dominates regardless of the similarity/dis-similarity between the ligand free and ligand bound conformations of the riboswitches (140,141). Therefore, a ligand bound stable state could be achieved through synergism between the induced fit/ lock-key model and the conformational selection model.

1.2.8 Kinetic and thermodynamic control of riboswitches

The regulation of gene expression by riboswitches can be under kinetic or thermodynamic control (Figure 1.11). The two modes of regulation depend on several factors like rate of aptamer folding, rate of ligand association/dissociation, ligand concentration, speed of transcription, transcriptional pausing by RNA polymerase (RNAP), competition between alternative RNA conformations etc (142). The elongation time taken by RNAP from the aptamer end to the termination decision point as well as the time taken by the ligand and aptamer to achieve equilibrium are the major regulators. Therefore, translationally and transcriptionally regulated riboswitches exhibit different controls of ligand induced signal transmission. In case of translationally operating riboswitches, a riboswitch can attain equilibrium with the ligand as RNAP arrives at a termination decision point later and therefore, the two competing conformations of the aptamer can coexist. Upon ligand binding, the equilibrium is shifted towards the thermodynamically more favourable ligand bound conformation. In case of riboswitches operating via a transcription attenuation mechanism, RNAP reaches the termination

decision point before the riboswitch achieves thermodynamic equilibrium with its ligand. Therefore, a higher ligand concentration is required to assure ligand binding and appropriate formation of the downstream regulatory elements. Such riboswitches exhibit a large discrepancy in the ligand concentration needed for 50% transcription termination and their apparent K_D values (ligand concentration needed for 50% ligand-RNA complex formation at equilibrium) (81,142).

A riboswitch however, can also switch between the kinetic and thermodynamic control depending on the environmental conditions that alter the intracellular levels of NTPs affecting thereby the elongation and pausing durations by RNAP during transcription (142).

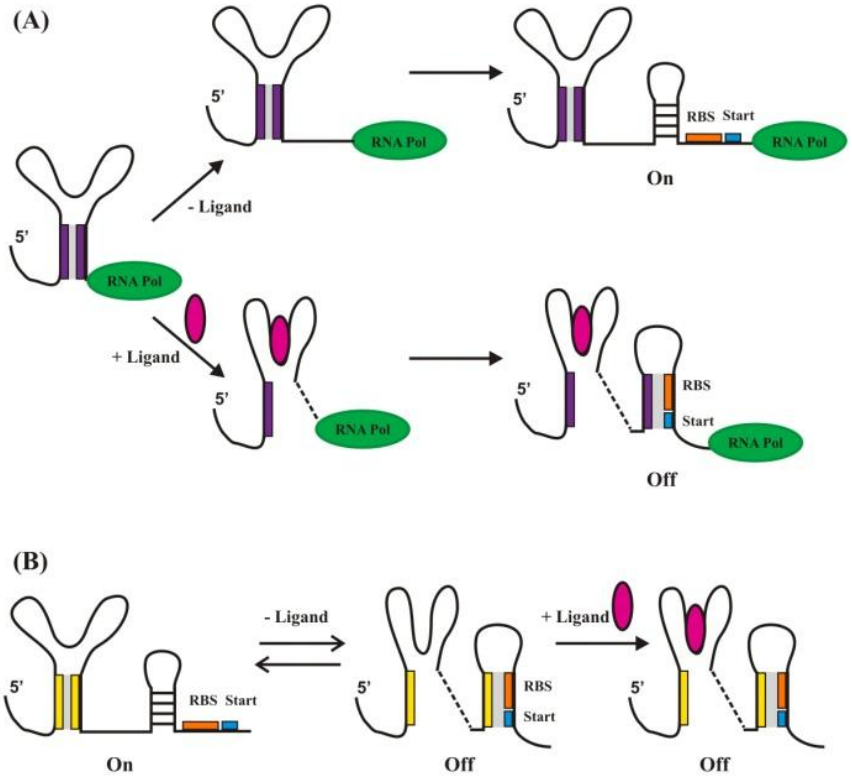

Figure 1.11: Regulation of gene expression by riboswitches: (A) In a kinetic mode of regulation, the 'translation on' conformation of the riboswitch is formed in the absence of ligand. However, binding of the ligand (pink) stabilizes the aptamer domain in a 'translation off' state prior to the transcription of the expression platform by RNA polymerase (green). (B) Under thermodynamic control, the translation 'on' and 'off' states of the riboswitch exist in equilibrium prior to ligand binding and the translation 'off' state is stabilized upon ligand binding (pink). Helical regions are shown as rectangles along with the base paired (grey) regions within. The ribosome binding site (RBS) is indicated in orange and the start codon (AUG) in blue. Figure partially adapted from ref. (81).

1.3 Coenzyme B_{12}/AdoCbl riboswitches

Coenzyme B_{12} riboswitches are widely distributed in Gram positive and Gram negative prokaryotes ranging from 1 to 13 representatives per genome and belong to one of the first reported metabolite binding RNA elements (74,143,144). These riboswitches are located in the 5' UTR of genes coding for cobalamine synthesis and for porphyrin/cobalt transporters (77). In addition, this class of riboswitch also controls the expression of proteins for glutamate/succinate fermentation and coenzyme B_{12} independent ribonucleotide reductases (77).

A comparative sequence analysis of ~ 200 B_{12} riboswitches from 67 bacterial genomes led to the identification of the consensus sequence and pattern of secondary structural elements for the coenzyme B_{12} aptamer domain (Figure 1.12) (144). The coenzyme B_{12} aptamer consists of at least 10 base paired elements and ~ 57 nucleotides being conserved in > 90% of the representative sequences (143). The region of the aptamer from stem P1 to P6 and P10 to P11 is highly conserved whereas the region from P7 to P10 is highly variable with putative P8 pairing (143). The highly conserved B_{12} box is located between P1 and P7 and surprisingly contributes to only a small portion of the structural domain with 25 nucleotides (143). Coenzyme B_{12} aptamers are demonstrated to directly bind coenzyme B_{12} with high affinity and high

specificity as observed from its ability to reject close coenzyme B_{12} analogues. Moreover, the coenzyme B_{12} aptamers undergo conformational changes upon interaction with coenzyme B_{12}/AdoCbl (70,143).

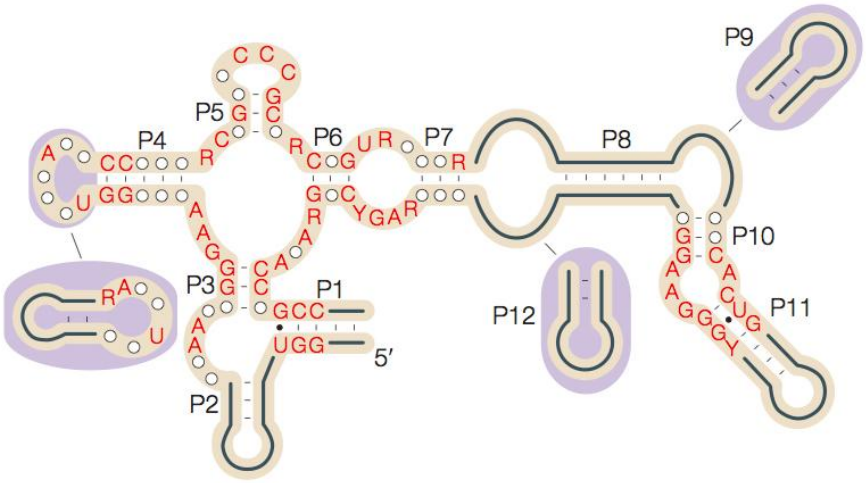

Figure 1.12: Consensus sequence for coenzyme B_{12} binding aptamer: The secondary structure of coenzyme B_{12} aptamer consists of distinct base-paired elements (P) and non-conserved regions (thick lines). Nucleotides in red are conserved in at least 90% of the representatives and a circle indicates a nucleotide of any base identity. The alternative secondary structural elements are marked in blue ovals. Figure taken from ref. (74).

The regulation of cobalamine metabolism is operated by coenzyme B_{12} riboswitches either at transcriptional, translational or at both levels simultaneously. From the sequence analysis, it was proposed that Gram positive bacteria undergo transcriptional mode of regulation due to the possibility of forming intrinsic terminator stem that stalls RNAP (Figure 1.13A) (144). In the absence of AdoCbl, the anti-terminator stem is formed resulting in gene transcription whereas, in the presence of AdoCbl, conformational changes in the aptamer lead to formation of an intrinsic terminator that aborts transcription. In Gram negative bacteria, a translational regulatory mechanism operates instead (Figure 1.13B) (70,143,144). In this case, the absence of AdoCbl leads to the formation of anti-anti-RBS stem that pairs with anti-RBS stem, freeing access to the RBS for effective translation. The presence of AdoCbl in contrast leads to the formation of an anti-RBS stem that sequesters the RBS and therefore, inhibits translation of the mRNA. A coupled transcription–translation mechanism is proposed for some cases and possible when the transcription terminator involves base pairing with RBS (74).

The era that led to the discovery of coenzyme B_{12} riboswitches consisted of extensive biochemical and genetic studies on the 5' UTRs of cob operon of *S. typhimurium*, the 5' UTR from *yvr* operon of *B. subtilis* and most importantly on the *btuB* gene of *S. typhimurium* and *E. coli.*

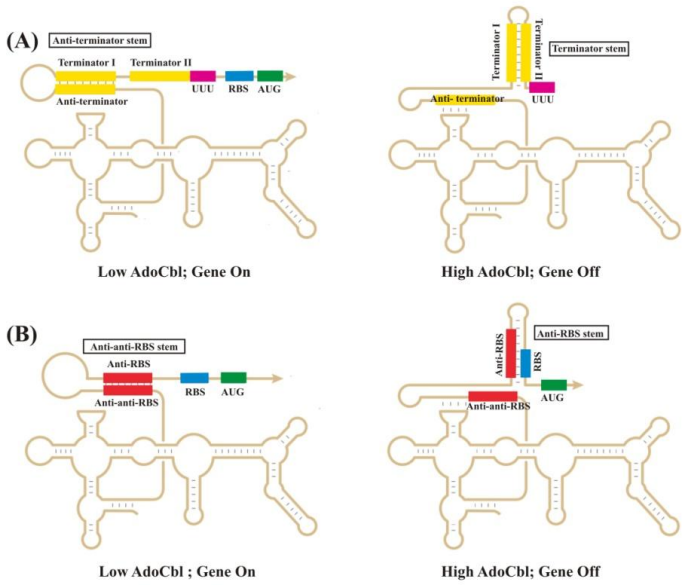

Figure 1.13: General mechanism for regulation of coenzyme B_{12}/AdoCbl ribosswitches: The regulation of gene expression mainly occurs at the transcriptional (A) or the translational (B) level. (A) In low AdoCbl conditions, terminator I stem is sequestered by anti-terminator stem whereas in high AdoCbl conditions, an intrinsic terminator is formed due to base pairing between terminator I and II and thereby leads to transcription termination. (B) In translational control, a hairpin formation occurs between anti-RBS (ribosome binding site) and anti-anti-RBS regions in low AdoCbl conditions. In high AdoCbl conditions, the anti-RBS region sequesters the RBS region and therefore, translation is inhibited. Anti-terminator and terminator (I and II) regions are indicated by yellow boxes. Anti-anti-RBS, anti-RBS and the RBS regions are shown by orange boxes. A stretch of U (needed for transcription terminator in bacteria) is shown in pink, the RBS in blue and the start codon (AUG) in green. Figure partially adapted from ref. (74).

1.3.1 *Salmonella typhimurium*

The *cob* operon of *S. typhimurium* codes for 20 proteins involved in the synthesis of coenzyme B_{12} whereas the *btuB* gene encodes an outer membrane cobalamine transporter, BtuB (145-149). The gene products for both *cob* and *btuB* are negatively regulated by cobalamine (148,150,151). It was suggested that the mRNA leader for *cob*/*btuB* directly binds AdoCbl as the search for mutations to identify a regulatory cobalamine binding protein failed (150-152). Moreover, both the *cob* and the *btuB* of *S. typhimurium* are proposed to be regulated by cobalamines at the translational level (151,153). The leader region of *cob* operon contains translational enhancer that forms pseudoknot interactions with the stem that sequester the RBS (153). These interactions release the RBS and therefore activate translation in the absence of cobalamine. Vitamin B_{12} ($VitB_{12}$) however, disrupts the translational enhancer therefore inhibits translation of mRNA (153). The direct interaction between the mRNA leader of *cob*/*btuB* and coenzyme B_{12} was proven with the help of in-line probing and equilibrium dialysis (143). The *cob* and *btuB* mRNA leader of *S. typhimurium* bind coenzyme B_{12} with an affinity of 200 nM and 400 nM respectively (143).

1.3.2 *Bacillus subtilis*

The phylogenetic analysis revealed a variant coenzyme B_{12} riboswitch at the upstream of 4 gene operon *yvr CABK* in *B. subtilis* (143). This operon is predicted to encode proteins involved in metal import and processing and therefore might undergo genetic modulation through cobalt containing coenzyme B_{12} (143). Structurally, the *yvr* coenzyme B_{12} aptamer lacks stems P8, P10 and P11 which are conserved in other bacterial genera (143). Notably, the *yvrC* leader exhibits poor discrimination against purinyl cobalamine and therefore, these studies for the first time predicted that the right half of the aptamer domain (P8-P11) might be responsible for the recognition and binding to the adenosyl moiety of cobalamine (143). Moreover, the *yvrC-lacZ* fusion represses the activity of *β-galactosidase* by ~ 3 fold in the presence of coenzyme B_{12} *in vivo* confirming the *yvrC* leader to be a functional coenzyme B_{12} riboswitch (143). The variant *yvrC* coenzyme B_{12} riboswitch led to the view that considerable changes can occur in the riboswitch structure to selectively respond to closely related metabolites.

1.4 The *btuB* riboswitch from *E. coli*

The *btuB* riboswitch from *E. coli* marked the hallmark of the riboswitch discovery being one of the first reported non-coding RNA elements in bacteria that directly binds a metabolite. It is situated at the 5' UTR of the gene *btuB* coding for an outer membrane B_{12} transporter BtuB (70). The protein BtuB binds extracellular $VitB_{12}$ with high affinity (K_D ~ 5 nM) and facilitate the energy dependent transfer of $VitB_{12}$ to periplasm (154-159).

The classical genetic and biochemical studies carried out on the *btuB* riboswitch from 1978 to 2002 led to the emergence of an RNA element involved in the regulation of coenzyme B_{12} levels in bacteria through direct interaction with coenzyme B_{12}/ AdoCbl.

1.4.1 1978-2000: Genetic and biochemical studies on the *btuB* riboswitch

In 1978, Kadner R.J reported the repression of the BtuB protein expression by addition of AdoCbl in a bacterial culture but attempts to obtain mutations in a gene for cobalamine responsive repressor were unsuccessful (160). The studies using *btuB-lacZ* fusion identified mutants that expressed BtuB constitutively in the presence of CN-Cbl/ $VitB_{12}$ and mapped to the unlinked locus *btuR* (161,162). The gene *btuR* encodes adenosyltransferase similar to *cobA* gene of *cob* operon and converts CN-Cbl to AdoCbl (162). Therefore, the regulatory system involving *btuB* was concluded to respond to intracellular levels of AdoCbl. Further, the *btuB-lacZ* fusions were used to identify *cis*-regulatory mutations that affect the expression of the *btuB-lacZ* and were linked to the *btuB*. The 5' end of the *btuB* transcript was then mapped by S1 nuclease assay on the mRNA isolated from the cells grown in the presence and absence of 5 µM CN-Cbl (163). The size of the protected fragment indicated the 5' end of *btuB* to be located at the G residue, 240 nucleotides upstream the translational start site (163). Moreover, the amount of the *btuB* mRNA was reduced when cells were grown with CN-Cbl indicating that Cbl mediated repression affects the mRNA synthesis or stability (163). The *btuB-lacZ* fusions also indicated that CN-Cbl induced repression is mediated by the sequences throughout the transcribed leader (163).

The role of transcribed sequences in the *btuB* gene was examined through a series of translational and transcriptional fusions of the *btuB* gene (163). The *btuB-phoA* translational fusions (carrying the *btuB* sequence from +368 to +1200) suggested that nucleotides distal to +368 do not play a major role in the CN-Cbl induced repression (163). The *btuB-lacZ* transcriptional fusions however, indicated that sequences between +156 to +365 strongly affect the expression of the gene and sequences from +250 to +313 are important for transcriptional repression of the gene (163). The translation initiation seemed to be a primary site of *btuB* regulation and needs integrity of most of the leader region (163-165). The control of translational fusion occurred in the absence of translated sequences and was proposed to include a RNA hairpin near to the Shine-Dalgarno (SD) sequence. Also, a conserved B_{12} box in the *btuB* leader sequence was found to be essential for BtuB expression as its deletion resulted in the very low and unregulated expression of BtuB (164).

Apart from the translational control, a possibility of coupled translational-transcriptional regulation of the *btuB* was evident when a transcriptional attenuator was identified in translated regulatory region (TRR) from nucleotides +241 to +350 that contained a putative Rho-independent terminator (165). The activity of the TRR in the *btuB* regulation was proven through *btuB-lacZ* fusions that carried several deletions in the *btuB* sequence. Deletions from +270 and upstream that disrupted the TRR eliminated the transcriptional control whereas deletions from +285 to +303 resulted in the reduced regulation by CN-Cbl (164,165). The deletions ending at +345 however exhibited a normal regulation by CN-Cbl. Moreover, deletions that cause complete loss in the transcriptional control retain the translational level regulation. The analysis of the *btuB* RNA levels through S1 nuclease protection assays under various conditions suggested that alteration of translation dramatically affects the expression of transcriptional fusion as well as the RNA levels and stability (165).

Therefore, the TRR was predicted to affect the *btuB* RNA levels and the negative action of the TRR can be eliminated by passage of ribosome through it.

Along with the translational and transcriptional regulation, the kinetics of RNA turnover indicated a possible of Cbl-dependent regulatory mechanism affecting the RNA stability. In S1 nuclease protection assay, the full length *btuB* mRNA was found to be long lived in non-repressing conditions and becomes labile in the presence of AdoCbl (165). However, the stability of the 165 nt fragment was not affected by AdoCbl indicating its contribution to the overall RNA stability (165). Moreover, two *rnc* mutants deficient in RNase III activity displayed a marked reduction in the 165 nt fragment and a increase in the Cbl induced 210 nt fragment but had no effect on the full length transcript (165). Therefore, it was proposed that RNA secondary structure is cleaved by RNase III at nt 165, immediately downstream the B_{12} box. The confirmation of Cbl induced changes in the secondary structure of the *btuB* RNA emerged with the observation when the amount of Cbl induced 210 nt fragment was greatly reduced in *hfq* mutants being deficient in RNA binding protein, host factor 1 that disrupts the RNA secondary structures (165).

These studies therefore, indicated that along with translation initiation, transcriptional regulation and alteration in the RNA stability could operate together to fine-tune the Cbl induced regulation of BtuB expression levels *via* 5' leader of the *btuB* mRNA.

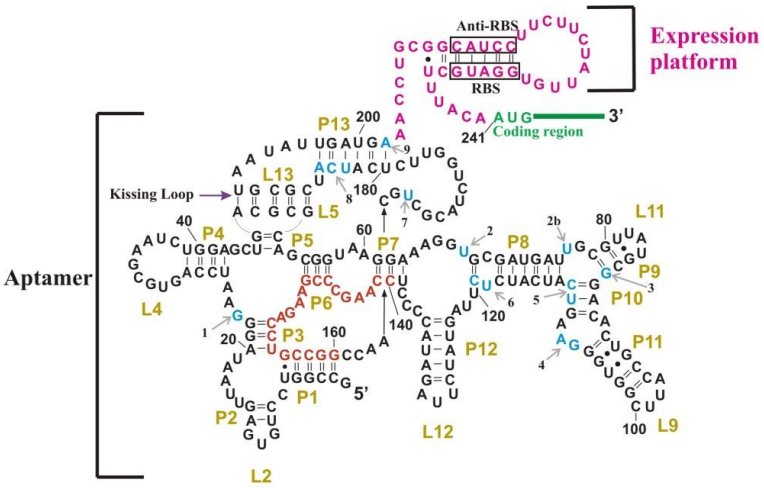

Figure 1.14: Secondary structure of the *btuB* riboswitch from *E.coli*: Shown is the secondary structure of the *btuB* riboswitch in the presence of AdoCbl. The aptamer region consists of 202 nucleotides with distinct base-paired elements (P) and intervening loops (L). A highly conserved B_{12} box (nucleotides 140-160) is indicated by nucleotides in red. The kissing loop interaction (between L5 and L13) is shown by an arrow in purple. Nucleotides (sites 1-9) undergoing modulation in the presence of cobalamine are shown in blue and indicated by arrows (grey). An expression platform consists of nucleotides (in pink) 203-240. The RBS (ribosome binding site) and the anti-RBS regions are marked by the boxes. The coding region begins at nucleotide 241 and is shown in green.

1.4.2 Pioneering insights into the secondary structure of the *btuB* riboswitch

In 2000, Nou and Kadner studied the translational regulatory process in detail with primer extension-inhibition assays that demonstrated the ability of ribosomes to bind the *btuB* mRNA (166). The assay measured the ability of bound ribosomes to prevent extension of a primer hybridized to the *btuB* RNA (downstream of the RBS) by reverse transcriptase. In the absence of ribosomes, the primer extension gave full length run off product as G315 (166). A major product whose formation was independent of ribosomes ended at position C161 in the B_{12} box (166). In the presence of 5 mM AdoCbl, a marked increase in the product ending at A202 was observed and therefore, the region upstream of A202 must be involved in AdoCbl binding (166). Moreover, the formation of the A202 product was independent of the presence of ribosomal subunits or $tRNA^{fMet}$ (initiator tRNA) excluding A202 from the ribosome binding (166). In the presence of the 30S ribosomal subunits and $tRNA^{fMet}$, a termination product was produced at position T256 indicating the region at its upstream (i.e. nt 203-255) affects the binding of ribosomes (166). The B_{12} box found within the *btuB* transcript (nt 141 to 161) is conserved among other Cbl regulated leader regions and its deletion caused marked reduction on the *btuB* expression, loss of Cbl dependent regulation and decreased stability of the *btuB* RNA *in vivo* (164-166). Moreover, the B_{12} box deleted RNA showed reduced binding to 30S ribosomal subunit (166). This mutant exhibited

decreased levels of C161 product whereas, product A202 was not made at all. Therefore, it was clear that the B_{12} box is needed for the formation of A202 product and to block ribosome access to the RNA (166). The formation of A202 product in the absence of ribosomes or other factors indicated that AdoCbl directly binds to the *btuB* RNA.

1.4.3 Direct interaction between the *btuB* riboswitch and coenzyme B_{12}

The very first evidence of the direct interaction between the *btuB* mRNA leader and coenzyme B_{12}/AdoCbl was established with the help of in-line probing by Nahvi *et al*. in 2002 (70). The probing data indicated AdoCbl specific conformational changes at eight sites within the *btuB* leader in the absence of any other accessory protein factors (70). With the help of computational models and structural probing data, a secondary structure was proposed for the 5' UTR of the *btuB* which was then revised in 2004 after comparison with other B_{12} riboswitch sequences (70,143). The *btuB* riboswitch therefore consists of a 202 nucleotide aptamer region and an expression platform lying between nucleotides 203-240 (Figure 1.14) (143). The *btuB* aptamer is highly structured with the conserved B_{12} box situated between nt 141 to 161 (143). A single point mutation on the B_{12} box eliminated not only the *in vitro* binding of the *btuB* RNA to AdoCbl but also the *in vivo* AdoCbl dependent regulation of *lacZ* expression (70). The shortened construct of the *btuB* including the highly conserved domain up to nucleotides 160 exhibited almost 100 fold loss in the binding affinity to AdoCbl (143). Therefore, structural elements within the non-conserved domain of the riboswitch assist in proper formation of a high affinity aptamer core. The secondary structure of the *btuB* riboswitch supported the translational regulation due to the presence of RBS sequestering hairpin in the expression platform (143,166). AdoCbl binding is predicted to alter the conformation of the *btuB* riboswitch in such a way that a pseudoknot is formed between loops L5 and L13 that disrupts the anti-anti-RBS/anti-RBS hairpin and sequesters the RBS through the formation of anti-RBS/RBS hairpin (70,143).

1.4.4 Role of RNA polymerase

In 2012 Perdizret *et al*. proposed that the transcriptional pausing by RNAP at strategic locations in the *btuB* riboswitch affects the folding and structural rearrangement of the full length riboswitch (Figure 1.15) (167). Pausing at these sites blocks the formation of alternative structures and acts as a chaperone to link the folding of the aptamer and the expression platform. It was proposed that in the AdoCbl free- apo /gene on state, the anti-anti-RBS region pairs with the anti-RBS region to form anti-aptamer whereas in AdoCbl bound or gene off state, the anti-anti-RBS is a part of the aptamer that allows anti-RBS to pair with the RBS in order to block translation (167). One of the identified pause sites (P_A) is located before the loop L13 and therefore, pausing here provides sufficient time for the aptamer to recognize the Cbl ligand. A successive pause site (P_B) releases L13/P13 to allow KL interaction before the RNAP proceeds transcription. Pausing at more distal pause site (P_C) is relevant in the absence of AdoCbl that allows refolding into the anti-aptamer conformation for appropriate gene regulatory response.

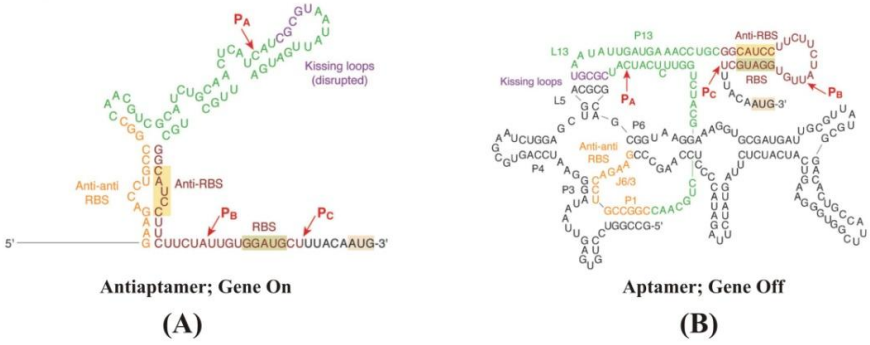

Figure 1.15: Proposed secondary structures of the *btuB* riboswitch in the ligand free (A) and ligand bound (B) forms: (A) In the absence of AdoCbl, an anti-aptamer is formed that releases the ribosome binding site (RBS) and thus, the *btuB* mRNA is translated (gene on state). (B) AdoCbl binding however leads to sequestration of the RBS, causing translation inhibition (gene off). The three transcriptional pause sites- P_A, P_B and P_C are shown in red. Figure taken from ref. (175).

1.4.5 Specificity towards AdoCbl

Although *in vivo* studies reported AdoCbl to be a sole regulator of the *btuB* expression, *in vitro* studies indicated the regulation of the *btuB* riboswitch by other cobalamines as well. In a primer extension assay, half maximal inhibition for ribosome binding was observed at 0.3 µM of AdoCbl and 3 µM of methyl-Cbl (166). Moreover, ribosome binding to the *btuB* RNA was inhibited in the presence of 30 µM of CN-Cbl, aquo-Cbl and dicyanocobinamide (166). Further, with the help of in-line probing, the modifications of cobalamine compounds were compared to its effects on the structural modulation of the RNA. It was found that the *btuB* RNA binds AdoCbl with a K_D of 300 nM and RNA does not undergo structural modulation in the absence of the adenosyl moiety (70). Precisely, the modifications of N1, N3 and N6 positions of the adenine ring disrupt binding whereas 2'-hydroxyl group of the adenosyl moiety is not crucial in molecular recognition (70). These studies also revealed that modification at position 13 of the corrin ring (13-epi-AdoCbl) renders the compound as inactive regulator *in vitro* and *in vivo* (70). Therefore, the *btuB* aptamer forms a tight binding pocket for AdoCbl and several contacts to AdoCbl are made to ensure high specificity.

Further in-line probing experiments involving cobalamine derivatives suggested that the corrin ring is the main determinant for the conformational alteration in the RNA structure (168). The axial moieties of cobalamine only affect the affinity of cobalamines for the riboswitch. AdoCbl and Ado-FactA both were found to bind the *btuB* aptamer in sub-micromolar range (168). Interestingly, vitamin B_{12} and Ado-Cobi lacking the upper and lower axial ligands respectively also induces the conformational alteration in the RNA although with a 1000 times lower binding affinity (168). The modification of the corrin ring side chains further suggested the interaction of the lower α-side of the corrin ring with the region between P6 to P12 of the *btuB* riboswitch and the modified side chains only affect the site 1 and 8 (169). The modification on the upper β-side of the corrin-ring however, leads to a completely different structural arrangement of the riboswitch and therefore should be crucial for the correct switching of the *btuB* RNA (169).

All these data together suggested that the *btuB* RNA interacts with AdoCbl such that different regions of the RNA help recognizing the functional moieties of AdoCbl via numerous contacts in order to impose high specificity and high affinity to its natural ligand, AdoCbl.

1.5 B_{12} riboswitches from *Desulfitobacterium*

The genus *Desulfitobacterium* includes obligate anaerobic bacteria isolated mostly from a polluted environment rich in organohalides (170). In routine cultures, *Desulfitobacterium hafniense* strain TCE1 could grow on the medium devoid of cobalamines indicating the *de novo* synthesis of cobalamines similar to a related strain *Desulfitobacterium hafniense* Y51. The corrinoid biosynthesis pathway in *D. hafniense* Y51 is organized into two main operons responsible for the synthesis of Ado-Cobi from factor II and addition of lower ligand to Ado-Cobi respectively (171-173). Both of these operons are proposed to be regulated by cobalamine riboswitches. The genome analysis of *D. hafniense* TCE1 as well revealed the presence of 16 conserved sequences similar to that of B_{12} riboswitches. These conserved sequences are located at the upstream of genes encoding cobalamine synthesis proteins and transporters and therefore were predicted to be cobalamine riboswitches. According to Rfam database, *D. hafniense* TCE1 currently ranks among the top ten bacteria with the highest number of riboswitches (173). *D. hafniense* TCE1 is therefore one of the model bacteria that can be explored in detail to understand the role of the predicted B_{12} riboswitch like sequences and the diversity of their secondary structural elements in the regulation of corrinoid metabolism in *Desulfitobacterium*.

1.6 Insights into the crystal structures of cobalamine riboswitches from thermophiles

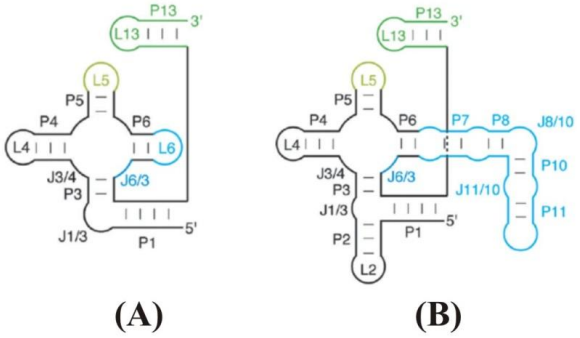

Figure 1.16: Secondary structures of cobalamine riboswitches: Shown are the secondary structural elements for AqCbl (A) and AdoCbl (B) class of cobalamine riboswitches. In comparison to AqCbl class of riboswitches, AdoCbl riboswitches consist of stem P2 (between P1 and P3) as well as the peripheral extension of P6 (stems P7-P11). Figure taken from ref. (175).

The molecular mechanism for cobalamine (Cbl) recognition by B_{12} riboswitches was provided by recently solved crystal structures of the B_{12} riboswitches from thermophilic bacteria (111,174). Batey and co-workers found a class of cobalamine riboswitches (marine and environmental [env] genomes from the ocean surface samples) that bind methylcobalamine (MeCbl) and aquocobalamine (AqCbl) with higher affinities and strongly discriminate against AdoCbl (174). This distinction is directly related to the secondary structures of these riboswitches that lack peripheral extension. The absence and presence of peripheral extension therefore respectively marks two classes of cobalamine riboswitch binding to MeCbl/AqCbl and AdoCbl (Figure 1.16) (174). The AdoCbl class differs from MeCbl/AqCbl class with respect to the presence of peripheral extension from stem P6 (P7 to P11) as well as an additional stem P2 between stem P1 and P3. Both classes however possess an evolutionarily conserved four way junction formed by stems P3-P4-P5-P6 as well a Cbl induced kissing loop (KL) interaction between loops L5 and L13 (174,175).

The crystal structures of AdoCbl riboswitches from *Thermoanaerobacter tengcongensis* (with L13/P13) and from *Symbiobacterium thermophilum* (without L13/P13) along with the crystal structures of much smaller *env8*AqCbl riboswitch recently provided first insights into the architecture of the cobalamine riboswitches and their recognition of AdoCbl (Figure 1.17) (111,174).

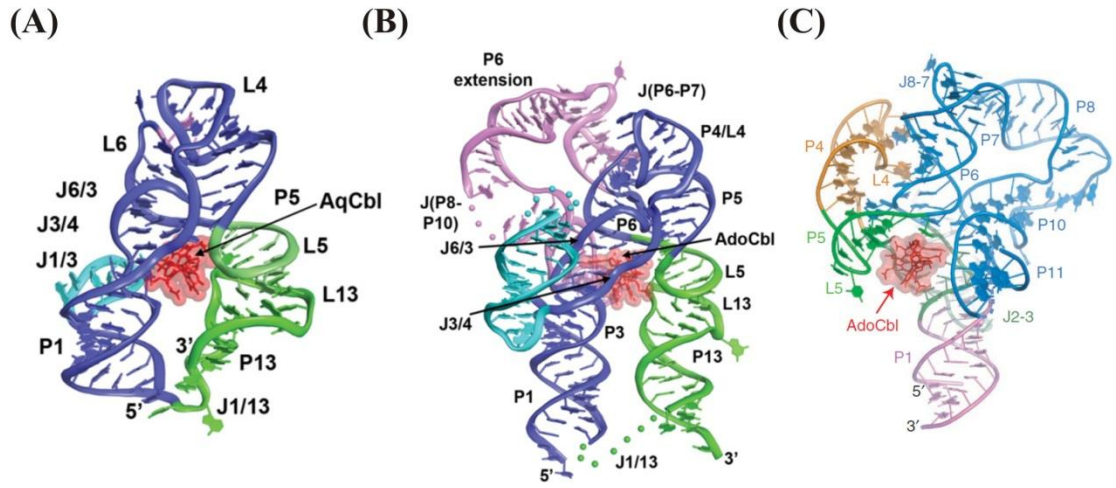

Figure 1.17: Crystal structures of B_{12} riboswitches from thermophilic bacteria: Shown are the representations of B_{12} riboswitches bound to AqCbl (A) (*env8*AqCbl) and to AdoCbl (B) (*T. tengcongensis*), (C) (*S. thermophilum*). The bound ligand is shown in red and indicated by the respective arrows. AdoCbl bound riboswitch from *S. thermophilum* (C) lacks the P13-L13 domain. Figure taken from ref. (111,174).

The crystal structures of ligand-bound B_{12} riboswitches suggest a similar global architecture with co-axial stacking of stems P1/P3/P6 and stems P4/P5/P13 (111,174). These stacks are joined by T-loop-T-loop motif through an interaction between L4 and L6 in AqCbl class whereas in AdoCbl class, T loop (L4) interacts with an internal loop between P6 and P7 (174). This core is flanked by class specific peripheral extensions that contain key cobalamine recognition element, J6/3.

The peripheral extensions alter the conformation at J6/3 and thereby confer specificity to cobalamine derivatives (Figure 1.18) (174). In the AqCbl class, the base pairing interaction between J6/3 and J1/3 alters the conformation at J6/3 to prevent the interaction with AdoCbl and establishes the selectivity for Cbl with small β-axial moieties (174). In the AdoCbl class however, J6/3 is placed further from J3/4 by a pair of conserved adenosines at J11/10 that allows the Hoogsteen face of conserved adenosine at J6/3 to interact with the adenine base of AdoCbl (111,174). Since the adenosines at J11/10 undergo a strong protection from chemical modification only in the presence of AdoCbl, it is proposed that the peripheral elements dock upon the core after initial cobalamine binding (174).

Interactions between RNA and cobalamine are mainly mediated through van der Walls shape complementarities (111,174). The ligand does not use its full hydrogen bonding potential to bind the RNA but hydrophobic packing and electrostatic interactions are most characteristic. Cobalamine is sandwiched between the minor grooves of the P3-P6 coaxial stack and the helix formed by base pairing between L5-L13 (KL interaction) (111,174). The superimposition of the RNA structures that lack P13/L13 with structures containing P13/L13 suggest an open cleft in the binding pocket, which is closed by the docking of P13/L13 through KL interaction with L5 and thereby encapsulate Cbl. The α-axial face of Cbl interacts with the KL where DMB and the amino propyl linker make contacts to the ribose-phosphate backbone of L5 and L13 through van der Waals interactions in addition to the interactions with propionamide and acetamide groups (174). The β-axial surface of Cbl projects towards the flat surface created by a stack of purines at J3/4 and J6/3 and therefore, the plane of corrin ring is perpendicular to the bases of the purine stack (174).

The crystal structures of B_{12} riboswitches therefore suggested that they are evolved to recognize distinct cobalamine derivatives through 'class-non-specific common interactions' as well as by 'class-specific unique interactions' displayed by a special organization of their secondary structural elements.

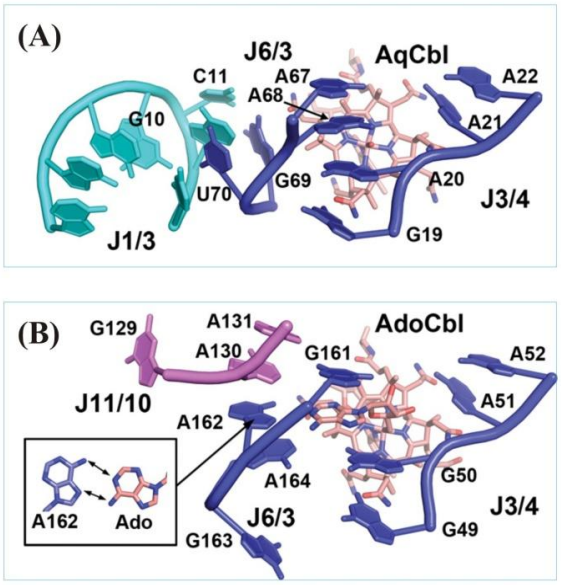

Figure 1.18: Recognition of cobalamines by B_{12} riboswitches: The specificity to cobalamines is determined by the conformation at J6/3. In AqCbl class (A), J6/3 interacts with J1/3 and therefore is placed closer to J3/4. A20 and A68 in J3/4 and J6/3 respectively occlude the adenosyl moiety of AdoCbl providing specificity to cobalamines with smaller β-axial groups. In contrast, the conserved adenosines at J11/10 in AdoCbl class (B) places J6/3 further from J3/4 and therefore the base pairing (shown in black box) between the Hoogsteen face of A168 (equivalent to A68 in AqCbl class) with the adenosyl moiety of AdoCbl is possible. Figure taken from ref. (174).

1.7 Riboswitches: Target for future antimicrobials

Riboswitches are not only known to recognize small ligands with high specificity and high affinity but also to regulate the metabolic pathways in bacteria essential for survival or pathogenesis. Moreover, except for the TPP riboswitch, the known riboswitches occur only in bacteria and not in eukaryotes. Therefore, riboswitches represent a promising target for the development of new antimicrobials (176,177). In total, four antimicrobials have been reported to target riboswitches in order to exert their effect on bacterial survival. Analogues of riboflavin and thiamine- roseoflavin and pyrithiamine respectively were reported to bind the FMN and TPP riboswitch ultimately leading to the impaired regulatory response (72,115,125,178-183). Also, two analogues of lysine namely L-Aminoethylcsyteine (AEC) and DL-4-Oxalysine inhibit the growth of Gram positive bacteria (184). These analogues bind the *lysC* riboswitch of *B. subtilis* and repress the expression of the reporter gene regulated by the lysine riboswitch (184).

The three dimensional structures of most of the riboswitches have been solved in their ligand free and ligand bound form providing a driving force for designing the antibiotics that target the riboswitches and impair the bacterial metabolic pathways.

1.8 Thesis Outline

The unparalleled power of riboswitches to control the gene expression in bacteria by recognizing their cognate ligands with high specificity and high affinity makes these RNA molecules a unique class of gene regulatory elements. Considering the phylogenetic conservation of riboswitches across the bacterial species, studying the structure of the riboswitches and their interaction with their ligands will immensely help in designing broad spectrum novel antibiotics.

This work focuses on the AdoCbl responsive riboswitches from the bacteria *E. coli* and *Desulfitobacterium*.

Previous reports on the *btuB* riboswitch from *E. coli* have convincingly demonstrated the direct interaction between AdoCbl and the *btuB* riboswitch (70,166,168). However, the information on the ligand free conformation was still missing and was crucial to investigate, as in the case of large RNAs the ligand binding pocket is mostly pre-organized for rapid recognition of its ligand (79,128). We hypothesized that the pre-folding of the ligand binding pocket of the *btuB* riboswitch should be a crucial factor in the ligand recognition as both, the *btuB* aptamer and its ligand, coenzyme B_{12} are highly complex molecules. As metal ions play indispensible role in the folding of the RNA, our work also aims at mapping such metal ion binding sites on the *btuB* riboswitch in order to investigate the implications of metal ion induced pre-folding of the *btuB* riboswitch. Along with the pre-organization of the aptamer, the key factors that control the riboswitch mediated gene regulation are the rates of ligand association and dissociation (142). The mode of ligand interaction with the riboswitch in turn dictates the possible kinetic or thermodynamic control of riboswitch activity and plays a vital role in the temporal gene regulation *in vivo* (81,142). The studies here also focus on the set of cobalamine riboswitches from *Desulfitobacterium hafniense* in order to correlate the structural diversity of these riboswitches to their role in corrinoid metabolism.

Section 2 describes the two classical methods used in this work, in-line probing and Tb^{3+} cleavage to explore the conformational changes in the RNA and to detect the metal ion binding sites on RNA respectively.

Section 3 deals with the elucidation of the pre-folding of the *btuB* aptamer. Since, the secondary and tertiary structure formation of the RNA is governed mainly by monovalent and divalent cations, the work here aims to explore the metal ion induced folding of the *btuB* aptamer and its contribution in the formation of ligand binding compatible conformation of the *btuB* riboswitch.

Section 4 focuses on the mapping of Mg^{2+} binding sites on the *btuB* aptamer in order to correlate the consequences of metal ion binding and the aptamer folding. An emphasis is given to locate the potential Mg^{2+} binding in the *btuB* aptamer which could be critical in organization of the native tertiary structure of the aptamer and might represent a strategy to prefold the aptamer not only in case of the *btuB* riboswitch but possibly for all AdoCbl riboswitches.

Section 5 concerns with the kinetics of interaction between the *btuB* riboswitch and AdoCbl studied by Surface Plasmon Resonance (SPR) spectroscopy. This work was carried out to confirm if the *btuB* riboswitch and AdoCbl follows a 1:1 interaction or some other mode of recognition. The kinetic parameters derived from SPR experiments helped to predict not only the mode of interaction between the *btuB* riboswitch and AdoCbl but also rationalize for the observed affinity differences of the *btuB* riboswitch towards AdoCbl and Vitamin B_{12}.

Section 6 is extended to the set of B_{12} riboswitches from an extremophile, *Desulfitobacterium*. The detection of 16 cobalamine riboswitch like sequences in the bacterium *Desulfitobacterium hafniense* TCE1 indicated the complex corrinoid metabolism. Therefore, this work focusses mainly on investigating if the cobalamine riboswitch like sequences found in the genome of *Desulfitobacterium hafniense* TCE1 represent the true B_{12} riboswitches or not. The diversity of

these cobalamine riboswitches in terms of their secondary structural elements and affinity to AdoCbl facilitate the prediction of their significance in the complex corrinoid metabolism.

1.9 References

1. Avery, O.T., Macleod, C.M. and McCarty, M. (1944) Studies on the Chemical Nature of the Substance Inducing Transformation of *Pneumococcal* Types: Induction of Transformation by a Desoxyribonucleic Acid Fraction Isolated from *Pneumococcus* Type Iii. *J Exp Med*, **79**, 137-158.
2. Watson, J.D. and Crick, F.H. (1953) Molecular structure of nucleic acids; a structure for deoxyribose nucleic acid. *Nature*, **171**, 737-738.
3. Watson, J.D. and Crick, F.H. (1953) The structure of DNA. *Cold Spring Harb Symp Quant Biol*, **18**, 123-131.
4. Hultin, T. (1957) The metabolic utilization of C14-formate in sea urchin embryos. *Exp Cell Res*, **12**, 518-525.
5. Hultin, T. and Von Der Decken, A. (1957) The incorporation *in vitro* of labeled amino acids into the proteins of regenerating rat liver. *Exp Cell Res*, **13**, 83-87.
6. Crick, F.H. (1958) On protein synthesis. *Symp Soc Exp Biol*, **12**, 138-163.
7. Bolton, D.C., McKinley, M.P. and Prusiner, S.B. (1982) Identification of a protein that purifies with the scrapie prion. *Science*, **218**, 1309-1311.
8. McKinley, M.P., Masiarz, F.R., Isaacs, S.T., Hearst, J.E. and Prusiner, S.B. (1983) Resistance of the scrapie agent to inactivation by psoralens. *Photochem Photobiol*, **37**, 539-545.
9. Prusiner, S.B. (1982) Novel proteinaceous infectious particles cause scrapie. *Science*, **216**, 136-144.
10. Chirico, W.J., Waters, M.G. and Blobel, G. (1988) 70K heat shock related proteins stimulate protein translocation into microsomes. *Nature*, **332**, 805-810.
11. Deshaies, R.J., Koch, B.D., Werner-Washburne, M., Craig, E.A. and Schekman, R. (1988) A subfamily of stress proteins facilitates translocation of secretory and mitochondrial precursor polypeptides. *Nature*, **332**, 800-805.
12. Schleyer, M. and Neupert, W. (1985) Transport of proteins into mitochondria: translocational intermediates spanning contact sites between outer and inner membranes. *Cell*, **43**, 339-350.
13. Baltimore, D. (1970) RNA-dependent DNA polymerase in virions of RNA tumour viruses. *Nature*, **226**, 1209-1211.
14. Temin, H.M. and Mizutani, S. (1970) RNA-dependent DNA polymerase in virions of Rous sarcoma virus. *Nature*, **226**, 1211-1213.
15. Gierer, A. and Schramm, G. (1956) Infectivity of ribonucleic acid from tobacco mosaic virus. *Nature*, **177**, 702-703.
16. Cech, T.R., Zaug, A.J. and Grabowski, P.J. (1981) *In vitro* splicing of the ribosomal RNA precursor of Tetrahymena: involvement of a guanosine nucleotide in the excision of the intervening sequence. *Cell*, **27**, 487-496.
17. Guerrier-Takada, C., Gardiner, K., Marsh, T., Pace, N. and Altman, S. (1983) The RNA moiety of ribonuclease P is the catalytic subunit of the enzyme. *Cell*, **35**, 849-857.
18. Gilbert, W. (1986) The origin of life: The RNA world. *Nature*, **319**, 618.
19. Ban, N., Nissen, P., Hansen, J., Moore, P.B. and Steitz, T.A. (2000) The complete atomic structure of the large ribosomal subunit at 2.4 A resolution. *Science*, **289**, 905-920.
20. Lee, R.C., Feinbaum, R.L. and Ambros, V. (1993) The *C. elegans* heterochronic gene lin-4 encodes small RNAs with antisense complementarity to lin-14. *Cell*, **75**, 843-854.
21. Mattick, J.S. and Makunin, I.V. (2006) Non-coding RNA. *Hum Mol Genet*, 15 Spec No 1, R17-29.

22. Nissen, P., Hansen, J., Ban, N., Moore, P.B. and Steitz, T.A. (2000) The structural basis of ribosome activity in peptide bond synthesis. *Science*, **289**, 920-930.
23. Reinhart, B.J., Slack, F.J., Basson, M., Pasquinelli, A.E., Bettinger, J.C., Rougvie, A.E., Horvitz, R.H. and Ruvkun, G. (2000) The 21-nucleotide let-7 RNA regulates developmental timing in *Caenorhabditis elegans*. *Nature*, **403**, 901-906.
24. Esteller, M. (2011) Non-coding RNAs in human disease. *Nature Rev Genet*, **12**, 861-874.
25. Wan, Y., Kertesz, M., Spitale, R.C., Segal, E. and Chang, H.Y. (2011) Understanding the transcriptome through RNA structure. *Nature Rev Genet*, **12**, 641-655.
26. Waters, L.S. and Storz, G. (2009) Regulatory RNAs in bacteria. *Cell*, **136**, 615-628.
27. Crick, F.H. (1966) Codon--anticodon pairing: the wobble hypothesis. *J Mol Biol*, **19**, 548-455.
28. Kim, S.H., Suddath, F.L., Quigley, G.J., McPherson, A., Sussman, J.L., Wang, A.H., Seeman, N.C. and Rich, A. (1974) Three-dimensional tertiary structure of yeast phenylalanine transfer RNA. *Science*, **185**, 435-440.
29. Leontis, N.B., Stombaugh, J. and Westhof, E. (2002) The non-Watson-Crick base pairs and their associated isostericity matrices. *Nucleic Acids Res*, **30**, 3497-3531.
30. Leontis, N.B. and Westhof, E. (2001) Geometric nomenclature and classification of RNA base pairs. *RNA*, **7**, 499-512.
31. Robertus, J.D., Ladner, J.E., Finch, J.T., Rhodes, D., Brown, R.S., Clark, B.F. and Klug, A. (1974) Structure of yeast phenylalanine tRNA at 3 Å resolution. *Nature*, **250**, 546-551.
32. Woese, C.R., Gutell, R., Gupta, R. and Noller, H.F. (1983) Detailed analysis of the higher-order structure of 16S-like ribosomal ribonucleic acids. *Microbiol Rev*, **47**, 621-669.
33. Batey, R.T., Rambo, R.P. and Doudna, J.A. (1999) Tertiary Motifs in RNA Structure and Folding. *Angew Chem Int Ed*, **38**, 2326-2343.
34. Zuker, M. (2003) Mfold web server for nucleic acid folding and hybridization prediction. *Nucleic Acids Res*, **31**, 3406-3415.
35. Ehresmann, C., Baudin, F., Mougel, M., Romby, P., Ebel, J.P. and Ehresmann, B. (1987) Probing the structure of RNAs in solution. *Nucleic Acids Res*, **15**, 9109-9128.
36. Butcher, S.E. and Pyle, A.M. (2011) The molecular interactions that stabilize RNA tertiary structure: RNA motifs, patterns, and networks. *Acc Chem Res*, **44**, 1302-1311.
37. Woodson, S.A. (2005) Metal ions and RNA folding: a highly charged topic with dynamic future. *Curr Opin Chem Biol*, **9**, 104-109.
38. Auffinger, P., Grover, N. and Westhof, E. (2011) Metal ion binding to RNA. *Met Ions Life Sci*, **9**, 1-35.
39. Draper, D.E. (2004) A guide to ions and RNA structure. *RNA*, **10**, 335-343.
40. Draper, D.E., Grilley, D. and Soto, A.M. (2005) Ions and RNA folding. *Annu Rev Biophys Biomol Struct*, **34**, 221-243.
41. Sigel, R.K.O. (2007) Intimate Relationships Between Metal Ions and Nucleic Acids. *Angew Chem Int Ed*, **46**, 654-656.
42. Lorsch, J.R. and Szostak, J.W. (1994) *In vitro* selection of RNA aptamers specific for cyanocobalamin. *Biochemistry*, **33**, 973-982.
43. Klein, D.J., Moore, P.B. and Steitz, T.A. (2004) The contribution of metal ions to the structural stability of the large ribosomal subunit. *RNA*, **10**, 1366-1379.
44. Pyle, A.M. (2002) Metal ions in the structure and function of RNA. *J Biol Inorg Chem*, **7**, 679-690.
45. Misra, V.K. and Draper, D.E. (1998) On the role of magnesium ions in RNA stability. *Biopolymers*, **48**, 113-135.

46. Misra, V.K. and Draper, D.E. (2002) The linkage between magnesium binding and RNA folding. *J Mol Biol*, **317**, 507-521.
47. Pyle, A.M. (1996) Role of metal ions in ribozymes. *Met Ions Biol Syst*, **32**, 479-520.
48. Sigel, R.K. and Pyle, A.M. (2007) Alternative roles for metal ions in enzyme catalysis and the implications for ribozyme chemistry. *Chem Rev*, **107**, 97-113.
49. Freisinger, E. and Sigel, R.K.O. (2007) From Nucleotides to Ribozymes - A Comparison of Their Metal Ion-Binding Properties. *Coord Chem Rev*, **251**, 1834-1851.
50. Ciesiolka, J., Marciniec, T. and Krzyzosiak, W. (1989) Probing the environment of lanthanide binding sites in yeast tRNA(Phe) by specific metal-ion-promoted cleavages. *Eur J Biochem*, **182**, 445-450.
51. Harris, D.A., Tinsley, R.A. and Walter, N.G. (2004) Terbium-mediated footprinting probes a catalytic conformational switch in the antigenomic hepatitis delta virus ribozyme. *J Mol Biol*, **341**, 389-403.
52. Sigel, R.K. and Pyle, A.M. (2003) Lanthanide ions as probes for metal ions in the structure and catalytic mechanism of ribozymes. *Met Ions Biol Syst*, **40**, 477-512.
53. Sigel, R.K., Vaidya, A. and Pyle, A.M. (2000) Metal ion binding sites in a group II intron core. *Nature Struct Biol*, **7**, 1111-1116.
54. Walter, N.G., Yang, N. and Burke, J.M. (2000) Probing non-selective cation binding in the hairpin ribozyme with Tb(III). *J Mol Biol*, **298**, 539-555.
55. Sigel, R.K.O. (2005) Group II intron Ribozymes and metal ions - A delicate relationship. *Eur J Inorg Chem*, 2281-2292.
56. Heppell, B., Blouin, S., Dussault, A.M., Mulhbacher, J., Ennifar, E., Penedo, J.C. and Lafontaine, D.A. (2011) Molecular insights into the ligand-controlled organization of the SAM-I riboswitch. *Nature Chem Biol*, **7**, 384-392.
57. Klein, D.J. and Ferre-D'Amare, A.R. (2006) Structural basis of *glmS* ribozyme activation by glucosamine-6-phosphate. *Science*, **313**, 1752-1756.
58. Lipfert, J., Sim, A.Y., Herschlag, D. and Doniach, S. (2010) Dissecting electrostatic screening, specific ion binding, and ligand binding in an energetic model for glycine riboswitch folding. *RNA*, **16**, 708-719.
59. Serganov, A., Huang, L. and Patel, D.J. (2009) Coenzyme recognition and gene regulation by a flavin mononucleotide riboswitch. *Nature*, **458**, 233-237.
60. Serganov, A., Polonskaia, A., Phan, A.T., Breaker, R.R. and Patel, D.J. (2006) Structural basis for gene regulation by a thiamine pyrophosphate-sensing riboswitch. *Nature*, **441**, 1167-1171.
61. Ramesh, A. and Winkler, W.C. (2010) Magnesium-sensing riboswitches in bacteria. *RNA Biol*, **7**, 77-83.
62. Aiba, H. (2007) Mechanism of RNA silencing by Hfq-binding small RNAs. *Curr Opin Microbiol*, **10**, 134-139.
63. Brantl, S. (2007) Regulatory mechanisms employed by cis-encoded antisense RNAs. *Curr Opin Microbiol*, **10**, 102-109.
64. Gottesman, S. (2005) Micros for microbes: non-coding regulatory RNAs in bacteria. *Trends Genet*, **21**, 399-404.
65. Wagner, E.G., Altuvia, S. and Romby, P. (2002) Antisense RNAs in bacteria and their genetic elements. *Adv Genet*, **46**, 361-398.
66. Storz, G., Vogel, J. and Wassarman, K.M. (2011) Regulation by small RNAs in bacteria: expanding frontiers. *Mol Cell*, **43**, 880-891.
67. Ellington, A.D. and Szostak, J.W. (1990) *In vitro* selection of RNA molecules that bind specific ligands. *Nature*, **346**, 818-822.

68. Gold, L., Singer, B., He, Y.Y. and Brody, E. (1997) SELEX and the evolution of genomes. *Curr Opin Genet Dev*, **7**, 848-851.
69. Mironov, A.S., Gusarov, I., Rafikov, R., Lopez, L.E., Shatalin, K., Kreneva, R.A., Perumov, D.A. and Nudler, E. (2002) Sensing small molecules by nascent RNA: A mechanism to control transcription in bacteria. *Cell*, **111**, 747-756.
70. Nahvi, A., Sudarsan, N., Ebert, M.S., Zou, X., Brown, K.L. and Breaker, R.R. (2002) Genetic control by a metabolite binding mRNA. *Chem Biol*, **9**, 1043-1049.
71. Winkler, W., Nahvi, A. and Breaker, R.R. (2002) Thiamine derivatives bind messenger RNAs directly to regulate bacterial gene expression. *Nature*, **419**, 952-956.
72. Winkler, W.C., Cohen-Chalamish, S. and Breaker, R.R. (2002) An mRNA structure that controls gene expression by binding FMN. *Proc Natl Acad Sci USA*, **99**, 15908-15913.
73. Barrick, J.E. and Breaker, R.R. (2007) The power of riboswitches. *Sci Am*, **296**, 50-57.
74. Mandal, M. and Breaker, R.R. (2004) Gene regulation by riboswitches. *Nature Rev Mol Cell Bio*, **5**, 451-463.
75. Nudler, E. and Mironov, A.S. (2004) The riboswitch control of bacterial metabolism. *Trends Biochem Sci*, **29**, 11-17.
76. Vitreschak, A.G., Rodionov, D.A., Mironov, A.A. and Gelfand, M.S. (2004) Riboswitches: the oldest mechanism for the regulation of gene expression? *Trends Genet*, **20**, 44-50.
77. Winkler, W.C. and Breaker, R.R. (2005) Regulation of bacterial gene expression by riboswitches. *Annu Rev Microbiol*, **59**, 487-517.
78. Roth, A. and Breaker, R.R. (2009) The structural and functional diversity of metabolite-binding riboswitches. *Annu Rev Biochem*, **78**, 305-334.
79. Montange, R.K. and Batey, R.T. (2008) Riboswitches: emerging themes in RNA structure and function. *Annu Rev Biophys*, **37**, 117-133.
80. Soukup, G.A. and Breaker, R.R. (1999) Relationship between internucleotide linkage geometry and the stability of RNA. *RNA*, **5**, 1308-1325.
81. Serganov, A. and Patel, D.J. (2012) Metabolite recognition principles and molecular mechanisms underlying riboswitch function. *Annu Rev Biophys*, **41**, 343-370.
82. Soukup, J.K. and Soukup, G.A. (2004) Riboswitches exert genetic control through metabolite-induced conformational change. *Curr Opin Struct Biol*, **14**, 344-349.
83. Bastet, L., Dube, A., Masse, E. and Lafontaine, D.A. (2011) New insights into riboswitch regulation mechanisms. *Mol Microbiol*, **80**, 1148-1154.
84. Winkler, W.C., Nahvi, A., Roth, A., Collins, J.A. and Breaker, R.R. (2004) Control of gene expression by a natural metabolite-responsive ribozyme. *Nature*, **428**, 281-286.
85. Hampel, K.J. and Tinsley, M.M. (2006) Evidence for preorganization of the *glmS* ribozyme ligand binding pocket. *Biochemistry*, **45**, 7861-7871.
86. Klein, D.J. and Ferre-D'Amare, A.R. (2006) Structural basis of *glmS* ribozyme activation by glucosamine-6-phosphate. *Science*, **313**, 1752-1756.
87. Brooks, K.M. and Hampel, K.J. (2011) Rapid steps in the *glmS* ribozyme catalytic pathway: cation and ligand requirements. *Biochemistry*, **50**, 2424-2433.
88. Lim, J., Grove, B.C., Roth, A. and Breaker, R.R. (2006) Characteristics of ligand recognition by a *glmS* self-cleaving ribozyme. *Angew Chem Int Ed*, **45**, 6689-6693.

89. McCarthy, T.J., Plog, M.A., Floy, S.A., Jansen, J.A., Soukup, J.K. and Soukup, G.A. (2005) Ligand requirements for *glmS* ribozyme self-cleavage. *Chem Biol*, **12**, 1221-1226.

90. Collins, J.A., Irnov, I., Baker, S. and Winkler, W.C. (2007) Mechanism of mRNA destabilization by the *glmS* ribozyme. *Genes Dev*, **21**, 3356-3368.

91. Komatsuzawa, H., Fujiwara, T., Nishi, H., Yamada, S., Ohara, M., McCallum, N., Berger-Bachi, B. and Sugai, M. (2004) The gate controlling cell wall synthesis in Staphylococcus aureus. *Mol Microbiol*, **53**, 1221-1231.

92. Cromie, M.J., Shi, Y., Latifi, T. and Groisman, E.A. (2006) An RNA sensor for intracellular Mg^{2+}. *Cell*, **125**, 71-84.

93. Spinelli, S.V., Pontel, L.B., Garcia Vescovi, E. and Soncini, F.C. (2008) Regulation of magnesium homeostasis in Salmonella: Mg^{2+} targets the mgtA transcript for degradation by RNase E. *FEMS Microbiol Lett*, **280**, 226-234.

94. Loh, E., Dussurget, O., Gripenland, J., Vaitkevicius, K., Tiensuu, T., Mandin, P., Repoila, F., Buchrieser, C., Cossart, P. and Johansson, J. (2009) A trans-acting riboswitch controls expression of the virulence regulator PrfA in *Listeria monocytogenes*. *Cell*, **139**, 770-779.

95. Cheah, M.T., Wachter, A., Sudarsan, N. and Breaker, R.R. (2007) Control of alternative RNA splicing and gene expression by eukaryotic riboswitches. *Nature*, **447**, 497-500.

96. Kubodera, T., Watanabe, M., Yoshiuchi, K., Yamashita, N., Nishimura, A., Nakai, S., Gomi, K. and Hanamoto, H. (2003) Thiamine-regulated gene expression of *Aspergillus oryzae thiA* requires splicing of the intron containing a riboswitch-like domain in the 5'-UTR. *FEBS Lett*, **555**, 516-520.

97. Sudarsan, N., Barrick, J.E. and Breaker, R.R. (2003) Metabolite-binding RNA domains are present in the genes of eukaryotes. *RNA*, **9**, 644-647.

98. Wachter, A., Tunc-Ozdemir, M., Grove, B.C., Green, P.J., Shintani, D.K. and Breaker, R.R. (2007) Riboswitch control of gene expression in plants by splicing and alternative 3' end processing of mRNAs. *Plant Cell*, **19**, 3437-3450.

99. Barrick, J.E., Corbino, K.A., Winkler, W.C., Nahvi, A., Mandal, M., Collins, J., Lee, M., Roth, A., Sudarsan, N., Jona, I. *et al.* (2004) New RNA motifs suggest an expanded scope for riboswitches in bacterial genetic control. *Proc Natl Acad Sci USA*, **101**, 6421-6426.

100. Mandal, M., Lee, M., Barrick, J.E., Weinberg, Z., Emilsson, G.M., Ruzzo, W.L. and Breaker, R.R. (2004) A glycine-dependent riboswitch that uses cooperative binding to control gene expression. *Science*, **306**, 275-279.

101. Butler, E.B., Xiong, Y., Wang, J. and Strobel, S.A. (2011) Structural basis of cooperative ligand binding by the glycine riboswitch. *Chem Biol*, **18**, 293-298.

102. Sudarsan, N., Hammond, M.C., Block, K.F., Welz, R., Barrick, J.E., Roth, A. and Breaker, R.R. (2006) Tandem riboswitch architectures exhibit complex gene control functions. *Science*, **314**, 300-304.

103. Gonzalez, J.C., Peariso, K., Penner-Hahn, J.E. and Matthews, R.G. (1996) Cobalamin-independent methionine synthase from Escherichia coli: a zinc metalloenzyme. *Biochemistry*, **35**, 12228-12234.

104. Pejchal, R. and Ludwig, M.L. (2005) Cobalamin-independent methionine synthase (MetE): a face-to-face double barrel that evolved by gene duplication. *PLoS Biol*, **3**, e31.

105. Mandal, M. and Breaker, R.R. (2004) Adenine riboswitches and gene activation by disruption of a transcription terminator. *Nature Struct Mol Biol*, **11**, 29-35.

106. Johansen, L.E., Nygaard, P., Lassen, C., Agerso, Y. and Saxild, H.H. (2003) Definition of a second *Bacillus subtilis pur* regulon comprising the *pur* and *xpt-pbuX* operons plus *pbuG*, *nupG* (*yxjA*), and *pbuE* (*ydhL*). *J Bacteriol*, **185**, 5200-5209.

107. Rodionov, D.A., Vitreschak, A.G., Mironov, A.A. and Gelfand, M.S. (2003) Regulation of lysine biosynthesis and transport genes in bacteria: yet another RNA riboswitch? *Nucleic Acids Res*, **31**, 6748-6757.

108. Klein, D.J., Schmeing, T.M., Moore, P.B. and Steitz, T.A. (2001) The kink-turn: a new RNA secondary structure motif. *EMBO J*, **20**, 4214-4221.

109. Nagaswamy, U. and Fox, G.E. (2002) Frequent occurrence of the T-loop RNA folding motif in ribosomal RNAs. *RNA*, **8**, 1112-1119.

110. Nissen, P., Ippolito, J.A., Ban, N., Moore, P.B. and Steitz, T.A. (2001) RNA tertiary interactions in the large ribosomal subunit: the A-minor motif. *Proc Natl Acad Sci USA*, **98**, 4899-4903.

111. Peselis, A. and Serganov, A. (2012) Structural insights into ligand binding and gene expression control by an adenosylcobalamin riboswitch. *Nature Struct Mol Biol*, **19**, 1182-1184.

112. Edwards, T.E., Klein, D.J. and Ferre-D'Amare, A.R. (2007) Riboswitches: small-molecule recognition by gene regulatory RNAs. *Curr Opin Struct Biol*, **17**, 273-279.

113. Serganov, A., Huang, L. and Patel, D.J. (2008) Structural insights into amino acid binding and gene control by a lysine riboswitch. *Nature*, **455**, 1263-1267.

114. Serganov, A., Polonskaia, A., Phan, A.T., Breaker, R.R. and Patel, D.J. (2006) Structural basis for gene regulation by a thiamine pyrophosphate-sensing riboswitch. *Nature*, **441**, 1167-1171.

115. Thore, S., Leibundgut, M. and Ban, N. (2006) Structure of the eukaryotic thiamine pyrophosphate riboswitch with its regulatory ligand. *Science*, **312**, 1208-1211.

116. Batey, R.T., Gilbert, S.D. and Montange, R.K. (2004) Structure of a natural guanine-responsive riboswitch complexed with the metabolite hypoxanthine. *Nature*, **432**, 411-415.

117. Cochrane, J.C., Lipchock, S.V. and Strobel, S.A. (2007) Structural investigation of the *glmS* ribozyme bound to its catalytic cofactor. *Chem Biol*, **14**, 97-105.

118. Gilbert, S.D., Rambo, R.P., Van Tyne, D. and Batey, R.T. (2008) Structure of the SAM-II riboswitch bound to S-adenosylmethionine. *Nature Struct Mol Biol*, **15**, 177-182.

119. Gilbert, S.D., Stoddard, C.D., Wise, S.J. and Batey, R.T. (2006) Thermodynamic and kinetic characterization of ligand binding to the purine riboswitch aptamer domain. *J Mol Biol*, **359**, 754-768.

120. Lemay, J.F., Penedo, J.C., Tremblay, R., Lilley, D.M. and Lafontaine, D.A. (2006) Folding of the adenine riboswitch. *Chem Biol*, **13**, 857-868.

121. Noeske, J., Buck, J., Furtig, B., Nasiri, H.R., Schwalbe, H. and Wohnert, J. (2007) Interplay of 'induced fit' and preorganization in the ligand induced folding of the aptamer domain of the guanine binding riboswitch. *Nucleic Acids Res*, **35**, 572-583.

122. Rieder, R., Lang, K., Graber, D. and Micura, R. (2007) Ligand-induced folding of the adenosine deaminase A-riboswitch and implications on riboswitch translational control. *ChemBioChem*, **8**, 896-902.

123. Serganov, A., Yuan, Y.R., Pikovskaya, O., Polonskaia, A., Malinina, L., Phan, A.T., Hobartner, C., Micura, R., Breaker, R.R. and Patel, D.J. (2004) Structural basis for discriminative regulation of gene expression by adenine- and guanine-sensing mRNAs. *Chem Biol*, **11**, 1729-1741.

124. Dann, C.E., 3rd, Wakeman, C.A., Sieling, C.L., Baker, S.C., Irnov, I. and Winkler, W.C. (2007) Structure and mechanism of a metal-sensing regulatory RNA. *Cell*, **130**, 878-892.

125. Edwards, T.E. and Ferre-D'Amare, A.R. (2006) Crystal structures of the thi-box riboswitch bound to thiamine pyrophosphate analogs reveal adaptive RNA-small molecule recognition. *Structure*, **14**, 1459-1468.

126. Montange, R.K. and Batey, R.T. (2006) Structure of the S-adenosylmethionine riboswitch regulatory mRNA element. *Nature*, **441**, 1172-1175.

127. Huang, L., Ishibe-Murakami, S., Patel, D.J. and Serganov, A. (2011) Long-range pseudoknot interactions dictate the regulatory response in the tetrahydrofolate riboswitch. *Proc Natl Acad Sci USA*, **108**, 14801-14806.
128. Baird, N.J. and Ferre-D'Amare, A.R. (2010) Idiosyncratically tuned switching behavior of riboswitch aptamer domains revealed by comparative small-angle X-ray scattering analysis. *RNA*, **16**, 598-609.
129. Baird, N.J., Kulshina, N. and Ferre-D'Amare, A.R. (2010) Riboswitch function: flipping the switch or tuning the dimmer? *RNA Biol*, **7**, 328-332.
130. Klein, D.J., Edwards, T.E. and Ferre-D'Amare, A.R. (2009) Cocrystal structure of a class I preQ1 riboswitch reveals a pseudoknot recognizing an essential hypermodified nucleobase. *Nature Struct Mol Biol*, **16**, 343-344.
131. Kulshina, N., Baird, N.J. and Ferre-D'Amare, A.R. (2009) Recognition of the bacterial second messenger cyclic diguanylate by its cognate riboswitch. *Nature Struct Mol Biol*, **16**, 1212-1217.
132. Smith, K.D., Lipchock, S.V., Ames, T.D., Wang, J., Breaker, R.R. and Strobel, S.A. (2009) Structural basis of ligand binding by a c-di-GMP riboswitch. *Nature Struct Mol Biol*, **16**, 1218-1223.
133. Winkler, W.C., Nahvi, A., Sudarsan, N., Barrick, J.E. and Breaker, R.R. (2003) An mRNA structure that controls gene expression by binding S-adenosylmethionine. *Nature Struct Biol*, **10**, 701-707.
134. Sudarsan, N., Wickiser, J.K., Nakamura, S., Ebert, M.S. and Breaker, R.R. (2003) An mRNA structure in bacteria that controls gene expression by binding lysine. *Genes Dev.*, **17**, 2688-2697.
135. Greenleaf, W.J., Frieda, K.L., Foster, D.A., Woodside, M.T. and Block, S.M. (2008) Direct observation of hierarchical folding in single riboswitch aptamers. *Science*, **319**, 630-633.
136. Haller, A., Rieder, U., Aigner, M., Blanchard, S.C. and Micura, R. (2011) Conformational capture of the SAM-II riboswitch. *Nature Chem Biol*, **7**, 393-400.
137. Boehr, D.D., Nussinov, R. and Wright, P.E. (2009) The role of dynamic conformational ensembles in biomolecular recognition. *Nature Chem Biol*, **5**, 789-796.
138. Lang, K., Rieder, R. and Micura, R. (2007) Ligand-induced folding of the *thiM* TPP riboswitch investigated by a structure-based fluorescence spectroscopic approach. *Nucleic Acids Res*, **35**, 5370-5378.
139. Garst, A.D., Heroux, A., Rambo, R.P. and Batey, R.T. (2008) Crystal structure of the lysine riboswitch regulatory mRNA element. *J Biol Chem*, **283**, 22347-22351.
140. Stoddard, C.D., Montange, R.K., Hennelly, S.P., Rambo, R.P., Sanbonmatsu, K.Y. and Batey, R.T. (2010) Free state conformational sampling of the SAM-I riboswitch aptamer domain. *Structure*, **18**, 787-797.
141. Vicens, Q., Mondragon, E. and Batey, R.T. (2011) Molecular sensing by the aptamer domain of the FMN riboswitch: a general model for ligand binding by conformational selection. *Nucleic Acids Res*, **39**, 8586-8598.
142. Zhang, J., Lau, M.W. and Ferre-D'Amare, A.R. (2010) Ribozymes and riboswitches: modulation of RNA function by small molecules. *Biochemistry*, **49**, 9123-9131.
143. Nahvi, A., Barrick, J.E. and Breaker, R.R. (2004) Coenzyme B_{12} riboswitches are widespread genetic control elements in prokaryotes. *Nucleic Acids Res*, **32**, 143-150.
144. Vitreschak, A.G., Rodionov, D.A., Mironov, A.A. and Gelfand, M.S. (2003) Regulation of the vitamin B_{12} metabolism and transport in bacteria by a conserved RNA structural element. *RNA*, **9**, 1084-1097.
145. Chen, P., Ailion, M., Weyand, N. and Roth, J. (1995) The end of the *cob* operon: evidence that the last gene (*cobT*) catalyzes synthesis of the lower ligand of vitamin B_{12}, dimethylbenzimidazole. *J Bacteriol*, **177**, 1461-1469.
146. Jeter, R.M., Olivera, B.M. and Roth, J.R. (1984) *Salmonella typhimurium* synthesizes cobalamin (vitamin B_{12}) *de novo* under anaerobic growth conditions. *J Bacteriol*, **159**, 206-213.

147. Jeter, R.M. and Roth, J.R. (1987) Cobalamin (vitamin B_{12}) biosynthetic genes of *Salmonella typhimurium*. *J Bacteriol*, **169**, 3189-3198.

148. Ravnum, S. and Andersson, D.I. (1997) Vitamin B_{12} repression of the *btuB* gene in *Salmonella typhimurium* is mediated via a translational control which requires leader and coding sequences. *Mol Microbiol*, **23**, 35-42.

149. Roth, J.R., Lawrence, J.G., Rubenfield, M., Kieffer-Higgins, S. and Church, G.M. (1993) Characterization of the cobalamin (vitamin B_{12}) biosynthetic genes of *Salmonella typhimurium*. *J Bacteriol*, **175**, 3303-3316.

150. Richter-Dahlfors, A.A. and Andersson, D.I. (1992) Cobalamin (vitaminB_{12}) repression of the *Cob* operon in *Salmonella typhimurium* requires sequences within the leader and the first translated open reading frame. *Mol Microbiol*, **6**, 743-749.

151. Richter-Dahlfors, A.A., Ravnum, S. and Andersson, D.I. (1994) Vitamin B_{12} Repression of the *Cob* Operon in *Salmonella typhimurium* - Translational Control of the Cbia Gene. *Mol Microbiol*, **13**, 541-553.

152. Ailion, M. and Roth, J.R. (1997) Repression of the *cob* operon of *Salmonella typhimurium* by adenosylcobalamin is influenced by mutations in the *pdu* operon. *J Bacteriol*, **179**, 6084-6091.

153. Ravnum, S. and Andersson, D.I. (2001) An adenosyl-cobalamin (coenzyme B_{12})-repressed translational enhancer in the *cob* mRNA of *Salmonella typhimurium*. *Mol Microbiol*, **39**, 1585-1594.

154. Bradbeer, C. (1993) The proton motive force drives the outer membrane transport of cobalamin in *Escherichia coli*. *J Bacteriol*, **175**, 3146-3150.

155. Bradbeer, C., Reynolds, P.R., Bauler, G.M. and Fernandez, M.T. (1986) A requirement for calcium in the transport of cobalamin across the outer membrane of *Escherichia coli*. *J Biol Chem*, **261**, 2520-2523.

156. Chimento, D.P., Mohanty, A.K., Kadner, R.J. and Wiener, M.C. (2003) Substrate-induced transmembrane signaling in the cobalamin transporter BtuB. *Nature Struct Biol*, **10**, 394-401.

157. Gudmundsdottir, A., Bradbeer, C. and Kadner, R.J. (1988) Altered binding and transport of vitamin B_{12} resulting from insertion mutations in the *Escherichia coli btuB* gene. *J Biol Chem*, **263**, 14224-14230.

158. Heller, K. and Kadner, R.J. (1985) Nucleotide sequence of the gene for the vitamin B_{12} receptor protein in the outer membrane of *Escherichia coli*. *J Bacteriol*, **161**, 904-908.

159. Reynolds, P.R., Mottur, G.P. and Bradbeer, C. (1980) Transport of vitamin B_{12} in *Escherichia coli*. Some observations on the roles of the gene products of BtuC and TonB. *J Biol Chem*, **255**, 4313-4319.

160. Kadner, R.J. (1978) Repression of Synthesis of Vitamin B_{12} Receptor in *Escherichia coli*. *J Bacteriol*, **136**, 1050-1057.

161. Lundrigan, M.D., De Veaux, L.C., Mann, B.J. and Kadner, R.J. (1987) Separate regulatory systems for the repression of *metE* and *btuB* by vitamin B_{12} in *Escherichia coli*. *Mol Gen Genet*, **206**, 401-407.

162. Lundrigan, M.D. and Kadner, R.J. (1989) Altered cobalamin metabolism in *Escherichia coli btuR* mutants affects *btuB* regulation. *J Bacteriol*, **171**, 154-161.

163. Lundrigan, M.D., Koster, W. and Kadner, R.J. (1991) Transcribed Sequences of the *Escherichia coli btub* Gene-Control Its Expression and Regulation by Vitamin B_{12}. *Proc Natl Acad Sci USA*, **88**, 1479-1483.

164. Franklund, C.V. and Kadner, R.J. (1997) Multiple transcribed elements control expression of the *Escherichia coli btuB* gene. *J Bacteriol*, **179**, 4039-4042.

165. Nou, X.W. and Kadner, R.J. (1998) Coupled changes in translation and transcription during cobalamin-dependent regulation of *btuB* expression in *Escherichia coli*. *J Bacteriol*, **180**, 6719-6728.

166. Nou, X.W. and Kadner, R.J. (2000) Adenosylcobalamin inhibits ribosome binding to *btuB* RNA. *Proc Natl Acad Sci USA*, **97**, 7190-7195.

167. Perdrizet, G.A., 2nd, Artsimovitch, I., Furman, R., Sosnick, T.R. and Pan, T. (2012) Transcriptional pausing coordinates folding of the aptamer domain and the expression platform of a riboswitch. *Proc Natl Acad Sci USA*, **109**, 3323-3328.

168. Gallo, S., Oberhuber, M., Sigel, R.K. and Krautler, B. (2008) The corrin moiety of coenzyme B_{12} is the determinant for switching the *btuB* riboswitch of *E. coli*. *ChemBioChem*, **9**, 1408-1414.

169. Gallo, S., Mundwiler, S., Alberto, R. and Sigel, R.K. (2010) The change of corrin-amides to carboxylates leads to altered structures of the B_{12}-responding *btuB* riboswitch. *Chem Commun*, **47**, 403-405.

170. Villemur, R., Lanthier, M., Beaudet, R. and Lepine, F. (2006) The *Desulfitobacterium* genus. *FEMS Microbiol Rev*, **30**, 706-733.

171. Nonaka, H., Keresztes, G., Shinoda, Y., Ikenaga, Y., Abe, M., Naito, K., Inatomi, K., Furukawa, K., Inui, M. and Yukawa, H. (2006) Complete genome sequence of the dehalorespiring bacterium *Desulfitobacterium hafniense* Y51 and comparison with *Dehalococcoides ethenogenes* 195. *J Bacteriol*, **188**, 2262-2274.

172. Reinhold, A., Westermann, M., Seifert, J., von Bergen, M., Schubert, T. and Diekert, G. (2012) Impact of vitamin B_{12} on formation of the tetrachloroethene reductive dehalogenase in *Desulfitobacterium hafniense* strain Y51. *Appl Environ Microbiol*, **78**, 8025-8032.

173. Choudhary, P.K., Duret, A., Rohrbach-Brandt, E., Holliger, C., Sigel, R.K.O. and Maillard, J. (2013) Corrinoid biosynthesis and diversity of cobalamine riboswitches in the organohalide respirer *Desulfitobacterium hafniense*. *J. Bacteriol*, accepted.

174. Johnson Jr, J.E., Reyes, F.E., Polaski, J.T. and Batey, R.T. (2012) B_{12} cofactors directly stabilize an mRNA regulatory switch. *Nature*, **492**, 133-137.

175. Souliere, M.F., Haller, A., Santner, T. and Micura, R. (2013) New insights into gene regulation--high-resolution structures of cobalamin riboswitches. *Angew Chem Int Ed*, **52**, 1874-1877.

176. Blount, K.F. and Breaker, R.R. (2006) Riboswitches as antibacterial drug targets. *Nature Biotechnol*, **24**, 1558-1564.

177. Deigan, K.E. and Ferre-D'Amare, A.R. (2011) Riboswitches: discovery of drugs that target bacterial gene-regulatory RNAs. *Acc Chem Res*, **44**, 1329-1338.

178. Gelfand, M.S., Mironov, A.A., Jomantas, J., Kozlov, Y.I. and Perumov, D.A. (1999) A conserved RNA structure element involved in the regulation of bacterial riboflavin synthesis genes. *Trends Genet*, **15**, 439-442.

179. Lee, E.R., Blount, K.F. and Breaker, R.R. (2009) Roseoflavin is a natural antibacterial compound that binds to FMN riboswitches and regulates gene expression. *RNA Biol*, **6**, 187-194.

180. Otani, S., Takatsu, M., Nakano, M., Kasai, S. and Miura, R. (1974) Letter: Roseoflavin, a new antimicrobial pigment from Streptomyces. *J Antibiot (Tokyo)*, **27**, 86-87.

181. Ott, E., Stolz, J., Lehmann, M. and Mack, M. (2009) The RFN riboswitch of *Bacillus subtilis* is a target for the antibiotic roseoflavin produced by *Streptomyces davawensis*. *RNA Biol*, **6**, 276-280.

182. Robbins, W.J. (1941) The Pyridine Analog of Thiamin and the Growth of Fungi. *Proc Natl Acad Sci USA*, **27**, 419-422.

183. Sudarsan, N., Cohen-Chalamish, S., Nakamura, S., Emilsson, G.M. and Breaker, R.R. (2005) Thiamine pyrophosphate riboswitches are targets for the antimicrobial compound pyrithiamine. *Chem Biol*, **12**, 1325-1335.

184. Blount, K.F., Wang, J.X., Lim, J., Sudarsan, N. and Breaker, R.R. (2007) Antibacterial lysine analogs that target lysine riboswitches. *Nature Chem Biol*, **3**, 44-49.

2 Monitoring global structural changes and specific metal-ion binding sites in RNA by in-line probing and Tb(III) cleavage

Pallavi K. Choudhary, Sofia Gallo, Roland K.O. Sigel

Institute of Inorganic Chemistry, Winterthurerstrasse 190, University of Zurich, CH-8057 Zurich, Switzerland

In press: Methods Mol Biol, 2014 (at the time of thesis submission, September 2013)

Key words:

RNA, riboswitch, folding, ribozymes, metal ions, in-line probing, terbium cleavage

2.1 Abstract

In this chapter we describe the use of two methods, in-line probing as well as terbium(III) cleavage. Both methods can be applied to RNAs of any size, structure and function. Aside from revealing directly metal ion binding sites, these techniques also provide structural information for longer RNA sequences that are out of range to be analyzed with other techniques such as NMR. The cleavage pattern derived from in-line probing experiments reflects local and overall conformational changes in RNA upon the addition of metal-ions, metal complexes or other ligands. On the other side, terbium(III) cleavage experiments are applied to locate specific metal ion binding sites in RNA molecules.

2.2 Introduction

To reach full activity for their versatile tasks, RNA molecules have to fold into highly specific and complex tertiary structures. However, a close packing of the RNA strand is only possible upon binding to positively charged ions, i.e. mostly metal ions that allow neutralization of the negative charge of the sugar-phosphate backbone. Generally, in the first step of folding, monovalent metal ions like K^+ and Na^+ allow a pre-organization of the RNA by binding non-specifically to the backbone (1-3). At this stage, the RNA is mainly arranged in thermodynamically stable helical parts separated by random-coil regions. Upon binding to divalent metal ions such as Mg^{2+}, the pre-folded domains are then oriented correctly in three-dimensional space to give the complex and functional tertiary structure (4, 5).

Given the large variety of structures and functions RNA can achieve, it is highly intriguing to investigate this class of molecules more closely. However, despite the continuous progress over the past decades to develop methods and tools to efficiently study, e.g., structural details, the investigation of the folding mechanism, conformational changes, or metal ion binding sites of small and large RNA molecules still remains challenging.

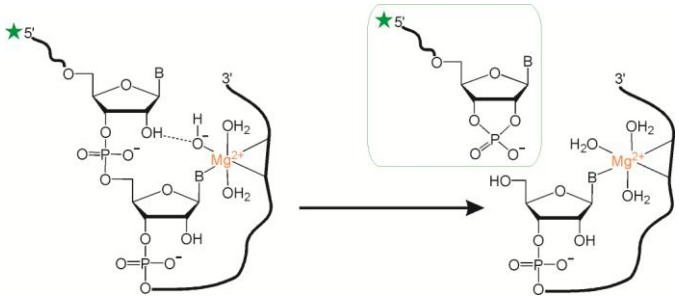

Figure 2.1: Schematic view of the self-cleavage reaction in RNA: The 2'-OH of the ribose attacks the neighboring bridging phosphate in a Mg^{2+}-assisted reaction cleaving one phosphodiester linkage. The solvated metal ion hydroxo complex (orange) coordinates to the RNA and acts as a base-catalyst by activating the attacking 2'-OH. Cleavage can also occur in the absence of any metal ion if the geometry is ideal and the cleavage sites are therefore not necessarily identical with metal-binding sites. By using 5'-labeled RNA (indicated as green asterisk), the 5'-cleavage products (green) can be detected on a denaturing polyacrylamide gel (the ^{32}P label can also be attached to the 3'-end).

The two methods described in this chapter, in-line probing and terbium(III) cleavage, are convenient techniques to study large RNA molecules. Both techniques exploit the inherent instability of RNA due to its 2'-OH group. In a spontaneous intramolecular nucleophilic reaction the 2'-OH group attacks the adjacent phosphodiester linkage leading to self-cleavage of the RNA backbone (Figure 2.1). This reaction can be accelerated by the presence of divalent metal ions (6) or acid/base catalysis (7). Interestingly, the cleavage rate is not only dependent on external factors but is also proportional to the "in-line character" of the phosphate linkage, a fact that is exploited in the in-line probing assay.

For an ideal "in-line geometry" the incoming 2'-OH group and the leaving 5'-OH are situated exactly opposite to each other of the central phosphorous. Such a geometry is however difficult to adopt in stable base-paired regions such as double helices, and hence these regions are generally more protected than unstructured regions of the RNA (8). In contrary, single stranded regions are inherently more dynamic and consequently take up more commonly an "in-line geometry", thus being cleaved also more efficiently. The differences in cleavage intensities therefore provide direct information on the flexibility or rigidity of a specific RNA region.

Each RNA molecule subjected to in-line probing shows a distinct pattern of cleavage products. As this pattern is defined by the secondary and tertiary structure of the RNA, the pattern is altered by structural changes of the RNA molecule (8). In-line probing is thus an ideal method to detect structural changes of RNA independent of their size. It is important to note that the cleavage sites detected by in-line probing do not necessarily coincide with specific metal binding sites. Therefore this technique is mainly used to investigate structural changes in RNA upon interactions with metal ion complexes or other ligands, as e.g. in so-called riboswitches (9).

Apart from detecting conformational changes in RNA, the knowledge on the specific location of metal ion binding sites is

crucial to understand folding, structure and mechanism of any RNA (10-13). Mg(II) is the key player in such metal ion interactions, but its spectroscopic detection is highly challenging and Mg(II) catalyzed hydrolytic cleavage of the RNA is very slow and often inefficient. As a way out, lanthanide(III) ions are often applied to map the metal ion binding sites on RNA, their higher charge leading to higher affinities (14-16). Importantly, the addition of small amounts of Ln(III) ions usually does not affect the activity of ribozymes. Terbium(III) has been used in the past to mimic earth alkaline ions, e.g. mostly Ca(II) (16), but also Mg(II) having similar properties (17, 18). Cleavage reactions with Tb(III) can be carried out at physiological pH because the Tb(III)-aqua species $[Tb(H_2O)_n]^{3+}$ has a pK_a value of ~ 7.9 in contrast to hydrated Mg(II) with a pK_a of 11.4 (17). Consequently, the acid-base assisted hydrolytic cleavage of the backbone is much faster with Tb(III) compared to Mg(II). It is assumed that Tb(III) replaces Mg(II) at its specific binding sites within the folded RNA tertiary structure and indeed it has been shown that the respective cleavage patterns are alike (17). The $Tb(OH)(aq)^{2+}$ complex activates a 2'-OH close-by and subsequently the intramolecular nucleophilic attack of the neighboring 3'-5'-phosphodiester bond can occur as described in Figure 2.1. While application of lower micromolar Tb(III) concentrations can specifically detect high affinity metal ion binding sites, high milimolar concentrations of Tb(III) cleave the RNA backbone at single stranded and non-Watson-Crick base-paired regions, thereby revealing the secondary and tertiary structure of the RNA (15, 16, 19).

In this chapter we describe both, in-line probing and terbium(III) cleavage, and show their practical application using the example of the 202 nt long *btuB* riboswitch of *E. coli*, a natural aptamer sequence that recognizes coenzyme B_{12} (AdoCbl) (20, 21).

2.3 Materials

All solutions must be prepared using freshly autoclaved (121 °C, 15 min, 210 kPa) bi-distilled water that is additionally filtered, e.g., through 0.2 µm Filtropur syringe filters from Sarstedt or 0.22 µm Steritop™ bottle top filter units from Millipore. In the following we refer to this as "ultrapure water". If not stated otherwise, the buffers were prepared using this ultrapure water before being filtered again using the above mentioned filtering systems. All consumables such as reaction tubes and pipette tips must be purchased as DNase/RNase-free items or otherwise need to be autoclaved (121 °C, 20 min, 210 kPa) before usage, as has to be done with all glass-ware. All chemicals are at least puriss p.a. or biograde and are purchased from usual suppliers such as Sigma-Aldrich or Brunschwig Chemie. Polyacrylamide gels were prepared using Long Ranger™ Gel Solution from Lonza. ^{32}P-γ-ATP was purchased from Perkin Elmer as a batch of 5 mCi (6000 Ci/mmol). RNase T1 of a concentration of 1000 U/µL was purchased from Fermentas/Thermo Scientific.

Centrifuges used are a Sorvall RC6+, as well as standard table top centrifuges from Eppendorf (5415D/R, 5804R). All vertical gel electrophoresis apparatuses are home made and power supplies are from Thermo (EC 600-90; 4'000V, 300 W, 300 mA maximum). The gels are dried on Whatmann™ Chromatography paper from GE Healthcare on gel driers from Uniequip or Biometra. Screening is performed using Storage Phosphor Screens from GE Healthcare. Phosphoimaging is performed on a Storm860 PhosphoImager from Amersham Biosciences, now part of GE Healthcare, or with a Typhoon scanner FLA 9000 from GE Healthcare. The gels are analyzed with the ImageQuant TL software from GE Healthcare and the intensity changes evaluated with Origin9, OriginLab® Corporation.

2.3.1 General stock solutions for polyacrylamide gel electrophoresis (PAGE)

1. Denaturing electrophoresis buffer (1X TBE): The 1X TBE buffer was prepared by dilution from 10X TBE buffer (National Diagnostics) which is: Tris-borate-EDTA; 0.89 M Tris, 0.89 M boric acid pH 8.3 and 20 mM Na_2H_2EDTA. The 1X TBE buffer is prepared by dilution with bi-distilled water followed by autoclaving (121 °C, 15 min, 210 kPa). The autoclaved buffer can be stored at r.t. for several weeks. Approximately 1 L of 1X TBE buffer is needed to run 1 or 2 gels

using one gel apparatus.

2. Denaturing 10% electrophoresis gel solutions (7M urea), 100 mL: 84 g urea (Eurobio), 20 mL Long Ranger™ Gel Solution and 10 mL 10X TBE buffer (National Diagnostics) are diluted with bi-distilled water followed by filtration with 0.22 µm Steritop™ bottle top filter units (Note 1, Figure 2.2). The gel solutions are best prepared one day before use and stored in the dark at 4 °C. The gel solutions should be cool when used for casting the gels (Note 2). For a gel with the dimensions of 30 cm x 45 cm x 0.5 mm roughly 80 mL of gel-solution is needed, although we advise to prepare 100 mL. Gel solutions can be stored a couple of weeks in the dark at 4 °C.

3. Formamide loading buffer: 82% (v/v) formamide, 0.16% (w/v) xylene cynol (XC), 0.16% (w/v) bromophenol blue (BB), 10 mM EDTA (pH 8.0 at 20 °C) (Note 3). The formamide loading buffer should be stored at 4 °C.

2.3.2 Buffers and solutions needed for in-line probing assays

1. 20X Tris buffer, 1 M (pH 8.3 at 25 °C): The buffer can be stored at r.t. and should be used within a few weeks.
2. 10X $MgCl_2$: (Note 4). The solution can be stored at r.t. and should be used within a few weeks.
3. 10X KCl: (Note 4). The solution can be stored at r.t. and should be used within a few weeks.

2.3.3 Buffers and solutions needed for Tb(III) cleavage assays

1. 5 mM Sodium cacodylate buffer (pH 5.5 at 25 °C): Prepare 21.40 gL^{-1} (100 mM) aqueous solution of sodium cacodylate trihydrate. Adjust the pH to 5.5 using a concentrated HCl-solution (32%) and dilute the 100 mM stock solution to 5 mM for further use. The buffer can be stored at r.t. and should be used within a few weeks.

2. 500 mM $TbCl_3$ solution: Dissolve 0.2 g of anhydrous $TbCl_3$ in 2 ml of 5 mM sodium cacodylate buffer (pH 5.5 at 25 °C); store at –20 °C.

3. 10X $TbCl_3$ solutions: 10X $TbCl_3$ solutions of the required concentrations are prepared in 5 mM sodium cacodylate buffer (pH 5.5 at 25 °C) by diluting the original stock of 500 mM $TbCl_3$. All $TbCl_3$ solutions have to be stored at –20 °C.

4. 10X MOPS, 250 mM (pH 7.0 at 25 °C): Adjust the pH to 7.0 by addition of a concentrated KOH-solution (e.g. 3M). The buffer should be stored in the dark at r.t. and used within a few weeks.

5. 2X Quenching buffer / colorless gel loading solution: 82% (v/v) Formamide and 10 mM EDTA (pH 8.0 at 20°C). The colorless loading buffer should be stored at 4 °C.

6. 3 M Sodium acetate (pH 5.2 at 25 °C).

7. 100% (v/v) Ethanol

8. Formamide loading buffer as described in Section 2.2.1.

2.3.4 Solutions needed for the control experiments

1. 10X Sodium carbonate (Na_2CO_3) buffer: 0.5 M Na_2CO_3 (pH 9.0 at 23 °C), 10 mM EDTA (pH 8.0 at 20 °C). The buffer can be stored at r.t. and used within a few weeks.

2. 10X Sodium citrate buffer: 0.25 M trisodium citrate (pH 5.0 at 23°C). Adjust the pH by addition of concentrated HCl. The buffer can be stored at r.t. and used within a few weeks.

3. 2X Quenching buffer as described in Section 2.2.3.

4. 1 U/µL RNase T1-solution: RNase T1 stock with a concentration of 1000U/µL was diluted to a final concentration of 1 U/µL in a buffer containing 50 mM Tris-HCl (pH 7.4 at 20 °C) and 50 % (v/v) glycerol. The RNase T1-solution should be stored at –20 °C and used before its expiry date given by the company.

2.4 Methods

Both in-line probing and terbium(III) cleavage are applied on RNA which is singularly labeled either at its 5'- or 3'-end. Although other labeling strategies are feasible, labeling with ^{32}P is still the most applied technique since it allows gel-experiments with very high resolution. For the description of the *in-vitro* transcription with T7 polymerase (22, 23) and the 5'-end labeling (24, 25) or 3'-end labeling of RNA (26) we refer to the literature.

Table 2.1: Practical example of a positive and negative control experiment for in-line probing.

Reagent	c_{stock}	c_{final}	$V_{negcontrol}$	$V_{poscontrol}$
^{32}P-RNA[1]	300 nM	30 nM	1 µL	1 µL
Tris-HCl, pH 8.3	1 M	50 mM	0.5 µL	0.5 µL
KCl	1 M	100 mM	1 µL	1 µL
$MgCl_2$	200 mM	20 mM	1 µL	1 µL
Coenzyme B_{12}	100 µM	10 µM	–	1 µL
Water			6.5 µL	5.5 µL

[[1]This concentration indicates the total concentration of the RNA after labeling. The concentration of the actually labeled RNA molecules is however lower and varies depending on the RNA sequence (Note 5)].

2.4.1 In-line probing assay

In-line probing reactions are performed in a total volume of 10 µL. If ^{32}P labeled RNA is used, the concentration of the labeled RNA should be around 2-3 nM or 20'000-40'000 cpm per reaction, while the total RNA concentration can vary depending on the experiment (Note 5). Although some RNA sequences might be folded correctly after *in-vitro* transcription and isolation, it is advisable to refold the RNA directly prior to the experiment. The refolding protocol has to be adapted to the specific sequence. The refolding protocol used in our laboratory for the *btuB* aptamer sequence is described in Note 6.

Negative and positive controls:

1. Mix ^{32}P labeled RNA (2-3 nM) with the adequate amount of Tris buffer (1 M, pH 8.3 at 25 °C), $MgCl_2$ (200 mM) and KCl (1 M) to reach a total volume of 10 µL (Note 7).
2. For the positive control add the desired amount of ligand (in our case this would be 1 µL of AdoCbl (0.1 mM)).
3. If needed, adjust the final concentrations with ultrapure water to a total volume of 10 µL.
4. Incubate at 25 °C for 40 hours.
5. Quench the reaction by adding 10 µL formamide loading buffer and analyze the reaction mixture by denaturing polyacrylamide gel electrophoresis.

For a practical example of the negative and positive control, please see Table 2.1.

2.4.2 Terbium(III) cleavage assay

The total volume of the reaction mixture is 10 µL.

1. Mix together ^{32}P labeled RNA (about 2-3 nM or 20'000-40'000 cpm per lane) and unlabeled RNA (1-1.5 µM) (Note 8) with 1 µL of 10X MOPS buffer (pH 7.0 at 25 °C) (Note 9) and KCl at its required concentration.
2. Keep the samples at 90 °C for 45 seconds for full denaturation of the RNA.

3. Cool the samples at room temperature for 1 min.
4. Add the required concentration of $MgCl_2$ from an appropriate stock for RNA folding.
5. Incubate the samples at the required temperature (varies with the system) (Note 10) for 15 minutes for a complete folding of the RNA.
6. Add 1 µL of $TbCl_3$ from the desired 10X stock solution except for the negative control.
7. Incubate the reaction mixture on ice for an optimized time period (generally ranges from 30 minutes to 2 hours) (Notes 11 and 12).
8. Quench the reaction by adding 10 µL of quench buffer / colorless gel loading buffer.
9. Add 3 M sodium acetate (pH 5.2 at 25 °C) to reach the final concentration of 0.3 M followed by the addition of 2.5 volumes of ice-cold ethanol (Note 13).
10. Incubate the samples at –20 °C overnight.
11. Centrifuge the samples at 15'000 g for 30 minutes at 4 °C.
12. Decant the supernatant carefully and dry the pellet in a speedvac evaporator (Note 14).
13. Dissolve the pellet in 5 µL of formamide loading buffer.

2.4.3 Controls and ladders

The same controls and ladders are used for both in-line probing and Tb(III) cleavage. For each control or ladder the equal amount and concentration of ^{32}P labeled RNA is needed as applied in the experimental lanes. The total volume of the control and ladders is 10µL. The control and ladders should be freshly made prior to loading on the gel.

2.4.3.1 Non-reacted RNA as a control

This control is crucial to check the inherent extent of degradation of the RNA sample. In an ideal case, this lane should only show the full-length RNA band. If this is the case, all cleavage products seen in the other lanes are "real" and can be evaluated unambiguously (Figure 2.3).

1. Dilute ^{32}P labeled RNA in ultrapure water.
2. Add 10 µL of formamide loading buffer and store the sample in liquid nitrogen until it is loaded on the gel.

2.4.3.2 RNase T1 ladder

1. Dilute ^{32}P labeled RNA in 2x quenching buffer (colorless gel loading solution), e.g. dilute 1 µL of ^{32}P labeled RNA in 7 µL 2x quenching buffer.
2. Add 1 µL of 0.25 M sodium citrate buffer.
3. Add 1 µL of RNase T1 (1U/µL) and mix gently by pipetting up and down (Note 15).
4. Incubate the mixture at 55 °C for 5 minutes (Note 16).
5. Immediately add 3 µL formamide loading buffer and 7 µL of ultrapure water and load the sample directly on the gel. If the sample cannot be loaded immediately, it should be stored in liquid nitrogen until loaded on the gel.

2.4.3.3 Alkaline hydrolysis ladder

1. Dilute ^{32}P labeled RNA in ultrapure water, e.g. dilute 1 µL of ^{32}P labeled RNA in 8 µL ultrapure water.
2. Add 1 µL of 0.5 M Na_2CO_3 buffer.
3. Incubate the mixture at 90 °C for 5 minutes (Note 17).

4. Immediately add 10 µL formamide loading buffer and load the sample directly on the gel. If the sample cannot be loaded immediately, it should be stored in liquid nitrogen until loaded on the gel.

2.4.4 Separation of cleavage products by denaturing PAGE:

1. Analyze the cleavage products of the respective experiment (from Sections 2.4.1 and 2.4.2) and the applicable controls (from Section 2.4.3) by denaturing PAGE (see Section 2.3.1).
2. Run the gel at 15-20 Watts until the lower dye Bromophenol Blue reaches the lower end of the gel (Note 16).
3. Preheat the gel dryers and set up the vacuum pump (Note 18).
4. Remove first the spacers and then the glass plate on the top with the help of a spatula.
5. Put Whatmann™ Chromatography paper on the gel, tap it gently and lift it up quickly turning it with the gel being now on the top (Note 19).
6. Cover the gel with plastic foil.
7. Put the gel on the gel dryer (paper pointing down) and dry under vacuum at 90 °C for 60-90 min (Note 20).
8. Switch off the heating mode of the gel dryer and cool the gel for about 1 hour under vacuum. To prevent breaking of the gel, the vacuum should not be released until the gel is cooled down to around 40 °C.
9. Carefully release the vacuum and put the gel for exposure overnight.
10. Scan the gel using a PhosphoImager (see Section 2.3) and analyze the gel with the respective software, e.g. ImageQuant TL from GE Healthcare.

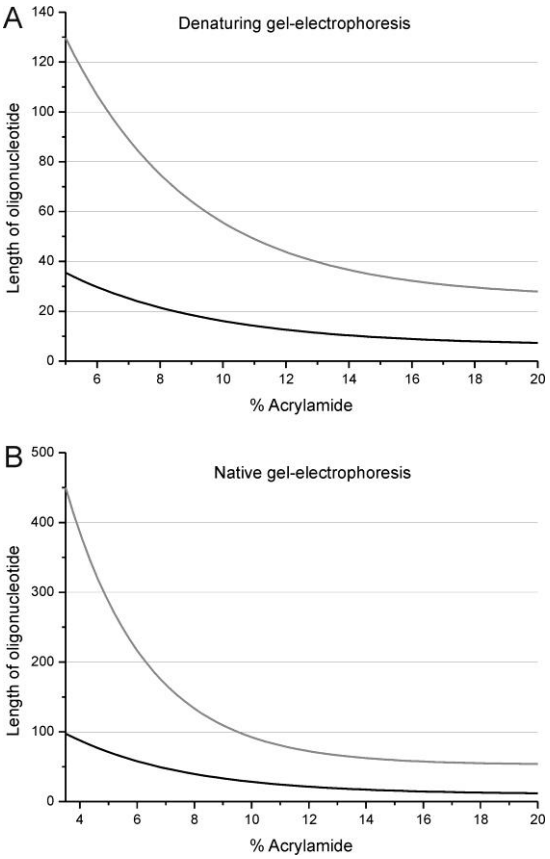

Figure 2.2: Dye mobility for selecting the appropriate acrylamide percentage of denaturing and native gels: The mobility of bromophenol blue (black, bottom curve) and xylene cyanol (grey, top curve) is shown relative to the length of a single stranded oligonucleotide on denaturing (top, 7M urea) and native (bottom) polyacrylamide gels of different percentage (31). Note that these mobilities can be used only as an approximation. The percentage of acrylamide in the gel should be chosen such that the oligonucleotide of interest migrates between the two dyes or above xylene cyanol. Aberration in migration speed of the oligonucleotide in both denaturing and native gels can however arise from its primary, secondary and tertiary structure as well as the ratio between acrylamide and bisacrylamide.

2.4.5 Quantification

1. Draw a rectangle around the band of a cleavage-site to be analyzed (Figure 2.3A). The whole band has to be included within the rectangle. However, if other bands are close by, care has to be taken not to include intensity deriving from other bands.
2. Copy this rectangle and place it on the second lane of the same site. Always use identical rectangles to quantify the bands of the same site.
3. For background-correction choose two sites within the cleavage-pattern that do not change in intensity. Take two single bands or areas to get references R1 and R2 (see also Section 2.4.5.1). It is important to determine these two sites for all lanes of interest.

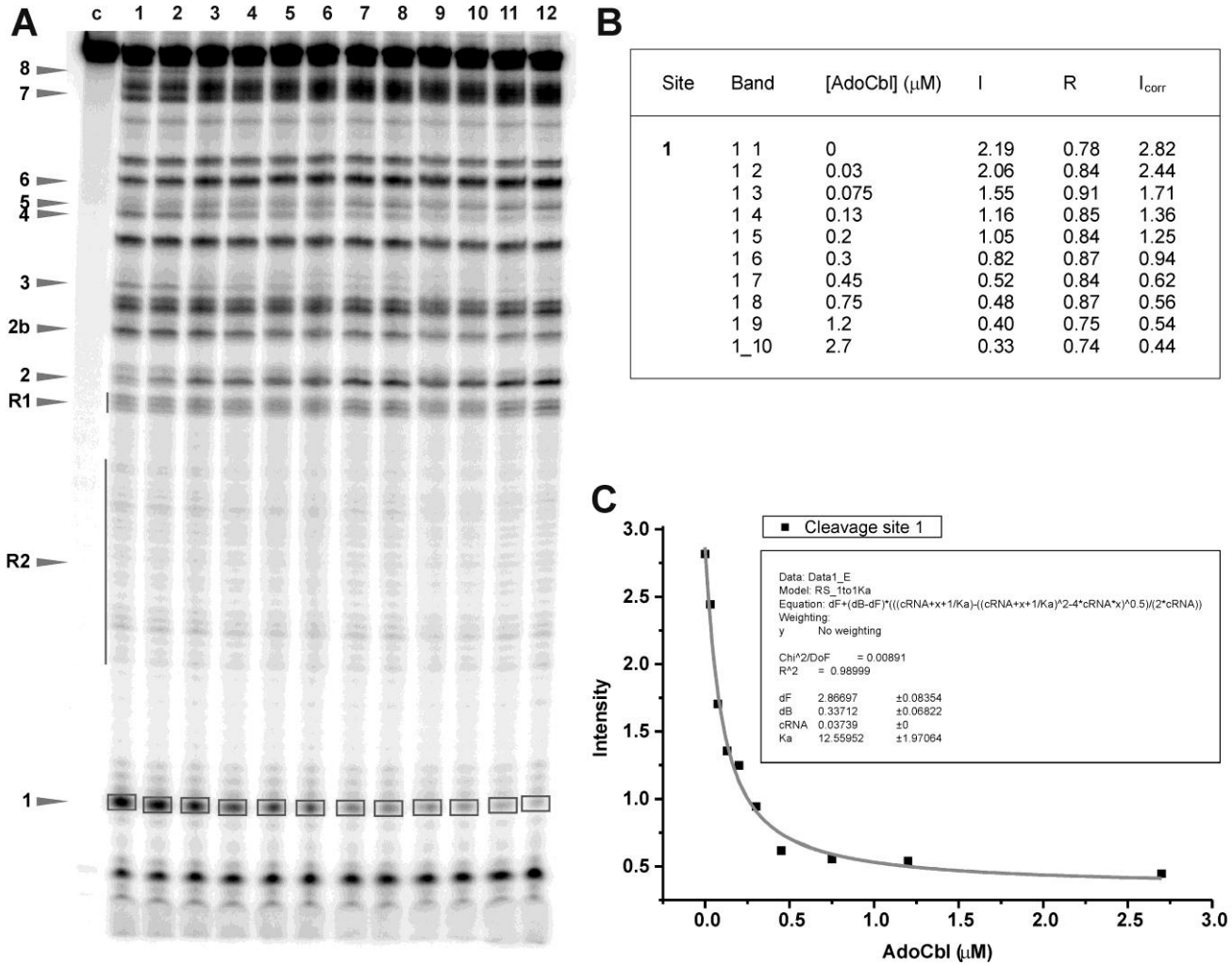

Figure 2.3: Example of the quantification of an in-line probing experiment, using a titration-experiment of the *btuB* aptamer sequence with coenzyme B_{12}. (A) Evaluation of the polyacrylamide gel. The arrows indicate the nine specific cleavage sites as well as the two constant regions R1 and R2 that are marked with a line and are used for background correction. The grey boxes frame the evaluated intensities at site 1. Lane c is the non-reacted RNA. The coenzyme B_{12} concentration is increasing from lane 1 to 12. (B) Evaluation of cleavage site 1 to obtain the corrected intensities I_{corr}. (C) Plot of the intensity changes at site 1 after background correction. The data is fit to a 1:1 binding isoterm (32) yielding the affinity constant between the RNA and its ligand.

2.4.5.1 Evaluation of the in-line probing experiments

1. To adjust the intensity of the different lanes calculate the relative intensity of each lane by the average of the two regions R1 and R2 (Figure 2.3A and B).

$$A = (R1+R2)/2 \quad (1)$$

2. Out of these averages *A*, determine the most intensive lane *X*.
3. Divide all averages *A* by *X* to get a correction factor *R* for each lane.

$$R = A/X \quad (2)$$

4. Adjust the intensities of each band *I* by dividing with the correction factor *R* of the corresponding lane. This procedure gives the corrected intensity I_{corr} (Figure 2.3B).

$$I_{corr} = I/R \quad (3)$$

5. Plot the intensities I_{corr} of the single bands versus the ligand concentration (or what is applicable) to quantify the intensity changes at each cleavage site using Origin9 or a respective program.

6. Fit the plot to a suitable fitting curve leading to the K_a-values for the interaction between the RNA and its ligand (Figure 2.3C, Note 21).

2.4.5.2 Evaluation of Terbium(III) cleavage experiments

1. To correct for the background and to adjust the intensity of each band, perform steps 1-4 as described in Section 2.3.5.1.
4. Determine I_{corr} for the corresponding site at 0 mM $TbCl_3$. This corrected cleavage intensity corresponds to $I_{corr(0)}$.
5. The final relative cleavage intensity I_R (compared to the absence of Tb(III)) of each band is calculated by taking the extent of cleavage at 0 mM $TbCl_3$ at the corresponding cleavage site into account. I_R is calculated by subtracting $I_{corr(0)}$ from I_{corr} at each applied $TbCl_3$ concentration:

$$I_R = I_{corr} - I_{corr(0)}. \quad (4)$$

6. The relative cleavage intensity of zero indicates a similar extent of cleavage as the control. Therefore only positive I_R values should be taken into account while I_R values of zero should be disregarded.
7. Classify the final calculated relative cleavage intensities I_R into categories from weak to (very) strong Tb(III) cleavage sites depending on the lowest and the highest observed cleavage intensity (Figure 2.4).
8. Compare the analyzed data to complementary experiments to confirm the accordance with Mg(II) binding sites (Note 22) (17, 27-30). A competition experiment can be set up in a similar way as the terbium cleavage assay, but here the Mg(II) concentration is increased in the presence of a constant Tb(III) concentration. Sites that involve Mg(II) binding exhibit a decrease in the cleavage intensity by Tb(III) with increasing Mg(II) concentration.

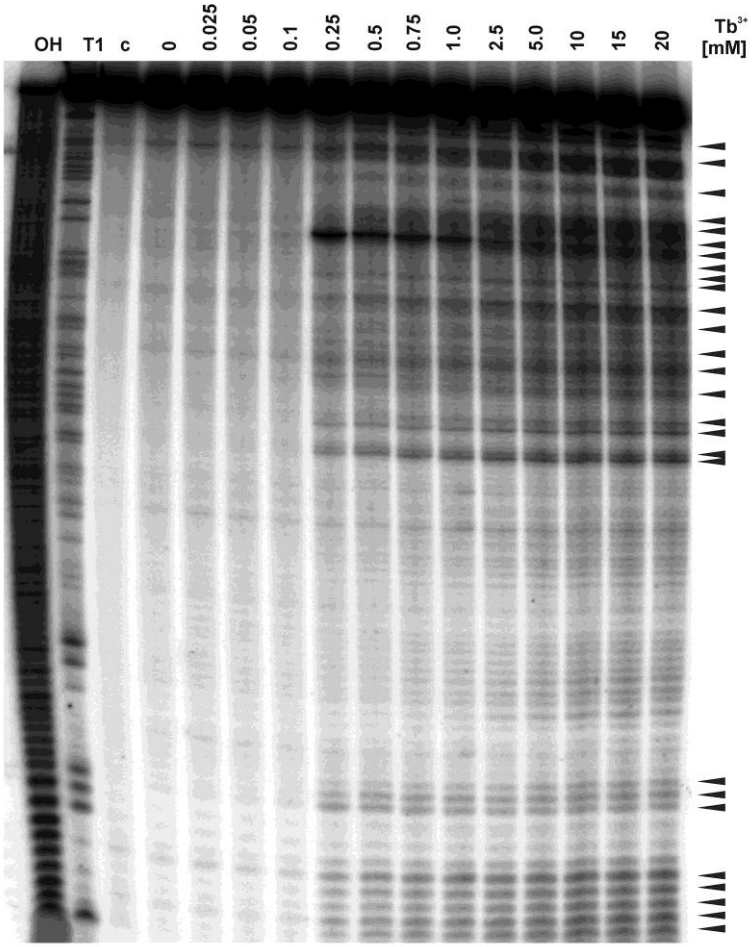

Figure 2.4: Tb(III)-mediated footprinting of the *btuB* riboswitch: Footprint of the ^{32}P labeled *btuB* riboswitch incubated with 0-20 mM Tb(III) after folding with 20 mM $MgCl_2$. Lanes 1 and 2 indicate alkaline hydrolysis and RNase T1 ladder, respectively. Lane 3, c, is the control to check for non specific degradation of the RNA used in the experiment. Lane 4 represents a second control to detect degradation of RNA under the employed reaction conditions but in the absence of Tb(III). The Tb(III) concentration increases from lanes 5 to 16. Tb(III) mediated cleavage of the RNA at specific nucleotides is indicated by arrows and can be categorized into weak, intermediate and strong cleavage sites.

2.5 Notes

1. The percentage of the polyacrylamide gel solution has to be adapted depending of the length of the RNA analyzed (Figure 2.2). For 200 nt long RNA we use a 10% gel solution. For smaller sequences the percentage has to be increased (e.g. for a 60 nt RNA use a polyacrylamide percentage of 18%). The Long Ranger^{TM} Gel Solution described in Section 2 gives a higher resolution, although also other gel solutions can be used that have a ratio of acrylamide/bisacrylamide = 29:1.
2. The best resolution of the gels is achieved if the gel is packed the evening before. After polymerization of the gel, wet towels and plastic foil are wrapped on the sides of the plates to prevent the gel from drying, while the combs are left inside and removed only the next day. The gel is then kept at 4 °C to fully polymerize overnight. For RNA of 100-200 nt in length, the dimensions of the gels needed for in-line probing experiments is normally 30 cm x 45 cm and can hold 20 pockets of 1 cm width. For terbium cleavage experiments with large RNAs (> 200 nt) we advise to use gel plates of 90 cm in length to allow good resolution at each nucleotide.
3. For small volumes it is advised to use formamide loading buffer over urea loading buffer as urea loading buffer tends to crystallize easily. Urea loading buffer can be rapidly brought back into solution by shortly heating in the microwave.
4. The concentrations of the $MgCl_2$ and KCl solutions have to be adapted to the RNA sequence. For the *btuB* riboswitch we use a final concentration of 20 mM $MgCl_2$ and 100 mM KCl to reach a complete folding and therefore prepare a 200 mM $MgCl_2$ and a 1 M KCl solution respectively.
5. The ratio between labeled and unlabeled RNA varies depending on the sequence and the labeling method. For the 5'-end labeling of the *btuB* RNA, the ratio normally lies between 3 and 20. If desired, additional unlabeled RNA can be added to the reaction volume, although we don't advise to do so for the regular experiments.
6. Refolding of the aptamer region of the *btuB* riboswitch for in-line probing experiments:
    a) Dilute the RNA to a desired concentration in ultrapure water containing 100 mM KCl.
    b) Heat the sample at 90 °C for 1 min.
    c) Cool the sample at room temperature for 1 min.
    d) Add $MgCl_2$ (1M) and Tris-HCl (1M, pH 8.3 at 25 °C) to reach a concentration of 20 mM and 50 mM respectively.
    e) Incubate at 37 °C for 15 min.
7. If many reactions need to be done contemporaneously (e.g. for a titration) it is easiest and safest to add the labeled RNA at the end.
8. Addition of unlabeled RNA reduces the non-specific cleavage by Tb(III) and also helps to precipitate the labeled RNA.
9. The pH of the Tb(III) cleavage reaction should be maintained between 7-7.5 to form sufficient amounts of the $Tb(OH)(aq)^{2+}$ species responsible for the cleavage.
10. The temperature and the time required for RNA folding after addition of $MgCl_2$ should be adjusted according to the system under investigation.
11. We recommend the Tb(III) cleavage reactions to be carried out at 4 °C (on ice bath) since it helps reducing the background degradation of the RNA although the cleavage reaction can also be carried out at higher temperatures (25 °C to 45 °C) and needs to be optimized carefully for an individual system.
12. For the cleavage reaction with Tb(III), the incubation time varies depending upon the target RNA under investigation and should be optimized for single hit cleavage reactions where 90% of the full length RNA should

remain uncleaved.

13. Instead of 3 M sodium acetate (pH 5.2), sodium chloride can be added to the samples to a final concentration of 200 mM to facilitate the precipitation of cleavage products.
14. Avoid excessive drying of the pellet in a speedvac evaporator as it makes the pellet difficult to redissolve in loading buffer.
15. The amount of RNase T1 can vary depending on the RNA used, e.g. higher amounts are needed for very stable and GC rich sequences.
16. The incubation-time needed for both ladders varies depending on the RNA sequence and should be optimized before.
17. The power of 15 Watt is recommended only when the first and last two pockets are not loaded with samples (e.g., only 16 pockets are used out of the possible 20). To reach a uniform running-pattern, we clamp aluminum plates to the front of the mounted gels. In this way the generated heat is distributed evenly over the whole surface preventing the so-called "smiley-effect". In the absence of aluminum plates, it is advised to run the gel at lower Watt (around 8 Watt) for longer times.
18. To preheat the gel dryer, for us it works best to set the dryer to 90 °C and switch it on 10 min prior to demounting the gels.
19. Gels of up to 12% acrylamide stick perfectly on Whatmann™ chromatography paper. Gels of higher percentage (e.g. 18%) need to be transferred to the plastic foil first. In a second step they are covered with the Whatmann™ chromatography paper and then put into the dryer with the paper pointing down.
20. Care should be taken while drying 15-18% polyacrylamide gels as excessive drying can curl up the gels.
21. All experiments should be done at least three times and the binding constants given as the averaged value (arithmetic or weighted mean, as applicable).
22. For example, cleavage studies can be performed also with other metal ions, e.g. Mn(II), Pb(II), Zn(II), any Ln(III), or Mg(II) itself (27-30). Note that some differences most likely will occur due to the different coordination properties. With Mg(II), the bands are usually only very weak, but help to verify real binding sites in combination with the Tb(III) data.

2.6 Acknowledgements

Financial support by the European Research Council (ERC Starting Grant to RKOS), the Swiss National Science Foundation, the Swiss State Secretariat for Education, Research, and Innovation (COST Action CM1105), and the University of Zurich is gratefully acknowledged.

2.7 References

1. Das, R. (2003) The fastest global events in RNA folding: electrostatic relaxation and tertiary collapse of the Tetrahymena ribozyme. *J Mol Biol* 332, 311-319.
2. Woodson, S. A. (2005) Metal ions and RNA folding: a highly charged topic with dynamic future. *Curr Opin Chem Biol* 9, 104-109.
3. Shimann, R., Draper, D. E. (2000) Stabilization of RNA tertiary structure by monovalent cations. *J Mol Biol* 302, 79-91.
4. Batey, R. T., Rambo, R. P., Doudna, J. A. (1999) Tertiary Motifs in RNA Structure and Folding. *Angew Chem Int Ed* 38, 2326-2343.

5. Costa, M., Michel, F. (1995) Frequent use of the same tertiary motif by self-folding RNAs. *EMBO J* 14, 1276-1285.
6. Cech, T., Golden, B. L. (1999) *in* "The RNA world" (Gesteland, R. F., Cech, T. R., and Atkins, J. F., Eds.), pp. 321-349, Cold Spring Harbor Laboratory Press, Cold Springs Harbor, New York.
7. Oivanen, M., Kuusela, S., Lonnberg, H. (1998) Kinetics and Mechanisms for the Cleavage and Isomerization of the Phosphodiester Bonds of RNA by Bronsted Acids and Bases. *Chem Rev* 98, 961-990.
8. Soukup, G. A., Breaker, R. R. (1999) Relationship between internucleotide linkage geometry and the stability of RNA. *RNA* 5, 1308-1325.
9. Roth, A., Breaker, R. R. (2009) The Structural and Functional Diversity of Metabolite-Binding Riboswitches. *Annu Rev Biochem* 78, 305-334.
10. Pyle, A. M. (2002) Metal ions in the structure and function of RNA. *J Biol Inorg Chem* 7, 679-690.
11. Freisinger, E., Sigel, R. K. O. (2007) From Nucleotides to Ribozymes - A Comparison of Their Metal Ion-Binding Properties. *Coord Chem Rev* 251, 1834-1851.
12. Schnabl, J., Sigel, R. K. (2010) Controlling ribozyme activity by metal ions. *Curr Opin Chem Biol* 14, 269-275.
13. Sigel, H., Sigel, R. K. O. (Eds.) (2013).
14. Ciesiolka, J., Marciniec, T., Krzyzosiak, W. (1989) Probing the environment of lanthanide binding sites in yeast tRNA(Phe) by specific metal-ion-promoted cleavages. *Eur J Biochem* 182, 445-450.
15. Walter, N. G., Yang, N., Burke, J. M. (2000) Probing non-selective cation binding in the hairpin ribozyme with Tb(III). *J Mol Biol* 298, 539-555.
16. Sigel, R. K., Pyle, A. M. (2003) Lanthanide ions as probes for metal ions in the structure and catalytic mechanism of ribozymes. *Met Ions Biol Syst* 40, 477-512.
17. Sigel, R. K., Vaidya, A., Pyle, A. M. (2000) Metal ion binding sites in a group II intron core. *Nat Struct Biol* 7, 1111-1116.
18. Saito, H., Suga, H. (2002) Outersphere and innersphere coordinated metal ions in an aminoacyl-tRNA synthetase ribozyme. *Nucleic Acids Res* 30, 5151-5159.
19. Harris, D. A., Tinsley, R. A., Walter, N. G. (2004) Terbium-mediated footprinting probes a catalytic conformational switch in the antigenomic hepatitis delta virus ribozyme. *J Mol Biol* 341, 389-403.
20. Nahvi, A., Barrick, J. E., Breaker, R. R. (2004) Coenzyme B_{12} riboswitches are widespread genetic control elements in prokaryotes. *Nucleic Acids Res* 32, 143-150.
21. Gallo, S., Oberhuber, M., Sigel, R. K. O., Kräutler, B. (2008) The corrin moiety of coenzyme B_{12} is the determinant for switching the *btuB* riboswitch of *E. coli*. *ChemBioChem* 9, 1408-1414.
22. Beckert, B., Masquida, B. (2011) Synthesis of RNA by in vitro transcription. *Methods Mol Biol* 703, 29-41.
23. Gallo, S., Furler, M., Sigel, R. K. O. (2005) *In vitro* transcription and purification of RNAs of different size. *Chimia* 59, 812-816.
24. Hilario, E. (2002) End labeling procedures. An overview. *Methods Mol Biol* 179, 13-18.
25. Hilario, E. (2004) End labeling procedures: an overview. *Mol Biotechnol* 28, 77-80.
26. Huang, Z., Szostak, J. W. (1996) A simple method for 3'-labeling of RNA. *Nucleic Acids Res* 24, 4360-4361.
27. Erat, M. C., Sigel, R. K. (2011) Methods to detect and characterize metal ion binding sites in RNA. *Met Ions Life Sci* 9, 37-100.
28. Pechlaner, M., Sigel, R. K. (2012) Characterization of metal ion-nucleic acid interactions in solution. *Met Ions Life Sci* 10, 1-42.

29. Hertweck, M., Mueller, M. W. (2001) Mapping divalent metal ion binding sites in a group II intron by Mn(2+)- and Zn(2+)-induced site-specific RNA cleavage. *Eur J Biochem* 268, 4610-4620.
30. Dorner, S., Barta, A. (1999) Probing ribosome structure by europium-induced RNA cleavage. *Biol Chem* 380, 243-251.
31. Sambrook, J., Russel, D. W. (2001) Molecular Cloning: A Laboratory Manual, Cold Spring Harbor Laboratory Press, NY.
32. Sigel, R. K. O., Freisinger, E., Lippert, B. (2000) Effects of N7-methylation, N7-platination, and C8-hydroxylation of guanine on H-bond formation with cytosine: platinum coordination strengthens the Watson-Crick pair. *J Biol Inorg Chem* 5, 287-299.

3 Mg^{2+} induced conformational changes in the *btuB* riboswitch from *E. coli*

Pallavi K. Choudhary and Roland K. O. Sigel

Institute of Inorganic Chemistry, Winterthurerstrasse 190, University of Zürich, 8057 Zürich, Switzerland

Under revision in: The RNA journal, 2013, manuscript id: RNA/2013/039909 (at the time of thesis submission, September 2013)

Keywords: Mg^{2+}, RNA, folding, riboswitch, coenzyme B_{12}

3.1 Abstract

With its vital role in the stabilization of tertiary structural elements of RNA, Mg^{2+} has also been shown to modulate the function of riboswitches by facilitating the ligand-riboswitch interactions. Here, we discuss the structural folding attained by the *btuB* riboswitch from *E. coli* in response to Mg^{2+} and how it affects the ligand binding competent conformation of the RNA. The *btuB* riboswitch notably adopts different conformational states depending upon the concentration of Mg^{2+}. With the help of in-line probing, we show the existence of at least two specific conformations, one being achieved in the complete absence of Mg^{2+} (or low Mg^{2+} concentration) and the other appearing above ~0.5 mM Mg^{2+}. Distinct regions of the riboswitch exhibit different dissociation constants towards Mg^{2+} indicating a stepwise folding of the *btuB* RNA. Increasing the Mg^{2+} concentration drives the transition from one conformation towards the other. The conformational state existing above 0.5 mM Mg^{2+} defines the binding competent conformation of the *btuB* riboswitch which can productively interact with the ligand, coenzyme B_{12} (adenosyl-cobalamine, AdoCbl), and switch the RNA conformation. Moreover, raising the Mg^{2+} concentration enhances the ratio of switched RNA in the presence of AdoCbl. The lack of a AdoCbl induced conformational switch experienced by the *btuB* riboswitch in absence of Mg^{2+} indicates a crucial role played by Mg^{2+} for defining an active conformation of the riboswitch.

3.2 Introduction

Riboswitches are highly conserved RNA elements present in the non-coding regions of various mRNAs exerting their response on genetic regulation by binding small metabolites (1-4). Metabolite binding to the aptamer region of the riboswitch alters its conformation accompanied by the structural changes in the downstream expression platform (5). These conformational changes regulate the gene expression either at the transcriptional or translational level (6,7), due to intron splicing (8), activation of self cleavage (9), or due to *trans* regulation (10,11). The *btuB* riboswitch of *E. coli* is placed in the 5'UTR of the *btuB* gene encoding the cobalamine transporter BtuB, an outer membrane protein (12,13). At high cellular concentration, the ligand AdoCbl interacts with the *btuB* aptamer inducing thereby a structural switch in the RNA (2). The co-ordinated conformational switch in the aptamer and the expression platform of the riboswitch can result in the attenuation of transcription or inhibition of translation of the *btuB* mRNA to maintain adequate levels of AdoCbl in the cytosol (5,14). Apart from AdoCbl, this riboswitch also interacts with Vitamin B_{12} and other cobalamine derivatives although with reduced affinity (2,15).

To bind its ligand, a riboswitch needs to adopt its so-called binding competent conformation (16). In most cases, such a competent structure can be achieved by Mg^{2+} assisted folding of the riboswitch. Mg^{2+} favors the formation and stabilization of the tertiary structure of the polyanionic RNA by reducing the strong electrostatic repulsions experienced by the closely positioned phosphodiester groups (17-24). Divalent metal ions like Mg^{2+} have been reported to be playing indispensable roles in case of riboswitches in the formation of an active tertiary structure (25-28). In some cases, Mg^{2+} also facilitates the interaction of ligand with its riboswitch (28-31), e.g., the SAM I riboswitch (32) requires both divalent metal ions and its ligand to induce a conformational alteration. In contrast, the binding of guanine to the *xpt* G riboswitch can take place at high monovalent ion concentration but absence of Mg^{2+} although 2 mM Mg^{2+} drives the complex formation to completion (33).

Given the diverse activities attributed to Mg^{2+} for an efficient functioning of riboswitches, we focused our interest on the roles of Mg^{2+} in one of the most complex riboswitches, the *btuB* riboswitch from *E. coli*. Although the mechanism for AdoCbl binding to B_{12} riboswitches has been studied previously (15,34-36) the metal ion induced folding and functioning of coenzyme B_{12} riboswitches remains unsolved.

Here we describe the influence of Mg^{2+} on the pre-organization of the binding competent structure for the *btuB* aptamer.

At the same time, we deduce the riboswitch folding by establishing the affinity constants of different regions to Mg^{2+}. Our results suggest that the formation of a binding competent conformation is crucial for the *btuB* aptamer to recognize AdoCbl. Furthermore, we have also defined the influence of Mg^{2+} in AdoCbl induced conformational switch of the aptamer. Our studies provide an insight into the Mg^{2+} dependent folding of the *btuB* riboswitch as well as indicate the relevance of Mg^{2+} in regulation of conformational switch of the *btuB* RNA by AdoCbl.

3.3 Results

3.3.1 Mg^{2+} dependent conformational states of the ligand free *btuB* aptamer

To observe the dependence of the *btuB* riboswitch folding on Mg^{2+}, we have used the well established technique of in-line probing (37,38). This technique has been used previously to distinguish the ligand induced changes in various riboswitches (2,4,39,40). The in-line nucleophilic attack itself depends on the local geometry taken up by the involved nucleotides and thereby represents the overall RNA conformation (41). Hence, to detect any metal ion induced conformational alteration in the ligand free RNA, we subjected the *btuB* aptamer to in-line probing by varying Mg^{2+} concentrations in the complete absence of AdoCbl.

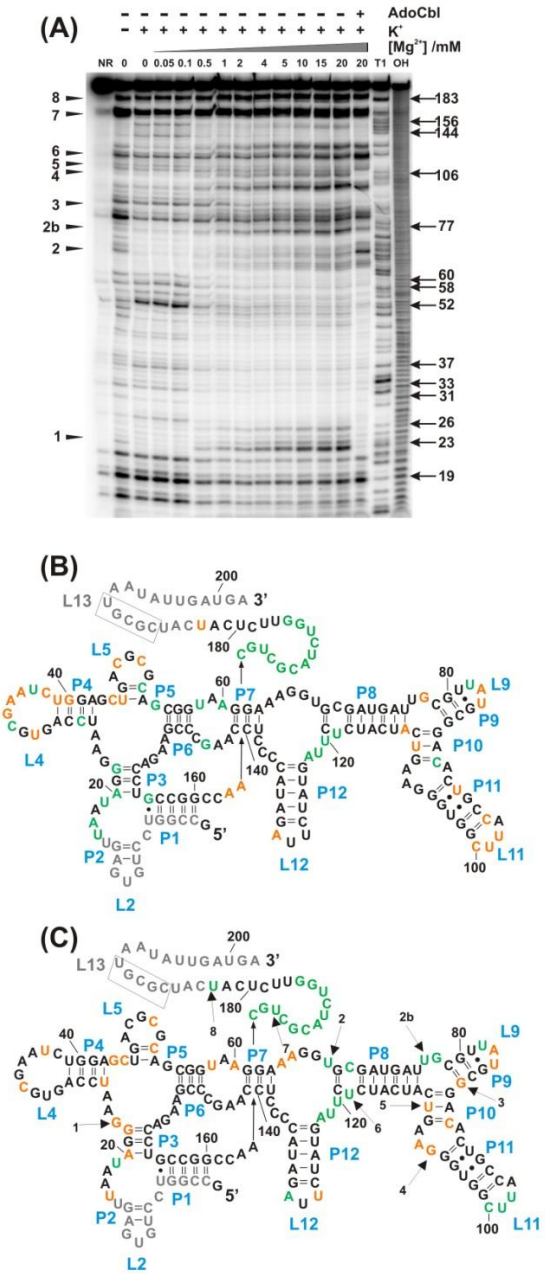

Figure 3.1: Mg^{2+} induced conformational changes in the *btuB* aptamer: (A) In-line probing of the *btuB* aptamer in the absence of AdoCbl by varying the Mg^{2+} concentration from 0-20mM in the absence and presence of 100 mM KCl. Lane 14 with 20 mM Mg^{2+} and 500 µM AdoCbl serves as a reference to map the AdoCbl interacting sites 1-8. Nucleotides 19-183 indicate the sites of the most visible changes at Mg^{2+} > 0.1 mM. NR, *btuB* in plain water; T1, RNase T1 ladder; OH, alkaline hydrolysis ladder. Structural changes detected by in-line probing experiments in the absence of AdoCbl are mapped on the secondary structure of the *btuB* aptamer in the absence (B) and in the presence of 2 mM Mg^{2+} (C). Shown are the nucleotides undergoing strong cleavage (green), intermediate cleavage (orange) and complete protection (black). Nucleotides in grey could not be mapped from the gel. Black arrows in (C) indicate the sites modulated by AdoCbl.

As seen in Figure 3.1A, the *btuB* RNA is almost completely unstructured in water only. Addition of Tris-HCl (pH 8.3) that includes ~25 mM K^+ leads to first structuring i.e. in the absence of further monovalent and divalent cations some nucleotides show a marked protection from the cleavage (Figure 3.1A, lanes 1and 2). The addition of 100 mM KCl induces distinct structural changes in some of the region of the RNA as summarized in Figure 3.1B. With the addition of Mg^{2+} up to 0.1 mM, the cleavage pattern and thus the structure remains unchanged indicating that the critical Mg^{2+} sites have K_D values smaller than 100 µM. Generally, a rather unspecific and relatively high background cleavage at all positions can be observed at low Mg^{2+} concentration. This is true especially for the loop regions indicating the absence of tertiary contacts.

Upon increase in Mg^{2+} concentration above 0.5 mM, the change in the geometry is noticeable at several nucleotides (Figure 3.1C). In the region encompassing nucleotides 16-30, most of the residues exhibit a relative protection from the cleavage except for nucleotides U19, G23, U26 (Figure 3.1C). Further changes can be seen at loop L4, which after addition of more than 0.5 mM Mg^{2+} displays less cleavage. Interestingly, some of the nucleotides in this loop like U31, A35, and A36 were found to be conserved in the consensus sequence of the coenzyme B_{12} aptamer (42) adding further to its importance in the function of the riboswitch. Moreover, the L4 interacts with an internal loop between P6 and P7 (T-loop-T-loop motif) in the crystal structure of *Tte*AdoCbl riboswitch (35). The *btuB* riboswitch probably undergoes a similar interaction explaining the observed partial protection from the cleavage at L4.

At Mg^{2+} concentration of 0.5 mM, nucleotides at the junction of P6/7, P7/8 (C52, G54,U58, A60) and in the region around stems P8-P11 (G106, A107, A112) show a decreasing susceptibility for cleavage as compared to the absence of Mg^{2+} (Figure 3.1A). Another interesting change takes place at L11 that takes up more flexible conformation with increasing Mg^{2+} concentration. From the conserved B_{12} box situated between nucleotides 140-160, only G144 and G156 undergo a Mg^{2+} dependent structural transition towards a more rigid geometry.

Interesting to note are the changes seen at the nucleotides (sites 1-8) reported to be modulated upon interaction with AdoCbl (2,15). As can be seen from Figure 3.1A, G23 (site 1) is less prone for in-line cleavage in the presence of up to 0.1 mM Mg^{2+} whereas at Mg^{2+} concentration > 0.1 mM along with monovalent cations, G23 takes up a dynamic geometry and undergoes a distinct cleavage. G23 therefore attains two different geometries, one in the presence of 0-0.1 mM Mg^{2+} or at high Mg^{2+} / AdoCbl and a second at 0.5-20 mM Mg^{2+}. Site 2b (U77), site 3 (G87), site 4 (G106) and site 8 (U183) are relatively protected from cleavage at 0-0.1 mM Mg^{2+} as compared to 0.5-20 mM Mg^{2+} (Figure 3.1A) whereas site 2 (U68), site 5 (G110), site 6 (U118) and site 7 (U167) do not change their geometry dramatically with increase in Mg^{2+} concentration. All of these sites (sites 1-8) switch their geometries in the presence of AdoCbl. The geometry displayed by sites 1-8 prior to ligand binding therefore could be important for the recognition by the ligand.

The structural changes observed between 0.1 and 0.5 mM Mg^{2+} persist when the Mg^{2+} concentration is raised to 20 mM. Although we could observe that the in-line nucleophilic cleavage is enhanced with Mg^{2+}, the intensity of cleavage increases only at specific intranucleotide linkages keeping otherwise the pattern of cleavage and thereby the conformation of RNA the same from 0.5 to 20 mM Mg^{2+}. It is important to note that the sites undergoing in-line cleavage may not correspond to specific Mg^{2+} binding sites of the RNA. Hence, the change in cleavage pattern of the *btuB* aptamer probably reflects the overall conformational change brought about by Mg^{2+}. However, metal ion binding at certain sites of cleavage cannot be ruled out.

3.3.2 The *btuB* aptamer is structured in the absence of divalent cations

To investigate the extent to which Mg^{2+}-introduced conformational alterations affect the stabilization of RNA, thermal denaturation studies of the *btuB* aptamer were carried out. 1 mM Mg^{2+} stabilizes the structure of the *btuB* RNA considerably as reflected by an increase of almost 10°C in the melting temperature of the RNA (Figure 3.2A). Nevertheless, the transition seen in the absence of Mg^{2+} suggests that the *btuB* RNA adopts a specific secondary structure even in absence of divalent cations. This is in agreement with our in-line probing data as some of the nucleotides do not change their geometry regardless of Mg^{2+}. CD spectra of the *btuB* aptamer (Figure 3.2B) indicate that the RNA forms A-form helices already in the absence of Mg^{2+} as the addition of Mg^{2+} does not lead to any significant increase in the large positive ellipticity at 265nm confirming the presence of secondary structural elements at high monovalent cation concentration.

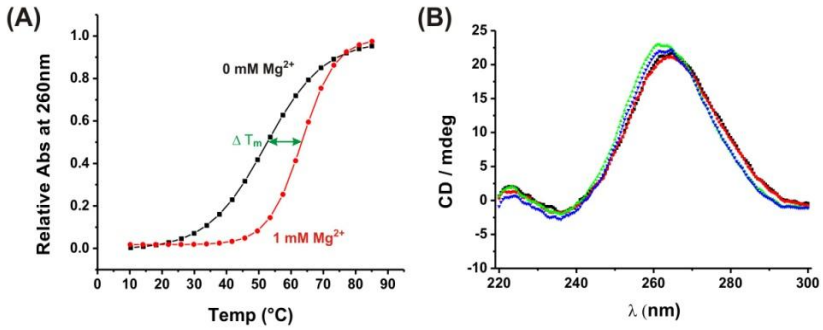

Figure 3.2: Structural changes in the *btuB* aptamer induced by K^+ and Mg^{2+}: (A) Mg^{2+} induced stabilization of the *btuB* riboswitch folded in 100 mM KCl as indicated by the increase of the melting temperature from 52.8 ± 0.13 (no Mg^{2+}, black curve) to 63.3 ± 0.10 in the presence of 1 mM Mg^{2+} (red curve). (B) CD spectra of the *btuB* aptamer renatured in 100 mM KCl and 0 mM (black), 0.1 mM (red), 1.5 mM (green), or 20 mM (blue) $MgCl_2$.

3.3.3 Mg^{2+} induces a hierarchical folding of the ligand free *btuB* aptamer

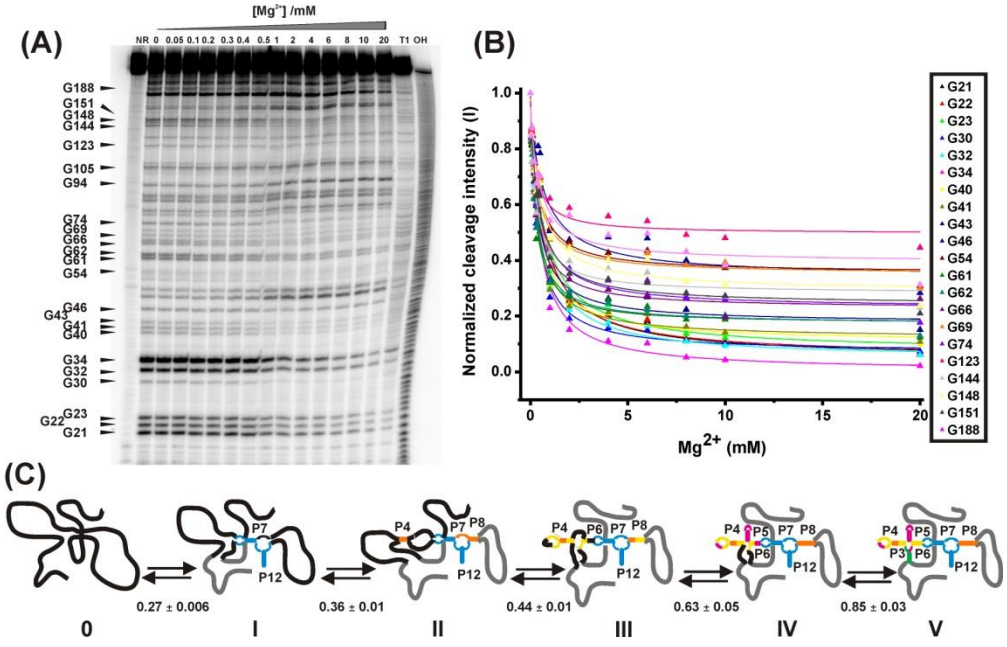

Figure 3.3: Mg^{2+} induced folding transition for the *btuB* aptamer: (A) Partial RNaseT1 digestion of the *btuB* aptamer subjected to renaturation in varying Mg^{2+} concentration (0-20 mM). Arrows indicate the corresponding guanine residues. NR, *btuB* in plain water; T1, RNaseT1 ladder under denaturing conditions; OH, alkaline hydrolysis ladder. (B) The relative intensity of cleavage as detected in the RNase T1 assay is plotted (Δ) against the Mg^{2+} concentration and the data points were fitted according a 1:1 binding model (—) to obtain the respective dissociation constants K_D (60). The K_D values for G94 and G105 are not considered due to large error associated with the values. (C) The proposed folding pathway for the *btuB* aptamer as a function of the Mg^{2+} concentration indicated by the five stages of folding as I (blue), II (orange), III (yellow), IV (pink), V(green). This pathway is based on categorizing the K_D values of the individual guanine residues towards Mg^{2+} into the following five categories: 0.1-0.3 mM, 0.3-0.4 mM, 0.4-0.5 mM, 0.5-0.75 mM, 0.75-1 mM. The folding stages for the regions indicated in grey could not be predicted.

As the in-line probing shows a structural transition in the *btuB* aptamer at Mg^{2+} concentrations between 0.1 and 0.5 mM, we determined the Mg^{2+} concentration needed for a folding transition of the *btuB* aptamer using RNase T1 (43,44). This ribonuclease cleaves 3' of unpaired guanine residues in RNA and hence, the folding of RNA by varying the Mg^{2+} concentrations should be reflected in protection of specific guanine residues.

Most guanine residues were found to be sensitive to the increasing concentration of Mg^{2+} (Figure 3.3A). Interestingly, the observed Mg^{2+} concentration required for structural transition of individual RNA domains varies with K_D values ranging from 0.26 to 0.91 mM (Figure 3.3B and Table 3.1). These distinct affinities exhibited by the different guanines suggest a stepwise folding of the aptamer into its complete secondary structure as the regions having lower dissociation constant to fold before the other regions as indicated in Figure 3.3C. Starting from a completely unfolded RNA, stems P7 and P12 undergo the first level of folding along with their associated loops. The second stage of folding is marked by the folding of stem P8 and the onset of folding for stem P4. In the next step, there is a complete folding of stem P4 along with its loop, stem P6 and probably some of the regions surrounding nucleotide G188. Stems P5 and P3 along with their associated regions undergo the fourth and fifth level of folding respectively due to their high K_D for Mg^{2+}.

On average 0.48 ± 0.04/ (~0.5) mM Mg^{2+} is required for the guanine residues to undergo a transition in their geometries when the final RNA concentration is 1 µM. Considering the half maximal Mg^{2+} concentration needed for a transition in folding (~0.5 mM), it can be said that the *btuB* aptamer achieves its complete secondary structure at Mg^{2+} concentration of ~1.0 mM. The pre-organization of the base-paired elements at the Mg^{2+} concentration of ~1.0 mM might facilitate the rapid folding of the *btuB* RNA to its native form.

Table 3.1: Dissociation constants K_D of Mg^{2+} as determined by partial RNaseT1 digestion. The individual K_D values for each guanine site are the weighted mean of K_D values obtained from two independent titration experiments of RNase T1 probing and all errors given correspond to one standard deviation. The arithmetic mean is K_D = 0.48 ± 0.04 mM representing the mid point for the overall requirement of Mg^{2+} for folding.

Guanine	K_D [mM]	Guanine	K_D [mM]	Guanine	K_D [mM]
G21	0.83 ± 0.15	G41	0.39 ± 0.03	G69	0.35 ± 0.07[a]
G22	0.80 ± 0.14	G43	0.36 ± 0.01	G74	0.45 ± 0.02
G23	0.91 ± 0.19	G46	0.74 ± 0.28[a]	G123	0.27 ± 0.06
G30	0.41 ± 0.04	G54	0.40 ± 0.09[a]	G144	0.28 ± 0.04
G32	0.70 ± 0.11	G61	0.26 ± 0.001	G148	0.54 ± 0.01
G34	0.53 ± 0.08	G62	0.29 ± 0.004	G151	0.41 ± 0.003
G40	0.48 ± 0.05	G66	0.31 ± 0.05[a]	G188	0.47 ± 0.14[a]

[[a] Only one of the two titration experiment yielded a satisfactory fit to calculate the K_D value].

3.3.4 Mg^{2+} drives the switch in RNA conformation upon AdoCbl binding

We defined the ligand compatible structure of the *btuB* aptamer with the help of in-line probing done in the presence of AdoCbl by varying the Mg^{2+} concentrations (Figure 3.4A). Up to concentrations of 0.1 mM Mg^{2+}, the cleavage pattern in the presence of AdoCbl remains almost unchanged as compared to the one in the absence of the ligand (Figure 3.4A, lanes 3-6). Under these conditions AdoCbl fails to switch the RNA as evident from the absence of any intensity changes at the classical nine sites previously reported (2,15). However, raising the Mg^{2+} concentration from 0.5 to 5 mM does lead to an enhanced conformational switch of the *btuB* aptamer in the presence of AdoCbl (Figure 3.4A, lanes 7-14). The extent of

switching for most of the sites modulated by AdoCbl at 5 mM Mg^{2+} appears similar to that at 20 mM Mg^{2+} (Figure 3.4B) indicating that the proportion of the switched RNA is almost same at these Mg^{2+} concentrations.

The cleavage pattern of the *btuB* aptamer with 100 mM KCl and in the absence of Mg^{2+} remains unaltered irrespective of the presence of AdoCbl, meaning that the secondary structure does not change much in the presence of AdoCbl (Figure 3.4C). Both in the absence and presence of AdoCbl, we see the same influence of Mg^{2+} to fold the RNA only at concentration higher than 0.1 mM. Above 0.5 mM Mg^{2+}, the presence of AdoCbl affects the cleavage pattern at the AdoCbl modulated sites (sites 1-8) similar to earlier observation with 20 mM Mg^{2+} (15,42). On the contrary, binding of AdoCbl definitely makes the *btuB* aptamer more compact. This can be seen in native gel electrophoresis where the species of RNA in the presence of AdoCbl migrates faster compared to the one in the absence of the ligand (Figure 3.4D). Therefore, the formation of new tertiary interactions is likely that enable the RNA to adopt a more compact conformation in its switched form. Taking the recently published crystal structures of AdoCbl riboswitches into account (35,36), the ligand induced compaction in the *btuB* aptamer can be a result of a kissing loop (KL) interaction between L5 and L13, the close packing of the coaxial stems P3-P6/ P4-P5 and the specific tertiary interactions mediated by peripheral elements (P7-P12) with the ligand binding pocket.

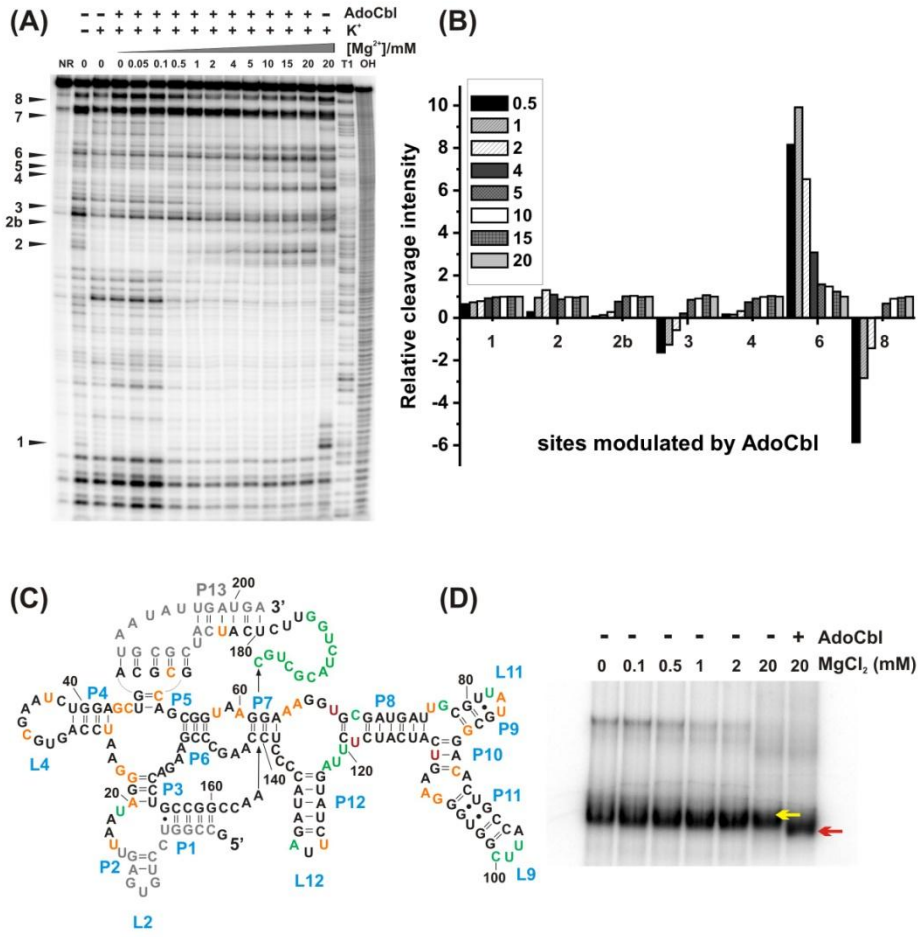

Figure 3.4: Detection of the binding competent conformation of the *btuB* aptamer: (A) In-line probing of the *btuB* aptamer in the presence of 500 µM AdoCbl and 100 mM KCl by varying the Mg^{2+} concentration (0-20mM). Sites 1-8 represent nucleotides modulated by AdoCbl. NR, *btuB* in plain water; T1, RNase T1 ladder; OH, alkaline hydrolysis ladder. (B) Mg^{2+} dependent relative maximal changes at the sites (1-8) modulated by AdoCbl. The difference between the intensity changes in the presence and absence of AdoCbl at each Mg^{2+} concentration were normalized to the difference at 20 mM Mg^{2+}. Data for site 5 and site 7 could not be evaluated. (C) Structural changes induced by AdoCbl along with Mg^{2+} (>0.1 mM). Superposition of structural changes detected by in-line probing experiment in the presence of AdoCbl on the secondary structure of the *btuB* aptamer indicating nucleotides undergoing strong cleavage (green), intermediate cleavage (orange), or complete protection (black). Residues marked in red indicate the position of nucleotides undergoing enhanced cleavage by AdoCbl. Nucleotides in grey could not be mapped from the gel. (D) The native gel electrophoresis of the *btuB* riboswitch indicating the faster migration of the RNA species incubated with AdoCbl (100 µM) (red arrow) compared to the one in the absence of AdoCbl (yellow arrow).

3.4 Discussion

3.4.1 Pre-organization of the *btuB* aptamer with Mg^{2+}

I. Mg^{2+}: A driving factor for the binding competent conformation

The stabilization of the tertiary structure of a specific RNA by Mg^{2+} influences its activity as reported for many different RNAs such as transfer RNA, catalytic ribozymes or riboswitches (45-49). The *btuB* riboswitch is no exception and undergoes Mg^{2+} dependent folding. In the presence of monovalent cations, two conformations exist for the *btuB* aptamer with respect to its secondary structure: One in the complete absence of Mg^{2+} or at Mg^{2+} concentrations of < 0.5 mM and the second achieved at > 0.5 mM Mg^{2+}. The high monovalent cation concentration changes the geometry at some nucleotides. Interestingly, these nucleotides undergo further change in their geometries with Mg^{2+} concentrations above 0.5 mM. Such geometrical alterations brought about by Mg^{2+} have a great impact on the overall conformation of the RNA as this conformation corresponds to the binding competent conformation of the *btuB* aptamer.

II. Folding of the *btuB* aptamer: A stepwise transition

It is possible that the Mg^{2+} induced structural transition of the *btuB* aptamer as seen in in-line probing represents an average conformation of the molecule on macroscopic scale. There could be transient folding intermediates which remain undetected by this method taking into consideration the time frame of 40 hours over which the cleavage reaction takes place. Although (from the in-line probing cleavage pattern) we could observe only one transition in the conformational change of the *btuB* aptamer taking place at Mg^{2+} concentrations above 0.1 mM Mg^{2+}, the existence of more than one folding intermediate cannot be excluded as distinctive regions of the RNA exhibit different affinities (K_D) towards Mg^{2+}. The *btuB* aptamer is therefore predicted to undergo a hierarchical folding of its structural elements as also observed for the aptamer of *pbuE* adenine riboswitch (50). The here proposed folding pathway is solely based on the dissociation constants (K_D) of different regions of the riboswitch towards Mg^{2+} from *in vitro* studies however the folding scheme might be different under conditions of *in vivo* co-transcriptional folding.

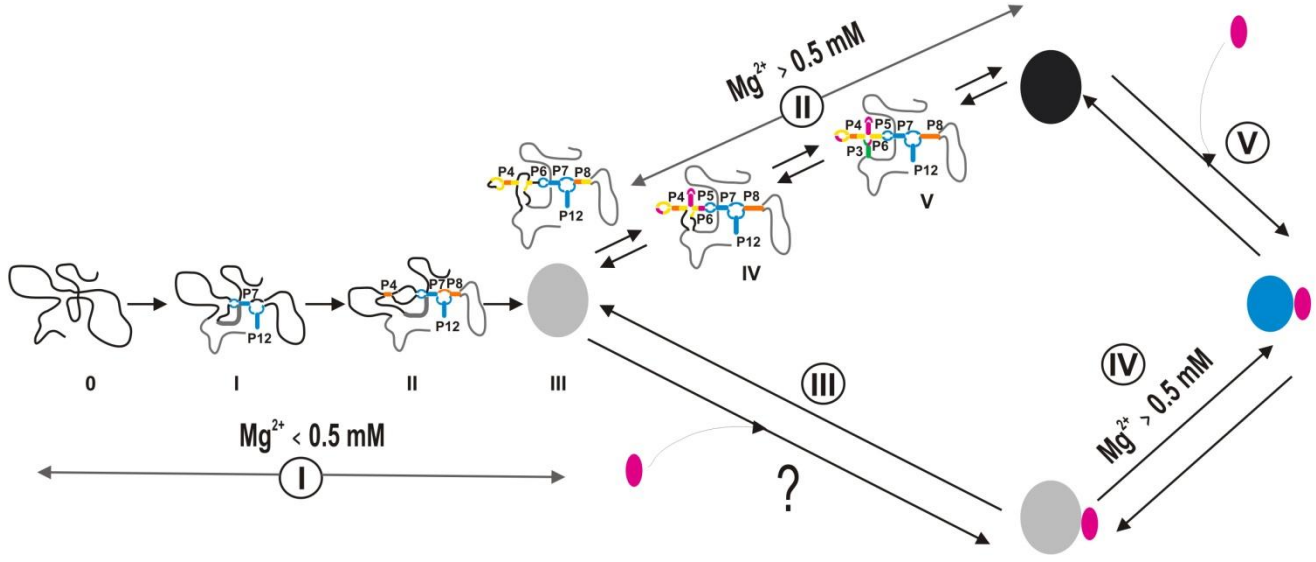

Figure 3.5: A model pathway for the folding and interaction between the *btuB* riboswitch and AdoCbl: The unfolded RNA begins to fold leading to the formation of binding incompetent conformation (grey) at Mg^{2+} concentration <0.5 mM (Pathway I). A binding competent conformation of the RNA (black) is achieved at Mg^{2+} concentrations >0.5 mM (Pathway II). AdoCbl (pink) may or may not bind to the binding incompetent conformation (grey) (Pathway III) but it does switch the RNA comformation at Mg^{2+}>0.5 mM (Pathway IV). AdoCbl not only binds the binding competent conformation but also switches its conformation making it more compact (blue) (Pathway V).

3.4.2 Binding of AdoCbl to the *btuB* aptamer

I. No switching of the *btuB* riboswitch by AdoCbl in the absence of Mg^{2+}

Our data provides strong evidence that the *btuB* riboswitch cannot be switched by its ligand in the absence of Mg^{2+}. Based on our observations, we propose the following two possibilities regarding the recognition and switching of the *btuB* riboswitch by its ligand as shown in Figure 3.5.

1. A binding competent conformation of the *btuB* aptamer is needed for AdoCbl recognition, which can only be achieved at Mg^{2+} concentrations above ~0.5 mM. Below 0.5 mM Mg^{2+}, a binding incompatible structure of the RNA is formed which fails to bind AdoCbl.

2. The aptamers of adenine binding (*add* A) and guanine binding (*xpt* G) riboswitches are known to bind their ligand independent of Mg^{2+} (33). As in in-line probing experiments, AdoCbl binding is monitored by accompanied switching of the RNA, it is possible that AdoCbl binds to the *btuB* aptamer below 0.5 mM Mg^{2+} but is unable to switch its conformation. In this case Mg^{2+} plays an important role in concert with the ligand to switch the structure of the riboswitch.

If a specific RNA is pre-organized, it can interact with its ligand in a classical induced fit manner circumventing thereby the entropic cost to the free energy of binding (51). The global architecture of the riboswitch achieved *via* RNA-RNA tertiary interactions is crucial for recognition of its ligand (26,52-54). We predict also for the *btuB* riboswitch that the Mg^{2+} induced folding transitions prepare the riboswitch for encountering its large and complex ligand. Although we do not know the exact nature of the tertiary interaction(s) accomplished by Mg^{2+} binding, the specific association of Mg^{2+} is crucial for an active *btuB* riboswitch. Moreover, the switched conformation (+ AdoCbl/ Mg^{2+}) of the *btuB* aptamer has a more compact conformation than the one in the absence of AdoCbl indicating new or altered tertiary contacts induced by ligand binding rather than a drastic rearrangement of the secondary structural elements.

II. Has Mg^{2+} any role in the conformational switch of the *btuB* aptamer along with AdoCbl?

Our studies indicate a strong connection between the Mg^{2+} concentration and AdoCbl induced conformational switching of the *btuB* RNA. The observed situation of Mg^{2+} aided switching of the RNA can be explained by two possibilities. As Mg^{2+} can assist the interaction of RNA with a ligand (55), it is probable that Mg^{2+} facilitates the binding of the complex AdoCbl to the *btuB* riboswitch. Increasing Mg^{2+} concentration possibly can also increase the riboswitch's affinity for AdoCbl, a phenomenon observed earlier with TPP and guanine binding riboswitches (52,56). In both cases, the switching of the *btuB* riboswitch by AdoCbl could be a concerted effect induced by the ligand along with Mg^{2+}. This concerted mechanism of switching by Mg^{2+} and ligand has been proposed also for the SAM I riboswitch (32) and remains a topic for further investigation in case of the *btuB* riboswitch. The mapping of Mg^{2+} binding sites from the in-line nucleophilic cleavage pattern can be indistinct and therefore, detection of such metal ion binding sites in the *btuB* riboswitch will help in predicting their implication not only in folding of the riboswitch but also in switching the structure of the riboswitch upon ligand binding.

3.4.3 Mg^{2+} dependent in-line probing and NAIM on the *btuB* riboswitch

The recently published NAIM (nucleotide analog interference mapping) study on the *btuB* riboswitch from *E. coli* does not indicate the distinct folding transitions with increasing Mg^{2+} concentration except at 15 mM Mg^{2+} where the KL interaction between L5 and L13 is predicted in the absence of ligand (35). Our current data in contrast clearly indicate conformational changes in the RNA as a function of Mg^{2+} in the absence of AdoCbl. In the presence of ligand however the structural changes in the RNA are evident at physiological Mg^{2+} concentration in NAIM as well as in in-line probing.

Altogether, our data suggests that the complex *btuB* riboswitch from *E. coli* belongs to the group of riboswitches involving Mg^{2+} as a key player for riboswitch function. Therefore, the activity of the *btuB* riboswitch can be modulated by Mg^{2+}

independently or along with its ligand, coenzyme B_{12}.

3.5 Materials and methods

3.5.1 Materials

Nucleoside 5'-triphosphates (ATP, GTP, CTP) were purchased from GE healthcare and Sigma-Aldrich (UTP). Coenzyme B_{12} (Sigma-Aldrich) was used without any further purification. Homemade T7 RNA polymerase was used for *in-vitro* RNA transcription (57). RNase T1 (Fermentas) 1000 U/µL was diluted to 0.05 U/µL in a buffer containing 50 mM Tris-HCl (pH 7.4) and 50% (v/v) glycerol. Denaturing polyacrylamide gels were prepared using Long Ranger™ gel solution (Lonza, Rockland ME, USA). Deionized water was further purified by Milipore-filtration and autoclaved before use. All the buffers, salt solutions and gel solutions were filtered through 0.2 µm filters. All other chemicals were at least puriss p.a and were purchased from Sigma-Aldrich. Gels were analyzed by Storm860 PhosphoImager and ImageQuant software (GE-Healthcare).

3.5.2 Preparation of the RNA

The *btuB* RNA was obtained by *in vitro* transcription from plasmid pPC1 by homemade T7 RNA polymerase (57). The plasmid pPC1 is based on the plasmid pSG2 (58) that contains the natural 202 nucleotide *btuB* aptamer sequence. In addition, pPC1 contains a newly introduced GGA sequence 5' to the *btuB* aptamer sequence for efficient transcription (57) and a GAGCUCG sequence at the 3' end stemming from digestion with the restriction enzyme EcoR1 (Promega). These additional nucleotides have no effect on the aptamer's ability to switch (Supplementary Figure S3.1). The *btuB* RNA was purified by 10% denaturing PAGE after *in vitro* transciption, electroeluted and concentrated using a Vivaspin concentrator (5000 MWCO) as described earlier (57). The RNA was stored in water at –20°C.

3.5.3 In-line probing

In-line probing experiments were carried out using ^{32}P-5'-labelled RNA at a final concentration of 7 nM. The RNA was incubated for 40 hrs at 25°C in 50 mM Tris-HCl (pH 8.3) and 100 mM KCl with varying concentrations of $MgCl_2$. In the presence of AdoCbl the incubation was done in the dark. The reaction was quenched by formamide loading buffer. RNase T1 ladder and alkaline hydrolysis ladder were prepared as described (37). The cleaved bands were separated by 10% denaturing PAGE and were analyzed with ImageQuant.

3.5.4 UV melting experiments

2.7 µM of RNA along with 100 mM KCl was heated to 90°C followed by addition of the respective $MgCl_2$ concentration. The sample was incubated at room temperature for 20 minutes and degassed prior to measurement. The samples were then transferred to a cuvette with a diameter of 1 mm and covered with a layer of 100 µL paraffin oil to prevent evaporation. The UV melting curves were recorded using a Cary 100 Bio UV-Visible spectrophotometer (Varian Inc.). The samples were subjected to thermal denaturation from 10-85°C at the rate of 0.5°/minute. The data was fitted to the Boltzmann equation [$y = A2 + (A1-A2) / 1+ \exp((x-x0)/dx))$] to derive the melting temperature x0.

3.5.5 Partial RNase T1 digestion

6 nM of ^{32}P-5'-labelled RNA along with 1 µM of unlabelled RNA along with 50 mM Tris-HCl (pH 7.5) was heated to 90°C for 1 min. The sample was cooled at room temperature for 1 min followed by the addition of 100 mM KCl and $MgCl_2$ (0-20 mM). The sample was incubated at 37°C for 10 minutes followed by addition of 1 µL of 0.05 U/µL of RNase

T1 (Fermentas) and subsequent incubation of further 10 minutes at 37°C. 10 µL of formamide loading buffer (82% (v/v) Formamide, 0.16% (w/v) Xylene Cynol, 0.16% (w/v) Bromophenol blue, 10 mM EDTA (pH 8.0)) was added for quenching the reaction and the samples were immediately loaded on 10% denaturing PAGE. The data was analyzed with ImageQuant.

3.5.6 Evaluation of data and calculation of K_D

The relative cleavage intensity at the guanine residues is calculated according to (59). The normalized cleavage intensities were plotted against Mg^{2+} concentration and the data points were fitted to a 1:1 binding isoterm (60) to derive the dissociation constant K_D.

3.5.7 Native gel electrophoresis

20 nM of ^{32}P-5'-labelled RNA and 1 µM of unlabelled RNA along with 50 mM Tris-HCl (pH 7.5) and 100 mM KCl was denatured at 90°C for 1 min followed by the addition of respective concentrations of $MgCl_2$. The sample was then incubated at 37°C for 15 min. AdoCbl (100 µM) was then added to the sample followed by subsequent incubation at 37°C for 30 min. Along with the equal volume of 60% glycerol, the samples were loaded on a 6% native gel and run in a buffer containing 3 mM MgOAc, 66 mM HEPES and 34 mM Tris-HCl (pH 7.5) inside the refrigerator at 4°C.

3.5.8 CD spectroscopy

0.2 µM RNA in 50 mM of Tris-HCl (pH 7.5) was denatured at 90°C for 1 minute. The sample was then cooled to room temperature for 10 minutes followed by the addition of 100 mM KCl and the respective amount of $MgCl_2$ and incubated at 25°C for 30 minutes. The CD spectra were recorded using a Jasco J-810 spectropolarimeter at a 0.5 nm data pitch and a scanning speed of 100 nm/min. Consecutive three accumulations were collected for each sample.

3.6 Acknowledgements

We thank Dr. Sofia Gallo for careful reading and valuable comments on our manuscript as well as for providing the plasmid pSG2 for the cloning purpose. Financial support by the Swiss National Science Foundation (R.K.O.S.), the University of Zurich, the European Research Council (ERC starting grant to R.K.O.S.), as well as within the COST Action CM1105 is gratefully acknowledged.

3.7 Supplementary information

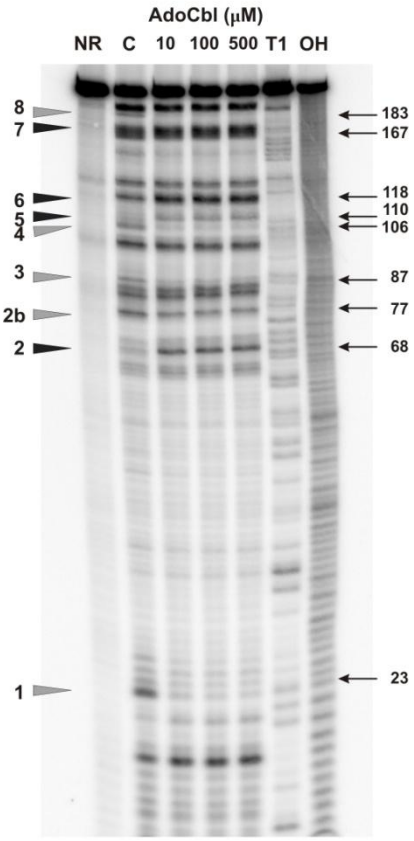

Figure S3.1: Switching of the modified 212 nucleotide long *btuB* aptamer construct in the presence of AdoCbl: The cleavage sites correspond to the ones observed for the classical 202 nucleotide *btuB* riboswitch. The black and the grey arrows indicate the sites undergoing increase and decrease in cleavage intensity respectively upon interaction with AdoCbl. NR, *btuB* in plain water; C, *btuB* incubated in the absence of AdoCbl; T1, RNase T1 ladder; OH, alkaline hydrolysis ladder. To enable straight forward comparison with previous data, the additional nucleotides at the 5' end have not been accounted for in the numbering scheme.

3.8 References

1. Mironov, A.S., Gusarov, I., Rafikov, R., Lopez, L.E., Shatalin, K., Kreneva, R.A., Perumov, D.A. and Nudler, E. (2002) Sensing small molecules by nascent RNA: a mechanism to control transcription in bacteria. *Cell*, **111**, 747-756.
2. Nahvi, A., Sudarsan, N., Ebert, M.S., Zou, X., Brown, K.L. and Breaker, R.R. (2002) Genetic control by a metabolite binding mRNA. *Chem Biol*, **9**, 1043.
3. Sudarsan, N., Barrick, J.E. and Breaker, R.R. (2003) Metabolite-binding RNA domains are present in the genes of eukaryotes. *RNA*, **9**, 644-647.
4. Winkler, W., Nahvi, A. and Breaker, R.R. (2002) Thiamine derivatives bind messenger RNAs directly to regulate bacterial gene expression. *Nature*, **419**, 952-956.
5. Mandal, M. and Breaker, R.R. (2004) Gene regulation by riboswitches. *Nat Rev Mol Cell Biol*, **5**, 451-463.
6. Soukup, J.K. and Soukup, G.A. (2004) Riboswitches exert genetic control through metabolite-induced conformational change. *Curr Opin Struct Biol*, **14**, 344-349.
7. Winkler, W.C. and Breaker, R.R. (2003) Genetic control by metabolite-binding riboswitches. *Chembiochem*, **4**, 1024-1032.
8. Kubodera, T., Watanabe, M., Yoshiuchi, K., Yamashita, N., Nishimura, A., Nakai, S., Gomi, K. and Hanamoto, H. (2003) Thiamine-regulated gene expression of *Aspergillus oryzae thiA* requires splicing of the intron containing a riboswitch-like domain in the 5'-UTR. *FEBS Lett*, **555**, 516-520.
9. Winkler, W.C., Nahvi, A., Roth, A., Collins, J.A. and Breaker, R.R. (2004) Control of gene expression by a natural metabolite-responsive ribozyme. *Nature*, **428**, 281-286.
10. Bastet, L., Dube, A., Masse, E. and Lafontaine, D.A. (2011) New insights into riboswitch regulation mechanisms. *Mol Microbiol*, **80**, 1148-1154.
11. Loh, E., Dussurget, O., Gripenland, J., Vaitkevicius, K., Tiensuu, T., Mandin, P., Repoila, F., Buchrieser, C., Cossart, P. and Johansson, J. (2009) A trans-acting riboswitch controls expression of the virulence regulator PrfA in Listeria monocytogenes. *Cell*, **139**, 770-779.
12. Gudmundsdottir, A., Bradbeer, C. and Kadner, R.J. (1988) Altered binding and transport of vitamin B_{12} resulting from insertion mutations in the *Escherichia coli btuB* gene. *J Biol Chem*, **263**, 14224-14230.
13. Reynolds, P.R., Mottur, G.P. and Bradbeer, C. (1980) Transport of vitamin B_{12} in *Escherichia coli*. Some observations on the roles of the gene products of *BtuC* and *TonB*. *J Biol Chem*, **255**, 4313-4319.
14. Nou, X. and Kadner, R.J. (2000) Adenosylcobalamin inhibits ribosome binding to *btuB* RNA. *Proc Natl Acad Sci USA*, **97**, 7190-7195.
15. Gallo, S., Oberhuber, M., Sigel, R.K. and Krautler, B. (2008) The corrin moiety of coenzyme B_{12} is the determinant for switching the *btuB* riboswitch of *E. coli*. *Chembiochem*, **9**, 1408-1414.
16. Montange, R.K. and Batey, R.T. (2008) Riboswitches: emerging themes in RNA structure and function. *Annu Rev Biophys*, **37**, 117-133.
17. Chu, V.B., Bai, Y., Lipfert, J., Herschlag, D. and Doniach, S. (2008) A repulsive field: advances in the electrostatics of the ion atmosphere. *Curr Opin Chem Biol*, **12**, 619-625.
18. Draper, D.E. (2004) A guide to ions and RNA structure. *RNA*, **10**, 335-343.
19. Freisinger, E. and Sigel, R.K.O. (2007) From Nucleotides to Ribozymes - A Comparison of Their Metal Ion-Binding Properties. *Coord. Chem. Rev.*, **251**, 1834-1851.
20. Sigel, R.K. and Pyle, A.M. (2007) Alternative roles for metal ions in enzyme catalysis and the implications for ribozyme chemistry. *Chem Rev*, **107**, 97-113.

21. Woodson, S.A. (2005) Metal ions and RNA folding: a highly charged topic with a dynamic future. *Curr Opin Chem Biol*, **9**, 104-109.
22. Pyle, A.M. (2002) Metal ions in the structure and function of RNA. *J Biol Inorg Chem*, **7**, 679-690.
23. Draper, D.E., Grilley, D. and Soto, A.M. (2005) Ions and RNA folding. *Annu Rev Biophys Biomol Struct*, **34**, 221-243.
24. Sigel, H. and Sigel, R.K.O. (2013).
25. Lemay, J.F., Penedo, J.C., Tremblay, R., Lilley, D.M. and Lafontaine, D.A. (2006) Folding of the adenine riboswitch. *Chem Biol*, **13**, 857-868.
26. Noeske, J., Schwalbe, H. and Wohnert, J. (2007) Metal-ion binding and metal-ion induced folding of the adenine-sensing riboswitch aptamer domain. *Nucleic Acids Res*, **35**, 5262-5273.
27. Ramesh, A., Wakeman, C.A. and Winkler, W.C. (2011) Insights into metalloregulation by M-box riboswitch RNAs via structural analysis of manganese-bound complexes. *J Mol Biol*, **407**, 556-570.
28. Serganov, A., Huang, L. and Patel, D.J. (2009) Coenzyme recognition and gene regulation by a flavin mononucleotide riboswitch. *Nature*, **458**, 233-237.
29. Klein, D.J. and Ferre-D'Amare, A.R. (2006) Structural basis of *glmS* ribozyme activation by glucosamine-6-phosphate. *Science*, **313**, 1752-1756.
30. Lipfert, J., Sim, A.Y., Herschlag, D. and Doniach, S. (2010) Dissecting electrostatic screening, specific ion binding, and ligand binding in an energetic model for glycine riboswitch folding. *RNA*, **16**, 708-719.
31. Serganov, A., Polonskaia, A., Phan, A.T., Breaker, R.R. and Patel, D.J. (2006) Structural basis for gene regulation by a thiamine pyrophosphate-sensing riboswitch. *Nature*, **441**, 1167-1171.
32. Heppell, B., Blouin, S., Dussault, A.M., Mulhbacher, J., Ennifar, E., Penedo, J.C. and Lafontaine, D.A. (2011) Molecular insights into the ligand-controlled organization of the SAM-I riboswitch. *Nat Chem Biol*, **7**, 384-392.
33. Serganov, A., Yuan, Y.R., Pikovskaya, O., Polonskaia, A., Malinina, L., Phan, A.T., Hobartner, C., Micura, R., Breaker, R.R. and Patel, D.J. (2004) Structural basis for discriminative regulation of gene expression by adenine- and guanine-sensing mRNAs. *Chem Biol*, **11**, 1729-1741.
34. Gallo, S., Mundwiler, S., Alberto, R. and Sigel, R.K. (2010) The change of corrin-amides to carboxylates leads to altered structures of the B_{12}-responding *btuB* riboswitch. *Chem Commun (Camb)*, **47**, 403-405.
35. Johnson Jr, J.E., Reyes, F.E., Polaski, J.T. and Batey, R.T. (2012) B_{12} cofactors directly stabilize an mRNA regulatory switch. *Nature*, **492**, 133-137.
36. Peselis, A. and Serganov, A. (2012) Structural insights into ligand binding and gene expression control by an adenosylcobalamin riboswitch. *Nat Struct Mol Biol*.
37. Regulski, E.E. and Breaker, R.R. (2008) In-line probing analysis of riboswitches. *Methods Mol Biol*, **419**, 53-67.
38. Choudhary, P.K., Gallo, S. and Sigel, R.K.O. (2014) Monitoring Global Structural Changes and Specific Metal Binding Sites in RNA by in-line Probing and Tb(III) Cleavage. *MIMB, in press*.
39. Mandal, M., Boese, B., Barrick, J.E., Winkler, W.C. and Breaker, R.R. (2003) Riboswitches control fundamental biochemical pathways in Bacillus subtilis and other bacteria. *Cell*, **113**, 577-586.
40. Sudarsan, N., Wickiser, J.K., Nakamura, S., Ebert, M.S. and Breaker, R.R. (2003) An mRNA structure in bacteria that controls gene expression by binding lysine. *Genes Dev*, **17**, 2688-2697.
41. Soukup, G.A. and Breaker, R.R. (1999) Relationship between internucleotide linkage geometry and the stability of RNA. *RNA*, **5**, 1308-1325.
42. Nahvi, A., Barrick, J.E. and Breaker, R.R. (2004) Coenzyme B_{12} riboswitches are widespread genetic control elements in prokaryotes. *Nucleic Acids Res*, **32**, 143-150.

43. Chauhan, S., Caliskan, G., Briber, R.M., Perez-Salas, U., Rangan, P., Thirumalai, D. and Woodson, S.A. (2005) RNA tertiary interactions mediate native collapse of a bacterial group I ribozyme. *J Mol Biol*, **353**, 1199-1209.
44. Rangan, P., Masquida, B., Westhof, E. and Woodson, S.A. (2003) Assembly of core helices and rapid tertiary folding of a small bacterial group I ribozyme. *Proc Natl Acad Sci USA*, **100**, 1574-1579.
45. Baird, N.J., Kulshina, N. and Ferre-D'Amare, A.R. (2010) Riboswitch function: flipping the switch or tuning the dimmer? *RNA Biol*, **7**, 328-332.
46. Cate, J.H., Gooding, A.R., Podell, E., Zhou, K., Golden, B.L., Kundrot, C.E., Cech, T.R. and Doudna, J.A. (1996) Crystal structure of a group I ribozyme domain: principles of RNA packing. *Science*, **273**, 1678-1685.
47. Cole, P.E., Yang, S.K. and Crothers, D.M. (1972) Conformational changes of transfer ribonucleic acid. Equilibrium phase diagrams. *Biochemistry*, **11**, 4358-4368.
48. Lindahl, T., Adams, A. and Fresco, J.R. (1966) Renaturation of transfer ribonucleic acids through site binding of magnesium. *Proc Natl Acad Sci USA*, **55**, 941-948.
49. Pyle, A.M. (1993) Ribozymes: a distinct class of metalloenzymes. *Science*, **261**, 709-714.
50. Greenleaf, W.J., Frieda, K.L., Foster, D.A., Woodside, M.T. and Block, S.M. (2008) Direct observation of hierarchical folding in single riboswitch aptamers. *Science*, **319**, 630-633.
51. Noeske, J., Buck, J., Furtig, B., Nasiri, H.R., Schwalbe, H. and Wohnert, J. (2007) Interplay of 'induced fit' and preorganization in the ligand induced folding of the aptamer domain of the guanine binding riboswitch. *Nucleic Acids Res*, **35**, 572-583.
52. Batey, R.T., Gilbert, S.D. and Montange, R.K. (2004) Structure of a natural guanine-responsive riboswitch complexed with the metabolite hypoxanthine. *Nature*, **432**, 411-415.
53. Buck, J., Noeske, J., Wohnert, J. and Schwalbe, H. (2010) Dissecting the influence of Mg^{2+} on 3D architecture and ligand-binding of the guanine-sensing riboswitch aptamer domain. *Nucleic Acids Res*, **38**, 4143-4153.
54. Hampel, K.J. and Tinsley, M.M. (2006) Evidence for preorganization of the *glmS* ribozyme ligand binding pocket. *Biochemistry*, **45**, 7861-7871.
55. Ferre-D'Amare, A.R. and Winkler, W.C. (2011) The roles of metal ions in regulation by riboswitches. *Met Ions Life Sci*, **9**, 141-173.
56. Yamauchi, T., Miyoshi, D., Kubodera, T., Nishimura, A., Nakai, S. and Sugimoto, N. (2005) Roles of Mg^{2+} in TPP-dependent riboswitch. *FEBS Lett*, **579**, 2583-2588.
57. Gallo, S., Furler, M. and Sigel, R.K.O. (2005) *In vitro* transcription and purification of RNAs of different size. *Chimia*, **59**, 812-816.
58. Gallo, S. (2008) *Dissertation, University of Zurich*
59. Harris, D.A. and Walter, N.G. (2003) Probing RNA structure and metal-binding sites using terbium(III) footprinting. *Curr Protoc Nucleic Acid Chem*, Chapter 6, Unit 6 8.
60. Sigel, R.K.O., Freisinger, E. and Lippert, B. (2000) Effects of N7-methylation, N7-platination, and C8-hydroxylation of guanine on H-bond formation with cytosine: platinum coordination strengthens the Watson-Crick pair. *J Biol Inorg Chem*, **5**, 287-299.

3.9 Additional experiments

3.9.1 RNase A digestion of the *btuB* RNA

The influence of Mg^{2+} on folding of the *btuB* RNA was checked by digestion with RNase A as well. RNase A cleaves the phosphodiester bond between the 5' ribose of a nucleotide and the phosphate group attached to the 3' ribose of the adjacent pyrimidine nucleotide within the single stranded RNA regions. Therefore, RNase A was employed to check the Mg^{2+} induced conformational changes at the pyrimidines within the *btuB* riboswitch.

The partial digestion of the *btuB* RNA with RNase A showed cleavage of the pyrimidine nucleotides as expected (Figure 3.6). However, the cleavage with RNase A did not show a trend of Mg^{2+} induced conformational changes at pyrimidines of the *btuB* riboswitch, unlike the RNase T1 digestion. The extent of RNA cleavage was almost the same in the presence or absence of 20 mM Mg^{2+} (Figure 3.6, full length RNA bands in lane 3 and 16). Also, there was no clear trend observed with respect to the cleavage of RNA and the divalent metal ion concentration. Therefore, RNase A activity remains the same at all Mg^{2+} concentrations however, the changes in the cleavage pattern at the pyrimidines were not evident. RNase A cleavage on the *btuB* RNA was repeated at least three times under similar conditions as in Figure 3.6 but the Mg^{2+} dependent conformational changes at the pyrimidines were never evident. This enzyme was therefore disregarded for structural probing of the *btuB* riboswitch.

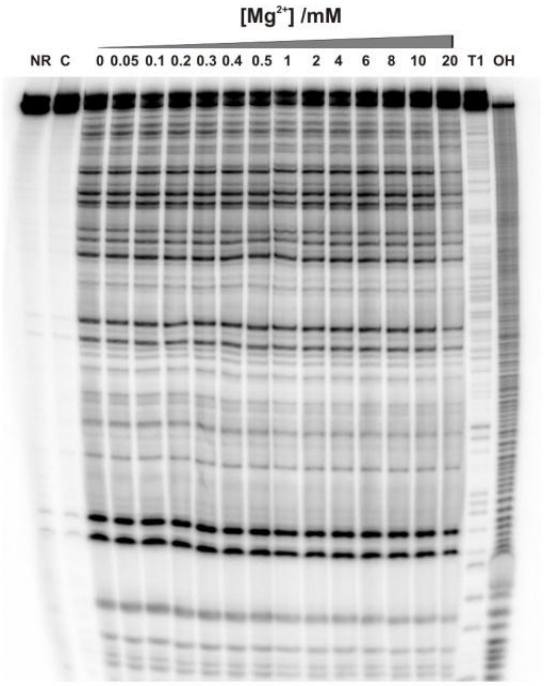

Figure 3.6: Partial RNase A digestion of the *btuB* RNA: The RNase A digestion was carried out on the *btuB* RNA refolded with increasing Mg^{2+} concentration as indicated. NR: RNA in water; C: RNA in buffer heated to 90 °C and incubated at 37 °C to check for the degradation at the employed reaction conditions; T1: RNase T1 ladder; OH: Alkaline hydrolysis ladder.

3.9.2 RNase V1 digestion of the *btuB* RNA

RNase V1 is the most frequently used enzyme for structural probing of RNA. RNase V1 cleaves specifically the double stranded regions within the A-form RNA without any base specificity and therefore helps in assigning the base paired and single stranded regions within the native conformation of RNA.

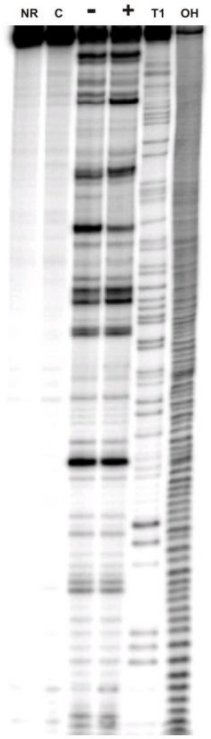

RNase V1 digestion on the *btuB* riboswitch was carried out in the presence of 20 mM Mg^{2+} to observe AdoCbl induced changes within the *btuB* riboswitch in its native conformation. As seen from Figure 3.7 and 3.8, the presence of AdoCbl does alter the pattern of protection at some nucleotides however the pattern does not match to the earlier reported modulations. The regions J2/3, J3/4, L4-P4, L5-P5, J6/7, P8, P9, P11 and L13 are cleaved by RNase V1 partially/strongly both in the absence and presence of AdoCbl. The cleavage mainly at L5, L13, L4 and J6/7 could be due to the kissing loop interaction between L5 and L13 and the T loop receptor interaction between L4 and J6/7. However, in the RNase V1 probing, these interactions do not appear to be introduced by AdoCbl as seen with other probing methods.

Figure 3.7: RNase V1 digestion of the *btuB* RNA: The *btuB* RNA was digested by RNase V1 in the absence (-) and presence (+) of 500 µM of AdoCbl. NR: RNA in water; C: RNA in buffer heated to 90 °C and incubated at 37 °C to check for the degradation at the employed reaction conditions; T1: RNase T1 ladder; OH: Alkaline hydrolysis ladder.

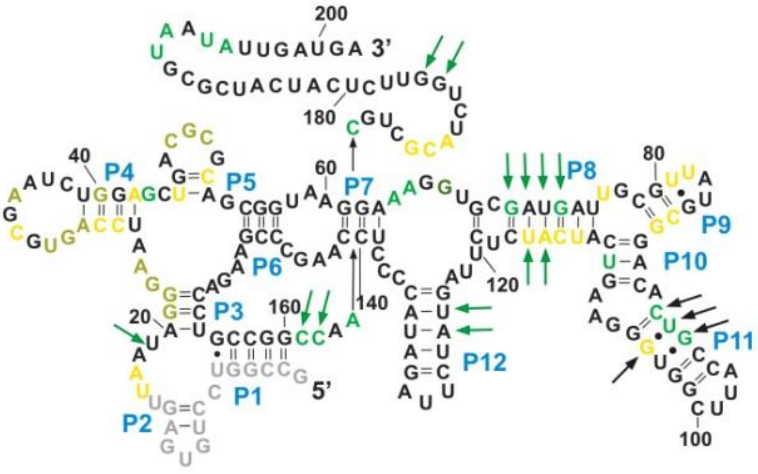

Figure 3.8: Interpretation of RNase V1 digestion on the secondary structure of the *btuB* riboswith: Nucleotides in black show complete protection with RNase V1 diegstion whereas nucleotides in yellow/light green shows partial protection. Nucleotides in green are cleaved strongly by RNase V1. The green and black arrows indicate AdoCbl induced increase and decrease in the cleavage by RNase V1.

4 Metal ion binding cores in the *btuB* riboswitch of *E. coli*

Pallavi K. Choudhary and Roland K. O. Sigel

Institute of Inorganic Chemistry, Winterthurerstrasse 190, University of Zürich, 8057 Zürich, Switzerland

To be submitted

Keywords: riboswitch, Tb(III), metal ion binding, tertiary interactions, coenzyme B_{12}.

4.1 Abstract

Riboswitches are RNA elements that bind their specific ligands in order to regulate the gene expression controlling cellular levels of the ligand. Most often, a pre-organization of the riboswitch is essential to facilitate ligand recognition and is brought about by Mg(II) assisted tertiary interactions within the secondary structural elements of the RNA. To predict the possible Mg(II) mediated tertiary interactions, we here report the Mg(II) binding pockets in the classical *btuB* riboswitch from *E. coli*. We detected an ensemble of weak, intermediate and strong Mg(II) binding sites distributed over the entire aptamer with the help of the well known Mg(II) mimic, the lanthanide ion Terbium(III). Our studies show that Mg(II) binding at strategic locations on the *btuB* riboswitch might facilitate the assembly of the ligand binding pocket as some of the Mg(II) binding sites involve conserved bases of the coenzyme B_{12} (Adenosylcobalamine, AdoCbl) riboswitches. Binding of AdoCbl to the *btuB* riboswitch however does not lead to drastic alterations in the metal ion binding cores. Comparison of the Mg(II) binding sites in the *btuB* riboswitch of *E. coli* with the recently published crystal structure of the *S. thermophilum* coenzyme B_{12} riboswitch identified a common set of tertiary interactions that might depend on Mg(II) to pre-organize the aptamer tertiary fold. Moreover, the Tb(III) mediated footprints of the riboswitch's structure in its ligand free and ligand bound state indicate that AdoCbl probably alters the riboswitch structure by inducing several local changes but keeping the global conformation of the *btuB* RNA fairly unchanged.

4.2 Introduction

Riboswitches are a class of non-coding RNA that bind small molecules/metabolites with high affinity and specificity (1-3). The two functional domains of the riboswitch, the aptamer and the downstream expression platform undergo *in tune* structural changes upon ligand binding to the aptamer region (4). This conformational switch in the riboswitch attained by ligand binding ultimately regulates gene expression mainly at the transcriptional or translational level (5,6). Recently, also other regulatory mechanisms involving splicing, self cleavage of the RNA and *trans* regulation have been proposed (7-10).

The *btuB* riboswitch from *E. coli* belongs to the class of coenzyme B_{12} riboswitches recognizing and regulating the concentration of coenzyme B_{12} (AdoCbl) inside the cell by altering the expression of the outer membrane B_{12} transporter, BtuB (11-14). The secondary structure of the *btuB* aptamer consists of a 4 way junction common with the other B_{12} riboswitches and a varying peripheral region (12). The recently solved crystal structure of AdoCbl riboswitches from thermophiles has established the role of a four way junction in constituting the ligand binding pocket/the receptor core whereas the peripheral elements stabilize the binding pocket further upon ligand binding and are crucial for specificity towards AdoCbl (15,16).

In most cases, the aptamer is pre-organized to facilitate an interaction with its cognate ligand as was observed for adenine, lysine, FMN, SAM I and glucosamine-6 phosphate binding riboswitches (17-20). The divalent metal ions Mg(II) are crucial to assemble the active tertiary structure of the polyanionic RNA not only by shielding the negatively charged sugar-phosphate backbone but also by stabilizing specific tertiary interactions within the 3D architecture (21-23). These interactions are mediated by Mg(II) either through outer sphere or inner sphere co-ordination where the contacts to the RNA are made *via* water molecules or directly to the metal ion (24).

Our earlier studies (25) indicated that the *btuB* riboswitch is prefolded by Mg(II) already in the absence of its ligand, AdoCbl. It was also observed that AdoCbl could not switch the RNA conformation in the absence of Mg(II) indicating an essential role of Mg(II) in the pre-organization of the aptamer to enable ligand binding. The tertiary interactions induced by Mg(II) that constitute the ligand free state of the riboswitch remain unidentified as the recently crystallized coenzyme B_{12} riboswitches represent the ligand bound structure (26,27). Therefore, it is crucial to locate Mg(II) binding sites in the *btuB* riboswitch in order to understand the Mg(II) aided pre-organization of the RNA in the absence of AdoCbl.

A promising method to map metal ion binding sites in large nucleic acids makes use of a lanthanide probe that gives insight into the binding properties of metal ions (26-31). Lanthanides, specifically terbium(III) (Tb(III)) has been used repeatedly as a mimic of Mg(II) (29,32). The ionic radius of hydrated Tb(III) (0.91 Å) is similar to the ionic radius of hydrated Mg(II) (0.71 Å) and both ions have similar preferences for co-ordination to oxygen ligands (33). It has been shown that Tb(III) can replace Mg(II) at its specific binding site within the tertiary structure of the RNA (34). Most importantly, the Tb(III) aqua species $[Tb(H_2O)_n]^{3+}$ can catalyze the cleavage of RNA backbone at physiological pH due to its lower pK_a (~ 7.9) as compared to hydrated Mg(II) (pK_a ~ 11.4) (34,35) and therefore, the cleavage reactions can be carried out at near native pH.

Our current studies elucidate the Mg(II) binding sites in the classical *btuB* riboswitch of *E. coli* in the ligand-free and ligand-bound state. With the help of Tb(III), we could locate the Mg(II) binding sites on the ligand free *btuB* aptamer. In order to establish the role of Mg(II) assisted tertiary interactions (if any) for the ligand bound form, we also characterized Mg(II) binding on the AdoCbl induced altered conformation of the *btuB* riboswitch. Furthermore, we compared our data to the consensus sequence (12) and to the two known crystal structures of the AdoCbl riboswitches (15,16) to observe a common set of Mg(II) mediated tertiary interactions crucial for the pre-organization of the AdoCbl aptamer.

4.3 Results

4.3.1 Tb(III) cleavage in the ligand free *btuB* aptamer

To look for specific metal ion binding sites on the ligand free *btuB* aptamer, Tb(III) cleavage was carried out with the RNA pre-folded in 20 mM $MgCl_2$ by varying the Tb(III) concentrations. As shown in Figure 4.1, Tb(III) concentrations up to 0.1 mM were unable to cleave the RNA indicating that the general binding strength (K_D) of the major metal ion binding sites is higher than 100 µM. As soon as the concentration of Tb(III) is raised to 0.25 mM, Tb(III) facilitated backbone cleavage becomes evident (Figure 4.1). Tb(III) mediated cleavage at lower micromolar concentrations indicate specific metal ion binding sites (29,35). Therefore, the cleavage intensities at 0.5 mM Tb(III) with respect to the cleavage intensities at 0 mM Tb(III) were used to map the specific metal ion binding sites. Comparison of the cleavage intensities (Figure 4.2A) indicate that the *btuB* aptamer offers Mg(II) binding sites of various strengths (Figure 4.2B).

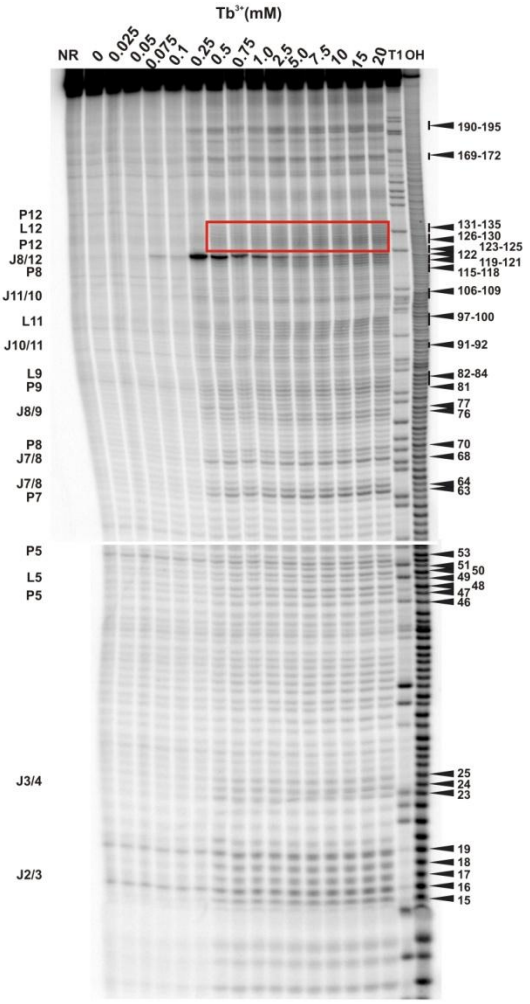

4.3.1.1 Specific metal ion binding sites in the *btuB* riboswitch

I. Weak to intermediate metal ion binding

The strength of Tb(III) cleavage depends on the geometry of the binding nucleotides, precisely on the accessibility of the ribose 2'-hydroxyl group (35). Weak to intermediate Tb(III) cleavage indicates a less favourable Tb(III) accessibility to the 2'- hydroxyl group due to geometry constraints. Weak Tb(III) cleavage sites in the *btuB* riboswitch are located around regions J7/8, P8, J8/9, P9, J10/11, J11/10 and in the region proximal to nucleotides 169-172 whereas intermediate Tb(III) cleavage sites are located at J3/4, P7, L9, L11, L12 and around nucleotides190-195 (Figure 4.2B). Regions P5, L5 and P12 have both weak and intermediate cleavage sites. Interestingly, some of the nucleotides in J3/4, P5, L5, P7 and J11/10 are found to be conserved in the consensus sequence of the coenzyme B_{12} ribsowitches (12). Comparison to the recently published crystal structures of the coenzyme B_{12} riboswitches from thermophiles (15,16) indicates that the conserved nucleotides at J11/10 contact the nucleotides from stem J6/3 helping to create one of the coaxial stems of the receptor core. Also metal ion binding at L5 might be important for the observed kissing loop (KL) interaction between L5 and L13 (15,16).

Figure 4.1: Tb(III) cleavage on the ligand free and prefolded *btuB* riboswitch of *E. coli*: The nucleotides undergoing a distinct cleavage with 0.25 – 20 mM $TbCl_3$ are shown by arrows. A red box indicates the region P12 encompassing nucleotides 123-135. NR: Non-reacted RNA, T1: RNase T1 ladder, OH: Alkaline hydrolysis ladder.

II. Strong metal ion binding

The regions J2/3, J3/4 and J8/12 harbour strong Tb(III) cleavage sites involving also the conserved nucleotides at J2/3 and J3/4 (Figure 4.2B). Interestingly, metal ion binding at J2/3 and J3/4 in the *btuB* riboswitch could assist the tertiary interactions with P1 and J6/3- P3 respectively, similar to the one reported in *S. thermophilum* AdoCbl riboswitch (16). Interesting to note is the cleavage pattern at region P12 (Figure 4.1 and Figure 4.2B). Although the nucleotides of P12 are proposed to undergo base pairing (12), partial cleavage due to Tb(III) is evident in this region. The region P12 therefore appears to be in a partially dynamic conformation accessible for Tb(III) cleavage contrary to the proposed helical counterpart. Nucleotide A122 which lies within this region exhibits the strongest cleavage due to Tb(III) from 0.25 - 1 mM Tb(III). Noticeably, the cleavage at nucleotide A122 decreases with increase in Tb(III) concentration (Figure 4.2C). Probably the geometry at A122 is altered at high Tb(III) concentrations thereby inhibiting the cleavage by Tb(III).

In general, the proposed helical regions of the *btuB* RNA (except for stem P12) were not found to be cleaved by Tb(III). This does not exclude their involvement in metal ion binding since the helical regions in RNA generally disfavour the attack by 2'-hydroxyl group (34) and therefore, binding sites in such regions remain undetected.

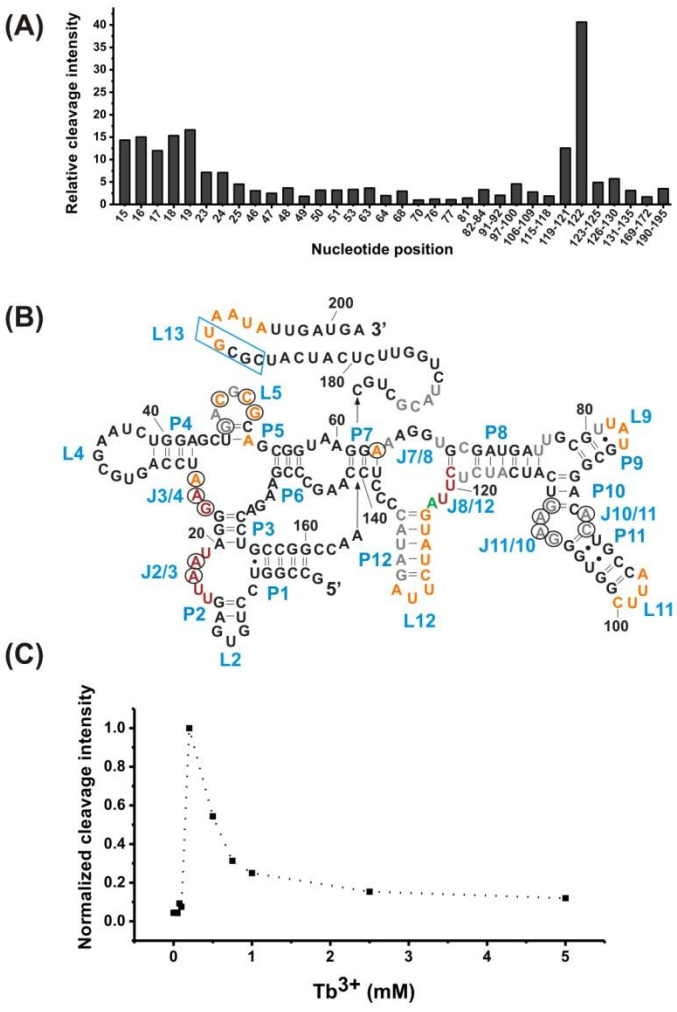

Figure 4.2: Mapping the Mg(II) binding sites on the ligand free *btuB* riboswitch of *E. coli*: (A) The relative intensity of cleavage displayed by nucleotides at 0.5 mM $TbCl_3$. (B) The nucleotides undergoing weak cleavage (grey), intermediate cleavage (orange), strong cleavage (red) and the strongest cleavage (green) were mapped by dividing the relative cleavage intensities into the following categories 1-3 fold, 3-6 fold, 6-40 fold and above 40 fold respectively. Nucleotides in black circle indicate the conserved bases from the consensus sequence of AdoCbl riboswitches (12). A blue box indicates the L13 region. (C) The change in cleavage intensity as a function of $TbCl_3$ concentration for nucleotide A122 (J8/12).

4.3.2 Competition between Tb(III) and Mg(II) confirms specific metal ion binding sites

Competing Tb(III) with increasing Mg(II) concentration ideally results in the decrease of Tb(III) cleavage intensity at the nucleotides involved in Mg(II) binding (35). Such a competition experiment not only confirms the specific metal ion binding sites but also helps eliminating the sites which show non-specific Tb(III) binding. In competition experiment with 500 µM Tb(III) and increasing concentrations of Mg(II), we observed a general decrease in cleavage intensities of the mapped Mg(II) binding nucleotides (Supplementary Figure S4.1). All of the mapped Mg(II) binding nucleotides exhibit a variation with respect to the observed decrease in cleavage intensity upon increasing Mg(II) concentrations (Figure 4.3A). This could be due to their different affinities towards Mg(II) requiring also different Mg(II) concentrations in order to compete with Tb(III). In general, nucleotides 82-84, 91-92, 97-100 and 106-109 exhibit a less pronounced competition with Tb(III) since the observed decrease in the cleavage intensity does not change drastically with increase in Mg(II) concentration (Figure 4.3A). These nucleotides belong to the peripheral structural elements (L9, J10/11, P11, J11/10) of the aptamer and therefore, this region of the *btuB* aptamer probably has a lower affinity towards Mg(II) than the other half of the aptamer. Interestingly, at all Mg(II) concentrations studied (20-100 mM), nucleotide A122 is always strongly cleaved by Tb(III). The evident strong cleavage due to Tb(III) as well as the distinctive decrease in the cleavage intensity with increasing Mg(II) suggests of a strong Mg(II) binding site at A122. The competition experiments thus confirm that the mapped metal ion binding sites on the *btuB* riboswitch are indeed specific Mg(II) binding sites.

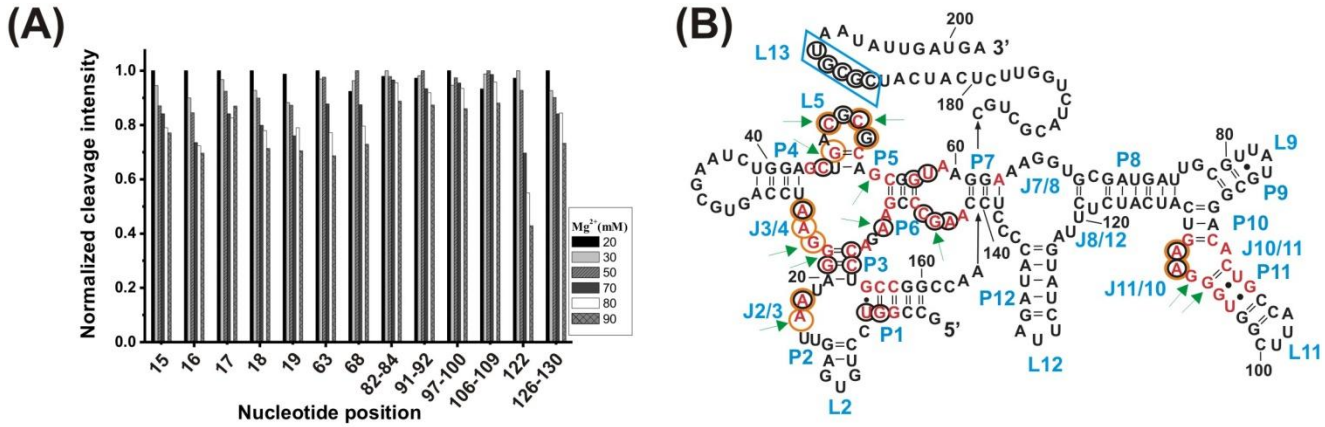

Figure 4.3: Competition between Mg(II) and Tb(III) for the specific binding sites: (A) Decrease in the cleavage intensities of the mapped Mg(II) binding sites as a function of $MgCl_2$ concentration in the presence of 500 µM $TbCl_3$. (B) Mapping of the metal ion binding sites on the consensus sequence of AdoCbl riboswitches. Shown is the proposed secondary structure of the *btuB* riboswitch with nucleotides in red representing the conserved bases in the consensus sequence of AdoCbl riboswitches. The nucleotides circled in black and marked by green arrows indicate the bases undergoing the tertiary interactions and metal ion binding sites in *S. thermophilum* respectively (16) [See Supplementary Figure S4.3]. The nucleotides circled in orange correspond to Mg(II) binding sites mapped by Tb(III) on the *btuB* riboswitch.

4.3.3 The relation between the conserved nucleotides, metal ion binding and tertiary interactions

Since some of the metal ion binding sites found in the *btuB* riboswitch correspond to the conserved bases of the aptamer (Figure 4.2B), finding a correlation between the conserved nucleotides and metal ion binding sites could provide the basis for Mg(II) mediated tertiary interactions in coenzyme B_{12} riboswitches. Therefore we compared the metal ion binding of the *btuB* riboswitch (*E. coli*) to the AdoCbl riboswitch from *S. thermophilum* (16).

Table 4.1: Contact map for Nitrogen atoms (N1 to N6) of Iridium hexammine ions (IRI A303-A309) in the crystal structure of AdoCbl riboswitch (*S. thermophilum*) (PDB ID: 4GXY) (16)**.**

Iridium hexammine	**$[Ir(NH_3)_6]^{3+}$ (A303)**			**$[Ir(NH_3)_6]^{3+}$ (A304)**			**$[Ir(NH_3)_6]^{3+}$ (A305)**		**$[Ir(NH_3)_6]^{3+}$ (A306)**			**$[Ir(NH_3)_6]^{3+}$ (A307)**			**$[Ir(NH_3)_6]^{3+}$ (A308)**				**$[Ir(NH_3)_6]^{3+}$ (A309)**		
N1													+						+		
N2		+	+ +			+		+			+						+				+
N3	+	+																+ +			
N4				+	+ +				+ +			+ + +	+		+	+			+	+	
N5						+			+				+	+							
N6			+ +				+			+								+		+	
Bases	**U**	**U**	**A**	**G**	**G**	**C**	**U**	**G**	**G**	**C**	**C**	**C**	**A**	**G**	**G**	**C**	**G**	**G**	**G**	**G**	**A**
	34	**35**	**38**	**64**	**65**	**67**	**100**	**101**	**65**	**68**	**69**	**72**	**73**	**151**	**103**	**104**	**122**	**123**	**41**	**42**	**157**
Regions	**J2/3**			**L5**			**J8/10**		**L5**			**J5/6; J7/6**			**J10/11; J11/10**				**J3/4; J6/3**		

[Contacts to the surrounding atoms are indicated by: + = OP1; + = OP2; + = O4; + = O5; + = N7; + = O6. The conserved nucleotides are indicated by the bases in red]

Bases / **Ligands**	**G 96**	**G 97**	**G 98**	**G 130**	**G 65**	**U 66**
O2'					+ (4.252 Å)	
O4'				+ (4.518 Å)		
O6	+ (5.197 Å)	+ (3.352 Å)	+ (3.546 Å)			
N7		+ (5.25 Å)	+ (5.432 Å)	+ (4.534 Å)		
OP1				+ (3.65 Å)		+ (5.343 Å)
OP2				+ (4.874 Å)		

Table 4.2: Outer sphere coordination for Mg(II) ions in the crystal structure of the AdoCbl riboswitch (*S. thermophilum*) (16) **as identified by MINAS** (35).

[Contacts to ions, Mg A310 and Mg A311 are indicated by (+) and (+) respectively along with the distances (Å). The conserved nucleotide G 65 is indicated in red].

The crystal structure of the AdoCbl riboswitch from *S. thermophilum* (PDB ID: 4GXY) (16) reveals the presence of two Mg(II) ions (Mg A310 and Mg A311) and seven Iridium hexammine ions $[Ir(NH_3)_6]^{3+}$ at a resolution of 3.05 Å. The contact maps for the seven $[Ir(NH_3)_6]^{3+}$ indicate hydrogen bonds not only with specific nucleobase atoms like O4 of pyrimidines and O6 and N7 of guanine but also with phosphate oxygens (Table 4.1). To characterize Mg(II) binding, we applied MINAS (36) to look for the nearest contacting nucleobases (Table 4.2). Both the Mg(II) ions interact with the nearby bases *via* outer sphere co-ordination since all distances are larger than 2.7 Å (Supplementary Figure S4.2 and Table. 4.2). One of the Mg(II) ions (A310) contacts a guanine quartet at L8 and P8 (Supplementary Figure S4.2A) whereas the other Mg(II) ion (A311) is placed in proximity to L5 (Supplementary Figure S4.2B). Interestingly, out of the 25 residues involved in metal ion binding (for both $[Ir(NH_3)_6]^{3+}$ and Mg(II)), 13 were found to be conserved in the consensus sequence of coenzyme B_{12} riboswitches (12). Furthermore, the binding of $[Ir(NH_3)_6]^{3+}$ at non-conserved residues namely U34, U35, U38, G64, C72, U100, G101, G103, C104 involves the adjacent vicinity to the conserved bases at J2/3, J4/5, P5 and J10/11 (16).

The mapped regions of Mg(II) binding on the *btuB* riboswitch (except for regions P5-P7 and P7-P3) overlap with the $[Ir(NH_3)_6]^{3+}$ binding and match to some of the conserved nucleotides undergoing tertiary interactions (J2/3, J3/4, L5, J10/11) in case of the *S. thermophilum* AdoCbl riboswitch (Figure 4.3B and Supplementary Figure S4.3) (16). Upon closer view, these interactions mainly found at the nucleotides involved in the T-loop-pseudoknot (T-loop-PK) interactions between L4 and J6/7-J7/6, the L5-L13 KL interaction, as well as at the long range tertiary interaction between J11/10 with J5/6 and J6/3 predicted to stabilize the receptor binding pocket in the AdoCbl riboswitch from *S. thermophilum* (16). A significant overlap between the nucleobases undergoing tertiary interactions and their involvement in metal ion binding suggests that some of the conserved nucleotides in AdoCbl riboswitches probably undergo tertiary interactions in the ligand free form mediated by Mg(II) binding.

4.3.4 Metal ion binding sites in the switched RNA conformation

The *btuB* riboswitch is proposed to undergo a conformational change upon AdoCbl binding mainly through the proposed pseudoknot formation (between L5 and L13) disrupting thereby the anti-terminator stem (2,37). We attempted to visualize the ligand induced conformational change in the *btuB* riboswitch in terms of metal ion binding properties and see if metal ion binding is altered in the presence of ligand. To observe the same, the *btuB* riboswitch was prefolded in 20 mM $MgCl_2$ and was then incubated with AdoCbl for 30 minutes before the addition of 0.5 mM Tb(III). The incubation time of 30 minutes with AdoCbl was adequate for a structural switch in the RNA (Supplementary Figure S4.4). Indeed the conformational switch appears instantaneously upon addition of AdoCbl. In the presence of AdoCbl, Tb(III) mediated cleavage of the RNA was evident from 0.25 mM Tb(III) onwards as observed also for the ligand free RNA (Figure 4.4). Interestingly, at Tb(III) concentrations between 0.25 mM to 1 mM, the strongest cleavage is again observed at nucleotide A122 (J8/12). However in the presence of AdoCbl, the cleavage intensity of A122 achieves its maximum at 1mM Tb(III) as compared to the maximal cleavage at 0.25 mM in the absence of AdoCbl (Figure 4.5A). It is possible that the interaction with AdoCbl decreases the metal ion affinity at A122.

The overall cleavage pattern for the switched RNA (+ AdoCbl) at higher Tb(III) concentrations (from 2.5 mM to 20 mM) remains the same as the one in the absence of AdoCbl except for the nucleotides modulated by AdoCbl as reported previously (2,37). Nucleotides G23, G87, G106 and U183 undergo relative decrease in cleavage whereas nucleotides U68, U110, U118 and U167 exhibit increase in the cleavage intensity as expected (Figure 4.5B) (2). However, U77 displays an increase in cleavage intensity contrary to observation from the in-line probing experiments (37). The AdoCbl dependent increase in the cleavage at U77 is confirmed from the experiment where the *btuB* riboswitch was incubated with varying AdoCbl concentration prior to Tb(III) cleavage with 0.5 mM Tb(III) (Supplementary Figure S4.5). Since the Tb(III) cleavage is carried out at a neutral pH (pH 7.0) compared to in-line probing (pH 8.3), it is possible that U77 adopts a dynamic geometry accessible for Tb(III) binding at pH 7.0 in the presence of AdoCbl.

There is a marked decrease in the cleavage intensity at nucleotides 63 (P7), 90-93 (P10-P11) and 149-152 (J6/3) along with the earlier reported sites modulated by AdoCbl (Figure 4.4 and Figure 4.5B). This could be due to AdoCbl induced tertiary interactions between P10-P11 and J6/3 in the *btuB* riboswitch similar to the one observed in AdoCbl riboswitches from thermophiles (15,16).

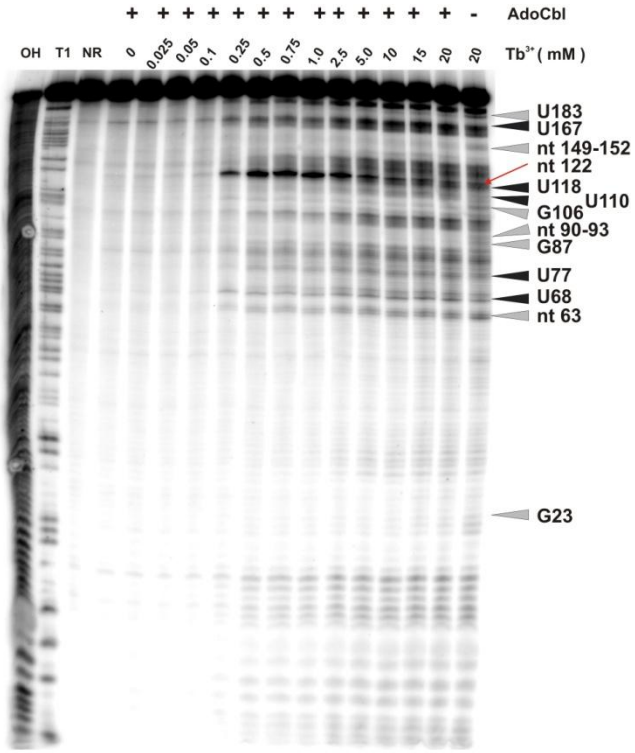

Figure 4.4: Tb(III) cleavage in the *btuB* riboswitch in the presence of AdoCbl: A concentration dependent $TbCl_3$ (0-20 mM) cleavage is observed on the prefolded *btuB* riboswitch incubated with 100 µM AdoCbl. Arrows in grey and black indicate the nucleotides undergoing decreasing and increasing cleavage in the presence of AdoCbl. The red arrow shows nucleotide A122 displaying strongest cleavage by $TbCl_3$. OH: Alkaline hydrolysis ladder, T1: RNase T1 ladder, NR: non-reacted RNA.

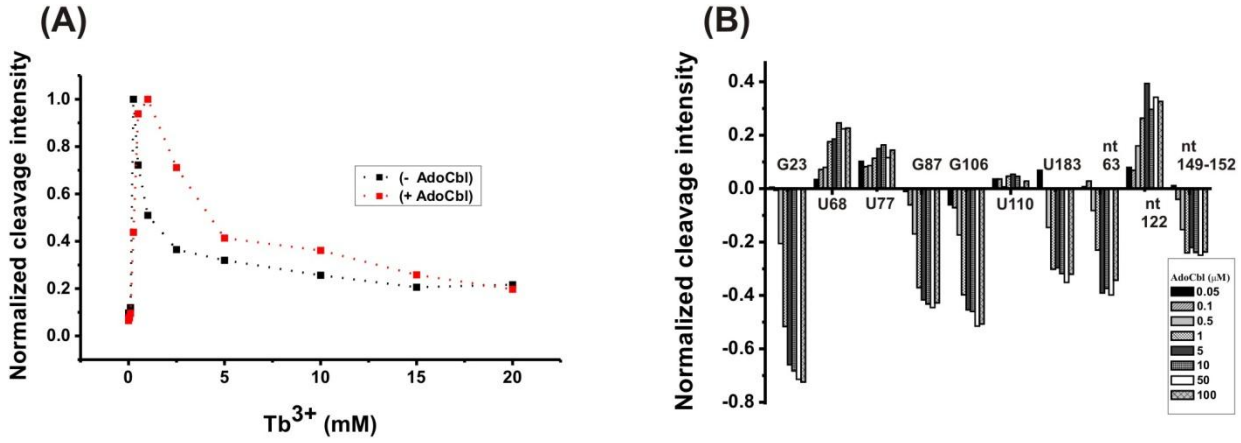

Figure 4.5: Tb(III) dependent changes in the ligand bound conformation of the *btuB* riboswitch: (A) $TbCl_3$ concentration dependent changes at nucleotide A122 in the absence and presence of 100 µM AdoCbl. (B) AdoCbl concentration depdendent changes at the indicated nucleotides on the *btuB* riboswitch incubated with 0.05 to 100 µM AdoCbl in the presence of 0.5 mM $TbCl_3$.

4.3.5 Footprints of the secondary and tertiary structures of the *btuB* riboswitch

Tb(III) cleavage is a useful tool to investigate the native conformation of RNAs as Tb(III) catalyzes the backbone cleavage of RNA at physiological pH (38). This can be achieved by high millimolar concentration of Tb(III) that cleaves RNA in sequence-independent manner producing a footprinting pattern of solvent accessible regions that involve single-stranded and non-Watson-Crick base paired elements (38). We compared the cleavage pattern at 20 mM Tb(III) in the absence and the presence of AdoCbl (Figure 4.4, lanes 16 and 17) to get an insight into the arrangement of the riboswitch domains at native pH.

In the absence of AdoCbl (Figure 4.6A), the strongly cleaved regions correspond to proposed single stranded regions. These regions mainly involve the junctions (J2/3, J3/4, L5, J7/8, J8/12) and the loops (L9, L11, L12) along with the nucleotides 169-172 and192-196 surrounding stem P13. The other proposed single stranded regions of the riboswitch like L4, J6/7, J7/8 and nucleotides 177-184 (surrounding stem P13) display relative protection from the cleavage indicating either surface occlusion within the folded RNA or their involvement in tertiary interactions that constrain the geometry for cleavage.

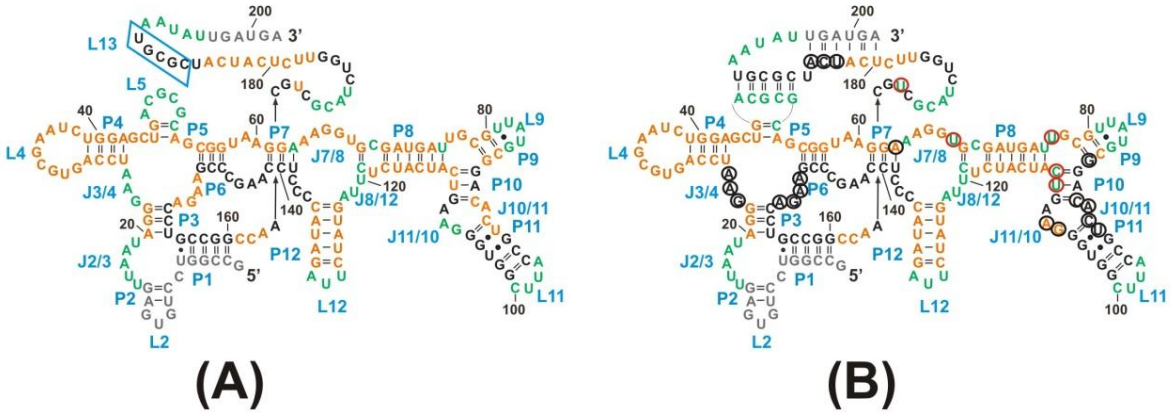

Figure 4.6: The structural footprint of the *btuB* aptamer obtained by Tb(III) cleavage in the absence (A) and presence (B) of AdoCbl. Nucleotides undergoing strong cleavage are shown in green, partial protection in orange and complete protection in black in the presence of 20 mM $TbCl_3$. Nucleotides circled in black and red indicate the sites undergoing decrease and increase in the cleavage intensity in the presence of 100 µM AdoCbl and 20 mM $TbCl_3$.

We observed a marked protection from cleavage at the conserved B_{12} box (140-160), P9-P11, J10/11 and J11/10 as well as at the regions encompassing nucleotides 164-168, 173-176, 186-190. Most protected regions like the B_{12} box and the peripheral face of the aptamer (at P8-P11and P13-L13) include not only the proposed helical regions but also tertiary interactions with other parts of the aptamer explaining the observed protection from the cleavage. Also, a clear protection from the cleavage is evident for the region encompassing nucleotides 20-22 and 26-62 that constitute a part of the receptor core in thermophilic AdoCbl riboswitches (15,16). With the addition of AdoCbl, the overall global conformation of the molecule appears similar as to the one in the absence of the ligand except for the sites reported to be modulated by AdoCbl (Figure 4.6B). AdoCbl binding therefore appears to introduce only small local changes in the RNA probably to access the binding pocket.

4.4 Discussion

The recent reports on the crystal structures of the AdoCbl riboswitches from *T. tengcongensis* and *S. thermophilum* indicated an overall similar tertiary fold needed for ligand recognition (15,16). The *btuB* riboswitch from *E. coli* has a similar secondary structure as that of the crystallized riboswitches but is distinguished by an additional stem P12 at the

periphery (12). Therefore structural organization of the *btuB* riboswitch can be compared to the tertiary structure adopted by the AdoCbl riboswitches from thermophiles (15,16). Since both of the crystallized coenzyme B_{12} riboswitches show the riboswitch structure in ligand bound form, the actual pre-organization of the ligand binding pocket/receptor core and of the peripheral elements in the ligand free state of AdoCbl riboswitches remains an interesting issue to be solved.

4.4.1 Mg(II) binding and tertiary contacts in AdoCbl riboswitches

The structure of the crystallized AdoCbl riboswitches in the ligand bound form involves tertiary structural elements such as coaxial stems (P3-P6 and P4-P6), kissing loop (L5 and L13), T loop-PK domain interaction (between L4 and J6-7-J7-6) and the long range tertiary interaction (between J10/11 and J6/3) (15,16). In addition, the AdoCbl riboswitch of *S. thermophilum* shows minor groove interactions of J2/3 with P1 and a zipper formation between J3/4, J6/3 and P3 (16). The formation of tertiary motifs like coaxial stems, KL and pseudoknot interactions are largely dependent on Mg(II) for their stabilization (39). Mg(II) binding on the *btuB* riboswitch takes place at regions J2/3, J3/4, P5-L5, P7, L9, J10/11-P11, L11, L11/10, J8/12, P12-L12, L13. Taken together, Mg(II) binding on the *btuB* riboswitch certainly involves regions undergoing also tertiary interactions in the AdoCbl riboswitches from thermophiles (15,16). Since Mg(II) binding to the *btuB* riboswitch is similar in the ligand bound and ligand free form, the ligand binding pocket of the *btuB* riboswitch seems to be pre-organized by Mg(II) to allow optimal binding to AdoCbl. An assembly of the ligand binding pocket solely by Mg(II) mediated tertiary interactions has been observed for the adenine riboswitch, the *glmS* ribozyme and lysine binding riboswitches (17,18,40). Also, Mg(II) mediated pre-compaction of the RNA conformation in the absence of the ligand has been reported by SAXS studies for the glycine, c-di-GMP, TPP, lysine and SAM I riboswicthes (17). Therefore, Mg(II) mediated pre-organization to achieve an active tertiary structure of the ligand- free aptamer seems to be a common phenomenon in riboswitches and probably holds true for the AdoCbl riboswitches as well.

4.4.2 Association between conserved bases of the aptamer and tertiary interactions in AdoCbl riboswitches

The aptamers for each class of riboswitches are more conserved than the expression platform and therefore the three dimensional structure of the apatmer is mostly accomplished by tertiary contacts between the conserved residues (41). Analysis of the crystallized AdoCbl riboswitches from thermophiles revealed the key tertiary interactions within the conserved bases of the aptamer. Interestingly, we observe Mg(II) binding on the *btuB* riboswitch at/around a set of conserved residues (J2/3, J3/4, P5, L5, P7, J10/11, P11 and J11/10) that undergoes the proposed tertiary interactions. It is therefore possible that AdoCbl riboswitches undergo a similar set of tertiary contacts mediated possibly by Mg(II) binding using a group of conserved bases. Also, the derepressed mutations (in case of the *S. thermophilum* AdoCbl riboswitch) leading to a loss of B_{12} induced repression involve the conserved nucleotides further supporting our observation (16). . Moreover, our earlier studies (25) indicated that the *btuB* riboswitch can not be switched by AdoCbl in the absence of Mg(II) reinforcing the crucial function of Mg(II) mediated pre-folding of the *btuB* riboswitch. Therefore, we propose that Mg(II) mediated tertiary interactions are crucial for arranging and stabilizing the structural motifs in case of the *btuB* riboswitch in its ligand free form and may also have similar implications for the other members of AdoCbl riboswitch class.

4.4.3 Metal ion binding at the peripheral elements of the *btuB* aptamer

In the case of the AdoCbl riboswitches of thermophiles, specificity to AdoCbl has been proposed to be acquired through the long range interaction between J6/3 and J11/10 upon ligand binding (15,16). Therefore, the peripheral elements gain a vital role for creating a tight binding pocket for AdoCbl by flanking the receptor core. Although AdoCbl binding does not alter the metal ion binding cores drastically in case of the *btuB* riboswitch, the observed Mg(II) binding to the conserved

adenosine residues of J11/10 might aid its interaction with J6/3 upon ligand binding. Located at the peripheral region of the *btuB* riboswitch is a nucleotide A122 that appears to have the best geometry for metal mediated cleavage. The strong cleavage at A122 is evident both in the ligand free and ligand bound forms at low micromolar Tb(III) concentrations. A122 is located at J8/12 region of the *btuB* apatmer and since both of the crystallized AdoCbl riboswitches (15,16) lack this peripheral part, it is difficult at present to predict the role of A122 in the overall structure of the *btuB* riboswitch of *E. coli*.

4.4.4 Insights from the footprints of the *btuB* structure in the ligand free and ligand bound forms

The footprints of the *btuB* structure generated with Tb(III) indicate the possible surface accessible and surface occluded regions in a folded RNA. The ligand binding pocket along with a part of the peripheral domain should constitute the inner core of the molecule as these regions are fairly protected from Tb(III) cleavage. Most of the dynamic region (loops and junction points) in contrast seems to be located at/on the surface of the molecule. The observed cleavage pattern at stem P12 indicates a partial dynamic geometry adopted by P12 in the overall tertiary structure of the RNA. The biochemical data for AdoCbl riboswitches with and without stem P12 does not correlate to the affinity for AdoCbl (12). Therefore, we predict that stem P12 might be involved in stabilizing the overall binding pocket but may not necessarily contribute towards the specificity to AdoCbl. Interestingly, at near native pH the switched RNA (+AdoCbl) does not undergo a drastic change in the conformation except for the reported nucleotides undergoing modulation with AdoCbl (2,37). Therefore the *btuB* riboswitch most probably undergoes local conformational changes upon AdoCbl binding at 20 mM Mg(II). However, the nature of the conformational changes in RNA varies with Mg(II) concentration e.g. the lysine riboswitch exhibits either global or local conformational changes upon ligand binding at physiological and above physiological concentrations of Mg(II) respectively (40). Although our structural probing data (25) suggests that AdoCbl induces local changes in the *btuB* riboswitch at both physiological and at relatively higher Mg(II) concentrations, the possible microscopic structural transitions need to be dissected to confirm the exact nature of Mg(II) dependent conformational changes.

To sum up, we show that the presence of specific Mg(II) binding sites and the pre-organization of the *btuB* aptamer in its ligand free form suggest Mg(II) mediated tertiary interactions within the aptamer most probably with a set of conserved bases. These tertiary interactions could be common in AdoCbl riboswitches in order to facilitate the interaction with their complex ligand, AdoCbl. A pre-organized binding pocket benefits the riboswitch not only with a rapid recognition of the ligand but also with the prompt transmission of a regulatory signal (17). Stressing the role of Mg(II) in the functioning of the *btuB* riboswitch, our studies open further opportunities to explore the ligand free state of the AdoCbl riboswitches in Mg(II) dependent manner.

4.5 Materials and methods

4.5.1 Materials

Nucleoside 5'-triphosphate (ATP, GTP, CTP) and UTP were purchased from GE healthcare and Sigma-Aldrich respectively. Homemade T7 RNA polymerase (42) was used for *in-vitro* RNA transcription. RNase T1 1000 U/µL was purchased from Fermentas and was diluted to 1U/µL in a buffer containing 50 mM Tris-HCl (pH 7.4) and 50% (v/v) glycerol. Coenzyme B_{12} (Sigma-Aldrich) and anhydrous $TbCl_3$ (Sigma-Aldrich) were used without any further purification. Denaturing polyacrylamide gels were prepared using Long Ranger™ gel solution, Lonza, Rockland ME (USA). All the buffers, salt solutions and gel solutions were filtered through 0.2 µm filters. All other chemicals were at

least puriss p.a. and were purchased from Sigma-Aldrich. Gels were scanned by Storm860 PhosphoImager and analyzed by imageQuant software (GE Healthcare).

4.5.2 Methods

4.5.2.1 Preparation of RNA

The *btuB* RNA was obtained by *in vitro* transcription from plasmid pPC1 by homemade T7 RNA polymerase (42). The plasmid pPC1 is based on the plasmid pSG2 (43) that contains the natural 202 nucleotide *btuB* aptamer sequence. In addition, pPC1 contains a newly introduced GGA sequence 5' to the *btuB* aptamer sequence for efficient transcription (42) and a GAGCUCG sequence at 3' end stemming from digestion with EcoR1 (Promega). These additional nucleotides still render the aptamer active (Supplementary Fig 5). After *in-vitro* transcription of the plasmid DNA, the *btuB* RNA was purified by 10% denaturing PAGE, electroeluted, precipitated with ethanol and concentrated with Vivaspin concentrator (5000MWCO). The RNA was stored in water at -20°C.

4.5.2.2 Tb^{3+} stock solutions

$TbCl_3$ stock solutions were prepared as described in (32,44).

4.5.2.3 Tb^{3+} mediated cleavage reaction

In a total volume of 10 µL, 1 µM of unlabeled RNA along with 10 nM of ^{32}P-5' labeled RNA was denatured at 90°C for 45 seconds in a reaction buffer containing 25mM MOPS, pH 7.0 and 100 mM KCl followed by the addition of 20 mM $MgCl_2$ and incubation at 37°C for 15 minutes. For the samples with ligand, AdoCbl was added to the RNA sample folded in 20 mM $MgCl_2$ and the samples were further incubated at 37°C for 30 minutes. For the competition experiments with $MgCl_2$, the RNA was folded in various $MgCl_2$ concentrations after denaturation and before the addition of $TbCl_3$. The cleavage reactions were performed over 1hour on ice. Subsequently, quench buffer (80% formamide (v/v), 10mM EDTA) was added to the samples to stop the reaction. The samples were precipitated with 2.5 volumes of ethanol, resuspended in 5µL of formamide loading buffer (80% formamide (v/v), 10 mM EDTA ; pH 8.0 at 20° C, 2% Bromophenol blue, 2% Xylene Cyanol) and the cleavage products were separated by 10% denaturing PAGE. RNase T1 ladder and alkaline hydrolysis ladder were prepared as described in (43,44).

4.5.2.4 Analysis of data

The final relative cleavage intensities of the nucleotides with respect to cleavage intensities at 0 mM Tb(III) concentration are calculated as described in (44).

4.6 Acknowledgements

We thank Joachim Schnabl for providing the data related to the MINAS database. We thank Dr. Sofia Gallo for providing the plasmid pSG2 as well as for highly valuable comments on the manuscript. This work was supported by the Swiss National Science Foundation and a European research Council (ERC) Starting Grant to RKOS.

4.7 Supplementary information

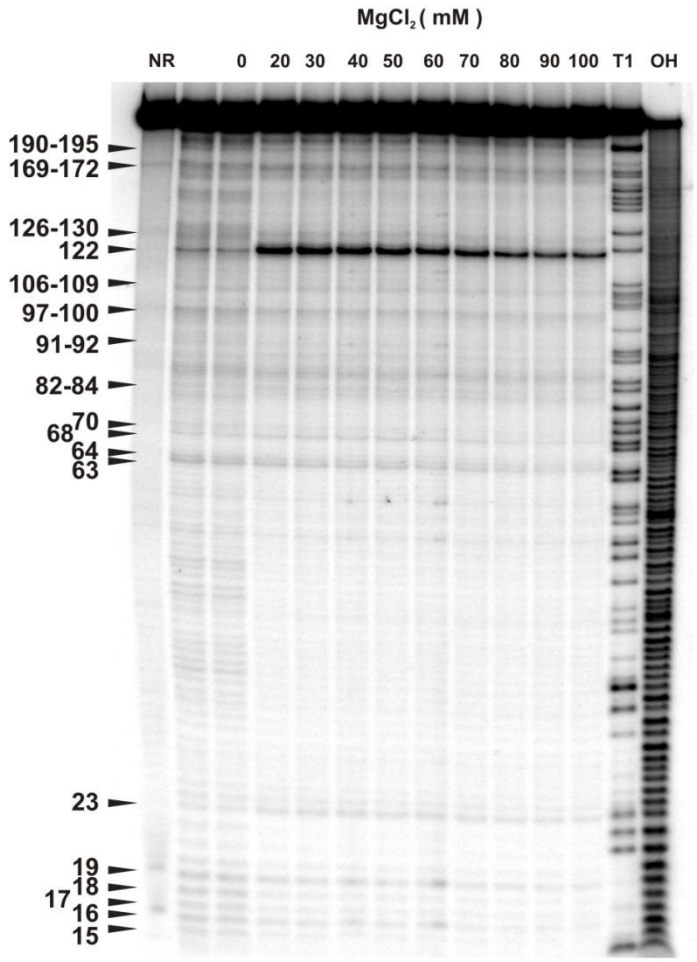

Figure S4.1: Competition experiment between Mg(II) and Tb(III) for the metal ion binding sites in the *btuB* aptamer: Arrows indicate the nucleotides undergoing a distinct decrease in the cleavage by 500 µM $TbCl_3$ with increase in Mg(II) concentration from 20 – 100 mM. NR: Non-reacted RNA, T1: RNase T1 ladder, OH: Alkaline hydrolysis ladder.

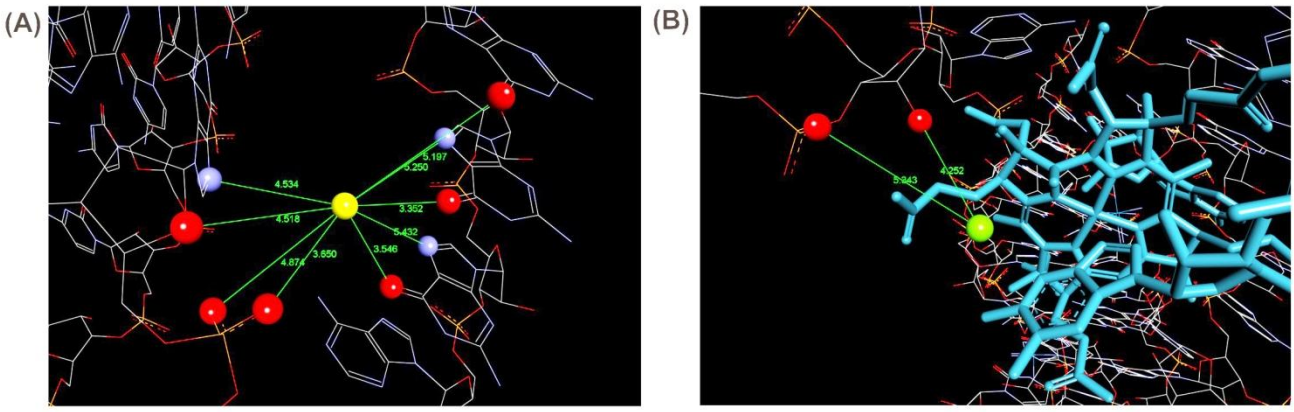

Figure S4.2: Mg(II) binding sites detected by MINAS (35) in the AdoCbl riboswitch of *S. thermophilum* (16)**:** Shown are the bases predicted by MINAS contacting in a outer sphere manner to the two magnesium ions, Mg A310 (A) and Mg A311 (B) appeared in the crystal structure of the AdoCbl riboswitch from *S. thermophilum* (PDB ID: 4GXY).

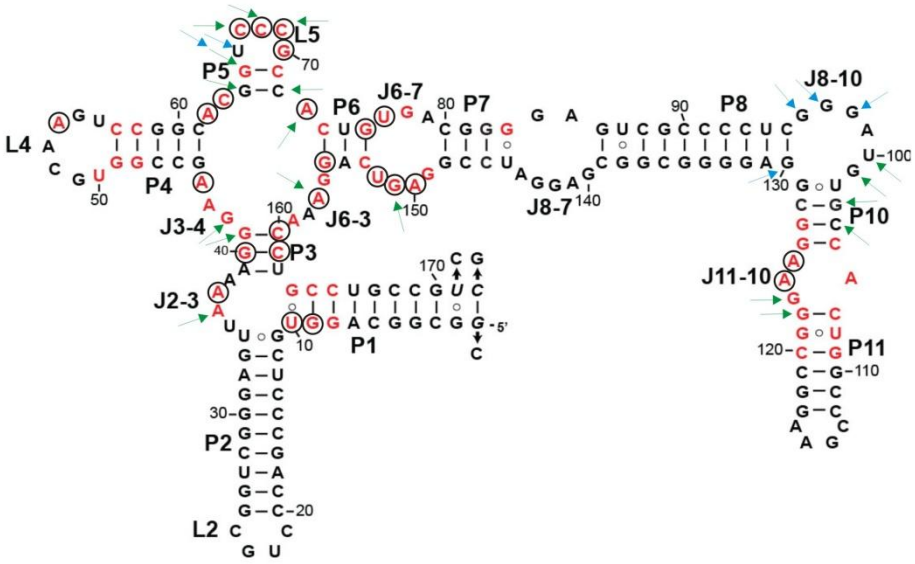

Figure S4.3: Metal ion binding and tertiary contacts in AdoCbl riboswitch of *S. thermophilum* (16): Shown is the secondary structure of the crystallized AdoCbl riboswitch of *S. thermophilum.* Nucleotides in red are conserved in at least 90% of AdoCbl aptamer sequences. The green and blue arrows indicate the sites of $[Ir(NH_3)_6]^{3+}$ binding identified from the crystal structure and MINAS respectively. The black circles indicate the conserved nucleotides undergoing tertiary contacts in the crystal structure.

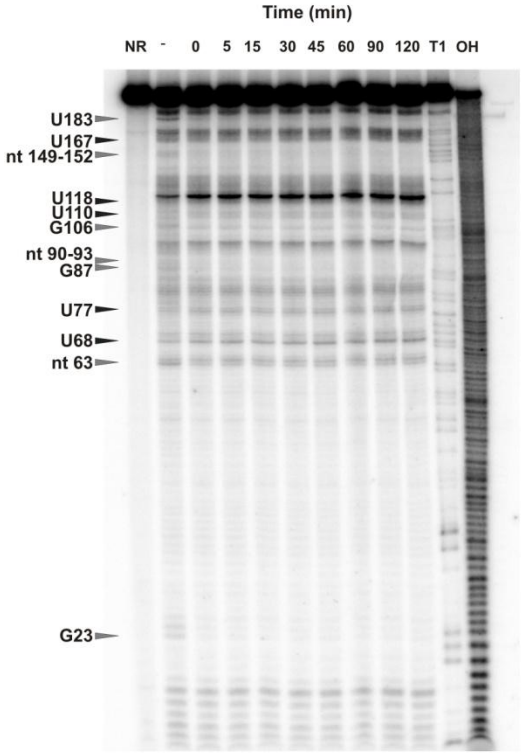

Figure S4.4: Tb(III) cleavage on the AdoCbl bound *btuB* aptamer indicating an instantaneous structural switch: The prefolded *btuB* riboswitch was incubated with 100 µM AdoCbl for an indicated time period before the addition of 0.5 mM $TbCl_3$. The grey and black arrows indicate the sites undergoing decrease and increase in the cleavage intensity upon incubation with AdoCbl respectively and represent similar pattern to the one observed in in- line probing experiments (2,37). Time of 0 minute implies an instant addition of 1mM Tb after the addition of AdoCbl. NR: non-reacted RNA, T1: RNase T1 ladder, OH: Alkaline hydrolysis ladder.

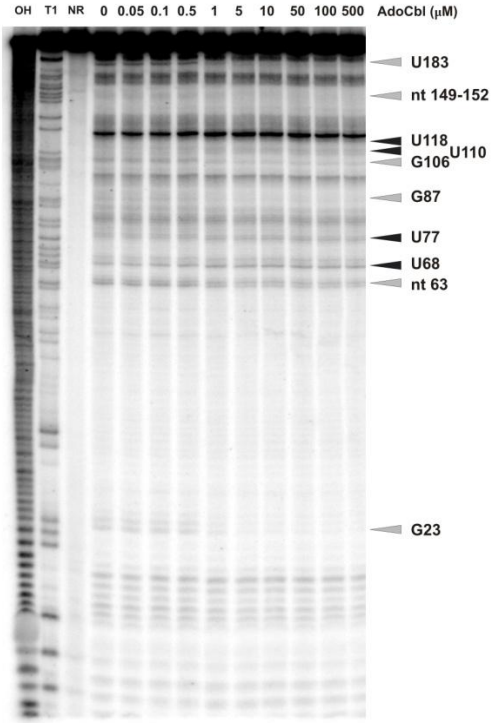

Figure S4.5: AdoCbl dependent Tb(III) cleavage of the *btuB* aptamer: The prefolded *btuB* aptamer was incubated with an indicated concentration of AdoCbl for 30 minutes before the addition of 0.5 mM $TbCl_3$. The grey and black arrows indicate the sites undergoing decrease and increase in the cleavage intensity upon incubation with AdoCbl respectively. OH: Alkaline hydrolysis ladder, T1: RNase T1 ladder, NR: non-reacted RNA.

4.8 References

1. Mironov, A.S., Gusarov, I., Rafikov, R., Lopez, L.E., Shatalin, K., Kreneva, R.A., Perumov, D.A. and Nudler, E. (2002) Sensing small molecules by nascent RNA: a mechanism to control transcription in bacteria. *Cell*, **111**, 747-756.
2. Nahvi, A., Sudarsan, N., Ebert, M.S., Zou, X., Brown, K.L. and Breaker, R.R. (2002) Genetic control by a metabolite binding mRNA. *Chem Biol*, **9**, 1043.
3. Winkler, W., Nahvi, A. and Breaker, R.R. (2002) Thiamine derivatives bind messenger RNAs directly to regulate bacterial gene expression. *Nature*, **419**, 952-956.
4. Mandal, M. and Breaker, R.R. (2004) Gene regulation by riboswitches. *Nat Rev Mol Cell Biol*, **5**, 451-463.
5. Winkler, W.C. and Breaker, R.R. (2003) Genetic control by metabolite-binding riboswitches. *Chembiochem*, **4**, 1024-1032.
6. Winkler, W.C., Nahvi, A., Roth, A., Collins, J.A. and Breaker, R.R. (2004) Control of gene expression by a natural metabolite-responsive ribozyme. *Nature*, **428**, 281-286.
7. Bastet, L., Dube, A., Masse, E. and Lafontaine, D.A. (2011) New insights into riboswitch regulation mechanisms. *Mol Microbiol*, **80**, 1148-1154.
8. Kubodera, T., Watanabe, M., Yoshiuchi, K., Yamashita, N., Nishimura, A., Nakai, S., Gomi, K. and Hanamoto, H. (2003) Thiamine-regulated gene expression of Aspergillus oryzae thiA requires splicing of the intron containing a riboswitch-like domain in the 5'-UTR. *FEBS Lett*, **555**, 516-520.
9. Loh, E., Dussurget, O., Gripenland, J., Vaitkevicius, K., Tiensuu, T., Mandin, P., Repoila, F., Buchrieser, C., Cossart, P. and Johansson, J. (2009) A trans-acting riboswitch controls expression of the virulence regulator PrfA in Listeria monocytogenes. *Cell*, **139**, 770-779.

10. Soukup, J.K. and Soukup, G.A. (2004) Riboswitches exert genetic control through metabolite-induced conformational change. *Curr Opin Struct Biol*, **14**, 344-349.
11. Gudmundsdottir, A., Bradbeer, C. and Kadner, R.J. (1988) Altered binding and transport of vitamin B12 resulting from insertion mutations in the Escherichia coli btuB gene. *J Biol Chem*, **263**, 14224-14230.
12. Nahvi, A., Barrick, J.E. and Breaker, R.R. (2004) Coenzyme B12 riboswitches are widespread genetic control elements in prokaryotes. *Nucleic Acids Res*, **32**, 143-150.
13. Nou, X. and Kadner, R.J. (2000) Adenosylcobalamin inhibits ribosome binding to btuB RNA. *Proc Natl Acad Sci U S A*, **97**, 7190-7195.
14. Reynolds, P.R., Mottur, G.P. and Bradbeer, C. (1980) Transport of vitamin B12 in Escherichia coli. Some observations on the roles of the gene products of BtuC and TonB. *J Biol Chem*, **255**, 4313-4319.
15. Johnson Jr, J.E., Reyes, F.E., Polaski, J.T. and Batey, R.T. (2012) B(12) cofactors directly stabilize an mRNA regulatory switch. *Nature*, **492**, 133-137.
16. Peselis, A. and Serganov, A. (2012) Structural insights into ligand binding and gene expression control by an adenosylcobalamin riboswitch. *Nat Struct Mol Biol*, **19**, 1182-1184.
17. Baird, N.J. and Ferre-D'Amare, A.R. (2010) Idiosyncratically tuned switching behavior of riboswitch aptamer domains revealed by comparative small-angle X-ray scattering analysis. *RNA*, **16**, 598-609.
18. Garst, A.D., Heroux, A., Rambo, R.P. and Batey, R.T. (2008) Crystal structure of the lysine riboswitch regulatory mRNA element. *J Biol Chem*, **283**, 22347-22351.
19. Heppell, B., Blouin, S., Dussault, A.M., Mulhbacher, J., Ennifar, E., Penedo, J.C. and Lafontaine, D.A. (2011) Molecular insights into the ligand-controlled organization of the SAM-I riboswitch. *Nat Chem Biol*, **7**, 384-392.
20. Noeske, J., Schwalbe, H. and Wohnert, J. (2007) Metal-ion binding and metal-ion induced folding of the adenine-sensing riboswitch aptamer domain. *Nucleic Acids Res*, **35**, 5262-5273.
21. Misra, V.K. and Draper, D.E. (1998) On the role of magnesium ions in RNA stability. *Biopolymers*, **48**, 113-135.
22. Pyle, A.M. (2002) Metal ions in the structure and function of RNA. *J Biol Inorg Chem*, **7**, 679-690.
23. Woodson, S.A. (2005) Metal ions and RNA folding: a highly charged topic with a dynamic future. *Curr Opin Chem Biol*, **9**, 104-109.
24. Erat, M.C. and Sigel, R.K.0. (2011) Methods to detect and characterize metal ion binding sites in RNA. *Met Ions Life Sci*, **9**, 37-100.
25. Choudhary, P.K. and Sigel, R.K.O. (2013) Mg^{2+} induced conformational changes in the *btuB* riboswitch from *E. coli*. *in revision*.
26. Ciesiolka, J., Marciniec, T. and Krzyzosiak, W. (1989) Probing the environment of lanthanide binding sites in yeast tRNA(Phe) by specific metal-ion-promoted cleavages. *Eur J Biochem*, **182**, 445-450.
27. Dorner, S. and Barta, A. (1999) Probing ribosome structure by europium-induced RNA cleavage. *Biol Chem*, **380**, 243-251.
28. Kaye, N.M., Zahler, N.H., Christian, E.L. and Harris, M.E. (2002) Conservation of helical structure contributes to functional metal ion interactions in the catalytic domain of ribonuclease P RNA. *J Mol Biol*, **324**, 429-442.
29. Sigel, R.K.O. and Pyle, A.M. (2003) Lanthanide ions as probes for metal ions in the structure and catalytic mechanism of ribozymes. *Met Ions Biol Syst*, **40**, 477-512.
30. Waldsich, C. and Pyle, A.M. (2008) A kinetic intermediate that regulates proper folding of a group II intron RNA. *J Mol Biol*, **375**, 572-580.
31. Walter, N.G., Yang, N. and Burke, J.M. (2000) Probing non-selective cation binding in the hairpin ribozyme with Tb(III). *J Mol Biol*, **298**, 539-555.

32. Choudhary, P.K., Gallo, S. and Sigel, R.K.O. (2014) Monitoring Global Structural Changes and Specific Metal Binding Sites in RNA by in-line Probing and Tb(III) Cleavage. *Methods Mol Biol, in press*.
33. Saito, H. and Suga, H. (2002) Outersphere and innersphere coordinated metal ions in an aminoacyl-tRNA synthetase ribozyme. *Nucleic Acids Res*, **30**, 5151-5159.
34. Sigel, R.K.O., Vaidya, A. and Pyle, A.M. (2000) Metal ion binding sites in a group II intron core. *Nat Struct Biol*, **7**, 1111-1116.
35. Harris, D.A. and Walter, N.G. (2003) Probing RNA structure and metal-binding sites using terbium(III) footprinting. *Curr Protoc Nucleic Acid Chem*, **Chapter 6**, Unit 6 8.
36. Schnabl, J., Suter, P. and Sigel, R.K.0. (2011) MINAS--a database of Metal Ions in Nucleic AcidS. *Nucleic Acids Res*, **40**, D434-438.
37. Gallo, S., Oberhuber, M., Sigel, R.K.0. and Kräutler, B. (2008) The corrin moiety of coenzyme B12 is the determinant for switching the btuB riboswitch of E. coli. *Chembiochem*, **9**, 1408-1414.
38. Harris, D.A., Tinsley, R.A. and Walter, N.G. (2004) Terbium-mediated footprinting probes a catalytic conformational switch in the antigenomic hepatitis delta virus ribozyme. *J Mol Biol*, **341**, 389-403.
39. Batey, R.T., Rambo, R.P. and Doudna, J.A. (1999) Tertiary Motifs in RNA Structure and Folding. *Angew Chem Int Ed Engl*, **38**, 2326-2343.
40. Fiegland, L.R., Garst, A.D., Batey, R.T. and Nesbitt, D.J. (2012) Single-Molecule Studies of the Lysine Riboswitch Reveal Effector-Dependent Conformational Dynamics of the Aptamer Domain. *Biochemistry*.
41. Roth, A. and Breaker, R.R. (2009) The structural and functional diversity of metabolite-binding riboswitches. *Annu Rev Biochem*, **78**, 305-334.
42. Gallo, S., Furler, M. and Sigel, R.K.O. (2005) *In vitro* transcription and purification of RNAs of different size. *Chimia*, **59**, 812-816.
43. Gallo, S. (2008) *Dissertation, University of Zurich*
44. Regulski, E.E. and Breaker, R.R. (2008) In-line probing analysis of riboswitches. *Methods Mol Biol*, **419**, 53-67.

4.9 Additional experiments: Fluorescence studies with Tb(III)

The interaction between the *btuB* riboswitch, Tb(III) and AdoCbl was studied also with the help of fluorescence emission by Tb(III). Tb(III) bound to RNA undergoes FRET due to energy transfer through nearby guanines and therefore emits fluorescence at 545 nm. The fluorescence intensity of Tb(III) bound to the *btuB* RNA decreases with increase in concentration of AdoCbl (Figure 4.7A). To confirm if the quenching of Tb(III) fluorescence is due to the Co(II) of the corrin ring of AdoCbl, the fluorescence emission of Tb(III) is studied under different conditions.

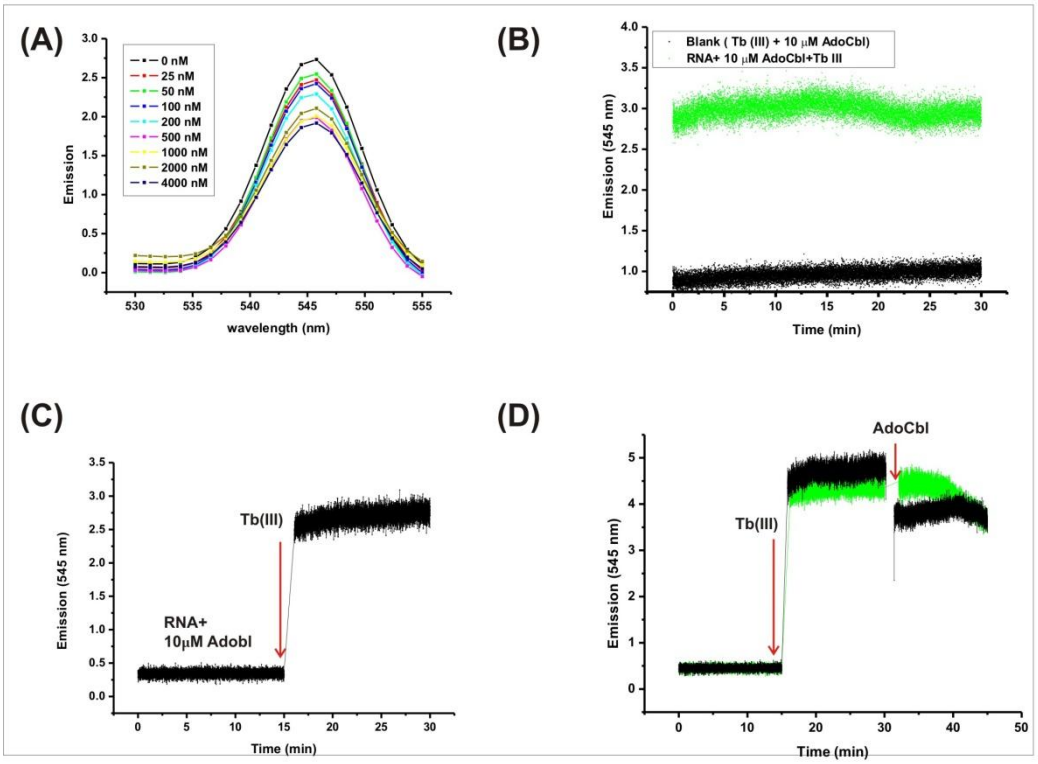

Figure 4.7: Fluorescence studies with Tb(III): The fluorescence emission by Tb(III) at 545 nm was measured (A) when the *btuB* riboswitch was incubated with 0-4000 nM of AdoCbl and 1 mM Tb(III). (B) shows the emission by Tb(III) for the complex of RNA, AdoCbl and Tb(III) (green spectrum) in comparison to the sample containing only Tb(III) and AdoCbl (black spectrum). (C) indicates increase in fluorescence emission upon addition of Tb(III) to the complex of RNA and AdoCbl. (D) shows increase in emission upon addition of Tb(III) to the RNA and decrease in emission upon addition of AdoCbl to the complex of RNA and Tb(III). The green and black spectra indicate the addition of 10 nM and 10 μM AdoCbl respectively.

A complex of RNA+ Tb(III) + AdoCbl increases the fluorescence emission by the bound Tb(III) only in the presence of RNA (Figure 4.7B). However, the trend of fluorescence emission is different depending upon the sequence of complex formation between RNA, Tb(III) and AdoCbl. When Tb(III) is added to a complex of RNA-AdoCbl, the fluorescence emission by Tb(III) increases (Figure 4.7C). In contrast, when AdoCbl is added to a complex of RNA-Tb(III), the fluorescence intensity decreases (Figure 4.7D). Interestingly, 10 nM of AdoCbl shows less quenching of emission by Tb(III) in comparison to 10 μM AdoCbl (Figure 4.7D). In contrast to 10 μM AdoCbl, 10 nM of AdoCbl can not bind to the *btuB* RNA as the K_D of AdoCbl to the *btuB* RNA is ~ 90 nM. Therefore, it is obvious that binding of AdoCbl to the *btuB* riboswitch quenches the fluorescence emission by Tb(III) in the complex of RNA-Tb(III).

These experiments suggest that AdoCbl binding takes place in close proximity to metal ion binding sites on the *btuB* RNA as the quenching of Tb(III) fluorescence is AdoCbl concentration dependent. The Tb(III) cleavage experiments in the

presence of AdoCbl (Figure S4.4) suggest that the metal ion binding sites are not altered in the switched conformation of the *btuB* riboswitch. Therefore, the observed quenching of Tb(III) fluorescence can not be due to the displacement of Tb(III) from the RNA upon AdoCbl binding. However, these preliminary observations need complementary experiments to confirm if the quenching of Tb(III) fluorescence is due to AdoCbl binding to the *btuB* RNA.

5 Kinetics of the interaction between the *btuB* riboswitch and cobalamines

5.1 Introduction

Bio-molecular binding is defined by the way macromolecules assemble into complexes and dissociate over time (1). The characterisation of such a binding phenomenon involves not only the verification of an interaction but also the determination of some quantitative binding parameters such as dissociation constants, stoichiometry and kinetic constants. The bio-molecular interaction has been studied before by various methods like equilibrium dialysis, gel shift assays, spectroscopic measurements, calorimetry and related techniques (2). However, most of these methods require labeling of the molecules with a fluorescent or radioactive tag.

Recent advancements in the label-free optical detection methods to study bio-molecular interaction have led to the emergence of Surface Plasmon Resonance (SPR) sensors (3-6). SPR has several intrinsic features that allow for label-free, real-time monitoring of bio-molecular interactions (7-14). This technique has been widely used in the evaluation of macromolecular interactions (DNA-DNA/protein, RNA-protein, protein-protein/drug) in terms of affinity, binding enthalpy and binding kinetics (10,15-25).

5.2 Physical basis of SPR

SPR sensors exploit the phenomenon of total internal reflection of light in their designs and detect changes in the refractive index (RI) near a sensor surface when molecules interact with each other. Total internal reflection of light occurs when it strikes the interface between high RI medium (glass) and low RI medium (water) at an angle greater than the critical angle (26). This reflection is not total when the surface of glass is coated with a thin film of a noble metal (e.g. gold) as some of the light is lost into the metallic film leading to the oscillation of mobile electrons (or plasma) at the surface (24,27,28). These oscillating electrons are called surface plasmons. The electrons resonate when the wave vector of the incident light matches the wavelength of the surface plasmons resulting in a loss of energy and therefore a reduction in the intensity of reflected light (29,30). The angle at which this loss is greatest (the intensity of reflected beam reaches its minimum) is called as SPR angle (Figure 5.1A). An evanescent electrical field associated with the plasma wave travels for a short distance (~300 nm) into the medium from the metallic film (31). Therefore, the resonance frequency of the surface plasmon wave depends on the refractive index of the medium (31).

A sensor chip in SPR sensors consists of a glass film coated with a thin layer of gold usually modified with a 100-200 nm carboxy-methylated dextran layer (32). The dextran layer can be modified by various chemical labels to enhance immobilization of the biomolecule on the surface (14). A typical sensor chip generally has four flow cells/compartments where the experiments can be carried out (33). Depending upon the experimental conditions either three cells, two cells or a single cell can be used as sample compartments. One of the cells always serves as a reference and is essential to record the background noise involved in the experiments.

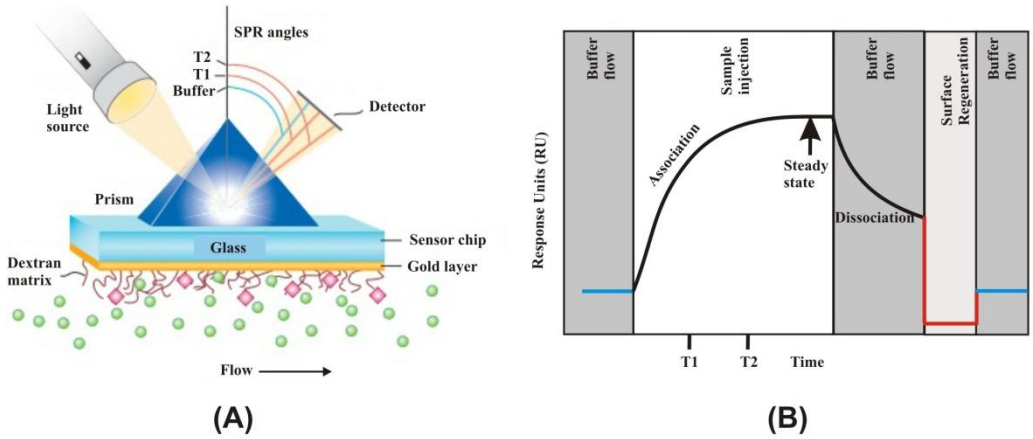

Figure 5.1: Basic concept of SPR: A) An optical unit for SPR: The reduced SPR angles at time points T1 and T2 are observed as analyte A (green) in the flow solution binds the ligand B (pink) immobilized on the dextran matrix. B) SPR sensorgram: The progress of the interaction between A and B is monitored over the given time period. A baseline (blue) represents a continuous flow of buffer. The signal (RU) increases as A binds to B (association) and reaches saturation (arrow) with increase in the concentration of bound B. The complex dissociates with an injection of buffer. The surface is regenerated to regain the baseline. (Figure partially adapted from (26)).

The experimental procedure involves immobilization of one reactant (ligand) on the surface of the sensor chip and monitoring its interaction with a second component (analyte) present in solution (14). Binding of an analyte to the ligand increases the refractive index at the surface thereby changing the SPR angle (26). This change is directly proportional to the amount of bound analyte and is expressed is terms of 'Response Units' (RU) where 1000 RU corresponds to a shift of 0.1° in SPR angle or to a change in RI of 10^{-3} (31,34). The change in RI upon analyte binding is measured in real time and the result (sensorgram) is plotted as response units versus time. The actual binding response is obtained by subtracting the background response from the control/reference cell harbouring either an irrelevant ligand or no ligand.

In a typical experiment, for which the sensorgram is shown in Figure 5.1B, initially the buffer flows over the sensor surface containing the immobilized ligand (base line) (14). When the analyte is injected, the upward slope of the curve indicates the association of the analyte with the immobilized ligand (14). After the steady state is achieved, the buffer is injected to dissociate the analyte as indicated by the downward curve (14). Before performing a new injection of an analyte, a regeneration solution is injected to normalize the sensor surface until the baseline is reached (14).

The basic experimental protocol to monitor the binding interaction between the two bio-molecules can be summarized as a four-step process:

1. Immobilization of one of the binding partners (ligand) on the sensor surface.
   (Careful immobilization of the ligand to the surface is important to avoid mass transport effects (35). Mass transport effects generate from the very high density of ligand where the binding rate of an analyte to ligand may exceed the rate at which it binds the surface or the analyte may bind the unoccupied ligand during the dissociation phase before diffusing out of the matrix. In both cases, the mass transport generates slower k_a (rate of association) and k_d (rate of dissociation) than the true k_a and k_d).
2. Injecting the second binding partner (analyte) and recording a real-time interaction curve.
3. Performing kinetics using a concentration series for an analyte.
4. Choosing an appropriate kinetic model and fit the raw data to extract the rate-constant estimates.

5.3 Aim of the project

Analysis of the riboswitch-ligand interaction in terms of their kinetic/thermodynamic parameters gives insights into the mode of gene expression regulated by riboswitches. A kinetic mode of regulation is associated with the speed of transcription, ligand association and with co-transcriptional folding of the aptamer whereas, the thermodynamic control depends upon the equilibrium between ligand association and dissociation as well as on the height of activation barrier between the bistable RNA structures (36). The *btuB* aptamer has been proposed to undergo co-transcriptional folding as the RNA polymerase (RNAP) pauses before continuing the transcription of the expression platform (37) (see section 1.4.4). The pausing of RNAP during transcription makes sure that the aptamer is folded correctly in order to transduce the regulatory signal upon ligand binding. Given this, it is crucial to investigate the kinetics of ligand binding to the *btuB* riboswitch in order to verify the kinetic/theromodynamic control of the regulation. Therefore to check for the possible regulatory mode of gene expression by the *btuB* riboswitch, we studied the kinetics of its interaction with its natural ligand, Adenosylcobalamine (AdoCbl) as well as with its non-physiological ligand, Vitamin B_{12} ($VitB_{12}$) by SPR.

5.4 Surface Plasmon Resonance with the *btuB* riboswitch

5.4.1 Immobilization of the binding partner

The essential requirement for SPR spectroscopy is the immobilization of one of the binding partners onto the sensor surface. Since the information on the essential groups of AdoCbl involved in the interaction with the *btuB* riboswitch was lacking at the time of experimentation (38,39), it was difficult to choose a strategy to modify AdoCbl to immobilize it on the surface such that binding to the *btuB* RNA remains unaltered. Alternatively, the expression platform of the *btuB* riboswitch is not involved in the metabolite recognition unlike the aptamer domain (40). Therefore, the region encompassing the expression platform is used to immobilize the *btuB* riboswitch on to the sensor surface. The natural expression platform of 37 nucleotides in length was added to the natural *btuB* aptamer (202 nt) by cloning. These additional 37 nucleotides do not hamper the folding of the aptamer region as observed from the in-line probing experiment (Figure 5.2). The 239 nucleotide long *btuB* riboswitch (pPC2) interacts with AdoCbl in a similar manner to that of 202 nucleotides *btuB* aptamer. With the exception of site 7, all other eight sites (sites 1-8) undergo the same modulation upon interaction with AdoCbl (Figure 5.2) compared to 202 nucleotides long *btuB* aptamer. The immobilization of the RNA to the sensor surface was achieved with the help of a DNA oligo carrying biotin at its 5' end and being complementary to the 25 nucleotides at the 3' end of the expression platform as shown in Figure 5.3. Since most of the expression platform region is hybridized to the biotinylated DNA oligo, the modified *btuB* RNA construct under study is expected to behave like a natural aptamer region. After hybridizing the biotinylated DNA oligo to the *btuB* RNA, the sample was injected on a sensor surface coated with streptavidin (Sensor chip SA) to form the high affinity streptavidin-biotin interaction.

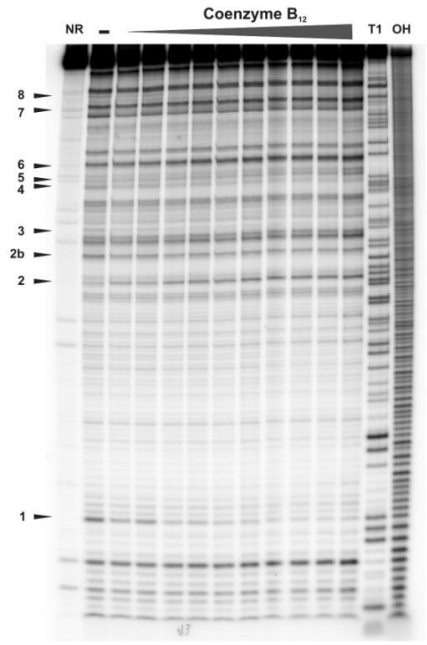

Figure 5.2: In-line probing with the modified *btuB* aptamer: 239 nt long *btuB* riboswitch includes the aptamer and an expression platform. This riboswitch undergoes a similar conformational switch (indicated by the AdoCbl modulated sites, 1-8) upon binding to AdoCbl as that of 202 nt long *btuB* aptamer except for changes at site 7.

The SPR detection system accurately records the binding of an analyte with molecular weight greater than 200 daltons (41). Although the analyte (AdoCbl) has a molecular mass of 1.6 kDa which is higher than the mass limit of the SPR, it is crucial to raise the surface density of the immobilized partner (the *btuB* RNA) to achieve a significant signal from the binding interaction. The RNA:oligo ratio was 1:10 during hybridization and therefore the surface should ideally also include the free DNA oligo (without RNA) along with the presence of RNA-DNA hybridized complex. To utilize the free DNA oligo and raise the RNA density on the surface, an 'RNA only' sample containing only the *btuB* RNA at a concentration of 30 µM was injected on the surface at the speed of 1µL/min to facilitate the hybridization of RNA to the free DNA oligo on the surface (Figure 5.4). This trick helped to raise the surface density of the RNA although much higher concentration of the sample is needed in comparison to the amount of substance involved in typical SPR experiments.

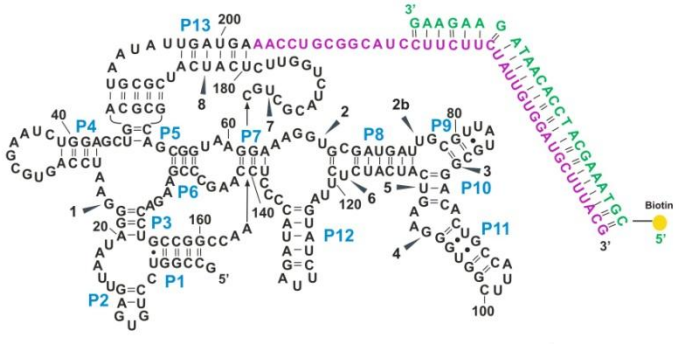

Figure 5.3: Hybridization of the modified *btuB* RNA to the DNA oligo: A DNA oligo (green) carrying biotin (yellow) at its 5' end is hybridized to the complementary 25 nucleotides at 3' end (purple) of the 239 nt *btuB* RNA. This construct facilitates the immobilization of the *btuB* RNA on the streptavidin coated sensor surface through high affinity biotin-streptavidin interaction. The arrows indicate the nucleotides (sites 1-8) undergoing the AdoCbl induced modulation by in-line probing (40, 46).

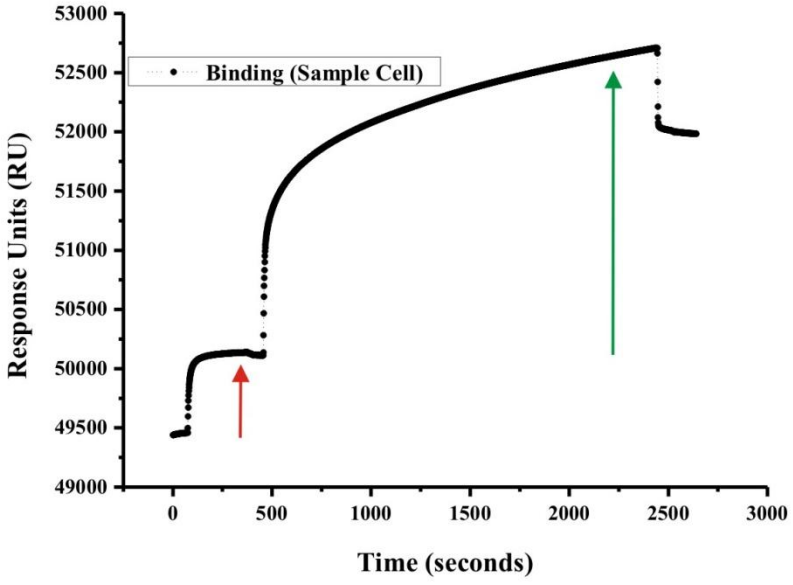

Figure 5.4: Immobilization of the *btuB* RNA on the sensor surface: The *btuB* RNA is immobilized on the sample flow cell of streptavidin chip in two steps. First a hybridized complex of *btuB* RNA-biotinylated DNA (1:10) is injected (indicated by red arrow), followed by the injection of 'RNA only' sample to utilize the unbound biotinlyated DNA oligo on the chip and thereby increases the surface density of the bound RNA (indicated by green arrow).

5.4.2 Control or Reference

The immobilization strategy in the experiments involved indirect coupling of the RNA to the streptavidin sensor surface with the use of biotinylated DNA oligo. Therefore, as a reference or control, the biotinylated DNA oligo was injected on the flow cell to normalize the response resulting from the binding of AdoCbl to the free DNA oligo. 1 µM of the biotinylated oligo was injected on the reference surface until saturation is achieved (Figure 5.5). The control cell exhibits negligible binding to AdoCbl in comparison to the surface with immobilized RNA (Figure 5.6). Therefore, we assume that even if the sample cell contains any free biotinylated DNA oligo (without bound RNA), the binding of AdoCbl should not generate any significant response. This control thus served as an optimum reference for our SPR experiments.

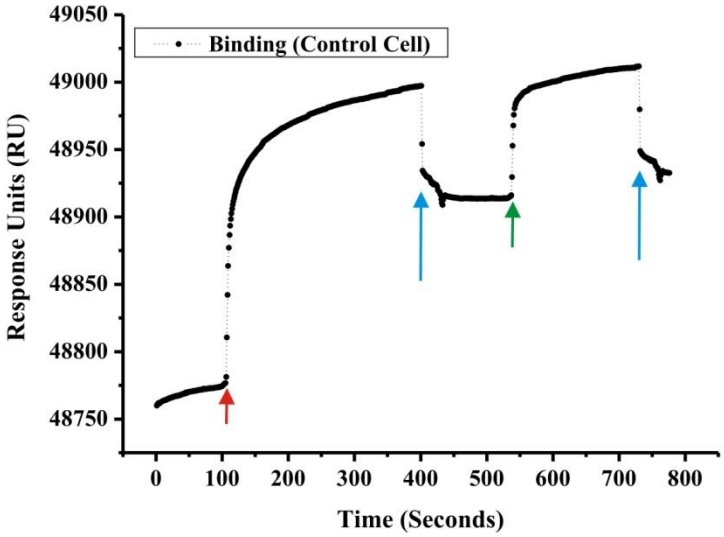

Figure 5.5: Preparation of control/reference flow cell: A sample containing biotinylated DNA oligo is injected in one of the flow cells of the streptavidin chip- control cell. Shown are the two injections of the sample on the control cell (indicated by red and green arrows) with the injection of running buffer in between and at the end of injection (blue arrow).

5.4.3 Regeneration of the surface

During the pilot run, it was found that the dissociation of AdoCbl from the surface is very slow even when the dissociation time was increased to 1200 seconds. To facilitate the dissociation of AdoCbl, regeneration of the surface was carried out by injecting 1 M NaCl as it was able to remove the analyte from the surface as well as to keep the surface active in terms of RNA density. So, in between every injection of AdoCbl, 1 M NaCl was injected to regenerate the surface.

5.4.4 Running buffer for the experiments

The buffer for SPR experiments consists of 50 mM Tris-HCl; pH 7.5, 100 mM KCl, 20 mM $MgCl_2$. The pH of the buffer was kept close to the physiological pH (pH 7.5). Since the SPR technique is highly sensitive to refractive index (RI) changes, it is crucial to avoid variations in the experimental conditions. Therefore, all the samples were prepared in 50 mM Tris-HCl; pH 7.5, 100 mM KCl, 20 mM $MgCl_2$.

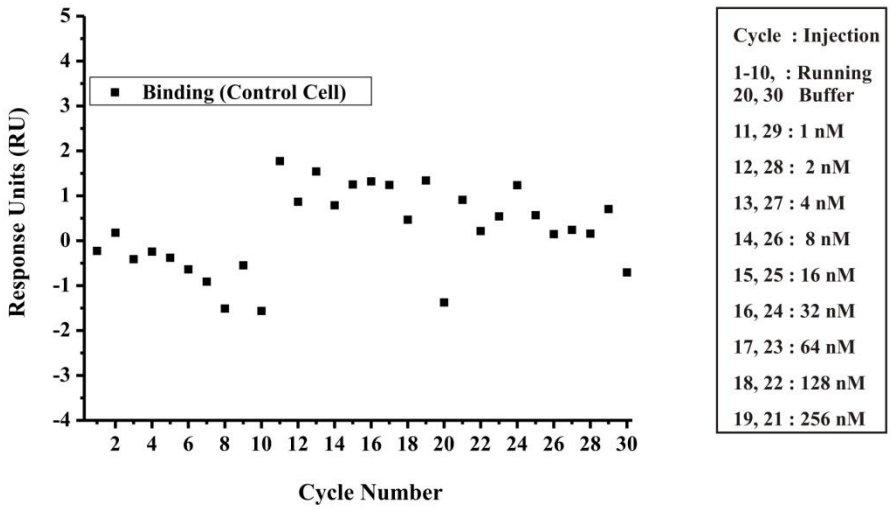

Figure 5.6: AdoCbl binding to control cell: The binding of AdoCbl in the given concentration range (1 to 256 nM) to the control cell is comparable to the binding response generated from injections of running buffer and therefore, is negligible.

5.5 Results

5.5.1 Binding kinetics between the *btuB* RNA and AdoCbl

With the immobilized *btuB* RNA on the surface, the kinetics studies were carried out by injecting AdoCbl in the concentration range of 1nM to 256 nM at the speed of 30 µL/min for 120 seconds. After a stability period of 300 seconds, running buffer is injected for 1200 seconds to follow the dissociation. Every injection of AdoCbl is then followed by injection of 1 M NaCl at the speed of 30 µL/min for 1 minute to ensure the surface regeneration. Moreover, each kinetics set up included two series of AdoCbl injections, once from low to high concentration and then from from high to low concentration. Such a set up helps to confirm the reproducibility of the binding interaction at the surface. The kinetics was carried out at 25 °C.

5.5.1.1 Binding and stability levels

[Note: The term 'binding level' referred in the following sections corresponds to the response units (RU) measured shortly before the end of the analyte injection whereas, the term 'stability level' indicates the response units measured just at the start of the dissociation phase and gives a clue on the rate of dissociation (k_d).]

During the kinetic run, several injections of running buffer were performed at the beginning to stabilize the sensor surface. Therefore, no significant binding can be seen either in the control cell or the sample cell up to cycle 10 (Figure 5.7). The surface also tends to get more stabilized with the continuous injections of running buffer as evident from the minimized fluctuations in the response units over the 10 cycles of running buffer injection (Figure 5.8). AdoCbl concentrations from 1 to 8 nM do not exhibit significant binding to the sample cell in comparison to the control cell. However, as the concentration of AdoCbl goes higher from 16 to 256 nM, the response units on the sample cell shows significant increase compared to the control cell (Figure 5.8). After the first series of AdoCbl injections from 1 to 256 nM, a control injection of running buffer was included to ensure the surface validity (Cycle number 20, Figure 5.7 and Figure 5.8). The running buffer injection drops down the response units drastically indicating the complete dissociation of AdoCbl from the surface with the regeneration conditions employed (Figure 5.8). In the second series, AdoCbl was injected in the reverse order from 256 nM to 1 nM. The reverse order was chosen for the second series in order to establish the concentration dependent binding of AdoCbl to the surface and also to confirm the complete dissociation of AdoCbl after every washout phase. In the second cycle, the general binding level to both the control cell and sample cell was higher than in the first cycle of

AdoCbl injections probably due to better stabilization of the surface through the first half of the kinetic run (Figure 5.7). However, the effective binding of AdoCbl to the sample cell after subtracting the response from the control cell is almost similar as for the first concentration series of AdoCbl (Figure 5.8).

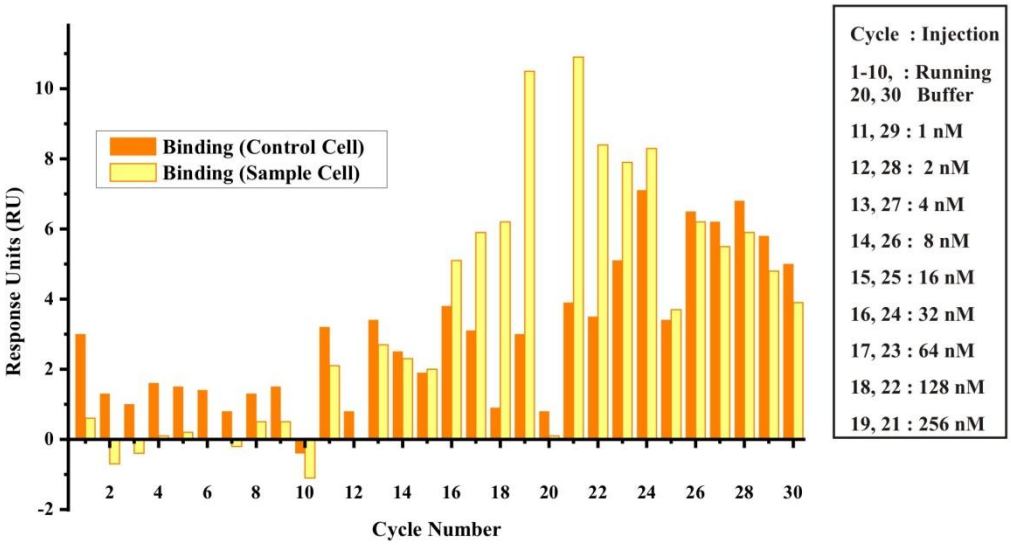

Figure 5.7: Comparison of binding responses during the *btuB*-AdoCbl kinetics: The binding of AdoCbl to the sample cell containing the *btuB* RNA is significantly higher than AdoCbl binding to the control cell. A concentration dependent binding is observed in the AdoCbl concentration range from 16-256 nM. The binding response for AdoCbl concentration series from 1-8 nM on the control and the sample cell is comparable to each other.

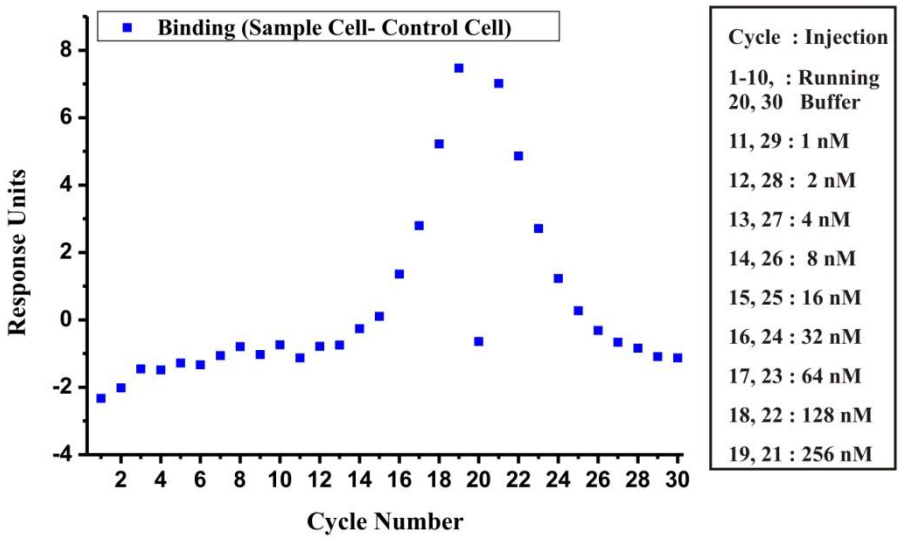

Figure 5.8: Concentration dependent binding of AdoCbl to the *btuB* RNA: The final binding response for AdoCbl in the sample cell (after subtracting the response from the control cell) exhibits a clear trend of concentration dependent increase in the RU from 16 to 256 nM. The response from 1-8 nM of AdoCbl was negligible and comparable to the binding response generated from the running buffer injection.

The stability level of the AdoCbl-bitionylated DNA oligo complex on the control cell (lacks RNA) is negligible in the concentration range of 1 to 8 nM (Figure 5.9). In contrast, a significant and concentration dependent stability of the RNA-AdoCbl complex is achieved on the sample cell with AdoCbl concentration from 16 to 256 nM (Figure 5.9).

When the binding and stability level of AdoCbl to the sample cell are compared after subtracting the corresponding levels from the control cell, it is observed that there is a concentration dependent increase in the binding and stability levels of AdoCbl on the surface (Figure 5.10). Although the binding levels for all concentrations of AdoCbl are slightly more than its stability levels, a markedly higher stability of AdoCbl on the RNA surface indicates a tight binding between the two.

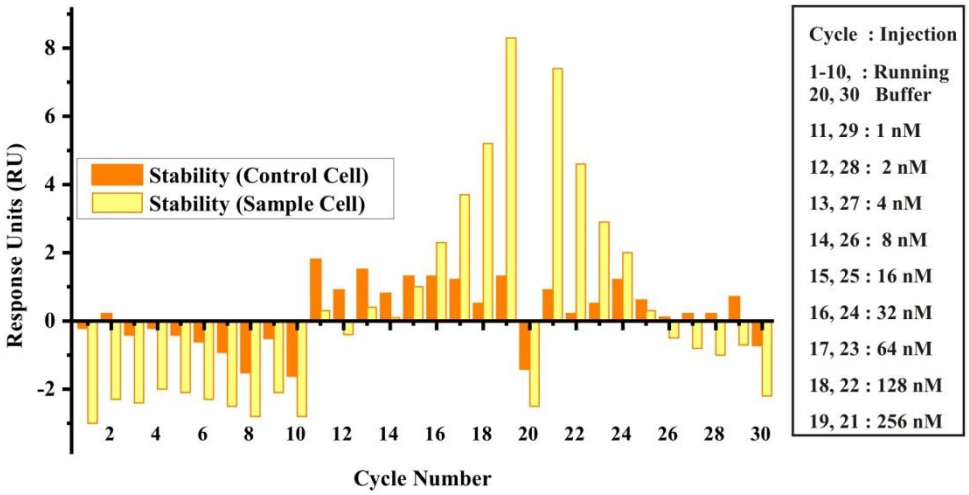

Figure 5.9: Stability of AdoCbl on the *btuB* RNA surface: During the kinetics, a high stability of the RNA-AdoCbl complex is observed on the sample cell in comparison to its stability on the control cell. AdoCbl concentration series injected in reverse order (Cycles 22 to 25: 256 to 16 nM) generates the similar stability level on the sample cell as the first concentration series (Cycles 15 to 19: 16 to 256 nM).

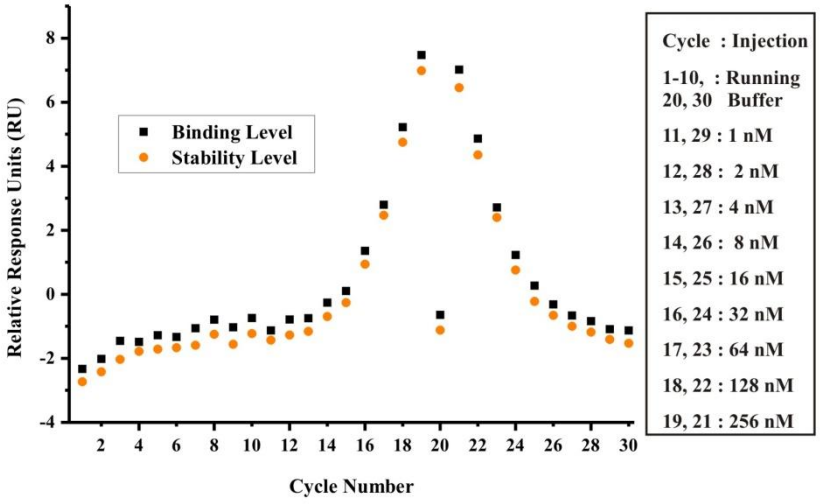

Figure 5.10: Comparison of binding and stability of the RNA-AdoCbl complex in the sample cell: Shown are the final binding and stability response on the sample cell after subtracting the respective responses from the control cell. The binding of AdoCbl to the sample cell is slightly stronger than its stability level however both binding and stability displays a similar trend of concentration dependent increase in the RU.

5.5.1.2 Derivation of the kinetic constants

All the sensorgrams (curves) were corrected for the bulk refractive index change and for non-specific binding from the control cell (with DNA oligo). The corrected sensograms were then evaluated with the Biacore evaluation software to analyze the kinetics of the interaction between the *btuB* riboswitch and AdoCbl by fitting the experimental data to different

kinetic models (42). The data from the corrected sensorgrams could be fitted to two different kinetic models as described below. These kinetic models are in turn compared to each other statistically in terms of Chi^2 value and the residual plot obtained after fitting the data to the kinetic models. The residual plot defines the difference between the experimental data points and fitted data points. Therefore, a residual plot close to zero (typically ± 1-2 RU) indicates an ideal fit to the corresponding kinetic model (43). The following kinetic models yielded a good fit to the acquired data:

I. 1:1 Langmuir binding model
II. Heterogenous ligand model

(I) 1:1 Langmuir binding model

This simplest model for kinetic evaluation is recommended by default unless the fit to the experimental data is poor. The 1:1 binding model assumes a simple bimolecular reaction with the following equilibrium between analyte A and ligand B (42,43):

$$A + B \underset{k_d}{\overset{k_a}{\rightleftharpoons}} AB$$

Table 5.1: Kinetic parameters derived from the 1:1 binding model for the interaction between the *btuB* riboswitch and AdoCbl. [Each value represents a weighted mean of the kinetic parameters derived from the two fitted kinetic experiments].

k_a (1/Ms)	k_d (1/s)	K_D (M)
32000 ± 61	$2.93 \times 10^{-4} \pm 5.90 \times 10^{-7}$	$9.16 \times 10^{-9} \pm 3.59 \times 10^{-11}$

In case of the 1:1 binding model, the rate of association between the *btuB* riboswitch and AdoCbl is in the order of $3*10^4$ $M^{-1}s^{-1}$ and falls within the range of k_a (10^4 to 10^5 $M^{-1}s^{-1}$) reported for most riboswitch aptamers (36). The rate of dissociation (k_d) however is extremely slow as indicated by the extended washout phase (Table 5.1 and Figure 5.11A). This slow k_d indicates a tight binding between the *btuB* riboswitch and AdoCbl suggesting a high affinity binding pocket provided by the riboswitch for AdoCbl. From the calculated k_d, only 0.03 % of the *btuB*- AdoCbl complex dissociates per second and therefore, approximately 30 minutes are needed for the system to reach an equilibrium. Considering the average half life of mRNA (~ 2 minutes) in the bacterial cell (44,45) , the dissociation of AdoCbl from the *btuB* riboswitch appears to be unattainable. Therefore, the only reaction that takes place between the *btuB* riboswitch and AdoCbl at a physiological time scale is the complex formation and a commitment to the switched conformation of the riboswitch. The equilibrium dissociation constant, K_D (k_d / k_a) or the affinity, K_A (k_a/ k_d) of AdoCbl for the riboswitch lies in the low nanomolar range (~ 8 nM). This affinity has been found to differ almost by 10 fold and 30 fold to the earlier reported apparent affinity values measured by in-line probing (90 nM) and ITC (250 nM) respectively (38,46). The observed bias in the affinity calculated from different methods could be due to the methodologies used in the determination of the K_D but it is evident from all the methods that the *btuB* riboswitch has an affinity towards AdoCbl in the lower nanomolar range.

The residual plot (the difference between the experimental data points and fitted data points) for the data fitted to the 1:1 Langmuir binding model lies very close to 0 in the range of -0.5 to +0.5 (Figure 5.11B). All the sensorgrams for AdoCbl concentration 16 to 256 nM exhibit a similar trend with respect to their residual plot and thus indicate a good fit to the 1:1 Langmuir binding model.

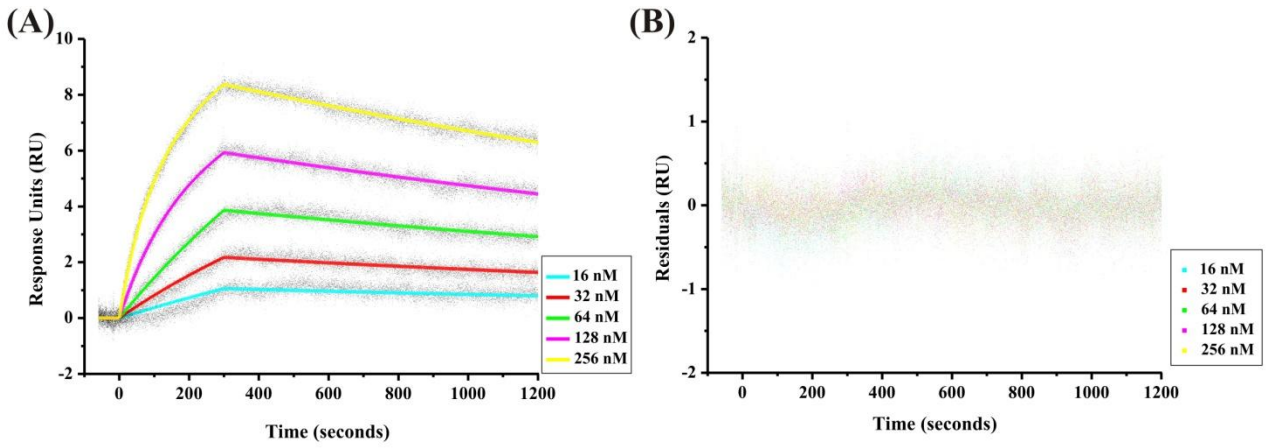

Figure 5.11: Kinetics of interaction between AdoCbl and the *btuB* RNA: A) Shown are the individual sensorgrams (dots) for each concentration of AdoCbl fitted to the 1:1 binding model (solid lines). AdoCbl concentration dependent increase in the rate of association (upward slope) and the slow rate of dissociation (downward slope) are evident. B) Residual plot: The residuals for the fit of the experimental data to the 1:1 binding model lies close to 0 and therefore, indicates a good fit of the data to the applied kinetic model.

(II) Heterogenous ligand Model

This kinetic model considers an interaction between one analyte and two independent ligands (43,47). The binding curve obtained is the sum of two independent reactions. This kinetic model was considered for the *btuB*-AdoCbl interaction due to consistent good fit of the experimental data (Figure 5.12A) and reproducible kinetic parameters. The heterogenous ligand model assumes the following equilibria between the analyte i.e. AdoCbl (A) and its ligands i.e. RNA (B1 and B2). (B1 and B2 can be the two possible RNA ligands i.e. two different conformations of the same RNA species).

$$\mathbf{A + B1} \underset{k_{d1}}{\overset{k_{a1}}{\rightleftharpoons}} \mathbf{AB1}$$

$$\mathbf{A + B2} \underset{k_{d2}}{\overset{k_{a2}}{\rightleftharpoons}} \mathbf{AB2}$$

The kinetic parameters derived from the heterogenous ligand model for the two different ligands exhibit a 4 fold difference in their k_a towards the *btuB* riboswitch (Table 5.2A and 5.2B). The k_d however remains the same for both the ligands (Table 5.2A and 5.2B). The differences in the k_a for both ligands are reflected in their equilibrium dissociation constant (K_D) towards AdoCbl where the ligand (ligand B2) with higher association rate exhibits 5 fold higher affinity for AdoCbl

(Table 5.2A and 5.2B). Interestingly, the kinetic parameters for the ligand with higher affinity to AdoCbl matches to the one derived from 1:1 binding model.

Table 5.2A and 5.2B: Kinetic parameters derived from the heterogenous ligand model for the interaction between the *btuB* riboswitch and AdoCbl. Table 5.2A and Table 5.2B respectively give the parameters for the interaction of AdoCbl with possible RNA ligands B1 and B2. Each value represents a weighted mean of the kinetic parameters derived from the two best fitted kinetic experiments.

Table 5.2A:

k_{a1} (1/Ms)	k_{d1} (1/s)	K_{D1} (M)
13500 ± 160	$3.11 \times 10^{-4} \pm 1.71 \times 10^{-6}$	$2.3 \times 10^{-8} \pm 4.0 \times 10^{-10}$

Table 5.2B:

k_{a2} (1/Ms)	k_{d2} (1/s)	K_{D2} (M)
49500 ± 406	$2.75 \times 10^{-4} \pm 1.71 \times 10^{-6}$	$5.56 \times 10^{-9} \pm 8.01 \times 10^{-11}$

The residuals for the fitting to heterogenous ligand model lies close to 0 (Figure 5.12B) suggesting a good fit of the experimental data to this kinetic model. The Chi^2 for the fitting to both of the above mentioned models (1:1 binding and heterogenous ligand binding) are almost equal (Table 5.3). Therefore, the kinetics between the *btuB* RNA and AdoCbl can be explained with two different possibilities of interaction (see section 5.6.1 and 5.6.2).

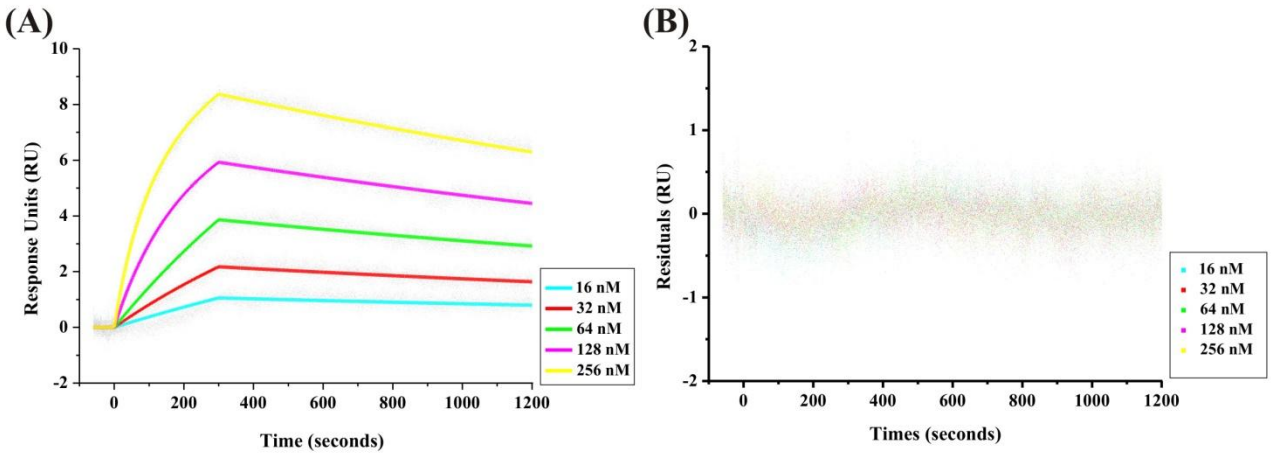

Figure 5.12: Heterogenous ligand binding model for AdoCbl-*btuB* kinetics: A) The individual sensorgrams (dots) for each concentration of AdoCbl are fitted to the heterogenous ligand binding model (solid lines). B) Residual plot: The residuals for the fit of the experimental data to heterogenous ligand binding model lies close to 0 indicating a good fit of the experimental data to the applied kinetic model.

Table 5.3: The Chi^2 for the fits of the *btuB*-AdoCbl kinetics data to the 1:1 binding model and heterogenous ligand model for the two experiments (1 and 2).

n	1: 1 binding	Het. ligand binding
1	0.0529	0.0462
2	0.0475	0.0445

5.5.2 SPR kinetics: The *btuB* RNA and Vitamin B_{12}

AdoCbl and $VitB_{12}$ are two related ligands of the B_{12} family. These metabolites have the same α-axial ligand, the DMB moiety and differ only in their β-axial ligand being cyanide for $VitB_{12}$ and adenosyl for AdoCbl (48). It has been established by in-line probing experiments that $VitB_{12}$ has 1000 fold lower affinity for the *btuB* riboswitch than AdoCbl (46). To better characterize the effect of the β-axial ligand of the analyte on its affinity towards the *btuB* riboswitch, the binding kinetics between the *btuB* RNA and $VitB_{12}$ were measured.

The experimental conditions for the $VitB_{12}$/*btuB* riboswitch interaction were kept the same as with AdoCbl except the B_{12} concentration. The immobilization of the *btuB* RNA on the sensor chip was done using the biotinylated oligo as described in section 5.4.1. Again the biotinylated DNA oligo was used as a reference/control. The $VitB_{12}$ stock solutions were prepared in running buffer (50 mM Tris-Cl; pH 7.5, 100 mM KCl, 20 mM $MgCl_2$). During the pilot experiment, it was observed that much higher concentration of $VitB_{12}$ is needed to obtain a similar value of response units as compared to the one observed in the case of AdoCbl. Therefore, the concentrations of $VitB_{12}$ in the range of 5.12 µM to 81.92 µM were used. The sensor surface was regenerated by 1 M NaCl as done with AdoCbl. The kinetics was carried out at 25 °C.

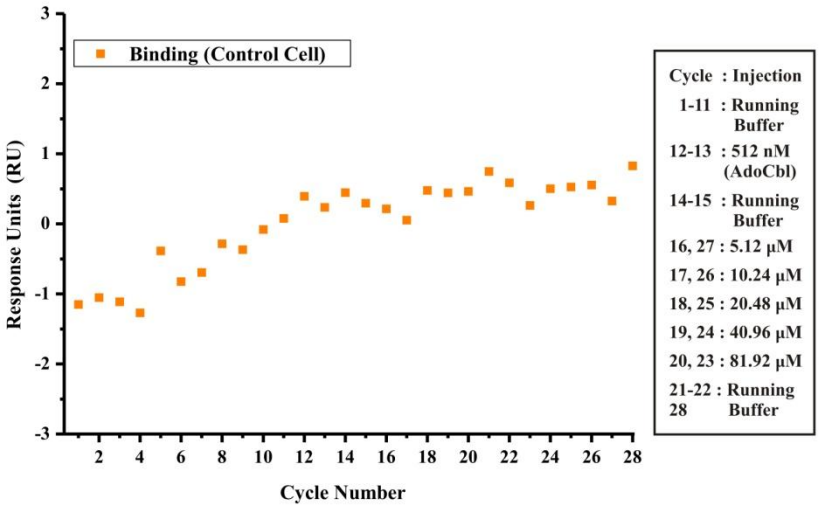

Figure 5.13: $VitB_{12}$ binding to the control cell: Binding of $VitB_{12}$ to the control cell is negligible for all the applied concentrations, indicated by the increase in RU being close to 0 and similar to the RU from the injections of running buffer.

5.5.2.1 Binding and Stability levels

The injections of running buffer as well as of $VitB_{12}$ into the control cell showed negligible binding as expected (Figure 5.13). However, $VitB_{12}$ in the applied concentration range (5.12 µM to 81.92 µM) does exhibit a significant and concentration dependent binding to the sample cell (after background correction from control cell) (Figure 5.14A). The injections of running buffer after the first half of the kinetic run (from 0 µM to 81.92 µM) drops down the binding of $VitB_{12}$ indicating a complete dissociation of $VitB_{12}$ from the surface (Cycle number 21 and 22, Figure 5.14A). The second half of the kinetic run with $VitB_{12}$ (from 81.92 µM to 0 µM) exhibits the same binding level as the first concentration series and thus confirms the validity of the sample (RNA) surface (Figure 5.14A). As an internal control, an AdoCbl concentration of 512 nM was injected twice before beginning the kinetic run with $VitB_{12}$ (Cycle number 12 and 13, Figure 5.14A). The binding levels for 512 nM of AdoCbl on the RNA surface were significantly higher than the binding level for 81.92 µM of $VitB_{12}$.

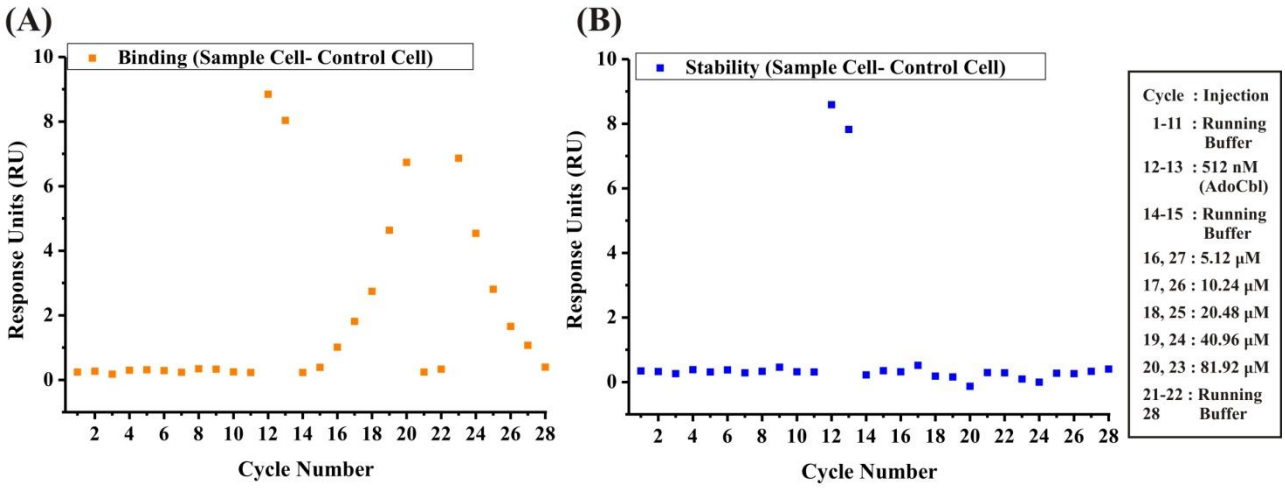

Figure 5.14: Binding and stability levels of $VitB_{12}$ on the *btuB* RNA surface: Shown are the final binding and stability responses after subtraction from the control cell responses. A) The concentration dependent and reproducible binding is observed for $VitB_{12}$ concentration from 5.12-81.92 µM in both orders of injections (low to high; high to low). An internal control of AdoCbl (512 nM) exhibits significantly higher levels of binding than by the highest comcentration (81.92 µM) of $VitB_{12}$. B) The stability levels of $VitB_{12}$ on the RNA surface are absolutely negligible. An internal control of AdoCbl (512 nM) in contrast has extremely higher stability on the sample cell in comparison to $VitB_{12}$. (The stability level indicates the response units measured just at the start of the dissociation phase and gives a clue on the rate of dissociation (k_d)).

A striking difference is observed when the stability levels (See 'Note' in Section 5.5.1.1) of the RNA-AdoCbl complex (512 nM) and the RNA-$VitB_{12}$ complex (5.12 µM to 81.92 µM) are compared on the sample cell (Figure 5.14B). The stability levels for the RNA-AdoCbl complex were almost same as the binding level indicating a tight binding to the *btuB* RNA to AdoCbl (Figure 5.15). In contrast, the stability levels of the RNA-$VitB_{12}$ complex for all the applied concentration series of $VitB_{12}$ were negligible (Figure 5.15). These differences in the binding and stability levels indicate a much higher affinity of AdoCbl to the *btuB* RNA in comparison to $VitB_{12}$.

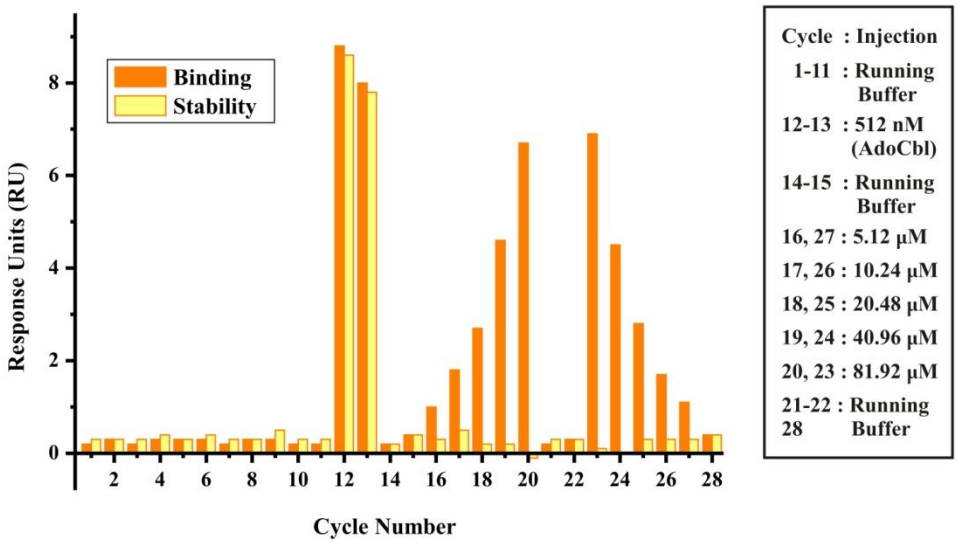

Figure 5.15: Comparison of binding and stability of the RNA-VitB$_{12}$ complex on the sample cell: Although a concentration dependent binding is observed for the VitB$_{12}$ concentration series, the stability levels for all the concentration were almost negligible with no clear trend. The binding and stability levels for an internal control of AdoCbl (512 nM) were almost similar indicating a tight binding of AdoCbl to the *btuB* RNA.

5.5.2.2 Derivation of the kinetic constants

After correcting the sensorgrams for bulk refractive index changes and non-specific binding to the control cell, the data was fitted to different kinetic models.

The kinetics between the *btuB* RNA and VitB$_{12}$ could only be fitted to the 1:1 binding model (Figure 5.16A) unlike the AdoCbl-*btuB* RNA interaction where the data could also be fitted to the heterogenous ligand binding model. Also, the residual plot for the fit to the 1:1 Langmuir binding model (for VitB$_{12}$-*btuB* interaction) lies close to 0 for almost the whole range of the observed kinetic phase (Figure 5.16B). (A fit of the data from the VitB$_{12}$-*btuB* RNA system to the heterogenous ligand model showed that the kinetic constants derived from the fits of independent experiments were not compatible with each other. Therefore, the heterogenous ligand model was disregarded for the interaction between VitB$_{12}$ and the *btuB* RNA).

As seen from Table 5.4, VitB$_{12}$ has nearly the same rate of association towards the riboswitch compared to AdoCbl differing only by a factor of two. Therefore, the pre-organized *btuB* riboswitch is able to recognize both the cobalamines possibly by a similar mechanism. However, the rate of dissociation (k_d) for VitB$_{12}$ from the *btuB* RNA is almost 10^4 fold faster than AdoCbl. The faster dissociation is evident in the washout phase with the rapid decrease in the response units (Figure 5.16A). The rapid dissociation of VitB$_{12}$ from the *btuB* riboswitch suggests that a conformationally switched riboswitch (after ligand binding) prefers AdoCbl over VitB$_{12}$. The evaluation of the kinetic constants indicate the equilibrium dissociation constant, K_D (k_d/ k_a) of the *btuB* riboswitch towards VitB$_{12}$ being 102 µM. Compared to AdoCbl, the affinity of the *btuB* riboswitch for VitB$_{12}$ is 10^5 and 10^3 fold low as calculated from SPR and in-line probing experiments respectively (46).

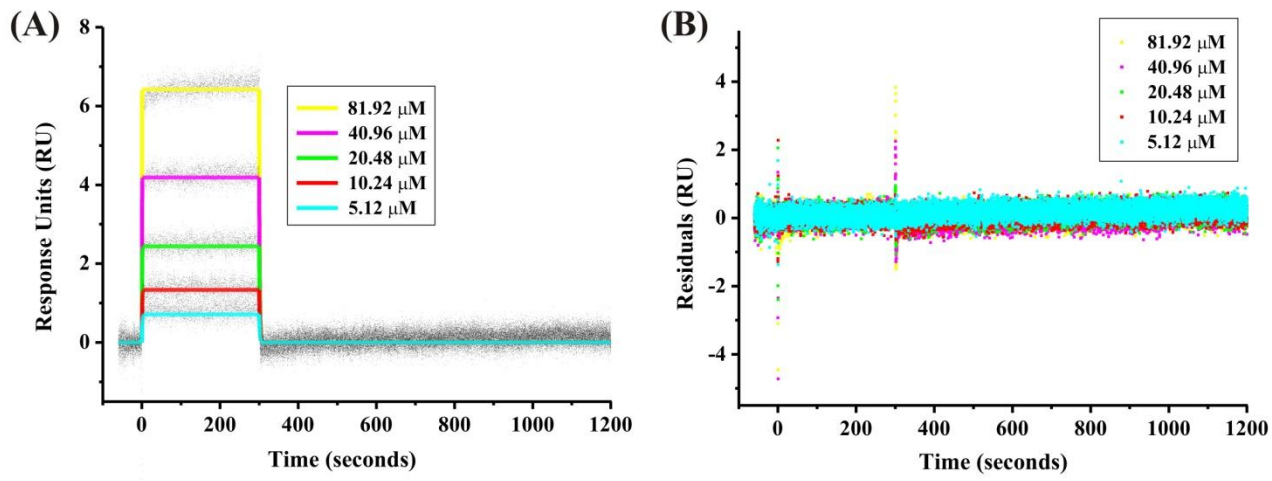

Figure 5.16: Kinetics of the *btuB*-VitB$_{12}$ interaction: A) Shown are the sensorgrams (dots) for each concentration of VitB$_{12}$ fitted to the 1:1 binding model (solid lines). A concentration dependent increase in the response units indicate the association of VitB$_{12}$ whereas the dissociation of VitB$_{12}$ from the *btuB* RNA is very fast (downward slope). B) Residual plot: The residuals for the fit of the experimental data to the 1:1 binding model lie close to 0 for all concentrations of VitB$_{12}$ except at the beginning and end of VitB$_{12}$ injection.

Table 5.4: Kinetic parameters derived from the 1:1 binding model for the interaction between the *btuB* riboswitch and VitB$_{12}$. Chi^2 is given for the fitting of the two independent experimental data (n1 and n2) to the 1:1 binding model. Each value represents a weighted mean of the kinetic parameters derived from the two fitted kinetic experiments.

k_a (1/Ms)	k_d (1/s)	K_D (M)	Chi^2
18900 ± 200	1.925 ± 0.02	1.02 x 10^{-4} ± 2.13 x 10^{-6}	n1= 0.0741 n2= 0.0609

5.6 Discussion

5.6.1 Interaction of cobalamines with the *btuB* riboswitch

SPR spectroscopy revealed the k_a and k_d for the *btuB*-AdoCbl/VitB$_{12}$ interaction. Interestingly, the 1:1 Langmuir binding model could be fitted to the experimental data for both AdoCbl-*btuB* and VitB$_{12}$-*btuB* interaction. In addition, the kinetic behaviour of AdoCbl binding to the *btuB* riboswitch can also be explained by a second kinetic model, the heterogenous ligand model (see Section 5.6.2).

Considering the 1:1 binding equilibrium, both AdoCbl and VitB$_{12}$ associate with the *btuB* riboswitch with an almost similar k_a. In contrast, the k_d for AdoCbl is much smaller than the k_d for VitB$_{12}$. It seems as if a general tight binding pocket is provided by the *btuB* riboswitch for the adenosyl moiety of AdoCbl as the presence of the adenosyl moiety reduces the dissociation rate by 10^4 fold. The varying rate of dissociation creates a difference in affinity (K_D= k_d / k_a) accounting to be a 10^4 fold higher affinity of AdoCbl than VitB$_{12}$.

A similar rate of association but drastically different rate of dissociation for AdoCbl and VitB$_{12}$ with the *btuB* riboswitch can be explained by the following model (Figure 5.17).

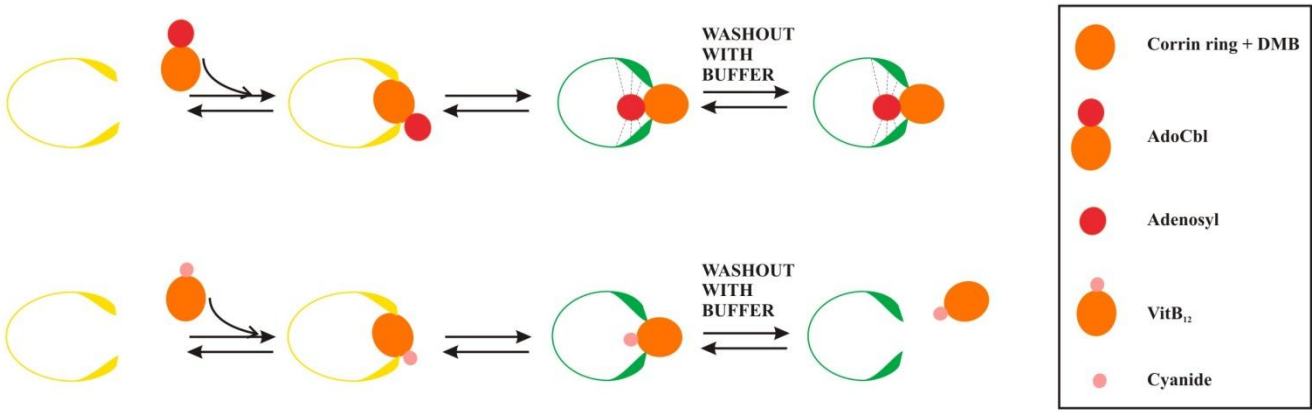

Figure 5.17: A model for interaction between cobalamines and the *btuB* riboswitch: The kinetic data indicates that a pre-organized *btuB* riboswitch (yellow) can interact with cobalamines irrespective of their β-axial groups and undergoes a conformational switch (green). The conformationally switched RNA (green) creates specific contacts (dotted lines) to the adenosyl moiety of AdoCbl but fails to coordinate to small β-axial groups like $VitB_{12}$. A tight binding between AdoCbl and the switched RNA is responsible for the lower dissociation rate observed for AdoCbl in comparison to $VitB_{12}$.

AdoCbl and $VitB_{12}$ differ only in their β-axial ligand. Therefore, it is possible that the pre-organized conformation of the riboswitch recognizes these metabolites by the side chains of the corrin ring/DMB moiety or both. The recently solved crystal structures of B_{12} riboswitches from thermophiles have proposed the interaction between the riboswitch and the corrin ring side chains/DMB (38). These contacts include van der Waals interactions between DMB and the amino propyl linker of cobalamine to the ribose phosphate backbone of loops L5 and L13 of the *btuB* RNA and also a direct hydrogen bond between 2'-hydroxyl group of cobalamine ribosyl moiety to the 2'-hydroxyl group of the conserved cytosine at L13. Contacts to the RNA are also made by propionamide and acetamide groups of the corrin ring (38,39). The α-axial side of cobalamine creates structure-specific contacts to the kissing loop (KL) interaction between L5 and L13 of RNA (Figure 5.18). Since the KL interaction within the B_{12} riboswitches occurs in the ligand bound form, we propose that the recognition of α-axial face of cobalamine could simultaneously promote the KL interaction in the *btuB* riboswitch leading to conformational change in the RNA. In this state, a tight binding pocket is provided for the adenosyl moiety of cobalamines. The binding pocket for AdoCbl mainly consists of a cavity created by J3/4 and J6/3 as observed from the crystal structures of the AdoCbl riboswitches (38,39). The peripheral region of the riboswitch stabilizes this pocket by A-minor triple-type interactions between the conserved adenosines at J11/10 with the residues from J6/3 and J5/6 (38,39). These interactions facilitate the Hoogsteen edge of one of the conserved Adenosines at J6/3 to base pair with the Watson-Crick face of the adenine base of AdoCbl (Figure 5.19) (38,39). Therefore, cobalamines lacking the adenosyl moiety as their β-axial ligand exhibit a reduced affinity to the riboswitch in the absence of specific interactions. This also explains the rapid dissociation of $VitB_{12}$ from the *btuB* riboswitch as observed in SPR experiments.

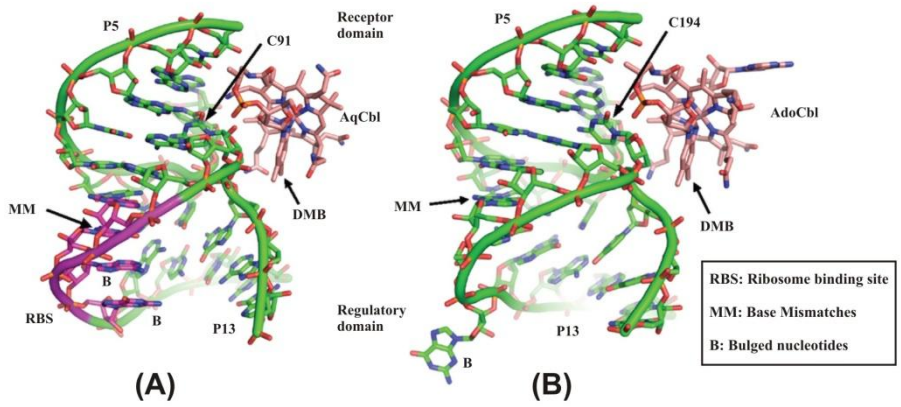

Figure 5.18: Interaction of cobalamines with the B_{12} riboswitches: A structure specific contact mediated by DMB moiety and the corrin side chain with the KL interaction of L5 and L13 for A) *env8* AqCbl B) *Tte* AdoCbl riboswitches. (Figure adapted from (38)).

A pre-organized *btuB* riboswitch thus could interact with cobalamines irrespective of their β-axial ligands and could lead to a similar conformational change in the riboswitch needed for gene regulation. Therefore, the adenosyl moiety of AdoCbl is not a mandatory requirement for the association or recognition of the *btuB* riboswitch. It is only required to create a high affinity contact to the *btuB* riboswitch. This also supports the earlier observations where a respective structural switch was observed in the *btuB* RNA with AdoCbl and $VitB_{12}$, but the affinity of $VitB_{12}$ towards the riboswitch was 1000 fold weaker than AdoCbl (46).

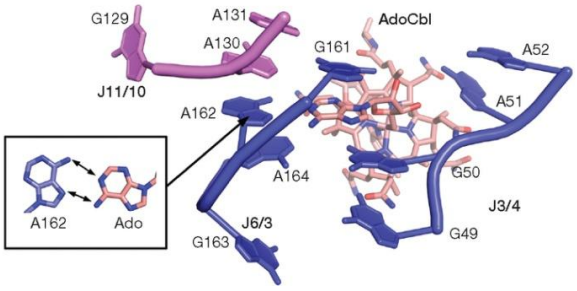

Figure 5.19: AdoCbl recognition by *Tte* AdoCbl riboswitch: J11/10 helps J6/3 to adopt a configuration that allows the Hoogsteen face of A162 to pair with adenosyl moiety of AdoCbl, an interaction responsible for high specificity of the riboswitch to AdoCbl. (Figure partially adapted from (38)).

5.6.2 Heterogenous ligand binding model and the *btuB*-AdoCbl interaction

As the kinetics between AdoCbl and the *btuB* riboswitch could be fitted to the heterogenous ligand model as well, an other possible mode of interaction can be proposed.

The heterogenous ligand model suggests the presence of two species (referred here as species B1 and B2) of the *btuB* RNA and both of these species bind AdoCbl. Species B2 exhibit an almost four times higher rate of association towards AdoCbl than species B1 while the dissociation rates are almost equivalent (Table 5.2A and 5.2B). Consequently, B2 exhibits a marked higher affinity towards AdoCbl than B1. Interestingly, the kinetic rates of B2 are the same as found with the 1:1 binding model. One explanation could be that B2 comprises the majority of the population.

The heterogenous ligand model could not be fitted to the experimental data for $VitB_{12}$-*btuB* riboswitch interaction. The *btuB*/AdoCbl data suggests that the *btuB* RNA exists in two conformations with one species having a higher affinity towards cobalamines than the other. Since, $VitB_{12}$ anyway has lower affinity for the *btuB* riboswitch than AdoCbl, the

binding by low affinity species can not be detected anymore by SPR. Therefore, only the binding by the high affinity species is recorded. This explains why the kinetics between the *btuB* riboswitch and $VitB_{12}$ could be fitted to a 1:1 binding model yielding the kinetic constants for the high affinity conformation.

Since SPR is a bulk method, it is difficult at present to describe the observed heterogeneity in the RNA population in more detail.

5.6.3 The regulation of the *btuB* riboswitch: Kinetic or thermodynamic control

The kinetic parameters for the *btuB*/AdoCbl interaction can help predict the mode of regulation for the *btuB* riboswitch since the riboswitch-mediated regulation of gene expression can be under kinetic or thermodynamic control (Figure 5.20) (36,49).

In case of the *btuB* riboswitch from *E. coli*, the expression of the transporter BtuB is regulated at the translational level (50,51). But before the translational regulation can operate, the pausing by RNAP at strategic pause sites after transcription of the aptamer region can play an important role in the overall regulation (37) (Section 1.4.4). The expression platform can compete with the aptamer for the formation of an RBS-anti-RBS hairpin and could lead to mis-regulation of the BtuB expression in the absence of AdoCbl. The pausing by RNAP allows a sufficiently long time window to co-ordinate tertiary folding of the aptamer region and the transcription of the expression platform (37,52). The kinetic parameters for the *btuB*-AdoCbl interaction obtained by SPR indicate extremely slow dissociation of AdoCbl from the *btuB* riboswitch. The bacterial mRNA has a half life of ~ 2 minutes and therefore, the *btuB* aptamer and AdoCbl would never reach an equilibrium state in the physiological time window needed for the gene regulation. Hence, the *btuB* riboswitch seems to be more under kinetic rather than thermodynamic control where factors like the rate of aptamer folding, the transcriptional pausing by RNAP, and the rate of ligand association along with the ligand concentration controls the final outcome of the genetic decision. However, information on the half life of RNAP pausing on the *btuB* riboswitch is lacking at present. This information is necessary to correlate the kinetic parameters of AdoCbl interaction to folding of the *btuB* riboswitch and awaits further investigations.

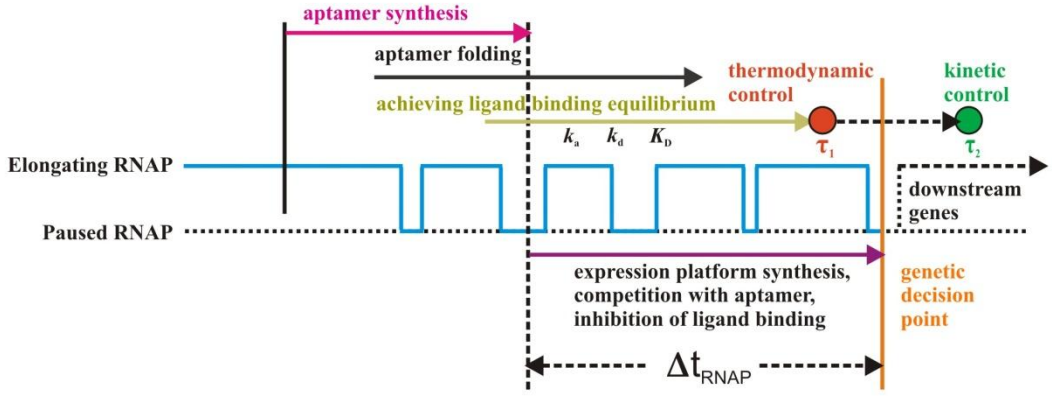

Figure 5.20: Kinetic and thermodynamic regulation of riboswitch function: The kinetic or thermodynamic regulation of riboswitch activity depends upon the Δt_{RNAP} (time taken by RNAP for elongation from the aptamer end to the termination decision point) and on τ (time constant for the equilibrium between ligand association and dissociation). When $\Delta t_{RNAP} > \tau$ (τ_1), RNAP reaches the termination decision point after ligand and aptamer achieves equilibrium leading to the thermodynamic control whereas a kinetic mode of regulation is evident when $\Delta t_{RNAP} < \tau$ (τ_2). (Figure adapted from (36)).

5.7 Experimental section

5.7.1 Materials

All chemicals were purchased from Sigma-Aldrich (Switzerland) except for Vitamin B_{12} that was obtained from Calbiochem (USA). All salt solutions, buffers and stock solutions were prepared using filtered ultrapure water and further filtered through 0.2 µm filters before use. The biotinylated DNA oligonucleotide was purchased from W.M. Keck Oligonucleotide Synthesis Facility, Yale University at 1 micromole scale and was purified further by PAGE. The streptavidin sensor chip (SA) was obtained from Biacore (GE Healthcare). The SPR experiments were performed with a Biacore T100 (Functional Genomics Centre, UZH and ETH, Zurich).

5.7.2 Sample preparation

5.7.2.1 Biotinylated DNA oligo for the control flow cell

DNA Oligo Sequence: 5' Biotin- CGT AAA GCA TCC ACA ATA GAA GAA G-3'.

Biotinylated DNA oligo at a final concentration of 1 µM was added to a buffer containing 50 mM Tris-HCl; pH 7.5, 100 mM KCl, 20 mM $MgCl_2$. 50 µL of the sample is needed for a single injection on a flow cell 1 (reference/ control cell) for 5 minutes at the flow rate of 10 µL/ minute.

5.7.2.2 Biotinylated RNA for the sample flow cell

A. Construction of plasmid pPC2: The 202 nucleotide *btuB* sequence from the genome of *E. coli* DH5α was extended at its 3' end by colony PCR with the two primers pSG2_5 and btuB 239 to include the 37 nucleotides long expression platform at the 3' end as well as additional nucleotides GGA at the 5' end (for better transcription yields) (see Section 8.2.1.2). After digestion of plasmid by *EcoRI*, the RNA was transcribed *in vitro* from the plasmid template using T7 RNAP (see Section 8.2.3). The RNA was purified by 10% denaturing PAGE, electroelution and was subsequently concentrated with the help of *Vivaspin*.

The terminal 25 nucleotides from the 3' end of the RNA were hybridized to the complementary biotinylated DNA oligo to create the biotinylated DNA- RNA complex.

B. Sample preparation: pPC2 RNA at a final concentration of 0.1µM was mixed with filtered ultrapure water and 50 mM (final concentration) Tris-HCl, pH 7.5. The sample is heated to 90 °C for 1 min. The biotinylated DNA oligo at the final concentration of 1 µM (RNA: DNA oligo is 1:10), KCl (final concentration, 100 mM) and $MgCl_2$ (final concentration 20 mM) were added to the sample. The sample is further kept at 55°C for 2 minutes. The sample is then kept at 37 °C for 15 minutes to allow RNA folding.

In total, 50 µL of the sample is needed for a single injection on the flow cell 2 (sample cell) for 5 minutes at the flow rate of 10 µL/minute.

5.7.2.3 RNA only (without the DNA oligo) for the sample flow cell

After immobilization of the hybridized RNA-DNA complex on the sample cell, the RNA alone was injected on the same sample flow cell to utilize the excess of unbound DNA oligo.

pPC2 RNA at a final concentration of 30 µM was mixed with distilled water and 50 mM (final concentration) Tris-HCl, pH 7.5. The sample was heated to 90 °C for 1 minute followed by the addition of KCl and $MgCl_2$ at the final concentration of 100 mM and 20 mM respectively. The sample is subsequently kept at 37°C for 15 minutes to allow the RNA folding.

The RNA sample is injected on the flow cell 2 (sample cell) at the flow rate of 1 µL/minute for 10 minutes. Sometimes, the injections were repeated for two or three times depending on the level of immobilization achieved. Therefore, the sample was prepared in the total volume of 30-50 µL.

[Note: The immobilization of the bio-molecules on the sensor surface depends on the intrinsic properties of the sensor surface and needs to be monitored for every new surface used in the experiments. Therefore, the injections need to be repeated several times to achieve significant immobilization of the bio-molecules. In the SPR experiments carried out here, the observed range for the increase in response units (RU) upon immobilization is indicated in Table 5.5].

Table 5.5: The range of the maximum response units achieved through immobilization of the indicated biomolecules on the streptavidin sensor surface.

Flow cell Number	Type of flow cell	Immobilized molecule	Increase in RU
1	Reference/ Control	Biotinylated DNA oligo	500- 2500
2	Sample	Hybridized RNA-DNA complex	1000- 3900
2	Sample	RNA alone	1100 - 4250

[Note: The RNA alone sample is injected on the flow cell 2 after the injection of the hybridized RNA-DNA complex to utilize the free biotinlyted DNA oligo].

5.7.3 AdoCbl and Vitamin B_{12} stock solutions

10 mM (w/v) AdoCbl and 5 mM (w/v) $VitB_{12}$ stock solutions were prepared in filtered ultrapure water. These stock solutions were checked for their accurate concentrations by monitoring the UV-Vis spectra at appropriate dilution. The concentration series of AdoCbl and of $VitB_{12}$ used in the SPR experiments were prepared by serial dilution of the 10 mM and 5 mM stock solutions in buffer containing 50 mM Tris-HCl; pH 7.5, 100 mM KCl and 20 mM $MgCl_2$.

5.7.4 Surface Plasmon Resonance

A. Instrument: Biacore T100 (Functional Genomics Centre, UZH and ETH, Zurich)

B. Senor Chip: Streptavidin coated chip- SA (Biacore).

C. Running buffer: 50 mM Tris-HCl; pH 7.5,100 mM KCl and 20 mM $MgCl_2$.

5.7.4.1 Immobilization of the samples on the sensor chip

I. Place the running buffer in the system.
II. Eject the autosampler (sample holder) and place all the required samples at the appropriate positions.
III. Command- Eject Chip-Insert the SA chip-dock the chip.
IV. Prime the system. (This step flushes running buffer through the system).

V. Begin ‘Manual Run’ on flow cells 1 and 2 or the flow cells 3 and 4 (Out of the four flow cells on the SA chip, two flow cells were needed for the experiment, one as a control and another for the RNA immobilization).
VI. Condition the SA chip on flow cell 1 and 2 by injecting conditioning solution (1 M NaCl, 50 mM NaOH) at the flow rate of 30 µL/ minute for 60 seconds. Perform this step three times.
VII. End the manual run.
VIII. Begin a new manual run only on flow cell 1.
IX. Inject 1 µM of biotinylated DNA oligo sample on the flow cell 1 at the flow rate of 10 µL/ minute for 5 minutes. Repeat the injection if needed.
X. End the manual run on flow cell 1.
XI. Begin the new manual run on flow cell 2.
XII. Inject the biotinylated DNA- RNA sample on flow cell 2 at the flow rate of 10 µL/ minute for 5 minutes. Repeat the injection if needed.
XIII. Change the flow rate to 1 µL/ minute.
XIV. Inject the RNA only sample on flow cell 2 for 10 minutes. Check for the immobilization levels and repeat the injection if necessary.
XV. End the manual run on flow cell 2.
XVI. This procedure completes the immobilization of the samples on the sensor surface.

5.7.4.2 Setup for the kinetics

Before running the kinetics on the surface, check the activity of the surface by trial injections of the appropriate concentration of analyte to confirm the significant binding levels achieved from the interaction. See also Reference (43) for more details.

For the kinetics, follow the commands in the given sequence:

I. Run- Wizard- Assay- Kinetics/Affinity- New- Flow path (2-1) or (4-3)
II. Enter the contact time, the flow rate and the dissociation time.
III. Run at least ten start up cycles with the running buffer for the better stabilization of the sensor surface.
IV. Enter the concentration series under the study including the zero concentration (i.e. running buffer only).
V. Fill the vials with the appropriate solutions and place those in the autosampler. Dark conditions were observed while working with AdoCbl samples.
VI. Run the kinetics at 25 °C.

5.7.4.3 Evaluation of the data

I. Open the Biacore evaluation software.
II. Open the kinetics data- Kinetics/Affinity- Surface bound.
III. Select the sensorgrams and correct for blank subtraction.
IV. Go to Affinity/Kinetics- Choose the models and enter the parameters for fitting the data to the models (select for RI change, global/ local Rmax).
V. Perform the fitting and choose the best fitted model to analyze the interaction.

5.7.5 Calculation of K_D

The K_D was calculated from the kinetic parameters of the two fitted experiments to the given model. The weighted mean of k_a and k_d with their absolute errors (E) were calculated from the derived k_a and k_d of the two best fitted experiments. The fractional error for the k_a and the k_d is calculated from their weighted mean and absolute error as E_{ka} / k_a and E_{kd} /k_d respectively. These fractional errors (for k_a and k_d) were added to give a combined fractional error, E_c. The K_D is the ratio of the weighted mean of k_d and weighted mean of k_a ($K_D = k_d/ k_a$). The final error is represented as K_D* E_c.

5.8 References

1. Piehler, J. (2005) New methodologies for measuring protein interactions *in vivo* and *in vitro*. *Curr Opin Struct Biol*, **15 (1)**, 4-14.
2. Cantor, C.R. and Schimmel, P.R. (1980) *Biophysical Chemistry*, **Vol. III**, W. H. Freeman, San Fransisco.
3. Jonsson, U., Fagerstam, L., Ivarsson, B., Johnsson, B., Karlsson, R., Lundh, K., Lofas, S., Persson, B., Roos, H., Ronnberg, I. *et al.* (1991) Real-time biospecific interaction analysis using surface plasmon resonance and a sensor chip technology. *Biotechniques*, **11**, 620-627.
4. Liedberg, B., Nylander, C. and Lundstrom, I. (1995) Biosensing with surface plasmon resonance--how it all started. *Biosens Bioelectron*, **10**, i-ix.
5. Malmqvist, M. (1993) Biospecific interaction analysis using biosensor technology. *Nature*, **361**, 186-187.
6. Szabo, A., Stolz, L. and Granzow, R. (1995) Surface plasmon resonance and its use in biomolecular interaction analysis (BIA). *Curr Opin Struct Biol*, **5**, 699-705.
7. Fisher, R.J. and Fivash, M. (1994) Surface plasmon resonance based methods for measuring the kinetics and binding affinities of biomolecular interactions. *Curr Opin Biotechnol*, **5**, 389-395.
8. Malmqvist, M. (1993) Surface plasmon resonance for detection and measurement of antibody-antigen affinity and kinetics. *Curr Opin Immunol*, **5**, 282-286.
9. Morton, T.A. and Myszka, D.G. (1998) Kinetic analysis of macromolecular interactions using surface plasmon resonance biosensors. *Methods Enzymol*, **295**, 268-294.
10. Myszka, D.G. and Rich, R.L. (2000) Implementing surface plasmon resonance biosensors in drug discovery. *Pharm Sci Technolo Today*, **3**, 310-317.
11. O'Shannessy, D.J. (1994) Determination of kinetic rate and equilibrium binding constants for macromolecular interactions: a critique of the surface plasmon resonance literature. *Curr Opin Biotechnol*, **5**, 65-71.
12. O'Shannessy, D.J., Brigham-Burke, M., Soneson, K.K., Hensley, P. and Brooks, I. (1994) Determination of rate and equilibrium binding constants for macromolecular interactions by surface plasmon resonance. *Methods Enzymol*, **240**, 323-349.
13. Roos, H., Karlsson, R., Nilshans, H. and Persson, A. (1998) Thermodynamic analysis of protein interactions with biosensor technology. *J Mol Recognit*, **11**, 204-210.
14. Torreri, P., Ceccarini, M., Macioce, P. and Petrucci, T.C. (2005) Biomolecular interactions by Surface Plasmon Resonance technology. *Ann Ist Super Sanita*, **41**, 437-441.
15. Baird, C.L., Courtenay, E.S. and Myszka, D.G. (2002) Surface plasmon resonance characterization of drug/liposome interactions. *Anal Biochem*, **310**, 93-99.

16. Cannon, M.J., Myszka, D.G., Bagnato, J.D., Alpers, D.H., West, F.G. and Grissom, C.B. (2002) Equilibrium and kinetic analyses of the interactions between vitamin B_{12} binding proteins and cobalamins by surface plasmon resonance. *Anal Biochem*, **305**, 1-9.
17. de Mol, N.J., Dekker, F.J., Broutin, I., Fischer, M.J. and Liskamp, R.M. (2005) Surface plasmon resonance thermodynamic and kinetic analysis as a strategic tool in drug design. Distinct ways for phosphopeptides to plug into Src- and Grb2 SH2 domains. *J Med Chem*, **48**, 753-763.
18. Fagerstam, L.G., Frostell, A., Karlsson, R., Kullman, M., Larsson, A., Malmqvist, M. and Butt, H. (1990) Detection of antigen-antibody interactions by surface plasmon resonance. Application to epitope mapping. *J Mol Recognit*, **3**, 208-214.
19. Katsamba, P.S., Park, S. and Laird-Offringa, I.A. (2002) Kinetic studies of RNA-protein interactions using surface plasmon resonance. *Methods*, **26**, 95-104.
20. Margulies, D.H., Plaksin, D., Khilko, S.N. and Jelonek, M.T. (1996) Studying interactions involving the T-cell antigen receptor by surface plasmon resonance. *Curr Opin Immunol*, **8**, 262-270.
21. Myszka, D.G., Arulanantham, P.R., Sana, T., Wu, Z., Morton, T.A. and Ciardelli, T.L. (1996) Kinetic analysis of ligand binding to interleukin-2 receptor complexes created on an optical biosensor surface. *Protein Sci*, **5**, 2468-2478.
22. Ohlson, S. (2008) Designing transient binding drugs: a new concept for drug discovery. *Drug Discov Today*, **13**, 433-439.
23. Roden, L.D. and Myszka, D.G. (1996) Global analysis of a macromolecular interaction measured on BIAcore. *Biochem Biophys Res Commun*, **225**, 1073-1077.
24. Salamon, Z., Macleod, H.A. and Tollin, G. (1997) Surface plasmon resonance spectroscopy as a tool for investigating the biochemical and biophysical properties of membrane protein systems. I: Theoretical principles. *Biochim Biophys Acta*, **1331**, 117-129.
25. Tseng, M.C. and Chu, Y.H. (2005) Using surface plasmon resonance to directly identify molecules in a tripeptide library that bind tightly to a vancomycin chip. *Anal Biochem*, **336**, 172-177.
26. Wilson, D.W. (2002) Analyzing Biomolecular Interactions. *Science*, **295**, 2103-2105.
27. Kretschmann, E. and Raether, H. (1968) Radiative decay of non-radiative surface plasmons excited by light. *Z. Naturforsch*, **23A**, 2135-2136.
28. Otto, A. (1968) Excitation of surface plasma waves in silver by the method of frustrated total reflection. *Z. Physik*, **216**, 398-410.
29. Daghestani, H.N. and Day, B.W. (2010) Theory and applications of surface plasmon resonance, resonant mirror, resonant waveguide grating, and dual polarization interferometry biosensors. *Sensors (Basel)*, **10**, 9630-9646.
30. Homola, J. (2003) Present and future of surface plasmon resonance biosensors. *Anal Bioanal Chem*, **377**, 528-539.
31. Fagerstam, L.G., Frostell-Karlsson, A., Karlsson, R., Persson, B. and Ronnberg, I. (1992) Biospecific interaction analysis using surface plasmon resonance detection applied to kinetic, binding site and concentration analysis. *J Chromatogr*, **597**, 397-410.
32. Johnsson, B., Lofas, S. and Lindquist, G. (1991) Immobilization of proteins to a carboxymethyldextran-modified gold surface for biospecific interaction analysis in surface plasmon resonance sensors. *Anal Biochem*, **198**, 268-277.
33. Sjolander, S. and Urbaniczky, C. (1991) Integrated fluid handling system for biomolecular interaction analysis. *Anal Chem*, **63**, 2338-2345.

34. Stenberg, E., Persson, B., Roos, H. and Urbaniczky, C. (1991) Quantitative determination of surface concentration of protein with surface plasmon resonance by using rediolabeled proteins. *J Colloid Interface Sci*, **143**, 513-526.
35. Myszka, D.G., He, X., Dembo, M., Morton, T.A. and Goldstein, B. (1998) Extending the range of rate constants available from BIACORE: interpreting mass transport-influenced binding data. *Biophys J*, **75**, 583-594.
36. Zhang, J., Lau, M.W. and Ferre-D'Amare, A.R. (2010) Ribozymes and riboswitches: modulation of RNA function by small molecules. *Biochemistry*, **49**, 9123-9131.
37. Perdrizet, G.A., 2nd, Artsimovitch, I., Furman, R., Sosnick, T.R. and Pan, T. (2012) Transcriptional pausing coordinates folding of the aptamer domain and the expression platform of a riboswitch. *Proc Natl Acad Sci USA*, **109**, 3323-3328.
38. Johnson, J.E., Jr., Reyes, F.E., Polaski, J.T. and Batey, R.T. (2012) B_{12} cofactors directly stabilize an mRNA regulatory switch. *Nature*, **492**, 133-137.
39. Peselis, A. and Serganov, A. (2012) Structural insights into ligand binding and gene expression control by an adenosylcobalamin riboswitch. *Nat Struct Mol Biol*, **19**, 1182-1184.
40. Nahvi, A., Sudarsan, N., Ebert, M.S., Zou, X., Brown, K.L. and Breaker, R.R. (2002) Genetic control by a metabolite binding mRNA. *Chem Biol*, **9**, 1043-1049.
41. Karlsson, R. and Stahlberg, R. (1995) Surface plasmon resonance detection and multispot sensing for direct monitoring of interactions involving low-molecular-weight analytes and for determination of low affinities. *Anal Biochem*, **228**, 274-280.
42. Hahnefeld, C., Drewianka, S. and Herberg, F.W. (2004) Determination of kinetic data using surface plasmon resonance biosensors. *Methods Mol Med*, **94**, 299-320.
43. Biacore. Biacore T100 software handbook, GE Healthcare, BR-1006-48 AE 07/2008.
44. Blundell, M., Craig, E. and Kennell, D. (1972) Decay rates of different mRNA in *E. coli* and models of decay. *Nature New Biol*, **238**, 46-49.
45. Pedersen, M., Nissen, S., Mitarai, N., Lo Svenningsen, S., Sneppen, K. and Pedersen, S. (2011) The functional half-life of an mRNA depends on the ribosome spacing in an early coding region. *J Mol Biol*, **407**, 35-44.
46. Gallo, S., Oberhuber, M., Sigel, R.K. and Krautler, B. (2008) The corrin moiety of coenzyme B_{12} is the determinant for switching the *btuB* riboswitch of *E. coli*. *Chembiochem*, **9**, 1408-1414.
47. Straume, D., Johansen, R.F., Bjoras, M., Nes, I.F. and Diep, D.B. (2009) DNA binding kinetics of two response regulators, PlnC and PlnD, from the bacteriocin regulon of Lactobacillus plantarum C11. *BMC Biochem*, **10**, 17.
48. Gruber, K., Puffer, B. and Krautler, B. (2011) Vitamin B_{12}-derivatives-enzyme cofactors and ligands of proteins and nucleic acids. *Chem Soc Rev*, **40**, 4346-4363.
49. Serganov, A. and Patel, D.J. (2012) Metabolite recognition principles and molecular mechanisms underlying riboswitch function. *Annu Rev Biophys*, **41**, 343-370.
50. Mandal, M. and Breaker, R.R. (2004) Gene regulation by riboswitches. *Nature Rev Mol Cell Bio*, **5**, 451-463.
51. Nou, X.W. and Kadner, R.J. (2000) Adenosylcobalamin inhibits ribosome binding to *btuB* RNA. *P Natl Acad Sci USA*, **97**, 7190-7195.
52. Wickiser, J.K., Winkler, W.C., Breaker, R.R. and Crothers, D.M. (2005) The speed of RNA transcription and metabolite binding kinetics operate an FMN riboswitch. *Mol Cell*, **18**, 49-60.

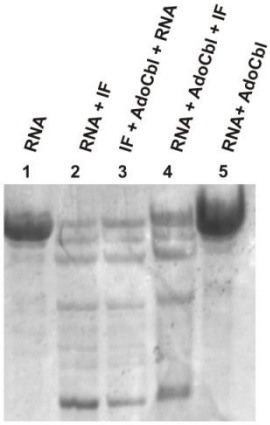

Figure 5.21: In-line probing of the *btuB* riboswitch with intrinsic factor: The *btuB* riboswitch (10 µM) was incubated with 3.2 units of intrinsic factor (IF) and 200 nM of AdoCbl followed by in-line probing for 20 hours at pH 7.5. Lane 1: RNA in reaction buffer; Lane 2: RNA incubated with IF; Lane 3: IF incubated with AdoCbl for 20 minutes followed by addition of the RNA; Lane 4: RNA incubated with AdoCbl for 20 minutes followed by addition of IF; Lane 5: RNA incubated with AdoCbl.

5.9 Additional experiments

5.9.1 Competition experiments between AdoCbl and intrinsic factor to bind the *btuB* riboswitch

The mode of interaction between the *btuB* riboswitch and AdoCbl was attempted first with the use of intrinsic factor (IF), a protein that binds to AdoCbl. The aim behind this study was to set up a competition between the intrinsic factor and the *btuB* RNA to bind AdoCbl and to check if the proportion of the switched RNA remains the same or gets altered.

In the pilot in-line probing experiment, the intrinsic factor degraded the *btuB* RNA even though the incubation for in-line cleavage reaction was done only for 20 hours instead of 40 hours (Figure 5.21). Although the *btuB* RNA was cleaved upon addition of IF, the cleavage was less when the *btuB* RNA was incubated with AdoCbl before the addition of IF. To avoid problems with the cleavage of the RNA, the IF (MW = 57 KDa) was purified by 30 kDa Vivaspin centrifugation to remove any contamination.

The in-line probing experiment was carried out with the purified IF at pH 7.5 for 20 hours (Figure 5.22) to compare degradation of RNA to the experiment carried out with the non-purified protein (Figure 5.21). The purified protein degraded the RNA much less than the non-purified protein. The lanes 1-3 in Figure 5.22 indicate the addition of *btuB* RNA to a complex of IF + AdoCbl (with varying ratios). Increased proportion of IF over AdoCbl increases RNA cleavage as evident from the full-length band (lanes 1-3, Figure 5.22). The lanes 4 and 5 in Figure 5.22 indicate the cleavage of *btuB* RNA but the presence of IF (lane 4) cleaves the RNA more than in the absence of IF. The *btuB* RNA is cleaved also when IF is added to the complex of RNA-AdoCbl (lane 6, Figure 5.22). Lanes 7 and 8 represent the in-line probing reactions carried out at pH 8.3 in the absence and presence of AdoCbl. These controls exhibit less cleavage of the *btuB* RNA but as the incubation was carried out only for 20 hours, the AdoCbl induced changes in the *btuB* RNA are not visible.

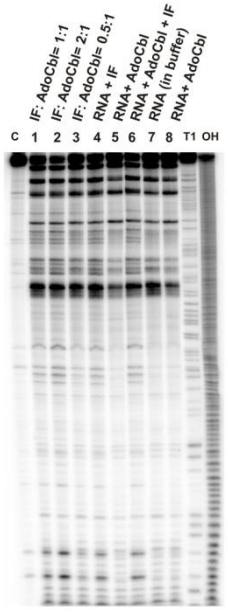

Figure 5.22: In-line probing of the *btuB* riboswitch with the purified intrinsic factor: In-line probing of 8 nM of 5' ^{32}P labelled *btuB* riboswitch with the purified IF: C: RNA in water. Lanes 1-3 indicate IF incubated with AdoCbl followed by addition of the RNA. The 1:1 ratio indicates 3.2 units of IF and 200 nM of AdoCbl. Lanes 4 : RNA incubated with 3.2 Units of IF; Lanes 5 and 8: RNA incubated with 200 nM of AdoCbl; Lane 6: RNA incubated with 200 nM of AdoCbl followed by addition of 3.2 units of IF; Lane 7 indicates RNA in the reaction buffer.

5.9.2 Laser photolysis of AdoCbl

As an alternative to the competition experiments with IF, laser photolysis of AdoCbl was carried out to study the mode of interaction between the *btuB* riboswitch and AdoCbl.

The relatively weak Co-C bond of AdoCbl undergoes photolysis upon exposure to light. This property of AdoCbl was exploited in order to study its interaction with the *btuB* RNA. The aim of this experiment was to photolyse AdoCbl in a time dependent manner after its interaction with the *btuB* RNA and to check if the proportion of the switched RNA changes.

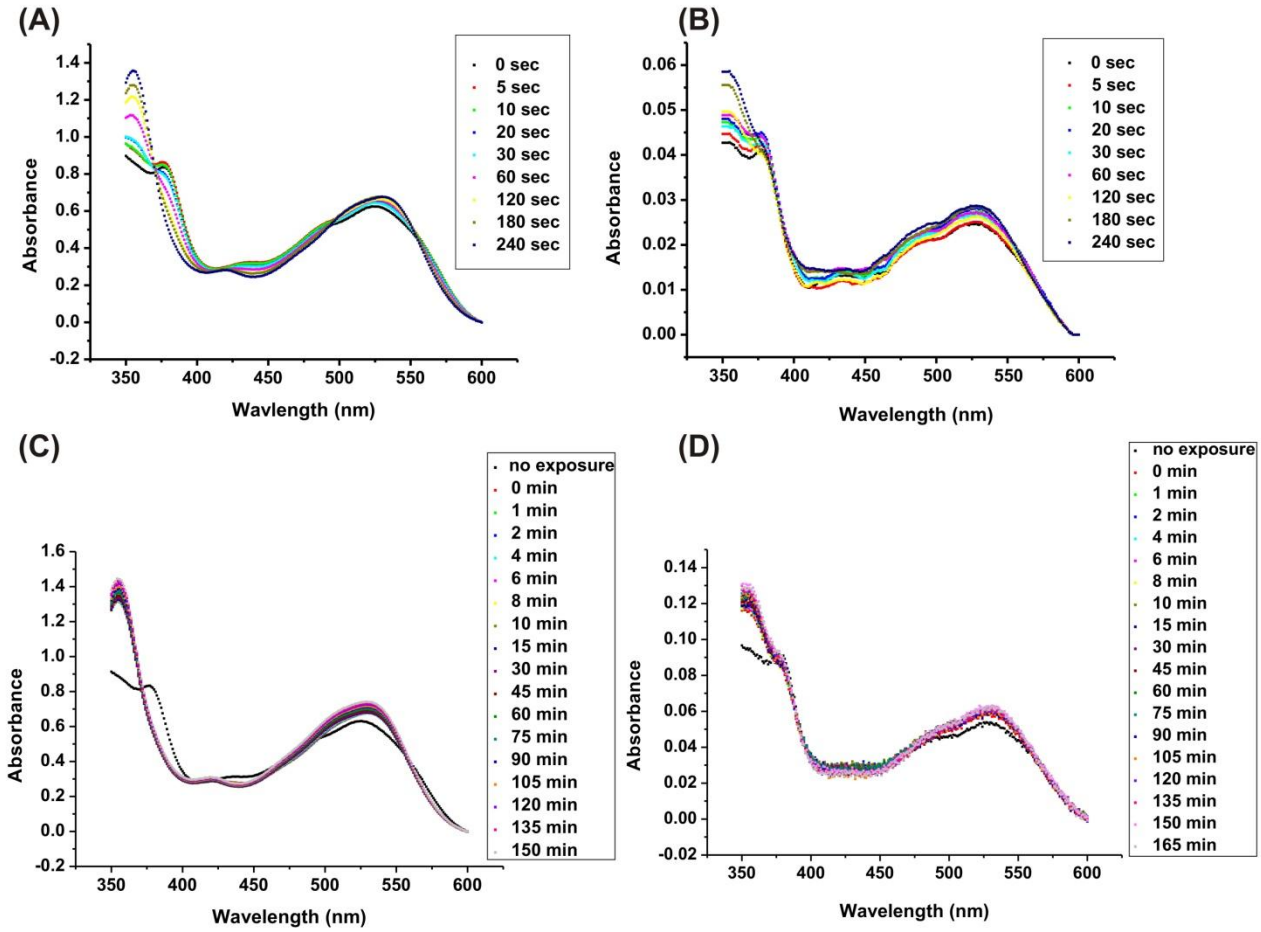

Figure 5.23: Laser photolysis of AdoCbl: shown are the UV-Vis spectra of 5 µM of AdoCbl after photolysis with red laser. (A) and (B) indicates the spectra of photolysed AdoCbl in the absence and presence of the 5 µM *btuB* RNA respectively after exposure to red laser for the indicated time period. The stability of photolysed product was checked by recording spectra of 5 µM AdoCbl after exposure to laser for 180 seconds in the absence (C) and presence of 5 µM *btuB* RNA(D) for an indicated time period.

The photolysis of AdoCbl was carried out with the help of a red laser (wavelength 650 nm). The laser mediated photolysis of AdoCbl was evident as the absorbance at 350 nm increases with increased exposure to laser (Figure 5.23 A). In the presence of the *btuB* RNA, the relative intensity of absorbance at 350 nm is less when compared to the one in the absence of the RNA, indicating a protection of AdoCbl when bound to the RNA (Figure 5.23 B). The photolysis of AdoCbl in the presence of the *btuB* RNA is evident after 180 seconds of laser exposure (Figure 5.23 B). The UV-Vis spectrum for AdoCbl was also observed for a certain time period after exposure to laser for 180 seconds both in absence (Figure 5.23 C) and presence of the *btuB* RNA (Figure 5.23 D). AdoCbl remains in the cleaved state both in the absence and presence of

the *btuB* RNA for almost up to 165 minutes. This is evident as the absorbance at 350 nm remains almost constant for the observed time period.

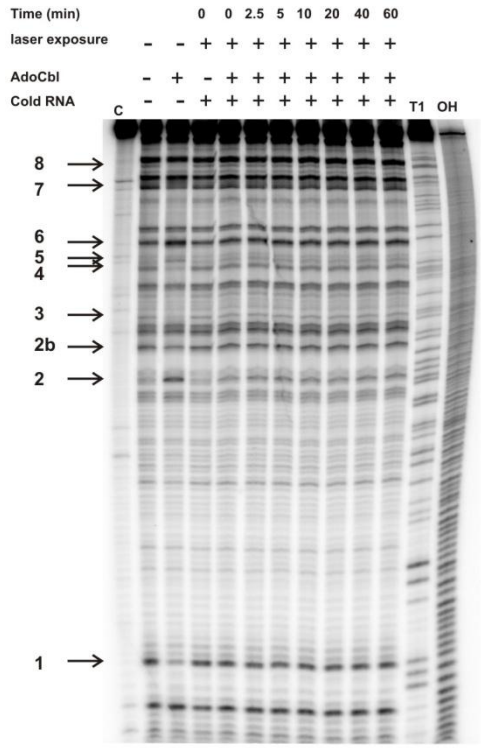

Figure 5.24: In-line probing of the *btuB* riboswitch with laser treated AdoCbl: The in-line probing was carried out with 8 nM of 5' ^{32}P labelled and 10 µM of the cold *btuB* RNA incubated with 1 µM of AdoCbl for 0-60 minutes. After the incubation, the samples were exposed to the laser for 180 seconds followed by in-line probing for 40 hours. Sites 1- 8 indicate AdoCbl induced modulations on the *btuB* riboswitch. C: RNA in water; T1: RNase T1 ladder; OH: Alkaline hydrolysis ladder.

An in-line probing experiment was carried out with the *btuB* riboswitch in combination with laser photolysis of AdoCbl. The ratio of the *btuB* RNA: AdoCbl was kept to 10:1 in order to have limited AdoCbl over the RNA. The first two lanes in Figure 5.24 represent the control in-line probing experiments (excess AdoCbl over RNA) and display AdoCbl induced changes in the *btuB* riboswitch (sites 1-8). The laser treatment does not alter the cleavage pattern of the RNA (lane 3, Figure 5.24). Lanes 4-10 indicate laser photolysis of AdoCbl for 180 seconds after interaction with the *btuB* RNA for the indicated time period (0-60 minutes) followed by 40 hours of in-line cleavage reaction. Except for site 2, the other AdoCbl induced changes on the *btuB* RNA were not evident in lanes 4-10. Also the intensity of cleavage at site 2 remains unaltered with increase in the incubation time between AdoCbl and the *btuB* RNA. Although, this experiment did not give much insight into the mode of interaction between the *btuB* riboswitch and AdoCbl, it certainly suggests that for complete switching of the *btuB* riboswitch an intact AdoCbl is necessary. Moreover, in the laser treated samples, the pattern of RNA cleavage remains almost the same in the absence and presence of AdoCbl - indicating that the *btuB* riboswitch probably falls back to the unswitched state upon the photolysis of AdoCbl.

6 Diversity of cobalamin riboswitches in the corrinoid-producing organohalide respirer *Desulfitobacterium hafniense*

Pallavi K. Choudhary[1], Aurélie Duret[2], Emmanuelle Rohrbach-Brandt[2], Christof Holliger[2], Roland K. O. Sigel[1], Julien Maillard[2#]

[1] *Institute of Inorganic Chemistry, University of Zurich, Winterthurerstrasse 190, 8057 Zurich, Switzerland.*

[2] *Ecole Polytechnique Fédérale de Lausanne (EPFL), School of Architecture, Civil and Environmental Engineering, Laboratory for Environmental Biotechnology, Station 6, CH-1015 Lausanne, Switzerland.*

Accepted in: J. Bacteriology, 2013, manuscript id: JB00730-13 (at the time of thesis submission, September 2013)

Key words: corrinoid, cobalamin riboswitches, *Desulfitobacterium*, in-line probing.

6.1 Abstract

The strategic adaptation of prokaryotes in polluted niches involves the efficient regulation of their metabolism. The obligate anaerobe and metabolically versatile *Desulfitobacterium hafniense* reductively dechlorinates halogenated organic compounds (so-called organohalides). Some *D. hafniense* strains carry out organohalide respiration (OHR), a process which requires the use of corrinoid as a cofactor in reductive dehalogenases, the key enzymes in OHR. We report here the diversity of the cobalamin riboswitches that possibly regulate the corrinoid metabolism for *D. hafniense*. The analysis of available *D. hafniense* genomes indicates the presence of eighteen cobalamin riboswitches located upstream of genes whose products are mainly involved in corrinoid biosynthesis and transport. To get insight into their function, the secondary structures of three of these RNA elements were predicted by Mfold as well as analyzed by in-line probing. These RNA elements display diversity in their structural elements as well as exhibit varying affinities towards adenosylcobalamin that possibly relates to their role in the regulation of corrinoid metabolism. Furthermore, adenosylcobalamin-induced *in vivo* repression of RNA synthesis of the downstream located genes indicates that the corrinoid transporters and biosynthetic enzymes in *D. hafniense* strain TCE1 are regulated at the transcriptional level. Taken together, the riboswitch-mediated regulation of the complex corrinoid metabolism in *D. hafniense* could be of crucial significance in environments polluted with organohalides to monitor their intracellular corrinoid level as well as to co-exist with corrinoid-auxotroph OHR bacteria.

6.2 Introduction

Corrinoids such as adenosylcobalamin (AdoCbl) represent the most complex of all cofactors and are the results of around 30 enzymatic reactions (1). The peculiarity of corrinoid-mediated enzymatic reactions and their mechanisms (see (2, 3) for reviews) has maintained the use of corrinoids in central metabolism. While most organisms (except higher plants) require corrinoids in their metabolism, only certain prokaryotes are able to synthesize them *de novo*. Depending on the presence of molecular oxygen, two routes were identified for corrinoid biosynthesis, namely the aerobic and the anaerobic pathways which differ mostly through the mechanism of tetrapyrrole ring contraction and the time for cobalt insertion (1). Salvaging corrinoid from the environment represents a cost-effective alternative to *de novo* synthesis. Escalante-Semerena and co-workers have described this process in many details in recent years (4-7). Their dedicated transporters and remodelling pathways allow the recycling of various forms of incomplete corrinoids into the final required cofactor.

The bacterial genus *Desulfitobacterium* belongs to the Gram-positive Firmicutes. Members of this genus are obligate anaerobic bacteria, most of which have been isolated from environments polluted with organohalides (8). Organohalide respiration (OHR, formerly named dehalo- or halorespiration) is the energy metabolism using organohalides, mostly chlorinated organic compounds, as terminal electron acceptors. The key catalytic enzyme in OHR is the reductive dehalogenase, a complex redox enzyme harbouring a corrinoid and two Fe/S clusters as cofactors (9). Unlike in well-known corrinoid-dependent enzymes, the electron-transfer reaction catalyzed by corrinoid-dependent reductive dehalogenases is yet mechanistically unresolved (10-12). Noteworthy, a new corrinoid, norpseudovitamin B_{12}, has been discovered in the tetrachloroethene reductive dehalogenase of *Sulfurospirillum multivorans* (13). So far only the genomes of *D. hafniense* strains Y51 (14) and DCB-2 (15) have been published, however several additional members of this genus are currently part of sequencing projects (http://jgi.doe.gov/).

Corrinoid metabolism in bacteria is largely regulated by RNA regulatory elements known as riboswitches (RS). RS are a class of non-coding RNAs that bind their cognate ligand with high specificity and affinity (16-18). Structurally, a riboswitch consists of an evolutionarily conserved aptamer domain and a variable expression platform (19, 20). Ligand binding to the aptamer brings about structural changes in both the aptamer and in the downstream expression platform leading to regulation of gene expression at various levels (21-25). Riboswitches sensing corrinoids (B_{12} derivatives), commonly named cobalamin riboswitches (abbreviated Cbl-RS in the present study), are prevalent throughout the bacterial kingdom and constitute the most complex class of riboswitches discovered so far (26, 27). These riboswitches mainly regulate the gene products associated with corrinoid biosynthesis and transport, porphyrin and cobalt transport, B_{12}-independent ribonucleotide reductase as well as enzymes involved in glutamate and succinate fermentation (28). Regulation of these gene products can take place either at translational or transcriptional level (29-31).

The aptamer of cobalamin riboswitches consists of a well organized secondary structure divided into distinct stems and loops. All of the cobalamin binding aptamers consist of a central four way junction that mostly forms the core ligand binding pocket (26, 32, 33). Cbl-RS were recently divided into two classes: i) aquocobalamin (AqCbl) and ii) adenosylcobalamin (AdoCbl) riboswitches depending on their cognate metabolite (32). In contrast to the AdoCbl class, the AqCbl class lacks the peripheral domain of the aptamer (stem P7-P11) (32). The solved crystal structure of two classes of Cbl-RS has indicated that the peripheral region of aptamers affects the conformation of the ligand-binding pocket making it more specific to bind AdoCbl (32, 33). Since the secondary structural elements define the specificity of Cbl-RS to a particular corrinoid derivative, it is of interest to explore Cbl-RS with diverse secondary structural elements.

The present study aims to reconsider the corrinoid biosynthesis pathway of *Desulfitobacterium* and to specifically investigate the diversity of cobalamin riboswitches. A combination of genome analysis, in-line probing experiments and *in vivo* transcription analysis reveals the complexity of the corrinoid metabolism in this bacterial genus.

6.3 Material & Methods

6.3.1 Bacterial strains, plasmids and growth conditions

E. coli DH5a was used to clone the DNA of cobalamin riboswitches for *in vitro* transcription, and their downstream genes for constructing the standards for quantitative PCR. *E. coli* was cultivated in Luria-Bertani (LB) medium, competent cells preparation and transformation were performed following standard procedures (34). Transformants containing derivatives of the pSG2 plasmid (35) or the pGEM-T Easy vector (Promega) were cultivated in LB medium supplemented with 100 µg/mL ampicillin. *Desulfitobacterium hafniense* strain TCE1 (DSM 12704) was cultivated as described in (36, 37) with the following modifications. Strain TCE1 was routinely cultivated with hydrogen and tetrachloroethene as electron donor and acceptor, respectively, and in absence of any corrinoid in the medium. For corrinoid pulse experiments, strain TCE1 was transferred to a medium containing 20 mM lactate in place of hydrogen. Half-way in the growth curve, corrinoid derivatives were added to a final concentration of 1 mg/L (0.63 µM), the cultures were incubated one more hour before collecting the biomass. Non-pulsed cultures were used as controls.

6.3.2 Genome analysis of cobalamin riboswitches and downstream genes

The Rfam database (http://rfam.sanger.ac.uk/) was initially used to identify distinct cobalamin riboswitches (Cbl-RS). Additional members of these riboswitch subfamilies were further detected in finished and unfinished genomes using Blast search (38). Sequence alignment and tree analysis were done using ClustalX 2.0 (39) and MEGA4 (40). Cbl-RS sequences were initially aligned based on conserved nucleotides. Then, predicted secondary RNA structures were identified in each riboswitch which allowed a manual correction of the alignment on the basis of conserved hairpins. The structure of *E. coli btuB* RS was used here as a model (26). Secondary structure prediction using Zucker Mfold (http://mfold.rna.albany.edu/?q=mfold/RNA-Folding-Form) (41) was further applied here. Potential transcription terminators were identified in the expression platform of Cbl-RS using ARNold (42).

6.3.3 Cloning and *in vitro* transcription of cobalamin riboswitches

Genomic DNA of *D. hafniense* strain TCE1 was obtained as described previously (43), and used as template for the amplification of three selected Cbl-RS sequences corresponding to RS07, RS08 and RS16. The primers used are listed in Table S1 (Supplementary information). Standard procedure of PCR amplification, ligation in the vector pSG2 (35), transformation and sequencing were applied as described earlier (43, 44). The RNA of the riboswitches RS07, RS08 and RS16 were obtained by *in vitro* transcription of the corresponding pSG2 plasmid derivatives by T7 RNA polymerase (45). The RNA was isolated by 10% acrylamide denaturing PAGE, purified by electroelution and concentrated by centrifugation using Vivaspin devices as described in (45). The RNA was stored in water at -20°C.

6.3.4 In-line probing

Ten nM of ^{32}P-5'- labelled RNA was incubated in the dark for 40 h in a buffer containing 50 mM Tris-HCl (pH 8.3), 20 mM $MgCl_2$ and 100 mM KCl in the absence or presence of AdoCbl. The reaction was quenched by the addition of equal volume of formamide gel loading buffer (82% (v/v formamide, 0.16% (w/v) xylene cynol, 0.16% (w/v) bromophenol blue,

10 mM EDTA, pH 8.0) and the samples were loaded on denaturing PAGE (10% acrylamide, 7 M urea). The RNase T1 and alkaline hydrolysis ladder were prepared as described in (46).

6.3.5 Calculation of apparent dissociation constants (K_D)

From the titration gels of in-line probing, the changes at each of the AdoCbl modulated sites for the aptamers of RS07, RS08 and RS16 riboswitches were plotted against the respective AdoCbl concentration after the background correction. The data points were then fitted to 1:1 binding isoterm (47) to derive the association constants (K_A) of AdoCbl to the modulated sites. The derived association constants are converted to the dissociation constants (K_D). The individual value of the affinity constants correspond to the weighted mean of the K_A values calculated from at least two titration gels for RS07, RS08 and RS16 unless otherwise indicated.

6.3.6 Reverse-transcription quantitative PCR

Partial genes (*Desulfitobacterium rpoB*, *btuF*, *cobT* and *cbi[ET]*) were cloned into the vector pGEM-T Easy (Promega) as described above to establish quantitative PCR (qPCR) standards. One µg of plasmids were linearized by 2 h digestion at 37°C with 5 units of *Sca*I restriction enzyme (Promega), dephosphorylated by 1 h incubation at 37°C with shrimp alkaline phosphatase (TaKaRa), and finally purified using the PCR purification kit (Qiagen). DNA concentration was measured with a NanoDrop ND-1000 apparatus. Standards were prepared by serial dilution from 10^7 to 10^2 copy number / µL. RNA extraction and reverse transcription (RT) were performed as described previously (48). Runs of qPCR consisted of the standard dilution series targeting a single gene and samples in triplicates. Each 10 µL qPCR reaction mixture was composed of 5 µL of KAPA SYBR® FAST Universal 2X qPCR Master Mix, 0.2 µL of each primer at 10 µM, 2.1 µL of sterile water and 2.5 µL of DNA template. The program consisted of 15 min of initial denaturation at 94°C, followed by 40 cycles of 30 s denaturation at 94°C, 20 s primer annealing at 60°C, and 30 s of elongation at 72°C after which acquisition of the fluorescence was done. A melting curve ranging from 50 to 99°C was added at the end for quality assessment. The reaction was run in the RotorGene RG3000 machine (Corbett Research). Data were analyzed using the RotorGene 6 software. The normalized repression factor (R_F) for a given target gene upon addition of a corrinoid was defined as the ratio of transcript copy numbers of a target gene (normalized with *rpoB* copy number measured in the culture batch) obtained without and with addition of the corrinoid.

6.4 Results

6.4.1 *De novo* synthesis of corrinoid by *Desulfitobacterium hafniense*

The corrinoid cofactor is essential for organohalide respiration and little is known so far on the corrinoid metabolism of the versatile OHR bacterial genus *D. hafniense*. In the present study, *D. hafniense* strain TCE1 was routinely cultivated for more than 40 successive culture transfers in a medium devoid of corrinoid under OHR conditions, which requires the corrinoid-dependent reductive dehalogenase. Figure 6.1 depicts the identical growth curves of strain TCE1 cultivated in presence or absence of corrinoid in the medium. This clearly confirmed the ability of *D. hafniense* to *de novo* synthesize corrinoid cofactors, as already suggested by the genome analysis and experimental data from *D. hafniense* strain Y51 (14, 49). The nomenclature of genes and proteins involved in corrinoid biosynthesis proposed by Nonaka *et al*. (14) was reconsidered here on the one hand to match the anaerobic pathway described by Roessner *et al*. (50) and more recently by Moore and Warren (1), and on the other to include the accessory steps responsible for synthesizing the nucleotide loop of cobalamin. This analysis was performed on the available genomes of *D. hafniense* strain Y51 (14) as well as strain DCB-2

(15), and the presence of these genes was also verified in the draft version of the genome of *D. hafniense* strain TCE1 (www.jgi.doe.gov; JGI project ID 403245) (Table 6.1).

The corrinoid biosynthesis pathway in *D. hafniense* (with *Dha*Y51 taken as example here) is organized in two main operons: DSY4071-4057 for major steps from Factor II to adenosylcobinamide (AdoCbi) and DSY2114-2116 for building up the nucleotide loop in adenosylcobalamin (AdoCbl). Both operons are predicted to be regulated by cobalamin riboswitches (Cbl-RS). The conversion of Co-precorrin-6B to Co-precorrin-8 is likely to be catalyzed by a single enzyme resulting from the fused domain of CbiE and CbiT (DSY4071, named here Cbi[ET]). Multiple cobalamin adenosyltransferases (CobA) are encoded in *D. hafniense* genomes, one of them (DSY4059) being part of the major biosynthetic operon. An additional CobA protein (DSY1561) is also shared by the three strains and is part of the methylmalonyl-CoA mutase operon, while another one (DSY3879) is under the regulation of a Cbl-RS.

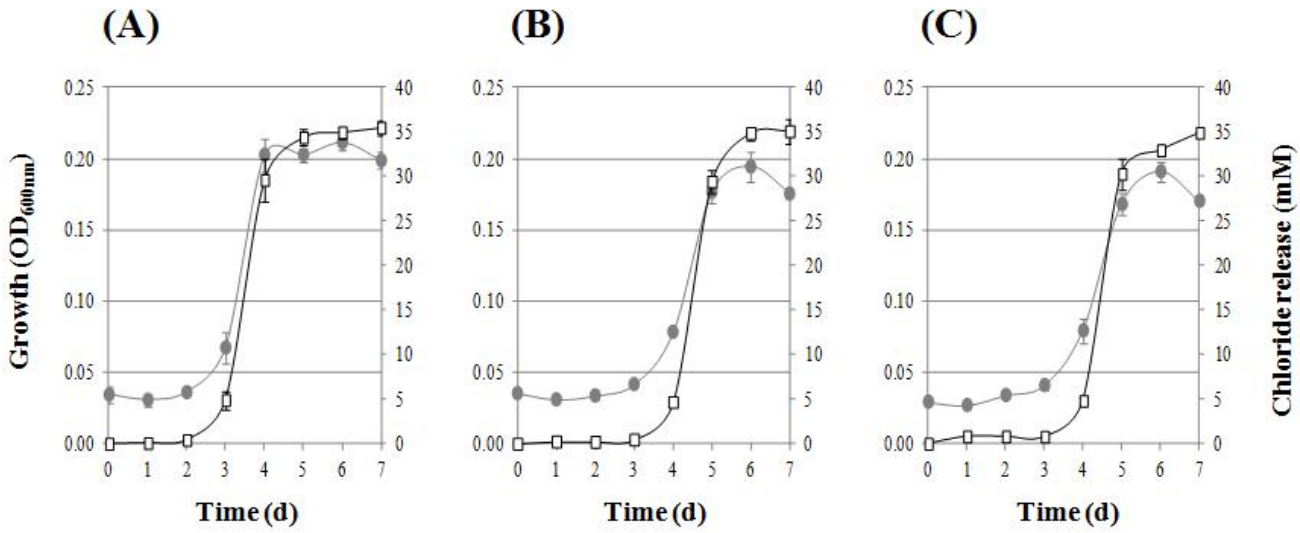

Figure 6.1: Growth curve of *D. hafniense* strain TCE1 in the presence or absence of CNCbl: Strain TCE1 was routinely cultivated in a medium containing 250 µg/L of CNCbl (A) and in a medium devoid of CNCbl (B) for more than 40 transfers. The inoculum used for (B) was also cultivated in a medium containing CNCbl (C). Triplicate cultures were performed and averaged. Grey circles indicate growth measured by optical density (600 nm), white squares show the concentration of chloride release in the culture supernatant upon PCE dechlorination.

6.4.2 Diversity of cobalamin riboswitches in *Desulfitobacterium hafniense* genomes

The initial analysis of *D. hafniense* strain Y51 genome for the presence of cobalamin riboswitches (Cbl-RS) using the Rfam online database revealed a high number of 16 different Cbl-RS. Members of these Cbl-RS subfamilies were also identified in two other *D. hafniense* genomes, namely strain DCB-2 (15), and strain TCE1 (Table 6.2). The latter was selected and used as model organism in the present study. Further analysis of the corresponding Rfam entries allowed extending to the complete riboswitch sequence, including both the aptamer domain and the expression platform. While strain TCE1 harbours the same diversity as strain Y51, strain DCB-2 showed 12 Cbl-RS from which 10 are identical to those of strains Y51 and TCE1. Two additional riboswitches were identified in strain DCB-2 making a total of 18 distinct Cbl-RS in *D. hafniense* (RS01-RS18, Figure S6.1). The sequence alignment of the 18 Cbl-RS along with the well characterized *E. coli btuB* riboswitch was manually corrected to align the conserved predicted secondary structures present in the aptamer domain (Figure 6.2 and Figure S6.2). While most of *D. hafniense* Cbl-RS contain both the core and peripheral regions (32), two of them, RS07 and RS18 only display the core region without the peripheral region bulging

from P7 (Figure 6.2). Another remarkable feature of those riboswitches compared with the structure of *E. coli btuB* is the absence of a P12 structure and in most cases of P9 as well. The expression platforms are very diverse in sequence and length (66-277 nt), all of them being significantly longer that the 34 nucleotides found in the *E. coli btuB* riboswitch which operates at translational level (31).

Table 6.1: Corrinoid biosynthesis pathway in *Desulfitobacterium hafniense.*

Biosynthetic steps	Gene [a]	*Dha*Y51 (DSY#)	*Dha*DCB-2 (Dhaf_#)	*Dha*TCE1 [b]	Annotated function in corrinoid biosynthesis
Precorrin-2					
↓	*cysG/sirC*	2227	3356	yes	Precorrin-2 dehydrogenase
Factor II					
↓	*cbiX*^{S}	4064	1302	yes	Sirohydrochlorin cobaltochelatase
Co(II)-factor II					
↓	*cbiL*	4070	1297	yes	Factor II C(20)-methyltransferase
Co(II)-factor III					
↓	*cbiH*	4066	1300	yes	Factor III C(17)-methyltransferase
Co(II)-precorrin-4					
↓	*cbiF*	4068	1298	yes	Precorrin-4 C(11)-methyltransferase
Co(II)-precorrin-5A					
↓	*cbiG*	4067	1299	yes	Precorrin-5A hydrolase
Co(II)-precorrin-5B					
↓	*cbiD*	4072	1295	yes	Precorrin-6A synthase
Co(II)-precorrin-6A					
↓	*cbiJ*	4065	1301	yes	Precorrin-6A reductase
Co(II)-precorrin-6B					
↓	*cbi[ET]*	4071	1296	yes	Precorrin-6Y C(5,15)-methyltransferase
Co(II)-precorrin-8					
↓	*cbiC*	4063	1303	yes	Precorrin-8X methylmutase
Cobyrinic acid					
↓	*cbiA*	4060 [c]	1306 [c]	yes	Cobyrinic acid a,c-diamide synthase
Cob(II)yrinic acid *a,c*-diamide					
↓	unknown	-	-	-	Cobyrinic acid a,c-diamide reductase
Cob(I)yrinic acid *a,c*-diamide					
↓	*cobA*	4059 [d]	1307 [d]	yes	Cob(I)alamin adenosyltransferase
Ado-cob(I)yrinic acid *a,c*-diamide					
↓	*cbiP*	4062	1304	yes	Adenosylcobyric acid synthase
Ado-cobyric acid					
↓	*cbiB*	4061	1305	yes	Adenosylcobinamide-phosphate synthase
↓	*pduX*	4058	1308	yes	L-threonine kinase
↓	*cobD*	4057	1309	yes	L-threonine-3-O-phosphate decarboxylase
Ado-cobinamide					
↓	*cobU*	2115	3286	yes	Cobinamide phosphate guanylyltransferase
Ado-cobinamide-GDP					
↓	*cobS*	2116	3287	yes	Cobalamin (5'-phosphate) synthase
↓	*cobC*	1979	3137	yes	Alpha-ribazole-5-phosphate phosphatase
↓	*cobT*	2114	3285	yes	Nicotinate-nucleotide-DMB phosphoribosyltransferase
Ado-cobalamin					

[a] Gene nomenclature for the anaerobic corrinoid biosynthesis pathway was taken from references (1,51).
[b] The draft version of *D. hafniense* strain TCE1 genome was analyzed for the presence of the genes, no locus was yet assigned.
[c] Additional candidates for *cbiA*: DSY0318, Dhaf_0262.
[d] Additional candidates for *cobA*: DSY1561 (also present in *Dha*DCB-2, Dhaf_2689, and *Dha*TCE1), DSY1853, DSY3879.
Underlined gene loci are located directly downstream of cobalamin riboswitches.

Typical transcription terminators were identified in most of them (Figure S6.2), suggesting that the regulation mechanism is taking place at the transcriptional rather than translational level. While most of the expression platforms end with a clear

ribosome binding site and start codon, two of them (RS04 and RS12) are directly followed by a second Cbl-RS and constitute tandem riboswitches (51), and another one (RS18) seems to be disrupted by the presence of a copy of IS*Dha8*, a common insertion sequence found in *D. hafniense* genomes (J. Maillard, unpublished data).

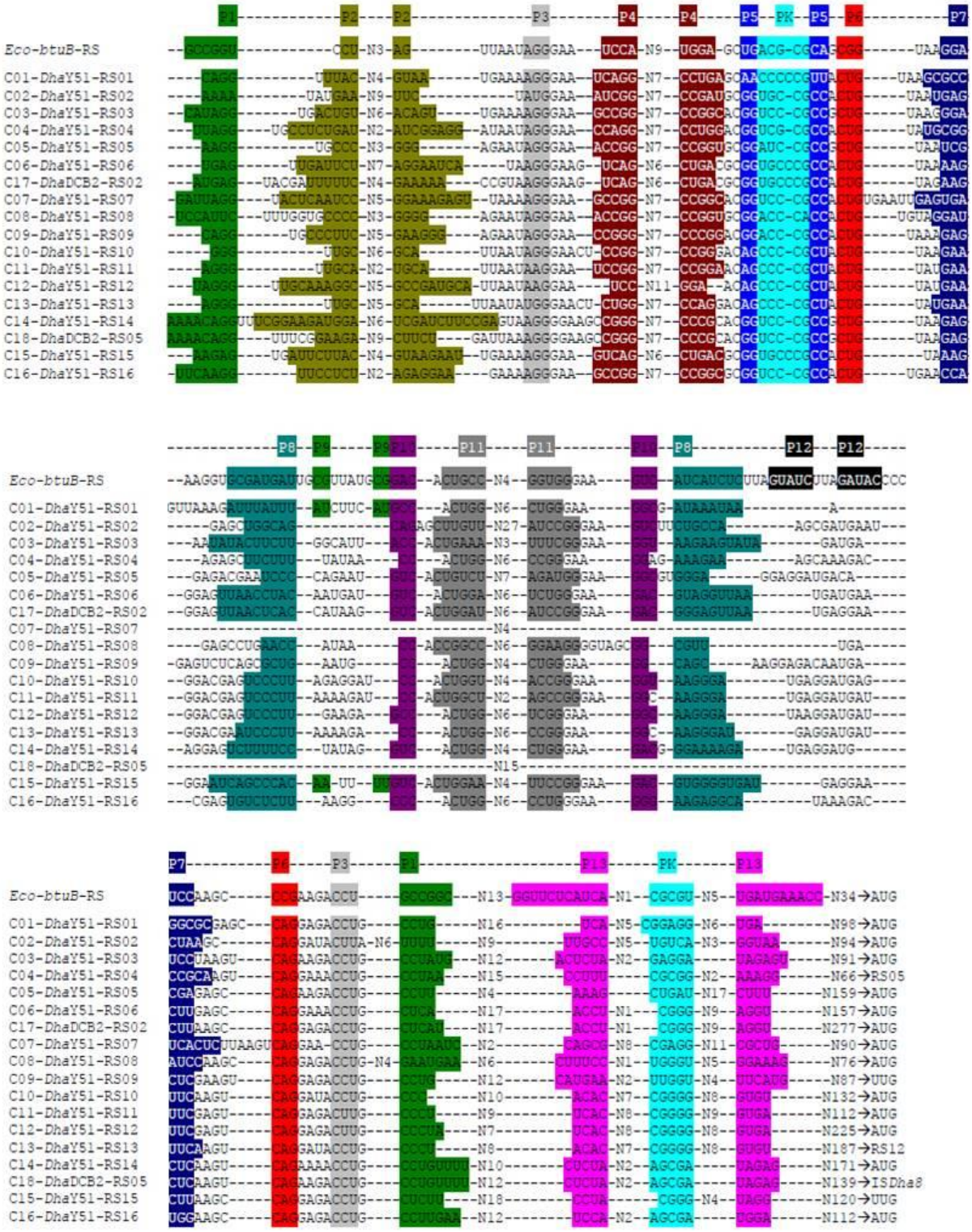

Figure 6.2: Sequence alignment of the aptamer of cobalamin riboswitch classes found in the genomes of *Desulfitobacterium hafniense*: Predicted secondary structures (shaded in colour boxes) were manually aligned to *E. coli btuB* riboswitch according to (56). Nucleotide stretches that are not participating in secondary structures are indicated as N#, where # is the number of nucleotides in the stretch. An extended version of this figure (including the expression platforms) is given in Figure S6.2 (Supplementary information).

Table 6.2: Cobalamin riboswitches of *Desulfitobacterium hafniense.*

Cluster	Present in [a]			Aptamer [b]	EP [c]	Operon [d]	COG [e]	Predicted function
	*Dha*Y51	*Dha*DCB-2	*Dha*TCE1	(nt)	(nt)			
C01	yes	yes	yes	189	98	DSY0087-0089	COG0614	ABC-type metal ions transporter
C02	yes	no	yes	205	94	DSY0362-0366	COG1348	Nitrogenase (*nif*) - ABC-type transporter
C03	yes	yes	yes	188	91	DSY0397-0395	COG1328	Anaerobic ribonucleoside triphosphate reductase
C04	yes	yes	yes	186	66 [f]	DSY1435-1439	COG0747	ABC-type nickel/dipeptide/oligopeptide transporter
C05	yes	yes	yes	184	159			
C06	yes	yes	yes	195	157	DSY1479-1482	-	ECF-type cobalt transporter
C07	yes	yes	yes	154	90	DSY2084-2086	COG0614	ABC-type metal ions transporter (*btu*)
C08	yes	yes	yes	186	76	DSY2114-2116	COG2038	NaMN:DMB phosphoribosyltransferase (*cobTUS*)
C09	yes	yes	yes	186	87	DSY2725-2720	-	Alpha-ribazole kinase and transporter (*cblST*)
C10	yes	yes	yes	184	132	DSY3840	-	Hypothetical protein
C11	yes	no	yes	184	112	DSY3859-3855	COG0811	MotA/TolQ/ExbB-type membrane transporter
C12	yes	no	yes	195	225	DSY3861	COG2207	AraC-type transcription regulator
C13	yes	no	yes	184	187 [f]			
C14	yes	no	yes	199	171	DSY3874-3872	COG0614	ABC-type metal ions transporter
C15	yes	no	yes	193	120	DSY3879	COG2109	Cob(I)alamin adenosyltransferase (*cobA*)
C16	yes	yes	yes	180	112	DSY4071-4057	COG2242	Precorrin-6Y C(5,15)-methyltransferase (*cbi[ET]*)
C17	no	yes	no	200	277	Dhaf_0035-0039	COG0747	ABC-type nickel/dipeptide/oligopeptide transporter
C18	no	yes	no	154	139 [g]	Dhaf_1527	COG3666	Transposase (IS*Dha8*)

[a] The member of the corresponding cluster that were used in sequence analysis and secondary structure alignments are underlined.
[b] Nucleotide length of the aptamer domain (from the first nucleotide of P1 to the last of P13; *E. coli btuB*: 206 nt).
[c] Nucleotide length of the expression platform (EP).
[d] Gene operon (locus tag of the representative member) located directly downstream of the riboswitch.
[e] COG number of the first gene located directly downstream of the riboswitch.
[f] Nucleotide length separating the first Cbl-RS from the second one in tandem Cbl-RS. Note that C13-C12 tandem RS are on the complementary DNA strand.
[g] Nucleotide length separating the DhaDCB2-Cbl-RS05 from the insertion sequence IS*Dha8*.

The predicted operons of *D. hafniense* that are under the regulation of Cbl riboswitches code for different metabolic pathways, most of which are related to corrinoid metabolism as expected (Table 6.2). RS08, RS15 and RS16 are directly linked to the corrinoid biosynthetic pathway by regulating the *cobTUS* operon, *cobA* and a predicted 15-gene operon encoding the major route to corrinoid, respectively (Table 6.1). Five riboswitches (RS01, RS04, RS07, RS14 and RS17) are involved in the regulation of ABC-type transporters, three of them likely transporting corrinoids (COG0614). In addition, RS02 regulates a *nifHE* operon possibly co-transcribed with another ABC-type transporter. A predicted ECF-type cobalt transporter is regulated by the RS06 and RS09 is located directly upstream of *cblS*, an alpha-ribazole kinase potentially involved in the production of the nucleotide loop of corrinoids (52). The riboswitch RS11 regulates an uncharacterized transporter operon, while the tandem riboswitch RS12-13 is likely to regulate a transcriptional regulator of the AraC-type.

6.4.3 *In vitro* activity of selected cobalamin riboswitches

Out of the 18 riboswitches involved in corrinoid metabolism of *D. hafniense*, the sequences from RS07, RS08 and RS16 were selected for confirming the activity of these sequences as riboswitches *in vitro*. These three riboswitch sequences fairly represent a diverse set of the genes involved in corrinoid metabolism in case of *D. hafniense*. The *in vitro* activity of the riboswitch sequences was confirmed by a classical method of in-line probing that exploits the spontaneous RNA cleavage to detect ligand-dependent structural alterations in the riboswitch in the absence of any accessory factors (29, 46). As adenosylcobalamin (AdoCbl/coenzyme B_{12}) is an active product of the corrinoid metabolism in the cell (30, 53), it is

used as a ligand in in-line probing experiments to measure its influence on the conformation of predicted riboswitches sequences.

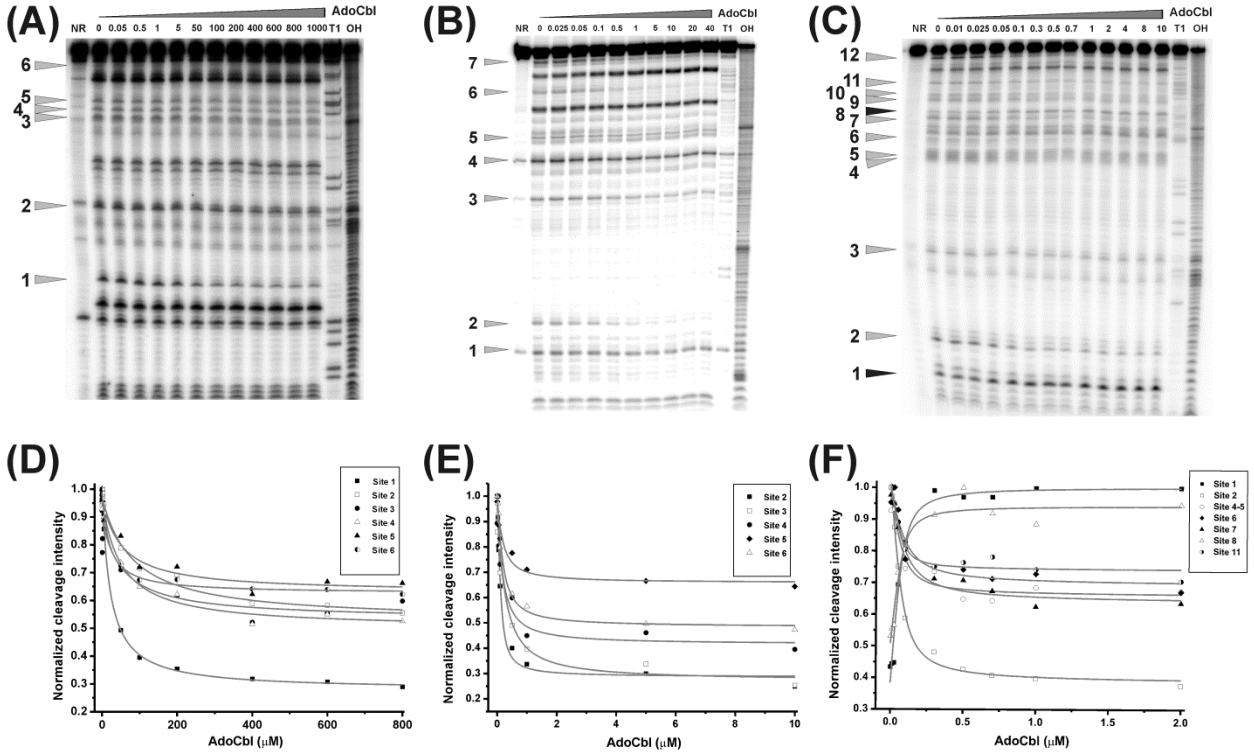

Figure 6.3: In-line probing and determination of the apparent K_D^{AdoCbl} of riboswitches RS07, RS08 and RS16: The titration with AdoCbl was carried out by in-line probing for the aptamers of RS07 (A), RS08 (B) and RS16 (C) with the indicated concentration range of AdoCbl (in µM). The grey and black arrows respectively indicate the decrease and increase in the cleavage intensity of the corresponding sites in the presence of AdoCbl. NR: RNA in pure water, T1: RNase T1 ladder, OH: Alkaline hydrolysis ladder. The normalized cleavage intensities at the cleavage sites for RS07 (D), RS08 (E) and RS16 (F) are plotted against AdoCbl concentrations. The data points for indicated sites are fitted to 1:1 binding isoterm (gray lines) to derive the apparent K_D.

As seen in Figure 6.3, in-line probing in the absence and presence of AdoCbl for the aptamer sequences of RS07, RS08 and RS16 reveals distinct changes in the riboswitch conformation. In the presence of AdoCbl, ligand-induced modifications occur at six, seven and twelve sites for the aptamers of RS07, RS08 and RS16 respectively. Therefore, the aptamer of RS07, RS08 and RS16 undergoes a conformational change upon direct interaction with AdoCbl. Noticeably, AdoCbl-induced conformational changes lead to a decrease in the cleavage intensity at the modulated sites for all three aptamer sequences except for sites 1 and 8 in the case of RS16 aptamer. Since the modulated cleavage intensities correspond to the geometry alterations at the corresponding nucleotides (54), it is probable that binding of AdoCbl leads to more structured regions in all three aptamer sequences compared to the ligand-free RNA conformation.

Table 6.3: Apparent association constants (K_A) of selected *D. hafniense* cobalamin riboswitches for AdoCbl.

Sites RS07	K_A -RS07 (1/µM)	Sites RS08	K_A -RS08 (1/µM)	Sites RS16	K_A -RS16 (1/µM)
Site 1	0.050 ± 0.008	Site 2	5.07 ± 1.66 [a]	Site 1	40.70 ± 5.85
Site 2	0.011 ± 0.000	Site 3	3.56 ± 0.86 [a]	Site 2	41.60 ± 8.06
Site 3	0.017 ± 0.001	Site 4	2.68 ± 1.80	Site 4-5	34.02 ± 17.14 [b]
Site 4	0.018 ± 0.002	Site 5	2.58 ± 1.51	Site 6	35.52 ± 2.66
Site 5	0.017 ± 0.001	Site 6	4.76 ± 1.02 [a]	Site 7	19.36 ± 2.05
Site 6	0.058 ± 0.020			Site 8	59.44 ± 40.64 [b]
				Site 11	65.54 ± 39.87 [b]
Average K_A (1/µM)	0.011 ± 0.003 [c]		3.85 ± 0.44		36.95 ± 4.34 [d]
K_D (µM)	90.91 ± 22.56		0.26 ± 0.03		0.027 ± 0.003

[a] average derived from three titrations; [b] value derived from one titration; [c] average excluding sites 1 and 6; [d] average excluding site 7

The relative affinity of riboswitches to AdoCbl helps to predict their role in the regulation of corrinoid metabolism. The apparent K_D value for ligand-aptamer complex formation can be derived from in-line probing by quantifying the ligand induced changes in the RNA cleavage over a range of AdoCbl concentration (55). We thus performed AdoCbl titration with the aptamer sequences from RS07, RS08 and RS16 and quantified the concentration dependent changes observed by in-line probing (Figure 6.3, Table 6.3, and Tables S6.2-S6.4, Supplementary information). In the case of the aptamer RS07, AdoCbl induces changes in the band intensity only at higher concentration (Figure 6.3, panels A and D) and therefore binds with weaker apparent affinity to RS07 than RS08 and RS16 (Table 6.3). Since the peripheral elements are essential to provide specificity to AdoCbl, the absence of peripheral stems P8- P11 in RS07 probably leads to its observed weaker affinity to AdoCbl. The aptamers of RS08 and RS16 have an affinity for AdoCbl in the mid and lower nanomolar range, respectively. Consequently, the cleavage sites are modulated at nanomolar concentrations of AdoCbl (Figure 6.3, panels B, C, E, and F). In comparison to the classical *btuB* riboswitch of *E. coli* (K_D = 90 nM) (56), the aptamers of RS07 and RS08 have almost 1000 and 30 fold lower affinity for AdoCbl. In contrast, RS16 aptamer has 3-fold higher affinity for AdoCbl than the *btuB* riboswitch with a K_D = 27 ± 3 nM.

To map the AdoCbl-induced conformational changes, the secondary structure of riboswitches was predicted using RNA secondary structure prediction algorithm by the Zucker Mfold program (41). The secondary structure was then refined by comparison with the alignment data (Figure S6.2) and the recently published crystal structures of Cbl-RS (32, 33) to yield a similar set of secondary structural elements (Figure 6.4 and Figure S6.3, Supplementary information). The predicted structures of RS07, RS08 and RS16 share the central four-way junction formed by stems P3-P4-P5-P6. Moreover, the peripheral elements P10, P11 and J11/10 in case of RS08 as well as RS16 are similar to *btuB* riboswitch and the secondary structure of the crystallized AdoCbl riboswitches. The sequences at loop L5 and L13 for RS07, RS08 and RS16 also indicate a strong possibility of AdoCbl induced kissing loop (KL) interaction similar to the one observed in crystal structure of the AdoCbl riboswitches (32, 33). The secondary structure for the aptamers of RS07, RS08 and RS16 therefore consist of the core region from stems P1-P6 similar to the known AdoCbl riboswitches whereas the non-conserved peripheral elements vary as indicated in Figure S6.3. The aptamer of RS07 lacks the peripheral elements from P8 to P12 whereas the aptamer of RS08 and RS16 carries P6 extension from P7-P11 with the absence of stems P9 and P12 in comparison to the classical *btuB* riboswitch from *E. coli*. When the ligand induced changes from in-line probing are mapped on the secondary structures of the riboswitches, these changes are scattered over the core region as well as in the peripheral domains for all three aptamers (Figure 6.4).

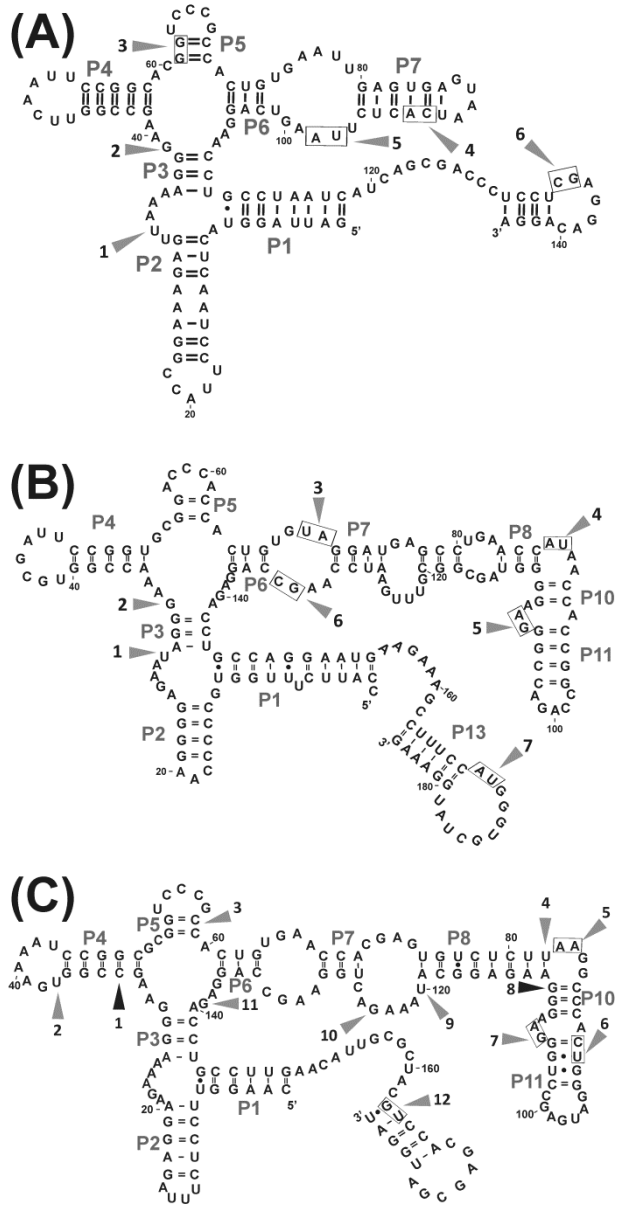

Figure 6.4: Mapping of AdoCbl induced changes on the secondary structures of the aptamers: The predicted secondary structure for the aptamer of RS07 (A), RS08 (B) and RS16 (C) is marked by the corresponding stems P1-P7 (A) and P1-P11 (B and C). The grey and black arrows respectively indicate the nucleotides undergoing decrease and increase in the cleavage intensity in the presence of AdoCbl in in-line probing. A rectangular box represents the group of nucleotides showing the indicated change marked by an arrow.

Therefore, the secondary structural elements from P1-P6 (core region) as well as from peripheral extension (P7-P11) are likely to be involved in the binding pocket for AdoCbl.

6.4.4 Corrinoid-dependent transcriptional repression of *D. hafniense btuF*, *cobT* and *cbi[ET]* genes

The three genes located directly downstream of the riboswitches RS07, RS08 and RS16 were targeted on RNA level to assess *in vivo* transcription regulation mediated by corrinoids in *D. hafniense* strain TCE1. Cultures of strain TCE1 routinely growing in absence of corrinoid in the medium were spiked with AdoCbl and CNCbl (1 mg/L (0.63 µM) final concentration) for 1 h before RNA was extracted. RT-qPCR targeting *btuF* (downstream of RS07), *cobT* (RS08), and *cbi[ET]* (RS16) along with *rpoB* (a constitutively expressed gene used to correct batch-dependent variations of transcription) clearly confirmed the reactivity of these riboswitches to AdoCbl, for which a normalized repression factor (R_F, as defined in the Material & Methods section) of 15.5, 9.0, and 13.0 for *btuF* (RS07), *cobT* (RS08) and *cbi[ET]* (RS16), respectively, was calculated (Figure 6.5, and Table S6.5, Supplementary information). In contrast, only a slight repression was obtained with CNCbl (R_F of 1.5, 1.8 and 2.1, respectively), strongly indicating that the upper adenosyl ligand in AdoCbl makes a significant contribution to riboswitch activity *in vivo*.

6.5 Discussion

The first published genome of *Desulfitobacterium* has revealed a full set of corrinoid biosynthetic genes (14). Recently Reinhold and co-workers have confirmed this genetic trait by cultivating *D. hafniense* strain Y51 without any addition of corrinoid in the medium (49). Confronting this knowledge with the well-characterized corrinoid anaerobic biosynthetic pathway (1), we re-annotated the full pathway and extended it to include the genomes of *D. hafniense* strains DCB-2 and TCE1, thus suggesting that *D. hafniense*, in contrast to *Dehalococcoides mccartyi*, is a versatile and corrinoid-prototroph OHR bacterium. It would be interesting to test whether *Desulfitobacterium*/*Dehalococcoides* co-cultures such as those

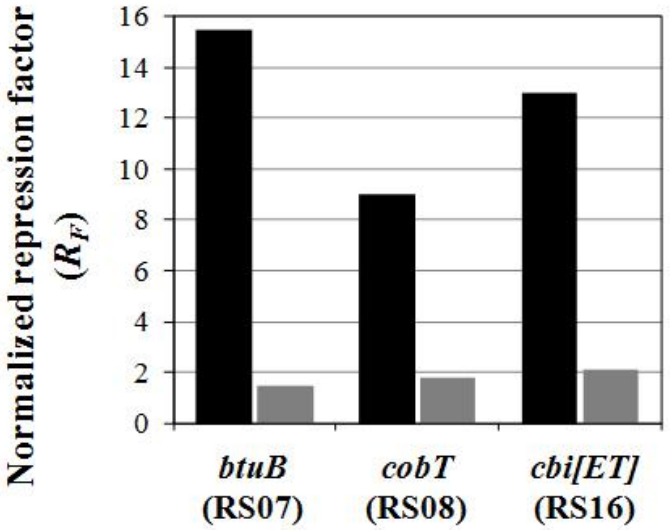

Figure 6.5: Corrinoid-mediated transcriptional repression of selected Cbl-RS dependent genes: The effect of corrinoid addition to *D. hafniense* strain TCE1 cultures routinely growing in absence of corrinoid was analyzed by quantitative RT-PCR on RNA extracted before and after addition of AdoCbl (black bars) or CNCbl (grey bars). The values are expressed as corrected repression factors (corr. R_F) which correspond to the ratio of gene copy number obtained before/after corrinoid addition corrected by the ratio obtained for the constitutive *rpoB* gene. For details, see Table S6.5 (Supplementary information).

obtained previously (57), would allow the latter to fully dechlorinate PCE without corrinoid addition in the medium, as it was shown in recent studies with *Geobacter* and other corrinoid producing bacteria (58, 59). Other OHR bacteria such as *Sulfurospirillum multivorans* (13), *Geobacter lovleyi* (60) and *Dehalobacter restrictus* (61) display a large variety of relationship to corrinoid biosynthesis, furthermore emphasizing the importance of studying individual model organisms.

Some particular features were identified among the corrinoid biosynthesis proteins of *D. hafniense*. The cobalt-chelatase protein CbiX of *Desulfitobacterium* is of archaeal type (Type IIa, $CbiX^S$), as initially postulated by Brindley *et al*. (62). While all classical proteins involved in synthesizing the nucleotide loop of cobalamin are encoded in the genomes of *D. hafniense* (CobU, CobT, CobS, CobC), the alternative pathway for synthesis of alpha-ribazole-5'-P described for *Listeria innocua* (52) is also present. Indeed, CblT (DSY2724) and CblS (DSY2725) respectively involved in alpha-ribazole transport across the membrane and alpha-ribazole phosphorylation, show 29% and 33% sequence identity with the characterized proteins of *L. innocua*, respectively, and are located in a predicted 6-gene operon (DSY2725-2720). While CblT in *L. innocua* was considered as a stand-alone transporter protein (52), CblT in *D. hafniense* could be part of an ECF-type complex with DSY2722 (CbiQ permease homolog) and DSY2723 (CbiO ATPase homolog) as previously suggested (63) for the specific transport of alpha-ribazole.

Besides *de novo* corrinoid biosynthesis, *D. hafniense* genomes harbour several putative corrinoid transporters (J. Maillard, unpublished data) suggesting that the corrinoid salvaging pathway is an alternative. Five operons among these transporter systems are regulated by cobalamin riboswitches, thus indicating their involvement in corrinoid transport. Furthermore, the BtuF homolog (corresponding to DSY2084 in *D. hafniense* strain Y51) was shown here to be down-regulated upon addition of AdoCbl due to the presence of the cobalamin riboswitch RS07.

A rich variety and apparent redundancy of corrinoid-dependent enzymes are also encoded in *D. hafniense* genomes. Next to the methylmalonyl-CoA mutase (DSY1563-5), the corrinoid-FeS protein of the Wood-Ljundahl pathway (DSY1648/1651, (64)), the glutamate mutase (DSY3235-6), the ethanolamine ammonia lyase (DSY4961-2) and the PCE reductive dehalogenase (DSY2839), a set of 15 different methyl-transferases were already identified in strain Y51 (14). Among the latter three are likely to be part of methylamine methyl-transferase systems and nine components of *O*-demethylases (J. Maillard, unpublished data), some of them being the subject of recent studies in *D. hafniense* strain DCB-2 (65-67). These multiple corrinoid-dependent pathways must have represented an ideal metabolic background for the likely recent acquisition of OHR metabolism by *D. hafniense* strain TCE1 (43).

The regulation of cobalamin transport and the synthesis of active cobalamin cofactor are achieved via cobalamin riboswitches (Cbl-RS) (27, 29, 53). The diversity of Cbl-RS has been explored in bacterial genera with 66 genomes predicted to contain approximately 200 Cbl-RS all together. Out of these Cbl-RS, 174 are complete (containing the core and peripheral structural elements) whereas 23 lack the peripheral region of the aptamer (27). The peripheral region of Cbl-RS, mainly stems P10 and P11, help creating a tight binding pocket for adenosylcobalamin as observed from the crystal structures of Cbl-RS from thermophilic prokaryotes (32, 33). Johnson *et al*. proposed that the Cbl-RS with or without the peripheral regions (stems P8 to P12) bind tightly to adenosylcobalamin or aquocobalamin, respectively (32). Here, all the 18 predicted Cbl-RS subfamilies from *D. hafniense* genomes contain the P1 to P7 secondary structural elements that constitute the ligand binding core but vary in terms of their organization at the peripheral region. Both aptamers, RS07 and RS18 lack the peripheral elements from stems P8 to P12, whereas the individual P9 and P12 secondary elements present in *E. coli btuB* Cbl-RS are missing in all other riboswitches in *D. hafniense*. Compared to the *E. coli btuB* Cbl-RS and to the crystal structures, all the predicted riboswitch sequences in *Desulfitobacterium* retain the structural elements involved in the kissing loop interaction (between L5 and L13) formed upon corrinoid binding (29, 32, 33). Therefore, all Cbl-RS in *Desulfitobacterium* probably undergo a similar tertiary conformational change upon binding to AdoCbl.

Although the AdoCbl induced structural changes could be similar for all three riboswitches studied here, their affinity to AdoCbl seems to vary. The apparent low affinity of RS07 to AdoCbl could be explained by the lack of peripheral structural elements as already suggested for a similar riboswitch (32), and rises the hypothesis of another physiologically relevant corrinoid ligand for RS07. However, *in vivo* the low affinity seemed to be overcome as the transcription of RS07 downstream located *btuF* gene was repressed when 0.63 µM of AdoCbl was added to the medium. A reason for the discrepancy between *in vitro* and *in vivo* data may reside in the actual physiological concentration and nature of the corrinoid sensed *in vivo* by the bacterial cells. Indeed, during the cellular uptake of AdoCbl by *D. hafniense* the corrinoid might be concentrated within the cell by the action of active transport and subjected to chemical transformation. The large difference in the *in vitro* measured affinities of the riboswitches RS07, RS08 and RS16 could also reflect the function of the gene products encoded in the corresponding downstream operons (the BtuFCD transporter, the synthesis of the nucleotide loop and the upper pathway of the corrinoid biosynthesis, respectively). Due to the large energetic cost of *de novo* corrinoid biosynthesis, it is reasonable to think that the expression of the upper pathway (regulated by RS16) should be the most rapidly shut down (K_D = 27 nM), while the synthesis of the nucleotide loop (RS08) might be required to remodel the lower ligand of the corrinoid and adapt it to the specific use by the bacterium (K_D = 260 nM). It also makes sense to see the production of corrinoid transporters (RS07) as the least sensitive event (K_D = 90 µM).

The mode of gene expression regulation of cobalamin riboswitches differs in Gram-negative and Gram-positive bacteria being executed at the translational and transcriptional level, respectively (27, 30, 68). All of the three aptamers studied here (RS07, RS08 and RS16) undergo a substantial transcriptional repression with AdoCbl (with up to 15-fold decrease in transcription), strongly arguing for a regulation at the level of transcription. This is in correlation with the identification of transcriptional terminators in the expression platform of those riboswitches, a feature that is shared by all but three riboswitches in *D. hafniense*.

D. hafniense available genomes with 16 cobalamin riboswitches in strains Y51 and TCE1 rank in the top-10 of bacteria with the highest number riboswitches according to Rfam database (RF00174, August 2012). The top-3 strains in this list, *Desulfosporosinus meridei* DSM 13257 (22 Cbl-RS), *Desulfotomaculum acetoxidans* DSM 771 (21 Cbl-RS), and *Desulfosporosinus orientis* DSM 765 (19 Cbl-RS) belong to the same phylogenetic group as *D. hafniense*, but were not yet recognized for their richness in Cbl-RS (69, 70). As highlighted in the present study, the diversity of cobalamin

riboswitches and the variety of metabolic traits regulated by those elements open future research directions for functional characterization of the rich corrinoid metabolism of *D. hafniense*.

6.6 Acknowledgements

Financial support by the European Research Council (ERC Starting Grant MIRNA 259092 to RKOS), the Swiss National Science Foundation (to RKOS) and UZH is gratefully acknowledged. AD was supported by the Swiss National Science Foundation grants 3100A0-108197 and 3100A0-120627. We are thankful to Dr. Maria Pechlaner for providing us the VARNA depicted secondary structures of the AdoCbl riboswitches.

6.7 References

1. Moore, S.J. and Warren, M.J. (2012) The anaerobic biosynthesis of vitamin B_{12}. *Biochem Soc Trans*, **40**, 581-586.
2. Gruber, K., Puffer, B. and Kräutler, B. (2011) Vitamin B_{12}-derivatives-enzyme cofactors and ligands of proteins and nucleic acids. *Chem Soc Rev*, **40**, 4346-4363.
3. Matthews, R.G. (2009) Cobalamin- and corrinoid-dependent enzymes. *Met Ions Life Sci*, **6**, 53-114.
4. Escalante-Semerena, J.C. (2007) Conversion of cobinamide into adenosylcobamide in bacteria and archaea. *J Bacteriol*, **189**, 4555-4560.
5. Gray, M.J. and Escalante-Semerena, J.C. (2009) The cobinamide amidohydrolase (cobyric acid-forming) CbiZ enzyme: a critical activity of the cobamide remodelling system of *Rhodobacter sphaeroides*. *Mol Microbiol*, **74**, 1198-1210.
6. Gray, M.J. and Escalante-Semerena, J.C. (2009) *In vivo* analysis of cobinamide salvaging in *Rhodobacter sphaeroides* strain 2.4.1. *J Bacteriol*, **191**, 3842-3851.
7. Gray, M.J., Tavares, N.K. and Escalante-Semerena, J.C. (2008) The genome of *Rhodobacter sphaeroides* strain 2.4.1 encodes functional cobinamide salvaging systems of archaeal and bacterial origins. *Mol Microbiol*, **70**, 824-836.
8. Villemur, R., Lanthier, M., Beaudet, R. and Lepine, F. (2006) The *Desulfitobacterium* genus. *FEMS Microbiol Rev*, **30**, 706-733.
9. Futagami, T., Goto, M. and Furukawa, K. (2008) Biochemical and genetic bases of dehalorespiration. *Chem Rec*, **8**, 1-12.
10. Banerjee, R. and Ragsdale, S.W. (2003) The many faces of vitamin B_{12}: catalysis by cobalamin-dependent enzymes. *Annu Rev Biochem*, **72**, 209-247.
11. Costentin, C., Robert, M. and Saveant, J.M. (2005) Does catalysis of reductive dechlorination of tetra- and trichloroethylenes by vitamin B_{12} and corrinoid-based dehalogenases follow an electron transfer mechanism? *J Am Chem Soc*, **127**, 12154-12155.
12. Kräutler, B. (2005) Vitamin B_{12}: chemistry and biochemistry. *Biochem Soc Trans*, **33**, 806-810.
13. Kräutler, B., Fieber, W., Ostermann, S., Fasching, M., Ongania, K.H., Gruber, K., Kratky, C., Mikl, C., Siebert, A. and Diekert, G. (2003) The cofactor of tetrachloroethene reductive dehalogenase of *Dehalospirillum multivorans* is norpseudo-B_{12}, a new type of a natural corrinoid. *Helvetica Chimica Acta*, **86**, 3698-3716.
14. Nonaka, H., Keresztes, G., Shinoda, Y., Ikenaga, Y., Abe, M., Naito, K., Inatomi, K., Furukawa, K., Inui, M. and Yukawa, H. (2006) Complete genome sequence of the dehalorespiring bacterium *Desulfitobacterium hafniense* Y51 and comparison with *Dehalococcoides ethenogenes* 195. *J Bacteriol*, **188**, 2262-2274.

15. Kim, S.H., Harzman, C., Davis, J.K., Hutcheson, R., Broderick, J.B., Marsh, T.L. and Tiedje, J.M. (2012) Genome sequence of *Desulfitobacterium hafniense* DCB-2, a Gram-positive anaerobe capable of dehalogenation and metal reduction. *BMC Microbiol*, **12**, 21.
16. Mironov, A.S., Gusarov, I., Rafikov, R., Lopez, L.E., Shatalin, K., Kreneva, R.A., Perumov, D.A. and Nudler, E. (2002) Sensing small molecules by nascent RNA: a mechanism to control transcription in bacteria. *Cell*, **111**, 747-756.
17. Sudarsan, N., Wickiser, J.K., Nakamura, S., Ebert, M.S. and Breaker, R.R. (2003) An mRNA structure in bacteria that controls gene expression by binding lysine. *Genes Dev*, **17**, 2688-2697.
18. Winkler, W., Nahvi, A. and Breaker, R.R. (2002) Thiamine derivatives bind messenger RNAs directly to regulate bacterial gene expression. *Nature*, **419**, 952-956.
19. Mandal, M. and Breaker, R.R. (2004) Gene regulation by riboswitches. *Nat Rev Mol Cell Biol*, **5**, 451-463.
20. Roth, A. and Breaker, R.R. (2009) The structural and functional diversity of metabolite-binding riboswitches. *Annu Rev Biochem*, **78**, 305-334.
21. Kubodera, T., Watanabe, M., Yoshiuchi, K., Yamashita, N., Nishimura, A., Nakai, S., Gomi, K. and Hanamoto, H. (2003) Thiamine-regulated gene expression of *Aspergillus oryzae thiA* requires splicing of the intron containing a riboswitch-like domain in the 5'-UTR. *FEBS Lett*, **555**, 516-520.
22. Loh, E., Dussurget, O., Gripenland, J., Vaitkevicius, K., Tiensuu, T., Mandin, P., Repoila, F., Buchrieser, C., Cossart, P. and Johansson, J. (2009) A trans-acting riboswitch controls expression of the virulence regulator PrfA in Listeria monocytogenes. *Cell*, **139**, 770-779.
23. Soukup, G.A. (2004) Aptamers meet allostery. *Chem Biol*, **11**, 1031-1032.
24. Winkler, W.C., Nahvi, A., Roth, A., Collins, J.A. and Breaker, R.R. (2004) Control of gene expression by a natural metabolite-responsive ribozyme. *Nature*, **428**, 281-286.
25. Winkler, W.C., Nahvi, A., Sudarsan, N., Barrick, J.E. and Breaker, R.R. (2003) An mRNA structure that controls gene expression by binding S-adenosylmethionine. *Nat Struct Biol*, **10**, 701-707.
26. Nahvi, A., Barrick, J.E. and Breaker, R.R. (2004) Coenzyme B_{12} riboswitches are widespread genetic control elements in prokaryotes. *Nucleic Acids Res*, **32**, 143-150.
27. Vitreschak, A.G., Rodionov, D.A., Mironov, A.A. and Gelfand, M.S. (2003) Regulation of the vitamin B_{12} metabolism and transport in bacteria by a conserved RNA structural element. *RNA*, **9**, 1084-1097.
28. Winkler, W.C. and Breaker, R.R. (2005) Regulation of bacterial gene expression by riboswitches. *Annu Rev Microbiol*, **59**, 487-517.
29. Nahvi, A., Sudarsan, N., Ebert, M.S., Zou, X., Brown, K.L. and Breaker, R.R. (2002) Genetic control by a metabolite binding mRNA. *Chem Biol*, **9**, 1043.
30. Nou, X. and Kadner, R.J. (2000) Adenosylcobalamin inhibits ribosome binding to *btuB* RNA. *Proc Natl Acad Sci USA*, **97**, 7190-7195.
31. Perdrizet, G.A., 2nd, Artsimovitch, I., Furman, R., Sosnick, T.R. and Pan, T. (2012) Transcriptional pausing coordinates folding of the aptamer domain and the expression platform of a riboswitch. *Proc Natl Acad Sci USA*, 109, 3323-3328.
32. Johnson Jr, J.E., Reyes, F.E., Polaski, J.T. and Batey, R.T. (2012) B_{12} cofactors directly stabilize an mRNA regulatory switch. *Nature*, **492**, 133-137.
33. Peselis, A. and Serganov, A. (2012) Structural insights into ligand binding and gene expression control by an adenosylcobalamin riboswitch. *Nat Struct Mol Biol*, **19**, 1182-1184.

34. Sambrook, J., Fritsch, E.F. and Maniatis, T. (1989) *Molecular cloning : a laboratory manual*. 2nd ed. Cold Spring Harbor Laboratory, New York.
35. Gallo, S., Oberhuber, M., Sigel, R.K.O. and Kräutler, B. (2008) The corrin moiety of coenzyme B_{12} is the determinant for switching the *btuB* riboswitch of *E. coli*. *Chembiochem*, **9**, 1408-1414.
36. Holliger, C., Hahn, D., Harmsen, H., Ludwig, W., Schumacher, W., Tindall, B., Vazquez, F., Weiss, N. and Zehnder, A.J. (1998) *Dehalobacter restrictus* gen. nov. and sp. nov., a strictly anaerobic bacterium that reductively dechlorinates tetra- and trichloroethene in an anaerobic respiration. *Arch Microbiol*, **169**, 313-321.
37. Maillard, J., Schumacher, W., Vazquez, F., Regeard, C., Hagen, W.R. and Holliger, C. (2003) Characterization of the corrinoid iron-sulfur protein tetrachloroethene reductive dehalogenase of Dehalobacter restrictus. *Appl Environ Microbiol*, **69**, 4628-4638.
38. Altschul, S., Gish, W., Miller, W., Myers, E. and Lipman, D. (1990) Basic alignment search tools. *J Mol Biol*, **215**, 403 - 410.
39. Larkin, M.A., Blackshields, G., Brown, N.P., Chenna, R., McGettigan, P.A., McWilliam, H., Valentin, F., Wallace, I.M., Wilm, A., Lopez, R. *et al.* (2007) Clustal W and Clustal X version 2.0. *Bioinformatics*, **23**, 2947-2948.
40. Tamura, K., Dudley, J., Nei, M. and Kumar, S. (2007) MEGA4: Molecular Evolutionary Genetics Analysis (MEGA) software version 4.0. *Mol Biol Evol*, **24**, 1596-1599.
41. Zuker, M. (2003) Mfold web server for nucleic acid folding and hybridization prediction. *Nucleic Acids Res*, **31**, 3406-3415.
42. Naville, M., Ghuillot-Gaudeffroy, A., Marchais, A. and Gautheret, D. (2011) ARNold: a web tool for the prediction of Rho-independent transcription terminators. *RNA Biol*, **8**, 11-13.
43. Duret, A., Holliger, C. and Maillard, J. (2012) The physiological opportunism of *Desulfitobacterium hafniense* strain TCE1 towards organohalide respiration with tetrachloroethene. *Appl Environ Microbiol*, **78**, 6121-6127.
44. Gallo, S. (2008), University of Zurich, Zurich.
45. Maillard, J., Genevaux, P. and Holliger, C. (2011) Redundancy and specificity of multiple Trigger Factor chaperones in *Desulfitobacteria*. *Microbiology*, **157**, 2410-2421.
46. Gallo, S., Furler, M. and Sigel, R.K.O. (2005) *In vitro* transcription and purification of RNAs of different size. *Chimia*, **59**, 812-816.
47. Choudhary, P.K., Gallo, S. and Sigel, R.K.O. (2014) Monitoring global structural changes and specific metal binding sites in RNA by in-line probing and Tb(III) cleavage. *Methods Mol Biol*, *in press.*
48. Sigel, R.K.O., Freisinger, E. and Lippert, B. (2000) Effects of N7-methylation, N7-platination, and C8-hydroxylation of guanine on H-bond formation with cytosine: platinum coordination strengthens the Watson-Crick pair. *J Biol Inorg Chem*, **5**, 287-299.
49. Prat, L., Maillard, J., Rohrbach-Brandt, E. and Holliger, C. (2012) An unusual tandem-domain rhodanese harbouring two active sites identified in *Desulfitobacterium hafniense*. *FEBS J*, **279**, 2754-2767.
50. Reinhold, A., Westermann, M., Seifert, J., von Bergen, M., Schubert, T. and Diekert, G. (2012) Impact of vitamin B_{12} on formation of the tetrachloroethene reductive dehalogenase in *Desulfitobacterium hafniense* strain Y51. *Appl Environ Microbiol*, **78**, 8025-8032.
51. Roessner, C.A. and Scott, A.I. (2006) Fine-tuning our knowledge of the anaerobic route to cobalamin (vitamin B_{12}). *J Bacteriol*, **188**, 7331-7334.

52. Brindley, A.A., Raux, E., Leech, H.K., Schubert, H.L. and Warren, M.J. (2003) A story of chelatase evolution: identification and characterization of a small 13-15-kDa "ancestral" cobaltochelatase ($CbiX^S$) in the archaea. *J Biol Chem*, **278**, 22388-22395.

53. Gray, M.J. and Escalante-Semerena, J.C. (2010) A new pathway for the synthesis of alpha-ribazole-phosphate in *Listeria innocua*. *Mol Microbiol*, **77**, 1429-1438.

54. Sudarsan, N., Hammond, M.C., Block, K.F., Welz, R., Barrick, J.E., Roth, A. and Breaker, R.R. (2006) Tandem riboswitch architectures exhibit complex gene control functions. *Science*, **314**, 300-304.

55. Rodionov, D.A., Vitreschak, A.G., Mironov, A.A. and Gelfand, M.S. (2003) Comparative genomics of the vitamin B_{12} metabolism and regulation in prokaryotes. *J Biol Chem*, **278**, 41148-41159.

56. Soukup, G.A. and Breaker, R.R. (1999) Relationship between internucleotide linkage geometry and the stability of RNA. *RNA*, **5**, 1308-1325.

57. Soukup, G.A., DeRose, E.C., Koizumi, M. and Breaker, R.R. (2001) Generating new ligand-binding RNAs by affinity maturation and disintegration of allosteric ribozymes. *RNA*, **7**, 524-536.

58. Rouzeau-Szynalski, K., Maillard, J. and Holliger, C. (2011) Frequent concomitant presence of *Desulfitobacterium* spp. and "*Dehalococcoides*" spp. in chloroethene-dechlorinating microbial communities. *Appl Microbiol Biotechnol*, **90**, 361-368.

59. Yan, J., Im, J., Yang, Y. and Loffler, F.E. (2013) Guided cobalamin biosynthesis supports *Dehalococcoides mccartyi* reductive dechlorination activity. *Philos Trans R Soc Lond B Biol Sci*, **368**, 20120320.

60. Yan, J., Ritalahti, K.M., Wagner, D.D. and Loffler, F.E. (2012) Unexpected specificity of interspecies cobamide transfer from *Geobacter* spp. to organohalide-respiring *Dehalococcoides mccartyi* strains. *Appl Environ Microbiol*, **78**, 6630-6636.

61. Wagner, D.D., Hug, L.A., Hatt, J.K., Spitzmiller, M.R., Padilla-Crespo, E., Ritalahti, K.M., Edwards, E.A., Konstantinidis, K.T. and Loffler, F.E. (2012) Genomic determinants of organohalide-respiration in *Geobacter lovleyi*, an unusual member of the *Geobacteraceae*. *BMC Genomics*, **13**, 200.

62. Rupakula, A., Kruse, T., Boeren, S., Holliger, C., Smidt, H. and Maillard, J. (2013) The restricted metabolism of the obligate organohalide respiring bacterium *Dehalobacter restrictus*: lessons from tiered functional genomics. *Philos Trans R Soc Lond B Biol Sci*, **368**, 20120325.

63. Prat, L., Maillard, J., Grimaud, R. and Holliger, C. (2011) Physiological adaptation of *Desulfitobacterium hafniense* strain TCE1 to tetrachloroethene respiration. *Appl Environ Microbiol*, **77**, 3853-3859.

64. Kreher, S., Schilhabel, A. and Diekert, G. (2008) Enzymes involved in the anoxic utilization of phenyl methyl ethers by *Desulfitobacterium hafniense* DCB2 and *Desulfitobacterium hafniense* PCE-S. *Arch Microbiol*, **190**, 489-495.

65. Neumann, A., Engelmann, T., Schmitz, R., Greiser, Y., Orthaus, A. and Diekert, G. (2004) Phenyl methyl ethers: novel electron donors for respiratory growth of *Desulfitobacterium hafniense* and *Desulfitobacterium* sp. strain PCE-S. *Arch Microbiol*, **181**, 245-249.

66. Studenik, S., Vogel, M. and Diekert, G. (2012) Characterization of an *O*-demethylase of *Desulfitobacterium hafniense* DCB-2. *J Bacteriol*, **194**, 3317-3326.

67. Kadner, R.J. (1978) Repression of synthesis of the vitamin B_{12} receptor in *Escherichia coli*. *J Bacteriol*, **136**, 1050-1057.

68. Luan, B., Carr, R., Caffrey, M. and Aksimentiev, A. (2010) The effect of calcium on the conformation of cobalamin transporter BtuB. *Proteins*, **78**, 1153-1162.

69. Bradbeer, C., Kenley, J.S., Di Masi, D.R. and Leighton, M. (1978) Transport of vitamin B_{12} in *Escherichia coli*. Corrinoid specificities of the periplasmic B_{12}-binding protein and of energy-dependent B_{12} transport. *J Biol Chem*, **253**, 1347-1352.

70. Cadieux, N., Bradbeer, C., Reeger-Schneider, E., Koster, W., Mohanty, A.K., Wiener, M.C. and Kadner, R.J. (2002) Identification of the periplasmic cobalamin-binding protein BtuF of *Escherichia coli*. *J Bacteriol*, **184**, 706-717.

71. Ravnum, S. and Andersson, D.I. (1997) Vitamin B_{12} repression of the *btuB* gene in *Salmonella typhimurium* is mediated via a translational control which requires leader and coding sequences. *Mol Microbiol*, **23**, 35-42.

72. Pester, M., Brambilla, E., Alazard, D., Rattei, T., Weinmaier, T., Han, J., Lucas, S., Lapidus, A., Cheng, J.F., Goodwin, L. *et al.* (2012) Complete genome sequences of *Desulfosporosinus orientis* DSM765T, *Desulfosporosinus youngiae* DSM17734T, *Desulfosporosinus meridiei* DSM13257T, and *Desulfosporosinus acidiphilus* DSM22704T. *J Bacteriol*, **194**, 6300-6301.

73. Spring, S., Lapidus, A., Schroder, M., Gleim, D., Sims, D., Meincke, L., Glavina Del Rio, T., Tice, H., Copeland, A., Cheng, J.F. *et al.* (2009) Complete genome sequence of *Desulfotomaculum acetoxidans* type strain (5575). *Stand Genomic Sci*, **1**, 242-253.

74. Kazanov, M.D., Vitreschak, A.G. and Gelfand, M.S. (2007) Abundance and functional diversity of riboswitches in microbial communities. *BMC Genomics*, **8**, 347.

6.8 Supplementary information

6.8.1 Supplementary Tables

Table S6.1: **Oligonucleotides used in this study.**

Name	Sequence [a]	Experiment / Target	Reference
RS07-f	GCCAAGCTTGCATGCTAATACGACTCACTATAG**G**ATTAGGT ACTCAATCCTTACCGGAAAGAG	Cloning / Cbl-RS07	This study
RS07-r	GCCCGGAATTCTCCTGTCCTCGAGGAGGGTCGC	Cloning / Cbl-RS07	This study
RS08-f	GCCAAGCTTGCATGCTAATACGACTCACTATAGGA**C**CATTC TTTGGTGCCCCCAAGGGGAGAATAG	Cloning / Cbl-RS08	This study
RS08-r	GCCCGGAATTCCTTTCCATAGCACCCATGGAAAGG	Cloning / Cbl-RS08	This study
RS16-f	GCCAAGCTTGCATGCTAATACGACTCACTATAGGA**C**AAGGT TCCTCTTTAGAGGAAGAAAAGG	Cloning / Cbl-RS16	This study
RS16-r	GCCCGGAATTCATCCATCGCTCGTGGACGTAGC	Cloning / Cbl-RS16	This study
pSG2-f	GGAGAAAATACCGCATCAGG	Sequencing / pSG2 plasmid	(1)
pSG2-r	TGTTGTGTGGAATTGTGAGC	Sequencing / pSG2 plasmid	(1)
rpoB-f	GACGGGTCAAGACTTATGAAGC	qPCR / *rpoB* (DSY0643)	This study
rpoB-r	CTCATCATCAACAGCTTCTTCG	qPCR / *rpoB* (DSY0643)	This study
btuF-f	CAGGGTATGGATTGAAGTGGAT	qPCR / *btuF* (DSY2084)	This study
btuF-r	GAGGGTTCTTCTCAATCACCTG	qPCR / *btuF* (DSY2084)	This study
cobT-f	GAATACACGGTCTTGACGAACA	qPCR / *cobT* (DSY2114)	This study
cobT-r	TAGAACATTTGCGGGGTTACTT	qPCR / *cobT* (DSY2114)	This study
cbi[ET]-f	GTTGGCTGAATACAGATGCTGA	qPCR / *cbi[ET]* (DSY4071)	This study
cbi[ET]-r	ACATCACCGCGTATAAACTCCT	qPCR / *cbi[ET]* (DSY4071)	This study

[a] Underlined nucleotides correspond to target of restriction enzymes used for cloning. Nucleotides in bold indicate the first nucleotide of the corresponding riboswitch sequence.

Tables S6.2-S6.4: Affinities (K_A) of the modulated cleavage sites of RS07, RS08 and RS16 towards AdoCbl.

Table S6.2: **RS07**

Sites (RS 07)	K_A (μM^{-1})	Average K_A (μM^{-1})
Site 1	0.060 ± 0.010 0.044 ± 0.005	0.050 ± 0.008
Site 2	0.011 ± 0.005 0.011 ± 0.002	0.011 ± 0.000
Site 3	0.017 ± 0.005 0.019 ± 0.013	0.017 ± 0.001
Site 4	0.022 ± 0.007 0.017 ± 0.004	0.018 ± 0.002
Site 5	0.016 ± 0.009 0.017 ± 0.006	0.017 ± 0.001
Site 6	0.096 ± 0.030 0.056 ± 0.007	0.058 ± 0.020

Table S6.3: RS08

Sites (RS 08)	K_A (μM^{-1})	Average K_A (μM^{-1})
Site 2	4.94 ± 0.65	5.07 ± 1.66
	6.61 ± 3.42	
	10.40 ± 5.34	
Site 3	3.29 ± 0.66	3.56 ± 0.86
	5.85 ± 2.20	
	4.48 ± 2.54	
Site 4	6.03 ± 3.77	2.68 ± 1.80
	2.45 ± 1.27	
Site 5	2.45 ± 0.68	2.58 ± 1.51
	5.47 ± 3.22	
Site 6	3.62 ± 0.87	4.76 ± 1.02
	5.91 ± 1.10	
	6.79 ± 1.92	

Table S6.4: RS16

Sites (RS16)	K_A (μM^{-1})	Average K_A(μM^{-1})
Site 1	35.41 ± 23.55	40.70 ± 5.85
	47.11 ± 25.91	
Site 2	55.55 ± 18.43	41.60 ± 8.06
	39.42 ± 7.27	
Site 4-5	34.02 ± 17.14	34.02 ± 17.14
Site 6	38.17 ± 26.95	35.52 ± 2.66
	32.85 ± 27.08	
Site 7	18.02 ± 6.70	19.36 ± 2.05
	22.13 ± 9.62	
Site 8	59.44 ± 40.64	59.44 ± 40.64
Site 11	65.54 ± 39.87	65.54 ± 39.87

[Given are the affinities (K_A) of AdoCbl towards the indicated cleavage sites of RS07, RS08 and RS16 derived from 1:1 binding isoterm (2) from one, two or three titration experiments. The K_A values at the indicated cleavage sites are considered for calculating the final affinity values (K_D) since AdoCbl-induced changes at these sites could be fitted well to the 1:1 binding isoterm. The average K_A values indicate the weighted mean and relative error of the individual K_A values].

Table S6.5: **Quantitative RT-PCR of selected Cbl-RS down-regulated gene targets (expressed as transcript copy number/mL of sample).**

Exp. [a]	Corrinoid	*rpoB*	*btuF* (RS07)	*cobT* (RS08)	*cbi[ET]* (RS16)
1	None	3663001	118294	964590	14021
		± 345358	± 14034	± 10489	± 2592
1	AdoCbl	6314752	13183	183922	1861
		± 136053	± 993	± 5153	± 203
	None/AdoCbl	0.58	8.97	5.24	7.53
	R_F [b]	**1.0**	**15.5**	**9.0**	**13.0**
2	None	7698255	185793	433574	23792
		± 1467148	± 9878	± 25091	± 6316
2	CNCbl	8492874	138160	262043	12253
		± 620797	± 15211	± 6676	± 1976
	None/CNCbl	0.91	1.34	1.65	1.94
	R_F [b]	**1.0**	**1.5**	**1.8**	**2.1**

[a] Two separate pulse experiments were conducted for each of which a non-pulsed control was included.

[b] Normalized repression factors (R_F) were calculated between non-pulsed and pulsed cultures after correcting the gene transcript copy number by the constitutively expressed *rpoB*.

6.8.2 Supplemetary Figures

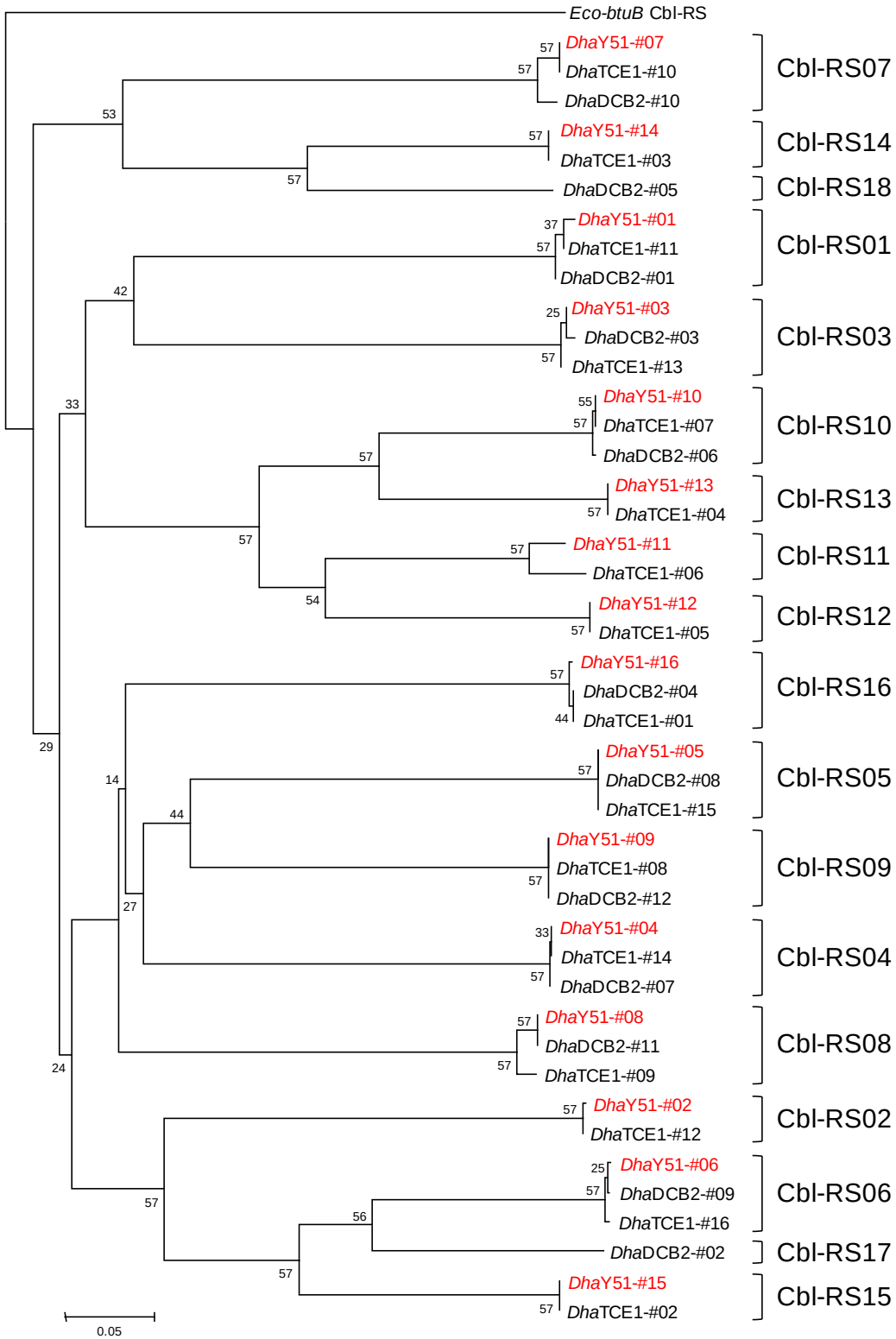

Figure S6.1: **Likelihood sequence analysis of cobalamin riboswitches (Cbl-RS) present in *Desulfitobacterium hafniense* (*Dha*) strains Y51, DCB-2 and TCE1:** The riboswitch sequence including the expression platform were aligned initially with ClustalX, and then manually corrected to align secondary structures as those found in *E. coli btuB* Cbl-RS (3). Cbl-RS1 to RS16 were defined by the riboswitches found in *D. hafniense* strain Y51 (shown in red), with two additional ones identified in strain DCB-2 (RS17 and RS18). The scale bar represents 5% divergence.

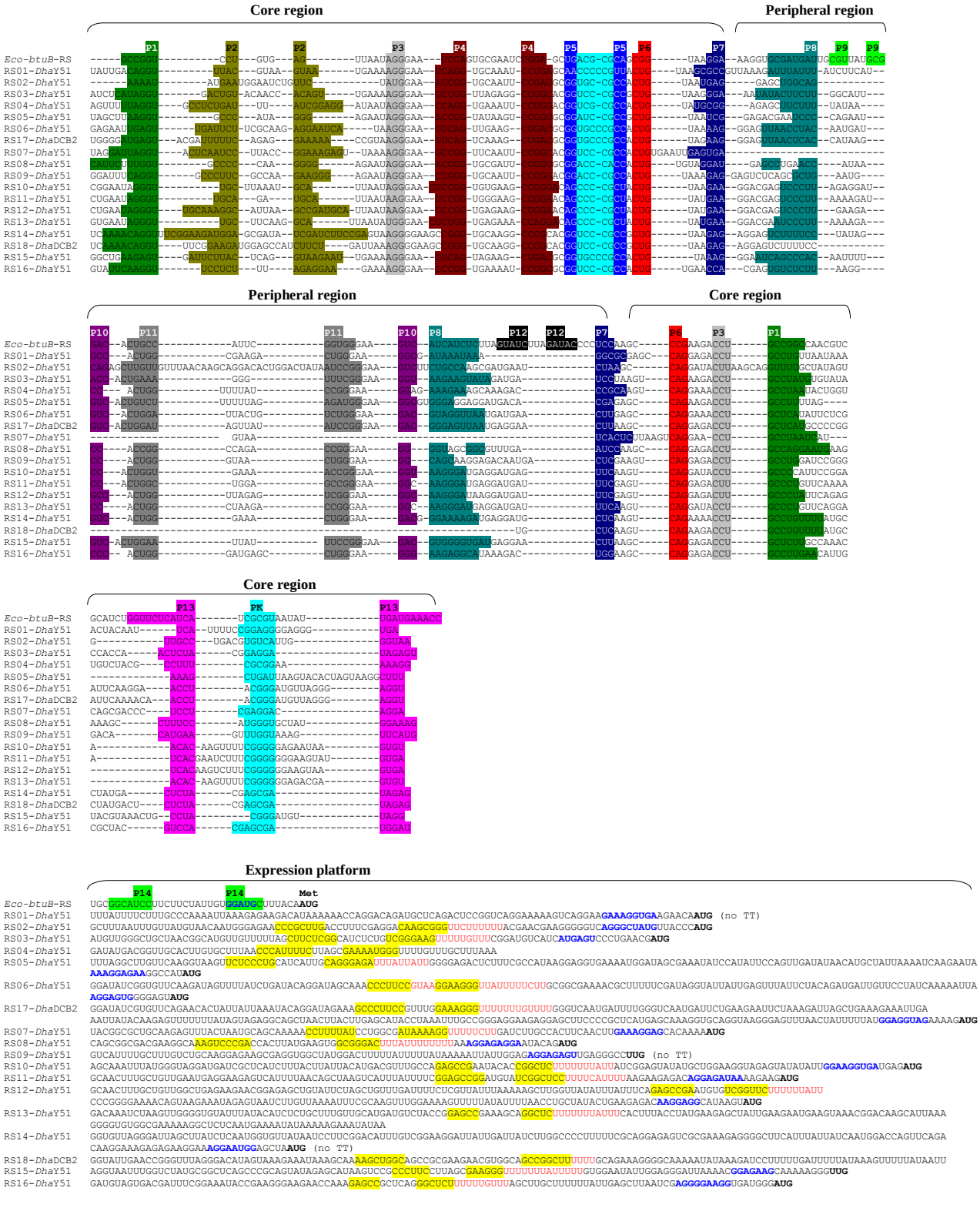

Figure S6.2: Complete sequence alignment of representative cobalamin riboswitches (Cbl-RS, incl. expression platform) from *Desulfitobacterium hafniense* (*Dha*): The riboswitches were initially aligned with ClustalX using default parameters, and then manually corrected to position conserved secondary structures. *E. coli btuB* P14 hairpin (shaded in light green) was taken from Perdrizet *et al*. (4). Putative transcription terminators were identified in most *Dha* Cbl-RS and are shaded in yellow (hairpin) and written in red (poly U).

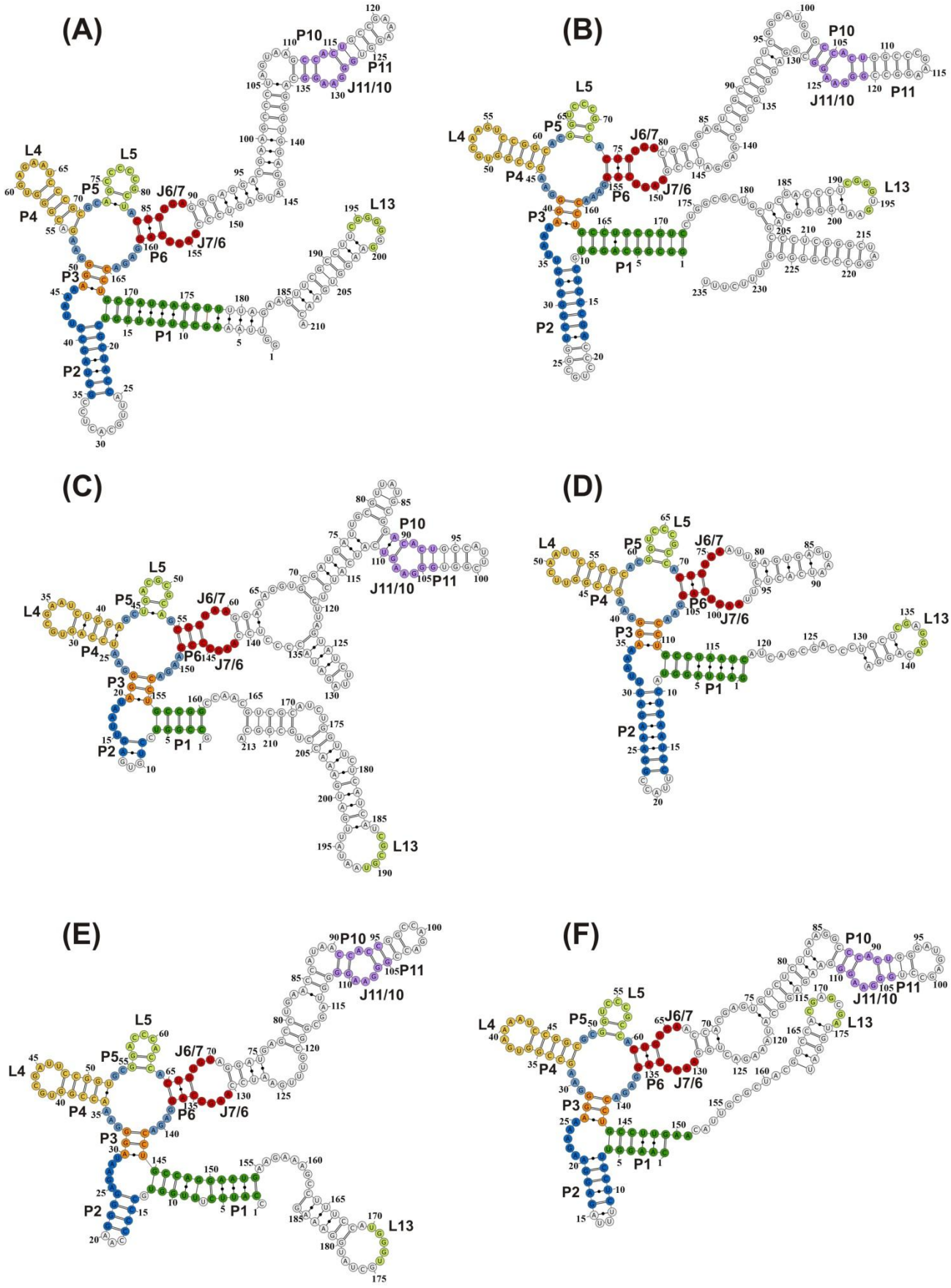

Figure S6.3: Comparsion of the secondary structures of AdoCbl riboswitches: Shown are the secondary structures of AdoCbl riboswitches for (A) *T. tengcongensis* (5), (B) *S. thermophilum* (6), (C) *E. coli btuB*) (7), (D) RS07, (E) RS08 and (F) RS16, showing a similarity at the core region (P3-P4-P5-P6), the peripheral region (P10-P11-J11/10) and the possible kissing-loop (KL) interaction between L5 and L13. The secondary structures were depicted with the help of the VARNA software (8).

6.9 Supplementary References

1. Gallo, S. (2008) Investigations on the interaction between coenzyme B_{12} derivatives and the *btuB* riboswitch of *E. coli*. PhD thesis. University of Zurich, Zurich.
2. Sigel, RKO., Freisinger, E., and Lippert, B. (2000) Effects of N7-methylation, N7-platination, and C8-hydroxylation of guanine on H-bond formation with cytosine: platinum coordination strengthens the Watson-Crick pair. *J Biol Inorg Chem***, 5**, 287-299.
3. Gallo, S., Oberhuber, M., Sigel, RKO., and Kräutler, B. (2008) The corrin moiety of coenzyme B_{12} is the determinant for switching the *btuB* riboswitch of *E. coli*. *Chembiochem*, **9**,1408-1414.
4. Perdrizet, GA., 2nd., Artsimovitch, I., Furman, R., Sosnick, TR., and Pan, T. (2012) Transcriptional pausing coordinates folding of the aptamer domain and the expression platform of a riboswitch. *Proc Natl Acad Sci U S A*, **109**, 3323-3328.
5. Johnson, Jr JE., Reyes, FE., Polaski, JT., and Batey, RT. (2012) B_{12} cofactors directly stabilize an mRNA regulatory switch. *Nature*, **492**, 133-137.
6. Peselis, A., and Serganov, A. (2012) Structural insights into ligand binding and gene expression control by an adenosylcobalamin riboswitch. *Nat Struct Mol Biol*, **19**, 1182-1184.
7. Nahvi, A., Barrick, JE., and Breaker, RR. (2004) Coenzyme B_{12} riboswitches are widespread genetic control elements in prokaryotes. *Nucleic Acids Res*, **32**, 143-150.
8. Darty, K., Denise, A., and Ponty, Y. (2009) VARNA: Interactive drawing and editing of the RNA secondary structure. *Bioinformatics*, **25**, 1974-1975.

6.10 Additional experiments : In-line probing of RS08 and RS16 riboswitches with dicyanocobinamide and adenosylcobinamide

RS08 and RS16 riboswitches are involved in the *de novo* synthesis of AdoCbl in bacterium, *D. hafniense*. RS08 is located at the upstream of genes *DSY2114-2116*, which are predicted to encode CobTUS proteins responsible for building up the lower ligand (DMB) of AdoCbl (Table 6.1). In contrast, RS16 is situated upstream of *cbi[ET]* (a fused gene in *Desulfitobacterium*), which is also the first gene (in a long series of genes) responsible for the overall biosynthetic pathway of cobalamine except for the addition of the lower ligand (Table 6.1).

In comparison to AdoCbl, dicyanocobinamide (DiCN-Cobi) lacks both the apical ligands whereas adenosylcobinamide (AdoCobi) lacks only the lower ligand. Therefore, we hypothesized that a high concentration of DiCN-Cobi and AdoCobi should not switch the RS08 riboswitch whereas they can probably switch the RS16 riboswitch.

To check the effect of DiCN-Cobi and AdoCobi on RS08 and RS16 riboswitches, in-line probing of these RNAs was carried out in the presence of these cobalamine ligands. As seen from Figure 6.6, in the presence of DiCN-Cobi, both the RS08 (Figure 6.6A) and RS16 riboswitch (Figure 6.6B) do not show modulation at any position in comparison to RNA incubated in the absence of DiCN-Cobi. Only at a higher concentration of DiCN-Cobi (1 mM), changes are observed at some nucleotides (marked by arrows in Figure 6.6). However, there is no clear trend observed in the modulation at these nucleotides with respect to increasing concentration of DiCN-Cobi. Therefore, the changes in RNA structure at 1 mM DiCN-Cobi appears to be non-specific for both RS08 and RS16.

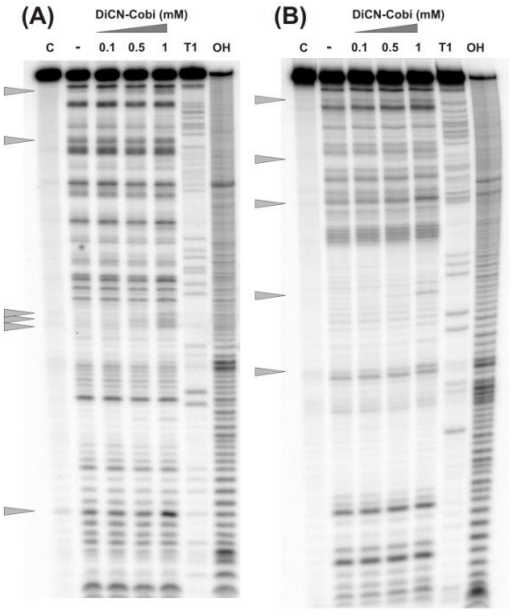

Figure 6.6: In-line probing experiments with DiCN-Cobi: The C08 (A) and C16 (B) riboswitches were incubated with DiCN-Cobi and subjected to in-line probing. The arrows indicate the nucleotides undergoing modulation with 1 mM DiCN-Cobi. Lane (-): RNA incubated in buffer only; C: RNA in water; T1: RNase T1 ladder; OH: Alkaline hydrolysis ladder.

In the presence of AdoCobi, the in line probing pattern for RS08 riboswitch shows changes at sites 2, 3, 5 and 6 (Figure 6.7A). AdoCobi acts as a substrate for a reaction involving the attachment of a lower ligand and this reaction is regulated by RS08. Therefore, RS08 was not expected to undergo a switch at all. However, the observed modulation at sites 2, 3, 5 and 6 in the presence of AdoCobi suggests an interaction of these sites or their nearby regions with AdoCobi. In the case of the RS16 riboswitch, only sites 2, 4, 5 and 6 undergo modulation in the presence of AdoCobi however, the most evident modulations at these sites are visible only at 5 µM of AdoCobi (Figure 6.7B).

AdoCobi was expected to switch only the RS16 riboswith and not the RS08 riboswitch. Some of the nucleotides from both of these riboswitches undergo modulation in the presence of AdoCobi, suggesting an incomplete switch of the RNA. However, the incomplete switch does not correspond to the misfolded RNA as most of the nucleotides in RS08 and RS16 riboswitches are cleaved similar to the RNAs incubated with AdoCbl (Figure 6.7 A and B).

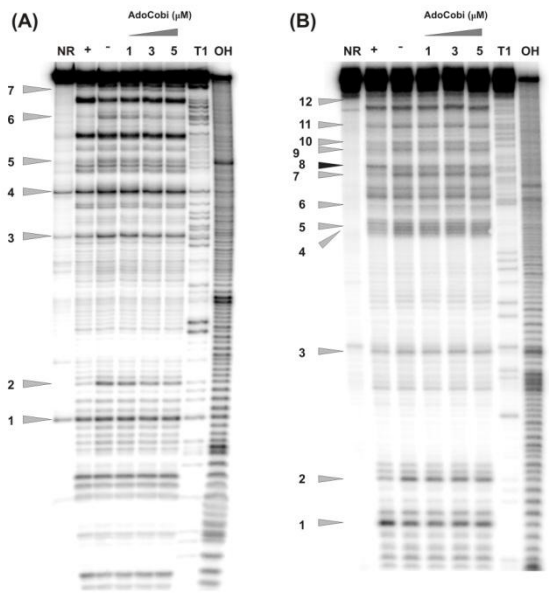

Figure 6.7: In-line probing experiments with AdoCobi: In-line probing was carried out on C08 (A) and C16 (B) RNA incubated with AdoCobi. The arrows indicate the nucleotides undergoing modulation with 100 μM AdoCbl (+) (A) and 10 μM AdoCbl (+) (B). Lane (-): RNA incubated in buffer only; NR: RNA in water; T1: RNase T1 ladder; OH: Alkaline hydrolysis ladder.

The highest concentration of AdoCobi used in the titration was 5 μM and therefore the in-line probing of RS08 and RS16 with higher concentration of AdoCobi than 5 μM can help to confirm the observed results and awaits further experiments.

Therefore, corrinoids that lack both the apical ligands e.g. DiCN-Cobi does not alter the conformation of RS08 and RS16 riboswitches. In contrast, corrinoids like AdoCobi that carries the adenosyl group as the upper apical ligand does interact with RS08 and RS16 riboswitches as the changes are evident at some of the cleavage sites in in-line probing experiments. However, the interaction of AdoCobi leads to the incomplete switch of these riboswitches unlike AdoCbl. The riboswitches RS08 and RS16 are folded similar to the RNA incubated with AdoCbl. Therefore, the interaction with AdoCobi does not lead to the misfolding of the RS08 and RS16 riboswitches. These riboswitches only fail to undergo a complete switch in the presence of AdoCobi.

7 Modification of the *btuB* riboswitch for FRET studies

In order to study the folding of the *btuB* riboswitch both in the absence and presence of AdoCbl on a real time scale, the *btuB* riboswitch was modified. The idea was to attach two fluorescent dyes, Cy3 and Cy5, to the modified *btuB* riboswitch and use the complex for single molecule FRET (smFRET) experiments. Since these dyes are attached to DNA oligonucleotides, complementary sequences are needed in the *btuB* riboswitch to hybridize the fluorophore containing DNA oligos (Cardo L, et al., 2012, *Methods Mol Biol*, 848, 227-51).

In a first attempt, loops L4 and L11 in the *btuB* riboswitch were replaced with modified loop sequences as shown in Figure 8.1A. At the time of designing these constructs, no information was available for the interaction between different regions of the *btuB* riboswitch. Therefore, we had to hunt for the best modification of the loops in such a way that the folding and the switching of the *btuB* riboswitch is not affected. Although L4 carried some of the conserved nucleotides, L4 and L11 are situated apart in the secondary structure and were therefore considered for the modifications.

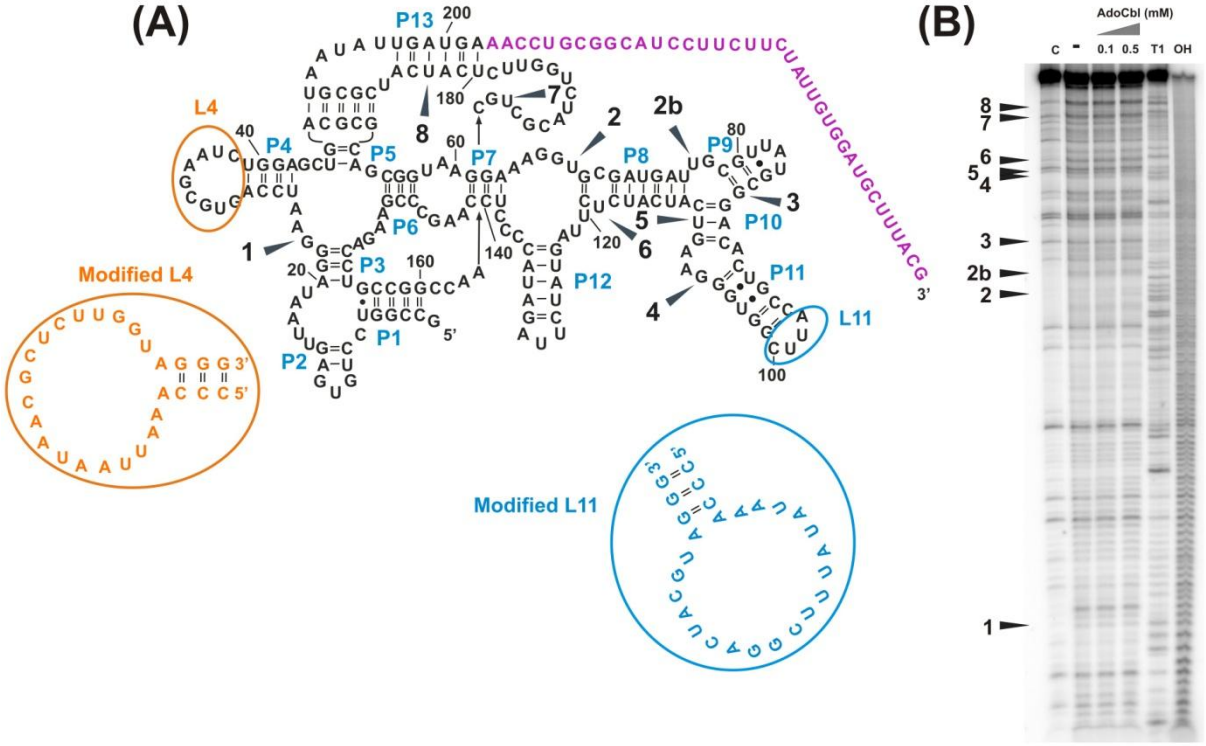

Figure 8.1: The modified *btuB* riboswitch, pPC3: (A) The *btuB* riboswitch was modified at loops L4 (orange) and L11 (blue) with modified sequences as indicated. The *btuB* riboswitch is also extended at the 3' end to include 37 nucleotides (in purple) from the expression platform. (B) In-line probing of the modified *btuB* riboswitch, pPC3 RNA in the presence of AdoCbl indicating absence of ligand induced changes at sites 1-8. Lane (-): RNA incubated in buffer only; C: RNA in water; T1: RNase T1 ladder; OH: Alkaline hydrolysis ladder.

The first modified RNA, pPC3 RNA carries 37 nucleotides of the expression platform along with the modified L4 and L11. This RNA was tested by in-line probing in order to confirm the folding of the *btuB* RNA and its switch in the presence of AdoCbl. As seen from Figure 8.1B, we could not observe AdoCbl induced modulations at any of the nucleotides in pPC3 RNA. We assume that the modification of L4 affects the folding of the *btuB* riboswitch and therefore, in the next attempt, the loop L4 was not modified and kept as it is in the *btuB* riboswitch.

In the next set of modification, only loop L11 was modified in a similar way to that of pPC3 RNA. This new modified RNA, pPC4 RNA carries the modified L11 and 37 nucleotides of the expression platform (Figure 8.2A). The extended 37 nucleotides of the pPC4 RNA can be used to attach the Cy3 containing oligo whereas L11 can be hybridized to the Cy5-DNA oligo (Figure 8.2A). To confirm that the modifications do not affect the folding of the RNA, in-line probing was carried out with pPC4 RNA in the presence of AdoCbl (Figure 8.2B). The AdoCbl induced changes were evident at the expected nucleotides (sites 1-8) in the case of pPC4 RNA. This result confirms that the incapability of the pPC3 construct to switch is due to modified L4 and therefore L4 plays a crucial role in folding of the *btuB* riboswitch.

Since pPC4 RNA showed a normal switching in the presence of AdoCbl, this RNA was used for further investigations. In-line probing was carried out with pPC4 RNA in the presence of fluorophore containing oligos and AdoCbl. This experiment was carried out to check if the binding of fluorophore containing oligos affect RNA folding. As seen from Figure 8.3A, the presence of both, Cy3-DNA and Cy5-DNA do not affect the switching of the *btuB* riboswitch since the changes are evident at sites 1-8 in the presence of AdoCbl. Interestingly, nucleotide 151 is cleaved only in the presence of Cy3-DNA (black box, Figure 8.3A). Since Cy3-DNA binds to the expression platform, it is expected that G151 is probably involved in interaction with the expression platform and is released when Cy3-DNA hybridizes to the expression platform.

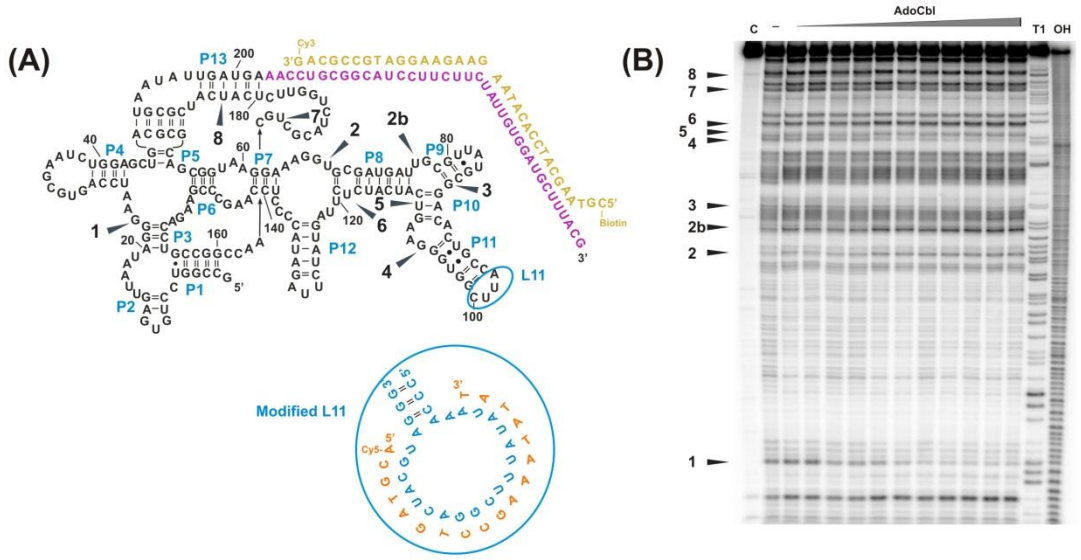

Figure 8.2: The modified *btuB* riboswitch, pPC4: (A) The modified *btuB* riboswitch pPC4 contains modified loop L11 (blue) and the extended 3' end (purple). The 5' Cy5-DNA oligo is indicated in orange and 5' Biotin-3' Cy3 DNA oligo is indicated in yellow. (B) In-line probing of pPC4 RNA incubated with AdoCbl showing the AdoCbl induced changes at sites 1-8. Lane (-): RNA incubated in buffer only; C: RNA in water; T1: RNase T1 ladder; OH: Alkaline hydrolysis ladder.

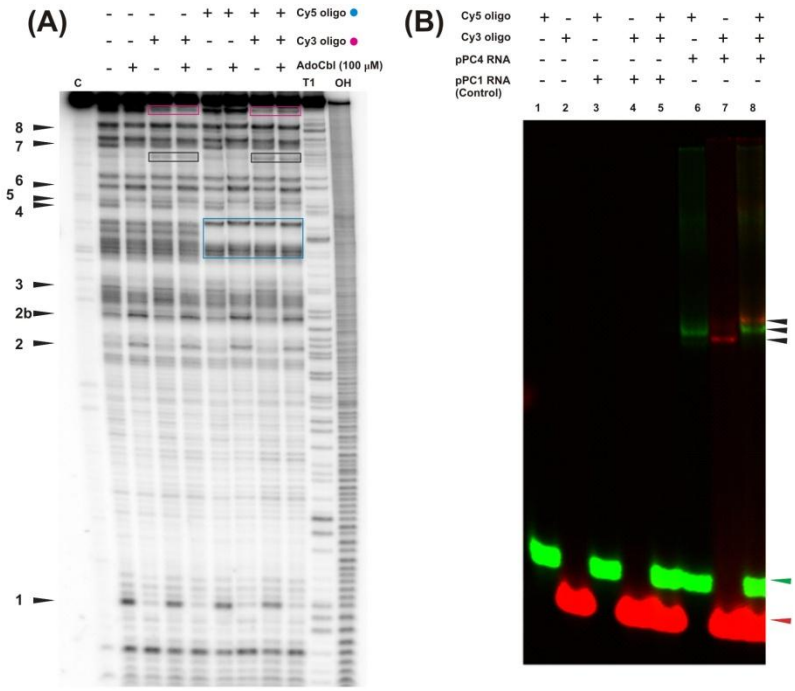

Figure 8.3: Analysis of pPC4 RNA bound to the fluorophore containing DNA: (A) In-line probing of pPC4 RNA in the presence of Cy5-DNA, Cy3-DNA and AdoCbl. Sites 1-8 (marked by arrows) indicate the nucleotides undergoing AdoCbl induced changes. Pink and blue boxes indicate the regions of the *btuB* riboswitch hybridising to the Cy3-DNA and Cy5-DNA respectively. Black boxes indicate changes at nucleotide G151. (B) Native gel electrophoresis of pPC4 RNA bound to Cy3-DNA and Cy5-DNA, indicated by black arrows. The green and red arrows show unbound Cy5-DNA and Cy3-DNA respectively.

The hybridisation of Cy3-DNA to the expression platform region appears to be complete since a clear protection of this region is observed in the presence of Cy3-DNA only (pink box, Figure 8.3A). The region of the *btuB* RNA hybridized to the Cy5-DNA on the other hand does not indicate a complete protection (blue box, Figure 8.3A). Although the Cy5-DNA hybridizes to the modified L11, the local distortions at the modified L11 region prevent the complete protection of this region in in-line cleavage reaction. Native gel electrophoresis shows that Cy3-DNA and Cy5-DNA both bind to the modified *btuB* construct pPC4 RNA (Figure 8.3B).

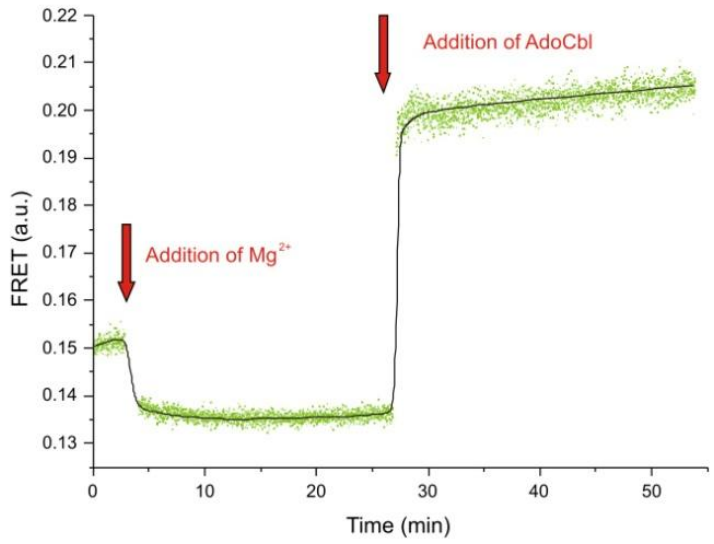

In a bulk FRET experiment (Figure 8.4) (with pPC4 RNA and the Cy3-Cy5 oligos), the addition of 20 mM Mg^{2+} reduces the FRET signal between the dyes however the addition of 150 μM AdoCbl increases the FRET signal. This experiment suggested that addition of 20 mM Mg^{2+} folds the *btuB* riboswitch in such a way that the regions bound to the fluorophore containing DNAs moves apart from each other, as observed from decrease in the FRET signal. In contrast, these regions close up in the presence of AdoCbl.

Figure 8.4: Bulk FRET measurement with pPC4 RNA: shown is the FRET between Cy3-DNA and Cy5-DNA bound to the modified *btuB* riboswitch, pPC4 RNA after addition of 20 mM Mg^{2+} and 150 μM of AdoCbl, indicated by red arrows.

8 Additional Materials and Methods

8.1 Materials

All primers and oligonucleotide sequences were purchased from Microsynth, Balgach (Switzerland). The flurophore and biotinylated DNA oligos were purchased from W.M. Keck Oligonucleotide Synthesis Facility, Yale University at a 1 micromole scale. The nucleoside 5'-triphosphates (ATP, GTP, CTP) were obtained from GE Healthcare, Glattburg (Switzerland) except for UTP which was purchased from Sigma-Aldrich, Buchs (Switzerland). The *in vitro* transcription of RNA was carried out using homemade T7 RNA polymerase (Gallo S, et al., 2005, *Chimia*, 59, 812-816). The *Taq* polymerase and *SphI* were purchased from MP Biomedicals, Illkirch (France). RNase A and RNase V1 were obtained from Fermentas. All the other enzymes like *pfu*, *EcoRI* and *BgIII* were from Promega, Madison (USA). The Shrimp Alkaline Phosphatase (SAP), the Thermosensitive SAP (TSAP) and the T4 polynucleotide kinase were obtained from Promega, Madison (USA). Intrinsic factor was purchased from Sigma-Alrich, Buchs (Switzerland). Dicyanocobinamide and Adenosylcobinamide were provided by Dr. Sofia Gallo. ^{32}P-γ-ATP was purchased from PerkinElmer, Schwerzenbach (Switzerland). Aqueous acrylamide solution (AccuGel 29:1 acrylamide to bis-acrylamide) and TBE (Tris-borate-EDTA; 10X) buffer were obtained from National Diagnostics, Hussle Hull (UK). Polyacrylamide gels for in-line probing, RNase T1 probing and for Tb(III) cleavage experiments were prepared using Long Ranger Gel solution, Lonza (Switzerland). The Perfectprep Gel Cleanup Kit from Eppendorf AG, Hamburg (Germany) was used to purify the PCR products. Plasmid minipreps were isolated using the High Pure Plasmid Isolation Kit from Roche, Basel (Switzerland) and plasmid maxipreps using the HiSpeed Plasmid Maxi Kit from Qiagen, Hilden (Germany). Sequencing of the plasmids was carried out at Microsynth, Balgach (Switzerland). Phenol and choloroform: isoamyl alcohol (24:1) were purchased from Sigma-Aldrich, Buchs (Switzerland).

8.2 Methods

8.2.1 Preparation of the plasmids

8.2.1.1 Primer and oligonucleotide sequences

pSG2_5:

5'GCC[AAGCTT]$_{HindIII}$-[GCATGC]$_{SphI}$-TAATACGACTCACTATAGGA GCCGGTCCTGTGAGTTAATAGG 3'

pSG2_6:

5'CCATGATTAC[GAATTC]$_{EcoRI}$-[GAGCT]$_{SacI}$-CTCATCAAT ATTACGCGATGATGAGAACC 3'

btuB239:

5'GCCCG[GAATTC]$_{EcoRI}$ GTAAAGCATCCACAATAGAAGAAGGATGCC 3'

pPC2_5:

5'CCCAAATTAATAACGCTCTTGGTAGGGTGGGAGCTGACGCGCAGCGGTAAGGAA 3'

pPC2_14hgaI:

5'GGAGCTGACGCGCAGCGGTAAGGAAAGGTGCGATTGCGTTATGCGGACACT 3'

pPC2_15:

5'CCTGTGAGTT AATAGGGAAT CCAGTGCGAATCTGGAGCTGACGCGCAGCG 3'

pPC2_5:

5’CCCAAATTAATAACGCTCTTGGTAGGGTGGAGCTGACGCGCAGCGGTAAGGAA 3’

pPC4_1:

5’CGCGTAATATTGATG[AGATC]$_{BgIII}$-TGCGGCATCCTTCTTC 3’

pPC4_2:

5’GAAGAAGGATGCCGCA[GATCT]$_{BgIII}$-CATCAATATTACGCG 3’

Primer 154:

5’GCTGGCGAAAGGGGGATGTG3’

Oligonucleotides:

pPC2_4:

5’GCC[AAGCTT]$_{HindIII}$[GCATGC]$_{SphI}$TAATACGACTCACTATAGGAGCCGGTCCTGTGAGTTAATAGGGAATCCA[CCCAAATTAATAACGCTCTTGGTAGGG]$_{modified\ loop\ L4}$ TGGAG 3’

pPC2_13:

5’GGAAAGGTGCGATGATTGCGTTATGCGGACACTGCC[CCCAAATATATTTCGGACTACGTAGGG]$_{modified\ loop\ L11}$ GGTGGGAAGTCATCTCTTAGTATCTTA[GATACC]$_{EcoRI}$ 3‘

5’ Cy5 DNA oligo:

5’Cy5-ACGTAGTCCGAAATATAT 3’

5’ Biotin-3’Cy3 DNA oligo:

5’ Biotin-CGTAAGCATCCACAATAGAAGAAGGATGCCGCAG-Cy3 3’

5’ Biotin DNA oligo:

5’ Biotin-CGTAAAGCATCCACAATAGAAGAAG 3’

8.2.1.2 Construction of the plasmids

pPC1: pPC1 plasmid carries the insertion of the three nucleotides-‘GGA’ between the TATA box and the *btuB* coding sequence. This insertion was done to improve the transcription start site for the T7 RNA polymerase. The plasmid was created by performing PCR using the plasmid pSG2 as a template. The PCR reaction contained 500 ng of plasmid pSG2 along with 1.25 µL of forward primer (pSG2_5) (100 µM), 1.25 µL of reverse primer (pSG2_6) (100 µM), 1.0 µL of dNTP mix (dATP, dCTP, dGTP and dTTP; 10 mM each) and 0.5 µL of *Taq* DNA polymerase in 50 µL of 1X *Taq* buffer. The PCR reaction mixture was subjected to 40 cycles of melting for 1 minute at 90° C, annealing for 30 seconds at 56° C and elongation for 3 minutes at 73° C. The PCR products were isolated by 2% agarose gel electrophoresis and extracted from the gel using Perfectprep Gel Cleanup kit from Eppendorf. The PCR products and the plasmid pSG2 were digested first with *SphI* followed by digestion with *EcoR1*. Plasmid pPC1 is created by ligating the double digested PCR product and plasmid pSG2 using T4 DNA ligase. The transformants were selected with the help of an ampicillin resistance gene (marker) carried by plasmid pSG2.

pPC2: pPC2 plasmid contains the *btuB* aptamer along with 37 nucleotides of the expression platform at the 3’ end of the *btuB* aptamer and ‘GGA’ transcriptional start site. This plasmid carries a spontaneous mutation at nucleotide 99 of the

btuB sequence (T to C). However, this mutation does not affect the RNA with respect to RNA folding and AdoCbl binding. The plasmid was created by performing a colony PCR with *E. coli DH5α* cell. The PCR reaction mixture contained 0.4 µL of forward primer (pSG2_5) (10 µM), 0.4 µL of reverse primer (btuB239) (10 µM), 0.4 µL of dNTP mix (dATP, dCTP, dGTP and dTTP; 10 mM each) and 1 µL of *Pfu* DNA polymerase in 20 µL of 1x *Pfu* buffer. A single colony of *E. coli DH5α* cell was added to the reaction mixture and the PCR was performed for 40 cycles of melting for 1 minute at 90° C, annealing at 55° C and elongation at 68° C. The PCR products were isolated by 2% agarose gel electrophoresis and extracted from the gel using Perfectprep Gel Cleanup kit from Eppendorf. The PCR products and the plasmid pPC1 were digested first with *SphI* and then with *EcoRI* for ligation purpose to create plasmid pPC2.

pPC3: pPC3 plasmid contains modified loop sequences at loop L4 and loop L11 in the *btuB* riboswitch along with the 37 nucleotides of the expression platform and 'GGA' at the 5' end as a start site for T7 RNA polymerase. pPC3 plasmid was created in three steps each consisting of 40 cycles of PCR that involves melting for 1 minute at 90 °C, annealing at 55 °C and elongation at 68 °C. In the first step, the oligonucleotide pPC2_13 was extended at the 3' end with the primer btuB 239 and the plasmid pPC2 as a template. The reaction mixture contains 500 ng of pPC2, 1.25 µL of oligo pPC_13 (10 µM), 1.25 µL of primer btuB239 (10 µM), 2.0 µL of dNTP mix (dATP, dCTP, dGTP and dTTP; 10 mM each), 1.0 µL of *Pfu* DNA polymerase (3 U/ µL) in 50 µL of 1X *Pfu* buffer. The PCR product was then extended at the 5' end with the help of 1.25 µL of primer pPC2_5 (10 µM) and 1.25 µL of primer btuB 239 (10 µM) in 50 µL of 1X *pfu* buffer containing 2.0 µL of dNTP mix (dATP, dCTP, dGTP and dTTP; 10 mM each) and1.0 µL of *Pfu* DNA polymerase (3 U/ µL). The PCR product of the step 2 is further extended at the 5'end by 1.25 µL of oligonucleotide pPC2_4 (10 µM) and 1.25 µL of primer btuB 239 (10 µM) with 2.0 µL of dNTP mix (dATP, dCTP, dGTP and dTTP; 10 mM each) and 1.0 µL of *Pfu* DNA polymerase (3 U/ µL) in 1X *pfu* buffer. The PCR product of step 3 and the plasmid pPC2 were digested with *SphI* followed by digestion with *EcoRI*. The digested PCR product and the digested plasmid pPC2 were ligated together to generate plasmid pPC3.

pPC4: pPC4 plasmid was created to introduce a new loop sequence at the loop L11 in the *btuB* aptamer. Along with the modified loop, pPC4 also carries 37 nucleotides of the expression platform the 3' end of the *btuB* aptamer sequence and 'GGA' as a start site for T7 RNA polymerase. pPC4 was created in four steps, each with 40 cycles of PCR consisting of melting for 1 minute at 90° C, annealing at 55° C and elongation at 68 °C. In the first step, the oligonucleotide pPC_13 was extended at the 3' end with the primer btuB239 and plasmid pPC2 as a template. The reaction mixture contains 500 ng of pPC2, 1.25 µL of oligo pPC_13 (10 µM), 1.25 µL of primer btuB239 (10 µM), 2.0 µL of dNTP mix (dATP, dCTP, dGTP and dTTP; 10 mM each), 1.0 µL of *Pfu* DNA polymerase (3 U/ µL) in 50 µL of 1X *Pfu* buffer. The PCR product was used as a template in the second PCR and was extended at the 5' end with the primer pPC2_14hgaI. The reaction contains 20 µL of the PCR product (20 ng/µL), 1.25 µL of forward primer (pPC2_14hgaI) (10 µM), 1.25 µL of reverse primer (btuB239) (10 µM), 2.0 µL of dNTP mix (dATP, dCTP, dGTP and dTTP; 10 mM each) and 1 µL of *Pfu* DNA polymerase (3 U/ µL) in 50 µL of 1X *Pfu* buffer. The PCR product of step two is further extended at the 5' end in a reaction containing 1 µL of the PCR product (130 ng/ µL), 5 µL of forward primer pPC2_15 (10 µM), 5 µL of reverse primer (btuB239) (10 µM), 1 µL of dNTP mix (dATP, dCTP, dGTP and dTTP; 10 mM each) and 0.5 µL of of *Pfu* DNA polymerase (3 U/ µL) in 50 µL of 1X *Pfu* buffer. 1 µL of the PCR product (62 ng/ µL) of step 4 is further extended at the 5' end with 1 µL of forward primer (pSG2_5) (10 µM), 1 µL of reverse primer (btuB239) (10 µM), 1 µL of dNTP mix (dATP, dCTP, dGTP and dTTP; 10 mM each) and 5 µL of *Pfu* DNA polymerase (3 U/ µL) in 50 µL of 1X *Pfu* buffer. The PCR product of step 4 and the plasmid pPC2 were digested with *SphI* followed by digestion with *EcoRI*. The digested PCR product and the digested plasmid pPC2 were ligated together to generate plasmid pPC4.

pPC5: Plasmid pPC5 was created to introduce a new restriction site *BgIII* at the 3' end of the *btuB* aptamer sequence. pPC5 plasmid contains the modified loop L11 and 'GGA' as a transcriptional start site for the T7 RNA polymerase. The plasmid was created by using two overlapping primers- pPC4_1 and pPC4_2, each carrying a restriction enzyme site $[AGATCT]_{BgIII}$ in the middle of the sequence. The PCR was performed with 500 ng of pPC4, 1.25 µL of primer pPC4_1 (10 µM), 1.25 µL of primer pPC4_2 (10 µM), 2.0 µL of dNTP mix (dATP, dCTP, dGTP and dTTP; 10 mM each) and 1.0 µL of *Pfu* DNA polymerase (3 U/ µL) in 50 µL of 1X *Pfu* buffer. The reaction mixture for PCR was subjected to 18 cycles for melting at 95° C for 30 seconds, annealing at 55° C for 1 minute, extension at 68 °C for 4:30 minutes and further incubation at 68° C for 5 minutes. The PCR product was transferred to a new eppendorf tube and 1 µL of DpnI enzyme was added to the sample followed by incubation at 37° C for 60 minutes. The sample was further transformed into *E. coli DH5α* cells to isolate the transformants containing the plasmid pPC5.

[Plasmids RS07, RS08 and RS16 were constructed by Dr. Julien Maillard. See Table S6.1]

8.2.2 Large scale preparation of plasmids

Heat shock transformation: The plasmids were transformed into chemically competent cells of *E. coli* DH5α. The bacterial cells were thawed on ice for 10 minutes prior to the transformation. The transformation was carried out by adding 10 µL of plasmid to 50 µL of bacterial cells (with 0.4- 0.5 OD_{600nm}), and mixing together gently by pipetting. The mixture was kept on ice for 10 minutes followed by incubation at 37 °C for 3 minutes (0 rpm), and was further kept on ice for 3 minutes. 500 µL of Luria-Bertani (LB) medium (without ampicillin) was added to the mixture followed by incubation at 37 °C for 30 minutes (0 rpm). The sample was shortly centrifuged at 1300 g for 1.5 minutes and the cells were collected from the pellet. 50 µL of the harvested transformed cells were spread on the ampicillin containing LB agar plates and incubated overnight at 37 °C to select the transformed colonies.

Small Liquid Cultures: Bacterial colonies growing on ampicillin containing LB agar plate indicate successful transformation as they carry an ampicilin resistance marker from the plasmid. Such a bacterial colony is picked with a sterile pipette tip and swirled into a culture tube containing 3 mL of LB medium + 100 µg/ mL ampicillin. The cells were grown by incubation at 37 °C/ 210 rpm for 8 hours. Some part of this culture was used to isolate the plasmid by High speed plasmid isolation (mini prep) kit. The isolated plasmid was sent for sequencing by mixing with primer (primer 154).

The remaining part of the small liquid culture is used as a pre-culture of making large scale liquid cultures.

Large Liquid Cultures: 200 µL of the small liquid culture was added to 150 µL of LB medium containing 100 µg/ mL of ampicillin. The cells were grown by overnight incubation at 37 °C/ 210 rpm. The cells were harvested by centrifugation at 6000 g for 15 minutes at 4 °C. The plasmid was isolated using the HiSpeed plasmid Maxi Kit.

8.2.3 Preparation of the RNA

Linearization of plasmids: The isolated plasmids were linearized by digestion with restriction enzyme. All of the plasmids were linearized with the restriction enzyme *EcoRI* except for plasmid pPC5. Plasmid pPC5 was digested with *BgIII*. (Depending upon the concentration of the template needed for *in vitro* transcription, the plasmid was digested in multiple sets, and each set contains 100 µg of the plasmid to be digested). The digestion of the plasmid was confirmed by performing agarose gel electrophoresis and the digested plasmid was purified by phenol- chloroform extraction (see section 7.2.4) to obtain higher yields.

***In vitro* transcription:** *In vitro* transcription was carried out using the digested plasmid (as a template) and homemade T7 RNA polymerase using general protocols (Gallo S, et al., 2005, *Chimia*, 59, 812-816). The following conditions of *in vitro* transcription were optimized by carrying out the transcription trials in a total volume of 50 µL. For 1 mL of transcription, the digested plasmid (see Table 7.1) was mixed with NTPs (ATP, GTP, CTP and UTP, 5 mM each), triton-X-100 (0.01%), $MgCl_2$ (see Table 7.1) and the T7 RNA polymerase (~ 20 to 25 µL/ mL, depending on the batch) in 1X transcription buffer (See Appendix 1). The reaction mixture was incubated overnight at 37 °C/ 300 rpm.

Table 7.1: Shown are the concentrations of the digested plasmids and $MgCl_2$ used for the *in vitro* transcription of RNAs by T7 RNA polymerase.

Plasmid	Digested plasmid (µg/ mL)	$MgCl_2$ (mM)
pPC1	5	40
pPC2	15	20
pPC3	5	40
pPC4	15	20
pPC5	15	30
pRS07	10	30
pRS08	10	30
pRS16	15	30

Precipitation of the transcription products: After overnight transcription, the reaction mixture was centrifuged at 3300 g for 0.5 minute. The transcription products in the supernatant were precipitated by 250 mM NaCl followed by the addition of 3 volumes of absolute ethanol (ice cold) and the samples were kept at -80 °C for 2 hours.

Purification and concentration of RNA by PAGE, electroelution and *Vivaspin*: The precipitated transcription products were isolated by centrifugation at 9500 rpm/ 4 °C for 30 minutes. The pellet is dried in a speed vac evaporator and was dissolved in autoclaved distilled water. The RNA sample in water was mixed with the equal volume of urea loading buffer (see Appendix 1) and was loaded on 10% denaturing PAGE (run with 1X TBE buffer). The RNA band was located with UV shadowing at 254 nm, cut out from the gel and recovered by elctroelution at room temperature in 1X TBE buffer until the RNA was completely eluted from the gel pieces. The eluted RNA was precipitated by 250 mM NaCl and 3 volumes of absolute ethanol (ice-cold). The samples were then kept overnight at -80 °C followed by centrifugation at 9500 rpm/ 4 °C for 30 minutes. The pellets were dissolved in water and concentrated by *Vivaspin* centrifugation. The RNA was stored in water at -20 °C. The concentration of RNA was determined spectroscopically from absorbance at 260 nm using the extinction coefficient shown in Table 7.2. The purity of RNA was checked by 10% PAGE and subsequent staining with ethidium bromide (staining in 5 µL ethidium bromide/ 500 ml of water for 5 minutes, destaining for 5-10 minutes in water) followed by detection at 312 nm.

Table 7.2: Extinction coefficients of RNAs.

RNA	Extinction coefficient (mM^{-1} cm^{-1})
pPC1	2404.8
pPC2	2675.6
pPC3	3150.1
pPC4	2941.3
pPC5	2541.9
pRS07	1664.1
pRS08	2090.1
pRS16	2081.4

8.2.4 Radiolabeling of the RNA

Dephosphorylation of the RNA: All of the *in vitro* transcribed RNA (pPC1, pPC2, pPC3, and pPC4) carry a 5'-tri phosphate and therefore, need to be dephosphorylated for 5' end labeling. Dephosphorylation was carried out with 60 pmol of RNA in a total reaction volume of 50 µL either by SAP (Shrimp Alkaline Phosphatase) or by TSAP (Thermosensitive Shrimp Alkaline Phosphatase). For reaction with the SAP, 5 µL of the SAP (1 U/ µL) was added followed by incubation at 37 °C for 15 minutes. Another 5 µL of the SAP (1 U/ µL) was then added and the sample was incubated for 15 minutes more at 37 °C. Alternatively, 2 µL of the TSAP (1 MBU/ µL) can be added to dephosphorylate RNA followed by incubation of the sample at 37 °C for 30 minutes. (TSAP works more efficiently than SAP and is preferred for the dephosphorylation of RNA especially if it is used further for radiolabeling purpose). 600 pmol of the RNA was dephosphorylated in total. The RNA was subsequently purified by phenol-chloroform extraction and was dissolved in 24 µL of ME buffer (Appendix 1).

Phenol-chloroform extraction:

1. Add 1/20th of total volume of 5 M NaCl to the sample
2. Add equal volume of equilibrated phenol (pH 7.9). Vortex the sample and spin down at 10000rpm/ 4 °C for 3 minutes.
3. Take out the upper aqueous phase in to separate eppendorf and add equal volume of ME buffer (Appendix 1) to the phenol phase and repeat step 2.
4. Add equal volume of chloroform: isoamyl alcohol (24:1) to the collected aqueous phase and vortex the sample thoroughly. Spin down at 10000rpm/ 4 °C for 3 minutes.
5. Take the aqueous phase and repeat step 4 at least 2-3 times.
6. Pool together all the aqueous phase from step 5 and add 2.5 volumes of absolute ethanol (ice cold) and keep the samples overnight at -80 °C.
7. The RNA is recollected by centrifugation at 9500 rpm/ 4 °C for 45- 60 minutes. The pellet is dried in a speedvac evaporator and is dissolved in 24 µL of ME buffer.

5' end labeling of the RNA: The dephosphorylated RNA in 24 µL of ME buffer is mixed with 8 µL of ^{32}P-γ-ATP (3000 Ci/ mmol), 4 µL of T4 polynucleotide kinase (PNK, 10 u/ µL), 4 µL of PNK buffer (10X). The reaction mixture is incubated at 37 °C for 30 minutes followed by the addition of equal volume of formamide loading buffer (Appendix 1). The labeled RNA is separated by running the sample on 5% denaturing PAGE (7 M urea) for 2- 2.5 hours. The RNA is visualized by phosphoimaging the gel and the RNA band was cut out from the gel.

Elution of the RNA: The RNA excised from the gel band is crushed into small pieces by centrifugation at 9500 rpm/ 4 °C for 3 minutes. The eppendorf tubes containing the crushed RNA were shortly dipped in liquid nitrogen to freeze the crushed bands. 800 µL of elution buffer was then added to each tube, mixed well by short vortexing and soaked in the buffer for 2.5 hours at 4 °C with short vortexing in between. The samples were then centrifuged at 9500 rpm/ 4 °C for 3 minutes. 2.5 volumes of ethanol were added to the supernatant followed by overnight precipitation at -20 °C. The samples were centrifuged at 13000 rpm/ 4 °C for 30-45 minutes. The pellet was dried in a speedvac evaporator and was dissolved in 50-60 µL of water. The concentration of RNA was measured by scintillation counting as well as spectroscopically from absorbance at 260 nm. The RNA was stored at -20 °C.

8.2.5 Structural probing with RNaseA and RNase V1

6 nM of ^{32}P-5'-labelled *btuB* RNA along with 1 µM of unlabeled RNA in 50 mM Tris-HCl (pH 7.5) was heated to 90°C for 1 min. The sample was cooled at room temperature for 1 min followed by the addition of 100 mM KCl and $MgCl_2$ (0-20 mM). The sample was incubated at 37°C for 10 minutes. In the case of RNase V1 digestion, 500 µM of AdoCbl was added to the sample and the sample was incubated at 37 °C for 15 minutes. The partial digestion with RNase was carried out by addition of 1 µL of of RNase A (0.0002 ng/µL) and RNase V1 (0.001 U/ µL). All the samples were incubated for 10 minutes at 37°C/300 rpm. 10 µL of formamide loading buffer was then added to the samples for quenching the reaction and the samples were immediately loaded on 10% denaturing PAGE to separate the cleavage products.

8.2.6 Fluorescence studies with Tb(III)

The conditions for these experiments were kept similar to the Tb(III) cleavage experiments. The final volume of the sample was kept to 100 µL. 1 µM of the *btuB* RNA (pPC1 RNA) was mixed with 25 mM MOPS, 100 mM KCl, distilled water and was heated to 90 °C for 45 seconds followed by incubation at room temperature for 1 minute. 20 mM $MgCl_2$ was then added to the samples followed by incubation at 37 °C for 15 minutes. In case of samples with AdoCbl, required concentration of AdoCbl was added and the samples were incubated at 37 °C for 15 minutes. 1 mM of $TbCl_3$ was then added to the samples. Depending upon the sequence of additions, either 1 mM of $TbCl_3$ was first added to the RNA followed by the addition of AdoCbl or AdoCbl was added before the addition of $TbCl_3$. The samples were excited at 290 nm and the fluorescence emission by Tb(III) was recorded at 545 nm using Cary Eclipse fluorescence spectrophotometer.

8.2.7 Laser photolysis of AdoCbl and in-line probing

The photolysis of AdoCbl by laser was confirmed by measuring the UV-Vis spectra (350-600 nm). The samples for UV-Vis spectroscopy were prepared by mixing 50 mM Tris-HCl (pH 8.3), 100 mM KCl, 20 mM $MgCl_2$ and 5 µM AdoCbl. In case of the samples with *btuB* RNA, 5 µM of the RNA (pPC1) was added to the samples to keep 1:1 ratio of the RNA: AdoCbl. The samples were then exposed to red laser (wavelength 650 nm) for the indicated time points followed by measurement of UV-Vis spectra. For the in-line probing experiments, 8 nM of the 5'-^{32}P-labeled RNA and 10 µM of the cold RNA were mixed with 50 mM Tris-HCl (pH 8.3), 100 mM KCl and 20 mM $MgCl_2$. 1 µM of AdoCbl was then added to the samples to keep the ratio of RNA: AdoCbl as 10:1. The samples were then incubated for the indicated time periods following exposure to red laser for 180 seconds. All the samples were then incubated for 40 hours at room temperature in dark and were analyzed by 10% denaturing PAGE.

8.2.8 Native gel electrophoresis with fluorophore containing DNAs

Samples (5 µL) containing RNA (3 µM), Cy3-DNA (4.5 µM) and Cy5-DNA were denatured in a reaction buffer containing 50 mM Tris-HCl (pH 7.5) and 100 mM KCl. 20 mM $MgCl_2$ was then added to the samples followed by incubation at 37 °C for 15 minutes. An equal volume of 60% glycerol was added to all the samples and the samples were loaded on a 6% (w/v) gel (0.5 mm thin) containing 3 mM MgOAc, 66 mM HEPES and 34 mM Tris, pH (7.5). Electrophoresis was performed at 4 °C for 2-2.5 hours in a buffer containing 3 mM MgOAc, 66 mM HEPES and 34 mM Tris, pH (7.5). Fluorescence bands of Cy3 and Cy5 were detected on the gels by Typhoon molecular scanner.

8.2.9 Bulk FRET experiment

1 µM of RNA (pPC4) along with Cy3-DNA (1 µM) and Cy5-DNA (1 µM) were denatured at 90 °C for 1 minute in a buffer containing 50 mM MOPS; pH 7.5, 10 µM EDTA, 100 mM KCl. 20 mM $MgCl_2$ was then added to the samples followed by incubation at 37 °C for 15 minutes. For the samples containing AdoCbl, 150 µM of AdoCbl was added to the samples. The samples were excited at 550 nm and the emission was recorded at 560-880 nm. All the spectra were recorded at 37 °C. The maximum values for Cy3 (donor) emission at 565 nm and for Cy5 (acceptor) emission at 665 nm were used for calculating the FRET as $[I_A/ (I_A + I_D)]$.

8.2.10 Other experiments carried out with the 5' end labeled RNA

In-line probing: See section 2.4.1 and 3.5.3.

Partial RNase T1 digestion: See section 3.5.5.

Tb(III) cleavage: See section 2.4.2 and 4.5.2.3.

Native gel electrophoresis: See section 3.5.7.

9 Summary

Recently, a new target class has emerged for developing promising antibiotics i.e. riboswitches (1,2). These are non-coding RNA elements residing at the 5' UTR of mRNA and are well known to recognize small metabolites/divalent cation/secondary messenger with strong affinity and specificity (3,4). All riboswitches known so far (except for the TPP binding riboswitches) are reported to occur only in prokaryotes regulating essential metabolic pathways in bacteria (2). Therefore, targeting a riboswitch provides a solid platform for the development of promising anti-microbials.

It is mandatory to know how a given riboswitch interacts with its ligand in order to employ this riboswitch as a target in drug designing. The essential domains of the riboswitch along with the functional groups of ligand contribute to an effective interaction. However, it is the 'ligand free' form of the riboswitch that is responsible for ligand binding (5). Upon binding to their ligand, riboswitches undergo a conformational change that activates or represses the expression of the gene product associated with the bound ligand (3,4). The regulation of gene expression is mainly controlled at the level of transcription or translation of the mRNA. Nevertheless, other mechanisms like alternative splicing, self cleavage and *trans* regulation have also been proposed recently (6).

The structure of most riboswitches has been determined both in their ligand free and ligand bound form except for the class of AdoCbl riboswitches (2,7). The crystal structures of AdoCbl riboswitches from thermophilic bacteria were solved recently in their ligand bound form providing details on the network of interactions between AdoCbl derivatives and B_{12} riboswitches (8-10). However, insights into the ligand free forms of B_{12} riboswitches are still missing. The work here therefore focuses on the *btuB* riboswitch from *E. coli* as a classical member of AdoCbl riboswitch class in order to provide a framework for understanding the nature of AdoCbl riboswitches in more depth.

The *btuB* riboswitch is located in the 5' UTR of the *btuB* mRNA (coding for the B_{12} transporter, BtuB) and regulates the cellular levels of AdoCbl (11-14). Structurally, the *btuB* riboswitch consists of 202 nucleotide long aptamer domain and an expression platform composed of 38 nucleotides (13,15). When the concentration of AdoCbl rises in the cell, the aptamer domain of the *btuB* riboswitch binds to AdoCbl and undergoes a structural change in its conformation. This switch in the structure ultimately leads to the sequestration of the ribosome binding site within the expression platform (3). Translation of the *btuB* mRNA is thus inhibited and the expression of the BtuB transporter is down regulated (3).

To get insights into the ligand free form of the *btuB* riboswitch, our work aims to observe the conformational changes in the RNA prior to ligand binding. Since RNA folding is largely dependent on monovalent and divalent cations (16-21), the studies here highlight the metal ion dependent conformational differences within the ligand free form of the *btuB* riboswitch. Moreover, the specific interaction of divalent metal ions like Mg^{2+} with RNA is essential to fold it into its native tertiary structure (21-23). We therefore extended our studies to locate such crucial Mg^{2+} binding sites within the *btuB* aptamer. Along with the pre-folding of aptamer, the regulation of the riboswitch depends also on the mode of interaction between the riboswitch and its ligand (24). To determine the same, we have studied the kinetics of interaction of the *btuB* riboswitch with its two ligands, AdoCbl and VitaminB_{12}.

Together with the *btuB* riboswitch, our studies also emphasize the diversity of cobalamine riboswitches in the corrinoid metabolism of another model system, *Desulfitobacterium*.

Pre-folding of the *btuB* aptamer

A first part of the thesis deals with the metal ion induced folding of the *btuB* riboswitch in its ligand free form. We applied in-line probing to study the same. In-line nucleophilic cleavage of RNA is largely dependent on the geometry taken up by the nucleotides and therefore, the cleavage pattern reveals a specific RNA conformation in its tertiary structure (13,25,26). We observed two specific conformations of the *btuB* aptamer in its ligand free form. These conformations depend on the concentration of Mg^{2+} ions where one of the species exists at low Mg^{2+} concentration (0-0.1 mM) and the other species exists at high Mg^{2+} concentration (0.5-20 mM) (Figure S1). With the addition of AdoCbl, the conformation of the species at 0-0.1 mM Mg^{2+} does not change at all. On the other hand, the species existing at high Mg^{2+} concentration clearly shows the earlier reported AdoCbl induced changes at certain nucleotides indicating a switched conformation of the RNA (13,27). Therefore, it is evident that AdoCbl can not switch the conformation of the *btuB* aptamer in the absence of Mg^{2+} or at low Mg^{2+} concentration. These results also suggested that the RNA species existing at 0.5-20 mM Mg^{2+} is correctly folded in order to interact with AdoCbl. This species therefore represents the 'binding competent conformation' of the *btuB* aptamer and clearly undergoes a conformational switch upon binding AdoCbl (Figure S1). The interaction of AdoCbl with the binding competent conformation of the *btuB* aptamer results in a compaction of the RNA conformation as observed from native gel electrophoresis. Therefore, AdoCbl possibly introduces new/altered tertiary interactions within the *btuB* riboswitch such that the ligand bound form is more compact than the ligand free form of the riboswitch.

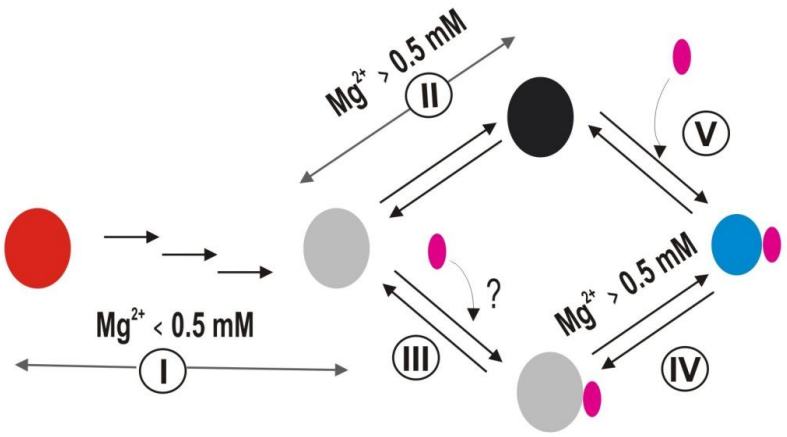

Figure S1: Mg^{2+} induced conformational changes in the *btuB* riboswitch: Shown is the model pathway for pre-folding of the *btuB* aptamer. The unfolded RNA (red) achieves binding 'incompetent' conformation (grey) at Mg^{2+} concentration < 0.5 mM (I) and binding 'competent' conformation (black) at Mg^{2+} concentration > 0.5 mM (II). Binding 'incompetent' conformation may or may not recognize AdoCbl (pink) (III) although it is able to undergo a AdoCbl induced conformational switch (blue) at Mg^{2+} concentration > 0.5 mM (IV). The binding competent conformation can switch its conformation (blue) in the presence of AdoCbl (V).

In-line probing however is able to detect only the conformational changes in RNA and does not indicate if the ligand is 'bound' to RNA in the absence of the expected conformational changes. Therefore, it could be that AdoCbl binds the conformation of the *btuB* aptamer at low Mg^{2+} concentration but is unable to switch its conformation (Figure S1). In this case, both Mg^{2+} and AdoCbl could interact with the *btuB* riboswitch in a concerted manner to facilitate the conformational switch. This phenomenon has been observed earlier in case of SAM I riboswitch (28) and needs further investigations to confirm the same in the *btuB* riboswitch.

As the *btuB* aptamer undergoes Mg^{2+} induced folding, we calculated the affinity of Mg^{2+} towards the different domains of the riboswitch in its ligand free form using the classical method of RNase T1 probing (29,30). Interestingly, Mg^{2+} has

distinct affinities towards different regions of the *btuB* riboswitch and therefore, the *btuB* riboswitch appears to follow a hierarchical mode of folding. With the help of dissociation constants (K_D) for Mg^{2+}, we propose a folding pathway for the *btuB* aptamer where domains with high affinity towards Mg^{2+} fold prior to other domains with lower affinity. Thus, in a ligand free *btuB* aptamer, stems P7 and P12 fold prior to the other regions followed by the folding of stems P8 and P4, P6, P5 and P3.

These studies suggested that Mg^{2+} plays a vital role in the pre-folding of the *btuB* riboswitch in order to interact with AdoCbl as in the absence of Mg^{2+}, AdoCbl fails to switch the conformation of the *btuB* riboswitch (31).

Mapping the Mg^{2+} binding sites on the *btuB* riboswitch

The interaction of Mg^{2+} with the *btuB* riboswitch is crucial to pre-fold the aptamer in order to recognize and bind AdoCbl. We have thus mapped the Mg^{2+} binding sites on the *btuB* riboswitch with the help of a Mg^{2+} mimic, the lanthanide ion terbium(III) (Tb^{3+}) (32-36). Of all the mapped Mg^{2+} binding nucleotides, nucleotide A122 at stem P12 exhibits the best geometry for M^{n+} binding and M^{n+} binding at A122 might be essential for the overall stabilization of the aptamer. Most of the M^{n+} binding sites over the *btuB* aptamer are concentrated mainly around the conserved bases near the regions J2/3, J3/4, P5, L5, P7, J10/11, P11 and J11/10 (Figure S2). Interestingly, the AdoCbl riboswitches from thermophiles involve tertiary interactions (coaxial stem, KL and pseudoknot interactions) near the regions involving the conserved nucleotides of the aptamer (Figure S2) (4,8,9,15). We therefore propose that the mapped M^{n+} binding sites in the *btuB* riboswitch are involved in tertiary interactions that assist folding of the aptamer prior to ligand binding. This specific interaction of Mg^{2+} with the *btuB* aptamer can be extrapolated to other members of AdoCbl riboswitches due to highly conserved bases of the aptamer within the consensus sequence of AdoCbl riboswitches (15). Interaction of AdoCbl with the *btuB* riboswitch however does not lead to the alterations in the metal ion binding properties and also does not affect the conformation of the RNA drastically. Therefore, AdoCbl appears to induce small localized changes in the *btuB* riboswitch without altering the global conformation of the RNA.

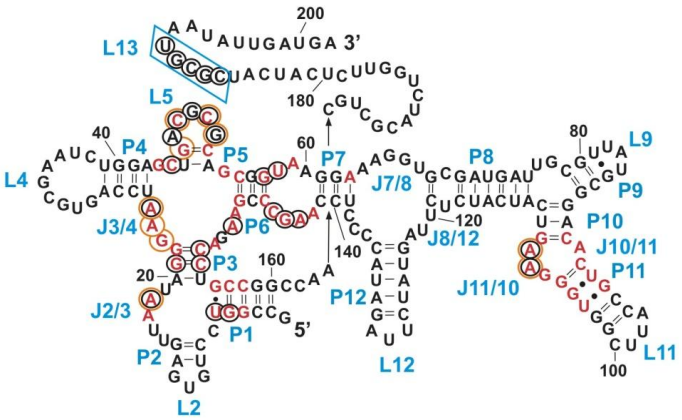

Figure S2: Mg^{2+} binding sites in the *btuB* aptamer: Shown is the secondary structure of the *btuB* riboswitch with conserved nucleotides indicated in red among AdoCbl riboswitches. Mg^{2+} binding sites (circled in orange) mostly coincide with bases (circled in black) undergoing tertiary interactions between regions J2/3, J3/4, L5 and J11/10 in the case of the AdoCbl riboswitch from *S. thermophilum* (9).

The kinetics of the interaction between the *btuB* riboswitch and cobalamines

This section provides insights into the kinetics of the interaction between the *btuB* riboswitch with its natural ligand (AdoCbl) and non-physiological ligand (Vitamin B_{12}) (Figure S3). The basic aim of this work was to establish the mode of interaction between AdoCbl and the *btuB* riboswitch as well as to find out why related ligands of the cobalamine family exhibit drastically different affinities towards the *btuB* riboswitch. With the help of SPR spectroscopy, we derived the rates of association (k_a) and dissociation (k_d) for the *btuB*-AdoCbl system as 3.2 x 10^4 ($M^{-1}s^{-1}$) and 2.93 x 10^{-4} (s^{-1}) respectively. Although the k_a falls within the range estimated for several other riboswitches (24), the k_d for dissociation of AdoCbl from the *btuB* riboswitch is extremely slow and apparently not achievable within the half life (~ 2 minutes) of the mRNA in bacterial cells.

The *btuB* -VitB_{12} interaction shows an almost identical k_a (1.89 x 10^4 $M^{-1}s^{-1}$) as the *btuB*-AdoCbl interaction (3.2 x 10^4 $M^{-1}s^{-1}$) however the k_d (1.925 s^{-1}) is 10^4 fold faster than in the *btuB*-AdoCbl system. This drastic difference in k_d is reflected in the dissociation constants (K_D) of the two ligands towards the *btuB* riboswitch. AdoCbl therefore binds the *btuB* riboswitch with 10^4 fold higher affinity than VitB_{12}. Interestingly, AdoCbl and VitB_{12} differ from each other only with respect to their β-axial moiety but share the α-axial group (37). Therefore, the similar rate of association suggests that AdoCbl and VitB_{12} are recognized by the *btuB* riboswitch possibly through a similar mechanism that involves contacts to α-axial side of cobalamines as well as to the corrin ring and its side chains. The association with cobalamine leads to the conformational rearrangement of the *btuB* riboswitch that provides a tight binding pocket to AdoCbl over the other cobalamines lacking the adenosyl moiety. This proposed mechanism strongly supports the earlier observation where a similar structural switch of the *btuB* riboswitch is achieved by AdoCbl and VitB_{12} although with 1000 fold differences in their affinity for the riboswitch (27).

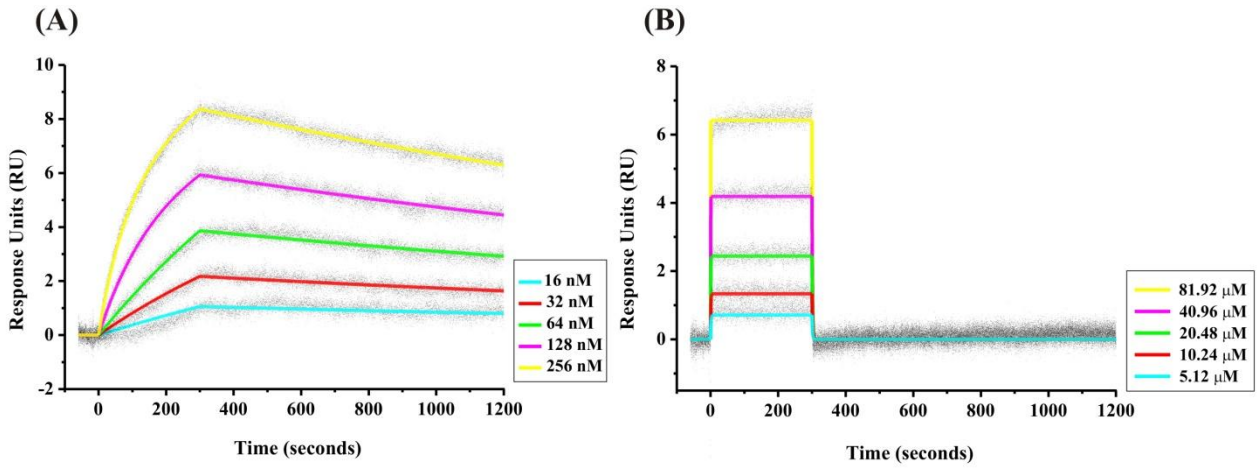

Figure S3: Kinetics of interaction between the *btuB* riboswitch and cobalamines: Shown are the sensorgrams (dots) for the kinetics of the *btuB* riboswitch with AdoCbl (A) and Vitamin B_{12} (B) fitted to the 1:1 binding model of interaction (solid lines). The downward slopes indicate the difference in the rate of dissociation between AdoCbl and Vitamin B_{12} towards the *btuB* riboswitch.

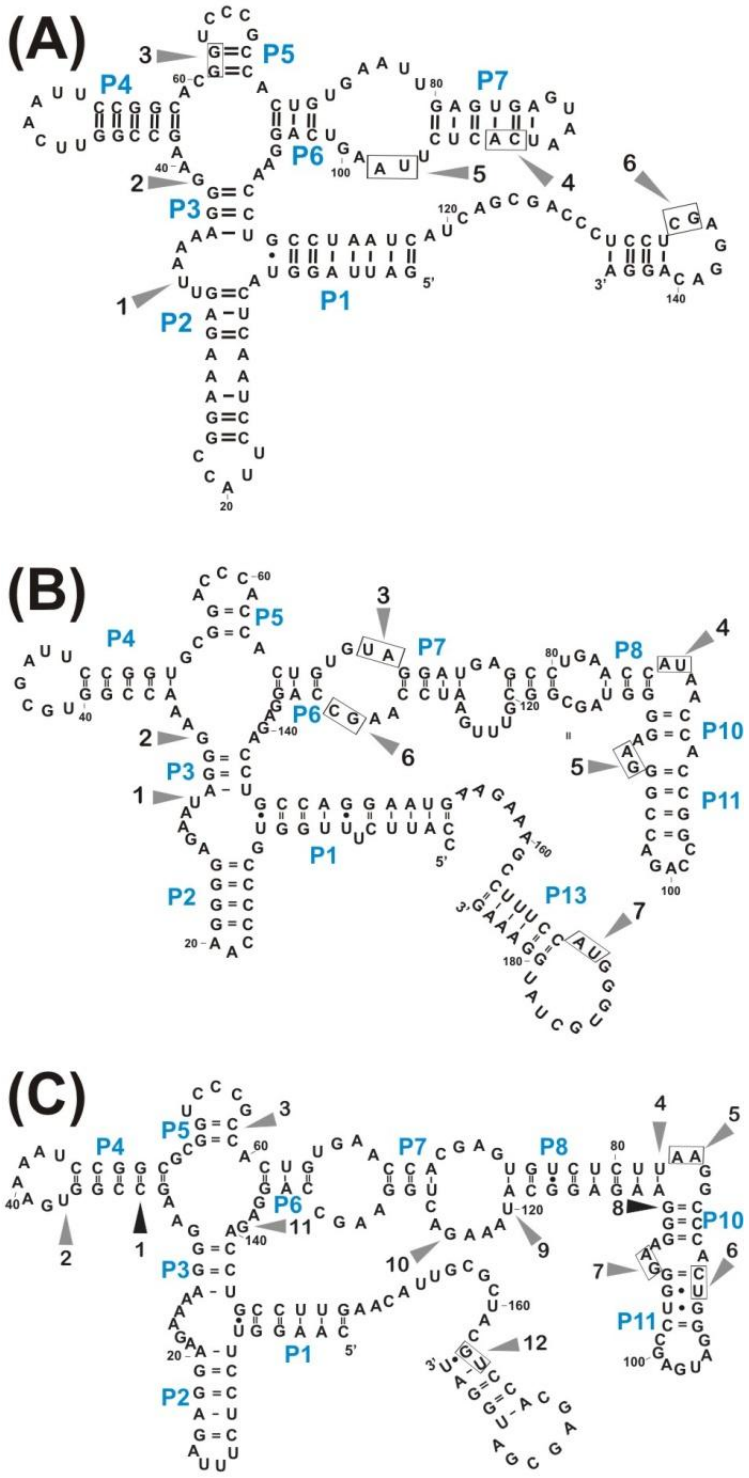

Figure S4: Secondary structural elements of the cobalamine riboswitches from *Desulfitobacterium*: Shown are the predicted secondary structures of riboswitches RS07 (A), RS08 (B) and RS16 (C). The grey and black arrows respectively indicate the nucleotides undergoing decrease and increase in the cleavage intensity in the presence of AdoCbl in in-line probing experiments. In comparison to the *btuB* riboswitch from *E. coli*, aptamer for RS07 lacks the peripheral structural elements from P8-P12 whereas the aptamers for RS08/RS16 lack stems P9 and P12.

The SPR studies led to another interesting hypothesis for the *btuB*-AdoCbl interaction. The kinetic data for the *btuB*-AdoCbl interaction could be fitted to two different kinetic models, i.e a 1:1 binding model and a heterogenous ligand binding model. The 1:1 binding model suggests a simple bimolecular reaction between AdoCbl and the *btuB* riboswitch. The heterogenous ligand model however indicates the presence of two RNA species, referred to as B1 and B2 where species B2 has a four fold higher affinity towards AdoCbl than species B1. Interestingly, the rate constants for the high affinity species (species B2) resemble the constants derived from 1:1 binding model for the *btuB*-AdoCbl interaction. As the interaction between the *btuB* riboswitch and $VitB_{12}$ could be fitted only to a 1:1 binding model, we propose that the 1:1 binding model reports the kinetic parameters only for the high affinity RNA species that occurs in majority. Therefore, species B2 seems to dominate the RNA population. If so, then the folded *btuB* riboswitch exists in two conformations, both being able to bind AdoCbl although with different affinities. It is however difficult to predict from the SPR experiments if both species undergo a similar structural switch by AdoCbl.

B_{12} riboswitches from *Desulfitobacterium*

Desulfitobacterium is another fascinating organism to explore further the diversity of B_{12} riboswitches. The genome of an obligate anaerobe like *Desulfitobacterium*, carries not only the full set of genes responsible for corrinoid biosynthesis but also the putative corrinoid transporters (38-40). As the cobalamine metabolism has been reported to be regulated by B_{12} riboswitches (41), our studies on *Desulfitobacterium* aims to understand the corrinoid metabolism in these bacteria in terms of their cobalamine riboswitches. This work has been carried out on *Desulfitobacterium hafniense* TCE1 as a representative member of the *Desulfitobacterium* group. Notably, this bacteria harbours 16 cobalamine riboswitches evident from the phylogenetic

analysis (42). Currently, *Desulfitobacterium hafniense* TCE1 has been reported as one of the top ten bacteria carrying the highest number of riboswitches in the Rfam database (RF00174, August 2012).

Out of the 16 predicted cobalamine riboswitches in *Desulfitobacterium hafniense* TCE1, we concentrated on riboswitches RS07, RS08 and RS16 to demonstrate their functionality *in vitro* as well as *in vivo*. RS07 is located upstream of the BtuF homolog and therefore must be involved in the regulation of B_{12} transport across the cell (43). RS08 and RS16 are situated upstream of the operons involved in cobalamine biosynthesis. In-line probing experiments indicated AdoCbl induced modification in all three riboswitches under study, however their affinity (K_D) towards AdoCbl varies. The secondary structural elements (predicted by mfold) of these riboswitches indicate the absence of peripheral structural elements (stems P8-P12) in RS07 and therefore justifies its lower affinity (89 µM) towards AdoCbl compared to RS08 and RS16 (Figure S4). The observed differences in the affinity to AdoCbl exhibited by RS08 and RS16 possibly relates to their role in corrinoid biosynthesis. The high affinity of AdoCbl to RS16 (30 nM) compared to RS08 (270 nM) probably represses the synthesis of α-axial ligand of AdoCbl.

The *in vivo* expression of mRNA for RS07, RS08 and RS16 is significantly repressed in the presence of AdoCbl. This repression is most probably exerted at the level of transcription as the expression platforms of RS07, RS08 and RS16 riboswitches carry transcriptional terminators. These studies on cobalamine riboswitches from *D. hafniense* TCE1 confirms the structural and functional diversity exhibited by B_{12} riboswitches possibly to fine tune the complex corrinoid metabolism in these bacteria.

Conclusion

This work focuses on B_{12} riboswitches in order to comprehend not only the high conservation of this RNA element across the prokaryotic world but also to understand their high specificity towards cobalamine ligands. Our work on the AdoCbl responsive *btuB* riboswitch from *E. coli* provides an insight into the significance of the aptamer architecture to the ligand binding potential for AdoCbl riboswitches. This work suggests that the divalent metal ion- Mg^{2+} facilitates the pre-folding of AdoCbl riboswitch to successfully recognize its complex ligand, AdoCbl. Moreover, the presence of Mg^{2+} binding sites near the conserved bases of the aptamer indicate that the mechanism of aptamer pre-organization in the case of the AdoCbl riboswitches might involve Mg^{2+} mediated interactions. The pre-folded aptamer probably interacts with cobalamine ligands in a similar way but does not provide a tight binding pocket to all cobalamines. This is evident from the rate constants for the *btuB*-AdoCbl/VitB_{12} interaction suggesting the rate of the dissociation (k_d) being a determining factor for the varying affinity of these cobalamines to the *btuB* riboswitch. In addition, our work on B_{12} riboswitches in *Desulfitobacterium* suggests that these riboswitches could harbour variable structural elements to alter their affinity towards AdoCbl and regulate cobalamine metabolism within the cell.

References

1. Blount, K.F. and Breaker, R.R. (2006) Riboswitches as antibacterial drug targets. *Nat Biotechnol*, **24**, 1558-1564.
2. Deigan, K.E. and Ferre-D'Amare, A.R. (2011) Riboswitches: discovery of drugs that target bacterial gene-regulatory RNAs. *Acc Chem Res*, **44**, 1329-1338.
3. Mandal, M. and Breaker, R.R. (2004) Gene regulation by riboswitches. *Nat Rev Mol Cell Bio*, **5**, 451-463.
4. Winkler, W.C. and Breaker, R.R. (2005) Regulation of bacterial gene expression by riboswitches. *Annu Rev Microbiol*, **59**, 487-517.
5. Montange, R.K. and Batey, R.T. (2008) Riboswitches: emerging themes in RNA structure and function. *Annu Rev Biophys*, **37**, 117-133.

6. Bastet, L., Dube, A., Masse, E. and Lafontaine, D.A. (2011) New insights into riboswitch regulation mechanisms. *Mol Microbiol*, **80**, 1148-1154.
7. Serganov, A. and Patel, D.J. (2012) Metabolite recognition principles and molecular mechanisms underlying riboswitch function. *Annu Rev Biophys*, **41**, 343-370.
8. Johnson Jr, J.E., Reyes, F.E., Polaski, J.T. and Batey, R.T. (2012) B_{12} cofactors directly stabilize an mRNA regulatory switch. *Nature*, **492**, 133-137.
9. Peselis, A. and Serganov, A. (2012) Structural insights into ligand binding and gene expression control by an adenosylcobalamin riboswitch. *Nat Struct Mol Biol*, **19**, 1182-1184.
10. Souliere, M.F., Haller, A., Santner, T. and Micura, R. (2013) New insights into gene regulation--high-resolution structures of cobalamin riboswitches. *Angew Chem Int Ed Engl*, **52**, 1874-1877.
11. Gudmundsdottir, A., Bradbeer, C. and Kadner, R.J. (1988) Altered binding and transport of vitamin B12 resulting from insertion mutations in the *Escherichia coli btuB* gene. *J Biol Chem*, **263**, 14224-14230.
12. Kadner, R.J. (1978) Repression of Synthesis of Vitamin-B_{12} Receptor in *Escherichia coli*. *J Bacteriol*, **136**, 1050-1057.
13. Nahvi, A., Sudarsan, N., Ebert, M.S., Zou, X., Brown, K.L. and Breaker, R.R. (2002) Genetic control by a metabolite binding mRNA. *Chem Biol*, **9**, 1043-1049.
14. Nou, X.W. and Kadner, R.J. (2000) Adenosylcobalamin inhibits ribosome binding to btuB RNA. *P Natl Acad Sci USA*, **97**, 7190-7195.
15. Nahvi, A., Barrick, J.E. and Breaker, R.R. (2004) Coenzyme B_{12} riboswitches are widespread genetic control elements in prokaryotes. *Nucleic Acids Res.*, **32**, 143-150.
16. Auffinger, P., Grover, N. and Westhof, E. (2011) Metal ion binding to RNA. *Met Ions Life Sci*, **9**, 1-35.
17. Draper, D.E. (2004) A guide to ions and RNA structure. *RNA*, **10**, 335-343.
18. Draper, D.E., Grilley, D. and Soto, A.M. (2005) Ions and RNA folding. *Annu Rev Biophys Biomol Struct*, **34**, 221-243.
19. Pyle, A.M. (2002) Metal ions in the structure and function of RNA. *J Biol Inorg Chem*, **7**, 679-690.
20. Sigel, R.K. and Pyle, A.M. (2007) Alternative roles for metal ions in enzyme catalysis and the implications for ribozyme chemistry. *Chem Rev*, **107**, 97-113.
21. Woodson, S.A. (2005) Metal ions and RNA folding: a highly charged topic with dynamic future. *Curr. Opin. Chem. Biol.*, **9**, 104-109.
22. Misra, V.K. and Draper, D.E. (1998) On the role of magnesium ions in RNA stability. *Biopolymers*, **48**, 113-135.
23. Misra, V.K. and Draper, D.E. (2002) The linkage between magnesium binding and RNA folding. *J Mol Biol*, **317**, 507-521.
24. Zhang, J., Lau, M.W. and Ferre-D'Amare, A.R. (2010) Ribozymes and riboswitches: modulation of RNA function by small molecules. *Biochemistry*, **49**, 9123-9131.
25. Choudhary, P.K., Gallo, S. and Sigel, R.K.O. (2014) Monitoring Global Structural Changes and Specific Metal Binding Sites in RNA by in-line Probing and Tb(III) Cleavage. *Methods Mol Biol, in press*.
26. Soukup, G.A. and Breaker, R.R. (1999) Relationship between internucleotide linkage geometry and the stability of RNA. *RNA*, **5**, 1308-1325.
27. Gallo, S., Oberhuber, M., Sigel, R.K.O. and Kräutler, B. (2008) The corrin moiety of coenzyme B_{12} is the determinant for switching the *btuB* riboswitch of *E. coli*. *Chembiochem*, **9**, 1408-1414.
28. Heppell, B., Blouin, S., Dussault, A.M., Mulhbacher, J., Ennifar, E., Penedo, J.C. and Lafontaine, D.A. (2011) Molecular insights into the ligand-controlled organization of the SAM-I riboswitch. *Nat Chem Biol*, **7**, 384-392.

29. Chauhan, S., Caliskan, G., Briber, R.M., Perez-Salas, U., Rangan, P., Thirumalai, D. and Woodson, S.A. (2005) RNA tertiary interactions mediate native collapse of a bacterial group I ribozyme. *J Mol Biol*, **353**, 1199-1209.
30. Rangan, P., Masquida, B., Westhof, E. and Woodson, S.A. (2003) Assembly of core helices and rapid tertiary folding of a small bacterial group I ribozyme. *Proc Natl Acad Sci USA*, **100**, 1574-1579.
31. Choudhary, P.K. and Sigel, R.K.O. (2013) Mg^{2+} induced conformational changes in the *btuB* riboswitch from *E. coli*. *in revision*.
32. Ciesiolka, J., Marciniec, T. and Krzyzosiak, W. (1989) Probing the environment of lanthanide binding sites in yeast tRNA(Phe) by specific metal-ion-promoted cleavages. *Eur J Biochem*, **182**, 445-450.
33. Harris, D.A., Tinsley, R.A. and Walter, N.G. (2004) Terbium-mediated footprinting probes a catalytic conformational switch in the antigenomic hepatitis delta virus ribozyme. *J Mol Biol*, **341**, 389-403.
34. Sigel, R.K.O. and Pyle, A.M. (2003) Lanthanide ions as probes for metal ions in the structure and catalytic mechanism of ribozymes. *Met Ions Biol Syst*, **40**, 477-512.
35. Sigel, R.K.O., Vaidya, A. and Pyle, A.M. (2000) Metal ion binding sites in a group II intron core. *Nat Struct Biol*, **7**, 1111-1116.
36. Walter, N.G., Yang, N. and Burke, J.M. (2000) Probing non-selective cation binding in the hairpin ribozyme with Tb(III). *J Mol Biol*, **298**, 539-555.
37. Gruber, K., Puffer, B. and Kräutler, B. (2011) Vitamin B_{12}-derivatives-enzyme cofactors and ligands of proteins and nucleic acids. *Chem Soc Rev*, **40**, 4346-4363.
38. Maillard, J. Unpublished data.
39. Nonaka, H., Keresztes, G., Shinoda, Y., Ikenaga, Y., Abe, M., Naito, K., Inatomi, K., Furukawa, K., Inui, M. and Yukawa, H. (2006) Complete genome sequence of the dehalorespiring bacterium *Desulfitobacterium hafniense* Y51 and comparison with *Dehalococcoides ethenogenes* 195. *J Bacteriol*, **188**, 2262-2274.
40. Villemur, R., Lanthier, M., Beaudet, R. and Lepine, F. (2006) The *Desulfitobacterium* genus. *FEMS Microbiol Rev*, **30**, 706-733.
41. Vitreschak, A.G., Rodionov, D.A., Mironov, A.A. and Gelfand, M.S. (2003) Regulation of the vitamin B_{12} metabolism and transport in bacteria by a conserved RNA structural element. *RNA*, **9**, 1084-1097.
42. Choudhary, P.K., Duret, A., Rohrbach-Brandt, E., Holliger, C., Sigel, R.K.O. and Maillard, J. (2013) Corrinoid biosynthesis and diversity of cobalamine riboswitches in the organohalide respirer *Desulfitobacterium hafniense*. *J. Bacteriol*, accepted.
43. Cadieux, N., Bradbeer, C., Reeger-Schneider, E., Koster, W., Mohanty, A.K., Wiener, M.C. and Kadner, R.J. (2002) Identification of the periplasmic cobalamin-binding protein BtuF of *Escherichia coli*. *J Bacteriol*, **184**, 706-717.

Zusammenfassung

Seit kurzem bildet sich eine neue Zielgruppe für die Entwicklung vielversprechende Antibiotika heraus: die Riboswitches (1,2). Riboswitches sind nicht-kodierende RNA-Elemente in der 5' UTR von mRNA und dafür bekannt, dass sie kleine Metabolite, zweiwertige Kationen und sekundäre Botenstoffe mit hoher Affinität und Spezifität erkennen (3,4). Alle bisher bekannten Riboswitches (mit Ausnahme der TPP-bindenden Riboswitches) wurden ausschließlich in Prokaryoten gefunden und regulieren essentielle Stoffwechselwege in Bakterien (2). Dadurch eignen sie sich besonders als Angriffspunkte für die Entwicklung vielversprechender anti-mikrobieller Wirkstoffe.

Das Wissen, wie ein Riboswitch mit seinem Liganden interagiert, ist unabdingbar für die Entwicklung von Wirkstoffen, die auf den Riboswitch abzielen. Zu einer stabilen Wechselwirkung tragen sowohl die entscheidenden Domänen des Riboswitches als auch die funktionellen Gruppen des Liganden bei. Jedoch ist es die Ligand-freie Form des Riboswitches, die das Binden des Liganden erlaubt (5). Wenn der Ligand bindet kommt es zu einer Konformationsänderung des Riboswitches, welche die Expression des mit dem gebundenen Liganden assoziierten Genprodukts aktiviert oder unterdrückt (3,4). Die Regulation der Genexpression wird hauptsächlich auf der Ebene von Transkription und Translation der mRNA kontrolliert. In letzter Zeit werden aber auch Mechanismen wie das alternative Spleissen, Selbstspaltung und *trans*-Regulation diskutiert (6).

Die Struktur der meisten Riboswitches wurde bereits in Ligand-gebundener und freier Form bestimmt, mit Ausnahme der Klasse der AdoCbl-Riboswitches (2,7). Kürzlich bestimmte Kristallstrukturen von AdoCbl-Riboswitches aus thermophilen Bakterien in der Ligand-gebunden Form zeigen den molekularen Mechanismus der Erkennung zwischen AdoCbl und den B_{12}-Riboswitches auf (8-10). Einblicke in die Ligand-freie Form der B_{12}-Riboswitches fehlen jedoch bisher noch. Die hier beschriebene Arbeit befasst sich daher mit dem *btuB*-Riboswitch aus *E. coli* als einem klassischen Mitglied der AdoCbl-Riboswitch Klasse um eine Basis für ein tieferes Verständnis der Natur der AdoCbl-Riboswitches aufzubauen.

Der *btuB*-Riboswitch findet sich in der 5' UTR der *btuB* mRNA (diese kodiert für den B_{12} Transporter BtuB) und reguliert den zellulären AdoCbl-Level (11-14). Er besteht aus einer 202 Nukleotide langen Aptamerdomäne und einer Expressionsplattform aus 38 Nukleotiden (13,15). Wenn die AdoCbl-Konzentration in der Zelle steigt bindet die Aptamerdomäne des *btuB*-Riboswitches das AdoCbl und vollzieht eine Strukturänderung. Dieses „Umschalten“ führt schlussendlich zur Sequestrierung der Ribosomenbindungsstelle in der Expressionsplattform (3). Dadurch wird die Translation der *btuB*- mRNA gehemmt und die Expression des BtuB-Transporters nach unten reguliert (3).

Um Erkenntnisse über die Ligand-freie Form des *btuB*-Riboswitchs zu gewinnen untersuchen wir in der vorliegenden Arbeit Konformationsänderungen der RNA vor der Bindung des Liganden. Da RNA-Faltung zu einem grossen Teil von ein- und zweiwertigen Kationen abhängt (16-21), beleuchten unsere Studien Metallionen-abhängige Konformationsänderungen in der Ligand-freien Form des *btuB*-Riboswitches. Auch für die Faltung der nativen Tertiärstruktur ist die spezifische Wechselwirkung von zweiwertigen Ionen wie Mg^{2+} mit der RNA wesentlich (21-23). Daher haben wir in unseren Studien auch die Lokalisierung solcher essentieller Mg^{2+}-Bindungsstellen im *btuB*-Aptamer untersucht. Abgesehen von der Vorfaltung des Aptamers wird die Regulation des Riboswitches auch von der Art der Wechselwirkung zwischen Riboswitch und Ligand bestimmt (24). Um diese zu bestimmen haben wir die Kinetik der Interaktion zwischen *btuB*-Riboswitch und zwei seiner Liganden, AdoCbl and Vitamin B_{12}, untersucht.

Zusammen mit dem *btuB*-Riboswitch zeigen unsere Studien auch die Diversität der Cobalamin-Riboswitches im Corrinoidstoffwechsel eines weiteren Modellsystems, des *Desulfitobacteriums,* auf.

Vorfaltung des *btuB*-Aptamer

Dieser Teil der Arbeit beschäftigt sich mit der Metallionen-induzierten Faltung des *btuB*-Riboswitches in seiner Liganden-freien Form. Um diese zu untersuchen setzen wir die Technik des *In-line Probing* ein. Nukleophile *in-line*-Spaltung von RNA hängt von der Geometrie der Nukleotide ab, weshalb das Spaltungsmuster spezifische RNA-Konformationen der Sekundärstruktur erkennen lassen kann (13,25,26). In seiner Ligand-freien Form beobachten wir zwei spezifische Konformationen des *btuB*-Aptamer. Diese Konformationen sind abhängig von der Konzentration der Mg^{2+}-Ionen, wobei eine der Spezies bei niedriger Mg^{2+}-Konzentration (0-0.1 mM) und die andere bei hoher Mg^{2+}-Konzentration (0.5-20 mM) vorkommt (Abbildung S1). Die Konformation der Spezies bei 0-0.1 mM Mg^{2+} zeigt keine Änderung bei Zugabe von AdoCbl. Die Spezies bei hoher Mg^{2+}-Konzentration andererseits zeigt deutlich die bereits beschriebenen AdoCbl-induzierten Änderungen bei bestimmten Nukleotiden, die ein Umschalten der RNA-Konformation anzeigen (13,27). Dadurch wird klar, dass AdoCbl ohne Mg^{2+} oder bei nur geringer Mg^{2+}-Konzentration die Konformation des *btuB*-Aptamer nicht umschalten kann. Ausserdem weisen die Ergebnisse darauf hin, dass die Spezies bei 0.5-20 mM Mg^{2+} korrekt gefaltet ist für die Interaktion mit AdoCbl. Diese Spezies stellt also die 'bindungskompetente Konformation' des *btuB*-Aptamer dar und erfährt eine Konformationsänderung bei der Bindung von AdoCbl (Abbildung S1). Die Wechselwirkung von AdoCbl mit der bindungskompeten Konformation des *btuB*-Aptamer führt zu einer Kompaktierung der RNA-Konformation, wie durch native Gelelektrophorese beobachtbar ist. AdoCbl führt möglicherweise zu neuen/veränderten tertiären Interaktionen im *btuB*-Riboswitch, die die Liganden-gebundene Form kompakter machen als die Liganden-freie Form.

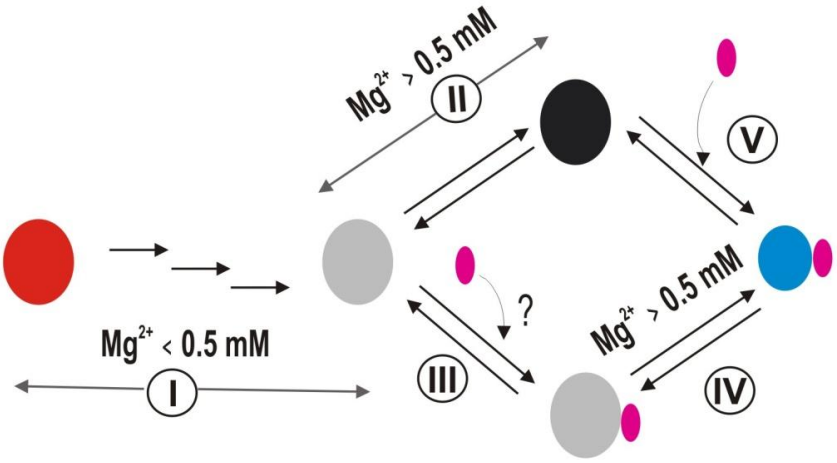

Abbildung S1: Mg^{2+}-induzierte Konformationsänderungen im *btuB* Riboswitch. Gezeigt ist ein Modellweg für die Vorfaltung des *btuB* Aptamer: Die ungefaltete RNA (rot) erreicht eine Bindungs-'inkompetente' Konformation (grau) bei Mg^{2+}-Konzentration < 0.5 mM (I) und Bindungs-'kompetente' Konformation (schwarz) bei Mg^{2+}-Konzentration > 0.5 mM (II). Die Bindungs-'inkompetente' Konformation könnte oder auch nicht AdoCbl (rosa) (III) erkennen, auch wenn sie die AdoCbl-induzierte Konformationsänderung (blau) nur bei Mg^{2+} Konzentrationen > 0.5 mM (IV) vollzieht. Die Bindungs-'kompetente' Konformation kann durch AdoCbl umgeschaltet werden (V).

In-line Probing kann jedoch nur Konformationsänderungen der RNA detektieren und zeigt nicht, ob der Ligand an die RNA gebunden ist, wenn keine Konformationsänderung erfolgt. Es wäre daher möglich, dass AdoCbl auch bei niedriger Mg^{2+}-Konzentration an das *btuB*-Aptamer bindet, aber dessen Konformation nicht umschalten kann (Abbildung S1). In diesem Fall könnten Mg^{2+} und AdoCbl gemeinsam zum Umschalten führen. Dieses Phänomen wurde zuvor im Fall des SAM I Riboswitches (28) beobachtet und müsste erst durch weitere Untersuchungen im *btuB*-Riboswitch bestätigt werden.

Da die Faltung des *btuB*-Aptamer Mg^{2+}-induziert ist haben wir Mg^{2+}-Affinitäten der verschiedenen Riboswitch-Domänen in der Ligand-freien Form mittels *RNase T1 Probing* bestimmt (29,30). Interessanterweise hat Mg^{2+} stark unterschiedliche Affinitäten zu verschiedenen Regionen des *btuB*-Riboswitch, was auf eine hierarchische Faltung hinweist. Mithilfe der Dissoziationskonstanten (K_D) für Mg^{2+} schlagen wir einen Faltungsweg des *btuB*-Aptamer vor, in dem die Domäne mit einer hohen Affinität für Mg^{2+} sich vor den anderen Domänen mit niedrigerer Affinität faltet. Das heisst, dass sich im Ligand-freien *btuB*-Aptamer erst die Stems P7 und P12 falten, gefolgt von Stems P8 und P4, P6, P5 und P3.

Diese Studien weisen auf eine wichtige Rolle von Mg^{2+} in der Vorfaltung des *btuB*-Riboswitch und für seine Interaktion mit AdoCbl hin, da AdoCbl ohne Mg^{2+} kein Umschalten des *btuB* Riboswitch bewirken kann (31).

Bestimmung der Mg^{2+}-Bindungsstellen im *btuB* Riboswitch

Die Wechselwirkung von Mg^{2+} mit dem *btuB*-Riboswitch ist von entscheidender Bedeutung für die Vorfaltung des Aptamers und die Erkennung und Bindung von AdoCbl. Daher haben wir mithilfe des Lanthanid Ions Terbium(III) (Tb^{3+}) (32-36), Mg^{2+}-Bindungsstellen auf dem *btuB*-Riboswitch lokalisiert. Unter allen Mg^{2+}-bindenden Nukleotiden besitzt Nukleotid A122 in der P12-Helix die beste Geometrie zur M^{n+}-Bindung wobei die M^{n+}-Bindung am A122 essentiell für die Stabilisierung des gesamten Aptamers sein könnte. Die meisten Bindungsstellen im *btuB*-Aptamer befinden sich in der Nähe der konservierten Basen in J2/3, J3/4, P5, L5, P7, J10/11, P11 und J11/10 (Abbildung S2). Interessanterweise gibt es in AdoCbl-Riboswitches von Thermophilen tertiäre Interaktionen (coaxial stem-, KL- und Pseudoknot-Interaktionen) in der Nähe dieser Regionen (Abbildung S2) (4,8,9,15). Es ist daher denkbar, dass die hier gefundenen M^{n+}-Ionen in die tertiären Wechselwirkung involviert sind und die Faltung des Aptamer vor der Ligandbindung unterstützen. Wegen der in der Konsensussequenz hoch-konservierten Basen im Aptamer der AdoCbl-Riboswitches (15) kann die Information über spezifische Interaktion von Mg^{2+} mit dem *btuB*-Aptamer auf andere Mitglieder der AdoCbl-Riboswitches übertragen werden. Interaktion von AdoCbl mit dem *btuB*-Riboswitch führt jedoch zu keinen Änderungen in den Metallbindungseigenschaften und beeinflusst auch die Konformation der RNA nicht stark. AdoCbl scheint daher kleine, lokalisierte Veränderungen im *btuB*-Riboswitch zu bewirken, ohne die globale Konformation der RNA zu ändern.

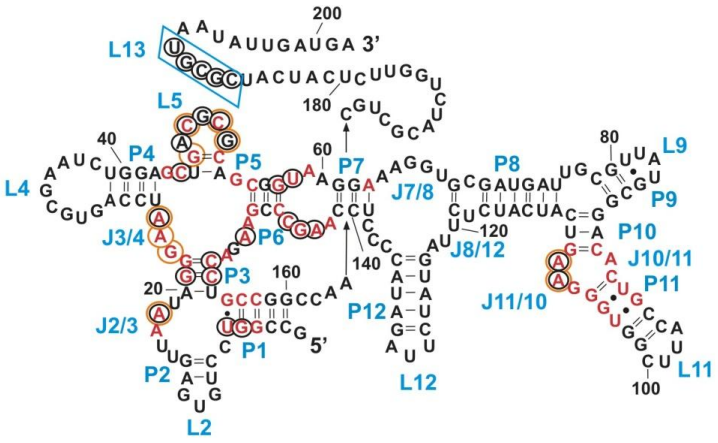

Abbildung S2: Mg^{2+}-Bindungsstellen im *btuB* Aptamer: Gezeigt ist die Sekundärstruktur des *btuB* Riboswitches mit Nukleotiden,die in der Konsensussequenz von AdoCbl Riboswitches konserviert sind (rot). Die Mg^{2+}-Bindungsstellen (orange eingekreist) am *btuB* Riboswitch finden sich bei den Basen (schwarz eingekreist), welche im Fall des AdoCbl Riboswitch von *S. Thermophilum* (9) tertiäre Interaktionen mit J2/3, J3/4, L5 and J11/10 eingehen.

Die Kinetik der Wechselwirkung – der *btuB*-Riboswitch und Cobalamines

Dieser Teil der Arbeit gibt Einblicke in die Kinetik der Wechselwirkungen zwischen dem *btuB*-Riboswitch und seinem natürlichen Liganden (AdoCbl) und einem nicht-physiologischen Liganden (Vitamin B_{12}) (Abbildung S3). Das grundlegende Ziel dieser Arbeit war die Art der Wechselwirkung zwischen AdoCbl und dem *btuB*-Riboswitch zu

bestimmen, sowie auch die drastisch unterschiedlichen Affinitäten von verschiedenen Liganden der Cobalamin-Familie zum *btuB*-Riboswitch zu erklären. Mithilfe von SPR-Spektroskopie haben wir die Geschwindigkeitskonstanten für die Assoziation (k_a = 3.2 x 10^4 $M^{-1}s^{-1}$ und die Dissoziationsrate (k_d = 2.93 x 10^{-4} s^{-1}) für das *btuB*-AdoCbl System bestimmt. Obwohl k_a im selben Bereich liegt wie für andere Riboswitches erwartete Geschwindigkeitskonstanten (24), zeigt k_d eine extrem langsame Dissoziation an, welche die Halbwertszeit von mRNA in einen Bakterienzelle (~ 2 Minuten) übersteigt.

Die kinetischen Parameter für die *btuB*- und $VitB_{12}$-Interaktion ergeben eine beinahe identische Assoziationsrate (k_a = 1.89 x 10^4 $M^{-1}s^{-1}$) wie bei der *btuB*-AdoCbl Interaktion (3.20 x 10^4 $M^{-1}s^{-1}$), während die Dissoziation (k_d = 1.925 s^{-1}) 10^4-mal schneller abläuft als im *btuB*-AdoCbl System. Dieser drastische Unterschied der k_d-Rate spiegelt sich in der Affinität (K_A) der zwei Liganden zum *btuB* Riboswitch. AdoCbl bindet den *btuB* Riboswitch mit 10^4 mal höherer Affinität als $VitaminB_{12}$. AdoCbl und $VitB_{12}$ unterscheiden sich nur in den β-axialen Resten, während die α-axialen gleich sind (37). Die ähnlichen Assoziationsraten weisen darauf hin, dass AdoCbl und $VitB_{12}$ vom *btuB* Riboswitch durch einen ähnlichen Mechanismus erkannt werden, und zwar sowohl über die α-axiale Seite als auch durch das Corrin Ringsystem und seine Seitenketten. Die Assoziation mit dem Cobalamin führt zu einer Konformationsänderung im *btuB* Riboswitch, wodurch eine Bindungstasche entsteht an die AdoCbl fester binden kann als andere Cobalamine ohne die Adenosylgruppe. Dieser Mechanismus stimmt mit früheren Beobachtungen überein, wo AdoCbl und $VitB_{12}$ ein ähnliches Umschalten der Struktur des *btuB* Riboswitches bewirken, jedoch mit 1000-fach unterschiedlicher Affinität für den Riboswitch (27).

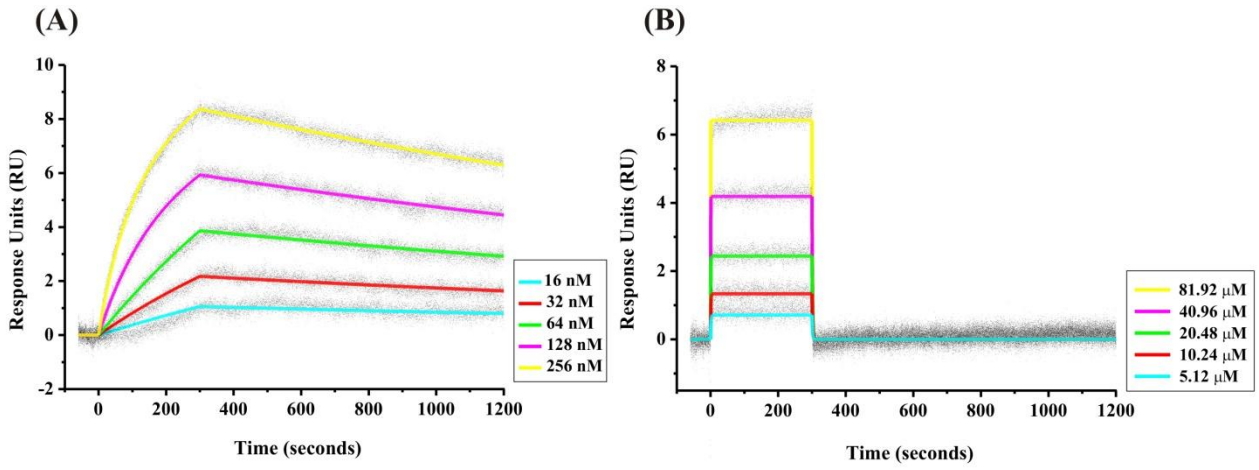

Abbildung S3: Kinetik der Wechselwirkung zwischen dem *btuB* Riboswitch und Cobalaminen: Gezeigt sind Sensogramme (schwarz gepunktet) der Kinetik des *btuB* Riboswitches mit AdoCbl (A) und Vitamin B_{12} (B), gefittet zu einem 1:1 Bindungsmodell (durchgezogene Linien). An der Steigung der abwärts fallenden Kurve zeigen sich die unterschiedlichen Dissoziationsraten von AdoCbl und Vitamin B_{12} vom *btuB* Riboswitch.

Die SPR Studien führten zu einer anderen interessanten Hypothese für *btuB*-AdoCbl Wechselwirkungen. Die kinetischen Daten für die *btuB*-AdoCbl Interaktion können mit zwei unterschiedlichen kinetischen Modellen – einem 1:1 Bindungsmodell und einem heterogenen Ligandenbindungsmodell – gefittet werden. Das 1:1 Bindungsmodell legt eine einfach bimolekulare Reaktion zwischen AdoCbl und dem *btuB* Riboswitch nahe. Das heterogene Ligandenbindungsmodell andererseits deutet auf die Präsenz von zwei RNA Spezies hin – Spezies B1 und B2 – wo Spezies B2 eine viermal stärkere Affinität zu AdoCbl hat als Spezies B1.

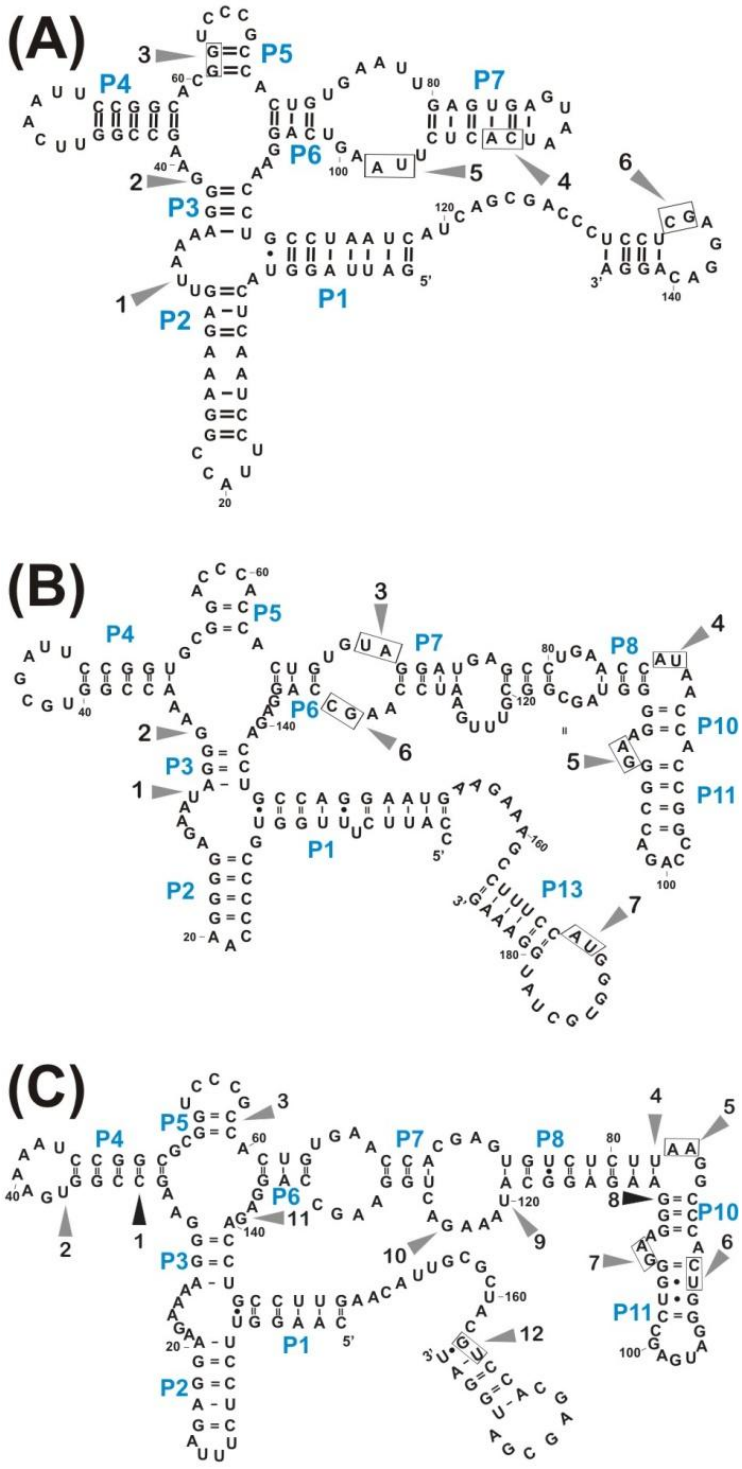

Abbildung S4: Sekundärstrukturelemente des Cobalamin-Riboswitches von *Desulfitobacterium*: Gezeigt ist die vorhergesagte Sekundärstruktur der Riboswitches RS07 (A), RS08 (B) und RS16 (C). Die grauen bzw. schwarzen Pfeile weisen auf Nukleotide, die in *In-line Probing* Experimenten in Gegenwart von AdoCbl stärker bzw. schwächer gespalten werden. Im Vergleich zum *btuB* Riboswitch von *E. coli* fehlen dem Aptamer von RS07 periphere Strukturelemente von P8-P12, während den Aptameren von RS08/RS16 P9 und P12 fehlen.

Die kinetischen Konstanten für die Hochaffinitätsspezies (Spezies B2) ähneln den Konstanten aus dem 1:1 Bindungsmodell für die *btuB*-AdoCbl Interaktion. Da die Interaktion zwischen dem *btuB* Riboswitch und VitB_{12} nur mit dem 1:1 Bindungsmodell gefittet werden kann, ist anzunehmen, dass das 1:1 Bindungsmodell nur die kinetischen Parameter für die Hochaffinitätsspezies der RNA anzeigt, die möglicherweise die Mehrheit ausmacht. Spezies B2 scheint daher die RNA Population zu dominieren. In diesem Fall würde der *btuB* Riboswitch in zwei Konformationen existieren, die beide im Stande sind AdoCbl zu binden, wenn auch mit unterschiedlicher Affinität. Aus den SPR Experimenten ist allerdings schwer vorherzusagen, ob beide Spezies durch AdoCbl ähnliche Strukturänderungen erfahren. Weitere Untersuchungen sind hier nötig.

B_{12} Riboswitches von *Desulfitobacterium*

Desulfitobacterium ist ein weiteres faszinierendes System um die Diversität von B_{12} Riboswitches zu untersuchen. Das Genom eines obligaten Anaeroben wie *Desulfitobacterium*, trägt nicht nur ein volles Set an Genen, die für die Corrinoid Biosynthese zuständig sind, sondern auch mögliche Corrinoid-Transporter (38-40). Da der Cobalamin-Stoffwechsel von B_{12} Riboswitches (41) reguliert wird, zielen unsere Studien an *Desulfitobacterium* darauf ab, den Corrinoid-Stoffwechsel in diesen Bakterien im Zusammenhang mit ihren Cobalamin-Riboswitches zu verstehen. In dieser Arbeit wurde *Desulfitobacterium hafniense* TCE1 als repräsentativem Mitglied der *Desulfitobacterium* Gruppe untersucht. Dieses Bakterium beherbergt 16 durch phylogenetische Analyse ersichtliche Cobalamin-Riboswitches (42). Gegenwärtig ist *Desulfitobacterium hafniense* TCE1 eines der Top 10 Bakterien mit der höchsten Anzahl an Riboswitches in der Rfam Datenbank (RF00174, August 2012).

Von den 16 vorhergesagten Cobalamin-Riboswitches in *Desulfitobacterium hafniense* TCE1 haben wir uns auf Riboswitches RS07, RS08 und RS16 konzentriert um ihre Funktionalität *in vitro* und *in vivo* zu bestimmen. RS07 findet sich upstream des BtuF Homologs und sollte daher an der Regulation des B_{12} Transports durch die Zelle beteiligt sein (43). RS08 und RS16 liegen upstream der Operons, die in die Cobalamin-Biosynthese involviert sind. *In-line Probing* Experimente zeigen AdoCbl-induzierte Modifikationen in allen drei untersuchten Riboswitches, jedoch mit unterschiedlicher Affinität (K_A) für AdoCbl. Die von mfold vorhergesagten Sekundärstrukturelemente dieser Riboswitches weisen auf ein Fehlen von peripheren Strukturelementen (Stems P8-P12) in RS07 hin, was die im Vergleich zu RS08 und RS16 niedrigere Affinität für AdoCbl von 89 µM erklärt (Abbildung S4). Die beobachteten Unterschiede zwischen RS08 und RS16 in der Affinität zu AdoCbl ist möglicherweise in ihrer Rolle in der Corrinoid-Biosynthese begründet. Die höhere Affinität von AdoCbl für RS16 (30 nM) im Vergleich zu RS08 (270 nM) hemmt vermutlich die Synthese des α-axialen Liganden von AdoCbl.

Die *in vivo* Expression der mRNA von RS07, RS08 und RS16 wird bedeutend vermindert wenn AdoCbl vorhanden ist. Diese Verminderung findet vermutlich auf dem Level der Transkription statt, da die Expressionsplattformen der RS07, RS08 und RS16 Riboswitches transkriptionelle Terminatoren beinhalten. Diese Studien an Cobalamin Riboswitches von *D. hafniense* TCE1 bestätigen die strukturelle und funktionelle Diversität der B_{12} Riboswitches, die ein genaue Regelung des komplexen Corrinoid-Stoffwechsel in Bakterien ermöglichen.

Fazit

Die hier präsentierte Arbeit beschäftigt sich mit B_{12} Riboswitches um nicht nur die hohe Konservierung dieses RNA-Elements in der prokaryotischen Welt, sondern auch seine hohe Spezifität für Cobalamin-Liganden zu verstehen. Unsere Arbeit am AdoCbl-bindenden *btuB*-Riboswitch von *E. coli* zeigt die Bedeutung der Aptamer-Architektur für das Bindungspotential von AdoCbl Riboswitches. Diese Arbeit weist darauf hin, dass das zweiwertige Metallion Mg^{2+} die Vorfaltung des AdoCbl-Riboswitches unterstützt, um eine erfolgreiche Erkennung des komplexen Liganden AdoCbl zu ermöglichen. Weiters weisen Mg^{2+} Bindungsstellen in der Nähe von konservierten Basen des Aptamer darauf hin, dass der Mechanismus der Aptamer-Preorganisation im Fall der AdoCbl-Riboswitches Mg^{2+}-vermittelte Interaktionen umfassen könnte. Das vorgefaltete Aptamer interagiert möglicherweise in ähnlicher Weise mit den Cobalamin-Liganden, birgt aber keine feste Bindungstasche für alle Cobalamine. Das zeigt sich in den Geschwindigkeitskonstanten für die *btuB*-AdoCbl/VitB_{12} Interaktion, wo die Dissoziationsrate (k_d) der entscheidende Faktor für Unterschiede in der Affinität dieser Cobalamine zum *btuB* Riboswitch ist. Unsere Arbeit an B_{12} Riboswitches von *Desulfitobacterium* weist darauf hin, dass diese Riboswitches Varianten von Strukturelementen beherbergen, welche die Affinität zu AdoCbl verändern und den Cobalamin-Stoffwechsel in der Zelle regulieren.

Referenzen:

1. Blount, K.F. and Breaker, R.R. (2006) Riboswitches as antibacterial drug targets. *Nat Biotechnol*, **24**, 1558-1564.
2. Deigan, K.E. and Ferre-D'Amare, A.R. (2011) Riboswitches: discovery of drugs that target bacterial gene-regulatory RNAs. *Acc Chem Res*, **44**, 1329-1338.
3. Mandal, M. and Breaker, R.R. (2004) Gene regulation by riboswitches. *Nat Rev Mol Cell Bio*, **5**, 451-463.
4. Winkler, W.C. and Breaker, R.R. (2005) Regulation of bacterial gene expression by riboswitches. *Annu Rev Microbiol*, **59**, 487-517.
5. Montange, R.K. and Batey, R.T. (2008) Riboswitches: emerging themes in RNA structure and function. *Annu Rev Biophys*, **37**, 117-133.

6. Bastet, L., Dube, A., Masse, E. and Lafontaine, D.A. (2011) New insights into riboswitch regulation mechanisms. *Mol Microbiol*, **80**, 1148-1154.
7. Serganov, A. and Patel, D.J. (2012) Metabolite recognition principles and molecular mechanisms underlying riboswitch function. *Annu Rev Biophys*, **41**, 343-370.
8. Johnson Jr, J.E., Reyes, F.E., Polaski, J.T. and Batey, R.T. (2012) B_{12} cofactors directly stabilize an mRNA regulatory switch. *Nature*, **492**, 133-137.
9. Peselis, A. and Serganov, A. (2012) Structural insights into ligand binding and gene expression control by an adenosylcobalamin riboswitch. *Nat Struct Mol Biol*, **19**, 1182-1184.
10. Souliere, M.F., Haller, A., Santner, T. and Micura, R. (2013) New insights into gene regulation--high-resolution structures of cobalamin riboswitches. *Angew Chem Int Ed Engl*, **52**, 1874-1877.
11. Gudmundsdottir, A., Bradbeer, C. and Kadner, R.J. (1988) Altered binding and transport of vitamin B12 resulting from insertion mutations in the *Escherichia coli btuB* gene. *J Biol Chem*, **263**, 14224-14230.
12. Kadner, R.J. (1978) Repression of Synthesis of Vitamin-B_{12} Receptor in *Escherichia coli*. *J Bacteriol*, **136**, 1050-1057.
13. Nahvi, A., Sudarsan, N., Ebert, M.S., Zou, X., Brown, K.L. and Breaker, R.R. (2002) Genetic control by a metabolite binding mRNA. *Chem Biol*, **9**, 1043-1049.
14. Nou, X.W. and Kadner, R.J. (2000) Adenosylcobalamin inhibits ribosome binding to btuB RNA. *P Natl Acad Sci USA*, **97**, 7190-7195.
15. Nahvi, A., Barrick, J.E. and Breaker, R.R. (2004) Coenzyme B_{12} riboswitches are widespread genetic control elements in prokaryotes. *Nucleic Acids Res.*, **32**, 143-150.
16. Auffinger, P., Grover, N. and Westhof, E. (2011) Metal ion binding to RNA. *Met Ions Life Sci*, **9**, 1-35.
17. Draper, D.E. (2004) A guide to ions and RNA structure. *RNA*, **10**, 335-343.
18. Draper, D.E., Grilley, D. and Soto, A.M. (2005) Ions and RNA folding. *Annu Rev Biophys Biomol Struct*, **34**, 221-243.
19. Pyle, A.M. (2002) Metal ions in the structure and function of RNA. *J Biol Inorg Chem*, **7**, 679-690.
20. Sigel, R.K. and Pyle, A.M. (2007) Alternative roles for metal ions in enzyme catalysis and the implications for ribozyme chemistry. *Chem Rev*, **107**, 97-113.
21. Woodson, S.A. (2005) Metal ions and RNA folding: a highly charged topic with dynamic future. *Curr. Opin. Chem. Biol.*, **9**, 104-109.
22. Misra, V.K. and Draper, D.E. (1998) On the role of magnesium ions in RNA stability. *Biopolymers*, **48**, 113-135.
23. Misra, V.K. and Draper, D.E. (2002) The linkage between magnesium binding and RNA folding. *J Mol Biol*, **317**, 507-521.
24. Zhang, J., Lau, M.W. and Ferre-D'Amare, A.R. (2010) Ribozymes and riboswitches: modulation of RNA function by small molecules. *Biochemistry*, **49**, 9123-9131.
25. Choudhary, P.K., Gallo, S. and Sigel, R.K.O. (2014) Monitoring Global Structural Changes and Specific Metal Binding Sites in RNA by in-line Probing and Tb(III) Cleavage. *Methods Mol Biol, in press*.
26. Soukup, G.A. and Breaker, R.R. (1999) Relationship between internucleotide linkage geometry and the stability of RNA. *RNA*, **5**, 1308-1325.
27. Gallo, S., Oberhuber, M., Sigel, R.K.O. and Kräutler, B. (2008) The corrin moiety of coenzyme B_{12} is the determinant for switching the *btuB* riboswitch of *E. coli*. *Chembiochem*, **9**, 1408-1414.
28. Heppell, B., Blouin, S., Dussault, A.M., Mulhbacher, J., Ennifar, E., Penedo, J.C. and Lafontaine, D.A. (2011) Molecular insights into the ligand-controlled organization of the SAM-I riboswitch. *Nat Chem Biol*, **7**, 384-392.

29. Chauhan, S., Caliskan, G., Briber, R.M., Perez-Salas, U., Rangan, P., Thirumalai, D. and Woodson, S.A. (2005) RNA tertiary interactions mediate native collapse of a bacterial group I ribozyme. *J Mol Biol*, **353**, 1199-1209.
30. Rangan, P., Masquida, B., Westhof, E. and Woodson, S.A. (2003) Assembly of core helices and rapid tertiary folding of a small bacterial group I ribozyme. *Proc Natl Acad Sci USA*, **100**, 1574-1579.
31. Choudhary, P.K. and Sigel, R.K.O. (2013) Mg^{2+} induced conformational changes in the *btuB* riboswitch from *E. coli*. *in revision*.
32. Ciesiolka, J., Marciniec, T. and Krzyzosiak, W. (1989) Probing the environment of lanthanide binding sites in yeast tRNA(Phe) by specific metal-ion-promoted cleavages. *Eur J Biochem*, **182**, 445-450.
33. Harris, D.A., Tinsley, R.A. and Walter, N.G. (2004) Terbium-mediated footprinting probes a catalytic conformational switch in the antigenomic hepatitis delta virus ribozyme. *J Mol Biol*, **341**, 389-403.
34. Sigel, R.K.O. and Pyle, A.M. (2003) Lanthanide ions as probes for metal ions in the structure and catalytic mechanism of ribozymes. *Met Ions Biol Syst*, **40**, 477-512.
35. Sigel, R.K.O., Vaidya, A. and Pyle, A.M. (2000) Metal ion binding sites in a group II intron core. *Nat Struct Biol*, **7**, 1111-1116.
36. Walter, N.G., Yang, N. and Burke, J.M. (2000) Probing non-selective cation binding in the hairpin ribozyme with Tb(III). *J Mol Biol*, **298**, 539-555.
37. Gruber, K., Puffer, B. and Kräutler, B. (2011) Vitamin B_{12}-derivatives-enzyme cofactors and ligands of proteins and nucleic acids. *Chem Soc Rev*, **40**, 4346-4363.
38. Maillard, J. Unpublished data.
39. Nonaka, H., Keresztes, G., Shinoda, Y., Ikenaga, Y., Abe, M., Naito, K., Inatomi, K., Furukawa, K., Inui, M. and Yukawa, H. (2006) Complete genome sequence of the dehalorespiring bacterium *Desulfitobacterium hafniense* Y51 and comparison with *Dehalococcoides ethenogenes* 195. *J Bacteriol*, **188**, 2262-2274.
40. Villemur, R., Lanthier, M., Beaudet, R. and Lepine, F. (2006) The *Desulfitobacterium* genus. *FEMS Microbiol Rev*, **30**, 706-733.
41. Vitreschak, A.G., Rodionov, D.A., Mironov, A.A. and Gelfand, M.S. (2003) Regulation of the vitamin B_{12} metabolism and transport in bacteria by a conserved RNA structural element. *RNA*, **9**, 1084-1097.
42. Choudhary, P.K., Duret, A., Rohrbach-Brandt, E., Holliger, C., Sigel, R.K.O. and Maillard, J. (2013) Corrinoid biosynthesis and diversity of cobalamine riboswitches in the organohalide respirer *Desulfitobacterium hafniense*. *J. Bacteriol*, accepted.
43. Cadieux, N., Bradbeer, C., Reeger-Schneider, E., Koster, W., Mohanty, A.K., Wiener, M.C. and Kadner, R.J. (2002) Identification of the periplasmic cobalamin-binding protein BtuF of *Escherichia coli*. *J Bacteriol*, **184**, 706-717.

10 **Appendices**

Appendix 1: Buffers

Appendix 2: Evaluation of Mg^{2+} concentration dependent partial RNase T1 digestion of the *btuB* RNA

Appendix 3: Evaluation of Tb^{3+} cleavage of the *btuB* RNA to map Mg^{2+} binding sites

Appendix 4: Evaluation of the in-line probing gel to determine the K_A of AdoCbl towards the RS07 RNA

Appendix 5: Plasmid Table pPC1

Appendix 6: Plasmid Table pPC2

Appendix 7: Plasmid Table pPC3

Appendix 8: Plasmid Table pPC4

Appendix 9: Plasmid Table pPC5

Appendix 10: Plasmid Table pRS07

Appendix 11: Plasmid Table pRS08

Appendix 12: Plasmid Table pRS16

Appendix 1: Buffers

Transcription Buffer for *in-vitro* transcription (10X, without $MgCl_2$)

400 mM Tris-HCl (pH 7.5), 20 mM spermidine, 50 mM DTT. Store at -20 °C.

Formamide loading buffer

82% (v/v) Formamide,10 mM EDTA (pH 8.0), 0.16% (w/v) XC and 0.16% (w/v) BB. Store at 4 °C.

Urea loading buffer for PAGE

11.8 M Urea, 8.3% sucrose, 42 mM Tris-HCl (pH 7.5), 0.8 mM EDTA (pH 8.0), 0.08% dye xylene cyanol (XC) and bromophenol blue (BB). Store at 4 °C.

Loading Buffer for native gel electrophoresis (PAGE)

60% glycerol in dd H_2O.

TBE buffer for electrophoresis and electro elution (10X)

0.89 M Tris-HCl (pH 8.3), 0.89 M boric acid, 0.002 M EDTA.

ME buffer

10 mM MOPS (pH 6.0), 1 µM EDTA (pH 8.0).

Elution buffer

10 mM Tris-HCl (pH 7.5), 200 mM NaCl, 1mM EDTA (pH 8.0).

Loading buffer for agarose gels (6X)

50 mM EDTA (pH 8.0), 30% (v/v) glycerol, 0.25% (w/v) BB, 0.25% (w/v) XC.

TAE buffer for Agarose gel electrophoresis (50X)

20 mM Tris, 1 M acetic acid, 50 mM EDTA (pH 8.0).

Appendix 2: Evaluation of the Mg^{2+} concentration dependent partial RNase T1 digestion of the *btuB* RNA

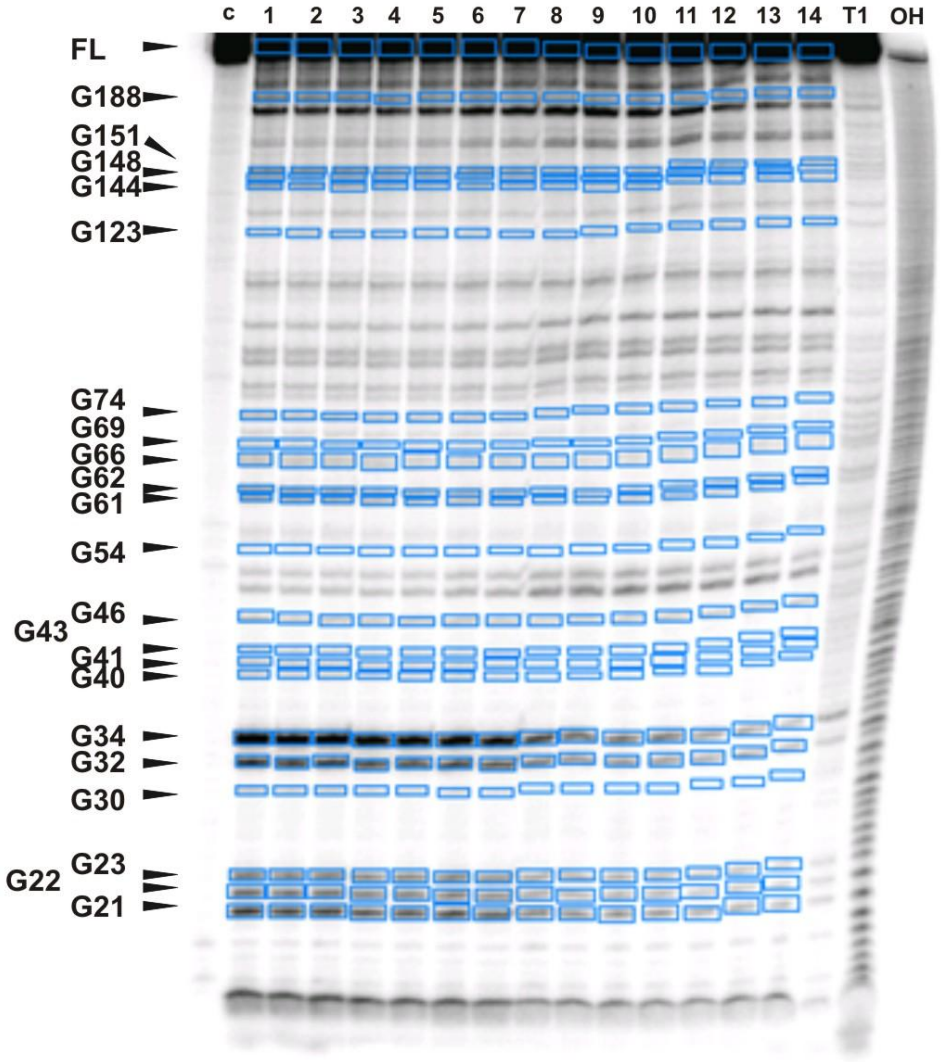

Figure A2.1: Evaluation of the PAGE gel for RNase T1 probing of the *btuB* RNA in Mg^{2+} dependent fashion: The typical gel shows the cleavage/protection at the guanine residues from the enzyme, RNase T1. The blue boxes mark the area of the band intensity used in the evaluation. The arrows indicate the subset of guanine residues analyzed in the experiments. The band FL corresponds to the full length RNA band, considered as a reference in the evaluation. The concentration of Mg^{2+} increases from lane 1 to 14 (see Table A2.1). Lane c is the unreacted RNA, lane T1 is RNase T1 ladder and lane OH corresponds to the alkaline hydrolysis ladder.

Table A2.1: Evaluation of the Gel.

Name of the Band	Band	Mg^{2+} concentration (mM)	Cleavage Intensity (Ic)	Full length band Intensity (I)	Cleaved Fraction Icc = (Ic / I)	Relative Cleavage Intensity Icc_R = (Icc (x mM) / Icc (0 mM))
Full length (FL)	FL. 1	0	12480905.28			
	FL. 2	0.05	12997891.93			
	FL. 3	0.1	13446398.51			
	FL. 4	0.2	13804966.51			
	FL. 5	0.3	14718298.52			
	FL. 6	0.4	14739663.74			
	FL. 7	0.5	13553753.07			
	FL. 8	1	16557185.18			
	FL. 9	2	17586912.27			
	FL. 10	4	19747288.5			
	FL. 11	6	19470632.46			
	FL. 12	8	20707474.7			
	FL. 13	10	21578485.42			
	FL. 14	20	22793231.65			
G 21	21. 1	0	982075.72	12480905.28	0.078686257	1
	21. 2	0.05	862028.16	12997891.93	0.066320613	0.842848745
	21. 3	0.1	899768.09	13446398.51	0.066915174	0.850404837
	21. 4	0.2	764821.61	13804966.51	0.055401917	0.70408632
	21. 5	0.3	728667.1	14718298.52	0.049507564	0.629176752
	21. 6	0.4	820785.23	14739663.74	0.055685479	0.707690018
	21. 7	0.5	716562.67	13553753.07	0.05286821	0.671886204
	21. 8	1	419715.32	16557185.18	0.025349437	0.322158377
	21. 9	2	355719.57	17586912.27	0.02022638	0.257050986
	21. 10	4	312828.82	19747288.5	0.015841609	0.201326247
	21. 11	6	276541.23	19470632.46	0.014202992	0.180501554
	21. 12	8	181582.55	20707474.7	0.008768937	0.111441791
	21. 13	10	179641.06	21578485.42	0.008325008	0.105800023
	21. 14	20	112778.9	22793231.65	0.004947912	0.062881525
G 22	22. 1	0	619382.58	12480905.28	0.049626415	1
	22. 2	0.05	545331.38	12997891.93	0.041955371	0.845424186
	22. 3	0.1	560102.62	13446398.51	0.041654471	0.839360884
	22. 4	0.2	491305.25	13804966.51	0.035589022	0.717138681
	22. 5	0.3	466090.47	14718298.52	0.031667415	0.638116121
	22. 6	0.4	500398.88	14739663.74	0.033949138	0.684094114
	22. 7	0.5	441733.74	13553753.07	0.032591249	0.656731887
	22. 8	1	271396.47	16557185.18	0.016391462	0.330297122
	22. 9	2	221775.92	17586912.27	0.012610282	0.254104229

Name of the Band	Band	Mg^{2+} concentration (mM)	Cleavage Intensity (Ic)	Full length band Intensity (I)	Cleaved Fraction Icc = (Ic / I)	Relative Cleavage Intensity Icc_R = (Icc (x mM) / Icc (0 mM))
	22. 10	4	200644.11	19747288.5	0.01016059	0.204741577
	22. 11	6	181062.47	19470632.46	0.00929926	0.187385284
	22. 12	8	121021.36	20707474.7	0.005844332	0.11776656
	22. 13	10	115353.39	21578485.42	0.005345759	0.10772004
	22. 14	20	71989.9	22793231.65	0.003158389	0.063643311
G 23	23. 1	0	542484.02	12480905.28	0.043465118	1
	23. 2	0.05	471169.23	12997891.93	0.036249665	0.833994404
	23. 3	0.1	495230.9	13446398.51	0.036830003	0.847346215
	23. 4	0.2	421648.22	13804966.51	0.030543227	0.702706631
	23. 5	0.3	417925.97	14718298.52	0.028394992	0.653282297
	23. 6	0.4	451200.54	14739663.74	0.030611318	0.704273216
	23. 7	0.5	394077.76	13553753.07	0.029075176	0.668931264
	23. 8	1	259112.84	16557185.18	0.015649571	0.360048964
	23. 9	2	220404.66	17586912.27	0.012532311	0.288330319
	23. 10	4	205781.23	19747288.5	0.010420733	0.239749343
	23. 11	6	178267.69	19470632.46	0.009155722	0.210645272
	23. 12	8	122943.44	20707474.7	0.005937153	0.136595804
	23. 13	10	114406.97	21578485.42	0.0053019	0.121980571
	23. 14	20	71960.4	22793231.65	0.003157095	0.072635144
G 30	30. 1	0	123876.24	12480905.28	0.009925261	1
	30. 2	0.05	108960.83	12997891.93	0.008382962	0.844608706
	30. 3	0.1	109451.62	13446398.51	0.008139847	0.820114118
	30. 4	0.2	89508.17	13804966.51	0.006483766	0.653258987
	30. 5	0.3	77755.3	14718298.52	0.0052829	0.532268134
	30. 6	0.4	80740.9	14739663.74	0.005477798	0.551904687
	30. 7	0.5	67775.38	13553753.07	0.005000488	0.50381427
	30. 8	1	43894.51	16557185.18	0.002651085	0.267104849
	30. 9	2	33374.62	17586912.27	0.001897696	0.191198643
	30. 10	4	30657.41	19747288.5	0.001552487	0.15641776
	30. 11	6	28892.41	19470632.46	0.001483897	0.149507088
	30. 12	8	22980.65	20707474.7	0.001109776	0.111813242
	30. 13	10	21686.53	21578485.42	0.001005007	0.101257495
	30. 14	20	16636.58	22793231.65	0.000729891	0.073538746
G 32	32. 1	0	1102157.06	12480905.28	0.088307461	1
	32. 2	0.05	953548.35	12997891.93	0.073361769	0.830753917
	32. 3	0.1	995562.71	13446398.51	0.074039358	0.838426976
	32. 4	0.2	820781.93	13804966.51	0.059455554	0.673278939
	32. 5	0.3	799056.49	14718298.52	0.054290004	0.614783887
	32. 6	0.4	864177.1	14739663.74	0.058629363	0.663923098

Name of the Band	Band	Mg^{2+} concentration (mM)	Cleavage Intensity (Ic)	Full length band Intensity (I)	Cleaved Fraction Icc = (Ic / I)	Relative Cleavage Intensity Icc_R = (Icc (x mM) / Icc (0 mM))
	32. 7	0.5	754323.82	13553753.07	0.05565424	0.630232584
	32. 8	1	443720.69	16557185.18	0.026799283	0.303476994
	32. 9	2	345226.81	17586912.27	0.019629757	0.222288768
	32. 10	4	308661.32	19747288.5	0.015630567	0.17700166
	32. 11	6	282744.48	19470632.46	0.014521587	0.164443487
	32. 12	8	199131.71	20707474.7	0.009616417	0.108896992
	32. 13	10	178225.7	21578485.42	0.008259417	0.093530223
	32. 14	20	121741.25	22793231.65	0.005341114	0.060483157
G 34	34. 1	0	3247082.71	12480905.28	0.260164038	1
	34. 2	0.05	2789659.87	12997891.93	0.214624024	0.824956539
	34. 3	0.1	2836229.47	13446398.51	0.21092856	0.810752176
	34. 4	0.2	2315833.82	13804966.51	0.167753672	0.644799617
	34. 5	0.3	2147871.55	14718298.52	0.145932055	0.560923241
	34. 6	0.4	2217508.51	14739663.74	0.150444986	0.578269725
	34. 7	0.5	1873428.45	13553753.07	0.138222118	0.531288332
	34. 8	1	986321.94	16557185.18	0.059570629	0.228973342
	34. 9	2	692177.85	17586912.27	0.039357554	0.151279763
	34. 10	4	567093.69	19747288.5	0.028717547	0.110382463
	34. 11	6	520706.49	19470632.46	0.026743173	0.102793503
	34. 12	8	280764.75	20707474.7	0.013558619	0.052115652
	34. 13	10	235415.7	21578485.42	0.010909742	0.041934088
	34. 14	20	125784.48	22793231.65	0.005518501	0.021211623
G 40	40. 1	0	109837.58	12480905.28	0.00880045	1
	40. 2	0.05	98869.36	12997891.93	0.007606569	0.864338648
	40. 3	0.1	101007.27	13446398.51	0.007511846	0.853575196
	40. 4	0.2	85529.58	13804966.51	0.006195566	0.7040056
	40. 5	0.3	78227.01	14718298.52	0.005314949	0.603940641
	40. 6	0.4	80746.16	14739663.74	0.005478155	0.622485778
	40. 7	0.5	66228.48	13553753.07	0.004886357	0.555239494
	40. 8	1	45687.73	16557185.18	0.00275939	0.313551011
	40. 9	2	37503.18	17586912.27	0.002132448	0.242311278
	40. 10	4	36603.06	19747288.5	0.001853574	0.210622641
	40. 11	6	36310.39	19470632.46	0.00186488	0.211907333
	40. 12	8	29043.98	20707474.7	0.001402584	0.15937644
	40. 13	10	26768.38	21578485.42	0.001240512	0.14096012
	40. 14	20	19560.26	22793231.65	0.000858161	0.097513299
G 41	41. 1	0	140104.2	12480905.28	0.011225484	1
	41. 2	0.05	122107.96	12997891.93	0.009394443	0.836885391
	41. 3	0.1	120374.39	13446398.51	0.008952166	0.797485974

Name of the Band	Band	Mg^{2+} concentration (mM)	Cleavage Intensity (Ic)	Full length band Intensity (I)	Cleaved Fraction Icc = (Ic / I)	Relative Cleavage Intensity Icc_R = (Icc (x mM) / Icc (0 mM))
	41. 4	0.2	100195.99	13804966.51	0.007257967	0.646561612
	41. 5	0.3	93152.92	14718298.52	0.006329055	0.563811329
	41. 6	0.4	98018.38	14739663.74	0.006649974	0.592399764
	41. 7	0.5	80211.26	13553753.07	0.005918011	0.527194295
	41. 8	1	54733.25	16557185.18	0.00330571	0.294482617
	41. 9	2	46526.94	17586912.27	0.002645543	0.235672998
	41. 10	4	47453.72	19747288.5	0.00240305	0.214070944
	41. 11	6	45494.54	19470632.46	0.002336572	0.208148915
	41. 12	8	37581.08	20707474.7	0.001814856	0.161672833
	41. 13	10	34267.28	21578485.42	0.00158803	0.141466499
	41. 14	20	27588.56	22793231.65	0.001210384	0.107824651
G 43	43. 1	0	105445.14	12480905.28	0.008448517	1
	43. 2	0.05	92981.4	12997891.93	0.007153575	0.846725577
	43. 3	0.1	92398.53	13446398.51	0.006871619	0.81335212
	43. 4	0.2	79684.98	13804966.51	0.005772197	0.683220093
	43. 5	0.3	74023.73	14718298.52	0.005029367	0.595295881
	43. 6	0.4	75868.24	14739663.74	0.005147216	0.609244971
	43. 7	0.5	61691.76	13553753.07	0.004551637	0.538749786
	43. 8	1	46003.99	16557185.18	0.002778491	0.328873222
	43. 9	2	41044.05	17586912.27	0.002333784	0.276235907
	43. 10	4	43891.84	19747288.5	0.002222677	0.263084848
	43. 11	6	44157.1	19470632.46	0.002267882	0.268435534
	43. 12	8	39113.88	20707474.7	0.001888877	0.22357502
	43. 13	10	35610.31	21578485.42	0.001650269	0.195332413
	43. 14	20	29159.4	22793231.65	0.001279301	0.151423123
G 46	46. 1	0	172508.06	12480905.28	0.013821759	1
	46. 2	0.05	153245.3	12997891.93	0.011790012	0.853003745
	46. 3	0.1	157318.93	13446398.51	0.011699708	0.846470255
	46. 4	0.2	150262.37	13804966.51	0.01088466	0.787501833
	46. 5	0.3	143077.16	14718298.52	0.009721039	0.703314223
	46. 6	0.4	164983.41	14739663.74	0.01119316	0.809821674
	46. 7	0.5	146985.07	13553753.07	0.010844603	0.784603698
	46. 8	1	115588.29	16557185.18	0.006981156	0.505084486
	46. 9	2	115116.61	17586912.27	0.006545584	0.47357099
	46. 10	4	131931.68	19747288.5	0.006681002	0.48336847
	46. 11	6	129005.95	19470632.46	0.006625668	0.479365063
	46. 12	8	114436.84	20707474.7	0.005526354	0.399830034
	46. 13	10	114014.74	21578485.42	0.005283723	0.382275741
	46. 14	20	89236.25	22793231.65	0.003915033	0.283251425

Name of the Band	Band	Mg^{2+} concentration (mM)	Cleavage Intensity (Ic)	Full length band Intensity (I)	Cleaved Fraction Icc = (Ic / I)	Relative Cleavage Intensity Icc_R = (Icc (x mM) / Icc (0 mM))
G 54	54. 1	0	59170.53	12480905.28	0.004740884	1
	54. 2	0.05	53836.09	12997891.93	0.004141909	0.873657514
	54. 3	0.1	52462.49	13446398.51	0.003901602	0.822969138
	54. 4	0.2	47742.78	13804966.51	0.003458377	0.729479303
	54. 5	0.3	44762.83	14718298.52	0.003041305	0.641505755
	54. 6	0.4	48516.83	14739663.74	0.003291583	0.694297288
	54. 7	0.5	44840.24	13553753.07	0.003308326	0.697828957
	54. 8	1	40307.72	16557185.18	0.002434455	0.513502255
	54. 9	2	38723.14	17586912.27	0.002201816	0.464431424
	54. 10	4	40005.72	19747288.5	0.002025884	0.427321996
	54. 11	6	40175.79	19470632.46	0.002063404	0.435236184
	54. 12	8	37632.42	20707474.7	0.001817335	0.383332495
	54. 13	10	38145.29	21578485.42	0.001767746	0.372872702
	54. 14	20	33166.3	22793231.65	0.001455094	0.306924635
G 61	61. 1	0	256921.44	12480905.28	0.020585161	1
	61. 2	0.05	217877.7	12997891.93	0.016762541	0.814302185
	61. 3	0.1	208985.79	13446398.51	0.015542139	0.755016632
	61. 4	0.2	176447.04	13804966.51	0.012781417	0.620904432
	61. 5	0.3	144518.11	14718298.52	0.009818941	0.476991243
	61. 6	0.4	159074.52	14739663.74	0.010792276	0.524274561
	61. 7	0.5	141075.35	13553753.07	0.010408582	0.505635208
	61. 8	1	108762.59	16557185.18	0.006568906	0.319108796
	61. 9	2	98200.56	17586912.27	0.005583729	0.271250225
	61. 10	4	105025.16	19747288.5	0.00531846	0.258363774
	61. 11	6	93822.22	19470632.46	0.004818653	0.234083814
	61. 12	8	80254.19	20707474.7	0.003875615	0.188272251
	61. 13	10	83427.64	21578485.42	0.003866242	0.187816931
	61. 14	20	57665.77	22793231.65	0.002529951	0.122901712
G 62	62. 1	0	264913.3	12480905.28	0.021225488	1
	62. 2	0.05	231352.72	12997891.93	0.017799249	0.838579058
	62. 3	0.1	222414.14	13446398.51	0.016540796	0.779289349
	62. 4	0.2	183541.37	13804966.51	0.013295314	0.626384405
	62. 5	0.3	161492.18	14718298.52	0.010972204	0.516935329
	62. 6	0.4	167484.11	14739663.74	0.011362818	0.535338353
	62. 7	0.5	153996.63	13553753.07	0.011361918	0.535295968
	62. 8	1	113567.81	16557185.18	0.006859125	0.323155141
	62. 9	2	107886.03	17586912.27	0.00613445	0.289013374
	62. 10	4	103447.45	19747288.5	0.005238565	0.246805392
	62. 11	6	91919.99	19470632.46	0.004720956	0.222419179
	62. 12	8	87886.56	20707474.7	0.004244195	0.199957478

Name of the Band	Band	Mg^{2+} concentration (mM)	Cleavage Intensity (Ic)	Full length band Intensity (I)	Cleaved Fraction Icc = (Ic / I)	Relative Cleavage Intensity Icc_R = (Icc (x mM) / Icc (0 mM))
	62. 13	10	92787.03	21578485.42	0.004299979	0.202585632
	62. 14	20	62809.28	22793231.65	0.002755611	0.129825569
G 66	66. 1	0	313163.56	12480905.28	0.025091414	1
	66. 2	0.05	281739.49	12997891.93	0.021675783	0.863872538
	66. 3	0.1	279492.57	13446398.51	0.020785682	0.828398216
	66. 4	0.2	237574.8	13804966.51	0.017209372	0.685866958
	66. 5	0.3	207410.13	14718298.52	0.014091991	0.561626023
	66. 6	0.4	214066.54	14739663.74	0.014523163	0.578810072
	66. 7	0.5	201519.37	13553753.07	0.01486816	0.592559675
	66. 8	1	157111.45	16557185.18	0.009489019	0.378177944
	66. 9	2	146349.96	17586912.27	0.008321527	0.331648377
	66. 10	4	146306.43	19747288.5	0.007408938	0.295277808
	66. 11	6	134652.5	19470632.46	0.006915672	0.275619048
	66. 12	8	139505.15	20707474.7	0.006736947	0.268496091
	66. 13	10	106382.58	21578485.42	0.00493003	0.196482749
	66. 14	20	149787.57	22793231.65	0.006571581	0.261905571
G 69	69. 1	0	100880.3	12480905.28	0.008082771	1
	69. 2	0.05	91471.46	12997891.93	0.007037407	0.870667656
	69. 3	0.1	93749.24	13446398.51	0.006972071	0.862584201
	69. 4	0.2	82800.58	13804966.51	0.005997883	0.742057816
	69. 5	0.3	75664.86	14718298.52	0.00514087	0.636028165
	69. 6	0.4	78392.52	14739663.74	0.005318474	0.65800133
	69. 7	0.5	75215.09	13553753.07	0.005549392	0.68657049
	69. 8	1	63536.03	16557185.18	0.003837369	0.474759092
	69. 9	2	63809.46	17586912.27	0.003628236	0.448885105
	69. 10	4	65290.3	19747288.5	0.003306292	0.409054256
	69. 11	6	67011.98	19470632.46	0.003441695	0.42580633
	69. 12	8	64052.39	20707474.7	0.003093201	0.382690712
	69. 13	10	68499.48	21578485.42	0.003174434	0.392740816
	69. 14	20	54931.42	22793231.65	0.002409988	0.298163614
G 74	74. 1	0	180391.1	12480905.28	0.014453367	1
	74. 2	0.05	160702.41	12997891.93	0.012363729	0.855422065
	74. 3	0.1	161948.1	13446398.51	0.012043976	0.833298997
	74. 4	0.2	142046.49	13804966.51	0.010289521	0.711911699
	74. 5	0.3	128521.23	14718298.52	0.008732071	0.604154823
	74. 6	0.4	134256.19	14739663.74	0.009108497	0.630199019
	74. 7	0.5	126522.6	13553753.07	0.009334876	0.645861682
	74. 8	1	102994.04	16557185.18	0.006220504	0.430384447
	74. 9	2	94266.22	17586912.27	0.005360021	0.37084931

Name of the Band	Band	Mg^{2+} concentration (mM)	Cleavage Intensity (Ic)	Full length band Intensity (I)	Cleaved Fraction Icc = (Ic / I)	Relative Cleavage Intensity Icc_R = (Icc (x mM) / Icc (0 mM))
	74. 10	4	93485.25	19747288.5	0.00473408	0.327541703
	74. 11	6	92040.76	19470632.46	0.004727158	0.327062775
	74. 12	8	79273.57	20707474.7	0.003828259	0.264869687
	74. 13	10	80467.37	21578485.42	0.003729056	0.258006014
	74. 14	20	58221.02	22793231.65	0.002554312	0.176727806
G 123	123. 1	0	142484.68	12480905.28	0.011416214	1
	123. 2	0.05	127993.57	12997891.93	0.009847256	0.862567611
	123. 3	0.1	130744.11	13446398.51	0.009723355	0.851714558
	123. 4	0.2	117447.02	13804966.51	0.008507592	0.7452201
	123. 5	0.3	111604.87	14718298.52	0.007582729	0.66420701
	123. 6	0.4	118253.71	14739663.74	0.008022823	0.702756894
	123. 7	0.5	108688.5	13553753.07	0.00801907	0.702428205
	123. 8	1	117560.14	16557185.18	0.007100249	0.621944318
	123. 9	2	118161.29	17586912.27	0.006718706	0.588523139
	123. 10	4	125890.77	19747288.5	0.006375091	0.558424334
	123. 11	6	120308.13	19470632.46	0.006178953	0.541243674
	123. 12	8	116166.01	20707474.7	0.005609859	0.491394
	123. 13	10	118334.46	21578485.42	0.005483909	0.480361498
	123. 14	20	116109.8	22793231.65	0.005094047	0.446211633
G 144	144. 1	0	282813.28	12480905.28	0.022659677	1
	144. 2	0.05	244455.28	12997891.93	0.018807302	0.829989864
	144. 3	0.1	229307.92	13446398.51	0.017053482	0.752591598
	144. 4	0.2	206630.14	13804966.51	0.014967812	0.660548333
	144. 5	0.3	189980.5	14718298.52	0.012907776	0.569636367
	144. 6	0.4	204675.19	14739663.74	0.013886015	0.612807278
	144. 7	0.5	183995.01	13553753.07	0.013575207	0.599090957
	144. 8	1	161109.88	16557185.18	0.009730511	0.429419693
	144. 9	2	158462	17586912.27	0.009010223	0.397632455
	144. 10	4	166080.01	19747288.5	0.008410269	0.371155739
	144. 11	6	157273.63	19470632.46	0.008077479	0.356469306
	144. 12	8	133511.14	20707474.7	0.006447485	0.284535627
	144. 13	10	131812.69	21578485.42	0.006108524	0.269576824
	144. 14	20	119028.83	22793231.65	0.005222113	0.230458403
G 148	148. 1	0	215420.44	12480905.28	0.017260001	1
	148. 2	0.05	191435.17	12997891.93	0.014728171	0.85331226
	148. 3	0.1	193937.2	13446398.51	0.014422985	0.835630574
	148. 4	0.2	172374.06	13804966.51	0.01248638	0.723428697
	148. 5	0.3	164294.65	14718298.52	0.011162612	0.646732957
	148. 6	0.4	185604.18	14739663.74	0.012592158	0.729557213

Name of the Band	Band	Mg^{2+} concentration (mM)	Cleavage Intensity (Ic)	Full length band Intensity (I)	Cleaved Fraction Icc = (Ic / I)	Relative Cleavage Intensity Icc_R = (Icc (x mM) / Icc (0 mM))
	148. 7	0.5	158223.53	13553753.07	0.01167378	0.67634873
	148. 8	1	136998.5	16557185.18	0.008274263	0.479389464
	148. 9	2	134717.91	17586912.27	0.007660123	0.443807787
	148. 10	4	136839.51	19747288.5	0.006929534	0.401479355
	148. 11	6	135853.64	19470632.46	0.006977361	0.404250345
	148. 12	8	116195.02	20707474.7	0.00561126	0.325101935
	148. 13	10	115331.7	21578485.42	0.005344754	0.309661286
	148. 14	20	93592.47	22793231.65	0.004106152	0.237899858
G 151	151. 1	0	370798.5	12480905.28	0.029709263	1
	151. 2	0.05	319389.43	12997891.93	0.024572402	0.827095649
	151. 3	0.1	330270.13	13446398.51	0.024561977	0.826744735
	151. 4	0.2	281225.92	13804966.51	0.020371358	0.68569046
	151. 5	0.3	276042.49	14718298.52	0.018755054	0.631286421
	151. 6	0.4	282360.29	14739663.74	0.019156495	0.644798713
	151. 7	0.5	254963.22	13553753.07	0.018811263	0.633178391
	151. 8	1	201190.89	16557185.18	0.012151274	0.409006231
	151. 9	2	183687.87	17586912.27	0.010444578	0.351559631
	151. 10	4	194994.68	19747288.5	0.009874504	0.332371219
	151. 11	6	184793.31	19470632.46	0.009490874	0.319458394
	151. 12	8	173476.13	20707474.7	0.008377464	0.281981557
	151. 13	10	174600.12	21578485.42	0.008091398	0.272352708
	151. 14	20	141996.87	22793231.65	0.006229782	0.209691577
G 188	188. 1	0	728385.74	12480905.28	0.058360009	1
	188. 2	0.05	642252.85	12997891.93	0.049412078	0.846677017
	188. 3	0.1	687775.89	13446398.51	0.05114945	0.876446925
	188. 4	0.2	608017.81	13804966.51	0.044043411	0.754684788
	188. 5	0.3	579945.31	14718298.52	0.039403013	0.675171475
	188. 6	0.4	611047.48	14739663.74	0.041455999	0.710349426
	188. 7	0.5	554527.18	13553753.07	0.040913183	0.701048269
	188. 8	1	524870.69	16557185.18	0.031700478	0.543188376
	188. 9	2	577046.64	17586912.27	0.03281114	0.562219587
	188. 10	4	565849.66	19747288.5	0.02865455	0.490996324
	188. 11	6	563753.66	19470632.46	0.02895405	0.496128263
	188. 12	8	521332.47	20707474.7	0.025176052	0.431392199
	188. 13	10	482677.08	21578485.42	0.022368441	0.383283718
	188. 14	20	416487.35	22793231.65	0.018272413	0.313098195

Figure A2.2: Determining the K_A of Mg^{2+} to the *btuB* RNA: The relative intensity changes at the guanine residues are plotted versus the Mg^{2+} concentration (black dots) and were fitted to a 1:1 binding isoterm [dF+(dB-dF)*(((cRNA+x+1/Ka)-((cRNA+x+1/Ka)^2-4*cRNA*x)^0.5)/(2*cRNA))] (grey lines) to derive the association constant (K_A) towards Mg^{2+}. Shown are the plots for the subset of guanine residues. (See Table A2.1)

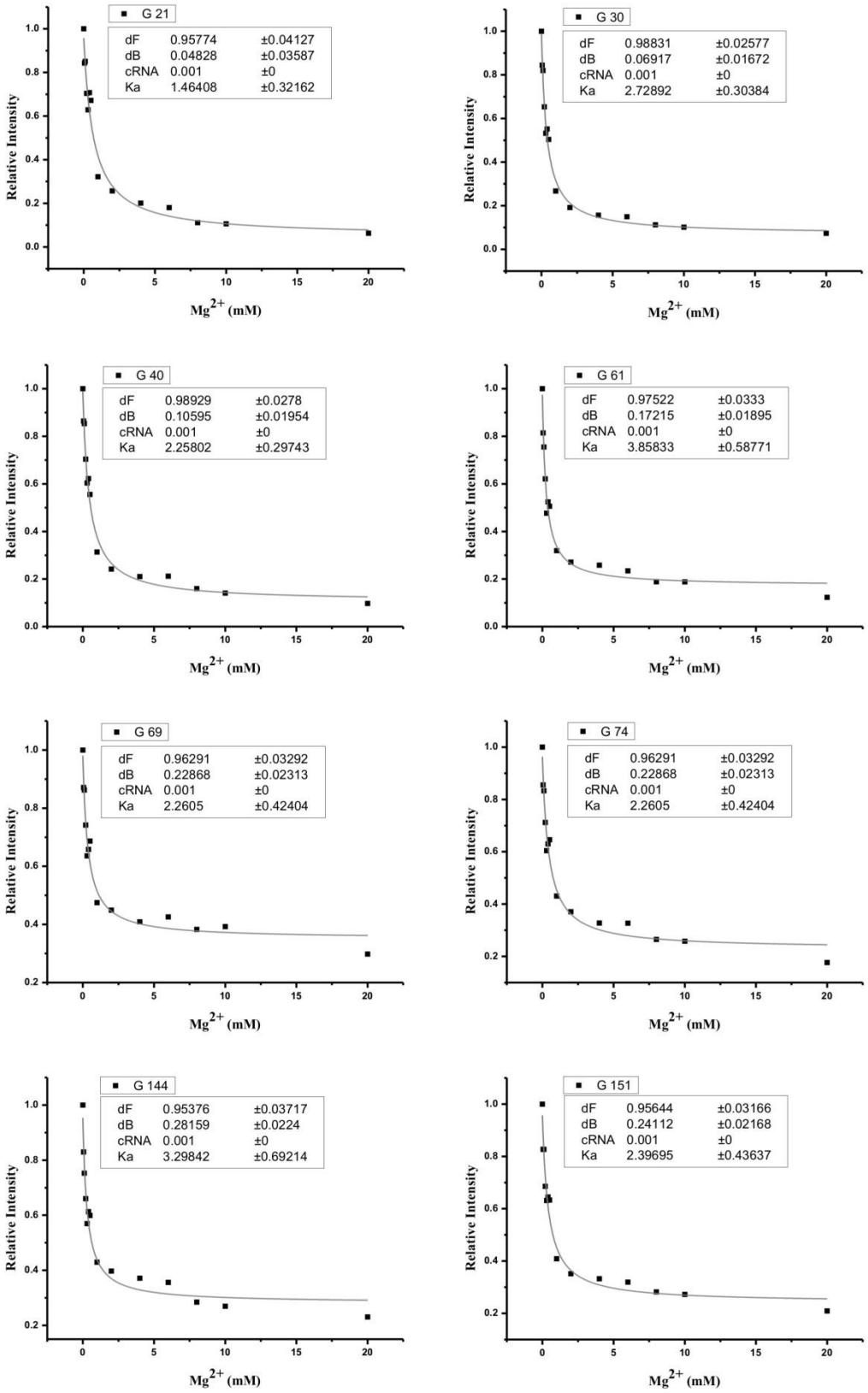

Appendix 3: Evaluation of Tb^{3+} cleavage in the *btuB* RNA to map metal ion binding sites

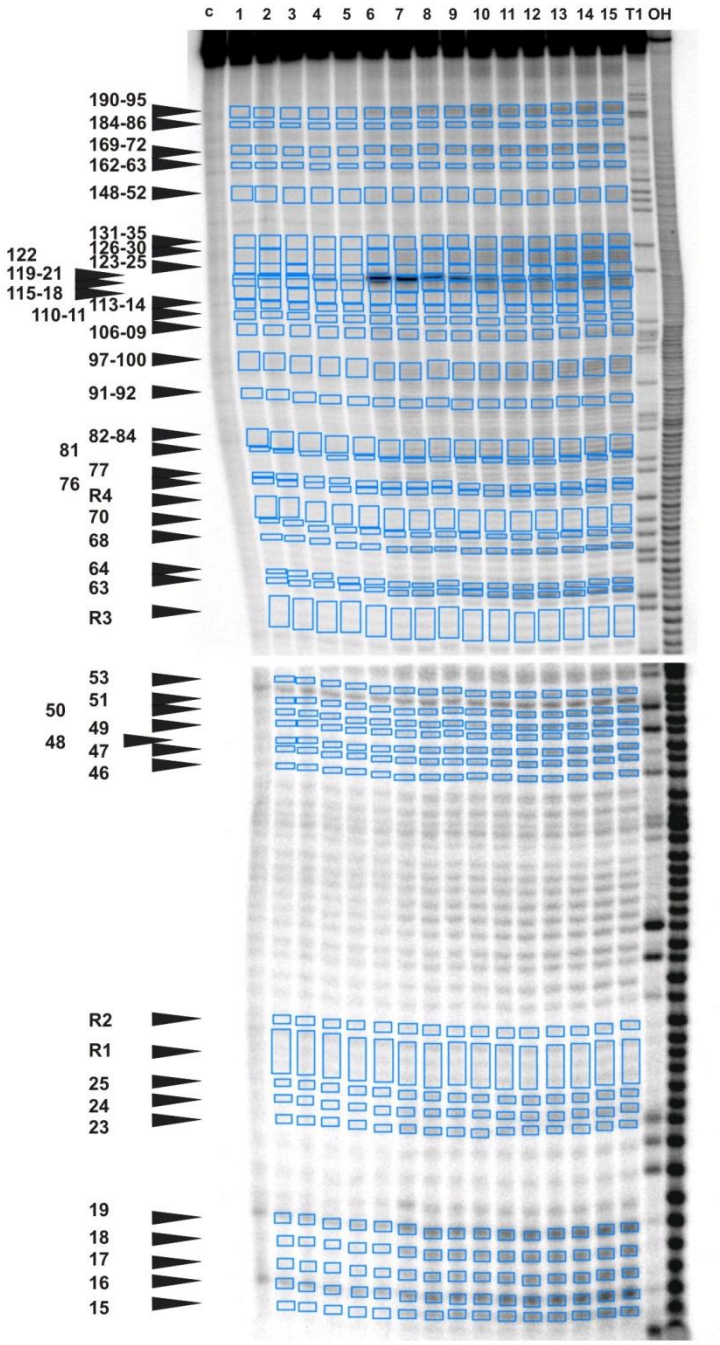

Figure A3.1: Evaluation of the PAGE gel for Tb^{3+} cleavage of the *btuB* RNA: The nucleotides marked by arrows are considered in the evaluation. The blue boxes mark the area of band intensity used in the evaluation. Bands R1, R2, R3 and R4 are used for background correction (see Table A3.1 and A3.2). The concentration of Tb^{3+} increases from lane 1 to 15 (see Table A3.3). Lane c is the unreacted RNA, lane T1 is RNase T1 ladder and lane OH corresponds to the alkaline hydrolysis ladder.

Table A3.1: Determination of the background correction factor from the control bands.

Control Bands (CB)	Tb^{3+} (mM)	Cleavage Intensity (I)	Max. cleavage intensity at CB (X)	Percentage relative to X, R_x= (I* 100/ X)
(For nucleotides 15-53)				
R1. 1	0	19095.17	**36848.09**	51.82
R1. 2	0.025	22443.75	**36848.09**	60.91
R1. 3	0.05	21037.61	**36848.09**	57.09
R1. 4	0.075	21162.43	**36848.09**	57.43
R1. 5	0.1	20810.09	**36848.09**	56.47
R1. 6	0.2	25964.96	**36848.09**	70.46
R1. 7	0.5	27923.6	**36848.09**	75.78
R1. 8	0.75	25528.66	**36848.09**	69.28
R1. 9	1	27969.85	**36848.09**	75.9
R1. 10	2.5	29815.95	**36848.09**	80.91
R1. 11	5	30538.65	**36848.09**	82.88
R1. 12	7.5	32531.6	**36848.09**	88.28
R1. 13	10	31639.45	**36848.09**	85.86
R1. 14	15	**36848.09**	**36848.09**	100
R1. 15	20	34891.57	**36848.09**	94.69
R2. 1	0	3675.51	**8167.27**	45
R2. 2	0.025	4456.3	**8167.27**	54.5629078
R2. 3	0.05	4181.87	**8167.27**	51.2
R2. 4	0.075	4347.07	**8167.27**	53.22
R2. 5	0.1	4355.38	**8167.27**	53.33
R2. 6	0.2	5291.6	**8167.27**	64.79
R2. 7	0.5	6059.53	**8167.27**	74.19
R2. 8	0.75	5350.87	**8167.27**	65.51
R2. 9	1	5978.57	**8167.27**	73.2
R2. 10	2.5	6415.64	**8167.27**	78.55
R2. 11	5	6727.05	**8167.27**	82.36
R2. 12	7.5	6836.58	**8167.27**	83.7
R2. 13	10	6637.44	**8167.27**	81.27
R2. 14	15	**8167.27**	**8167.27**	100
R2. 15	20	8001.73	**8167.27**	97.97
(For nucleotides 63-195)				
R3. 1	0	22681.68	**59194.84**	38.31698844
R3. 2	0.025	25313.37	**59194.84**	42.76279824
R3. 3	0.05	24945.54	**59194.84**	42.14140962
R3. 4	0.075	23875.61	**59194.84**	40.33393789
R3. 5	0.1	24237.51	**59194.84**	40.94530875
R3. 6	0.2	33991.38	**59194.84**	57.42287672
R3. 7	0.5	38642.81	**59194.84**	65.2807069
R3. 8	0.75	37052.95	**59194.84**	62.59489847

Control Bands (CB)	Tb^{3+} (mM)	Cleavage Intensity (I)	Max. cleavage intensity at CB (X)	Percentage relative to X, R_x= (I* 100/ X)
R3. 9	1	38535.01	**59194.84**	65.09859643
R3. 10	2.5	43793.6	**59194.84**	73.98212412
R3. 11	5	47027.17	**59194.84**	79.44471174
R3. 12	7.5	50714.59	**59194.84**	85.67400469
R3. 13	10	50565.28	**59194.84**	85.42176987
R3. 14	15	57906.05	**59194.84**	97.8228001
R3. 15	20	**59194.84**	**59194.84**	100
R4. 1	0	20455.04	**58950.06**	34.69892991
R4. 2	0.025	22629	**58950.06**	38.38672938
R4. 3	0.05	22602.64	**58950.06**	38.34201356
R4. 4	0.075	23063.03	**58950.06**	39.12299665
R4. 5	0.1	22337.54	**58950.06**	37.89231088
R4. 6	0.2	29687.46	**58950.06**	50.36035587
R4. 7	0.5	36074.46	**58950.06**	61.19495044
R4. 8	0.75	34424.91	**58950.06**	58.39673446
R4. 9	1	37599.64	**58950.06**	63.78219123
R4. 10	2.5	42924.85	**58950.06**	72.81561715
R4. 11	5	46405.69	**58950.06**	78.72034397
R4. 12	7.5	48978.19	**58950.06**	83.08420721
R4. 13	10	48868.13	**58950.06**	82.8975068
R4. 14	15	56474.44	**58950.06**	95.80047925
R4. 15	20	**58950.06**	**58950.06**	100

[Note: The PAGE gel involving nucleotides 15-53 and 63-195 (marked by arrows in Figure A3.1) was cut into two gels for the purpose of drying and phosphoimaging. Therefore, different control bands (R1, R2, R3, R4) are considered here to determine the correction factor R separately for the two gels].

Table A3.2: Calculation of the final correction factor.

Correction factor R = $(R_{x1}+R_{x2})/2$	R
$(R_{x1.1}+ R_{x\ 2.1})/2$ = R (0 mM)	48.41212467
$(R_{x1.2}+ R_{x\ 2.2})/2$ = R (0.025 mM)	57.7358818
$(R_{x1.3}+ R_{x\ 2.3})/2$ = R (0.05 mM)	54.14779933
$(R_{x1.4}+ R_{x\ 2.4})/2$ = R (0.075 mM)	55.32852424
$(R_{x1.5}+ R_{x\ 2.5})/2$ = R (0.1 mM)	54.90129998
$(R_{x1.6}+ R_{x\ 2.6})/2$ = R (0.2 mM)	67.62759449
$(R_{x1.7}+ R_{x\ 2.7})/2$ = R (0.5 mM)	74.98658197
$(R_{x1.8}+ R_{x\ 2.8})/2$ = R (0.75 mM)	67.39841997
$(R_{x1.9}+ R_{x\ 2.9})/2$ = R (1 mM)	74.55370278
$(R_{x1.10}+ R_{x\ 2.10})/2$ = R (2.5 mM)	79.73445839
$(R_{x1.11}+ R_{x\ 2.11})/2$ = R (5 mM)	82.62155722
$(R_{x1.12}+ R_{x\ 2.12})/2$ = R (7.5 mM)	85.99637809
$(R_{x1.13}+ R_{x\ 2.13})/2$ = R (10 mM)	83.56666532
$(R_{x1.14}+ R_{x\ 2.14})/2$ = R (15 mM)	100
$(R_{x1.15}+ R_{x\ 2.15})/2$ = R (20 mM)	96.33171878
$(R_{x3.1}+ R_{x\ 4.1})/2$ = R (0 mM)	34.69892991
$(R_{x3.2}+ R_{x\ 4.2})/2$ = R (0.025 mM)	38.38672938
$(R_{x3.3}+ R_{x\ 4.3})/2$ = R (0.05 mM)	38.34201356
$(R_{x3.4}+ R_{x\ 4.4})/2$ = R (0.075 mM)	39.12299665
$(R_{x3.5}+ R_{x\ 4.5})/2$ = R (0.1 mM)	37.89231088
$(R_{x3.6}+ R_{x\ 4.6})/2$ = R (0.2 mM)	50.36035587
$(R_{x3.7}+ R_{x\ 4.7})/2$ = R (0.5 mM)	61.19495044
$(R_{x3.8}+ R_{x\ 4.8})/2$ = R (0.75 mM)	58.39673446
$(R_{x3.9}+ R_{x\ 4.9})/2$ = R (1 mM)	63.78219123
$(R_{x3.10}+ R_{x\ 4.10})/2$ = R (2.5 mM)	72.81561715
$(R_{x3.11}+ R_{x\ 4.11})/2$ = R (5 mM)	78.72034397
$(R_{x3.12}+ R_{x\ 4.12})/2$ = R (7.5 mM)	83.08420721
$(R_{x3.13}+ R_{x\ 4.13})/2$ = R (10 mM)	82.8975068
$(R_{x3.14}+ R_{x\ 4.14})/2$ = R (15 mM)	95.80047925
$(R_{x3.15}+ R_{x\ 4.15})/2$ = R (20 mM)	100

Table A3.3: Determination of relative cleavage intensities from the background correction factor (R).

nt No.	Name of the Band	Tb^{3+} (mM)	Cleavage Intensity (I)	Correction factor (R)	Corrected cleavage Intensity (I_{corr} = I*100/ R)	I_{corr} / 1000	(I_{corr}) at 0 mM	$I_R = (I_{corr\ (x\ mM)} - I_{corr\ (0\ mM)})$
15	nt 15.1	0	3125.02	48.41212467	6455.035844	6.455035844	6.455035844	0
	nt 15.2	0.025	3460.85	57.7358818	5994.279281	5.994279281	6.455035844	-0.460756563
	nt 15.3	0.05	3573.87	54.14779933	6600.212833	6.600212833	6.455035844	0.145176989
	nt 15.4	0.075	4047.59	55.32852424	7315.557491	7.315557491	6.455035844	0.860521647
	nt 15.5	0.1	4115.91	54.90129998	7496.926304	7.496926304	6.455035844	1.04189046
	nt 15.6	0.2	10271.27	67.62759449	15187.98662	15.18798662	6.455035844	8.732950773
	nt 15.7	0.5	15595.29	74.98658197	20797.44081	20.79744081	6.455035844	14.34240496
	nt 15.8	0.75	15524.28	67.39841997	23033.59635	23.03359635	6.455035844	16.5785605
	nt 15.9	1	16250.45	74.55370278	21796.97238	21.79697238	6.455035844	15.34193653
	nt 15.10	2.5	21309.77	79.73445839	26725.92306	26.72592306	6.455035844	20.27088721
	nt 15.11	5	24075.36	82.62155722	29139.32006	29.13932006	6.455035844	22.68428422
	nt 15.12	7.5	26144.16	85.99637809	30401.46641	30.40146641	6.455035844	23.94643057
	nt 15.13	10	27961.64	83.56666532	33460.27976	33.46027976	6.455035844	27.00524392
	nt 15.14	15	31869.48	100	31869.48	31.86948	6.455035844	25.41444416
	nt 15.15	20	31228.84	96.33171878	32418.0243	32.4180243	6.455035844	25.96298845
16	nt 16.1	0	9177.65	48.41212467	18957.33778	18.95733778	18.95733778	0
	nt 16.2	0.025	9513.41	57.7358818	16477.46549	16.47746549	18.95733778	-2.479872289
	nt 16.3	0.05	10087.68	54.14779933	18629.8984	18.6298984	18.95733778	-0.327439383
	nt 16.4	0.075	10701.11	55.32852424	19341.03638	19.34103638	18.95733778	0.383698594
	nt 16.5	0.1	10350.2	54.90129998	18852.37691	18.85237691	18.95733778	-0.104960874
	nt 16.6	0.2	18437.58	67.62759449	27263.39764	27.26339764	18.95733778	8.306059859
	nt 16.7	0.5	25486.6	74.98658197	33988.21406	33.98821406	18.95733778	15.03087628
	nt 16.8	0.75	23164.16	67.39841997	34368.99561	34.36899561	18.95733778	15.41165783
	nt 16.9	1	25614.84	74.55370278	34357.56917	34.35756917	18.95733778	15.40023139
	nt 16.10	2.5	32478.55	79.73445839	40733.39263	40.73339263	18.95733778	21.77605485
	nt 16.11	5	34151.98	82.62155722	41335.4349	41.3354349	18.95733778	22.37809712
	nt 16.12	7.5	36478.08	85.99637809	42418.15854	42.41815854	18.95733778	23.46082076
	nt 16.13	10	39447.77	83.56666532	47205.15034	47.20515034	18.95733778	28.24781256
	nt 16.14	15	47502.89	100	47502.89	47.50289	18.95733778	28.54555222
	nt 16.15	20	46342.86	96.33171878	48107.58137	48.10758137	18.95733778	29.15024359
17	nt 17.1	0	4118.76	48.41212467	8507.703449	8.507703449	8.507703449	0
	nt 17.2	0.025	4508.39	57.7358818	7808.644918	7.808644918	8.507703449	-0.699058531
	nt 17.3	0.05	4266.78	54.14779933	7879.877027	7.879877027	8.507703449	-0.627826422
	nt 17.4	0.075	4785.7	55.32852424	8649.60717	8.64960717	8.507703449	0.141903721
	nt 17.5	0.1	5148.18	54.90129998	9377.155006	9.377155006	8.507703449	0.869451557
	nt 17.6	0.2	10675.09	67.62759449	15785.10973	15.78510973	8.507703449	7.277406284
	nt 17.7	0.5	15373.34	74.98658197	20501.45452	20.50145452	8.507703449	11.99375107
	nt 17.8	0.75	15022.64	67.39841997	22289.3059	22.2893059	8.507703449	13.78160245
	nt 17.9	1	16373.92	74.55370278	21962.58454	21.96258454	8.507703449	13.45488109

nt No.	Name of the Band	Tb^{3+} (mM)	Cleavage Intensity (I)	Correction factor (R)	Corrected cleavage Intensity (I_{corr} = I*100/ R)	I_{corr} / 1000	(I_{corr}) at 0 mM	$I_R = (I_{corr\ (x\ mM)} - I_{corr\ (0\ mM)})$
	nt 17.10	2.5	20395.93	79.73445839	25579.81883	25.57981883	8.507703449	17.07211538
	nt 17.11	5	23575.88	82.62155722	28534.7805	28.5347805	8.507703449	20.02707705
	nt 17.12	7.5	25443.18	85.99637809	29586.33906	29.58633906	8.507703449	21.07863561
	nt 17.13	10	26866	83.56666532	32149.18281	32.14918281	8.507703449	23.64147936
	nt 17.14	15	31728.62	100	31728.62	31.72862	8.507703449	23.22091655
	nt 17.15	20	31158.87	96.33171878	32345.38986	32.34538986	8.507703449	23.83768641
18	nt 18.1	0	3787.66	48.41212467	7823.783869	7.823783869	7.823783869	0
	nt 18.2	0.025	4269.28	57.7358818	7394.500382	7.394500382	7.823783869	-0.429283487
	nt 18.3	0.05	3848.82	54.14779933	7107.989702	7.107989702	7.823783869	-0.715794167
	nt 18.4	0.075	4702.81	55.32852424	8499.792945	8.499792945	7.823783869	0.676009076
	nt 18.5	0.1	4996.74	54.90129998	9101.314543	9.101314543	7.823783869	1.277530675
	nt 18.6	0.2	12669.95	67.62759449	18734.88196	18.73488196	7.823783869	10.91109809
	nt 18.7	0.5	17376.96	74.98658197	23173.42589	23.17342589	7.823783869	15.34964202
	nt 18.8	0.75	16582.65	67.39841997	24603.91506	24.60391506	7.823783869	16.78013119
	nt 18.9	1	17445.33	74.55370278	23399.68284	23.39968284	7.823783869	15.57589898
	nt 18.10	2.5	21566.65	79.73445839	27048.09243	27.04809243	7.823783869	19.22430856
	nt 18.11	5	23614.87	82.62155722	28581.97157	28.58197157	7.823783869	20.75818771
	nt 18.12	7.5	25591.28	85.99637809	29758.55561	29.75855561	7.823783869	21.93477175
	nt 18.13	10	26222.4	83.56666532	31379.01925	31.37901925	7.823783869	23.55523539
	nt 18.14	15	29413.14	100	29413.14	29.41314	7.823783869	21.58935613
	nt 18.15	20	29352.84	96.33171878	30470.58681	30.47058681	7.823783869	22.64680294
19	nt 19.1	0	7306.08	48.41212467	15091.42606	15.09142606	15.09142606	0
	nt 19.2	0.025	8541.13	57.7358818	14793.45207	14.79345207	15.09142606	-0.297973996
	nt 19.3	0.05	8498.97	54.14779933	15695.87334	15.69587334	15.09142606	0.604447277
	nt 19.4	0.075	9762.1	55.32852424	17643.88285	17.64388285	15.09142606	2.552456786
	nt 19.5	0.1	10194.92	54.90129998	18569.54207	18.56954207	15.09142606	3.47811601
	nt 19.6	0.2	18455.19	67.62759449	27289.43731	27.28943731	15.09142606	12.19801124
	nt 19.7	0.5	23785.46	74.98658197	31719.62153	31.71962153	15.09142606	16.62819547
	nt 19.8	0.75	21310.57	67.39841997	31618.7976	31.6187976	15.09142606	16.52737154
	nt 19.9	1	23331.37	74.55370278	31294.7166	31.2947166	15.09142606	16.20329054
	nt 19.10	2.5	29236.91	79.73445839	36667.84799	36.66784799	15.09142606	21.57642193
	nt 19.11	5	30262.82	82.62155722	36628.23725	36.62823725	15.09142606	21.53681119
	nt 19.12	7.5	32892.51	85.99637809	38248.71551	38.24871551	15.09142606	23.15728944
	nt 19.13	10	33449.74	83.56666532	40027.61134	40.02761134	15.09142606	24.93618527
	nt 19.14	15	37941.43	100	37941.43	37.94143	15.09142606	22.85000394
	nt 19.15	20	37241.61	96.33171878	38659.75867	38.65975867	15.09142606	23.5683326
23	nt 23.1	0	2419.86	48.41212467	4998.458582	4.998458582	4.998458582	0
	nt 23.2	0.025	3132.73	57.7358818	5425.967185	5.425967185	4.998458582	0.427508603
	nt 23.3	0.05	2905.14	54.14779933	5365.204193	5.365204193	4.998458582	0.366745611

nt No.	Name of the Band	Tb^{3+} (mM)	Cleavage Intensity (I)	Correction factor (R)	Corrected cleavage Intensity (I_{corr} = I*100/ R)	I_{corr} / 1000	(I_{corr}) at 0 mM	$I_R = (I_{corr\ (x\ mM)} - I_{corr\ (0\ mM)})$
	nt 23.4	0.075	3484.7	55.32852424	6298.197987	6.298197987	4.998458582	1.299739405
	nt 23.5	0.1	3678.88	54.90129998	6700.897795	6.700897795	4.998458582	1.702439213
	nt 23.6	0.2	9130.49	67.62759449	13501.13082	13.50113082	4.998458582	8.502672235
	nt 23.7	0.5	9101.63	74.98658197	12137.67818	12.13767818	4.998458582	7.139219601
	nt 23.8	0.75	8116.44	67.39841997	12042.47815	12.04247815	4.998458582	7.04401957
	nt 23.9	1	8683.17	74.55370278	11646.86619	11.64686619	4.998458582	6.648407604
	nt 23.10	2.5	10575.85	79.73445839	13263.83876	13.26383876	4.998458582	8.265380182
	nt 23.11	5	9785.3	82.62155722	11843.51921	11.84351921	4.998458582	6.845060626
	nt 23.12	7.5	9741.02	85.99637809	11327.24449	11.32724449	4.998458582	6.32878591
	nt 23.13	10	9856.7	83.56666532	11795.01415	11.79501415	4.998458582	6.79655557
	nt 23.14	15	12404.62	100	12404.62	12.40462	4.998458582	7.406161418
	nt 23.15	20	12207.24	96.33171878	12672.08782	12.67208782	4.998458582	7.673629235
24	nt 24.1	0	2779.23	48.41212467	5740.772625	5.740772625	5.740772625	0
	nt 24.2	0.025	3179.69	57.7358818	5507.303086	5.507303086	5.740772625	-0.233469539
	nt 24.3	0.05	2943.96	54.14779933	5436.896857	5.436896857	5.740772625	-0.303875768
	nt 24.4	0.075	3352.36	55.32852424	6059.008524	6.059008524	5.740772625	0.318235899
	nt 24.5	0.1	3682.83	54.90129998	6708.092524	6.708092524	5.740772625	0.967319899
	nt 24.6	0.2	7269.86	67.62759449	10749.84266	10.74984266	5.740772625	5.009070032
	nt 24.7	0.5	9613.18	74.98658197	12819.8669	12.8198669	5.740772625	7.079094273
	nt 24.8	0.75	9192.9	67.39841997	13639.63725	13.63963725	5.740772625	7.89886463
	nt 24.9	1	9470.82	74.55370278	12703.35295	12.70335295	5.740772625	6.962580323
	nt 24.10	2.5	10577.5	79.73445839	13265.90813	13.26590813	5.740772625	7.525135508
	nt 24.11	5	11681.99	82.62155722	14139.15495	14.13915495	5.740772625	8.398382327
	nt 24.12	7.5	13493.59	85.99637809	15690.88176	15.69088176	5.740772625	9.950109131
	nt 24.13	10	13438.17	83.56666532	16080.77808	16.08077808	5.740772625	10.34000546
	nt 24.14	15	16066.35	100	16066.35	16.06635	5.740772625	10.32557737
	nt 24.15	20	15318.06	96.33171878	15901.36685	15.90136685	5.740772625	10.16059423
25	nt 25.1	0	3324.38	48.41212467	6866.833511	6.866833511	6.866833511	0
	nt 25.2	0.025	3936.99	57.7358818	6818.965741	6.818965741	6.866833511	-0.04786777
	nt 25.3	0.05	3539.25	54.14779933	6536.276716	6.536276716	6.866833511	-0.330556795
	nt 25.4	0.075	3869.88	55.32852424	6994.366926	6.994366926	6.866833511	0.127533414
	nt 25.5	0.1	4115.01	54.90129998	7495.286999	7.495286999	6.866833511	0.628453488
	nt 25.6	0.2	6903.76	67.62759449	10208.49559	10.20849559	6.866833511	3.341662077
	nt 25.7	0.5	8546.69	74.98658197	11397.62578	11.39762578	6.866833511	4.530792271
	nt 25.8	0.75	8098.77	67.39841997	12016.26092	12.01626092	6.866833511	5.149427409
	nt 25.9	1	8628.19	74.55370278	11573.12069	11.57312069	6.866833511	4.706287176
	nt 25.10	2.5	9776.24	79.73445839	12260.99756	12.26099756	6.866833511	5.394164052
	nt 25.11	5	10817.13	82.62155722	13092.38214	13.09238214	6.866833511	6.225548627
	nt 25.12	7.5	11620.87	85.99637809	13513.20865	13.51320865	6.866833511	6.646375136
	nt 25.13	10	11844.76	83.56666532	14174.02496	14.17402496	6.866833511	7.307191449

nt No.	Name of the Band	Tb^{3+} (mM)	Cleavage Intensity (I)	Correction factor (R)	Corrected cleavage Intensity (I_{corr} = I*100/ R)	I_{corr} / 1000	(I_{corr}) at 0 mM	$I_R = (I_{corr\ (x\ mM)} - I_{corr\ (0\ mM)})$
	nt 25.14	15	13237.38	100	13237.38	13.23738	6.866833511	6.370546489
	nt 25.15	20	12937.42	96.33171878	13430.07284	13.43007284	6.866833511	6.563239328
46	nt 46.1	0	3572.18	48.41212467	7378.688758	7.378688758	7.378688758	0
	nt 46.2	0.025	3765.87	57.7358818	6522.581595	6.522581595	7.378688758	-0.856107162
	nt 46.3	0.05	3921.67	54.14779933	7242.528872	7.242528872	7.378688758	-0.136159886
	nt 46.4	0.075	3837.19	55.32852424	6935.283477	6.935283477	7.378688758	-0.44340528
	nt 46.5	0.1	3786.26	54.90129998	6896.485149	6.896485149	7.378688758	-0.482203609
	nt 46.6	0.2	5395.69	67.62759449	7978.533084	7.978533084	7.378688758	0.599844326
	nt 46.7	0.5	7834.33	74.98658197	10447.64249	10.44764249	7.378688758	3.068953732
	nt 46.8	0.75	7677.12	67.39841997	11390.65278	11.39065278	7.378688758	4.011964025
	nt 46.9	1	8115.88	74.55370278	10885.9516	10.8859516	7.378688758	3.507262841
	nt 46.10	2.5	9598.14	79.73445839	12037.63115	12.03763115	7.378688758	4.658942392
	nt 46.11	5	10985.23	82.62155722	13295.83993	13.29583993	7.378688758	5.917151177
	nt 46.12	7.5	11984.63	85.99637809	13936.20321	13.93620321	7.378688758	6.557514448
	nt 46.13	10	12350.81	83.56666532	14779.58939	14.77958939	7.378688758	7.400900632
	nt 46.14	15	14592.55	100	14592.55	14.59255	7.378688758	7.213861242
	nt 46.15	20	14371.2	96.33171878	14918.45073	14.91845073	7.378688758	7.539761968
47	nt 47.1	0	3760.32	48.41212467	7767.310412	7.767310412	7.767310412	0
	nt 47.2	0.025	4083.68	57.7358818	7073.036512	7.073036512	7.767310412	-0.6942739
	nt 47.3	0.05	4037.48	54.14779933	7456.406447	7.456406447	7.767310412	-0.310903966
	nt 47.4	0.075	4181.7	55.32852424	7557.946027	7.557946027	7.767310412	-0.209364385
	nt 47.5	0.1	4115.5	54.90129998	7496.17951	7.49617951	7.767310412	-0.271130903
	nt 47.6	0.2	6012.17	67.62759449	8890.113637	8.890113637	7.767310412	1.122803225
	nt 47.7	0.5	7688.78	74.98658197	10253.5411	10.2535411	7.767310412	2.486230685
	nt 47.8	0.75	7447.64	67.39841997	11050.17002	11.05017002	7.767310412	3.282859611
	nt 47.9	1	8949.17	74.55370278	12003.65598	12.00365598	7.767310412	4.236345564
	nt 47.10	2.5	10179.56	79.73445839	12766.82655	12.76682655	7.767310412	4.999516134
	nt 47.11	5	12259.11	82.62155722	14837.66515	14.83766515	7.767310412	7.070354734
	nt 47.12	7.5	13331.05	85.99637809	15501.8738	15.5018738	7.767310412	7.734563383
	nt 47.13	10	14003.22	83.56666532	16756.94483	16.75694483	7.767310412	8.989634414
	nt 47.14	15	16371.62	100	16371.62	16.37162	7.767310412	8.604309588
	nt 47.15	20	16000.57	96.33171878	16609.86662	16.60986662	7.767310412	8.842556205
48	nt 48.1	0	4056.21	48.41212467	8378.500279	8.378500279	8.378500279	0
	nt 48.2	0.025	4224.35	57.7358818	7316.680492	7.316680492	8.378500279	-1.061819787
	nt 48.3	0.05	4017.19	54.14779933	7418.934933	7.418934933	8.378500279	-0.959565345
	nt 48.4	0.075	4028.29	55.32852424	7280.674941	7.280674941	8.378500279	-1.097825337
	nt 48.5	0.1	3824.73	54.90129998	6966.556349	6.966556349	8.378500279	-1.411943929
	nt 48.6	0.2	6767.95	67.62759449	10007.6752	10.0076752	8.378500279	1.629174918
	nt 48.7	0.5	9029.98	74.98658197	12042.12775	12.04212775	8.378500279	3.663627476

nt No.	Name of the Band	Tb^{3+} (mM)	Cleavage Intensity (I)	Correction factor (R)	Corrected cleavage Intensity (I_{corr} = I*100/ R)	I_{corr} / 1000	(I_{corr}) at 0 mM	$I_R = (I_{corr\ (x\ mM)} - I_{corr\ (0\ mM)})$
	nt 48.8	0.75	8885.78	67.39841997	13183.95892	13.18395892	8.378500279	4.805458638
	nt 48.9	1	10091.66	74.55370278	13536.09495	13.53609495	8.378500279	5.157594675
	nt 48.10	2.5	12051.09	79.73445839	15114.03005	15.11403005	8.378500279	6.73552977
	nt 48.11	5	14178.5	82.62155722	17160.77556	17.16077556	8.378500279	8.782275282
	nt 48.12	7.5	15559.5	85.99637809	18093.20386	18.09320386	8.378500279	9.714703582
	nt 48.13	10	16645.23	83.56666532	19918.50451	19.91850451	8.378500279	11.54000423
	nt 48.14	15	19928.28	100	19928.28	19.92828	8.378500279	11.54977972
	nt 48.15	20	18737.26	96.33171878	19450.7689	19.4507689	8.378500279	11.07226862
49	nt 49.1	0	3886.33	48.41212467	8027.596448	8.027596448	8.027596448	0
	nt 49.2	0.025	4285.24	57.7358818	7422.143504	7.422143504	8.027596448	-0.605452944
	nt 49.3	0.05	4330.65	54.14779933	7997.831959	7.997831959	8.027596448	-0.029764489
	nt 49.4	0.075	4115.89	55.32852424	7439.001955	7.439001955	8.027596448	-0.588594493
	nt 49.5	0.1	4191.78	54.90129998	7635.119753	7.635119753	8.027596448	-0.392476695
	nt 49.6	0.2	5762.63	67.62759449	8521.122248	8.521122248	8.027596448	0.493525801
	nt 49.7	0.5	7382.45	74.98658197	9845.028011	9.845028011	8.027596448	1.817431563
	nt 49.8	0.75	7218.84	67.39841997	10710.69619	10.71069619	8.027596448	2.683099742
	nt 49.9	1	8044.19	74.55370278	10789.79273	10.78979273	8.027596448	2.762196278
	nt 49.10	2.5	9308.88	79.73445839	11674.85199	11.67485199	8.027596448	3.64725554
	nt 49.11	5	10755.63	82.62155722	13017.94636	13.01794636	8.027596448	4.990349911
	nt 49.12	7.5	11804.95	85.99637809	13727.26417	13.72726417	8.027596448	5.699667726
	nt 49.13	10	12064.38	83.56666532	14436.8331	14.4368331	8.027596448	6.409236653
	nt 49.14	15	14083.9	100	14083.9	14.0839	8.027596448	6.056303552
	nt 49.15	20	13540.7	96.33171878	14056.32555	14.05632555	8.027596448	6.028729102
50	nt 50.1	0	4323.77	48.41212467	8931.171747	8.931171747	8.931171747	0
	nt 50.2	0.025	4859.15	57.7358818	8416.170064	8.416170064	8.931171747	-0.515001682
	nt 50.3	0.05	5292.9	54.14779933	9774.912491	9.774912491	8.931171747	0.843740744
	nt 50.4	0.075	4730.28	55.32852424	8549.441838	8.549441838	8.931171747	-0.381729908
	nt 50.5	0.1	4789.49	54.90129998	8723.818928	8.723818928	8.931171747	-0.207352818
	nt 50.6	0.2	6635.57	67.62759449	9811.9267	9.8119267	8.931171747	0.880754953
	nt 50.7	0.5	9086.05	74.98658197	12116.90113	12.11690113	8.931171747	3.185729386
	nt 50.8	0.75	8835.15	67.39841997	13108.83846	13.10883846	8.931171747	4.177666715
	nt 50.9	1	10256.61	74.55370278	13757.34486	13.75734486	8.931171747	4.826173117
	nt 50.10	2.5	11988.12	79.73445839	15035.05541	15.03505541	8.931171747	6.103883664
	nt 50.11	5	14926.94	82.62155722	18066.64084	18.06664084	8.931171747	9.135469093
	nt 50.12	7.5	16615.09	85.99637809	19320.68579	19.32068579	8.931171747	10.38951404
	nt 50.13	10	17443.29	83.56666532	20873.50253	20.87350253	8.931171747	11.94233078
	nt 50.14	15	20513.51	100	20513.51	20.51351	8.931171747	11.58233825
	nt 50.15	20	20148.28	96.33171878	20915.52009	20.91552009	8.931171747	11.98434835
51	nt 51.1	0	4184.72	48.41212467	8643.95031	8.64395031	8.64395031	0

nt No.	Name of the Band	Tb^{3+} (mM)	Cleavage Intensity (I)	Correction factor (R)	Corrected cleavage Intensity (I_{corr} = I*100/ R)	I_{corr} / 1000	(I_{corr}) at 0 mM	$I_R = (I_{corr\ (x\ mM)} - I_{corr\ (0\ mM)})$
	nt 51.2	0.025	4901.96	57.7358818	8490.318061	8.490318061	8.64395031	-0.153632249
	nt 51.3	0.05	4845.14	54.14779933	8947.990611	8.947990611	8.64395031	0.304040301
	nt 51.4	0.075	4716.56	55.32852424	8524.644502	8.524644502	8.64395031	-0.119305808
	nt 51.5	0.1	4541.99	54.90129998	8273.009931	8.273009931	8.64395031	-0.370940379
	nt 51.6	0.2	6137.46	67.62759449	9075.378248	9.075378248	8.64395031	0.431427938
	nt 51.7	0.5	8876.05	74.98658197	11836.85103	11.83685103	8.64395031	3.192900719
	nt 51.8	0.75	8615.24	67.39841997	12782.55485	12.78255485	8.64395031	4.138604538
	nt 51.9	1	9715.31	74.55370278	13031.29105	13.03129105	8.64395031	4.387340743
	nt 51.10	2.5	11721.91	79.73445839	14701.1847	14.7011847	8.64395031	6.057234394
	nt 51.11	5	14111.02	82.62155722	17079.10196	17.07910196	8.64395031	8.435151651
	nt 51.12	7.5	15120.78	85.99637809	17583.04284	17.58304284	8.64395031	8.93909253
	nt 51.13	10	16382.01	83.56666532	19603.52245	19.60352245	8.64395031	10.95957215
	nt 51.14	15	18990.96	100	18990.96	18.99096	8.64395031	10.34700969
	nt 51.15	20	18535.37	96.33171878	19241.191	19.241191	8.64395031	10.59724069
53	nt 53.1	0	4588.8	48.41212467	9478.617251	9.478617251	9.478617251	0
	nt 53.2	0.025	5253.9	57.7358818	9099.886997	9.099886997	9.478617251	-0.378730254
	nt 53.3	0.05	5165.63	54.14779933	9539.870621	9.539870621	9.478617251	0.06125337
	nt 53.4	0.075	5223.88	55.32852424	9441.567567	9.441567567	9.478617251	-0.037049684
	nt 53.5	0.1	5216.55	54.90129998	9501.687577	9.501687577	9.478617251	0.023070326
	nt 53.6	0.2	8286.39	67.62759449	12252.97168	12.25297168	9.478617251	2.774354429
	nt 53.7	0.5	9611.97	74.98658197	12818.25328	12.81825328	9.478617251	3.339636025
	nt 53.8	0.75	9009.48	67.39841997	13367.49438	13.36749438	9.478617251	3.888877126
	nt 53.9	1	9899.93	74.55370278	13278.92463	13.27892463	9.478617251	3.800307377
	nt 53.10	2.5	11020.07	79.73445839	13820.96301	13.82096301	9.478617251	4.342345759
	nt 53.11	5	12360.97	82.62155722	14960.95016	14.96095016	9.478617251	5.482332912
	nt 53.12	7.5	13294.69	85.99637809	15459.59295	15.45959295	9.478617251	5.980975694
	nt 53.13	10	13535.06	83.56666532	16196.72144	16.19672144	9.478617251	6.718104192
	nt 53.14	15	15275.01	100	15275.01	15.27501	9.478617251	5.796392749
	nt 53.15	20	15315.2	96.33171878	15898.39795	15.89839795	9.478617251	6.419780695
63	nt 63.1	0	4409.01	34.69892991	12076.84598	1.207684598	1.207684598	0
	nt 63.2	0.025	4898.92	38.38672938	12073.81027	1.207381027	1.207684598	-0.000303571
	nt 63.3	0.05	5374.95	38.34201356	13356.66349	1.335666349	1.207684598	0.127981751
	nt 63.4	0.075	5762.39	39.12299665	14504.43573	1.450443573	1.207684598	0.242758975
	nt 63.5	0.1	5857.2	37.89231088	14858.89611	1.485889611	1.207684598	0.278205013
	nt 63.6	0.2	17024.66	50.36035587	31590.55373	3.159055373	1.207684598	1.951370775
	nt 63.7	0.5	30750.09	61.19495044	48626.10031	4.862610031	1.207684598	3.654925433
	nt 63.8	0.75	28968.63	58.39673446	47885.3443	4.78853443	1.207684598	3.580849832
	nt 63.9	1	33353.32	63.78219123	51758.40496	5.175840496	1.207684598	3.968155898
	nt 63.10	2.5	45855.74	72.81561715	62474.72148	6.247472148	1.207684598	5.03978755
	nt 63.11	5	50330.48	78.72034397	63642.98331	6.364298331	1.207684598	5.156613733

nt No.	Name of the Band	Tb^{3+} (mM)	Cleavage Intensity (I)	Correction factor (R)	Corrected cleavage Intensity (I_{corr} = I*100/ R)	I_{corr} / 1000	(I_{corr}) at 0 mM	$I_R = (I_{corr\ (x\ mM)} - I_{corr\ (0\ mM)})$
	nt 63.12	7.5	54043.61	83.08420721	64048.56912	6.404856912	1.207684598	5.197172314
	nt 63.13	10	55940.91	82.8975068	66469.9981	6.64699981	1.207684598	5.439315211
	nt 63.14	15	66385.51	95.80047925	68571.82692	6.857182692	1.207684598	5.649498094
	nt 63.15	20	66261.62	100	66261.62	6.626162	1.207684598	5.418477402
64	nt 64.1	0	5138.23	34.69892991	14074.27344	1.407427344	1.407427344	0
	nt 64.2	0.025	5411.65	38.38672938	13337.47751	1.333747751	1.407427344	-0.073679592
	nt 64.3	0.05	5749.37	38.34201356	14287.09111	1.428709111	1.407427344	0.021281768
	nt 64.4	0.075	6081.68	39.12299665	15308.11637	1.530811637	1.407427344	0.123384293
	nt 64.5	0.1	6183.66	37.89231088	15687.07942	1.568707942	1.407427344	0.161280598
	nt 64.6	0.2	13594.72	50.36035587	25226.03873	2.522603873	1.407427344	1.11517653
	nt 64.7	0.5	21333.74	61.19495044	33735.72504	3.373572504	1.407427344	1.96614516
	nt 64.8	0.75	20112.73	58.39673446	33246.48079	3.324648079	1.407427344	1.917220735
	nt 64.9	1	23072.24	63.78219123	35804.00216	3.580400216	1.407427344	2.172972873
	nt 64.10	2.5	30629.1	72.81561715	41729.66115	4.172966115	1.407427344	2.765538771
	nt 64.11	5	33659.19	78.72034397	42562.10685	4.256210685	1.407427344	2.848783341
	nt 64.12	7.5	36634.22	83.08420721	43416.22205	4.341622205	1.407427344	2.934194861
	nt 64.13	10	35730.37	82.8975068	42455.46999	4.245546999	1.407427344	2.838119656
	nt 64.14	15	41296.77	95.80047925	42656.82323	4.265682323	1.407427344	2.858254979
	nt 64.15	20	44304.12	100	44304.12	4.430412	1.407427344	3.022984656
68	nt 68.1	0	5197.93	34.69892991	14237.79942	1.423779942	1.423779942	0
	nt 68.2	0.025	5974.05	38.38672938	14723.56075	1.472356075	1.423779942	0.048576133
	nt 68.3	0.05	6048.22	38.34201356	15029.72851	1.502972851	1.423779942	0.079192909
	nt 68.4	0.075	6965.32	39.12299665	17532.31493	1.753231493	1.423779942	0.329451551
	nt 68.5	0.1	7005.46	37.89231088	17771.87092	1.777187092	1.423779942	0.35340715
	nt 68.6	0.2	20644.52	50.36035587	38307.47975	3.830747975	1.423779942	2.406968033
	nt 68.7	0.5	27752.49	61.19495044	43885.8996	4.38858996	1.423779942	2.964810018
	nt 68.8	0.75	24220.98	58.39673446	40037.44625	4.003744625	1.423779942	2.579964683
	nt 68.9	1	26639.15	63.78219123	41339.21042	4.133921042	1.423779942	2.7101411
	nt 68.10	2.5	34159.95	72.81561715	46540.1575	4.65401575	1.423779942	3.230235808
	nt 68.11	5	37961.82	78.72034397	48002.79029	4.800279029	1.423779942	3.376499087
	nt 68.12	7.5	41030.53	83.08420721	48626.40998	4.862640998	1.423779942	3.438861056
	nt 68.13	10	42212.96	82.8975068	50158.20034	5.015820034	1.423779942	3.592040092
	nt 68.14	15	48781.97	95.80047925	50388.53816	5.038853816	1.423779942	3.615073874
	nt 68.15	20	50317.16	100	50317.16	5.031716	1.423779942	3.607936058
70	nt 70.1	0	5853.18	34.69892991	16032.61352	1.603261352	1.603261352	0
	nt 70.2	0.025	6650.98	38.38672938	16391.91304	1.639191304	1.603261352	0.035929952
	nt 70.3	0.05	6350.84	38.34201356	15781.7343	1.57817343	1.603261352	-0.025087923
	nt 70.4	0.075	6433.06	39.12299665	16192.57032	1.619257032	1.603261352	0.01599568
	nt 70.5	0.1	6506.75	37.89231088	16506.7135	1.65067135	1.603261352	0.047409997

nt No.	Name of the Band	Tb^{3+} (mM)	Cleavage Intensity (I)	Correction factor (R)	Corrected cleavage Intensity (I_{corr} = I*100/ R)	I_{corr} / 1000	(I_{corr}) at 0 mM	$I_R = (I_{corr\ (x\ mM)} - I_{corr\ (0\ mM)})$
	nt 70.6	0.2	11068.77	50.36035587	20538.94606	2.053894606	1.603261352	0.450633253
	nt 70.7	0.5	16366.68	61.19495044	25881.15428	2.588115428	1.603261352	0.984854075
	nt 70.8	0.75	16295.45	58.39673446	26936.49074	2.693649074	1.603261352	1.090387722
	nt 70.9	1	18406.09	63.78219123	28562.96944	2.856296944	1.603261352	1.253035592
	nt 70.10	2.5	23240.55	72.81561715	31663.36185	3.166336185	1.603261352	1.563074832
	nt 70.11	5	25453.57	78.72034397	32186.08546	3.218608546	1.603261352	1.615347194
	nt 70.12	7.5	27186.17	83.08420721	32219.07804	3.221907804	1.603261352	1.618646452
	nt 70.13	10	28600.66	82.8975068	33983.81999	3.398381999	1.603261352	1.795120647
	nt 70.14	15	31265.09	95.80047925	32294.76342	3.229476342	1.603261352	1.62621499
	nt 70.15	20	32982.99	100	32982.99	3.298299	1.603261352	1.695037648
76	nt 76.1	0	6535.21	34.69892991	17900.78149	1.790078149	1.790078149	0
	nt 76.2	0.025	7242.84	38.38672938	17850.60299	1.785060299	1.790078149	-0.005017851
	nt 76.3	0.05	7475.17	38.34201356	18575.67609	1.857567609	1.790078149	0.06748946
	nt 76.4	0.075	7584.62	39.12299665	19091.14678	1.909114678	1.790078149	0.119036528
	nt 76.5	0.1	7792.65	37.89231088	19768.86171	1.976886171	1.790078149	0.186808022
	nt 76.6	0.2	13583.09	50.36035587	25204.45838	2.520445838	1.790078149	0.730367689
	nt 76.7	0.5	18851.63	61.19495044	29810.68515	2.981068515	1.790078149	1.190990365
	nt 76.8	0.75	18268.58	58.39673446	30198.08818	3.019808818	1.790078149	1.229730668
	nt 76.9	1	20374.09	63.78219123	31616.9545	3.16169545	1.790078149	1.371617301
	nt 76.10	2.5	26713.72	72.81561715	36395.27389	3.639527389	1.790078149	1.84944924
	nt 76.11	5	28191.95	78.72034397	35648.77194	3.564877194	1.790078149	1.774799045
	nt 76.12	7.5	32050.97	83.08420721	37984.48637	3.798448637	1.790078149	2.008370488
	nt 76.13	10	33611.33	82.8975068	39937.58845	3.993758845	1.790078149	2.203680695
	nt 76.14	15	36914.17	95.80047925	38129.88823	3.812988823	1.790078149	2.022910673
	nt 76.15	20	38552.93	100	38552.93	3.855293	1.790078149	2.065214851
77	nt 77.1	0	7092.55	34.69892991	19427.4075	1.94274075	1.94274075	0
	nt 77.2	0.025	7959.66	38.38672938	19617.26761	1.961726761	1.94274075	0.018986011
	nt 77.3	0.05	7729.14	38.34201356	19206.78742	1.920678742	1.94274075	-0.022062008
	nt 77.4	0.075	8290.47	39.12299665	20867.83249	2.086783249	1.94274075	0.144042498
	nt 77.5	0.1	8544.22	37.89231088	21675.48955	2.167548955	1.94274075	0.224808204
	nt 77.6	0.2	15366.18	50.36035587	28513.11773	2.851311773	1.94274075	0.908571022
	nt 77.7	0.5	19114.6	61.19495044	30226.52802	3.022652802	1.94274075	1.079912051
	nt 77.8	0.75	18431.09	58.39673446	30466.71832	3.046671832	1.94274075	1.103931082
	nt 77.9	1	20081.52	63.78219123	31162.93804	3.116293804	1.94274075	1.173553053
	nt 77.10	2.5	25885.08	72.81561715	35266.31919	3.526631919	1.94274075	1.583891169
	nt 77.11	5	27381.26	78.72034397	34623.65297	3.462365297	1.94274075	1.519624546
	nt 77.12	7.5	30438.61	83.08420721	36073.63417	3.607363417	1.94274075	1.664622667
	nt 77.13	10	31302.68	82.8975068	37194.40889	3.719440889	1.94274075	1.776700138
	nt 77.14	15	34915.13	95.80047925	36065.01255	3.606501255	1.94274075	1.663760505
	nt 77.15	20	35900.21	100	35900.21	3.590021	1.94274075	1.64728025

nt No.	Name of the Band	Tb^{3+} (mM)	Cleavage Intensity (I)	Correction factor (R)	Corrected cleavage Intensity (I_{corr} = I*100/ R)	I_{corr} / 1000	(I_{corr}) at 0 mM	$I_R = (I_{corr\ (x\ mM)} - I_{corr\ (0\ mM)})$
81	nt 81.1	0	6085.62	34.69892991	16669.29661	1.666929661	1.666929661	0
	nt 81.2	0.025	6470.78	38.38672938	15947.79462	1.594779462	1.666929661	-0.072150199
	nt 81.3	0.05	6528.27	38.34201356	16222.64497	1.622264497	1.666929661	-0.044665164
	nt 81.4	0.075	6706.02	39.12299665	16879.63433	1.687963433	1.666929661	0.021033772
	nt 81.5	0.1	7340.03	37.89231088	18620.62816	1.862062816	1.666929661	0.195133155
	nt 81.6	0.2	14132.12	50.36035587	26223.22538	2.622322538	1.666929661	0.955392877
	nt 81.7	0.5	19607	61.19495044	31005.17588	3.100517588	1.666929661	1.433587927
	nt 81.8	0.75	17960.6	58.39673446	29688.99512	2.968899512	1.666929661	1.301969852
	nt 81.9	1	20325.57	63.78219123	31541.66012	3.154166012	1.666929661	1.487236351
	nt 81.10	2.5	25250.56	72.81561715	34401.83722	3.440183722	1.666929661	1.773254062
	nt 81.11	5	26660.08	78.72034397	33711.71955	3.371171955	1.666929661	1.704242294
	nt 81.12	7.5	27619.11	83.08420721	32732.16715	3.273216715	1.666929661	1.606287054
	nt 81.13	10	29718.34	82.8975068	35311.86753	3.531186753	1.666929661	1.864257092
	nt 81.14	15	34549.94	95.80047925	35687.79551	3.568779551	1.666929661	1.901849891
	nt 81.15	20	35906.26	100	35906.26	3.590626	1.666929661	1.923696339
82-84	nt 82.1	0	33285.32	34.69892991	91172.77644	9.117277644	9.117277644	0
	nt 82.2	0.025	36550.79	38.38672938	90082.56997	9.008256997	9.117277644	-0.109020647
	nt 82.3	0.05	35666.49	38.34201356	88630.64862	8.863064862	9.117277644	-0.254212782
	nt 82.4	0.075	36621.53	39.12299665	92179.56925	9.217956925	9.117277644	0.100679281
	nt 82.5	0.1	36775.02	37.89231088	93293.0755	9.32930755	9.117277644	0.212029906
	nt 82.6	0.2	60247.78	50.36035587	111794.346	11.1794346	9.117277644	2.062156959
	nt 82.7	0.5	78518.43	61.19495044	124163.7034	12.41637034	9.117277644	3.299092692
	nt 82.8	0.75	75735.52	58.39673446	125191.3346	12.51913346	9.117277644	3.401855814
	nt 82.9	1	83061.96	63.78219123	128897.35	12.889735	9.117277644	3.77245736
	nt 82.10	2.5	102609.31	72.81561715	139796.8513	13.97968513	9.117277644	4.862407481
	nt 82.11	5	108490.21	78.72034397	137186.0675	13.71860675	9.117277644	4.601329101
	nt 82.12	7.5	114270.99	83.08420721	135425.6942	13.54256942	9.117277644	4.425291777
	nt 82.13	10	117250.65	82.8975068	139319.3368	13.93193368	9.117277644	4.814656038
	nt 82.14	15	137625.3	95.80047925	142157.803	14.2157803	9.117277644	5.098502655
	nt 82.15	20	141802.43	100	141802.43	14.180243	9.117277644	5.062965356
91-92	nt 91.1	0	14163.41	34.69892991	38795.40331	3.879540331	3.879540331	0
	nt 91.2	0.025	15757.13	38.38672938	38834.804	3.8834804	3.879540331	0.00394007
	nt 91.3	0.05	15227.74	38.34201356	37840.68668	3.784068668	3.879540331	-0.095471662
	nt 91.4	0.075	15687.6	39.12299665	39487.05067	3.948705067	3.879540331	0.069164736
	nt 91.5	0.1	15546.86	37.89231088	39440.20652	3.944020652	3.879540331	0.064480322
	nt 91.6	0.2	29308.29	50.36035587	54383.76507	5.438376507	3.879540331	1.558836177
	nt 91.7	0.5	37480.5	61.19495044	59269.11279	5.926911279	3.879540331	2.047370949
	nt 91.8	0.75	36655.43	58.39673446	60591.67748	6.059167748	3.879540331	2.179627417
	nt 91.9	1	40637.03	63.78219123	63061.42403	6.306142403	3.879540331	2.426602072

nt No.	Name of the Band	Tb^{3+} (mM)	Cleavage Intensity (I)	Correction factor (R)	Corrected cleavage Intensity (I_{corr} = I*100/ R)	I_{corr} / 1000	(I_{corr}) at 0 mM	$I_R = (I_{corr\ (x\ mM)} - I_{corr\ (0\ mM)})$
	nt 91.10	2.5	45620.39	72.81561715	62154.07622	6.215407622	3.879540331	2.335867292
	nt 91.11	5	49696.66	78.72034397	62841.51677	6.284151677	3.879540331	2.404611346
	nt 91.12	7.5	51885.91	83.08420721	61491.41949	6.149141949	3.879540331	2.269601618
	nt 91.13	10	53173.53	82.8975068	63181.74727	6.318174727	3.879540331	2.438634397
	nt 91.14	15	59202.49	95.80047925	61152.24388	6.115224388	3.879540331	2.235684058
	nt 91.15	20	59739.89	100	59739.89	5.973989	3.879540331	2.094448669
97-100	nt 97.1	0	37425.26	34.69892991	102512.6051	10.25126051	10.25126051	0
	nt 97.2	0.025	43264.07	38.38672938	106628.0267	10.66280267	10.25126051	0.411542168
	nt 97.3	0.05	41352.22	38.34201356	102759.5954	10.27595954	10.25126051	0.024699031
	nt 97.4	0.075	39625.81	39.12299665	99741.60274	9.974160274	10.25126051	-0.277100231
	nt 97.5	0.1	40500.43	37.89231088	102743.9189	10.27439189	10.25126051	0.023131388
	nt 97.6	0.2	79370.61	50.36035587	147278.214	14.7278214	10.25126051	4.476560899
	nt 97.7	0.5	93736.81	61.19495044	148229.0141	14.82290141	10.25126051	4.571640909
	nt 97.8	0.75	86062.13	58.39673446	142261.2918	14.22612918	10.25126051	3.974868677
	nt 97.9	1	97037.1	63.78219123	150584.2752	15.05842752	10.25126051	4.807167017
	nt 97.10	2.5	122697.28	72.81561715	167165.0789	16.71650789	10.25126051	6.465247384
	nt 97.11	5	133940.43	78.72034397	169367.9168	16.93679168	10.25126051	6.685531178
	nt 97.12	7.5	144010.26	83.08420721	170670.5213	17.06705213	10.25126051	6.815791626
	nt 97.13	10	150358.98	82.8975068	178659.2516	17.86592516	10.25126051	7.614664655
	nt 97.14	15	177157.84	95.80047925	182992.2937	18.29922937	10.25126051	8.047968864
	nt 97.15	20	165986.66	100	165986.66	16.598666	10.25126051	6.347405495
106-109	nt 106.1	0	20387.08	34.69892991	55842.83663	5.584283663	5.584283663	0
	nt 106.2	0.025	22300.46	38.38672938	54961.40435	5.496140435	5.584283663	-0.088143229
	nt 106.3	0.05	21244.67	38.34201356	52792.66005	5.279266005	5.584283663	-0.305017658
	nt 106.4	0.075	23750.32	39.12299665	59781.61664	5.978161664	5.584283663	0.393878
	nt 106.5	0.1	26208.94	37.89231088	66488.41029	6.648841029	5.584283663	1.064557365
	nt 106.6	0.2	51665.66	50.36035587	95869.5685	9.58695685	5.584283663	4.002673187
	nt 106.7	0.5	52804.73	61.19495044	83501.80756	8.350180756	5.584283663	2.765897093
	nt 106.8	0.75	49258.86	58.39673446	81425.23381	8.142523381	5.584283663	2.558239717
	nt 106.9	1	53691.7	63.78219123	83319.94392	8.331994392	5.584283663	2.747710728
	nt 106.10	2.5	64416.59	72.81561715	87762.37215	8.776237215	5.584283663	3.191953552
	nt 106.11	5	69571.16	78.72034397	87972.85809	8.797285809	5.584283663	3.213002146
	nt 106.12	7.5	73542.8	83.08420721	87157.59568	8.715759568	5.584283663	3.131475904
	nt 106.13	10	75469.99	82.8975068	89674.80314	8.967480314	5.584283663	3.38319665
	nt 106.14	15	85669.98	95.80047925	88491.40484	8.849140484	5.584283663	3.264856821
	nt 106.15	20	86128.01	100	86128.01	8.612801	5.584283663	3.028517337
110- 111	nt 111.1	0	18288.58	34.69892991	50094.77499	5.009477499	5.009477499	0
	nt 111.2	0.025	18541.25	38.38672938	45696.50753	4.569650753	5.009477499	-0.439826746
	nt 111.3	0.05	18395.18	38.34201356	45711.72366	4.571172366	5.009477499	-0.438305132

nt No.	Name of the Band	Tb^{3+} (mM)	Cleavage Intensity (I)	Correction factor (R)	Corrected cleavage Intensity (I_{corr} = I*100/ R)	I_{corr} / 1000	(I_{corr}) at 0 mM	$I_R = (I_{corr\ (x\ mM)} - I_{corr\ (0\ mM)})$
	nt 111.4	0.075	18540.13	39.12299665	46667.11624	4.666711624	5.009477499	-0.342765875
	nt 111.5	0.1	19019.09	37.89231088	48248.76776	4.824876776	5.009477499	-0.184600723
	nt 111.6	0.2	31890.38	50.36035587	59175.0298	5.91750298	5.009477499	0.908025481
	nt 111.7	0.5	34750.08	61.19495044	54951.41236	5.495141236	5.009477499	0.485663738
	nt 111.8	0.75	31603.38	58.39673446	52240.60414	5.224060414	5.009477499	0.214582915
	nt 111.9	1	33844.41	63.78219123	52520.48907	5.252048907	5.009477499	0.242571409
	nt 111.10	2.5	38986.05	72.81561715	53115.32679	5.311532679	5.009477499	0.302055181
	nt 111.11	5	41967.25	78.72034397	53067.66379	5.306766379	5.009477499	0.297288881
	nt 111.12	7.5	45061.55	83.08420721	53403.68269	5.340368269	5.009477499	0.330890771
	nt 111.13	10	45116.26	82.8975068	53607.95375	5.360795375	5.009477499	0.351317877
	nt 111.14	15	53164.85	95.80047925	54915.76238	5.491576238	5.009477499	0.482098739
	nt 111.15	20	52817.83	100	52817.83	5.281783	5.009477499	0.272305501
113-114	nt 113.1	0	19431.19	34.69892991	53224.53087	5.322453087	5.322453087	0
	nt 113.2	0.025	20141.86	38.38672938	49641.34873	4.964134873	5.322453087	-0.358318214
	nt 113.3	0.05	19884.1	38.34201356	49411.66569	4.941166569	5.322453087	-0.381286518
	nt 113.4	0.075	19621.59	39.12299665	49389.24491	4.938924491	5.322453087	-0.383528596
	nt 113.5	0.1	20543.98	37.89231088	52117.20013	5.211720013	5.322453087	-0.110733074
	nt 113.6	0.2	30042.17	50.36035587	55745.53533	5.574553533	5.322453087	0.252100446
	nt 113.7	0.5	33680.07	61.19495044	53259.37134	5.325937134	5.322453087	0.003484047
	nt 113.8	0.75	31316.69	58.39673446	51766.7036	5.17667036	5.322453087	-0.145782727
	nt 113.9	1	34687.77	63.78219123	53829.2334	5.38292334	5.322453087	0.060470253
	nt 113.10	2.5	38876.9	72.81561715	52966.61878	5.296661878	5.322453087	-0.025791209
	nt 113.11	5	42171.36	78.72034397	53325.76126	5.332576126	5.322453087	0.010123039
	nt 113.12	7.5	45495.88	83.08420721	53918.41912	5.391841912	5.322453087	0.069388826
	nt 113.13	10	46035.9	82.8975068	54700.68659	5.470068659	5.322453087	0.147615572
	nt 113.14	15	55718.95	95.80047925	57553.97821	5.755397821	5.322453087	0.432944734
	nt 113.15	20	53845.24	100	53845.24	5.384524	5.322453087	0.062070913
115-118	nt 115.1	0	29974.19	34.69892991	82103.16511	8.210316511	8.210316511	0
	nt 115.2	0.025	31064.82	38.38672938	76561.92441	7.656192441	8.210316511	-0.55412407
	nt 115.3	0.05	30754.12	38.34201356	76423.48892	7.642348892	8.210316511	-0.567967619
	nt 115.4	0.075	31006.66	39.12299665	78046.45417	7.804645417	8.210316511	-0.405671095
	nt 115.5	0.1	31773.2	37.89231088	80604.15865	8.060415865	8.210316511	-0.149900646
	nt 115.6	0.2	51300.32	50.36035587	95191.65229	9.519165229	8.210316511	1.308848718
	nt 115.7	0.5	63715.72	61.19495044	100755.7048	10.07557048	8.210316511	1.865253973
	nt 115.8	0.75	56387.53	58.39673446	93208.97426	9.320897426	8.210316511	1.110580915
	nt 115.9	1	62889.01	63.78219123	97592.52894	9.759252894	8.210316511	1.548936383
	nt 115.10	2.5	73971.5	72.81561715	100780.161	10.0780161	8.210316511	1.867699589
	nt 115.11	5	85637.73	78.72034397	108289.065	10.8289065	8.210316511	2.61858999
	nt 115.12	7.5	87136.72	83.08420721	103268.1243	10.32681243	8.210316511	2.116495917
	nt 115.13	10	83114.83	82.8975068	98758.53989	9.875853989	8.210316511	1.665537478

nt No.	Name of the Band	Tb^{3+} (mM)	Cleavage Intensity (I)	Correction factor (R)	Corrected cleavage Intensity (I_{corr} = I*100/ R)	I_{corr} / 1000	(I_{corr}) at 0 mM	$I_R = (I_{corr\ (x\ mM)} - I_{corr\ (0\ mM)})$
	nt 115.14	15	105836.21	95.80047925	109321.7823	10.93217823	8.210316511	2.721861722
	nt 115.15	20	104276.56	100	104276.56	10.427656	8.210316511	2.217339489
119-121	nt 119.1	0	32586.64	34.69892991	89259.00197	8.925900197	8.925900197	0
	nt 119.2	0.025	33637.97	38.38672938	82903.67421	8.290367421	8.925900197	-0.635532777
	nt 119.3	0.05	35200.45	38.34201356	87472.54679	8.747254679	8.925900197	-0.178645519
	nt 119.4	0.075	40433.97	39.12299665	101775.8116	10.17758116	8.925900197	1.251680962
	nt 119.5	0.1	41665.53	37.89231088	105699.6145	10.56996145	8.925900197	1.644061249
	nt 119.6	0.2	148533.1	50.36035587	275614.4837	27.56144837	8.925900197	18.63554817
	nt 119.7	0.5	135896.94	61.19495044	214898.1754	21.48981754	8.925900197	12.56391735
	nt 119.8	0.75	112621.63	58.39673446	186164.3277	18.61643277	8.925900197	9.690532571
	nt 119.9	1	113498.47	63.78219123	176129.386	17.6129386	8.925900197	8.687038404
	nt 119.10	2.5	147454.72	72.81561715	200895.0802	20.08950802	8.925900197	11.16360782
	nt 119.11	5	144673.84	78.72034397	182940.3333	18.29403333	8.925900197	9.368133129
	nt 119.12	7.5	153314.63	83.08420721	181697.3862	18.16973862	8.925900197	9.243838421
	nt 119.13	10	151560.79	82.8975068	180087.2639	18.00872639	8.925900197	9.082826194
	nt 119.14	15	185362.84	95.80047925	191467.5143	19.14675143	8.925900197	10.22085123
	nt 119.15	20	185830.12	100	185830.12	18.583012	8.925900197	9.657111803
122	nt 122.1	0	13096.63	34.69892991	35873.35555	3.587335555	3.587335555	0
	nt 122.2	0.025	14982.52	38.38672938	36925.71094	3.692571094	3.587335555	0.105235539
	nt 122.3	0.05	14187.11	38.34201356	35254.73803	3.525473803	3.587335555	-0.061861753
	nt 122.4	0.075	29938.79	39.12299665	75358.5327	7.53585327	3.587335555	3.948517715
	nt 122.5	0.1	24140.31	37.89231088	61240.58568	6.124058568	3.587335555	2.536723013
	nt 122.6	0.2	438746.77	50.36035587	814128.0595	81.41280595	3.587335555	77.8254704
	nt 122.7	0.5	279769.39	61.19495044	442408.2798	44.24082798	3.587335555	40.65349243
	nt 122.8	0.75	154348.22	58.39673446	255138.6675	25.51386675	3.587335555	21.92653119
	nt 122.9	1	131189.55	63.78219123	203582.7874	20.35827874	3.587335555	16.77094319
	nt 122.10	2.5	91650	72.81561715	124865.6815	12.48656815	3.587335555	8.89923259
	nt 122.11	5	77225.7	78.72034397	97652.03781	9.765203781	3.587335555	6.177868226
	nt 122.12	7.5	82908.37	83.08420721	98256.99036	9.825699036	3.587335555	6.238363481
	nt 122.13	10	76094.86	82.8975068	90417.28494	9.041728494	3.587335555	5.454392939
	nt 122.14	15	73563.8	95.80047925	75986.52419	7.598652419	3.587335555	4.011316864
	nt 122.15	20	81858.91	100	81858.91	8.185891	3.587335555	4.598555445
123-125	nt 123.1	0	22006.99	34.69892991	60279.97866	6.027997866	6.027997866	0
	nt 123.2	0.025	23546.65	38.38672938	58032.74693	5.803274693	6.027997866	-0.224723173
	nt 123.3	0.05	23441.52	38.34201356	58251.79664	5.825179664	6.027997866	-0.202818203
	nt 123.4	0.075	25509.75	39.12299665	64210.25464	6.421025464	6.027997866	0.393027598
	nt 123.5	0.1	25201.15	37.89231088	63931.7882	6.39317882	6.027997866	0.365180953
	nt 123.6	0.2	70542.43	50.36035587	130896.8534	13.08968534	6.027997866	7.061687478
	nt 123.7	0.5	69194.5	61.19495044	109419.4748	10.94194748	6.027997866	4.913949613

nt No.	Name of the Band	Tb^{3+} (mM)	Cleavage Intensity (I)	Correction factor (R)	Corrected cleavage Intensity (I_{corr} = I*100/ R)	I_{corr} / 1000	(I_{corr}) at 0 mM	$I_R = (I_{corr\ (x\ mM)} - I_{corr\ (0\ mM)})$
	nt 123.8	0.75	66562.04	58.39673446	110027.5092	11.00275092	6.027997866	4.974753049
	nt 123.9	1	68845.53	63.78219123	106835.9858	10.68359858	6.027997866	4.655600713
	nt 123.10	2.5	74741.43	72.81561715	101829.1281	10.18291281	6.027997866	4.154914943
	nt 123.11	5	75932.95	78.72034397	96017.35309	9.601735309	6.027997866	3.573737443
	nt 123.12	7.5	83457.09	83.08420721	98907.29353	9.890729353	6.027997866	3.862731487
	nt 123.13	10	81553.97	82.8975068	96903.89789	9.690389789	6.027997866	3.662391923
	nt 123.14	15	94620.33	95.80047925	97736.52251	9.773652251	6.027997866	3.745654385
	nt 123.15	20	97049.02	100	97049.02	9.704902	6.027997866	3.676904134
126-130	nt 126.1	0	46053.89	34.69892991	126147.5334	12.61475334	12.61475334	0
	nt 126.2	0.025	48178.89	38.38672938	118741.0239	11.87410239	12.61475334	-0.74065095
	nt 126.3	0.05	48479.82	38.34201356	120471.5657	12.04715657	12.61475334	-0.567596777
	nt 126.4	0.075	47225.85	39.12299665	118871.563	11.8871563	12.61475334	-0.727597042
	nt 126.5	0.1	49107.46	37.89231088	124578.7487	12.45787487	12.61475334	-0.156878477
	nt 126.6	0.2	80155.45	50.36035587	148734.5445	14.87345445	12.61475334	2.258701104
	nt 126.7	0.5	115932.29	61.19495044	183327.4362	18.33274362	12.61475334	5.717990277
	nt 126.8	0.75	115445.53	58.39673446	190832.2538	19.08322538	12.61475334	6.468472035
	nt 126.9	1	126865.55	63.78219123	196872.7105	19.68727105	12.61475334	7.072517709
	nt 126.10	2.5	154890.55	72.81561715	211025.7946	21.10257946	12.61475334	8.48782612
	nt 126.11	5	170389.21	78.72034397	215457.4653	21.54574653	12.61475334	8.930993188
	nt 126.12	7.5	185662.74	83.08420721	220034.0213	22.00340213	12.61475334	9.388648793
	nt 126.13	10	187947.9	82.8975068	223323.0842	22.33230842	12.61475334	9.71755508
	nt 126.14	15	224953.18	95.80047925	232361.7085	23.23617085	12.61475334	10.62141751
	nt 126.15	20	222299.28	100	222299.28	22.229928	12.61475334	9.615174658
131-135	nt 131.1	0	35283.24	34.69892991	96645.33652	9.664533652	9.664533652	0
	nt 131.2	0.025	38861.54	38.38672938	95777.61236	9.577761236	9.664533652	-0.086772416
	nt 131.3	0.05	37538.88	38.34201356	93283.50737	9.328350737	9.664533652	-0.336182915
	nt 131.4	0.075	36969	39.12299665	93054.1814	9.30541814	9.664533652	-0.359115512
	nt 131.5	0.1	36771.82	37.89231088	93284.95755	9.328495755	9.664533652	-0.336037897
	nt 131.6	0.2	53255.17	50.36035587	98819.02541	9.881902541	9.664533652	0.217368889
	nt 131.7	0.5	80714.17	61.19495044	127635.8972	12.76358972	9.664533652	3.09905607
	nt 131.8	0.75	82305.4	58.39673446	136051.3913	13.60513913	9.664533652	3.940605482
	nt 131.9	1	89053.21	63.78219123	138194.7017	13.81947017	9.664533652	4.154936513
	nt 131.10	2.5	110916.75	72.81561715	151115.0635	15.11150635	9.664533652	5.446972703
	nt 131.11	5	125174.12	78.72034397	158282.9019	15.82829019	9.664533652	6.163756541
	nt 131.12	7.5	131826.83	83.08420721	156231.6032	15.62316032	9.664533652	5.958626669
	nt 131.13	10	131767.45	82.8975068	156568.4604	15.65684604	9.664533652	5.992312385
	nt 131.14	15	150727.84	95.80047925	155691.8574	15.56918574	9.664533652	5.904652089
	nt 131.15	20	151228.14	100	151228.14	15.122814	9.664533652	5.458280348
148-152	nt 148.1	0	44510.81	34.69892991	121920.8387	12.19208387	12.19208387	0

nt No.	Name of the Band	Tb^{3+} (mM)	Cleavage Intensity (I)	Correction factor (R)	Corrected cleavage Intensity (I_{corr} = I*100/ R)	I_{corr} / 1000	(I_{corr}) at 0 mM	$I_R = (I_{corr\ (x\ mM)} - I_{corr\ (0\ mM)})$
	nt 148.2	0.025	48259.92	38.38672938	118940.7293	11.89407293	12.19208387	-0.298010932
	nt 148.3	0.05	45304.3	38.34201356	112580.45	11.258045	12.19208387	-0.934038865
	nt 148.4	0.075	46128.89	39.12299665	116110.4195	11.61104195	12.19208387	-0.581041918
	nt 148.5	0.1	47525.27	37.89231088	120564.9542	12.05649542	12.19208387	-0.135588445
	nt 148.6	0.2	68180.07	50.36035587	126513.3145	12.65133145	12.19208387	0.459247582
	nt 148.7	0.5	79221.2	61.19495044	125275.016	12.5275016	12.19208387	0.335417737
	nt 148.8	0.75	76637.87	58.39673446	126682.9253	12.66829253	12.19208387	0.476208668
	nt 148.9	1	83513.19	63.78219123	129597.5785	12.95975785	12.19208387	0.767673988
	nt 148.10	2.5	89872.11	72.81561715	122443.4507	12.24434507	12.19208387	0.052261207
	nt 148.11	5	99706.3	78.72034397	126078.7973	12.60787973	12.19208387	0.415795866
	nt 148.12	7.5	105332.9	83.08420721	124832.9178	12.48329178	12.19208387	0.291207918
	nt 148.13	10	105250.22	82.8975068	125060.2095	12.50602095	12.19208387	0.313937082
	nt 148.14	15	119546.06	95.80047925	123483.1477	12.34831477	12.19208387	0.156230904
	nt 148.15	20	122419.05	100	122419.05	12.241905	12.19208387	0.049821135
162-163	nt 162.1	0	18903.62	34.69892991	51779.44872	5.177944872	5.177944872	0
	nt 162.2	0.025	21031.9	38.38672938	51834.92897	5.183492897	5.177944872	0.005548025
	nt 162.3	0.05	20212.2	38.34201356	50226.98886	5.022698886	5.177944872	-0.155245986
	nt 162.4	0.075	19577.56	39.12299665	49278.41758	4.927841758	5.177944872	-0.250103114
	nt 162.5	0.1	19406.44	37.89231088	49231.42046	4.923142046	5.177944872	-0.254802826
	nt 162.6	0.2	26656.72	50.36035587	49463.57492	4.946357492	5.177944872	-0.231587381
	nt 162.7	0.5	32724.66	61.19495044	51748.55097	5.174855097	5.177944872	-0.003089775
	nt 162.8	0.75	32515.14	58.39673446	53747.74968	5.374774968	5.177944872	0.196830096
	nt 162.9	1	34766.66	63.78219123	53951.65661	5.395165661	5.177944872	0.217220789
	nt 162.10	2.5	41289.47	72.81561715	56253.54947	5.625354947	5.177944872	0.447410074
	nt 162.11	5	40029.51	78.72034397	50617.38805	5.061738805	5.177944872	-0.116206067
	nt 162.12	7.5	42860.62	83.08420721	50795.29999	5.079529999	5.177944872	-0.098414873
	nt 162.13	10	43222.77	82.8975068	51358.07479	5.135807479	5.177944872	-0.042137393
	nt 162.14	15	48159.84	95.80047925	49745.91915	4.974591915	5.177944872	-0.203352957
	nt 162.15	20	48047	100	48047	4.8047	5.177944872	-0.373244872
169-172	nt 169.1	0	37770.81	34.69892991	103459.111	10.3459111	10.3459111	0
	nt 169.2	0.025	43758.97	38.38672938	107847.7504	10.78477504	10.3459111	0.438863942
	nt 169.3	0.05	40256.45	38.34201356	100036.6247	10.00366247	10.3459111	-0.342248628
	nt 169.4	0.075	40566.89	39.12299665	102110.3828	10.21103828	10.3459111	-0.134872821
	nt 169.5	0.1	40799.31	37.89231088	103502.1356	10.35021356	10.3459111	0.004302465
	nt 169.6	0.2	61202.94	50.36035587	113566.7182	11.35667182	10.3459111	1.010760719
	nt 169.7	0.5	76101.14	61.19495044	120341.1654	12.03411654	10.3459111	1.688205443
	nt 169.8	0.75	71595.53	58.39673446	118347.9027	11.83479027	10.3459111	1.48887917
	nt 169.9	1	76149.88	63.78219123	118171.0345	11.81710345	10.3459111	1.471192347
	nt 169.10	2.5	100442.76	72.81561715	136845.1028	13.68451028	10.3459111	3.338599185
	nt 169.11	5	91204.27	78.72034397	115327.9649	11.53279649	10.3459111	1.186885396

nt No.	Name of the Band	Tb^{3+} (mM)	Cleavage Intensity (I)	Correction factor (R)	Corrected cleavage Intensity (I_{corr} = I*100/ R)	I_{corr} / 1000	(I_{corr}) at 0 mM	$I_R = (I_{corr\ (x\ mM)} - I_{corr\ (0\ mM)})$
	nt 169.12	7.5	94465.86	83.08420721	111954.0897	11.19540897	10.3459111	0.849497876
	nt 169.13	10	95125.9	82.8975068	113030.3099	11.30303099	10.3459111	0.957119889
	nt 169.14	15	108673.92	95.80047925	112252.9485	11.22529485	10.3459111	0.879383749
	nt 169.15	20	104821.08	100	104821.08	10.482108	10.3459111	0.136196902
184-186	nt 184.1	0	21910.54	34.69892991	60015.7897	6.00157897	6.00157897	0
	nt 184.2	0.025	25938.82	38.38672938	63928.45593	6.392845593	6.00157897	0.391266623
	nt 184.3	0.05	22987.93	38.34201356	57124.63285	5.712463285	6.00157897	-0.289115684
	nt 184.4	0.075	22696.37	39.12299665	57128.73302	5.712873302	6.00157897	-0.288705668
	nt 184.5	0.1	22674.75	37.89231088	57522.66521	5.752266521	6.00157897	-0.249312448
	nt 184.6	0.2	32779.48	50.36035587	60824.82259	6.082482259	6.00157897	0.080903289
	nt 184.7	0.5	40114.41	61.19495044	63434.19887	6.343419887	6.00157897	0.341840918
	nt 184.8	0.75	38317.29	58.39673446	63338.74347	6.333874347	6.00157897	0.332295377
	nt 184.9	1	39750.92	63.78219123	61686.33932	6.168633932	6.00157897	0.167054963
	nt 184.10	2.5	51344.83	72.81561715	69953.1608	6.99531608	6.00157897	0.99373711
	nt 184.11	5	47668.5	78.72034397	60276.90477	6.027690477	6.00157897	0.026111507
	nt 184.12	7.5	49902.22	83.08420721	59140.49389	5.914049389	6.00157897	-0.08752958
	nt 184.13	10	48199.46	82.8975068	57271.4676	5.72714676	6.00157897	-0.27443221
	nt 184.14	15	53446.3	95.80047925	55206.48156	5.520648156	6.00157897	-0.480930814
	nt 184.15	20	53961.96	100	53961.96	5.396196	6.00157897	-0.60538297
190-195	nt 190.1	0	50669.04	34.69892991	138789.0234	13.87890234	13.87890234	0
	nt 190.2	0.025	58392.66	38.38672938	143913.7398	14.39137398	13.87890234	0.512471637
	nt 190.3	0.05	52133.93	38.34201356	129551.9697	12.95519697	13.87890234	-0.923705372
	nt 190.4	0.075	51334.03	39.12299665	129212.2086	12.92122086	13.87890234	-0.957681481
	nt 190.5	0.1	52477.45	37.89231088	133127.9413	13.31279413	13.87890234	-0.566108207
	nt 190.6	0.2	85336.73	50.36035587	158348.8043	15.83488043	13.87890234	1.955978086
	nt 190.7	0.5	109977.69	61.19495044	173911.2369	17.39112369	13.87890234	3.512221346
	nt 190.8	0.75	100256.79	58.39673446	165725.1623	16.57251623	13.87890234	2.693613887
	nt 190.9	1	109218.97	63.78219123	169488.3651	16.94883651	13.87890234	3.069934175
	nt 190.10	2.5	149294.43	72.81561715	203401.5356	20.34015356	13.87890234	6.461251222
	nt 190.11	5	133674.02	78.72034397	169031.0409	16.90310409	13.87890234	3.024201751
	nt 190.12	7.5	141909.63	83.08420721	168181.0069	16.81810069	13.87890234	2.93919835
	nt 190.13	10	135996.15	82.8975068	161593.078	16.1593078	13.87890234	2.280405457
	nt 190.14	15	161371.23	95.80047925	166685.7731	16.66857731	13.87890234	2.789674966
	nt 190.15	20	157056.83	100	157056.83	15.705683	13.87890234	1.82678066

Table A3.4: Determination of the metal ion binding sites of various strengths from the I_R values.

Nucleotide No	I_R at (0.5 mM)
15	14.34240496
17	11.99375107
18	15.34964202
16	15.03087628
19	16.62819547
23	7.139219601
24	7.079094273
25	4.530792271
46	3.068953732
47	2.486230685
48	3.663627476
49	1.817431563
50	3.185729386
51	3.192900719
53	3.339636025
63	3.654925433
64	1.96614516
68	2.964810018
70	0.984854075
76	1.190990365
77	1.079912051
81	1.433587927
82-84	3.299092692
91-92	2.047370949
97-100	4.571640909
106-109	2.765897093
110-111	0.485663738
113-114	0.003484047
115-118	1.865253973
119-121	12.56391735
122	40.65349243
123-125	4.913949613
126-130	5.717990277
131-135	3.09905607
148-152	0.335417737
162-163	-0.003089775
169-172	1.688205443
184-186	0.341840918
190-195	3.512221346

Appendix 4: Evaluation of the in-line probing gel to determine the K_A of AdoCbl towards the RS07 RNA

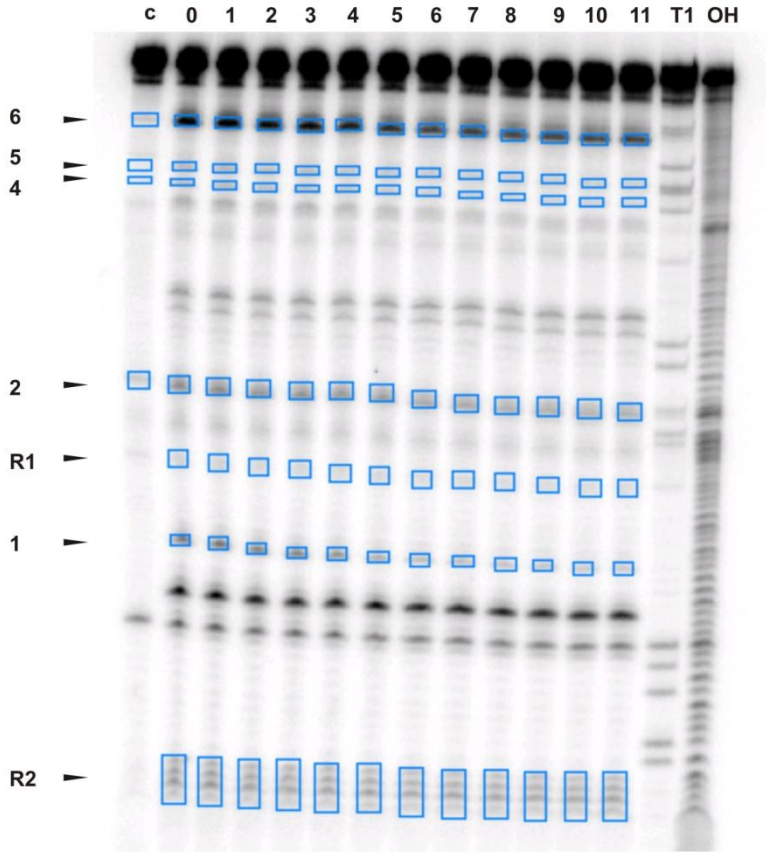

Figure A4.1: Evaluation of the PAGE gel of a typical titration experiments with AdoCbl and the RS07 RNA: Shown is the in-line probing gel of RS07 RNA. The arrows indicate the cleavage sites analyzed in the experiments. Bands R1 and R2 are used for background correction (see Table A4.1 and A4.2). The blue boxes indicate the area of the band intensity used in the evaluation. The concentration of AdoCbl increases from lane 0 to 11 (see Table A4.3). Lane c is the unreacted RNA, lane T1 is RNase T1 ladder and lane OH corresponds to the alkaline hydrolysis ladder.

Table A4.1: Determination of the background correction factor from the control bands.

Control Bands (CB)	AdoCbl concentration (µM)	Cleavage Intensity (I)	Max. cleavage intensity at CB (X)	Percentage relative to X, R_x= (I* 100/ X)
RECT-R1.0	0	53675.49	**58733.86**	91.38764249
RECT-R1.1	0.05	**58733.86**	**58733.86**	100
RECT-R1.2	0.5	50908.18	**58733.86**	86.67603321
RECT-R1.3	1	51473.06	**58733.86**	87.6377953
RECT-R1.4	5	44872.73	**58733.86**	76.40010379
RECT-R1.5	50	47786.27	**58733.86**	81.3606836
RECT-R1.6	100	42610.28	**58733.86**	72.54806682
RECT-R1.7	200	47116.92	**58733.86**	80.22105137
RECT-R1.8	400	43110.32	**58733.86**	73.39943263
RECT-R1.9	600	44480.85	**58733.86**	75.7328907
RECT-R1.10	800	41939.95	**58733.86**	71.40676605
RECT-R1.11	1000	44263.53	**58733.86**	75.36288267
RECT-R2.0	0	389443.99	**427463.66**	91.10575388
RECT-R2.1	0.05	**427463.66**	**427463.66**	100
RECT-R2.2	0.5	365989.86	**427463.66**	85.61894127
RECT-R2.3	1	366002.04	**427463.66**	85.62179063
RECT-R2.4	5	343289.85	**427463.66**	80.30854599
RECT-R2.5	50	346535.54	**427463.66**	81.06783627
RECT-R2.6	100	327092.48	**427463.66**	76.51936541
RECT-R2.7	200	352873.32	**427463.66**	82.55048394
RECT-R2.8	400	337219.07	**427463.66**	78.88835977
RECT-R2.9	600	346040.83	**427463.66**	80.95210479
RECT-R2.10	800	351442.89	**427463.66**	82.21585199
RECT-R2.11	1000	378171.89	**427463.66**	88.46878118

Table A4.2: Calculation of the final correction factor.

Correction factor R = (Rx1+Rx2)/2	R
$(R_{x1.0}+ R_{x\ 2.0})/2$ = R (0 µM)	91.2467
$(R_{x1.1}+ R_{x\ 2.1})/2$ = R (0.05 µM)	100
$(R_{x1.2}+ R_{x\ 2.2})/2$ = R (0.5 µM)	86.14749
$(R_{x1.3}+ R_{x\ 2.3})/2$ = R (1 µM)	86.62979
$(R_{x1.4}+ R_{x\ 2.4})/2$ = R (5 µM)	78.35432
$(R_{x1.5}+ R_{x\ 2.5})/2$ = R (50 µM)	81.21426
$(R_{x1.6}+ R_{x\ 2.6})/2$ = R (100 µM)	74.53372
$(R_{x1.7}+ R_{x\ 2.7})/2$ = R (200 µM)	81.38577
$(R_{x1.8}+ R_{x\ 2.8})/2$ = R (400 µM)	76.1439
$(R_{x1.9}+ R_{x\ 2.9})/2$ = R (600 µM)	78.3425
$(R_{x1.10}+ R_{x\ 2.10})/2$ = R (800 µM)	76.81131
$(R_{x1.11}+ R_{x\ 2.11})/2$ = R (1000 µM)	81.91583

Table A4.3: Determination of the relative intensities at the cleavage sites.

Sites	AdoCbl (µM)	Band	Cleavage Intensity (I)	Correction for cleavage band (C) = I- IC	Correction factor (R)	Corrected cleavage Intensity (I_{corr}= I*100/ R)	I_{corr} / 10000
Site 1	0	RECT- 1.0	193906.93	-	91.24669819	212508.4347	21.25084
	0.05	RECT- 1.1	221449.11	-	100	221449.11	22.144911
	0.5	RECT- 1.2	190757.86	-	86.14748724	221431.7168	22.143168
	1	RECT- 1.3	187541.61	-	86.62979297	216486.2729	21.648629
	5	RECT- 1.4	148717.45	-	78.35432489	189801.2014	18.980114
	50	RECT- 1.5	88720.87	-	81.21425993	109242.9705	10.924205
	100	RECT- 1.6	65203.16	-	74.53371612	87481.42907	8.7481407
	200	RECT- 1.7	63779.27	-	81.38576765	78366.61352	7.8366652
	400	RECT- 1.8	53577.9	-	76.1438962	70364.01166	7.0364066
	600	RECT- 1.9	53305.28	-	78.34249775	68041.33329	6.8041329
	800	RECT-1.10	49299.75	-	76.81130902	64182.9317	6.4182937
	1000	RECT-1.11	46825.63	-	81.91583193	57163.10132	5.7163132
Site 2	0	RECT- 2.0	282380.25	207931.79	91.24669819	227878.7004	22.787804
	0.05	RECT- 2.1	315761.5	241313.04	100	241313.04	24.131304
	0.5	RECT- 2.2	273166.12	198717.66	86.14748724	230671.4524	23.067124
	1	RECT- 2.3	278915.65	204467.19	86.62979297	236024.1009	23.602409
	5	RECT- 2.4	253374.5	178926.04	78.35432489	228355.0273	22.835573
	50	RECT- 2.5	228981.79	154533.33	81.21425993	190278.567	19.027857
	100	RECT- 2.6	203040.97	128592.51	74.53371612	172529.3152	17.252952
	200	RECT- 2.7	210263.1	135814.64	81.38576765	166877.6297	16.687797
	400	RECT- 2.8	182756.24	108307.78	76.1438962	142240.922	14.224092
	600	RECT- 2.9	184592.05	110143.59	78.34249775	140592.39	14.059239
	800	RECT-2.10	177201.33	102752.87	76.81130902	133773.101	13.377311
	1000	RECT-2.11	179355.38	104906.92	81.91583193	128066.7211	12.806611
		RECT- 2C	74448.46	74448.46			
Site 4	0	RECT- 4.0	68281	52106.15	91.24669819	57104.69643	5.7104643
	0.05	RECT- 4.1	77730.83	61555.98	100	61555.98	6.155598
	0.5	RECT- 4.2	68319.17	52144.32	86.14748724	60529.12473	6.0529173
	1	RECT- 4.3	65807.14	49632.29	86.62979297	57292.40288	5.7292488
	5	RECT- 4.4	59598.67	43423.82	78.35432489	55419.81258	5.5419858
	50	RECT- 4.5	52978.44	36803.59	81.21425993	45316.65994	4.5316694
	100	RECT- 4.6	45975.28	29800.43	74.53371612	39982.4825	3.9982485
	200	RECT- 4.7	47329.21	31154.36	81.38576765	38279.86256	3.8279856
	400	RECT- 4.8	40297.55	24122.7	76.1438962	31680.41196	3.1680496
	600	RECT- 4.9	42710.91	26536.06	78.34249775	33871.85852	3.3871852
	800	RECT-4.10	41011.35	24836.5	76.81130902	32334.43137	3.2334437
	1000	RECT-4.11	39911.51	23736.66	81.91583193	28976.88938	2.8976838
		RECT- 4C	16174.85	16174.85			
Site 5	0	RECT- 5.0	85980.71	69491.07	91.24669819	76157.35296	7.6157396

Sites	AdoCbl (µM)	Band	Cleavage Intensity (I)	Correction for cleavage band (C) = I- IC	Correction factor (R)	Corrected cleavage Intensity (I_{corr}= I*100/ R)	I_{corr} / 10000
	0.5	RECT- 5.2	82799.52	66309.88	86.14748724	76972.50625	7.6972525
	1	RECT- 5.3	82482.07	65992.43	86.62979297	76177.52247	7.6177547
	5	RECT- 5.4	71708.72	55219.08	78.35432489	70473.55724	7.0473524
	50	RECT- 5.5	70026.94	53537.3	81.21425993	65921.05874	6.5921074
	100	RECT- 5.6	58986.25	42496.61	74.53371612	57016.62578	5.7016678
	200	RECT- 5.7	62992.98	46503.34	81.38576765	57139.40083	5.7139483
	400	RECT- 5.8	54039.54	37549.9	76.1438962	49314.39271	4.9314371
	600	RECT- 5.9	57923.92	41434.28	78.34249775	52888.63796	5.2888696
	800	RECT-5.10	56800.04	40310.4	76.81130902	52479.77221	5.2479721
	1000	RECT-5.11	56403.59	39913.95	81.91583193	48725.56264	4.8725564
		RECT- 5C	16489.64	16489.64			
Site 6	0	RECT- 6.0	1276843.27	1196143.35	91.24669819	1310889.461	131.08861
	0.05	RECT- 6.1	1419797.39	1339097.47	100	1339097.47	133.90977
	0.5	RECT- 6.2	1218277.63	1137577.71	86.14748724	1320500.164	132.05064
	1	RECT- 6.3	1200457.61	1119757.69	86.62979297	1292578.052	129.25752
	5	RECT- 6.4	1039545.55	958845.63	78.35432489	1223730.319	122.37319
	50	RECT- 6.5	868526.52	787826.6	81.21425993	970059.446	97.005946
	100	RECT- 6.6	752383.25	671683.33	74.53371612	901180.5194	90.118094
	200	RECT- 6.7	816475.32	735775.4	81.38576765	904059.0526	90.405926
	400	RECT- 6.8	734652.24	653952.32	76.1438962	858837.4809	85.883709
	600	RECT- 6.9	750989.3	670289.38	78.34249775	855588.4727	85.558827
	800	RECT-6.10	720630.89	639930.97	76.81130902	833120.7711	83.312011
	1000	RECT-6.11	785743.34	705043.42	81.91583193	860692.4979	86.069279
		RECT- 6C	80699.92	80699.92			

Figure A4.2: Determining the K_A of AdoCbl to the RS07 RNA from in-line probing experiments: The intensity changes (black dots) (see Table A4.3) at each cleavage site are plotted against the AdoCbl concentration and were fitted (grey lines) to a 1:1 binding isoterm [dF+(dB-dF)*(((cRNA+x+1/Ka)-((cRNA+x+1/Ka)^2-4*cRNA*x)^0.5)/(2*cRNA))] to calculate the K_A values.

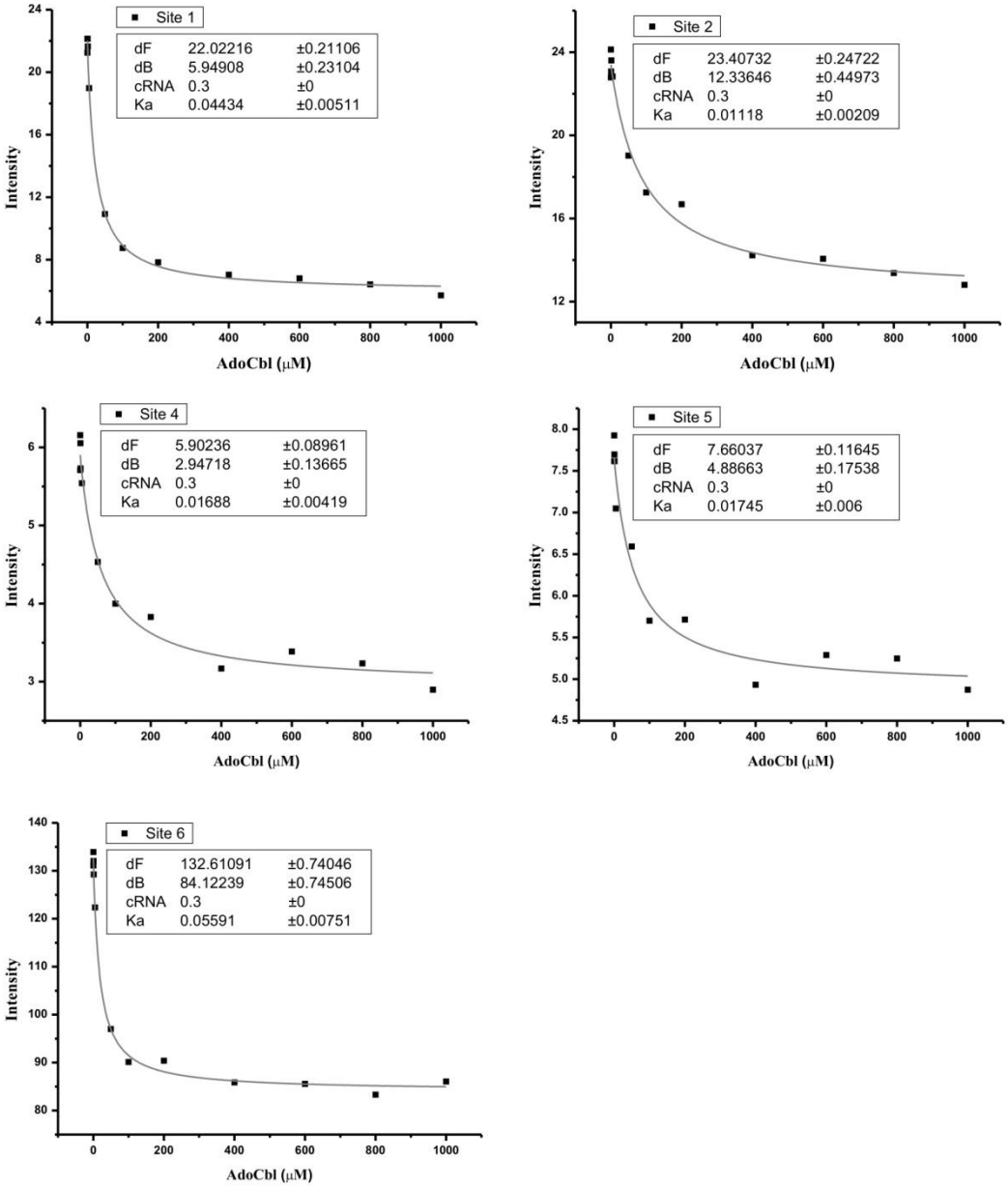

Appendix 5: Plasmid Table pPC1

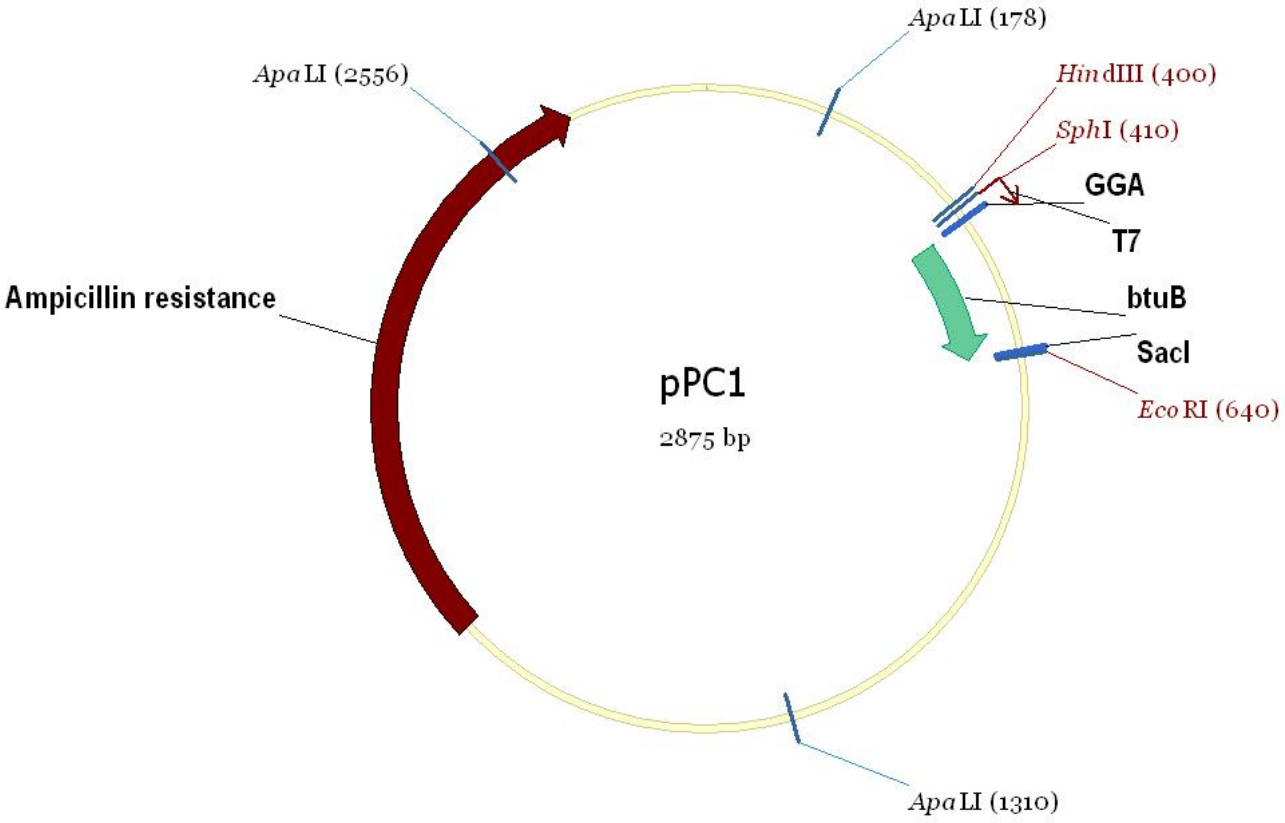


```
1     TCGCGCGTTT CGGTGATGAC GGTGAAAACC TCTGACACAT GCAGCTCCCG
51    GAGACGGTCA CAGCTTGTCT GTAAGCGGAT GCCGGGAGCA GACAAGCCCG
101   TCAGGGCGCG TCAGCGGGTG TTGGCGGGTG TCGGGGCTGG CTTAACTATG
151   CGGCATCAGA GCAGATTGTA CTGAGAGTGC ACCATATGCG GTGTGAAATA
201   CCGCACAGAT GCGTAAGGAG AAAATACCGC ATCAGGCGCC ATTCGCCATT
251   CAGGCTGCGC AACTGTTGGG AAGGGCGATC GGTGCGGGCC TCTTCGCTAT
301   TACGCCAGCT GGCGAAAGGG GGATGTGCTG CAAGGCGATT AAGTTGGGTA
351   ACGCCAGGGT TTTCCCAGTC ACGACGTTGT AAAACGACGG CCAGTGCCAA

          HindIII  SphI                              btuB

401   GCTTGCATGC TAATACGACT CACTATAGGA GCCGGTCCTG TGAGTTAATA
451   GGGAATCCAG TGCGAATCTG GAGCTGACGC GCAGCGGTAA GGAAAGGTGC
501   GATGATTGCG TTATGCGGAC ACTGCCATTC GGTGGGAAGT CATCATCTCT
551   TAGTATCTTA GATACCCCTC CAAGCCCGAA GACCTGCCGG CCAACGTCGC
601   ATCTGGTTCT CATCATCGCG TAATATTGAT GAGAGCTCGA ATTCGTAATC

                                          SacI       EcoRI

651   ATGGTCATAG CTGTTTCCTG TGTGAAATTG TTATCCGCTC ACAATTCCAC
701   ACAACATACG AGCCGGAAGC ATAAAGTGTA AAGCCTGGGG TGCCTAATGA
751   GTGAGCTAAC TCACATTAAT TGCGTTGCGC TCACTGCCCG CTTTCCAGTC
801   GGGAAACCTG TCGTGCCAGC TGCATTAATG AATCGGCCAA CGCGCGGGGA
```

```
851  GAGGCGGTTT GCGTATTGGG CGCTCTTCCG CTTCCTCGCT CACTGACTCG
901  CTGCGCTCGG TCGTTCGGCT GCGGCGAGCG GTATCAGCTC ACTCAAAGGC
951  GGTAATACGG TTATCCACAG AATCAGGGGA TAACGCAGGA AAGAACATGT
1001 GAGCAAAAGG CCAGCAAAAG GCCAGGAACC GTAAAAAGGC CGCGTTGCTG
1051 GCGTTTTTCC ATAGGCTCCG CCCCCCTGAC GAGCATCACA AAAATCGACG
1101 CTCAAGTCAG AGGTGGCGAA ACCCGACAGG ACTATAAAGA TACCAGGCGT
1151 TTCCCCCTGG AAGCTCCCTC GTGCGCTCTC CTGTTCCGAC CCTGCCGCTT
1201 ACCGGATACC TGTCCGCCTT TCTCCCTTCG GGAAGCGTGG CGCTTTCTCA
1251 TAGCTCACGC TGTAGGTATC TCAGTTCGGT GTAGGTCGTT CGCTCCAAGC
1301 TGGGCTGTGT GCACGAACCC CCCGTTCAGC CCGACCGCTG CGCCTTATCC
1351 GGTAACTATC GTCTTGAGTC CAACCCGGTA AGACACGACT TATCGCCACT
1401 GGCAGCAGCC ACTGGTAACA GGATTAGCAG AGCGAGGTAT GTAGGCGGTG
1451 CTACAGAGTT CTTGAAGTGG TGGCCTAACT ACGGCTACAC TAGAAGGACA
1501 GTATTTGGTA TCTGCGCTCT GCTGAAGCCA GTTACCTTCG GAAAAAGAGT
1551 TGGTAGCTCT TGATCCGGCA AACAAACCAC CGCTGGTAGC GGTGGTTTTT
1601 TTGTTTGCAA GCAGCAGATT ACGCGCAGAA AAAAAGGATC TCAAGAAGAT
1651 CCTTTGATCT TTTCTACGGG GTCTGACGCT CAGTGGAACG AAAACTCACG
1701 TTAAGGGATT TTGGTCATGA GATTATCAAA AAGGATCTTC ACCTAGATCC
1751 TTTTAAATTA AAAATGAAGT TTTAAATCAA TCTAAAGTAT ATATGAGTAA
1801 ACTTGGTCTG ACAGTTACCA ATGCTTAATC AGTGAGGCAC CTATCTCAGC
1851 GATCTGTCTA TTTCGTTCAT CCATAGTTGC CTGACTCCCC GTCGTGTAGA
1901 TAACTACGAT ACGGGAGGGC TTACCATCTG GCCCCAGTGC TGCAATGATA
1951 CCGCGAGACC CACGCTCACC GGCTCCAGAT TTATCAGCAA TAAACCAGCC
2001 AGCCGGAAGG GCCGAGCGCA GAAGTGGTCC TGCAACTTTA TCCGCCTCCA
2051 TCCAGTCTAT TAATTGTTGC CGGGAAGCTA GAGTAAGTAG TTCGCCAGTT
2101 AATAGTTTGC GCAACGTTGT TGCCATTGCT ACAGGCATCG TGGTGTCACG
2151 CTCGTCGTTT GGTATGGCTT CATTCAGCTC CGGTTCCCAA CGATCAAGGC
2201 GAGTTACATG ATCCCCCATG TTGTGCAAAA AAGCGGTTAG CTCCTTCGGT
2251 CCTCCGATCG TTGTCAGAAG TAAGTTGGCC GCAGTGTTAT CACTCATGGT
2301 TATGGCAGCA CTGCATAATT CTCTTACTGT CATGCCATCC GTAAGATGCT
2351 TTTCTGTGAC TGGTGAGTAC TCAACCAAGT CATTCTGAGA ATAGTGTATG
2401 CGGCGACCGA GTTGCTCTTG CCCGGCGTCA ATACGGGATA ATACCGCGCC
2451 ACATAGCAGA ACTTTAAAAG TGCTCATCAT TGGAAAACGT TCTTCGGGGC
2501 GAAAACTCTC AAGGATCTTA CCGCTGTTGA GATCCAGTTC GATGTAACCC
2551 ACTCGTGCAC CCAACTGATC TTCAGCATCT TTTACTTTCA CCAGCGTTTC
2601 TGGGTGAGCA AAAACAGGAA GGCAAAATGC CGCAAAAAAG GGAATAAGGG
2651 CGACACGGAA ATGTTGAATA CTCATACTCT TCCTTTTTCA ATATTATTGA
2701 AGCATTTATC AGGGTTATTG TCTCATGAGC GGATACATAT TTGAATGTAT
2751 TTAGAAAAAT AAACAAATAG GGGTTCCGCG CACATTTCCC CGAAAAGTGC
2801 CACCTGACGT CTAAGAAACC ATTATTATCA TGACATTAAC CTATAAAAAT
2851 AGGCGTATCA CGAGGCCCTT TCGTC
```

Appendix 6: Plasmid Table pPC2

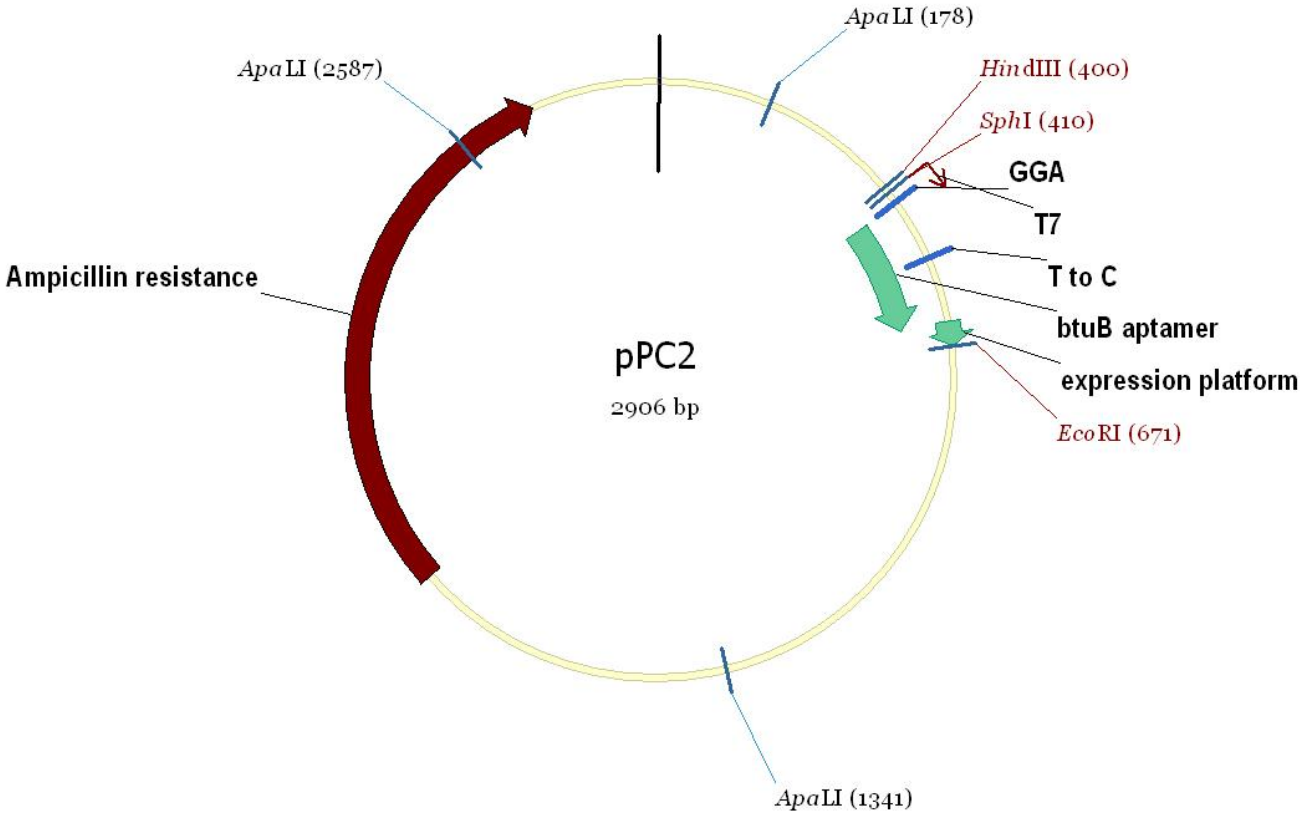


```
1     TCGCGCGTTT CGGTGATGAC GGTGAAAACC TCTGACACAT GCAGCTCCCG
      GAGACGGTCA CAGCTTGTCT GTAAGCGGAT GCCGGGAGCA GACAAGCCCG
101   TCAGGGCGCG TCAGCGGGTG TTGGCGGGTG TCGGGGCTGG CTTAACTATG
      CGGCATCAGA GCAGATTGTA CTGAGAGTGC ACCATATGCG GTGTGAAATA
201   CCGCACAGAT GCGTAAGGAG AAAATACCGC ATCAGGCGCC ATTCGCCATT
      CAGGCTGCGC AACTGTTGGG AAGGGCGATC GGTGCGGGCC TCTTCGCTAT
301   TACGCCAGCT GGCGAAAGGG GGATGTGCTG CAAGGCGATT AAGTTGGGTA
      ACGCCAGGGT TTTCCCAGTC ACGACGTTGT AAAACGACGG CCAGTGCCAA

        HindIII   SphI                                btuB
401   GCTTGCATGC TAATACGACT CACTATAGGA GCCGGTCCTG TGAGTTAATA
      GGGAATCCAG TGCGAATCTG GAGCTGACGC GCAGCGGTAA GGAAAGGTGC
                                  (T to C)
501   GATGATTGCG TTATGCGGAC ACTGCCATCC GGTGGGAAGT CATCATCTCT
      TAGTATCTTA GATACCCCTC CAAGCCCGAA GACCTGCCGG CCAACGTCGC
601   ATCTGGTTCT CATCATCGCG TAATATTGAT GAACCTGCG GCATCCTTCT
      TCTATTGTGG ATGCTTTACG AATTCGTAAT CATGGTCATA GCTGTTTCCT
        Expression platform    EcoRI

701   GTGTGAAATT GTTATCCGCT CACAATTCCA CACAACATAC GAGCCGGAAG
      CATAAAGTGT AAAGCCTGGG GTGCCTAATG AGTGAGCTAA CTCACATTAA
801   TTGCGTTGCG CTCACTGCCC GCTTTCCAGT CGGGAAACCT GTCGTGCCAG
      CTGCATTAAT GAATCGGCCA ACGCGCGGGG AGAGGCGGTT TGCGTATTGG
901   GCGCTCTTCC GCTTCCTCGC TCACTGACTC GCTGCGCTCG GTCGTTCGGC
      TGCGGCGAGC GGTATCAGCT CACTCAAAGG CGGTAATACG GTTATCCACA
1001  GAATCAGGGG ATAACGCAGG AAAGAACATG TGAGCAAAAG GCCAGCAAAA
      GGCCAGGAAC CGTAAAAAGG CCGCGTTGCT GGCGTTTTTC CATAGGCTCC
```

```
1101 GCCCCCCTGA CGAGCATCAC AAAAATCGAC GCTCAAGTCA GAGGTGGCGA
     AACCCGACAG GACTATAAAG ATACCAGGCG TTTCCCCCTG GAAGCTCCCT
1201 CGTGCGCTCT CCTGTTCCGA CCCTGCCGCT TACCGGATAC CTGTCCGCCT
     TTCTCCCTTC GGGAAGCGTG GCGCTTTCTC ATAGCTCACG CTGTAGGTAT
1301 CTCAGTTCGG TGTAGGTCGT TCGCTCCAAG CTGGGCTGTG TGCACGAACC
     CCCCGTTCAG CCCGACCGCT GCGCCTTATC CGGTAACTAT CGTCTTGAGT
1401 CCAACCCGGT AAGACACGAC TTATCGCCAC TGGCAGCAGC CACTGGTAAC
     AGGATTAGCA GAGCGAGGTA TGTAGGCGGT GCTACAGAGT TCTTGAAGTG
1501 GTGGCCTAAC TACGGCTACA CTAGAAGGAC AGTATTTGGT ATCTGCGCTC
     TGCTGAAGCC AGTTACCTTC GGAAAAAGAG TTGGTAGCTC TTGATCCGGC
1601 AAACAAACCA CCGCTGGTAG CGGTGGTTTT TTTGTTTGCA AGCAGCAGAT
     TACGCGCAGA AAAAAAGGAT CTCAAGAAGA TCCTTTGATC TTTTCTACGG
1701 GGTCTGACGC TCAGTGGAAC GAAAACTCAC GTTAAGGGAT TTTGGTCATG
     AGATTATCAA AAAGGATCTT CACCTAGATC CTTTTAAATT AAAAATGAAG
1801 TTTTAAATCA ATCTAAAGTA TATATGAGTA AACTTGGTCT GACAGTTACC
     AATGCTTAAT CAGTGAGGCA CCTATCTCAG CGATCTGTCT ATTTCGTTCA
1901 TCCATAGTTG CCTGACTCCC CGTCGTGTAG ATAACTACGA TACGGGAGGG
     CTTACCATCT GGCCCCAGTG CTGCAATGAT ACCGCGAGAC CCACGCTCAC
2001 CGGCTCCAGA TTTATCAGCA ATAAACCAGC CAGCCGGAAG GGCCGAGCGC
     AGAAGTGGTC CTGCAACTTT ATCCGCCTCC ATCCAGTCTA TTAATTGTTG
2101 CCGGGAAGCT AGAGTAAGTA GTTCGCCAGT TAATAGTTTG CGCAACGTTG
     TTGCCATTGC TACAGGCATC GTGGTGTCAC GCTCGTCGTT TGGTATGGCT
2201 TCATTCAGCT CCGGTTCCCA ACGATCAAGG CGAGTTACAT GATCCCCCAT
     GTTGTGCAAA AAAGCGGTTA GCTCCTTCGG TCCTCCGATC GTTGTCAGAA
2301 GTAAGTTGGC CGCAGTGTTA TCACTCATGG TTATGGCAGC ACTGCATAAT
     TCTCTTACTG TCATGCCATC CGTAAGATGC TTTTCTGTGA CTGGTGAGTA
2401 CTCAACCAAG TCATTCTGAG AATAGTGTAT GCGGCGACCG AGTTGCTCTT
     GCCCGGCGTC AATACGGGAT AATACCGCGC CACATAGCAG AACTTTAAAA
2501 GTGCTCATCA TTGGAAAACG TTCTTCGGGG CGAAAACTCT CAAGGATCTT
     ACCGCTGTTG AGATCCAGTT CGATGTAACC CACTCGTGCA CCCAACTGAT
2601 CTTCAGCATC TTTTACTTTC ACCAGCGTTT CTGGGTGAGC AAAAACAGGA
     AGGCAAAATG CCGCAAAAAA GGGAATAAGG GCGACACGGA AATGTTGAAT
2701 ACTCATACTC TTCCTTTTTC AATATTATTG AAGCATTTAT CAGGGTTATT
     GTCTCATGAG CGGATACATA TTTGAATGTA TTTAGAAAAA TAAACAAATA
2801 GGGGTTCCGC GCACATTTCC CCGAAAAGTG CCACCTGACG TCTAAGAAAC
     CATTATTATC ATGACATTAA CCTATAAAAA TAGGCGTATC ACGAGGCCCT
2901 TTCGTC
```

Appendix 7: Plasmid Table pPC3

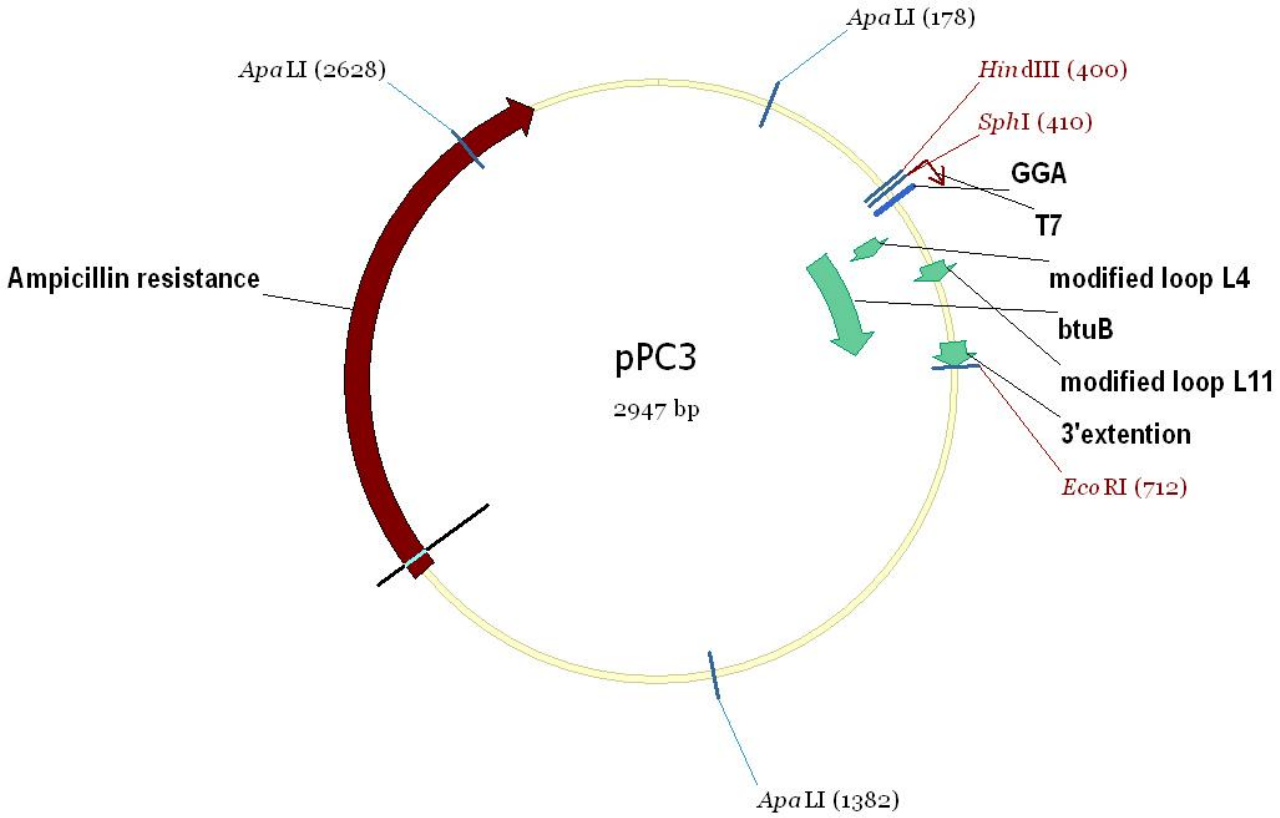


```
1     TCGCGCGTTT CGGTGATGAC GGTGAAAACC TCTGACACAT GCAGCTCCCG
      GAGACGGTCA CAGCTTGTCT GTAAGCGGAT GCCGGGAGCA GACAAGCCCG
101   TCAGGGCGCG TCAGCGGGTG TTGGCGGGTG TCGGGGCTGG CTTAACTATG
      CGGCATCAGA GCAGATTGTA CTGAGAGTGC ACCATATGCG GTGTGAAATA
201   CCGCACAGAT GCGTAAGGAG AAAATACCGC ATCAGGCGCC ATTCGCCATT
      CAGGCTGCGC AACTGTTGGG AAGGGCGATC GGTGCGGGCC TCTTCGCTAT
301   TACGCCAGCT GGCGAAAGGG GGATGTGCTG CAAGGCGATT AAGTTGGGTA
      ACGCCAGGGT TTTCCCAGTC ACGACGTTGT AAAACGACGG CCAGTGCCAA
            HindIII  SphI                          btuB
401   GCTTGCATGC TAATACGACT CACTATAGGA GCCGGTCCTG TGAGTTAATA
                                Modified L4
      GGGAATCCAC CCAAATTAAT AACGCTCTTG GTAGGGTGGA GCTGACGCGC
501   AGCGGTAAGG AAAGGTGCGA TGATTGCGTT ATGCGGACAC TGCCCCCAAA
       Modified L11
      TATATTTCGG ACTACGTAGG GGGTGGGAAG TCATCATCTC TTAGTATCTT
601   AGATACCCCT CCAAGCCCGA AGACCTGCCG GCCAACGTCG CATCTGGTTC
      TCATCATCGC GTAATATTGA TGAAACCTGC GGCATCCTTC TTCTATTGTG
      Expression platform  EcoRI
701   GATGCTTTAC GAATTCGTAA TCATGGTCAT AGCTGTTTCC TGTGTGAAAT
      TGTTATCCGC TCACAATTCC ACACAACATA CGAGCCGGAA GCATAAAGTG
801   TAAAGCCTGG GGTGCCTAAT GAGTGAGCTA ACTCACATTA ATTGCGTTGC
      GCTCACTGCC CGCTTTCCAG TCGGGAAACC TGTCGTGCCA GCTGCATTAA
901   TGAATCGGCC AACGCGCGGG GAGAGGCGGT TTGCGTATTG GGCGCTCTTC
```

```
     CGCTTCCTCG CTCACTGACT CGCTGCGCTC GGTCGTTCGG CTGCGGCGAG
1001 CGGTATCAGC TCACTCAAAG GCGGTAATAC GGTTATCCAC AGAATCAGGG
     GATAACGCAG GAAAGAACAT GTGAGCAAAA GGCCAGCAAA AGGCCAGGAA
1101 CCGTAAAAAG GCCGCGTTGC TGGCGTTTTT CCATAGGCTC CGCCCCCCTG
     ACGAGCATCA CAAAAATCGA CGCTCAAGTC AGAGGTGGCG AAACCCGACA
1201 GGACTATAAA GATACCAGGC GTTTCCCCCT GGAAGCTCCC TCGTGCGCTC
     TCCTGTTCCG ACCCTGCCGC TTACCGGATA CCTGTCCGCC TTTCTCCCTT
1301 CGGGAAGCGT GGCGCTTTCT CATAGCTCAC GCTGTAGGTA TCTCAGTTCG
     GTGTAGGTCG TTCGCTCCAA GCTGGGCTGT GTGCACGAAC CCCCCGTTCA
1401 GCCCGACCGC TGCGCCTTAT CCGGTAACTA TCGTCTTGAG TCCAACCCGG
     TAAGACACGA CTTATCGCCA CTGGCAGCAG CCACTGGTAA CAGGATTAGC
1501 AGAGCGAGGT ATGTAGGCGG TGCTACAGAG TTCTTGAAGT GGTGGCCTAA
     CTACGGCTAC ACTAGAAGGA CAGTATTTGG TATCTGCGCT CTGCTGAAGC
1601 CAGTTACCTT CGGAAAAAGA GTTGGTAGCT CTTGATCCGG CAAACAAACC
     ACCGCTGGTA GCGGTGGTTT TTTTGTTTGC AAGCAGCAGA TTACGCGCAG
1701 AAAAAAAGGA TCTCAAGAAG ATCCTTTGAT CTTTTCTACG GGGTCTGACG
     CTCAGTGGAA CGAAAACTCA CGTTAAGGGA TTTTGGTCAT GAGATTATCA
1801 AAAAGGATCT TCACCTAGAT CCTTTTAAAT TAAAAATGAA GTTTTAAATC
     AATCTAAAGT ATATATGAGT AAACTTGGTC TGACAGTTAC CAATGCTTAA
1901 TCAGTGAGGC ACCTATCTCA GCGATCTGTC TATTTCGTTC ATCCATAGTT
     GCCTGACTCC CCGTCGTGTA GATAACTACG ATACGGGAGG GCTTACCATC
2001 TGGCCCCAGT GCTGCAATGA TACCGCGAGA CCCACGCTCA CCGGCTCCAG
     ATTTATCAGC AATAAACCAG CCAGCCGGAA GGGCCGAGCG CAGAAGTGGT
2101 CCTGCAACTT TATCCGCCTC CATCCAGTCT ATTAATTGTT GCCGGGAAGC
     TAGAGTAAGT AGTTCGCCAG TTAATAGTTT GCGCAACGTT GTTGCCATTG
2201 CTACAGGCAT CGTGGTGTCA CGCTCGTCGT TTGGTATGGC TTCATTCAGC
     TCCGGTTCCC AACGATCAAG GCGAGTTACA TGATCCCCCA TGTTGTGCAA
2301 AAAAGCGGTT AGCTCCTTCG GTCCTCCGAT CGTTGTCAGA AGTAAGTTGG
     CCGCAGTGTT ATCACTCATG GTTATGGCAG CACTGCATAA TTCTCTTACT
2401 GTCATGCCAT CCGTAAGATG CTTTTCTGTG ACTGGTGAGT ACTCAACCAA
     GTCATTCTGA GAATAGTGTA TGCGGCGACC GAGTTGCTCT TGCCCGGCGT
2501 CAATACGGGA TAATACCGCG CCACATAGCA GAACTTTAAA AGTGCTCATC
     ATTGGAAAAC GTTCTTCGGG GCGAAAACTC TCAAGGATCT TACCGCTGTT
2601 GAGATCCAGT TCGATGTAAC CCACTCGTGC ACCCAACTGA TCTTCAGCAT
     CTTTTACTTT CACCAGCGTT TCTGGGTGAG CAAAAACAGG AAGGCAAAAT
2701 GCCGCAAAAA AGGGAATAAG GGCGACACGG AAATGTTGAA TACTCATACT
     CTTCCTTTTT CAATATTATT GAAGCATTTA TCAGGGTTAT TGTCTCATGA
2801 GCGGATACAT ATTTGAATGT ATTTAGAAAA ATAAACAAAT AGGGGTTCCG
     CGCACATTTC CCCGAAAAGT GCCACCTGAC GTCTAAGAAA CCATTATTAT
2901 CATGACATTA ACCTATAAAA ATAGGCGTAT CACGAGGCCC TTTCGTC
```

Appendix 8: Plasmid Table pPC4

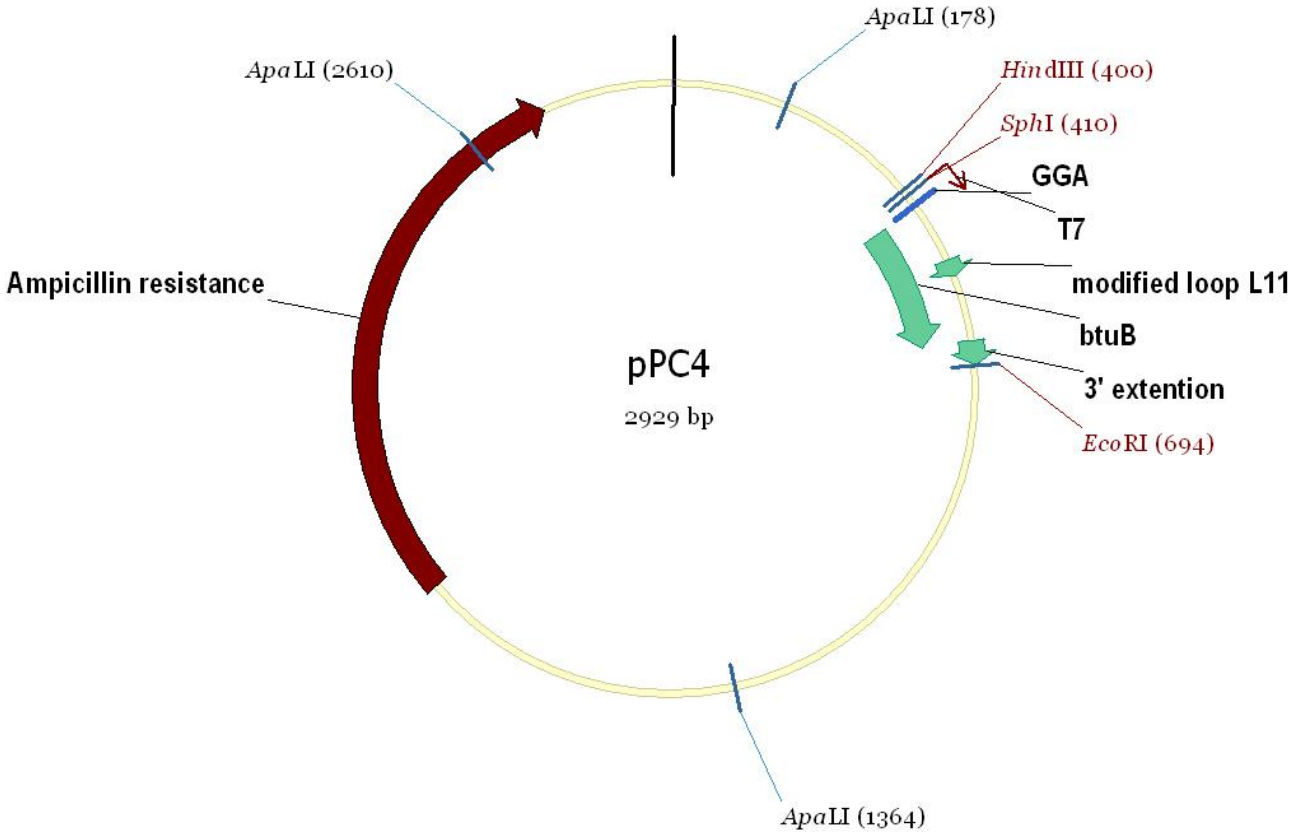


```
1     TCGCGCGTTT CGGTGATGAC GGTGAAAACC TCTGACACAT GCAGCTCCCG
      GAGACGGTCA CAGCTTGTCT GTAAGCGGAT GCCGGGAGCA GACAAGCCCG
101   TCAGGGCGCG TCAGCGGGTG TTGGCGGGTG TCGGGGCTGG CTTAACTATG
      CGGCATCAGA GCAGATTGTA CTGAGAGTGC ACCATATGCG GTGTGAAATA
201   CCGCACAGAT GCGTAAGGAG AAAATACCGC ATCAGGCGCC ATTCGCCATT
      CAGGCTGCGC AACTGTTGGG AAGGGCGATC GGTGCGGGCC TCTTCGCTAT
301   TACGCCAGCT GGCGAAAGGG GGATGTGCTG CAAGGCGATT AAGTTGGGTA
      ACGCCAGGGT TTTCCCAGTC ACGACGTTGT AAAACGACGG CCAGTGCCAA

          HindIII  SphI                                btuB
401   GCTTGCATGC TAATACGACT CACTATAGGA GCCGGTCCTG TGAGTTAATA
      GGGAATCCAG TGCGAATCTG GAGCTGACGC GCAGCGGTAA GGAAAGGTGC
                                        Modified L11
501   GATGATTGCG TTATGCGGAC ACTGCCCCCA AATATATTTC GGACTACGTA
      GGGGGTGGGA AGTCATCATC TCTTAGTATC TTAGATACCC CTCCAAGCCC
601   GAAGACCTGC CGGCCAACGT CGCATCTGGT TCTCATCATC GCGTAATATT
      GATGAAACCT GCGGCATCCT TCTTCTATTG TGGATGCTTT ACGAATTCGT
                Expression platform                  EcoRI
701   AATCATGGTC ATAGCTGTTT CCTGTGTGAA ATTGTTATCC GCTCACAATT
      CCACACAACA TACGAGCCGG AAGCATAAAG TGTAAAGCCT GGGGTGCCTA
801   ATGAGTGAGC TAACTCACAT TAATTGCGTT GCGCTCACTG CCCGCTTTCC
      AGTCGGGAAA CCTGTCGTGC CAGCTGCATT AATGAATCGG CCAACGCGCG
901   GGGAGAGGCG GTTTGCGTAT TGGGCGCTCT TCCGCTTCCT CGCTCACTGA
      CTCGCTGCGC TCGGTCGTTC GGCTGCGGCG AGCGGTATCA GCTCACTCAA
1001  AGGCGGTAAT ACGGTTATCC ACAGAATCAG GGGATAACGC AGGAAAGAAC
      ATGTGAGCAA AAGGCCAGCA AAAGGCCAGG AACCGTAAAA AGGCCGCGTT
1101  GCTGGCGTTT TTCCATAGGC TCCGCCCCCC TGACGAGCAT CACAAAAATC
```

```
     GACGCTCAAG TCAGAGGTGG CGAAACCCGA CAGGACTATA AAGATACCAG
1201 GCGTTTCCCC CTGGAAGCTC CCTCGTGCGC TCTCCTGTTC CGACCCTGCC
     GCTTACCGGA TACCTGTCCG CCTTTCTCCC TTCGGGAAGC GTGGCGCTTT
1301 CTCATAGCTC ACGCTGTAGG TATCTCAGTT CGGTGTAGGT CGTTCGCTCC
     AAGCTGGGCT GTGTGCACGA ACCCCCCGTT CAGCCCGACC GCTGCGCCTT
1401 ATCCGGTAAC TATCGTCTTG AGTCCAACCC GGTAAGACAC GACTTATCGC
     CACTGGCAGC AGCCACTGGT AACAGGATTA GCAGAGCGAG GTATGTAGGC
1501 GGTGCTACAG AGTTCTTGAA GTGGTGGCCT AACTACGGCT ACACTAGAAG
     GACAGTATTT GGTATCTGCG CTCTGCTGAA GCCAGTTACC TTCGGAAAAA
1601 GAGTTGGTAG CTCTTGATCC GGCAAACAAA CCACCGCTGG TAGCGGTGGT
     TTTTTTGTTT GCAAGCAGCA GATTACGCGC AGAAAAAAAG GATCTCAAGA
1701 AGATCCTTTG ATCTTTTCTA CGGGGTCTGA CGCTCAGTGG AACGAAAACT
     CACGTTAAGG GATTTTGGTC ATGAGATTAT CAAAAAGGAT CTTCACCTAG
1801 ATCCTTTTAA ATTAAAAATG AAGTTTTAAA TCAATCTAAA GTATATATGA
     GTAAACTTGG TCTGACAGTT ACCAATGCTT AATCAGTGAG GCACCTATCT
1901 CAGCGATCTG TCTATTTCGT TCATCCATAG TTGCCTGACT CCCCGTCGTG
     TAGATAACTA CGATACGGGA GGGCTTACCA TCTGGCCCCA GTGCTGCAAT
2001 GATACCGCGA GACCCACGCT CACCGGCTCC AGATTTATCA GCAATAAACC
     AGCCAGCCGG AAGGGCCGAG CGCAGAAGTG GTCCTGCAAC TTTATCCGCC
2101 TCCATCCAGT CTATTAATTG TTGCCGGGAA GCTAGAGTAA GTAGTTCGCC
     AGTTAATAGT TTGCGCAACG TTGTTGCCAT TGCTACAGGC ATCGTGGTGT
2201 CACGCTCGTC GTTTGGTATG GCTTCATTCA GCTCCGGTTC CCAACGATCA
     AGGCGAGTTA CATGATCCCC CATGTTGTGC AAAAAAGCGG TTAGCTCCTT
2301 CGGTCCTCCG ATCGTTGTCA GAAGTAAGTT GGCCGCAGTG TTATCACTCA
     TGGTTATGGC AGCACTGCAT AATTCTCTTA CTGTCATGCC ATCCGTAAGA
2401 TGCTTTTCTG TGACTGGTGA GTACTCAACC AAGTCATTCT GAGAATAGTG
     TATGCGGCGA CCGAGTTGCT CTTGCCCGGC GTCAATACGG GATAATACCG
2501 CGCCACATAG CAGAACTTTA AAAGTGCTCA TCATTGGAAA ACGTTCTTCG
     GGGCGAAAAC TCTCAAGGAT CTTACCGCTG TTGAGATCCA GTTCGATGTA
2601 ACCCACTCGT GCACCCAACT GATCTTCAGC ATCTTTTACT TTCACCAGCG
     TTTCTGGGTG AGCAAAAACA GGAAGGCAAA ATGCCGCAAA AAAGGGAATA
2701 AGGGCGACAC GGAAATGTTG AATACTCATA CTCTTCCTTT TTCAATATTA
     TTGAAGCATT TATCAGGGTT ATTGTCTCAT GAGCGGATAC ATATTTGAAT
2801 GTATTTAGAA AAATAAACAA ATAGGGGTTC CGCGCACATT TCCCCGAAAA
     GTGCCACCTG ACGTCTAAGA AACCATTATT ATCATGACAT TAACCTATAA
2901 AAATAGGCGT ATCACGAGGC CCTTTCGTC
```

Appendix 9: Plasmid Table pPC5

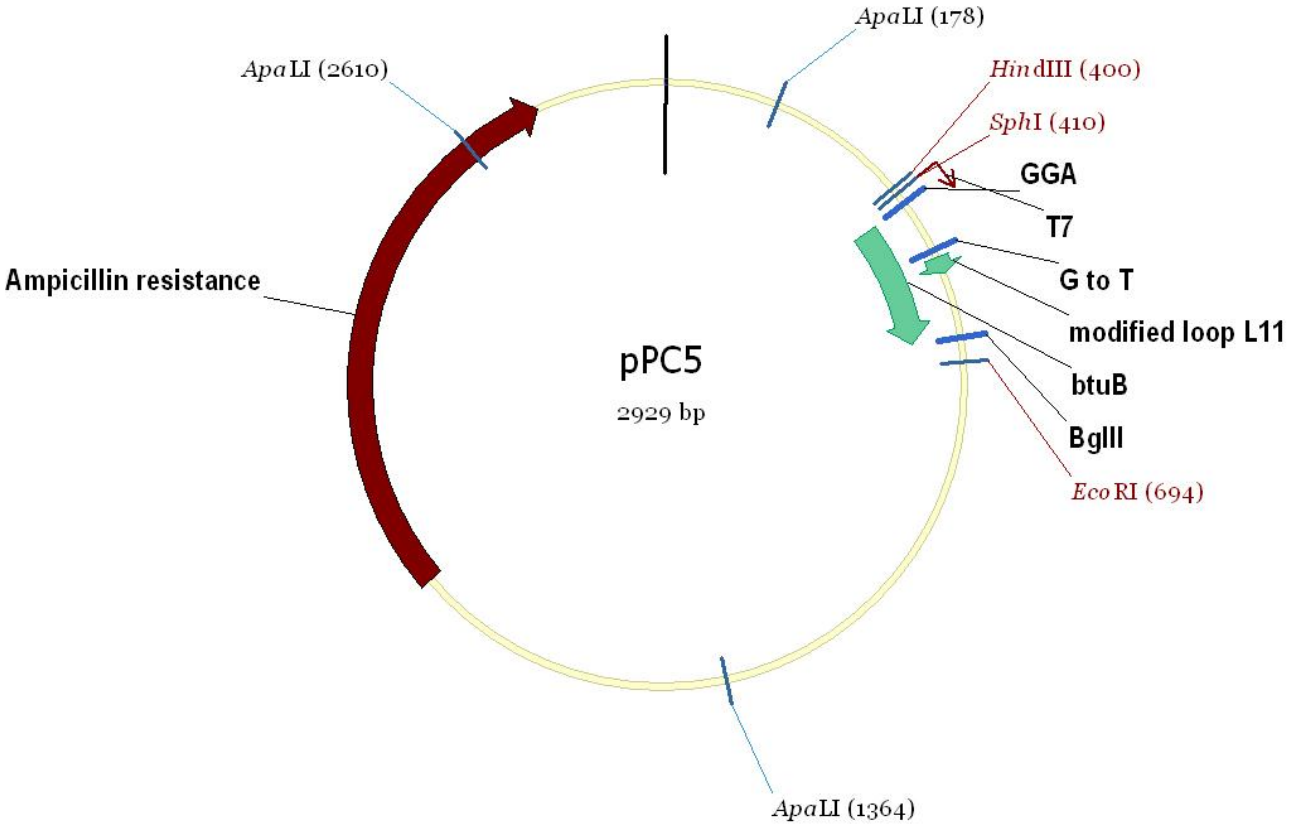


```
1     TCGCGCGTTT CGGTGATGAC GGTGAAAACC TCTGACACAT GCAGCTCCCG
      GAGACGGTCA CAGCTTGTCT GTAAGCGGAT GCCGGGAGCA GACAAGCCCG
101   TCAGGGCGCG TCAGCGGGTG TTGGCGGGTG TCGGGGCTGG CTTAACTATG
      CGGCATCAGA GCAGATTGTA CTGAGAGTGC ACCATATGCG GTGTGAAATA
201   CCGCACAGAT GCGTAAGGAG AAAATACCGC ATCAGGCGCC ATTCGCCATT
      CAGGCTGCGC AACTGTTGGG AAGGGCGATC GGTGCGGGCC TCTTCGCTAT
301   TACGCCAGCT GGCGAAAGGG GGATGTGCTG CAAGGCGATT AAGTTGGGTA
      ACGCCAGGGT TTTCCCAGTC ACGACGTTGT AAAACGACGG CCAGTGCCAA

          HindIII  SphI                                btuB
401   GCTTGCATGC TAATACGACT CACTATAGGA GCCGGTCCTG TGAGTTAATA
      GGGAATCCAG TGCGAATCTG GAGCTGACGC GCAGCGGTAA GGAAAGGTGC
                     G to T                 Modified L11
501   GATGATTGCG TTATTCGGAC ACTGCCCCCA AATATATTTC GGACTACGTA
      GGGGGTGGGA AGTCATCATC TCTTAGTATC TTAGATACCC CTCCAAGCCC
601   GAAGACCTGC CGGCCAACGT CGCATCTGGT TCTCATCATC GCGTAATATT
      GATGAGATCT GCGGCATCCT TCTTCTATTG TGGATGCTTT ACGAATTCGT
              BglII
701   AATCATGGTC ATAGCTGTTT CCTGTGTGAA ATTGTTATCC GCTCACAATT
      CCACACAACA TACGAGCCGG AAGCATAAAG TGTAAAGCCT GGGGTGCCTA
801   ATGAGTGAGC TAACTCACAT TAATTGCGTT GCGCTCACTG CCCGCTTTCC
      AGTCGGGAAA CCTGTCGTGC CAGCTGCATT AATGAATCGG CCAACGCGCG
901   GGGAGAGGCG GTTTGCGTAT TGGGCGCTCT TCCGCTTCCT CGCTCACTGA
      CTCGCTGCGC TCGGTCGTTC GGCTGCGGCG AGCGGTATCA GCTCACTCAA
1001  AGGCGGTAAT ACGGTTATCC ACAGAATCAG GGGATAACGC AGGAAAGAAC
      ATGTGAGCAA AAGGCCAGCA AAAGGCCAGG AACCGTAAAA AGGCCGCGTT
```

```
1101 GCTGGCGTTT TTCCATAGGC TCCGCCCCCC TGACGAGCAT CACAAAAATC
     GACGCTCAAG TCAGAGGTGG CGAAACCCGA CAGGACTATA AAGATACCAG
1201 GCGTTTCCCC CTGGAAGCTC CCTCGTGCGC TCTCCTGTTC CGACCCTGCC
     GCTTACCGGA TACCTGTCCG CCTTTCTCCC TTCGGGAAGC GTGGCGCTTT
1301 CTCATAGCTC ACGCTGTAGG TATCTCAGTT CGGTGTAGGT CGTTCGCTCC
     AAGCTGGGCT GTGTGCACGA ACCCCCCGTT CAGCCCGACC GCTGCGCCTT
1401 ATCCGGTAAC TATCGTCTTG AGTCCAACCC GGTAAGACAC GACTTATCGC
     CACTGGCAGC AGCCACTGGT AACAGGATTA GCAGAGCGAG GTATGTAGGC
1501 GGTGCTACAG AGTTCTTGAA GTGGTGGCCT AACTACGGCT ACACTAGAAG
     GACAGTATTT GGTATCTGCG CTCTGCTGAA GCCAGTTACC TTCGGAAAAA
1601 GAGTTGGTAG CTCTTGATCC GGCAAACAAA CCACCGCTGG TAGCGGTGGT
     TTTTTTGTTT GCAAGCAGCA GATTACGCGC AGAAAAAAAG GATCTCAAGA
1701 AGATCCTTTG ATCTTTTCTA CGGGGTCTGA CGCTCAGTGG AACGAAAACT
     CACGTTAAGG GATTTTGGTC ATGAGATTAT CAAAAAGGAT CTTCACCTAG
1801 ATCCTTTTAA ATTAAAAATG AAGTTTTAAA TCAATCTAAA GTATATATGA
     GTAAACTTGG TCTGACAGTT ACCAATGCTT AATCAGTGAG GCACCTATCT
1901 CAGCGATCTG TCTATTTCGT TCATCCATAG TTGCCTGACT CCCCGTCGTG
     TAGATAACTA CGATACGGGA GGGCTTACCA TCTGGCCCCA GTGCTGCAAT
2001 GATACCGCGA GACCCACGCT CACCGGCTCC AGATTTATCA GCAATAAACC
     AGCCAGCCGG AAGGGCCGAG CGCAGAAGTG GTCCTGCAAC TTTATCCGCC
2101 TCCATCCAGT CTATTAATTG TTGCCGGGAA GCTAGAGTAA GTAGTTCGCC
     AGTTAATAGT TTGCGCAACG TTGTTGCCAT TGCTACAGGC ATCGTGGTGT
2201 CACGCTCGTC GTTTGGTATG GCTTCATTCA GCTCCGGTTC CCAACGATCA
     AGGCGAGTTA CATGATCCCC CATGTTGTGC AAAAAAGCGG TTAGCTCCTT
2301 CGGTCCTCCG ATCGTTGTCA GAAGTAAGTT GGCCGCAGTG TTATCACTCA
     TGGTTATGGC AGCACTGCAT AATTCTCTTA CTGTCATGCC ATCCGTAAGA
2401 TGCTTTTCTG TGACTGGTGA GTACTCAACC AAGTCATTCT GAGAATAGTG
     TATGCGGCGA CCGAGTTGCT CTTGCCCGGC GTCAATACGG GATAATACCG
2501 CGCCACATAG CAGAACTTTA AAAGTGCTCA TCATTGGAAA ACGTTCTTCG
     GGGCGAAAAC TCTCAAGGAT CTTACCGCTG TTGAGATCCA GTTCGATGTA
2601 ACCCACTCGT GCACCCAACT GATCTTCAGC ATCTTTTACT TTCACCAGCG
     TTTCTGGGTG AGCAAAAACA GGAAGGCAAA ATGCCGCAAA AAAGGGAATA
2701 AGGGCGACAC GGAAATGTTG AATACTCATA CTCTTCCTTT TTCAATATTA
     TTGAAGCATT TATCAGGGTT ATTGTCTCAT GAGCGGATAC ATATTTGAAT
2801 GTATTTAGAA AAATAAACAA ATAGGGGTTC CGCGCACATT TCCCCGAAAA
     GTGCCACCTG ACGTCTAAGA AACCATTATT ATCATGACAT TAACCTATAA
2901 AAATAGGCGT ATCACGAGGC CCTTTCGTC
```

Appendix 10: Plasmid Table pRS07

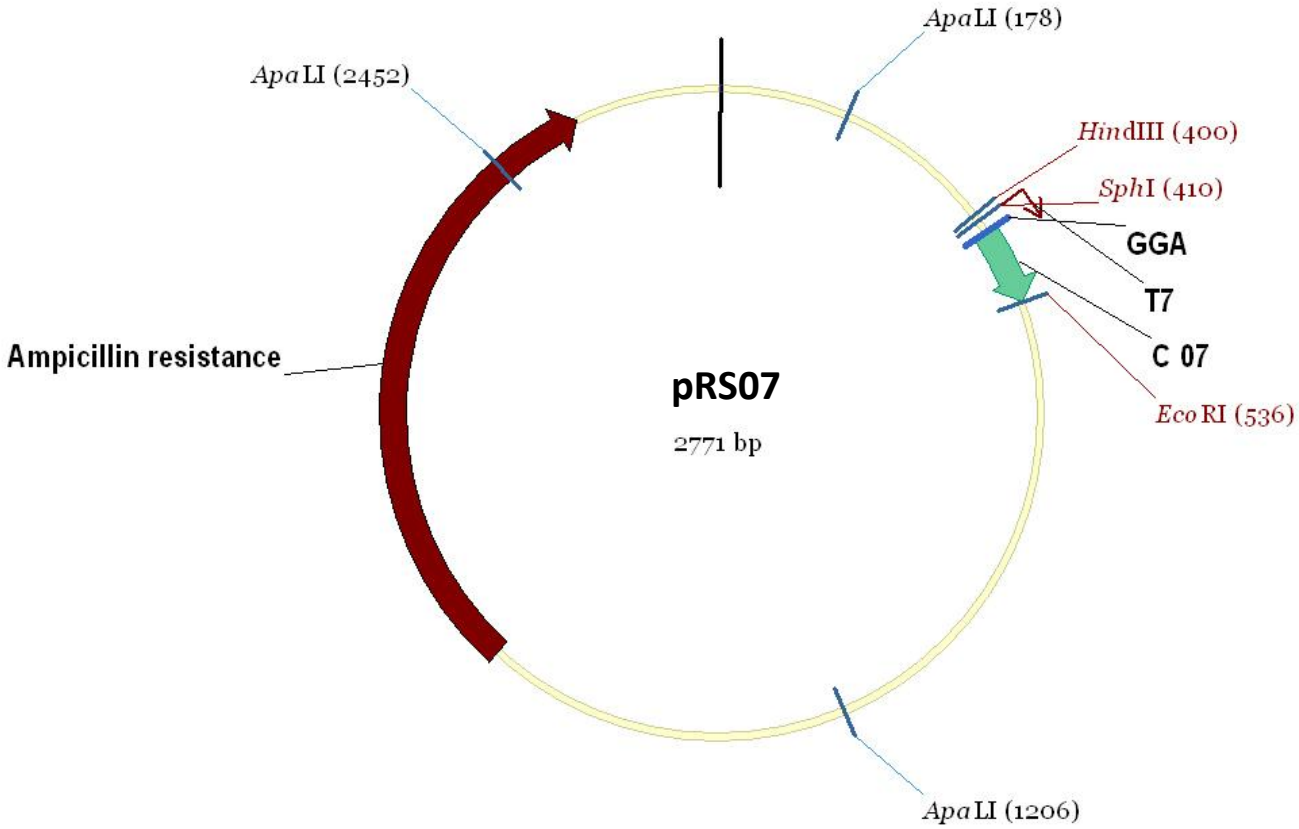


```
1     TCGCGCGTTT CGGTGATGAC GGTGAAAACC TCTGACACAT GCAGCTCCCG
      GAGACGGTCA CAGCTTGTCT GTAAGCGGAT GCCGGGAGCA GACAAGCCCG
101   TCAGGGCGCG TCAGCGGGTG TTGGCGGGTG TCGGGGCTGG CTTAACTATG
      CGGCATCAGA GCAGATTGTA CTGAGAGTGC ACCATATGCG GTGTGAAATA
201   CCGCACAGAT GCGTAAGGAG AAAATACCGC ATCAGGCGCC ATTCGCCATT
      CAGGCTGCGC AACTGTTGGG AAGGGCGATC GGTGCGGGCC TCTTCGCTAT
301   TACGCCAGCT GGCGAAAGGG GGATGTGCTG CAAGGCGATT AAGTTGGGTA
      ACGCCAGGGT TTTCCCAGTC ACGACGTTGT AAAACGACGG CCAGTGCCAA
       HindIII  SphI                              RS07
401   GCTTGCATGC TAATACGACT CACTATAGGA TTAGGTACTC AATCCTTACC
      GGAAAGAGTT AAAAGGGAAG CCGGTTCAAT TCCGGCACGG TCCCGCCACT
                                          EcoRI
501   GTGAATTGAG TGAGTAATCA CTCTTAAGTC AGGAGAATTC GTAATCATGG
      TCATAGCTGT TTCCTGTGTG AAATTGTTAT CCGCTCACAA TTCCACACAA
601   CATACGAGCC GGAAGCATAA AGTGTAAAGC CTGGGGTGCC TAATGAGTGA
      GCTAACTCAC ATTAATTGCG TTGCGCTCAC TGCCCGCTTT CCAGTCGGGA
701   AACCTGTCGT GCCAGCTGCA TTAATGAATC GGCCAACGCG CGGGGAGAGG
      CGGTTTGCGT ATTGGGCGCT CTTCCGCTTC CTCGCTCACT GACTCGCTGC
801   GCTCGGTCGT TCGGCTGCGG CGAGCGGTAT CAGCTCACTC AAAGGCGGTA
      ATACGGTTAT CCACAGAATC AGGGGATAAC GCAGGAAAGA ACATGTGAGC
901   AAAAGGCCAG CAAAAGGCCA GGAACCGTAA AAAGGCCGCG TTGCTGGCGT
      TTTTCCATAG GCTCCGCCCC CCTGACGAGC ATCACAAAAA TCGACGCTCA
1001  AGTCAGAGGT GGCGAAACCC GACAGGACTA TAAAGATACC AGGCGTTTCC
      CCCTGGAAGC TCCCTCGTGC GCTCTCCTGT TCCGACCCTG CCGCTTACCG
1101  GATACCTGTC CGCCTTTCTC CCTTCGGGAA GCGTGGCGCT TTCTCATAGC
      TCACGCTGTA GGTATCTCAG TTCGGTGTAG GTCGTTCGCT CCAAGCTGGG
1201  CTGTGTGCAC GAACCCCCCG TTCAGCCCGA CCGCTGCGCC TTATCCGGTA
```

```
     ACTATCGTCT TGAGTCCAAC CCGGTAAGAC ACGACTTATC GCCACTGGCA
1301 GCAGCCACTG GTAACAGGAT TAGCAGAGCG AGGTATGTAG GCGGTGCTAC
     AGAGTTCTTG AAGTGGTGGC CTAACTACGG CTACACTAGA AGGACAGTAT
1401 TTGGTATCTG CGCTCTGCTG AAGCCAGTTA CCTTCGGAAA AAGAGTTGGT
     AGCTCTTGAT CCGGCAAACA AACCACCGCT GGTAGCGGTG GTTTTTTTGT
1501 TTGCAAGCAG CAGATTACGC GCAGAAAAAA AGGATCTCAA GAAGATCCTT
     TGATCTTTTC TACGGGGTCT GACGCTCAGT GGAACGAAAA CTCACGTTAA
1601 GGGATTTTGG TCATGAGATT ATCAAAAAGG ATCTTCACCT AGATCCTTTT
     AAATTAAAAA TGAAGTTTTA AATCAATCTA AAGTATATAT GAGTAAACTT
1701 GGTCTGACAG TTACCAATGC TTAATCAGTG AGGCACCTAT CTCAGCGATC
     TGTCTATTTC GTTCATCCAT AGTTGCCTGA CTCCCCGTCG TGTAGATAAC
1801 TACGATACGG GAGGGCTTAC CATCTGGCCC CAGTGCTGCA ATGATACCGC
     GAGACCCACG CTCACCGGCT CCAGATTTAT CAGCAATAAA CCAGCCAGCC
1901 GGAAGGGCCG AGCGCAGAAG TGGTCCTGCA ACTTTATCCG CCTCCATCCA
     GTCTATTAAT TGTTGCCGGG AAGCTAGAGT AAGTAGTTCG CCAGTTAATA
2001 GTTTGCGCAA CGTTGTTGCC ATTGCTACAG GCATCGTGGT GTCACGCTCG
     TCGTTTGGTA TGGCTTCATT CAGCTCCGGT TCCCAACGAT CAAGGCGAGT
2101 TACATGATCC CCCATGTTGT GCAAAAAAGC GGTTAGCTCC TTCGGTCCTC
     CGATCGTTGT CAGAAGTAAG TTGGCCGCAG TGTTATCACT CATGGTTATG
2201 GCAGCACTGC ATAATTCTCT TACTGTCATG CCATCCGTAA GATGCTTTTC
     TGTGACTGGT GAGTACTCAA CCAAGTCATT CTGAGAATAG TGTATGCGGC
2301 GACCGAGTTG CTCTTGCCCG GCGTCAATAC GGGATAATAC CGCGCCACAT
     AGCAGAACTT TAAAAGTGCT CATCATTGGA AAACGTTCTT CGGGGCGAAA
2401 ACTCTCAAGG ATCTTACCGC TGTTGAGATC CAGTTCGATG TAACCCACTC
     GTGCACCCAA CTGATCTTCA GCATCTTTTA CTTTCACCAG CGTTTCTGGG
2501 TGAGCAAAAA CAGGAAGGCA AAATGCCGCA AAAAAGGGAA TAAGGGCGAC
     ACGGAAATGT TGAATACTCA TACTCTTCCT TTTTCAATAT TATTGAAGCA
2601 TTTATCAGGG TTATTGTCTC ATGAGCGGAT ACATATTTGA ATGTATTTAG
     AAAAATAAAC AAATAGGGGT TCCGCGCACA TTTCCCCGAA AAGTGCCACC
2701 TGACGTCTAA GAAACCATTA TTATCATGAC ATTAACCTAT AAAAATAGGC
     GTATCACGAG GCCCTTTCGT C
```

Appendix 11: Plasmid Table pRS08

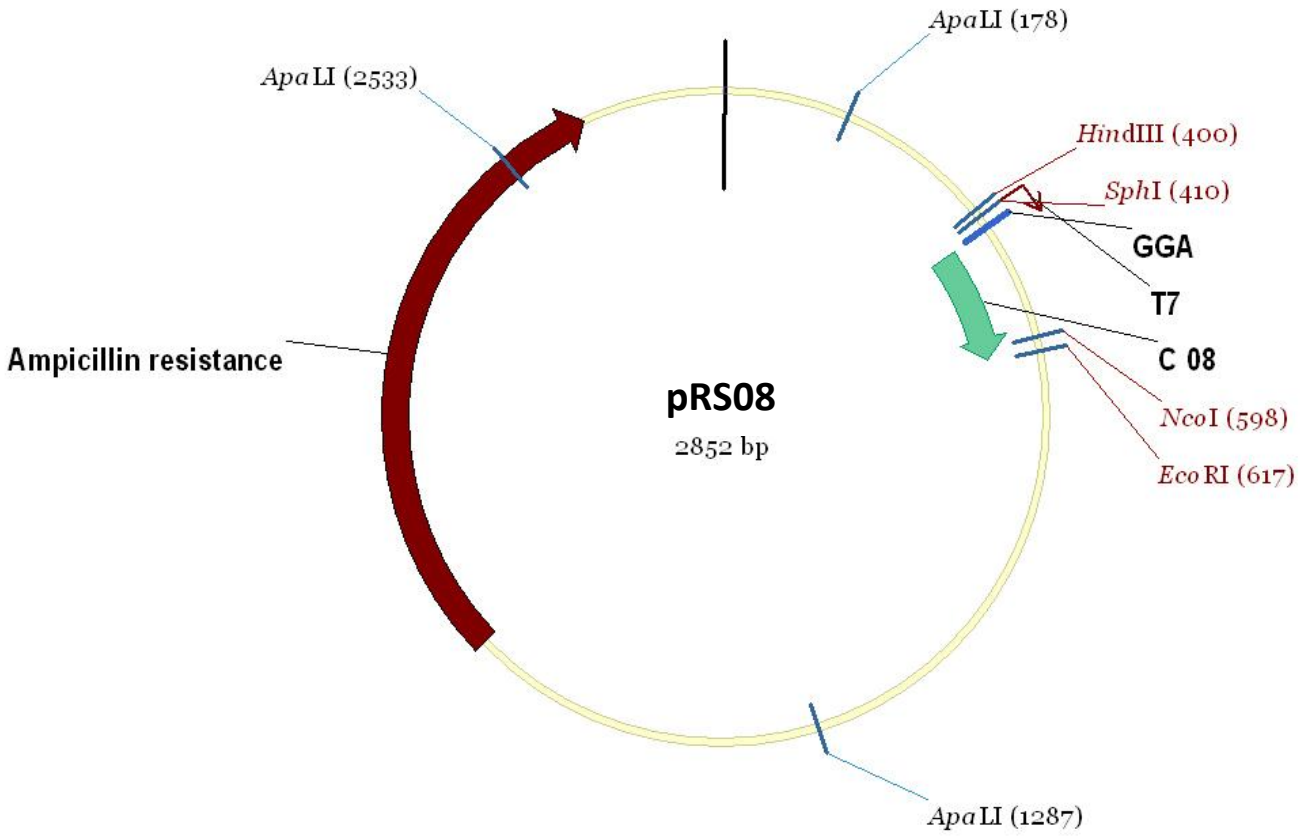


```
1     TCGCGCGTTT CGGTGATGAC GGTGAAAACC TCTGACACAT GCAGCTCCCG
      GAGACGGTCA CAGCTTGTCT GTAAGCGGAT GCCGGGAGCA GACAAGCCCG
101   TCAGGGCGCG TCAGCGGGTG TTGGCGGGTG TCGGGGCTGG CTTAACTATG
      CGGCATCAGA GCAGATTGTA CTGAGAGTGC ACCATATGCG GTGTGAAATA
201   CCGCACAGAT GCGTAAGGAG AAAATACCGC ATCAGGCGCC ATTCGCCATT
      CAGGCTGCGC AACTGTTGGG AAGGGCGATC GGTGCGGGCC TCTTCGCTAT
301   TACGCCAGCT GGCGAAAGGG GGATGTGCTG CAAGGCGATT AAGTTGGGTA
      ACGCCAGGGT TTTCCCAGTC ACGACGTTGT AAAACGACGG CCAGTGCCAA
        HindIII  SphI                              RS08
401   GCTTGCATGC TAATACGACT CACTATAGGA CCATTCTTTG GTGCCCCCAA
      GGGGAGAATA GGGAAACCGG TGCGATTCCG GTGCGGACCC ACCACTGTGT
501   AGGATGAGCC TGAACCATAA CCACCGGCCA GACCGGGAAG GGGTAGCGGC
      GTTTGAATCC AAGCCAGGAG ACCTGCCAGG AATGAAGAAA GCCTTTCCAT
        NcoI                  EcoRI
601   GGGTGCTATG GAAAGGAATT CGTAATCATG GTCATAGCTG TTTCCTGTGT
      GAAATTGTTA TCCGCTCACA ATTCCACACA ACATACGAGC CGGAAGCATA
701   AAGTGTAAAG CCTGGGGTGC CTAATGAGTG AGCTAACTCA CATTAATTGC
      GTTGCGCTCA CTGCCCGCTT TCCAGTCGGG AAACCTGTCG TGCCAGCTGC
801   ATTAATGAAT CGGCCAACGC GCGGGGAGAG GCGGTTTGCG TATTGGGCGC
      TCTTCCGCTT CCTCGCTCAC TGACTCGCTG CGCTCGGTCG TTCGGCTGCG
901   GCGAGCGGTA TCAGCTCACT CAAAGGCGGT AATACGGTTA TCCACAGAAT
      CAGGGGATAA CGCAGGAAAG AACATGTGAG CAAAAGGCCA GCAAAAGGCC
1001  AGGAACCGTA AAAAGGCCGC GTTGCTGGCG TTTTTCCATA GGCTCCGCCC
      CCCTGACGAG CATCACAAAA ATCGACGCTC AAGTCAGAGG TGGCGAAACC
1101  CGACAGGACT ATAAAGATAC CAGGCGTTTC CCCCTGGAAG CTCCCTCGTG
      CGCTCTCCTG TTCCGACCCT GCCGCTTACC GGATACCTGT CCGCCTTTCT
```

```
1201 CCCTTCGGGA AGCGTGGCGC TTTCTCATAG CTCACGCTGT AGGTATCTCA
     GTTCGGTGTA GGTCGTTCGC TCCAAGCTGG GCTGTGTGCA CGAACCCCCC
1301 GTTCAGCCCG ACCGCTGCGC CTTATCCGGT AACTATCGTC TTGAGTCCAA
     CCCGGTAAGA CACGACTTAT CGCCACTGGC AGCAGCCACT GGTAACAGGA
1401 TTAGCAGAGC GAGGTATGTA GGCGGTGCTA CAGAGTTCTT GAAGTGGTGG
     CCTAACTACG GCTACACTAG AAGGACAGTA TTTGGTATCT GCGCTCTGCT
1501 GAAGCCAGTT ACCTTCGGAA AAAGAGTTGG TAGCTCTTGA TCCGGCAAAC
     AAACCACCGC TGGTAGCGGT GGTTTTTTTG TTTGCAAGCA GCAGATTACG
1601 CGCAGAAAAA AAGGATCTCA AGAAGATCCT TTGATCTTTT CTACGGGGTC
     TGACGCTCAG TGGAACGAAA ACTCACGTTA AGGGATTTTG GTCATGAGAT
1701 TATCAAAAAG GATCTTCACC TAGATCCTTT TAAATTAAAA ATGAAGTTTT
     AAATCAATCT AAAGTATATA TGAGTAAACT TGGTCTGACA GTTACCAATG
1801 CTTAATCAGT GAGGCACCTA TCTCAGCGAT CTGTCTATTT CGTTCATCCA
     TAGTTGCCTG ACTCCCCGTC GTGTAGATAA CTACGATACG GGAGGGCTTA
1901 CCATCTGGCC CCAGTGCTGC AATGATACCG CGAGACCCAC GCTCACCGGC
     TCCAGATTTA TCAGCAATAA ACCAGCCAGC CGGAAGGGCC GAGCGCAGAA
2001 GTGGTCCTGC AACTTTATCC GCCTCCATCC AGTCTATTAA TTGTTGCCGG
     GAAGCTAGAG TAAGTAGTTC GCCAGTTAAT AGTTTGCGCA ACGTTGTTGC
2101 CATTGCTACA GGCATCGTGG TGTCACGCTC GTCGTTTGGT ATGGCTTCAT
     TCAGCTCCGG TTCCCAACGA TCAAGGCGAG TTACATGATC CCCCATGTTG
2201 TGCAAAAAAG CGGTTAGCTC CTTCGGTCCT CCGATCGTTG TCAGAAGTAA
     GTTGGCCGCA GTGTTATCAC TCATGGTTAT GGCAGCACTG CATAATTCTC
2301 TTACTGTCAT GCCATCCGTA AGATGCTTTT CTGTGACTGG TGAGTACTCA
     ACCAAGTCAT TCTGAGAATA GTGTATGCGG CGACCGAGTT GCTCTTGCCC
2401 GGCGTCAATA CGGGATAATA CCGCGCCACA TAGCAGAACT TTAAAAGTGC
     TCATCATTGG AAAACGTTCT TCGGGGCGAA AACTCTCAAG GATCTTACCG
2501 CTGTTGAGAT CCAGTTCGAT GTAACCCACT CGTGCACCCA ACTGATCTTC
     AGCATCTTTT ACTTTCACCA GCGTTTCTGG GTGAGCAAAA ACAGGAAGGC
2601 AAAATGCCGC AAAAAAGGGA ATAAGGGCGA CACGGAAATG TTGAATACTC
     ATACTCTTCC TTTTTCAATA TTATTGAAGC ATTTATCAGG GTTATTGTCT
2701 CATGAGCGGA TACATATTTG AATGTATTTA GAAAAATAAA CAAATAGGGG
     TTCCGCGCAC ATTTCCCCGA AAAGTGCCAC CTGACGTCTA AGAAACCATT
2801 ATTATCATGA CATTAACCTA TAAAAATAGG CGTATCACGA GGCCCTTTCG
     TC
```

Appendix 12: Plasmid Table pRS16

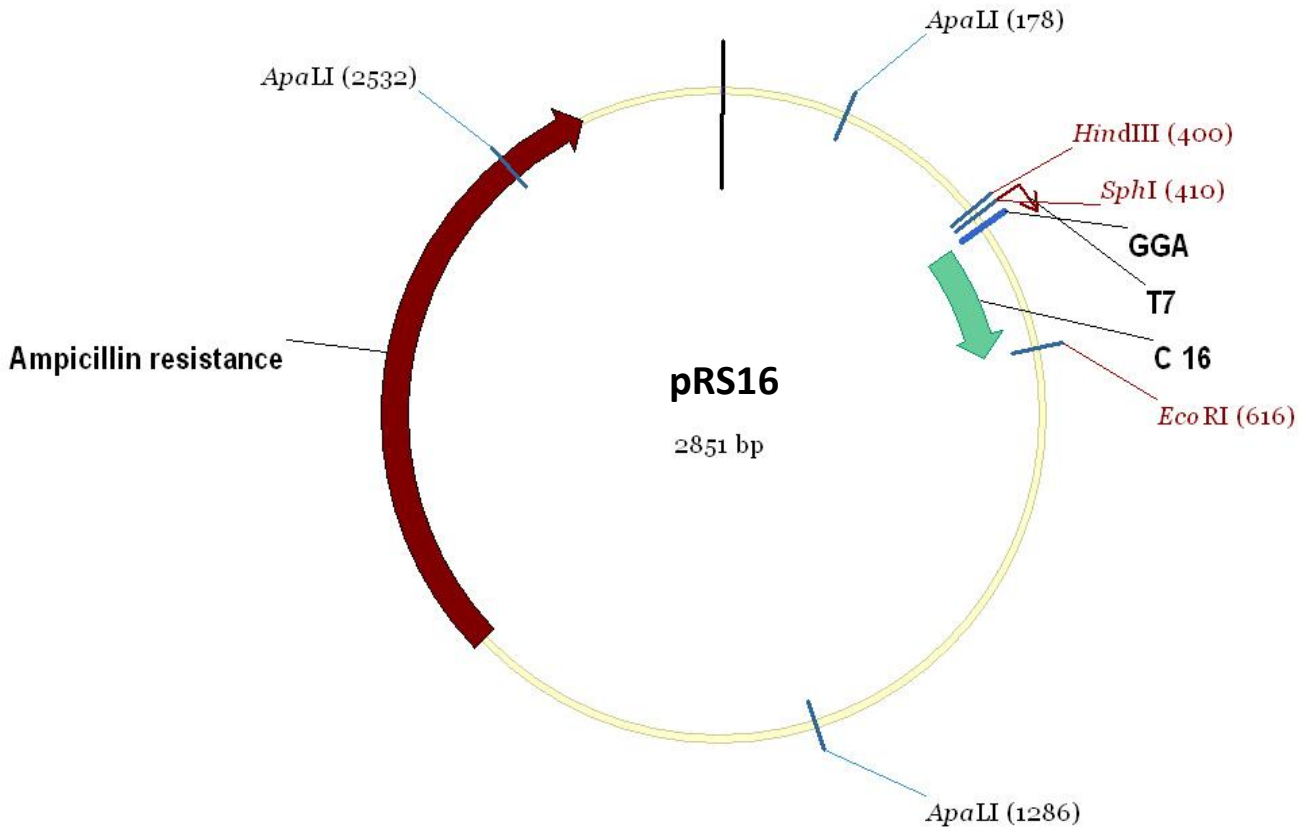


```
1     TCGCGCGTTT CGGTGATGAC GGTGAAAACC TCTGACACAT GCAGCTCCCG
      GAGACGGTCA CAGCTTGTCT GTAAGCGGAT GCCGGGAGCA GACAAGCCCG
101   TCAGGGCGCG TCAGCGGGTG TTGGCGGGTG TCGGGGCTGG CTTAACTATG
      CGGCATCAGA GCAGATTGTA CTGAGAGTGC ACCATATGCG GTGTGAAATA
201   CCGCACAGAT GCGTAAGGAG AAAATACCGC ATCAGGCGCC ATTCGCCATT
      CAGGCTGCGC AACTGTTGGG AAGGGCGATC GGTGCGGGCC TCTTCGCTAT
301   TACGCCAGCT GGCGAAAGGG GGATGTGCTG CAAGGCGATT AAGTTGGGTA
      ACGCCAGGGT TTTCCCAGTC ACGACGTTGT AAAACGACGG CCAGTGCCAA
        HindIII  SphI                              RS16
401   GCTTGCATGC TAATACGACT CACTATAGGA GTATTCAAGG TTCCTCTTTA
      GAGGAAGAAA AGGGAAGCCG GTGAAAATCC GGCGCGGTCC CGCCACTGTG
501   AACCACGAGT GTCTCTTAAG GCCCACTGGG ATGAGCCTGG GAAGGGAAGA
      GGCATAAAGA CTGGAAGCCA GGAGACCTGC CTTGAACATT GCGCTACGTC
                          EcoRI
601   CACGAGCGAT GGATGAATTC GTAATCATGG TCATAGCTGT TTCCTGTGTG
      AAATTGTTAT CCGCTCACAA TTCCACACAA CATACGAGCC GGAAGCATAA
701   AGTGTAAAGC CTGGGGTGCC TAATGAGTGA GCTAACTCAC ATTAATTGCG
      TTGCGCTCAC TGCCCGCTTT CCAGTCGGGA AACCTGTCGT GCCAGCTGCA
801   TTAATGAATC GGCCAACGCG CGGGGAGAGG CGGTTTGCGT ATTGGGCGCT
      CTTCCGCTTC CTCGCTCACT GACTCGCTGC GCTCGGTCGT TCGGCTGCGG
901   CGAGCGGTAT CAGCTCACTC AAAGGCGGTA ATACGGTTAT CCACAGAATC
      AGGGGATAAC GCAGGAAAGA ACATGTGAGC AAAAGGCCAG CAAAAGGCCA
1001  GGAACCGTAA AAAGGCCGCG TTGCTGGCGT TTTTCCATAG GCTCCGCCCC
      CCTGACGAGC ATCACAAAAA TCGACGCTCA AGTCAGAGGT GGCGAAACCC
1101  GACAGGACTA TAAAGATACC AGGCGTTTCC CCCTGGAAGC TCCCTCGTGC
      GCTCTCCTGT TCCGACCCTG CCGCTTACCG GATACCTGTC CGCCTTTCTC
1201  CCTTCGGGAA GCGTGGCGCT TTCTCATAGC TCACGCTGTA GGTATCTCAG
```

```
     TTCGGTGTAG GTCGTTCGCT CCAAGCTGGG CTGTGTGCAC GAACCCCCCG
1301 TTCAGCCCGA CCGCTGCGCC TTATCCGGTA ACTATCGTCT TGAGTCCAAC
     CCGGTAAGAC ACGACTTATC GCCACTGGCA GCAGCCACTG GTAACAGGAT
1401 TAGCAGAGCG AGGTATGTAG GCGGTGCTAC AGAGTTCTTG AAGTGGTGGC
     CTAACTACGG CTACACTAGA AGGACAGTAT TTGGTATCTG CGCTCTGCTG
1501 AAGCCAGTTA CCTTCGGAAA AAGAGTTGGT AGCTCTTGAT CCGGCAAACA
     AACCACCGCT GGTAGCGGTG GTTTTTTTGT TTGCAAGCAG CAGATTACGC
1601 GCAGAAAAAA AGGATCTCAA GAAGATCCTT TGATCTTTTC TACGGGGTCT
     GACGCTCAGT GGAACGAAAA CTCACGTTAA GGGATTTTGG TCATGAGATT
1701 ATCAAAAAGG ATCTTCACCT AGATCCTTTT AAATTAAAAA TGAAGTTTTA
     AATCAATCTA AAGTATATAT GAGTAAACTT GGTCTGACAG TTACCAATGC
1801 TTAATCAGTG AGGCACCTAT CTCAGCGATC TGTCTATTTC GTTCATCCAT
     AGTTGCCTGA CTCCCCGTCG TGTAGATAAC TACGATACGG GAGGGCTTAC
1901 CATCTGGCCC CAGTGCTGCA ATGATACCGC GAGACCCACG CTCACCGGCT
     CCAGATTTAT CAGCAATAAA CCAGCCAGCC GGAAGGGCCG AGCGCAGAAG
2001 TGGTCCTGCA ACTTTATCCG CCTCCATCCA GTCTATTAAT TGTTGCCGGG
     AAGCTAGAGT AAGTAGTTCG CCAGTTAATA GTTTGCGCAA CGTTGTTGCC
2101 ATTGCTACAG GCATCGTGGT GTCACGCTCG TCGTTTGGTA TGGCTTCATT
     CAGCTCCGGT TCCCAACGAT CAAGGCGAGT TACATGATCC CCCATGTTGT
2201 GCAAAAAAGC GGTTAGCTCC TTCGGTCCTC CGATCGTTGT CAGAAGTAAG
     TTGGCCGCAG TGTTATCACT CATGGTTATG GCAGCACTGC ATAATTCTCT
2301 TACTGTCATG CCATCCGTAA GATGCTTTTC TGTGACTGGT GAGTACTCAA
     CCAAGTCATT CTGAGAATAG TGTATGCGGC GACCGAGTTG CTCTTGCCCG
2401 GCGTCAATAC GGGATAATAC CGCGCCACAT AGCAGAACTT TAAAAGTGCT
     CATCATTGGA AAACGTTCTT CGGGGCGAAA ACTCTCAAGG ATCTTACCGC
2501 TGTTGAGATC CAGTTCGATG TAACCCACTC GTGCACCCAA CTGATCTTCA
     GCATCTTTTA CTTTCACCAG CGTTTCTGGG TGAGCAAAAA CAGGAAGGCA
2601 AAATGCCGCA AAAAAGGGAA TAAGGGCGAC ACGGAAATGT TGAATACTCA
     TACTCTTCCT TTTTCAATAT TATTGAAGCA TTTATCAGGG TTATTGTCTC
2701 ATGAGCGGAT ACATATTTGA ATGTATTTAG AAAAATAAAC AAATAGGGGT
     TCCGCGCACA TTTCCCCGAA AAGTGCCACC TGACGTCTAA GAAACCATTA
2801 TTATCATGAC ATTAACCTAT AAAAATAGGC GTATCACGAG GCCCTTTCGT
```

11 Curriculum Vitae

Personal Data:

Name	Pallavi Choudhary
Date of Birth	August 7, 1985
Place of birth	Pune, Maharashtra state, India
Nationality	Indian

Academic qualifications:

1990-1994	Modern Primary School, Pune, India.
1994-2000	Ahilyadevi High School for Girls, Pune, India.
2000-2002	Laxmanrao Apte Junior College, Pune, India.
2002-2005	Bachelor in Microbiology from University of Pune, India.
2005-2007	Master in Biochemistry from The Maharaja Sayajirao University of Baroda, India.
2008-2013	Ph.D. student in the group of Prof. Dr. Roland K. O. Sigel at the Institute of Inorganic Chemistry, University of Zürich, Switzerland.

Teaching experience:

December 2007-August 2008	Assistant lecturer at the Department of Biotechnology, Modern College, University of Pune, India.
September 2009-December 2009	Teaching assistant in the general chemistry laboratory course at the Department of Chemistry and Biochemistry, University of Zürich, Switzerland.

Academic Achievements:

- Awarded Dr. Dharmishta V. Shah Gold Medal in 2007 from The Maharaja Sayajirao University of Baroda, India for securing the first rank in Master of Biochemistry.
- Awarded Dr. Dharmishta V. Shah Scholarship for 2005-2007 from The Maharaja Sayajirao University of Baroda, India for securing the highest score in Bachelor of Science.
- Awarded UGC-NET Junior Research Fellowship in June 2007 from the University Grants Commission (UGC), India.

List of publications:

- Monitoring global structural changes and specific metal ion-binding sites in RNA by in-line probing and Tb(III) cleavage.
  Pallavi K. Choudhary, Sofia Gallo, Roland K. O. Sigel. (2014) *Methods Mol Biol*, **1086**, 143-158.

- Mg^{2+} induced conformational changes in the *btuB* riboswitch from *E. coli*.
  Pallavi K. Choudhary and Roland K. O. Sigel. (2014) *RNA*, **20**, 36-45.

- Corrinoid biosynthesis and diversity of cobalamin riboswitches in the organohalide respirer *Desulfitobacterium hafniense*.
  Pallavi K. Choudhary, Aurélie Duret, Emmanuelle Rohrbach-Brandt, Christof Holliger, Roland K. O. Sigel, Julien Maillard. (2013) *J. Bacteriol*, **195**, 5186-95.

- Metal ion binding cores for the *btuB* riboswitch of *E. coli*.
  Pallavi K. Choudhary and Roland K. O. Sigel, *to be submitted*.

Poster presentations:

- The role of Mg^{2+} ions and corrin side chains on the structural rearrangement of a coenzyme B_{12} responsive *btuB* riboswitch.
  Pallavi K. Choudhary, Sofia Gallo, Roger Alberto and Roland K. O. Sigel.
  Vitamin B_{12} and Corphins: The Gordon research conference, August 2-7, 2009, Oxford, UK.

- Insights into the interaction of the *btuB* riboswitch with its cognate metabolite, coenzyme B_{12}.
  Alessia H. Dürst, Pallavi K. Choudhary, Sofia Gallo and Roland K. O. Sigel.
  11th International symposium on Inorganic Biochemistry, September 4-8, 2010, Kudowa Dröj, Poland.

- Mg^{2+} dependent folding of the *btuB* riboswitch and kinetics of its interaction with coenzyme B_{12}.
  Pallavi K. Choudhary, Alessia H. Duerst and Roland K. O. Sigel.
  Nucleic Acids Conference, Zing conferences, November 10-13, 2010, Cancun, Mexico.

- Mg^{2+} dependent folding of the *btuB* riboswitch.
  Pallavi K. Choudhary and Roland K.O. Sigel.
  Fall meeting of the Swiss Chemical Society, September 6th, 2011, EPFL, Lausanne, Switzerland.

- Mg^{2+} dependent folding of the *btuB* riboswitch.
  Pallavi K. Choudhary and Roland K.O. Sigel.
  6th Annual Dorothy Crowfoot Hodgkin symposium, October 10th, 2011, Univeristy of Zürich, Switzerland.

- Metal ion binding sites in the *btuB* riboswitch and kinetics of its interaction with coenzyme B_{12}.
  Pallavi K. Choudhary and Roland K. O. Sigel.
  Swiss RNA Workshop, February 3rd, 2012, Bern, Switzerland.

- The kinetics of interaction between the *btuB* riboswitch and coenzyme B_{12}.
  Pallavi K. Choudhary and Roland K. O. Sigel.
  17th Annual meeting of the RNA Society, May 29-June 3, 2012, University of Michigan, Ann Arbor, Michigan, USA.

- The corrinoid metabolism in *Desulfitobacterium hafniense*- genetic and regulatory aspects.
  Julien Maillard, Pallavi K. Choudhary, Emmanuelle Rohrbach-Brandt, Aurélie Duret, Roland K. O. Sigel and Christhof Holliger.
  The 6th Swiss Molecular Microbiology Meeting, September 6-7, 2012, Villars-sur-Ollon, Switzerland.

- The kinetics of interaction between the *btuB* riboswitch and coenzyme B_{12}.
  Pallavi K. Choudhary and Roland K. O. Sigel.
  Fall meeting of the Swiss Chemical Society, September 12th, 2012, ETH, Zürich, Switzerland.